Arthritis &Rheumatology

In this **Issue**

Highlights from this issue of *A&R* | **By Lara C. Pullen, PhD**

Inflammation in Patients With Rheumatoid Arthritis and Fibromyalgia Associated with Pronociceptive Brain Connections

For patients with rheumatoid arthritis (RA), peripheral inflammation affects measures of brain functional connectivity as well as fibromyalgia (FM) status. These altera-

p. 41

tions in brain connectivity center on the insula, which is a multimodal sensory processing region that is critically involved in pain perception. In this issue, Kaplan et al (p. 41) report the results of their investigation into how peripheral inflammation, the principal nociceptive stimulus in RA, interacts with brain connectivity in RA patients with FM.

The group had previously identified the inferior parietal lobule (IPL) cluster as a region linked to levels of peripheral inflammation in patients with RA. In their current research, they expanded their investigation to the connectivity of the IPL and insula in patients with concomitant RA and FM. Their new results are the first neurobiologic evidence that FM in RA may be linked to peripheral inflammation via pronociceptive patterns of brain connectivity.
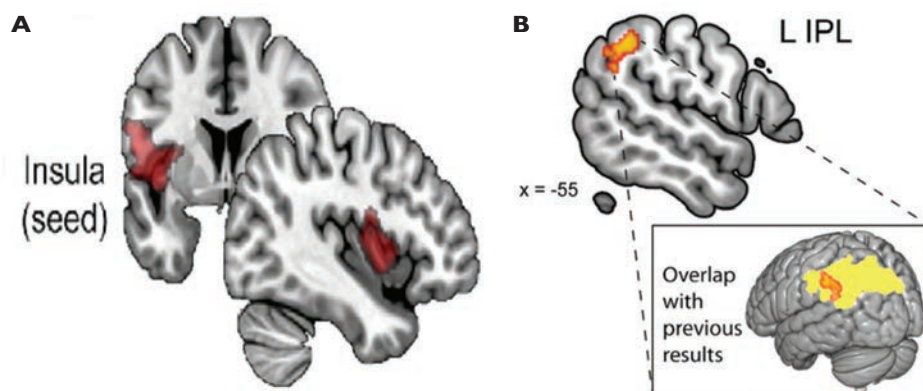

Figure 1. Correlation of higher levels of peripheral inflammation with increased brain connectivity between the left mid/posterior insula (**A**) and the left IPL (L IPL) (**B**) in RA patients with concomitant FM.

In this study, investigators examined patients with RA, some of whom had FM and some of whom did not. The 2 groups did not differ by age, sex, or erythrocyte sedimentation rate (ESR). They found that FM+ RA patients had increased functional connectivity of the insula–left IPL, left IPL–dorsal ACC, and left IPL–mPFC regions, and that these changes correlated with higher ESR levels. By performing post hoc interaction analyses, researchers were able to confirm the relationship between ESR and connectivity changes that occurred as FM scores increased. The findings suggest that, in patients with such "bottom-up" pain centralization, concomitant symptoms may partially respond to antiinflammatory treatments.

Tocilizumab Cardiovascular Risk Similar to That of Etanercept

Giles et al (p. 31) report the results of a cardiovascular (CV) safety trial of tocilizumab versus etanercept in rheumatoid arthritis. The ENTRACTE trial was designed to determine whether it was possible to rule out a relative risk for major adverse cardiovascular events

p. 31

(MACE) of 1.8 or higher in the tocilizumab group compared to the etanercept group. The investigators found that, by week 4, patients receiving tocilizumab had higher levels of low-density lipoprotein cholesterol (11.1% increase), high-density lipoprotein cholesterol (5.7% increase), and triglyceride (13.6% increase), compared to patients receiving etanercept. During a mean follow-up of 3.2 years, researchers documented 83 MACE in

the tocilizumab group and 78 MACE in the etanercept group, with an estimated hazard ratio for MACE of 1.05 (95% confidence interval 0.77–1.43). Sensitivity analyses and an on-treatment population analysis revealed similar results.

The investigators' results rule out a relative risk of 1.43 or higher for the occurrence of MACE in patients treated with tocilizumab. The investigators did note that adverse events such as serious infections and gastrointestinal perforation occurred more frequently in the tocilizumab group and concluded that their results should be interpreted in the context of the clinical efficacy and non-CV safety of tocilizumab.

Characterization of CD4+ T Cells in Patients with Idiopathic Inflammatory Myopathies

p. 179

In this issue, Galindo-Feria et al (p. 179) compare the peripheral blood mononuclear cells (PBMCs) and bronchoalveolar lavage (BAL) fluid cells from patients with idiopathic inflammatory myopathies (IIMs) and antisynthetase syndrome to those from patients with sarcoidosis and healthy controls. They report the presence of histidyl–transfer RNA synthetase (HisRS)–reactive CD4+ T cells in blood and BAL fluid cells of patients with IIM/antisynthetase syndrome relative to the comparator groups in both compartments. These patients also had antibodies to HisRS (anti–Jo-1) in BAL fluid and it was possible to identify germinal center-like structures in lung biopsy samples. The results suggest that immune activation against HisRS might take place within the lungs of patients with IIM/antisynthetase syndrome.

To investigate whether the presence and functionality of antigen-specific CD4+ T cells may vary in different compartments, the investigators analyzed T cell responses by measuring changes in CD40L expression in cells stimulated with HisRS protein or a HisRS-derived peptide (HisRS$_{11-23}$) compared to unstimulated cells. When they examined BAL fluid, they found that the highest frequencies of CD4+CD40L+ T cells were found in BAL fluid after stimulation with HisRS$_{11-23}$ with a median fold change of 7.8% (IQR 1.37-29.9%, whereas in PBMCs, the median fold change was 0.38% (IQR 0.02-5.89), suggesting an enrichment of antigen-specific T cells in the lung. Further experiments revealed that HisRS-specific CD4+CD40L+ T cells in BAL fluid presented a proinflammatory Th1 phenotype with an increased production of IFNγ, when compared to the corresponding CD4+CD40L T cells from PBMCs. The researchers concluded that there is an increased reactivity against the HisRS protein, and in particular the HisRS-derived peptide HisRS$_{11-23}$ in lung-derived T cells compared to blood-derived T cells. Taken together, the results suggest that immune activation against HisRS might take place within the lungs of patients with IIM/antisynthetase syndrome.

Gout: Primary Importance of Modifiable Risk Factors for Hyperuricemia, Uric Acid–Lowering Therapy Works

p. 157

As many studies measure serum uric acid (UA) levels in patients with gout, monosodium urate (MSU) deposits are central to the pathology of gout. In this issue, Choi et al (p. 157) report the results of their nationally representative study of men and women that investigated the role of 4 modifiable risk factors in hyperuricemia. They found that body mass index, the Dietary Approach to Stop Hypertension (DASH) diet, alcohol use, and diuretic use could be used to individually account for a substantial proportion of hyperuricemia cases. The investigators calculated the population attributable risks (PARs) of hyperuricemia cases for overweight/obesity (prevalence 60%), nonadherence to a DASH-style diet (prevalence 82%), alcohol use (prevalence 48%), and diuretic use (prevalence 8%) as 44%, 9%, 8%, and 12%, respectively.

The researchers determined that the corresponding serum urate variance explained by these risk factors was very small and, paradoxically, masked their high prevalences. For example, the serum urate variance explained by adherence to the DASH diet was just 0.1%, a finding that was similar to one previously reported in an analysis of 5 U.S. cohorts. The researchers also calculated corresponding variances of 8.9% for overweight/obesity, 0.5% for alcohol intake, and 5% for diuretic use. When they performed a simulation study, the variance neared 0% as exposure prevalence neared 100%. The authors concluded from real-life empirical evidence that these common modifiable risk factors have an important place in the primary prevention of hyperuricemia.
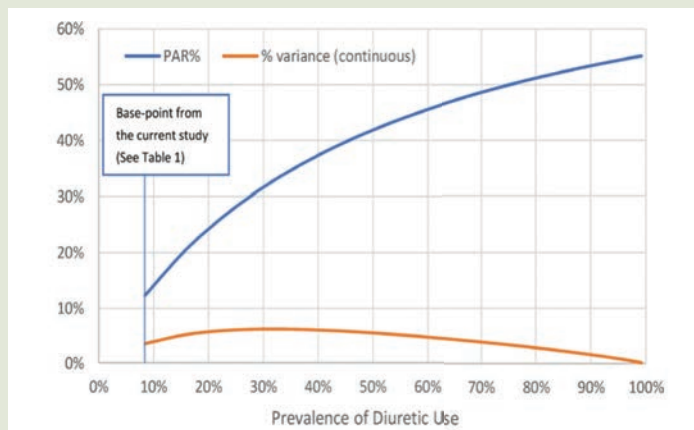

Figure 1. PAR versus variance explained according to the prevalence of diuretic use.

Also in this issue, Ellmann et al (p. 150) report that lifestyle intervention and xanthine oxidase inhibitors decrease MSU deposit burden. The team performed baseline and follow-up dual-energy computed tomography scans on 83 subjects with gout. Six subjects discontinued treatment, 24 underwent a lifestyle intervention, 29 were treated with allopurinol, 22 were treated with febuxostat, and 2 were treated with benzbromarone over the observation period. The investigators found that the mean serum UA level decreased from 7.2 to 5.8 mg/dl in the overall population. The patients who discontinued treatment had no change in MSU deposits or serum UA levels. In contrast, the burden of MSU deposits decreased in patients undergoing lifestyle intervention and in those treated with allopurinol or febuxostat. The results suggest that conventional gout therapy not only lowers serum UA levels but also reduces pathologic MSU deposits.
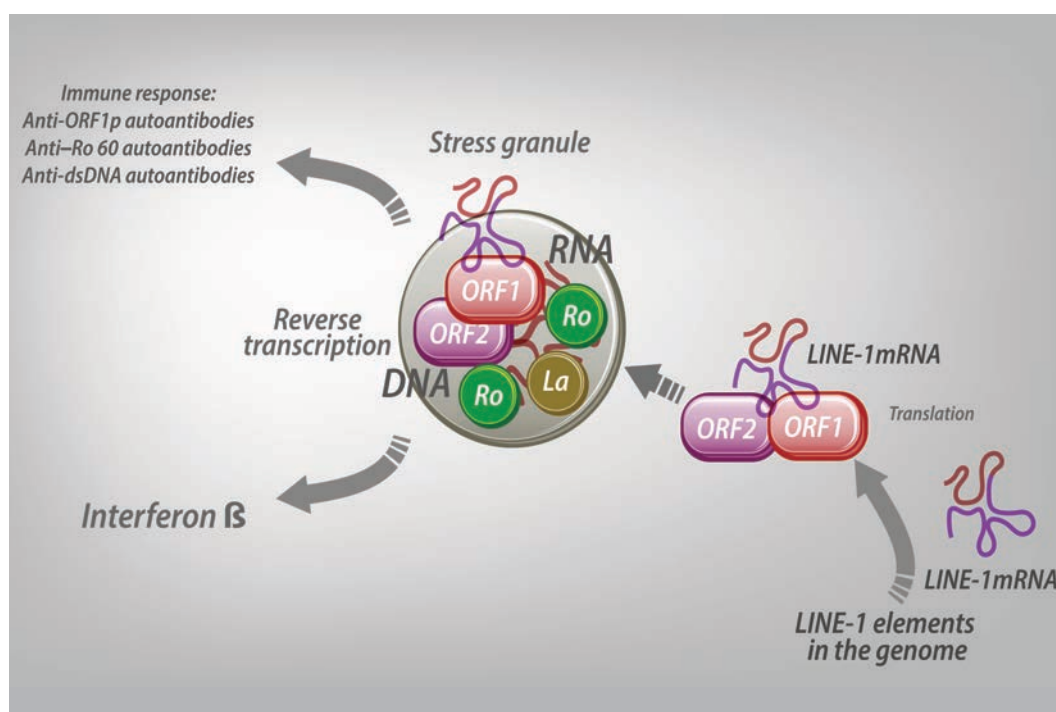
p. 150

Clinical **Connections**

High Prevalence and Disease Correlation of Autoantibodies Against p40 Encoded by Long Interspersed Nuclear Elements in SLE

CORRESPONDENCE
Tomas Mustelin, MD, PhD: tomas2@uw.edu

KEY POINTS

- Anti-ORF1p/p40 autoantibodies are prevalent and often high in lupus patients.

- Healthy subjects have low levels of these antibodies, but they gradually increase with age.

- Anti-ORF1p/p40 autoantibodies correlate with active disease.

- SLE patients also have autoantibodies against several p40-associated proteins, including Ro 60.

SUMMARY

Our genome contains half a million copies of the long interspersed nuclear element (LINE-1), a 6-kilobase sequence that encodes for 2 proteins and with the autonomous ability to replicate by a copy-and-paste mechanism. Carter et al demonstrated that systemic lupus erythematosus (SLE) patients have abundant autoantibodies against at least 1 of the 2 proteins encoded by LINE-1, the 40-kd open-reading frame 1p (ORF1p). These autoantibodies are higher in patients experiencing a flare compared to those with disease in remission, and they correlate with measures of disease activity, such as SLE Disease Activity Index score, complement consumption, anti–double-stranded DNA (anti-dsDNA) antibodies, other autoantibodies, and the presence of nephritis. Anti-p40 autoantibodies also correlate positively with type I interferons in the patient sera. Finally, LINE-1 proteins are located in macromolecular assemblies (known as stress granules) that also contain RNA-binding proteins, such as Ro 60, many of which are known SLE autoantigens. This aggregate appears to be of great interest to the autoimmune response in SLE.
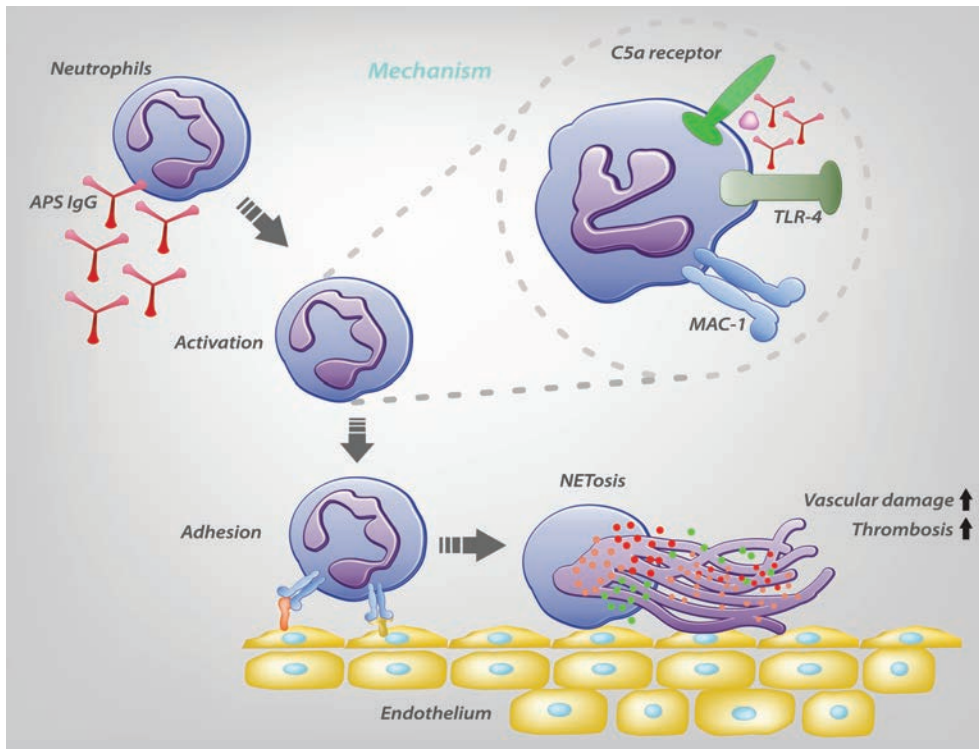
Increased Adhesive Potential of Antiphospholipid Syndrome Neutrophils Mediated by β_2 Integrin Mac-1

CORRESPONDENCE
Jason Knight, MD, PhD: jsknight@umich.edu
Omolola Eniola-Adefeso, PhD: lolaa@umich.edu

KEY POINTS

- The integrin Mac-1 is abnormally activated on the surface of APS neutrophils.

- Mac-1 activation in APS is dependent upon TLR-4 and complement-mediated signaling.

- Surface Mac-1 promotes the adhesion of APS neutrophils to a quiet endothelium, which could have implications for increased risk of thrombotic events.

- Upon adhering to endothelial cells, APS neutrophils are prone to release NETs, a process that can be neutralized by blockade of Mac-1.

SUMMARY

Antiphospholipid syndrome (APS) is an autoimmune thromboinflammatory disorder characterized by circulating antiphospholipid antibodies and a markedly increased risk of arterial and venous thrombotic events. While significant attention has been paid to activation of the endothelium as a trigger for leukocyte adhesion and thrombosis in APS, what the leukocytes bring to these adhesive interactions has received considerably less investigation. Sule et al characterized blood from APS patients in the context of cellular adhesion in a fluidic model of the human microvasculature. APS leukocytes, and especially neutrophils, are significantly more likely than control cells to adhere to a quiet, unstimulated endothelium—with the difference between APS and controls primarily mediated by the surface integrin Mac-1. Mac-1 activation in APS depends on antiphospholipid antibodies, via a signaling pathway that appears to involve both Toll-like receptor 4 (TLR-4) and the C5a receptor. Interestingly, activated Mac-1 also seems to favor the tendency of APS neutrophils to release prothrombotic neutrophil extracellular traps (NETs) upon their adherence to endothelial cells. These findings shed light on neutrophil adhesion as a potentially important player in APS-associated thrombosis, while revealing new therapeutic targets that may be pursued for the alleviation of various APS manifestations.

Arthritis & Rheumatology

An Official Journal of the American College of Rheumatology
www.arthritisrheum.org and wileyonlinelibrary.com

Arthritis & Rheumatology

Cover image: The figure on the cover (from Ellmann et al, pages 150–156) shows a 3-dimensional dual-energy computed tomography image of the first metatarsophalangeal joint of a patient with chronic tophaceous gout. Uric acid crystals in the periarticular area are visualized in green.

AMERICAN COLLEGE
of RHEUMATOLOGY
Empowering Rheumatology Professionals

EDITORIAL

Classification of IgG4-Related Disease: A Medical Marvel of Our Time

Sindhu R. Johnson[1] [ID] and Arthur Bookman[2]

In the course of our lifetime, we have watched a disease evolve from descriptions of disparate syndromes, identification of common pathologic features, to recognition of a unifying disease entity. As reported in this issue of *Arthritis & Rheumatology*, a team of multidisciplinary investigators has achieved international consensus on the development and validation of the 2019 American College of Rheumatology (ACR)/European League Against Rheumatism (EULAR) classification criteria for IgG4-related disease (1). The speed at which this evolutionary process has unfolded is remarkable.

Where we started: the blind men and the elephant

Case 1. A 45-year-old man is referred to the rheumatology clinic with facial swelling. The referring ear, nose, and throat specialist asks if this could be Sjögren's syndrome. On physical examination the patient is found to have hard painless swelling (tumefaction) of the lacrimal, parotid, and salivary glands. His serologic findings are negative.

Case 2. A 50-year-old woman presents to the emergency room with hoarseness, dysphagia, and dyspnea. Examination reveals a nontender, firm goiter. She is found to have hypothyroidism.

Case 3. A 53-year-old man is seen in the rheumatology clinic for low back pain. The pain is noninflammatory in nature. He has elevated blood pressure, an elevated creatinine level, and right leg swelling. Doppler ultrasound of the right leg reveals deep vein thrombosis.

Pattern recognition of cases that share common features is a foundation of medical practice. When the cause is unknown, we call such cases syndromes, often giving them eponymous names.

Case 1 of dacryosialoadopathy, first reported in 1888 by Johann von Mikulicz-Radecki, has been called von Mikulicz syndrome (2). Similar cases can present with a hard, non-neoplastic mass in the submandibular gland, otherwise known as a Küttner's tumor. Hermann Küttner reported 4 cases of submandibular gland masses as a consequence of chronic sclerosing sialadenitis in 1896 (3). Case 2 of chronic thyroiditis secondary to sclerotic infiltration of the thyroid gland, often leading to obstruction of surrounding structures, has been called Riedel's thyroiditis, as it was described by Bernhard Riedel in 1896 (4). Although frequently having normal thyroid function, a subset of these patients can have hypothyroidism. Case 3 of retroperitoneal fibrosis leading to ureteric obstruction, hydronephrosis, and renal injury was described by John Kelso Ormond in 1948 and is referred to as Ormond's disease (5). Compression of the inferior vena cava or iliac veins can lead to development of deep vein thrombosis.

These syndromes were thought to be unrelated and largely single organ system dominant. Each syndrome was treated by physicians with expertise in the specific involved body organs. This led to the classic elephant and the blind men scenario, with each specialist putting emphasis on the major clinical manifestation under consideration.

The paradigm shift: toward a common pathology

However, in the early 2000s, there was a paradigm shift in our perspective on these disparate syndromes. Kamisawa and colleagues published a report on a small pathologic study of 8 patients with autoimmune pancreatitis compared to control subjects. They documented the infiltration of IgG4-positive plasma cells (associated with CD4- or CD8-positive T lymphocytes) in the pancreas, but also in extrapancreatic sites including the bile duct, gallbladder, portal area of the liver, gastric mucosa, colonic mucosa, salivary glands, lymph nodes, and

[1]Sindhu R. Johnson, MD, PhD, Toronto Western Hospital, Mount Sinai Hospital, and University of Toronto, Toronto, Ontario, Canada; [2]Arthur Bookman, MD, Toronto Western Hospital and University of Toronto, Toronto, Ontario, Canada.

bone marrow (6). They suggested that autoimmune pancreatitis is not solely pancreatitis but an organ manifestation of an IgG4-related systemic disease.

From that point forward, investigators started to describe a common pathologic entity linking entities described by von Mikulicz, Küttner, Riedel, and Ormond and adding many other unsuspected examples of similar tissue findings (7). All of these syndromes shared a dense lymphoplasmacytic infiltrate with predominant IgG4-secreting plasma cells, obliterative phlebitis, and storiform fibrosis. Serum IgG4 levels were frequently, but not always, found to be elevated in such cases. Together these pathologic changes were noted to alter organ tissue architecture, causing enlargement and often disturbing function.

Toward a common nomenclature

These pathologic changes have been observed in nearly every organ of the body, including the aorta, bile ducts, breast, heart, kidneys, lungs, lymph nodes, meninges, pericardium, periorbital tissues, prostate, salivary glands, skin, and thyroid (8). It is impressive that we can now recognize them as a multiorgan disease process with unified pathology, but unknown etiology.

Numerous names have been used for this condition. These include IgG4-related sclerosing disease, IgG4-related autoimmune disease, IgG-associated multifocal systemic fibrosis, hyper-IgG4 disease, systemic IgG4-related plasmacytic syndrome, and IgG4-positive multiorgan lymphoproliferative syndrome. At a consensus meeting in 2010, Japanese investigators recommended the preferred use of "IgG4-related disease" (7). Concerns have been raised about the role of IgG4 in the pathogenesis of this disease and the ability to use serum IgG4 as a defining biomarker (9). Similar concerns relate to the imprecise use of the eponymous names, leading to confusion (9). At a subsequent international consensus meeting of multidisciplinary stakeholders in 2011, it was agreed that a shared nomenclature was indeed needed to facilitate communication and research. IgG4-related disease (IgG4-RD) was endorsed as the preferred diagnostic term (9).

Toward international agreement on classification

The ability to validly and reliably study the mechanisms underlying IgG4-RD, its epidemiology (e.g., prevalence, incidence, risk factors, survival), and response to existing or novel therapies is adversely affected by heterogeneity in clinical presentation and disease recognition. This heterogeneity not only adds to uncertainty around any conclusions made within a study, but also challenges comparison of findings across studies. The ACR and EULAR have long recognized the need for classification criteria

to identify more homogeneous groups of patients for inclusion in research studies (10–12).

With a balanced use of expert-based and data-driven methodology, the investigators have developed a system of classification that comprises entry, exclusion, and additive inclusion criteria. With a threshold score of ≥20 points, IgG4-RD can be classified. In the final validation cohort, the investigators observed reasonably high sensitivity of 82% and very high specificity of 97.8% (1). In the modern era of classification criteria development, their use of weighted criteria and a numeric point system confers an important advantage. It more accurately reflects physician thinking, with more emphasis put on some symptoms or signs than others (13–16)

We should remember that developing and validating criteria is not easy. Due to the potential biases that may affect criteria development, rigorous methodologic standards must be met before a criteria set is endorsed by either the ACR or EULAR (10,12,17,18). Furthermore, achieving international agreement on classification of disease is difficult (16). It is even harder with heterogeneous multisystem diseases, including others that we know well (e.g., systemic sclerosis, systemic lupus erythematosus) (13,19). It is particularly noteworthy that this group of investigators was able to achieve international consensus on a multisystem disease that is newly described.

Readers should be aware of some caveats. These criteria will not suffice for diagnosis (20). They were developed for research purposes. Reasonable precaution will be required, as the criteria necessitate judgment and diligence when used for any reason other than the assembly of a cohort for study and research. Unusual sites of infiltration have been reported, such as hypophysitis (21), thymus (22), temporal lobe (23), true ocular infiltrate (24), or aortic root involvement (25). Readers are reminded that classification criteria do not comprise the complete list of disease manifestations. Investigators will need to consider how patients with infrequent or excluded sites of infiltration may access innovative therapies in the setting of clinical trials. More importantly, a patient's not fulfilling classification criteria should not preclude a diagnosis of IgG4-RD, and should not be used by payers as justification to withhold appropriate therapy (20).

Landmark publication

The ACR/EULAR classification criteria for IgG4-related disease is a landmark publication. It represents a breathtaking rate of progress from misunderstood disease entities to the discovery of common pathology, the construction of international consensus on nomenclature, and then the development of validated, internationally accepted classification criteria. All of this has occurred within 16 years.

These classification criteria will form the inclusion criteria for basic, translational, and epidemiologic studies to better characterize the frequency and determinants of IgG4-related disease.

Furthermore, they position us to embark on studies of novel and innovative therapeutics to bring relief and maintained remission to this unique patient group. The participating investigators should be congratulated for moving the ball forward, to a point where we can make better inroads toward understanding and management of IgG4-related disease.

AUTHOR CONTRIBUTIONS

Drs. Johnson and Bookman drafted the article, revised it critically for important intellectual content, and approved the final version to be published.

REFERENCES

1. Wallace ZS, Naden RP, Chari S, Choi H, Della-Torre E, Dicaire JF, et al. The 2019 American College of Rheumatology/European League Against Rheumatism classification criteria for IgG4-related disease. Arthritis Rheumatol 2020;72:7–19.

2. Von Mikulicz-Radecki J. Über eine eigenartige symmetrische erkrankung der thränen- und mundspeicheldrüsen. Billroth T, editor. Stuttgart: Beitr. z. Chir. Festschr; 1892.

3. Küttner H. Über entzündliche tumoren der submaxillar-speicheldrüse. Bruns Beitr Klin Chir 1896;15:815–28.

4. Riedel BM. Die chronische, zur bildung eisenharter tumoren führende entzündung der schilddrüse. Verhandlungen der deutschen Gesellschaft für Chirurgie 1896;25:101–5.

5. Ormond JK. Bilateral ureteral obstruction due to envelopment and compression by an inflammatory retroperitoneal process. J Urol 1948;59:1072–9.

6. Kamisawa T, Funata N, Hayashi Y, Eishi Y, Koike M, Tsuruta K, et al. A new clinicopathological entity of IgG4-related autoimmune disease. J Gastroenterol 2003;38:982–4.

7. Umehara H, Okazaki K, Masaki Y, Kawano M, Yamamoto M, Saeki T, et al, and the Research Program for Intractable Disease by Ministry of Health, Labor and Welfare (MHLW) Japan G4 team. A novel clinical entity, IgG4-related disease (IgG4RD): general concept and details. Mod Rheumatol 2012;22:1–14.

8. Stone JH, Zen Y, Deshpande V. IgG4-related disease [review]. N Engl J Med 2012;366:539–51.

9. Stone JH, Khosroshahi A, Deshpande V, Chan JK, Heathcote JG, Aalberse R, et al. Recommendations for the nomenclature of IgG4-related disease and its individual organ system manifestations. Arthritis Rheum 2012;64:3061–7.

10. Felson DT, Anderson JJ. Methodological and statistical approaches to criteria development in rheumatic diseases. Baillieres Clin Rheumatol 1995;9:253–66.

11. Classification and Response Criteria Subcommittee of the American College of Rheumatology Committee on Quality Measures. Development of classification and response criteria for rheumatic diseases [editorial]. Arthritis Rheum 2006;55:348–52.

12. Johnson SR, Goek ON, Singh-Grewal D, Vlad SC, Feldman BM, Felson DT, et al. Classification criteria in rheumatic diseases: a review of methodologic properties. Arthritis Rheum 2007;57:1119–33.

13. Johnson SR, Khanna D, Daikh D, Cervera R, Costedoat-Chalumeau N, Gladman DD, et al. Use of consensus methodology to determine candidate items for systemic lupus erythematosus classification criteria. J Rheumatol 2019;46:721–6.

14. Tedeschi SK, Johnson SR, Boumpas DT, Daikh D, Dörner T, Diamond B, et al. Multicriteria decision analysis process to develop new classification criteria for systemic lupus erythematosus. Ann Rheum Dis 2019;78:634–40.

15. Johnson SR, Naden RP, Fransen J, van den Hoogen F, Pope JE, Baron M, et al. Multicriteria decision analysis methods with 1000minds for developing systemic sclerosis classification criteria. J Clin Epidemiol 2014;67:706–14.

16. Neogi T, Aletaha D, Silman AJ, Naden RL, Felson DT, Aggarwal R, et al. The 2010 American College of Rheumatology/European League Against Rheumatism classification criteria for rheumatoid arthritis: phase 2 methodological report. Arthritis Rheum 2010;62:2582–91.

17. Dougados M, Betteridge N, Burmester GR, Euller-Ziegler L, Guillemin F, Hirvonen J, et al. EULAR standardised operating procedures for the elaboration, evaluation, dissemination, and implementation of recommendations endorsed by the EULAR standing committees. Ann Rheum Dis 2004;63:1172–6.

18. Johnson SR, Grayson PC. Use of "provisional" designation for response criteria [editorial]. Arthritis Care Res (Hoboken) 2018;70:811–2.

19. Van den Hoogen F, Khanna D, Fransen J, Johnson SR, Baron M, Tyndall A, et al. 2013 classification criteria for systemic sclerosis: an American College of Rheumatology/European League Against Rheumatism collaborative initiative. Arthritis Rheum 2013;65:2737–47.

20. Aggarwal R, Ringold S, Khanna D, Neogi T, Johnson SR, Miller A, et al. Distinctions between diagnostic and classification criteria? [review]. Arthritis Care Res (Hoboken) 2015;67:891–7.

21. Uccella S, Amaglio C, Brouland JP, Bianconi E, Ippolito S, Messerer M, et al. Disease heterogeneity in IgG4-related hypophysitis: report of two histopathologically proven cases and review of the literature. Virchows Arch 2019;475:373–81.

22. Oda R, Okuda K, Murase T, Watanabe T, Sakane T, Tatematsu T, et al. Thymic inflammatory pseudotumor with multilocular thymic cyst caused by immunoglobulin G4-related disease. Thorac Cancer 2019;10:116–9.

23. Chan BW, Chan RC, Cupples J. IgG4-related disease presenting as a temporal lobe tumor [letter]. J Neurosurg Sci 2017;61:680–1.

24. Gange WS, Holland SM, De Alba F. IgG4-related ophthalmic disease presenting as choroidal and orbital lesions. Retin Cases Brief Rep 2019;13:283–6.

25. Hourai R, Ozawa H, Sohmiya K, Hirose Y, Katsumata T, Daimon M, et al. IgG4-positive plasmacytic infiltration in aortic wall and aortic valve surgical samples and its relation to preoperative serum IgG4 levels. Int Heart J 2019;60:688–94.

American College
of Rheumatology
Empowering Rheumatology Professionals

EDITORIAL

When Randomized Clinical Trials and Real-World Evidence Say the Same: Tocilizumab and Its Cardiovascular Safety

Seoyoung C. Kim [iD] and Sebastian Schneeweiss

In this issue of *Arthritis & Rheumatology*, Giles et al report much-awaited data from the ENTRACTE trial (1). The US Food and Drug Administration (FDA) required this postmarketing randomized controlled trial (RCT) to study the risk of major adverse cardiovascular events (MACE) in patients with rheumatoid arthritis (RA) treated with tocilizumab at 8 mg/kg monthly by intravenous infusion, compared to the risk in those treated with etanercept at 50 mg weekly by subcutaneous injection (1).

We always gain important clinical insights from a well-conducted RCT like ENTRACTE. It was designed to study cardiovascular (CV) outcomes in eligible patients who had active RA, were age ≥50 years, and had ≥1 CV disease (CVD) risk factor, history of a CVD event, or extraarticular RA. The final cohort of this RCT included a total of 3,080 RA patients (1,538 receiving tocilizumab and 1,542 receiving etanercept). In their primary intent-to-treat analysis over a mean follow-up period of 3.2 years, 83 MACE (5.4%) occurred in the tocilizumab group compared to 78 MACE (5.1%) in the etanercept group, resulting in a hazard ratio (HR) of 1.05 with a 95% confidence interval (95% CI) of 0.77–1.43. The authors concluded that the results of the ENTRACTE study ruled out a relative risk of MACE of 1.43 or higher in patients treated with tocilizumab compared to those treated with etanercept.

We all appreciate data from RCTs, but is a trial always necessary? Or can we answer some safety and effectiveness questions in a clinical patient population using data collected through the healthcare system? The FDA currently develops guidance documents on how real world evidence (RWE) studies can inform regulatory decision making, following a trend demanding more high-quality RWE to complement RCTs when they are done, and substitute for RCTs when they are not conducted (2).

While the ENTRACTE trial was still ongoing, a cohort study by Kim et al used data from 3 different administrative claims databases in the US to examine the CV safety of tocilizumab compared to tumor necrosis factor inhibitors (TNFi) among RA patients

(3). That cohort study, first presented at the American College of Rheumatology annual meeting in 2016, included a total of 28,038 RA patients with prior use of a TNFi (9,218 assigned to receive tocilizumab and 18,810 assigned to receive TNFi) and found no increased risk of CV events (i.e., hospitalization for myocardial infarction [MI] or stroke) associated with tocilizumab use compared to TNFi use in extensive propensity score–matched analyses (HR_{pooled} = 0.84, 95% CI 0.56–1.26). After the ENTRACTE trial was completed, another insurance claims data–based study was conducted by Xie et al (4). Using 2 of the 3 claims databases formerly studied by Kim et al (i.e., Medicare and Truven MarketScan) and a slightly different outcome definition and analytic strategy, Xie et al came to very similar conclusions with regard to the risk of CV events in comparing tocilizumab against any TNFi ($HR_{Medicare}$ = 0.79, 95% CI 0.63–0.98; $HR_{MarketScan}$ = 0.78, 95% CI 0.49–1.23) or against etanercept ($HR_{Medicare}$ = 0.90, 95% CI 0.66–1.25; $HR_{MarketScan}$ = 0.69, 95% CI 0.41–1.15). In another analysis by Xie et al in which prior use of a biologic disease-modifying antirheumatic drug was required, the HRs for risk of CV events associated with tocilizumab use compared to any TNFi were comparable to that in the study by Kim et al ($HR_{Medicare}$ = 0.79, 95% CI 0.65–0.96; $HR_{MarketScan}$ = 0.84, 95% CI 0.52–1.37 (see Supplementary Figure 2 in Xie et al [4]).

What can we learn from comparing the current RCT to these 2 RWE studies?

The ENTRACTE trial (1) is an interesting case study to discuss the complementarity of RCTs and RWE studies, 1 of which, the RWE study by Kim et al (3), publicly predicted the major findings before the results of the ENTRACTE trial were available, and the second of which, the RWE study by Xie et al (4), confirmed the trial findings post hoc. Both the ENTRACTE trial (1) and the 2 RWE studies using healthcare claims data

Seoyoung C. Kim, MD, ScD, MSCE, Sebastian Schneeweiss, MD, ScD: Brigham and Women's Hospital and Harvard Medical School, Boston, Massachusetts.

Address correspondence to Seoyoung C. Kim, MD, ScD, MSCE, 1620 Tremont Street, Suite 3-030, Boston, MA 02120. E-mail: sykim@bwh.harvard.edu.

(3,4) came to the same conclusion, that there is no increased risk of adverse CV events among patients treated with tocilizumab compared to patients treated with TNFi. The 2 RWE studies largely agreed in their point estimates, with overlapping 95% CIs, and the RCT showed a point estimate that was numerically different, although the 95% CI substantially overlapped with those in the RWE studies. The upper 95% confidence limits of both RWE studies were below 1.3, which is used as the FDA threshold for CV outcome trials in patients with diabetes (5).

Can we interpret the results from these studies as "nearly identical"? One may think the HR for MACE from the RCT (HR 1.05) (1) is not the same as the HRs of 0.84 and 0.90 in the cohort studies (3,4). Two general considerations are to be made. First, to what extent did the RWE studies emulate the RCT, and how do they differ and expand on the RCT findings? Second, were there any biases operating in the RWE study or the RCT that could result in numeric differences?

There are key differences between these studies. First, the RWE studies included patients with a wide age range, and included those with and those without existing CVD (3,4).

Second, the cohort study by Kim and colleagues limited its population to patients with prior TNFi use (3), and in the study by Xie and colleagues, 50% of patients had prior TNFi use (4). Although these populations are much more reflective of those found in clinical care than the RCT, it is a critical population difference.

Third, the ENTRACTE trial used etanercept as a comparator (1), whereas the study by Kim et al used the class of TNFi as a comparator group (3).

Fourth, the primary outcome in the ENTRACTE trial was defined as adjudicated MACE, including nonfatal MI, nonfatal stroke, and CV-related deaths in the RCT (1). In contrast, the RWE studies mostly relied on the claims-based algorithms to identify MI or stroke as the primary outcome with high specificity (3,4), but may have missed some marginal events.

Fifth, the primary analysis of the RCT data was an intent-to-treat analysis, with 10% of the follow-up time being misclassified because of treatment discontinuation, and its on-treatment analysis yielded a numerically different result (1). The RWE studies focused on on-treatment analyses, given the substantial lack of persistence of treatments, but also provided secondary analyses (3,4).

Sixth, the follow-up time was substantially shorter in the RWE studies than in the RCT, reflecting suboptimal adherence patterns in routine care (6).

In light of these key differences in the study populations and additional differences in the follow-up and analytic methods, the treatment effect estimates and their 95% CIs are reassuringly consistent. Nevertheless, it may be most reasonable to compare the overall clinical conclusion, that there is no increased CVD risk in patients treated with tocilizumab compared to patients treated with TNFi, across all studies, rather than comparing the exact point estimates.

Implications for RWE studies

Any RWE study that can be anchored in RCT evidence helps gain confidence in RWE findings (7,8). It provides confidence that biases are controlled and minimized. The 2 RWE studies (3,4) had a similar overall aim but were not designed to emulate the ENTRACTE trial completely. Systematic comparisons of RWE studies that emulate RCTs as closely as possible in terms of populations, exposure, and outcomes are ongoing and show promising early results (7,9,10). This will help identify those situations in which RWE studies are valid alternatives as opposed to those situations in which RWE studies would be misleading and should be avoided.

There are many examples of misleading RWE studies, such as the early claim that postmenopausal hormone replacement therapy would reduce coronary heart disease (11), which was later reanalyzed using a new user design that avoided survivorship bias (12), the findings of which yielded the same conclusion as the subsequent RCT, which did not find reduction in coronary heart disease with postmenopausal hormone replacement therapy (13). In other circumstances, apparent discrepancies between RCTs and RWE studies may be attributable to different patient populations or different measurement approaches, making a direct comparison less meaningful. Several RWE studies of RA patients have suggested potential CV benefits from treatment with methotrexate (14,15), which were discordant with the findings from the Cardiovascular Inflammation Reduction Trial (CIRT), which found no CV benefits from methotrexate (16). However, CIRT did not include any patients with RA or patients with any other systemic inflammatory diseases, resulting in a study population of patients with minimal systemic inflammation and a median C-reactive protein level of 1.5 mg/liter. Whether methotrexate has CV effects on patients with moderate-to-high systemic inflammation (e.g., patients with RA) remains to be determined in an RCT.

The advantages of RWE studies, if well done and allowing causal conclusions on treatment effects, are obvious. They include broader and often clinically more relevant population segments, and can ask many more questions than any single RCT can, because of their ability to access very large, longitudinal data sources. Not surprisingly, RWE studies that rely on already collected information are far more efficient than most trials. The ENTRACTE trial started patient enrollment in 2011 and ended in mid-2016 (ClinicalTrials.gov identifier: NCT01331837), whereas the RWE study by Kim et al (3) was registered in 2015 (EU PAS Registry identifier: EUPAS11327) and completed in spring 2016.

The limitations of RWE studies are equally obvious and are largely related to measurement issues when the study relies on secondary data, and related to the lack of baseline randomization,

which exposes studies to the risk of confounding bias (7). Hybrid designs and ever richer healthcare data sources will increasingly improve the situation. However, it is important to note that the analysis of real-world data requires experience with the data sources and training in pharmacoepidemiology. Steps that might improve confidence in RWE studies could include ways to improve transparency of data (17,18), preregistration of RWE studies (19), and systematic comparisons of RWE studies that emulate RCTs (see http://rctduplicate.org).

While the FDA and other regulatory agencies are quite experienced in designing and interpreting RWE studies that evaluate the safety of medical products, we are in a critical time period in which regulatory agencies need to re-evaluate their use of RWE for approval decisions (2). Rheumatology has now contributed another important case study to this complex decision.

AUTHOR CONTRIBUTIONS

Both authors were involved in drafting the article, revising it critically for important intellectual content, and approving the final version for publication.

REFERENCES

1. Giles JT, Sattar N, Gabriel S, Ridker PM, Gay S, Warne C, et al. Cardiovascular safety of tocilizumab versus etanercept in rheumatoid arthritis: a randomized controlled trial. Arthritis Rheumatol 2019; 72:31–40.

2. US Food and Drug Administration. Framework for FDA's real-world evidence program. December 2018. URL: https://www.fda.gov/media/120060/download.

3. Kim SC, Solomon DH, Rogers JR, Gale S, Klearman M, Sarsour K, et al. Cardiovascular safety of tocilizumab versus tumor necrosis factor inhibitors in patients with rheumatoid arthritis: a multi-database cohort study. Arthritis Rheumatol 2017;69:1154–64.

4. Xie F, Yun H, Levitan EB, Muntner P, Curtis JR. Tocilizumab and the risk of cardiovascular disease: direct comparison among biologic disease-modifying antirheumatic drugs for rheumatoid arthritis patients. Arthritis Care Res (Hoboken) 2019;71:1004–18.

5. US Department of Health and Human Services, Food and Drug Administration, Center for Drug Evaluation and Research (CDER). Guidance for industry: diabetes mellitus—evaluating cardiovascular risk in new antidiabetic therapies to treat type 2 diabetes. December 2008. URL: https://www.fda.gov/media/71297/download.

6. Bradley LA. Adherence with treatment regimens among adult rheumatoid arthritis patients: current status and future directions. Arthritis Care Res 1989;2:S33–9.

7. Franklin JM, Glynn RJ, Martin D, Schneeweiss S. Evaluating the use of nonrandomized real-world data analyses for regulatory decision making. Clin Pharmacol Ther 2019;105:867–77.

8. Schneeweiss S. Real-world evidence of treatment effects: the useful and the misleading. Clin Pharmacol Ther 2019;106:43–4.

9. Fralick M, Kesselheim AS, Avorn J, Schneeweiss S. Use of health care databases to support supplemental indications of approved medications. JAMA Intern Med 2018;178:55–63.

10. Patorno E, Schneeweiss S, Gopalakrishnan C, Martin D, Franklin JM. Using real-world data to predict findings of an ongoing phase IV cardiovascular outcome trial: cardiovascular safety of linagliptin versus glimepiride. Diabetes Care 2019;42:2204–10.

11. Grodstein F, Stampfer MJ, Manson JE, Colditz GA, Willett WC, Rosner B, et al. Postmenopausal estrogen and progestin use and the risk of cardiovascular disease. N Engl J Med 1996;335:453–61.

12. Ray WA. Evaluating medication effects outside of clinical trials: new-user designs. Am J Epidemiol 2003;158:915–20.

13. Hernán MA, Alonso A, Logan R, Grodstein F, Michels KB, Willett WC, et al. Observational studies analyzed like randomized experiments: an application to postmenopausal hormone therapy and coronary heart disease. Epidemiology 2008;19:766–79.

14. Westlake SL, Colebatch AN, Baird J, Kiely P, Quinn M, Choy E, et al. The effect of methotrexate on cardiovascular disease in patients with rheumatoid arthritis: a systematic literature review. Rheumatology (Oxford) 2010;49:295–307.

15. Micha R, Imamura F, Wyler von Ballmoos M, Solomon DH, Hernán MA, Ridker PM, et al. Systematic review and meta-analysis of methotrexate use and risk of cardiovascular disease. Am J Cardiol 2011;108:1362–70.

16. Ridker PM, Everett BM, Pradhan A, MacFadyen JG, Solomon DH, Zaharris E, et al. Low-dose methotrexate for the prevention of atherosclerotic events. N Engl J Med 2019;380:752–62.

17. Schneeweiss S, Rassen JA, Brown JS, Rothman KJ, Happe L, Arlett P, et al. Graphical depiction of longitudinal study designs in health care databases. Ann Intern Med 2019;170:398–406.

18. Wang SV, Schneeweiss S, Berger ML, Brown J, de Vries F, Douglas I, et al. Reporting to improve reproducibility and facilitate validity assessment for healthcare database studies V1.0. Pharmacoepidemiol Drug Saf 2017;26:1018–32.

19. Berger ML, Sox H, Willke RJ, Brixner DL, Eichler HG, Goettsch W, et al. Good practices for real-world data studies of treatment and/or comparative effectiveness: recommendations from the joint ISPOR-ISPE Special Task Force on real-world evidence in health care decision making. Pharmacoepidemiol Drug Saf 2017;26:1033–9.

AMERICAN COLLEGE
of RHEUMATOLOGY
Empowering Rheumatology Professionals

SPECIAL ARTICLE

The 2019 American College of Rheumatology/European League Against Rheumatism Classification Criteria for IgG4-Related Disease

Zachary S. Wallace,[1] iD Ray P. Naden,[2] Suresh Chari,[3] Hyon Choi,[1] iD Emanuel Della-Torre,[4] Jean-Francois Dicaire,[5] Phil A. Hart,[6] Dai Inoue,[7] Mitsuhiro Kawano,[8] Arezou Khosroshahi,[9] Kensuke Kubota,[10] Marco Lanzillotta,[11] Kazuichi Okazaki,[12] Cory A. Perugino,[1] Amita Sharma,[1] Takako Saeki,[13] Hiroshi Sekiguchi,[3] Nicolas Schleinitz,[14] James R. Stone,[1] Naoki Takahashi,[3] Hisanori Umehara,[15] George Webster,[16] Yoh Zen,[17] and John H. Stone,[1] iD for the American College of Rheumatology/European League Against Rheumatism IgG4-Related Disease Classification Criteria Working Group

Objective. IgG4-related disease (IgG4-RD) can cause fibroinflammatory lesions in nearly any organ. Correlation among clinical, serologic, radiologic, and pathologic data is required for diagnosis. This work was undertaken to develop and validate an international set of classification criteria for IgG4-RD.

Methods. An international multispecialty group of 86 physicians was assembled by the American College of Rheumatology (ACR) and the European League Against Rheumatism (EULAR). Investigators used consensus exercises, existing literature, derivation and validation cohorts of 1,879 subjects (1,086 cases, 793 mimickers), and multicriterion decision analysis to identify, weight, and test potential classification criteria. Two independent validation cohorts were included.

Results. A 3-step classification process was developed. First, it must be demonstrated that a potential IgG4-RD case has involvement of at least 1 of 11 possible organs in a manner consistent with IgG4-RD. Second, exclusion criteria consisting of a total of 32 clinical, serologic, radiologic, and pathologic items must be applied; the presence of any of these criteria eliminates the patient from IgG4-RD classification. Third, 8 weighted inclusion criteria domains, addressing clinical findings, serologic results, radiology assessments, and pathology interpretations, are applied. In the first validation cohort, a threshold of 20 points had a specificity of 99.2% (95% confidence interval [95% CI] 97.2–99.8%) and a sensitivity of 85.5% (95% CI 81.9–88.5%). In the second, the specificity was 97.8% (95% CI 93.7–99.2%) and the sensitivity was 82.0% (95% CI 77.0–86.1%). The criteria were shown to have robust test characteristics over a wide range of thresholds.

Conclusion. ACR/EULAR classification criteria for IgG4-RD have been developed and validated in a large cohort of patients. These criteria demonstrate excellent test performance and should contribute substantially to future clinical, epidemiologic, and basic science investigations.

Introduction

IgG4-related disease (IgG4-RD) is an immune-mediated condition associated with fibroinflammatory lesions that can occur at nearly any anatomic site (1,2). It often presents as a multiorgan disease and may be confused with malignancy, infection, or other immune-mediated conditions, such as Sjögren's syndrome or vasculitis, associated with antineutrophil cytoplasmic antibodies (ANCAs). Rheumatologists, internists, gastroenterologists, nephrologists, pulmonologists, neurologists, radiologists, pathologists, and other practitioners are often involved in the evaluation of patients with this condition. IgG4-RD can lead to organ dysfunction, organ failure, and death. Its epidemiology remains poorly described because of its relatively recent recognition as a discrete condition, yet the disease is now seen by both generalists and specialists all across the world.

IgG4-RD was first recognized as a distinct disease in 2003 (3,4). Over the next decade, it became clear that although the disease could affect virtually any organ, there are strong predilections for certain organs (1,5). These include the major salivary glands (submandibular, parotid, sublingual), the orbits and lacrimal glands, the pancreas and biliary tree, the lungs, the kidneys, the aorta and retroperitoneum, the meninges, and the thyroid gland (Riedel's thyroiditis) (6–8). Many of the early diagnoses of IgG4-RD relied on pathologic assessment of surgical resection specimens (9). These discoveries were often incidental findings made following resections of lesions with suspected malignancy. The large pathologic samples available from such procedures generally permitted identification of a full range of findings considered characteristic of IgG4-RD: a lymphoplasmacytic infiltrate, storiform fibrosis, obliterative phlebitis, and dramatic IgG4+ plasma cell infiltrates, among others (9). With growing recognition of this condition, however, the diagnosis is now made using increasingly small biopsy samples that frequently do not demonstrate the full spectrum of pathologic findings (7,9,10). In a subset of patients with classic combinations of clinical, serologic, or radiologic findings, clinical diagnoses are sometimes made in the absence of biopsy, but the threshold to perform biopsies of accessible sites when there is significant concern about malignancy or infection remains appropriately low.

Other cases diagnosed early in the course of IgG4-RD were identified because of striking elevations in serum IgG4 concen-

trations (4). However, it is now recognized that serum IgG4 levels are normal in a substantial percentage of patients with clinico-pathologic diagnoses of IgG4-RD (6,11,12). Although serum IgG4 concentrations can provide an important clue to the diagnosis and some guidance in the longitudinal assessment of disease activity, the centrality of IgG4 in the overall pathophysiology of this condition has been called into question (13). The presence of an elevated serum IgG4 level is no longer considered essential to the diagnosis of IgG4-RD. Indeed, certain organ systems and anatomic regions (e.g., the retroperitoneum) are less likely to be associated with a serum IgG4 elevation than are others (6).

Finally, the radiologic features of IgG4-RD have also been described with increasing thoroughness. Radiologic findings such as a sausage-shaped pancreas and periaortitis affecting the infrarenal aorta are now viewed as being strongly suggestive of IgG4-RD if detected in the proper clinical context (14,15). Nevertheless, radiologic findings in isolation—without reference to clinical, serologic, or pathologic data—are never sufficient for either clinical diagnosis or appropriate disease classification.

In short, although clinical, serologic, radiologic, and pathologic features all contribute to the classification of IgG4-RD, none of these approaches alone provides definitive evidence for the accurate classification of patients. The proper categorization of patients for both research studies and clinical purposes relies upon integration of data from all 4 domains of evidence. Given the recent recognition of IgG4-RD as a distinct condition, along with its multiorgan nature and the absence of a single diagnostic feature, classification criteria are now needed for the conduct of high-quality clinical and epidemiologic investigations in this disease.

Methods

This study was approved by the Partners HealthCare Institutional Review Board.

Study overview. The development and testing of the classification criteria for IgG4-RD was based on consensus-based and data-driven methods using prospectively collected data and decision analytics (16–19).

[1]Zachary S. Wallace, MD, Hyon Choi, MD, PhD, Cory A. Perugino, DO, Amita Sharma, MD, James R. Stone, MD, MPH, John H. Stone, MD, MPH: Massachusetts General Hospital, Boston; [2]Ray P. Naden, MD, FRACP: New Zealand Health Ministry, Auckland, New Zealand; [3]Suresh Chari, MD, Hiroshi Sekiguchi, MD, Naoki Takahashi, MD, PhD: Mayo Clinic, Rochester, Minnesota; [4]Emanuel Della-Torre, MD: IRCCS Ospedale San Raffaele, Milan, Italy; [5]Jean-Francois Dicaire: Pinnacle, Inc., Montreal, Quebec, Canada; [6]Phil A. Hart, MD: Ohio State University College of Medicine, Columbus; [7]Dai Inoue, MD, MPH: Kanazawa University, Kanazawa, Japan; [8]Mitsuhiro Kawano, MD, MPH: Kanazawa University Hospital, Kanazawa, Japan; [9]Arezou Khosroshahi, MD: Emory University,

Atlanta, Georgia; [10]Kensuke Kubota, MD: Yokohama City University, Yokohama, Japan; [11]Marco Lanzillotta, MD: IRCCS, Milan, Italy; [12]Kazuichi Okazaki, MD, PhD: Kansai Medical University, Hirakata, Japan; [13]Takako Saeki, MD, PhD: Nagaoka Red Cross Hospital, Nagaoka, Japan; [14]Nicolas Schleinitz, MD: Aix-Marseille University, Marseille, France; [15]Hisanori Umehara, MD, PhD: Kanazawa Medical University, Uchinada, Japan, and Hayashi Hospital, Echizen, Japan; [16]George Webster, MD, FRCP: University College London, London, UK; [17]Yoh Zen, MD, PhD, FRCP: Kobe University, Kobe, Japan.

Investigators. A Steering Committee composed of investigators from North America, Europe, and Asia was established. The Steering Committee directed the entire project and invited other investigators who were assigned to specific Advisory Groups addressing clinical, serologic, radiologic, and pathologic issues. In addition to members of the Steering Committee and the Advisory Groups, other investigators were invited to participate by submitting cases of IgG4-RD and of mimicking conditions to be used in the development and testing phases of the study. This full group of investigators is known as the American College of Rheumatology (ACR)/European League Against Rheumatism (EULAR) IgG4-RD Classification Criteria Working Group (Appendix A).

Item generation. Each Advisory Group consisted of a Steering Committee member and experts in the field being addressed by the specific Advisory Group. The Advisory Groups were tasked with using evidence- and consensus-based approaches to identify items that might be relevant to the classification of patients as having or not having IgG4-RD. These items comprised preliminary exclusion criteria and preliminary inclusion criteria. Preliminary exclusion criteria were defined as items that would lead to termination of consideration of the patient as an IgG4-RD case. In contrast, preliminary inclusion criteria could either increase or decrease the likelihood of classification of the patient as an IgG4-RD case. Preliminary inclusion criteria that demonstrated discriminatory ability to increase the likelihood of classification were later selected as inclusion criteria. A 24-member Steering Committee of the ACR/EULAR IgG4-RD Classification Criteria Development Group met in Boston in April 2016 to begin this process. At this initial Steering Committee meeting, 104 rounds of consensus-based decision-making were conducted. Consensus was achieved for 79 (76%) of these decisions, the process of which is described below. Item generation and the subsequent task of item reduction were continued through teleconferences and e-mail discussions.

Process of consensus. The rules regarding consensus were set out at the time of the first face-to-face meeting. Consensus was considered to have been reached when 80% of the members of the Steering Committee were in agreement on a given point. Discussion was permitted following achievement of the 80% threshold, however, if individuals in the minority wished to express the rationale behind their opinion. During discussions, evidence was presented by participants to support arguments. Discussants referred to the medical literature when relevant to illuminate a particular question. In some instances, in the setting of a persuasive argument by a member of the minority, discussion led to re-voting and occasionally to a change in the ultimate decision on a particular point.

Item reduction. Following item generation, the Steering Committee participated in 2 exercises to reduce the number of items. First, the Committee reviewed all proposed inclusion and exclusion criteria and reduced the potential criteria into 8–10 domains through the consensus process described above. Related items were clustered within domains that were independent of the other domains; for preliminary inclusion criteria, items contributed positive or negative weights toward classifying cases as IgG4-RD. For instance, biopsy immunohistochemistry results (e.g., IgG4+ plasma cells/high-power field [hpf] and IgG4+IgG+ plasma cells/hpf) were listed under an immunohistochemistry domain. Within each preliminary inclusion criteria domain, items were arranged by group members according to the degree to which they either increased or decreased the likelihood of classification as IgG4-RD (e.g., an infiltrate of ≥40 IgG4+ plasma cells/ hpf was positioned above an infiltrate of 0–9 IgG4+ plasma cells/ hpf). Definitions for each item were determined such that cases could be assigned clearly to only 1 item in a domain.

The Steering Committee then ranked each potential preliminary inclusion criteria item on a Likert scale from –5 ("Highly confident the patient does not have IgG4-RD if this item is present") to +5 ("Highly confident the patient has IgG4-RD if this item is present"). Items associated with an average confidence between –2.0 and +2.0 were deemed to have insufficient sensitivity or specificity and were excluded from further consideration.

Derivation case collection. Investigators were invited to submit cases of IgG4-RD or mimicking conditions that they had managed and to report the presence or absence of each preliminary item for each submitted case using standardized data collection forms. No identifying data on these patients were collected. Investigators were encouraged to submit data on a broad range of IgG4-RD cases, including cases in which they were highly confident in the diagnosis as well as those in which they were less confident. The investigator submitting the case proposed the initial classification of the case as IgG4-RD or as a mimicker of IgG4-RD. This initial classification of all cases was reviewed by a subset of the Steering Committee to confirm the appropriateness of the initial designation. Cases that appeared to be inappropriately classified by the investigator or cases with insufficient information on which to base a classification decision were discarded.

Approach to assigning relative weights to inclusion criteria items. Twenty of the submitted cases representing a combination of IgG4-RD and mimickers were selected for a Steering Committee exercise designed for 2 purposes. First, the exercise was used to assign preliminary weights to the inclusion criteria. Second, it fostered discussion and facilitated consensus on the definitions of individual items. Only cases that did not fulfill any of the exclusion criteria were selected for this exercise. The cases selected represented a broad range of manifestations in order to assess the performance of all potential criteria. Investigators were

asked to rank all cases in order from most likely to least likely to be classified as IgG4-RD. In addition, investigators were asked to indicate the point at which they would divide the cases into those that should be classified as IgG4-RD and those that were more likely to be mimickers.

The draft IgG4-RD classification criteria consisted of 8 domains and a total of 29 items. Once preliminary domains and items had been selected, the Steering Committee met in person for a 2-day session employing decision science theory and computer adaptive technology. A computer software program known as 1000minds (http://www.1000minds.com) was used. Investigators participated in a series of discrete, forced-choice experiments through pairwise rankings of alternatives that led to quantified weights for each item (20–22). During this exercise, investigators were presented with a series of paired scenarios (A and B), each of which contained the same 2 domains (e.g., serum IgG4 concentrations and salivary gland disease). Different combinations of the domains' items were grouped together in each scenario.

For each paired scenario choice, investigators selected the scenario they believed to contribute more toward classification of the patient as having IgG4-RD, assuming that all other aspects of the case were the same. The distribution of votes (percent who voted for A, B, or "equal probability") was presented for each pair of scenarios after each vote. Discussions and re-voting were pursued when necessary, using the same process of consensus described above. Consensus was considered to have been achieved when all participants either indicated complete agreement as to which scenario represented a higher probability of IgG4-RD or indicated that they could accept the majority opinion. During this phase of classification criteria development, 160 rounds of consensus-based decision-making were conducted. Based on this voting, the computer software assigned relative weights to each item. The specific weights assigned to each item were not revealed to investigators.

Scoring of weighted items. If >1 item was present within a given domain, only the highest-weighted item was scored. As an example from the Chest domain, if a patient had peribronchovascular and septal thickening evident on computed tomography of the chest (weighted 4 points) as well as a paravertebral band-like soft tissue mass in the thorax (weighted 10), only the weight of the paravertebral band-like soft tissue mass in the thorax would count in the patient's total classification criteria score.

Identifying a threshold for classifying IgG4-RD. Each derivation case that was not removed by an exclusion criterion was assigned a total score based on the aggregation of weighted inclusion criteria present. These cases were ranked and a preliminary threshold was identified based on targets of >90% for specificity and >80% for sensitivity. Cases around the threshold were selected for discussion among the investigators, who reached consensus on a cutoff point between the group of patients who should be classified as having IgG4-RD and those

who could not be confidently classified as having IgG4-RD. A preliminary threshold of 20 was selected by 2 of the investigators (RPN and JHS) after an in-person review of cases around this threshold revealed a common point at which cases were more likely to be classified by investigators as not clearly being IgG4-RD. This preliminary threshold was then tested in the first of 2 validation phases, using newly submitted cases of IgG4-RD and IgG4-RD mimickers. This preliminary threshold was not revealed to other investigators as the cases for the validation phase were collected.

Collection of IgG4-RD cases and mimickers for the first validation phase. Investigators were invited to submit a second set of data from cases of IgG4-RD or mimicking conditions. None of the cases in this second set had been included in the derivation set. The investigators reported the presence or absence of each finalized item using standardized data collection forms. For each case, investigators reported their confidence in the diagnosis on a scale of 0–3 in which 0 = uncertain, 1 = slightly confident, 2 = confident, and 3 = very confident.

Testing of the IgG4-RD classification criteria and other statistical analyses. We evaluated the performance of the preliminary classification criteria among those cases that fulfilled the entry criteria. To determine the test performance, we only analyzed cases in which investigators were at least "confident" or "very confident" in the diagnosis (IgG4-RD or mimicker); thus, a "confident" or "very confident" diagnosis was considered the gold standard for the purpose of assessing test performance. The number of patients with "confident" or "very confident" designations as either IgG4-RD cases or IgG4-RD mimickers was 771, or 85% of all of the patients included in the first validation phase.

We assessed the test performance of the classification criteria at the preliminary threshold of 20 as well as at a range of thresholds above and below 20. To determine the optimal threshold, we considered the goal of our classification criteria for use in clinical trials (specificity >90% and sensitivity >80%). We also considered other measures such as area under the curve (AUC) (23), Youden's criteria (24), distance from (0,1) on a receiver operating characteristic curve (ROC), difference between sensitivity and specificity, and the diagnostic odds ratio (positive likelihood ratio/negative likelihood ratio) (25).

Sensitivity analyses. We performed several sensitivity analyses to test the performance of the criteria. These sensitivity analyses included the following considerations: 1) if all cases, regardless of confidence level were included; 2) if all of the exclusion criteria were removed; 3) if information on serum IgG4 concentrations was not available; 4) if biopsies were not available; and 5) if the mimickers without data on serum IgG4 concentrations or biopsies were assumed to have the highest values for each item. Chi-square tests, Fisher's exact tests,

t-tests, and Wilcoxon rank sum tests were used to compare subgroups, as appropriate.

Testing the final threshold in a second validation cohort. Investigators were invited to submit another set of data from cases of IgG4-RD or mimicking conditions that they had managed but had not yet contributed to the previous derivation or validation cohorts. This second validation cohort was collected because minor changes in the some of the definitions of inclusion and exclusion criteria had been made after the derivation set of patients had been collected, in the interest of clarifying definitions for investigators. However, the definitions of inclusion criteria and exclusion criteria used in the 2 validation cohorts were exactly the same. Using the same approach as above, we assessed the performance of the classification criteria at the identified threshold of 20. We used all cases and mimickers for whom the diagnosis was considered "confident" or "very confident" by the investigator as the gold standard (n = 402 [83%]).

Table 1.   Exclusion criteria definitions

Clinical

Fever: Documented, recurrent temperature >38°C, with fever being a prominent part of the patient's overall presentation with the underlying disease, in the absence of any clinical features of infection.

No objective response to glucocorticoids: If the patient has been treated with prednisone at a minimum of 40 mg/day (~0.6 mg/kg/day) for a period of 4 weeks, it is assumed that the patient has not demonstrated an objective clinical response. An objective response includes unequivocal improvement of the clinical lesions, biochemical abnormalities, or radiologic findings. There are 2 additional points to consider with regard to glucocorticoid response: Improvement only in the serum IgG4 concentration should not be regarded as a clinical response without improvement in other aspects of the disease. Some forms of IgG4-related disease (IgG4-RD) associated with advanced fibrosis, e.g., some cases of retroperitoneal fibrosis or sclerosing mesenteritis, may not demonstrate obvious radiologic responses to glucocorticoids.

Serologic

Leukopenia and thrombocytopenia without alternative explanation: Reduction in the total white blood cell count and platelet count to levels below those normal for the reference laboratory, having no apparent explanation except for the underlying disease. Reductions in both the white blood cell count and platelet count are unusual in IgG4-RD but are typical of, for example, myelodysplastic syndromes, hematopoietic malignancies, and autoimmune conditions within the systemic lupus erythematosus spectrum.

Peripheral eosinophilia: To a concentration of >3,000 mm^3.

Positive antineutrophil cytoplasmic antibody (ANCA): Enzyme-linked immunosorbent assay results positive for ANCA targeted against proteinase 3 or myeloperoxidase.

Positive antibodies: Ro, La, double-stranded DNA, RNP, or Sm antibodies positive in titers greater than normal suggest an alternative diagnosis. Other autoantibody associated with high specificity for another immune-mediated condition that is a reasonable explanation for the patient's presentation. Such specific autoantibodies include antisynthetase antibodies (e.g., anti–Jo-1), anti–topoisomerase III (Scl-70), and anti–phospholipase A_2 receptor antibodies. This does not include autoantibodies of low specificity such as rheumatoid factor, antinuclear antibodies, antimitochondrial antibodies, anti–smooth muscle antibodies, and antiphospholipid antibodies.

Cryoglobulinemia: Cryoglobulinemia (type I, II, or III) occurring in a clinical context that provides a reasonable explanation for the patient's presentation.

Radiologic

Known radiologic findings suspicious for malignancy or infection that have not been investigated sufficiently: Such radiologic findings include mass lesions that have not been evaluated thoroughly, necrosis, cavitation, hypervascular or exophytic mass, bulky or matted lymphadenopathy, loculated abdominopelvic fluid collection, among others.

Rapid radiologic progression: Defined as significant worsening within a 4–6-week interval.

Long bone abnormalities consistent with Erdheim-Chester disease: Multifocal osteosclerotic lesions of the long bones, usually associated with bilateral diaphyseal involvement.

Splenomegaly: >14 cm in the absence of alternative explanation (e.g., portal hypertension).

Pathologic

Cellular infiltrates suspicious for malignancy that have not been investigated sufficiently: A high likelihood of malignancy may be suggested by cellular atypia, a monotypic nature of immunohistochemistry findings, or light chain restriction on in situ hybridization studies. If malignancy is suspected, this must be excluded by appropriate studies before inclusion.

Markers consistent with inflammatory myofibroblastic tumor: Known positivity for a marker suggestive of inflammatory myofibroblastic tumor, e.g., anaplastic lymphoma kinase 1 or ROS, a receptor tyrosine kinase that is encoded by the gene *ROS1*.

Prominent neutrophilic inflammation: Neutrophilic infiltrates are unusual in IgG4-RD, with the exception of occasional examples in the lung or near mucosal sites. Extensive neutrophilic infiltrates or neutrophilic abscesses strongly indicate the possibility of a non–IgG4-RD diagnosis.

Necrotizing vasculitis: Although vascular injury (e.g., obliterative phlebitis or arteritis) is a hallmark of IgG4-RD, the presence of fibrinoid necrosis within blood vessel walls provides strong evidence against IgG4-RD.

Prominent necrosis: Small foci of necrosis may rarely be present around the luminal surface of ductal organs, but zonal necrosis with no alternative explanation (e.g., stenting) provides strong evidence against IgG4-RD.

Primary granulomatous inflammation: Inflammation rich in epithelioid histiocytes, including multinucleated giant cell formation and granuloma formation, is highly atypical of IgG4-RD.

Pathologic features of a macrophage/histiocytic disorder: Example: known S100-positive macrophages demonstrating emperipolesis, a pathologic feature of Rosai-Dorfman disease.

Specific disease exclusions

Known diagnoses of the following diseases are exclusion criteria:
  Multicentric Castleman's disease
  Crohn's disease (if pancreatobiliary disease is present)
  Ulcerative colitis (if pancreatobiliary disease is present)
Hashimoto thyroiditis (if the thyroid is the only proposed disease manifestation). Patients with IgG4-RD can certainly have Hashimoto thyroiditis separately from IgG4-RD, but Hashimoto thyroiditis is part of the IgG4-RD spectrum.

Results

Research group. The Steering Committee consisted of investigators from North America, Europe, and Asia. There were 3 Advisory Groups: clinical and serologic, radiologic, and pathologic. A total of 86 investigators submitted cases for the derivation and/or validation sets.

Item generation and reduction. At the conclusion of item generation, definitions for the entry criteria, exclusion criteria, and inclusion criteria were established. The entry criteria were defined as 1) characteristic clinical or radiologic involvement of a typical organ (e.g., pancreas, bile ducts, orbits, lacrimal glands, major salivary glands, retroperitoneum, kidney, aorta, pachymeninges, or thyroid gland [Riedel's thyroiditis]) or 2) pathologic evidence of an inflammatory process accompanied by a lymphoplasmacytic infiltrate of uncertain etiology in one of these same organs. "Characteristic" involvement generally refers to enlargement of the organ or a tumor-like mass within an affected organ. It also includes 3 organ-specific features, with reference to 1) the bile ducts, where narrowing tends to occur, 2) the aorta, where wall thickening or aneurysmal dilatation is typical, and 3) the lungs, where thickening of the bronchovascular bundles is common.

Supplementary Tables 1 and 2 (on the *Arthritis & Rheumatology* web site at http://onlinelibrary.wiley.com/doi/10.1002/art.41120/abstract) list the preliminary exclusion criteria and the preliminary inclusion criteria. There was initially a total of 78 such criteria (51 preliminary exclusion criteria and 27 preliminary inclusion criteria). The preliminary exclusion criteria and preliminary inclusion criteria demonstrating the highest discrimination of IgG4-RD from disease mimickers were chosen as draft classification criteria. Complete definitions of the exclusion criteria and the inclusion criteria are shown in Table 1 and Table 2, respectively. Following the

consensus exercises and the Likert scale rating of the preliminary inclusion criteria, refined lists of exclusion and positive and negative inclusion criteria were created (Supplementary Table 2).

Derivation and validation cohorts. Table 3 describes the derivation cohort and the first and second validation cohorts used to develop and assess the performance of the classification criteria. A total of 1,879 patients were included in the overall IgG4-RD classification criteria effort, including 486 in the derivation cohort (272 IgG4-RD cases, 214 mimickers), 908 in the first validation cohort (493 cases, 415 mimickers), and 485 in the second validation cohort (321 cases, 164 mimickers). The patients' status as a case or mimicker, proposed by the submitting investigator, was confirmed by members of the Steering Committee. In both the derivation and validation cohorts, the majority of cases were male patients and typically in their sixth decade of life, consistent with the demographics of IgG4-RD and many of its mimicking conditions.

Classification criteria (Table 4). The derivation cohort was used to assess the relative performance of each proposed exclusion and inclusion criterion. The exclusion criteria are not designed to be a "laundry list" of evaluations that must be checked off as negative before a patient can be classified as having IgG4-RD. Rather, they serve as a reminder to the investigator of evaluations that might be appropriate to consider in specific clinical scenarios.

Criteria that did not distinguish IgG4-RD cases from mimickers were eliminated, and those that helped distinguish IgG4-RD cases from mimickers were retained. The final entry criteria and items were modified through in-person discussion after completion of the 1000minds program and review of the derivation cases (n = 486) ranked in order of points accrued by totaling the weights associated with each inclusion criteria item after cases fulfilling exclusion criteria had been excluded. A preliminary score of 20 was identified

Table 2. Inclusion criteria definitions

Immunostaining
IgG+ cells can be identified using either IgG staining or CD138 staining.

Head and neck gland involvement
A "set" of glands refers to both lacrimal glands or both submandibular glands, etc. If a gland has been surgically removed for the purpose of diagnosis, it can be considered to have been involved if confirmed by pathology.
Involvement of the lacrimal glands and the major salivary glands in IgG4-related disease is bilateral (but can be asymmetric). Involvement of the glands can be determined either by clinical examination or by a radiology study (e.g., positron emission tomography scan or computed tomography scan).

Chest
Peribronchovascular and septal thickening in the lung must be determined by a cross-sectional imaging study of the chest.
The paravertebral band-like soft tissue in the thorax is usually right-sided, located between T8 and T11, and does not encase the aorta.

Pancreas and biliary tree
Diffuse pancreas enlargement usually encompasses more than two-thirds of the pancreas.
The type of biliary involvement that is highly consistent with IgG4-related sclerosing cholangitis involves the proximal biliary tract (i.e., intrahepatic and extrapancreatic portions of the extrahepatic bile ducts). The bile duct walls often have smooth thickening.

Kidney
Hypocomplementemia pertains to low serum levels of C3, C4, or both.
Renal pelvic wall thickening can be either unilateral or bilateral, usually without severe stenosis or luminal irregularity.
Low-density areas in both renal cortices can be seen only on contrast-enhanced computed tomography and are usually patchy or round-shaped in appearance.

Retroperitoneum
The location of IgG4-related retroperitoneal fibrosis or periaortitis is typically circumferential or on the anterolateral sides of the aorta. The segment of aorta involved tends to be the infrarenal aorta, often extending to include the iliac vessels.

Table 3. Demographic and disease characteristics of the derivation and validation cohorts*

	Derivation cohort (n = 486)†	Validation cohort 1 (n = 908)†	Validation cohort 2 (n = 485)†
IgG4-related disease	272 (56)	493 (54)	321 (66)
Mimickers‡	214 (44)	415 (46)	164 (34)
Vasculitis	26 (12)	106 (26)	34 (21)
Malignancy	51 (24)	31 (7)	36 (22)
Sjögren's syndrome	13 (6)	59 (14)	8 (5)
Other pancreatitis	5 (2)	15 (4)	7 (4)
Other	119 (56)	204 (49)	79 (48)
Male sex	319 (66)	503 (55)	288 (59)
Age at diagnosis, mean ± SD years	58.2 ± 14.5	55.5 ± 16.5	56.4 ± 16.8
Select organ involvement			
Salivary glands	153 (31)	278 (31)	151 (31)
Orbit	101 (21)	188 (21)	146 (30)
Pulmonary	128 (26)	173 (19)	75 (15)
Lymph nodes	176 (36)	262 (29)	95 (20)
Aorta	52 (11)	97 (11)	37 (8)
Retroperitoneal fibrosis	78 (16)	108 (12)	50 (10)
Pancreas	132 (27)	269 (30)	160 (33)
Biliary	75 (15)	149 (16)	91 (19)
Renal	90 (19)	137 (15)	74 (15)
No. of organs involved, median (interquartile range)	2 (1–4)	2 (1–3)	2 (1–3)

* In validation cohort 1, the judgment of a case as being IgG4-related disease (IgG4-RD) or as being an IgG4-RD mimicker was "confident" or "very confident" in 771 cases (84.9% of all cases and mimickers included in that cohort). In validation cohort 2, the judgment of a case as being IgG4-RD or as being an IgG4-RD mimicker was "confident" or "very confident" in 431 cases (88.9% of all cases and mimickers included in that cohort). Except where indicated otherwise, values are the number (%).
† Includes all submitted cases and mimickers.
‡ Mimicker conditions are listed in Supplementary Table 5, on the *Arthritis & Rheumatology* web site at http://online library.wiley.com/doi/10.1002/art.41120/abstract.

as the cutoff point at or above which the majority of investigators considered the patient to have IgG4-RD; with this threshold, a sensitivity of >80% and high specificity were also achieved.

Validating the classification criteria. We then tested the performance of the classification criteria in the first validation cohort (n = 908). To determine the optimal cutoff, we assessed the test performance of criteria at various thresholds (Table 5). Given that the purpose of the criteria was to identify patients with IgG4-RD for enrollment in research studies, the ideal threshold would have excellent specificity while retaining good sensitivity (>80%). The preliminary threshold of 20 had a specificity of 99.2% (95% confidence interval [95% CI] 97.2–99.8%) and a sensitivity of 85.5% (95% CI 81.9–88.5%). Moreover, the threshold of 20 had excellent discrimination, with an AUC of 0.924 (95% CI 0.906–0.941). A threshold of either 21 or 22 had a specificity identical to that obtained with the threshold of 20, but sensitivity decreased at those thresholds, as reflected in other measures of threshold performance, including the AUC. A threshold of 20 also had the highest diagnostic odds ratio compared to other thresholds.

Because of the emphasis placed upon specificity, we considered the test characteristics obtained with a threshold of 20 superior to those of other potential thresholds. Of note, however, a threshold of 16 performed better in certain mea-

sures, including sensitivity (88.6%), Youden's criteria, distance from (0,1) on the ROC curve (0.12), and AUC (0.933 [95% CI 0.916–0.950]). The threshold of 16 was associated with a slightly lower specificity: 98.1% versus 99.2%. When comparing a threshold of 20 to a threshold of 16 with regard to the diagnostic odds ratio, a threshold of 20 was associated with superior test performance (761.5 versus 394.5). The consistent performance of these classification criteria across a range of thresholds suggests that the criteria will be robust when used in the clinic for purposes of research.

Analyses were then performed using the second validation cohort (n = 485). In this group the classification criteria had a specificity of 97.8% (95% CI 93.7–99.2%) and a sensitivity of 82.0% (95% CI 77.0–86.1%).

Sensitivity analyses with a threshold of 20. We performed a number of sensitivity analyses to assess the robustness of the classification criteria at a threshold of 20 in the first validation cohort. If all cases, regardless of confidence in the diagnosis, were included, the classification criteria performed very well, with a sensitivity of 83% and a specificity of 98.9%. The IgG4-RD classification criteria are the first of its kind in any rheumatic disease to incorporate absolute exclusion criteria. In a sensitivity analysis that removed exclusion criteria from the classification algorithm, we found that the specificity of the criteria decreased from 99.2%

Table 4. The 2019 American College of Rheumatology/European League Against Rheumatism classification criteria for IgG4-related disease

Step	Categorical assessment or numeric weight
Step 1. Entry criteria	**Yes**† or No
Characteristic* clinical or radiologic involvement of a typical organ (e.g., pancreas, salivary glands, bile ducts, orbits, kidney, lung, aorta, retroperitoneum, pachymeninges, or thyroid gland [Riedel's thyroiditis]) OR pathologic evidence of an inflammatory process accompanied by a lymphop-lasmacytic infiltrate of uncertain etiology in one of these same organs	
Step 2. Exclusion criteria: domains and items‡	Yes or **No**§
Clinical	
Fever	
No objective response to glucocorticoids	
Serologic	
Leukopenia and thrombocytopenia with no explanation	
Peripheral eosinophilia	
Positive antineutrophil cytoplasmic antibody (specifically against proteinase 3 or myeloperoxidase)	
Positive SSA/Ro or SSB/La antibody	
Positive double-stranded DNA, RNP, or Sm antibody	
Other disease-specific autoantibody	
Cryoglobulinemia	
Radiologic	
Known radiologic findings suspicious for malignancy or infection that have not been sufficiently investigated	
Rapid radiologic progression	
Long bone abnormalities consistent with Erdheim-Chester disease	
Splenomegaly	
Pathologic	
Cellular infiltrates suggesting malignancy that have not been sufficiently evaluated	
Markers consistent with inflammatory myofibroblastic tumor	
Prominent neutrophilic inflammation	
Necrotizing vasculitis	
Prominent necrosis	
Primarily granulomatous inflammation	
Pathologic features of macrophage/histiocytic disorder	
Known diagnosis of the following:	
Multicentric Castleman's disease	
Crohn's disease or ulcerative colitis (if only pancreatobiliary disease is present)	
Hashimoto thyroiditis (if only the thyroid is affected)	
If case meets entry criteria and does not meet any exclusion criteria, proceed to step 3.	
Step 3. Inclusion criteria: domains and items¶	
Histopathology	
Uninformative biopsy	0
Dense lymphocytic infiltrate	+4
Dense lymphocytic infiltrate and obliterative phlebitis	+6
Dense lymphocytic infiltrate and storiform fibrosis with or without obliterative phlebitis	+13
Immunostaining#	0–16, as follows: Assigned weight is 0 if the IgG4+:IgG+ ratio is 0–40% or indeterminate and the number of IgG4+ cells/hpf is 0–9.** Assigned weight is 7 if 1) the IgG4+:IgG+ ratio is ≥41% and the number of IgG4+ cells/hpf is 0–9 or indeterminate; or 2) the IgG4+:IgG+ ratio is 0–40% or indeterminate and the number of IgG4+ cells/hpf is ≥10 or indeterminate. Assigned weight is 14 if 1) the IgG4+:IgG+ ratio is 41–70% and the number of IgG4+ cells/hpf is ≥10; or 2) the IgG4+:IgG+ ratio is ≥71% and the number of IgG4+ cells/hpf is 10–50. Assigned weight is 16 if the IgG4+:IgG+ ratio is ≥71% and the number of IgG4+ cells/hpf is ≥51.

(Continued)

Table 4. *(Cont'd)*

Step	Categorical assessment or numeric weight
Serum IgG4 concentration	
Normal or not checked	0
> Normal but <2× upper limit of normal	+4
2–5× upper limit of normal	+6
>5× upper limit of normal	+11
Bilateral lacrimal, parotid, sublingual, and submandibular glands	
No set of glands involved	0
One set of glands involved	+6
Two or more sets of glands involved	+14
Chest	
Not checked or neither of the items listed is present	0
Peribronchovascular and septal thickening	+4
Paravertebral band-like soft tissue in the thorax	+10
Pancreas and biliary tree	
Not checked or none of the items listed is present	0
Diffuse pancreas enlargement (loss of lobulations)	+8
Diffuse pancreas enlargement and capsule-like rim with decreased enhancement	+11
Pancreas (either of above) and biliary tree involvement	+19
Kidney	
Not checked or none of the items listed is present	0
Hypocomplementemia	+6
Renal pelvis thickening/soft tissue	+8
Bilateral renal cortex low-density areas	+10
Retroperitoneum	
Not checked or neither of the items listed is present	0
Diffuse thickening of the abdominal aortic wall	+4
Circumferential or anterolateral soft tissue around the infrarenal aorta or iliac arteries	+8
Step 4: Total inclusion points	
A case meets the classification criteria for IgG4-RD if the entry criteria are met, no exclusion criteria are present, and the total points is ≥20.	

* Refers to enlargement or tumor-like mass in an affected organ except in 1) the bile ducts, where narrowing tends to occur, 2) the aorta, where wall thickening or aneurysmal dilatation is typical, and 3) the lungs, where thickening of the bronchovascular bundles is common.
† If entry criteria are not fulfilled, the patient cannot be further considered for classification as having IgG4-related disease (IgG4-RD).
‡ Assessment for the presence of exclusion criteria should be individualized depending on a patient's clinical scenario.
§ If exclusion criteria are met, the patient cannot be further considered for classification as having IgG4-RD.
¶ Only the highest-weighted item in each domain is scored.
# Biopsies from lymph nodes, mucosal surfaces of the gastrointestinal tract, and skin are not acceptable for use in weighting the immunostaining domain.
** "Indeterminate" refers to a situation in which the pathologist is unable to clearly quantify the number of positively staining cells within an infiltrate yet can still ascertain that the number of cells is at least 10/high-power field (hpf). For a number of reasons, most often pertaining to the quality of the immunostain, pathologists are sometimes unable to count the number of IgG4+ plasma cells with precision yet even so, can be confident in grouping cases into the appropriate immunostaining result category.

to 89.2%, while the sensitivity increased from 85.5% to 90.0%. As is typical of clinical practice, serum IgG4 concentrations were not measured, or biopsies not performed, in some cases of IgG4-RD (3% and 15%, respectively) and mimickers (36% and 16%, respectively). When exclusion and inclusion criteria related to biopsy results or serum IgG4 concentrations were removed from the classification algorithm, the classification criteria maintained excellent specificity in both scenarios (98.9% when biopsy criteria were removed, 99.3% when serum IgG4 concentrations were removed). The sensitivity decreased substantially in the absence of pathology data or serum IgG4 concentrations, to 48.6% and 75.0%, respectively. When we assumed the worst-case scenario in which all the mimickers without biopsy or serum IgG4 concentration data were assigned the highest weights for each (e.g., IgG4 concentrations >5 times the upper limit of normal), the specificity of the classification criteria remained high (92.7%).

Reasons for cases not achieving a classification of IgG4-RD. Of the 428 and 267 IgG4-RD cases from the first and second validation cohorts used to test the classification criteria, 62 (14%) and 48 (18%), respectively, did not fulfill the classification criteria. In both the first and second validation cohorts, the majority of these false-negative cases (43 [69%] and 39 [81%], respectively) did not achieve sufficient inclusion criteria points (Table 6), partly because they were less likely to have had biopsies compared to true-positive cases (65% versus 91% [P < 0.001] and 73% versus 88% [P = 0.007], respectively). Twenty false-negative cases in the first validation cohort

Table 5. Performance of various thresholds of the 2019 American College of Rheumatology/European League Against Rheumatism classification criteria for IgG4-related disease using validation cohort 1*

Threshold	Sensitivity (95% CI)	Specificity (95% CI)	AUC (95% CI)	Youden index	Distance to (0,1)	Specificity − sensitivity	Diagnostic odds ratio
14	0.89 (0.86–0.92)	0.95 (0.91–0.97)	0.92 (0.90–0.94)	0.84	0.12	0.06	142.4
15	0.89 (0.85–0.91)	0.97 (0.95–0.99)	0.93 (0.91–0.95)	0.86	0.12	0.09	286.1
16	0.89 (0.85–0.91)	0.98 (0.96–0.99)	0.93 (0.92–0.95)	0.87	0.12	0.10	394.5
17	0.88 (0.85–0.91)	0.98 (0.96–0.99)	0.93 (0.92–0.95)	0.86	0.12	0.10	385.6
18	0.88 (0.84–0.90)	0.98 (0.96–0.99)	0.93 (0.91–0.95)	0.86	0.13	0.11	360.8
19	0.86 (0.83–0.89)	0.99 (0.92–0.99)	0.93 (0.91–0.94)	0.85	0.14	0.12	408.3
20	0.86 (0.82–0.89)	0.99 (0.97–100.0)	0.92 (0.91–0.94)	0.85	0.15	0.14	761.5
21	0.83 (0.79–0.86)	0.99 (0.97–0.99)	0.91 (0.89–0.93)	0.82	0.18	0.17	607.2
22	0.82 (0.78–0.85)	0.99 (0.97–0.99)	0.91 (0.89–0.92)	0.81	0.18	0.18	578.8

* 95% CI = 95% confidence interval; AUC = area under the curve.

(32%) and 9 in the second validation cohort (19%) met at least 1 exclusion criterion. Of all of the IgG4-RD cases submitted in the first and second validation cohorts, 24 (4.9%) and 42 (8.7%), respectively, did not meet the initial entry criterion (characteristic organ involvement). In addition, 23 (5%) and 13 (4%) of the submitted IgG4-RD cases in the first and second validation cohorts, respectively, fulfilled at least 1 exclusion criterion, most often a clinical or serologic exclusion criterion (Table 7).

In the first validation cohort, 64 (20%) of 324 mimickers considered when deriving thresholds for the classification criteria did not meet entry criteria. Similarly, in the second validation cohort, 17 (10%) of the 164 mimickers did not meet entry criteria. Of those who met entry criteria in each validation cohort (260 and 147, respec-

tively), 258 (99%) and 144 (98%), respectively, did not fulfill the classification criteria (true-negatives). The majority of mimickers in both cohorts (201 [77%] and 93 [65%], respectively) were eliminated at the exclusion criteria stage (Table 7). Supplementary Tables 3 and 4 (on the *Arthritis & Rheumatology* web site at http://onlinelibrary. wiley.com/doi/10.1002/art.41120/abstract) list the inclusion criteria fulfilled by the cases classified as IgG4-RD and cases submitted as mimickers in the first and second validation cohorts.

Discussion

The 2019 ACR/EULAR IgG4-RD criteria represent a significant milestone in IgG4-RD, a multiorgan condition with myriad

Table 6. Comparison of differences in false-negative and true-positive IgG4-related disease cases from the validation cohorts*

	Validation cohort 1			Validation cohort 2		
	False-negatives (n = 62)	True-positives (n = 366)	P	False-negatives (n = 48)	True-positives (n = 219)	P
Male sex	38 (61)	244 (67)	0.4	29 (60)	150 (69)	0.3
Age at diagnosis, mean ± SD years	57.5 ± 14.9	60.5 ± 13.4	0.1	60.4 ± 15.9	58.8 ± 14.8	0.5
Age at symptom onset, mean ± SD years	55.6 ± 15.0	58.6 ± 14.0	0.1	57.9 ± 16.2	56.7 ± 15.3	0.6
No. of organs involved, median (interquartile range)	2 (1–3)	3 (2–4)	0.002	2 (1–3)	2 (2–4)	0.01
Biopsy performed	40 (65)	332 (91)	<0.001	35 (73)	193 (88)	0.007
Reason criteria not met						
Exclusion criteria present	20 (32)	–		9 (19)	–	
Clinical	7 (11)	–		4 (8)	–	
Serologic	7 (11)	–		3 (6)	–	
Radiologic	5 (8)	–		2 (4)	–	
Pathologic	2 (3)	–		0 (0)	–	
Inclusion criteria score <20	43 (69)	–		39 (81)	–	
Total points toward inclusion criteria, mean ± SD	22.9 ± 17.1	38.9 ± 12.2	<0.001	18.6 ± 11.9	37.9 ± 12.7	<0.001

* "Gold standard" cases and mimickers were used in this analysis. Except where indicated otherwise, values are the number (%).

Table 7. Percentage of validation cohort cases and mimickers fulfilling exclusion criteria*

	Validation cohort 1		Validation cohort 2	
Exclusion criteria met†	IgG4-RD	Mimicker	IgG4-RD	Mimicker
Clinical exclusion criteria	7 (2)	81 (31)	5 (2)	25 (17)
Fever	1 (<1)	44 (17)	4 (1)	15 (10)
No response to glucocorticoids	1 (<1)	23 (9)	0 (0)	9 (6)
Leukopenia and thrombocytopenia	1 (<1)	19 (7)	0 (0)	2 (1)
Peripheral eosinophilia (>3,000 mm³)	4 (1)	9 (4)	1 (<1)	4 (3)
Serologic exclusion criteria	7 (2)	108 (42)	5 (2)	32 (22)
Positive PR3- or MPO-ANCA	2 (1)	48 (19)	1 (<1)	26 (18)
Positive anti-Ro or anti-La	5 (1)	51 (20)	2 (1)	6 (4)
Positive extractable nuclear antigen (e.g., anti-Sm antibody)	0 (0)	6 (2)	1 (<1)	2 (1)
Other specific antibody positive	0 (0)	0 (0)	0 (0)	0 (0)
Cryoglobulins	0 (0)	10 (4)	1 (<1)	1 (1)
Radiologic exclusion criteria	5 (1)	24 (9)	2 (1)	20 (14)
Rapid radiographic progression	0 (0)	5 (2)	0 (0)	3 (2)
Long bone abnormalities (e.g., Erdheim-Chester disease)	0 (0)	3 (1)	0 (0)	1 (1)
Splenomegaly	3 (1)	14 (5)	0 (0)	3 (2)
Infectious/malignancy radiographic concern	2 (1)	4 (2)	2 (1)	13 (9)
Pathologic exclusion criteria	2 (1)	110 (42)	2 (1)	66 (45)
Malignant infiltrate on biopsy	1 (<1)	26 (10)	0 (0)	30 (20)
Inflammatory pseudotumor pathology	0 (0)	2 (1)	0 (0)	1 (1)
Prominent neutrophilic infiltrate	0 (0)	6 (2)	1 (<1)	9 (6)
Necrotizing vasculitis	0 (0)	36 (14)	0 (0)	11 (8)
Prominent necrosis	0 (0)	2 (1)	0 (0)	7 (5)
Primarily granulomatous inflammation	0 (0)	39 (15)	0 (0)	21 (14)
Prominent histiocytic infiltrate	1 (<1)	7 (3)	0 (0)	7 (5)
Multicentric Castleman's pathology	0 (0)	6 (2)	1 (<1)	2 (1)

* Includes all cases and mimickers fulfilling entry criteria. Values are the number (%). IgG4-RD = IgG4-related disease; PR3 = proteinase 3; MPO = myeloperoxidase; ANCA = antineutrophil cytoplasmic antibody.
† Total will sum to >100% because cases and mimickers could meet >1 exclusion criterion.

clinical presentations (3,4). Our approach reflects the fact that in clinical practice, information from clinical, serologic, radiologic, and pathologic evaluations must be integrated to arrive at a confident decision about whether to classify a patient as having IgG4-RD. The excellent sensitivity and specificity of these criteria will assist in the conduct of clinical trials and other studies of IgG4-RD. The purpose of these classification criteria is to facilitate the identification of more homogeneous groups of subjects for inclusion into clinical trials and observational studies (26–28).

No set of classification criteria can be constructed so as to include all patients within the spectrum of a disease. Accordingly, attempts to include all conceivable patients with clinical diagnoses of IgG4-RD would inevitably involve major sacrifices in specificity that would lead to the unacceptable inclusion of a significant percentage of false-positive cases. Our principal goal in constructing these classification criteria was to create a criteria set with the highest possible specificity while retaining moderately high sensitivity. The specificity of 97.8% achieved at a threshold of ≥20 points will include few false-positive cases: a highly desirable performance measure for clinical trials and other investigations. The sensitivity of 82.0% at this threshold also captures a broad spectrum of the patient population about whose IgG4-RD classification investigators are confident. The classification criteria for

IgG4-RD that we have developed demonstrate robust test characteristics across a range of thresholds, suggesting that they will have broad relevance to the field of IgG4-RD investigation.

These criteria are not intended for use in clinical practice as the basis of establishing the diagnosis of IgG4-RD (29). If the appropriate clinical diagnosis for a patient is IgG4-RD, then failure to fulfill the ACR/EULAR classification criteria should not prevent the management of that patient's condition accordingly. There might be a substantial likelihood of this when, for example, a representative biopsy sample is difficult to obtain (30). These criteria provide a useful framework for clinicians considering the diagnosis of IgG4-RD in a patient. They highlight findings such as bilateral salivary gland enlargement, common features of IgG4-related kidney disease, and typical pancreas abnormalities that increase the likelihood that a patient has IgG4-RD. They also describe findings that suggest alternative diagnoses are more likely, such as primary granulomatous inflammation, ANCA positivity, and fevers. However, the exclusion criteria should not be interpreted as a list of studies or tests a clinician must obtain on every patient.

An important strength of this criteria set is that a patient may be classified accurately as having IgG4-RD in many cases even in the absence of a biopsy. Although biopsies

are essential in many settings to establish the diagnosis of IgG4-RD and exclude mimickers, we aimed to develop criteria in which biopsy is not required when the diagnosis of IgG4-RD is straightforward on the basis of clinical, serologic, and radiologic findings. Such criteria are consistent with clinical practice (7,31), compatible with research, and essential to the appropriate diagnosis of patients in both clinical and research settings. The fact that the 2019 ACR/EULAR IgG4-RD classification criteria require neither a biopsy nor an elevated serum IgG4 level reflects important changes in the approaches whereby classifications of this disease are now assigned (and clinical diagnoses rendered). Nearly 20% of cases classified as IgG4-RD had a normal serum IgG4 concentration or did not have a serum IgG4 value available. Moreover, 9% of the IgG4-RD cases did not have a biopsy, 37% lacked the classic histopathologic findings, and >40% did not meet previously defined cutoffs for IgG4+ plasma cell infiltrates (9). These criteria reflect the reality of clinical care and clinical investigation in IgG4-RD; clinicians consider a combination of factors when determining whether to classify a patient as having this disease (10).

The 2019 IgG4-RD classification criteria are one of the first sets of classification criteria in rheumatology to include absolute exclusion criteria that are not based solely on having an alternative diagnosis, but rather focus on clinical, serologic, radiologic, and pathologic features. This approach has strong appeal, particularly when the common mimickers of IgG4-RD themselves pose challenges in classification because of their multiorgan nature. Our sensitivity analysis indicated that in the absence of exclusion criteria, the specificity of the classification criteria decreased by nearly 10%, yet was accompanied by only a small improvement in sensitivity.

Some patients with clinical diagnoses of IgG4-RD will not fulfill these classification criteria. There are several explanations for this. First, we excluded patients with disease that affected only organs or sites that are involved only infrequently in IgG4-RD (e.g., patients with pituitary, breast, skin, or prostate disease). We focused our classification criteria development efforts on patients with more typical and common manifestations because of the desire to enroll relatively homogeneous populations in clinical trials. Second, some patients were excluded because their clinical evaluations identified exclusion criteria. Again, for the purposes of clinical trials, the exclusion of exceptional cases is usually prudent. Third, some patients met the entry criteria and did not meet exclusion criteria but still failed to accrue sufficient inclusion points to be classified as having IgG4-RD. Patients considered with confidence by their investigators to have IgG4-RD who did not fulfill the classification criteria were significantly less likely to have had a biopsy. It is possible that in some of these cases, a biopsy showing typical features of IgG4-RD might be useful for achieving sufficient points for the patient to be classified as having IgG4-RD.

Our study has a number of strengths. First, a cohort of nearly 1,900 patients with either IgG4-RD or a mimicking condition was assembled by an international group of investigators. Second, the experts involved in the consensus exercises, decision analysis, and cohort development represented investigators from a variety of specialties (e.g., rheumatology, gastroenterology, pathology, and radiology) and from around the world, including the Americas, Europe, Asia, and Australia. Moreover, many investigators involved in cohort development were not involved in other aspects of the classification criteria development, minimizing any influence of circularity of reasoning. Such a bias can occur when the same investigators who define criteria also develop derivation and validation cohorts (22). Our design prevented this potential bias. Third, we applied multicriteria decision analysis to derive the weights for each inclusion criteria item. These weights can be adjusted easily if or when other tests or information relevant to diagnosis become available.

Despite these strengths, our study has certain limitations. First, although the derivation and validation sets included a wide range of IgG4-RD mimickers, the performance of these classification criteria might be further evaluated in specific populations enriched for malignant conditions, non–IgG4-RD pancreatobiliary diseases, and infections. Because of the specific exclusion criteria intended to address these groups of mimickers, however, the 2019 ACR/EULAR criteria should perform well under such circumstances. Second, the laboratory, imaging, and pathology findings were not assessed centrally. Although the sensitivity and specificity of certain results may consequently have varied between investigator sites, this is unlikely to have affected our results significantly because of the expertise of the research group overall.

In summary, these are the first classification criteria for IgG4-RD, developed and tested using a data-driven approach and multicriterion decision analysis. The criteria perform well over a wide range of thresholds. They represent a significant advance in this rapidly evolving field and should be used in future clinical trials and epidemiologic studies of IgG4-RD.

AUTHOR CONTRIBUTIONS

REFERENCES

1. Stone JH, Zen Y, Deshpande V. IgG4-related disease [review]. N Engl J Med 2012;366:539–51.

2. Kamisawa T, Zen Y, Pillai S, Stone JH. IgG4-related disease [review]. Lancet 2015;385:1460–71.

3. Kamisawa T, Funata N, Hayashi Y, Eishi Y, Koike M, Tsuruta K, et al. A new clinicopathological entity of IgG4-related autoimmune disease. J Gastroenterol 2003;38:982–4.

4. Hamano H, Kawa S, Horiuchi A, Unno H, Furuya N, Akamatsu T, et al. High serum IgG4 concentrations in patients with sclerosing pancreatitis. N Engl J Med 2001;344:732–8.

5. Stone JH, Khosroshahi A, Deshpande V, Chan JK, Heathcote JG, Aalberse R, et al. Recommendations for the nomenclature of IgG4-related disease and its individual organ system manifestations. Arthritis Rheum 2012;64:3061–7.

6. Wallace ZS, Deshpande V, Mattoo H, Mahajan VS, Kulikova M, Pillai S, et al. IgG4-related disease: clinical and laboratory features in one hundred twenty-five patients. Arthritis Rheumatol 2015;67:2466–75.

7. Sekiguchi H, Horie R, Kanai M, Suzuki R, Yi ES, Ryu JH. IgG4-related disease: retrospective analysis of one hundred sixty-six patients. Arthritis Rheumatol 2016;68:2290–9.

8. Kuroda N, Nao T, Fukuhara H, Karashima T, Inoue K, Taniguchi Y, et al. IgG4-related renal disease: clinical and pathological characteristics. Int J Clin Exp Pathol 2014;7:6379–85.

9. Deshpande V, Zen Y, Chan JK, Yi EE, Sato Y, Yoshino T, et al. Consensus statement on the pathology of IgG4-related disease. Mod Pathol 2012;25:1181–92.

10. Brito-Zerón P, Bosch X, Ramos-Casals M, Stone JH. IgG4-related disease: advances in the diagnosis and treatment. Best Pract Res Clin Rheumatol 2016;30:261–78.

11. Carruthers MN, Khosroshahi A, Augustin T, Deshpande V, Stone JH. The diagnostic utility of serum IgG4 concentrations in IgG4-related disease. Ann Rheum Dis 2015;74:14–8.

12. Hao M, Liu M, Fan G, Yang X, Li J. Diagnostic value of serum IgG4 for IgG4-related disease: a PRISMA-compliant systematic review and meta-analysis. Medicine (Baltimore) 2016;95:e3785.

13. Mahajan VS, Mattoo H, Deshpande V, Pillai SS, Stone JH. IgG4-related disease. Annu Rev Pathol 2014;9:315–47.

14. Chari ST. Diagnosis of autoimmune pancreatitis using its five cardinal features: introducing the Mayo Clinic's HISORt criteria. J Gastroenterol 2007;42 Suppl 18:39–41.

15. Perugino CA, Wallace ZS, Meyersohn N, Oliveira G, Stone JR, Stone JH. Large vessel involvement by IgG4-related disease. Medicine (Baltimore) 2016;95:e3344.

16. Fransen J, Johnson SR, van den Hoogen F, Baron M, Allanore Y, Carreira PE, et al. Items for revised classification criteria in systemic sclerosis: results of a consensus exercise. Arthritis Care Res (Hoboken) 2012;64:351–7.

17. Johnson SR, Khanna D, Daikh D, Cervera R, Costedoat-Chalumeau N, Gladman DD, et al. Use of consensus methodology to determine candidate items for systemic lupus erythematosus classification criteria. J Rheumatol 2019;46:721–6.

18. Johnson SR, Naden RP, Fransen J, van den Hoogen F, Pope JE, Baron M, et al. Multicriteria decision analysis methods with 1000Minds for developing systemic sclerosis classification criteria. J Clin Epidemiol 2014;67:706–14.

19. Tedeschi SK, Johnson SR, Boumpas DT, Daikh D, Dörner T, Diamond B, et al. Multicriteria decision analysis process to develop new classification criteria for systemic lupus erythematosus. Ann Rheum Dis 2019;78:634–40.

20. Neogi T, Jansen TL, Dalbeth N, Fransen J, Schumacher HR, Berendsen D, et al. 2015 gout classification criteria: an American College of Rheumatology/European League Against Rheumatism collaborative initiative. Arthritis Rheumatol 2015;67:2557–68.

21. Aletaha D, Neogi T, Silman AJ, Funovits J, Felson DT, Bingham CO III, et al. 2010 rheumatoid arthritis classification criteria: an American College of Rheumatology/European League Against Rheumatism collaborative initiative. Arthritis Rheum 2010;62:2569–81.

22. Van den Hoogen F, Khanna D, Fransen J, Johnson SR, Baron M, Tyndall A, et al. 2013 classification criteria for systemic sclerosis: an American College of Rheumatology/European League Against Rheumatism collaborative initiative. Arthritis Rheum 2013;65:2737–47.

23. Metz CE. Basic principles of ROC analysis. Semin Nucl Med 1978;8:283–98.

24. Youden WJ. Index for rating diagnostic tests. Cancer 1950;3:32–5.

25. Glas AS, Lijmer JG, Prins MH, Bonsel GJ, Bossuyt PM. The diagnostic odds ratio: a single indicator of test performance. J Clin Epidemiol 2003;56:1129–35.

26. Classification and Response Criteria Subcommittee of the American College of Rheumatology Committee on Quality Measures. Development of classification and response criteria for rheumatic diseases [editorial]. Arthritis Rheum 2006;55:348–52.

27. Johnson SR, Goek ON, Singh-Grewal D, Vlad SC, Feldman BM, Felson DT, et al. Classification criteria in rheumatic diseases: a review of methodologic properties. Arthritis Rheum 2007;57:1119–33.

28. Dougados M, Gossec L. Classification criteria for rheumatic diseases: why and how? [editorial]. Arthritis Rheum 2007;57:1112–5.

29. Aggarwal R, Ringold S, Khanna D, Neogi T, Johnson SR, Miller A, et al. Distinctions between diagnostic and classification criteria? [review]. Arthritis Care Res (Hoboken) 2015;67:891–7.

30. Felson DT, Anderson JJ. Methodological and statistical approaches to criteria development in rheumatic diseases. Baillieres Clin Rheumatol 1995;9:253–66.

31. Chari ST, Takahashi N, Levy MJ, Smyrk TC, Clain JE, Pearson RK, et al. A diagnostic strategy to distinguish autoimmune pancreatitis from pancreatic cancer. Clin Gastroenterol Hepatol 2009;7:1097–103.

APPENDIX A: THE AMERICAN COLLEGE OF RHEUMATOLOGY/EUROPEAN LEAGUE AGAINST RHEUMATISM IgG4-RELATED DISEASE CLASSIFICATION CRITERIA WORKING GROUP

Members of the ACR/EULAR IgG4-RD Classification Criteria Working Group are as follows: Drs. Takashi Akamizu, Mitsuhiro Akiyama, Lillian Barra, Adrian Bateman, Daniel Blockmans, Pilar Brito-Zeron, Corrado Campochiaro, Mollie Carruthers, Suresh Chari, Tsutomu Chiba, Hyon Choi, Lynn Cornell, Emma Culver, Saman Darabian, Emanuel Della-Torre, Vikram Deshpande, Mr. Jean-Francois Dicaire, Drs. Lingli Dong, Mikael Ebbo, Andreu Fernández-Codina, Judith A. Ferry, George Fragkoulis, Fabian Frost, Luca Frulloni, Phil A. Hart, Gabriela Hernandez-Molina, Dai Inoue, Haihan Ji, Karuna Keat, Terumi Kamisawa, Shigeyuki Kawa, Mitsuhiro Kawano, Arezou Khosroshahi, Hiroshi Kobayashi, Yuzo Kodama, Satoshi Kubo, Kensuke Kubota, Marco Lanzillotta, Haiyang Leng, Markus Lerch, Yanying Liu, Zhifu Liu, Matthias Löhr, Eduardo Martin-Nares, Ferran Martinez-Valle, Chiara Marvisi, Yasufumi Masaki, Shoko Matsui, Ichiro Mizushima, Ray P. Naden, Seiji Nakamura, Jan Nordeide, Kenji Notohara, Kazuichi Okazaki, Sergio Paira, Cory A. Perugino, Jovan Popovic, Manel Ramos-Casals, James Rosenbaum, Jay Ryu, Takako Saeki, Yasuharu Sato, Nicolas Schleinitz, Hiroshi Sekiguchi, Amita Sharma, Evgeniya V. Sokol, James R. Stone, John H. Stone, Wenwu Sun, Hiroki Takahashi, Naoki Takahashi, Masayuki Takahira, Yoshiya Tanaka, Hisanori Umehara, Augusto Vaglio, Alejandra Villamil, Yoko Wada, Zachary S. Wallace, George Webster, Kazunori Yamada, Motohisa Yamamoto, Joanne Yi, Yinlan Yi, Giuseppe Zamboni, Yoh Zen, Wen Zhang.

REVIEW

High-Density Lipoprotein in Lupus: Disease Biomarkers and Potential Therapeutic Strategy

Sang Yeop Kim,[1] [iD] Minzhi Yu,[1] [iD] Emily E. Morin,[1] Jukyung Kang,[1] Mariana J. Kaplan,[2] and Anna Schwendeman[1] [iD]

Systemic lupus erythematosus (SLE) patients exhibit accelerated development of atherosclerosis and increased incidents of cardiovascular disease (CVD) that cannot be explained by traditional risk factors alone. Accumulating evidence suggests that reduced levels of high-density lipoproteins (HDLs), along with altered HDL composition and function, may contribute to the accelerated atherosclerosis in SLE patients. Normally, HDLs play various atheroprotective roles through facilitating cholesterol efflux, inhibiting vascular inflammation, and scavenging oxidative species. However, systemic inflammation, oxidative stress, and autoimmunity in SLE patients induce changes in HDL size distribution and proteomic and lipidomic signatures. These compositional changes in HDLs result in the formation of proinflammatory, dysfunctional HDL. These lupus-altered HDLs have impaired antiatherogenic function with reduced cholesterol efflux capacities, impaired antioxidation abilities, and diminished antiinflammatory properties. In fact, dysfunctional HDL may promote atherogenesis by inducing inflammation. Thus, dysfunctional HDLs could be an important biomarker of accelerated atherosclerosis in lupus. Additionally, HDL-targeted therapies, especially infusion of reconstituted HDLs, may serve as a potential therapeutic intervention for SLE patients with CVD.

Introduction

Systemic lupus erythematosus (SLE) is an autoimmune syndrome with pleiotropic clinical manifestations, characterized by the synthesis of autoantibodies, the development of significant immune dysregulation, and organ damage. While life expectancy in SLE has improved due to the advancement of immunosuppressive therapies and improved treatments for infections and renal disease, mortality rates remain ~3-fold higher than in the general population (1). Of the many causes of mortality in SLE, accelerated atherosclerosis and cardiovascular disease (CVD) is recognized as one of the most prevalent (2). SLE patients showed a higher prevalence of coronary artery disease and atherosclerosis compared to controls, which could not be predicted by traditional risk factors alone (3). Since CVD-inflicted mortality accounts for

more than one-third of all deaths in SLE patients (4), it is clear that CVD continues to be a significant threat to SLE patients.

High-density lipoprotein (HDL) is the smallest lipoprotein and is well-known to exhibit various atheroprotective effects independent of cholesterol mobilization, including its antioxidative, antiinflammatory, antithrombotic, and antiapoptotic abilities (5). Thus, low levels of HDL have been associated with an increased risk of CVD. SLE patients with accelerated atherosclerosis exhibit decreased levels of HDL and the development of dysfunctional HDL (6–8). Such evidence suggests that HDL is likely a novel target for minimizing the risk of CVD in SLE patients, and several studies have recently proposed and investigated HDL-targeted therapies as a potential therapeutic intervention in SLE patients with CVD. In this review, we will discuss the quantitative and qualitative roles of HDL under both normal conditions and

[1]Sang Yeop Kim, PhD, Minzhi Yu, MS, Emily E. Morin, PhD, Jukyung Kang, PhD, Anna Schwendeman, PhD: University of Michigan, Ann Arbor; [2]Mariana J. Kaplan, MD: National Institute of Arthritis and Musculoskeletal and Skin Diseases, NIH, Bethesda, Maryland.

Dr. Kim and Ms Yu contributed equally to this work.

No potential conflicts of interest relevant to this article were reported.

Address correspondence to Anna Schwendeman, PhD, University of Michigan, North Campus Research Center, 2800 Plymouth Road, Ann Arbor, MI 48109. E-mail: annaschw@med.umich.edu.

Submitted for publication May 14, 2018; accepted in revised form July 23, 2019.

Highlights

- **There are quantitative and qualitative abnormalities in HDL of SLE patients including low HDL levels, altered HDL subclass distributions, proteomic and lipidomic changes, and presence of oxidized HDL particles.**

- **The cholesterol efflux, anti-inflammatory and anti-oxidative functions of HDL are impaired in SLE patients, possibly contributing to the accelerated atherosclerosis development.**

- **HDL targeted therapy which aims to restore levels and quality of HDL holds a potential in halting development of CVD in SLE patients.**

Figure 1. A brief summary of the role of high-density lipoprotein (HDL) in systemic lupus erythematosus (SLE). CVD = cardiovascular disease.

in patients with SLE, as well as the potential of HDL-targeted therapeutic interventions (Figure 1).

Structure and composition of HDLs

HDL is constantly remodeled in the bloodstream through interactions with other lipoproteins, enzymes, and contact with target cells, resulting in significant particle heterogeneity. HDL consists of a core of hydrophobic lipids, including cholesteryl esters and triglycerides, and a surface monolayer containing phospholipids, free cholesterol, and apolipoproteins. Apolipoprotein A-I (Apo A-I) is the most abundant protein associated with HDL, comprising 70% of the total HDL protein content (9). Apo A-I is a 28.1-kd, highly α-helical and amphipathic scaffold protein consisting of 243 amino acids that interact with lipids to ultimately define the size and shape of HDL species (9).

In addition to proteins, lipid species are another key component of the overall structure of HDL. A recent lipidome analysis by Kontush et al revealed that more than half of the total HDL mass is accounted for by lipid components, the majority being phospholipids—accounting for 40–60% of the total lipid mass (10). Of these phospholipids, phosphatidylcholines are the largest population, making up 33–45% of total lipid mass, and play critical roles in particle stability, cholesterol efflux, and molecular interactions with HDL-associated enzymes (10).

HDL can be classified into different subpopulations using various techniques. An overview of HDL classification, based on the publication by Rosenson et al (11), is shown in Table 1. Briefly, the use of density-gradient ultracentrifugation and non-denaturing gradient gel electrophoresis can distinguish HDL subpopulations on the basis of density and size, respectively;

from smallest to largest: HDL3c, HDL3b, HDL3a, HDL2a, and HDL2b (11). Apo A-I containing HDL subpopulations can also be defined on the basis of size and charge: pre–β-1 HDL (very small, discoidal HDL with Apo A-I and phospholipid), α-4 HDL (small, discoidal HDL with Apo A-I, phospholipid, and free cholesterol), α-3 HDL (medium-sized, spherical HDL with Apo A-I, Apo A-II, phospholipid, free cholesterol, cholesteryl ester, and triglyceride), α-2 HDL (large, spherical HDL with the same constituents as α-3 HDL), and α-1 HDL (very large, spherical HDL with the same constituents as α-3 HDL but nearly no Apo A-II) (11). Using more sophisticated techniques, such as nuclear magnetic resonance (NMR), 26 different HDL subpopulations have been identified, but they are simply described as small, medium, and large due to limited measurement precision (11). Recently, an NMR-based clinical analyzer called Vantera was developed to measure total HDL particle number in clinical laboratory settings (12).

Changes in HDL composition in SLE patients

Dyslipoproteinemia. Many SLE patients have increased levels of very low-density lipoproteins and low-density lipoproteins (LDLs) and decreased levels of HDL, considered the "lupus lipoprotein pattern." Low HDL cholesterol is one of the most prevalent dyslipidemia indicators observed in SLE patients, including pediatric populations (13–18). In a multiethnic US cohort study containing 546 SLE patients, 81% had low HDL cholesterol levels (<35 mg/dl) (17). In a recent Egyptian study, 45% of 221 SLE patients presented with low HDL cholesterol levels (<40 mg/dl) (18). In some instances, no significant differences in HDL cholesterol levels were found between SLE patients and controls, which may be explained by differences in the patient population (7). Nevertheless, other

Table 1. Classification of HDL*

Separation and analytical methods	Very small	Small	Medium	Large	Very large
Density					
Ultracentrifugation					
Classification	–	HDL3	–	HDL2	–
Range, $F_{1.2}$	–	0–3.5	–	3.5–9	–
Density-gradient ultracentrifugation					
Classification	HDL3c	HDL3b	HDL3a	HDL2a	HDL2b
Range, gm/ml	1.15–1.17	1.13–1.15	1.11–1.13	1.09–1.11	1.06–1.09
Size					
Nondenaturing gradient gel electrophoresis					
Classification	HDL3c	HDL3b	HDL3a	HDL2a	HDL2b
Range, nm	7.2–7.8	7.8–8.2	8.2–8.8	8.8–9.7	9.7–12.9
2-D gel electrophoresis					
Classification	pre–β-1	α-4	α-3	α-2	α-1
Range, nm	5.0–6.0	7.0–7.5	8.5–8.5	9.0–9.4	10.8–11.2
NMR					
Classification		Small	Medium	Large	
Range, nm	–	7.3–8.2	8.2–9.4	9.4–14	–

* HDL = high-density lipoprotein; 2-D = 2-dimensional; NMR = nuclear magnetic resonance.

HDL-related abnormalities were identified in those studies, such as reduced paraoxonase 1 (PON-1) activity (7).

It is noteworthy that HDL cholesterol, which is routinely determined in clinical laboratories, is usually considered synonymous to HDL particle level. However, it has been increasingly recognized that HDL cholesterol may not be an appropriate surrogate of HDL levels, since the cholesterol content of HDL does not correlate perfectly with the number of HDL particles (19). Alternatively, some studies determined HDL levels by measuring Apo A-I concentrations using immunochemistry methods, and lower Apo A-I levels were found in SLE patients relative to healthy subjects (13). Recently, direct measurement of HDL particle numbers has been made possible in clinical laboratories using NMR methods (12). Chung et al found that SLE patients

had lower numbers of large HDL particles compared to healthy volunteers when evaluated by NMR (20). Patients with active disease have lower HDL levels (21–24), while the use of prednisone and hydroxychloroquine correlates with higher HDL cholesterol (23,25). In contrast, simvastatin and atorvastatin have not been found to modify HDL cholesterol levels in SLE patients (26,27).

Changes in HDL size distribution in SLE patients. Lupus patients have been found to have a different distribution of HDL subfractions and HDL sizes compared to healthy controls (Table 2). However, the reported HDL changes vary between individual studies, likely due to the differences in patient inflammatory states as well as medications administered in each study to control SLE, both affecting HDL distribution. In

Table 2. Changes in lipoprotein profile and HDL composition in SLE patients*

Author, year (ref.)	Subjects	HDL changes
Delgado Alves et al, 2002 (35)	32 lupus patients and 20 matched controls	Decreased PON-1 activity Decreased HDL2 Decreased HDL3
McMahon et al, 2006 (38)	154 women with SLE	Increased proinflammatory HDL
Kiss et al, 2007 (7)	37 SLE patients	Decreased Apo A-I Decreased PON-I activity
Juárez-Rojas et al, 2008 (29)	30 women with uncomplicated SLE and 18 matched controls	Decreased cholesteryl ester Increased triglycerides Decreased Apo A-I Decreased HDL size Decreased HDL2b Increased HDL3b and HDL3c
Batuca et al, 2009 (34)	77 lupus patients	Decreased PON-1 activity
Smith et al, 2014 (39)	SLE patients and healthy controls	Increased oxidized Apo A-I
Marsillach et al, 2015 (60)	54 SLE patients and 25 matched healthy controls	Decreased PON-3
Gaál et al, 2016 (16)	51 SLE patients and 49 matched healthy controls	Increased SAA combination Decreased PON-I arylesterase activity
Han et al, 2016 (33)	18 SLE patients	Increased SAA combination

* HDL = high-density lipoprotein; SLE = systemic lupus erythematosus; PON-1 = paraoxonase 1; Apo A-I = apolipoprotein A-I; SAA = serum amyloid A.

addition, the analytical methodologies used to characterize HDL distribution differ between studies, further hindering comparison of the results. Hua et al reported that small HDL is less prevalent in SLE patients, while the overall HDL size is increased in SLE patients compared to healthy controls (28). Chung et al reported that SLE patients have a lesser proportion of large HDL; however, the overall sizes of HDL were no different between SLE and healthy individuals (20). Other studies have also reported no significant differences in HDL size between SLE patients and healthy controls (16). Juárez-Rojas et al reported that SLE patients tend to have lower proportions of HDL2b and higher proportions of HDL3b and HDL3c (29). Similar results were reported by Formiga et al, where SLE patients had higher levels of HDL3 cholesterol and lower levels of HDL2 cholesterol (30).

Proteomic and lipidomic changes in SLE HDL composition. HDL in SLE also has abnormal proteomic features, with changes in Apo A-I being the most noteworthy. In the study by Machado et al, female adolescents with SLE had a higher ratio of HDL cholesterol to Apo A-I compared to healthy controls, indicating that the HDL particles in those SLE patients had a lesser amount of Apo A-I (31). Juárez-Rojas et al reported lower Apo A-I and higher Apo E content in HDL particles isolated from women with SLE (29). However, in another study comparing 51 SLE patients to 49 healthy controls, SLE patients were found to have a higher ratio of Apo A-I to HDL, although the overall serum Apo A-I level was lower (16). Similar to proteomic alterations, the lipidome of HDL is also compromised in the SLE setting. Juárez-Rojas et al found that HDL isolated from SLE patients had less cholesteryl ester and more triglycerides compared to healthy controls (29). Moreover, lipid peroxidation is enhanced in SLE patients due to enhanced oxidative stress that promotes a significant increase in the production of oxidized lipids (32). Further, Gaál et al (16) and Han et al (33) found that SLE patients display significantly increased levels of serum amyloid A (SAA) compared to healthy subjects. Additionally, multiple studies confirmed a significant reduction in PON-1 and PON-3 activity in SLE patients (7,16,34,35). The abnormal lipoprotein profiles in SLE patients are summarized in Table 2.
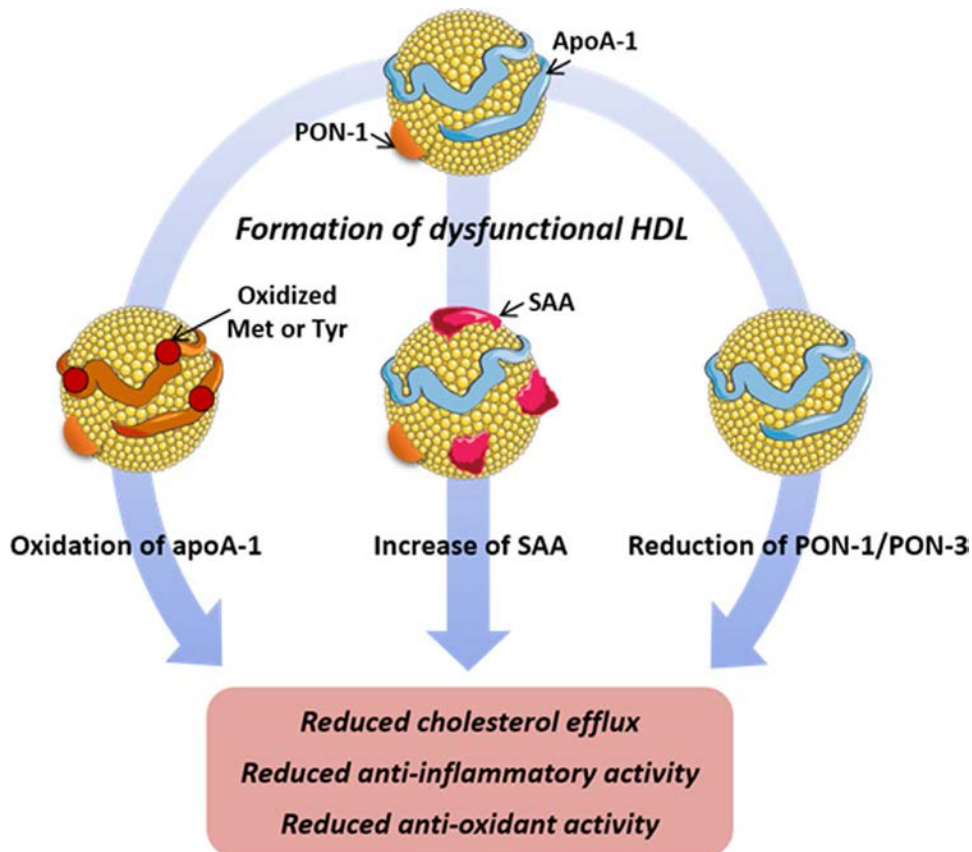
Figure 2. Formation of dysfunctional or proinflammatory high-density lipoprotein (HDL) in systemic lupus erythematosus (SLE). In SLE, multiple HDL proteomic changes occur, leading to the impairment of the function of HDL. Oxidation of apolipoprotein A-I (Apo A-I) methionine (Met) and tyrosine (Tyr) residues by chemical and enzymatic pathways leads to reduced ability of HDL to efflux cholesterol outside the cell and neutralize oxidized lipids. Increased levels of serum amyloid A (SAA) cause displacement of Apo A-I on HDL and reduced cholesterol efflux and antiinflammatory activity. Reduced levels and activity of HDL-associated paraoxonase 1 (PON-1) lead to the reduced antioxidant activity of HDL.

Proinflammatory HDL. HDL exerts antiinflammatory functions in healthy subjects. However, in the course of inflammatory disease such as SLE, the composition of HDL is altered and its function compromised. This can lead to the transformation of HDL into a dysfunctional, proinflammatory particle with reduced cholesterol efflux capacity unable to perform its normal antiinflammatory and antioxidative functions (Figure 2) (36). Compared to normal HDL, proinflammatory HDL is characterized by increased SAA content, decreased Apo A-I levels, increased Apo A-I oxidation, and decreased PON activity (16). Increased SAA content in HDL results in its displacement of Apo A-I, thus, reducing the atheroprotective properties of HDL (37). McMahon et al reported that 44.7% of SLE patients had increased levels of proinflammatory HDL in comparison to only 4.1% of controls and 20.1% of rheumatoid arthritis patients (38). Their subsequent study identified proinflammatory HDL to be associated with increased carotid intima-media thickness and plaque by carotid ultrasound, suggesting that dysfunctional proinflammatory HDL significantly contributes to the development of subclinical atherosclerosis in SLE (6).

Oxidized HDL. HDL also undergoes structural changes in SLE due to oxidation, and it has been found that SLE patients have elevated levels of oxidized HDL (Figure 2) (39). Myeloperoxidase (MPO) is the main oxidant enzyme responsible for the oxidation of HDL. MPO-catalyzed oxidation converts normal tyrosine on Apo A-I to 3-chlorotyrosine or 3-nitrotyrosine, leading to oxidized HDL (40). MPO also oxidizes 3 methionine residues of Apo A-I, methionine 86 (Met-86), Met-112, and Met-148, contributing significantly to enhancing levels of oxidized Apo A-I (41). In SLE patients, a high concentration of serum MPO is reported, implying a link between increased HDL oxidation and increased MPO levels in this disease. Recent studies found associations between HDL oxidation and elevated formation of neutrophil extracellular traps (NETs) (39). Under normal conditions, NETs play an important antimicrobial role; however, in SLE, NETs are dysregulated. It has been shown that the degradation of NETs is hindered in SLE patients, resulting in aberrant elevation of NETs and infiltration of netting neutrophils in tissues (42).

Carlucci et al demonstrated that SLE patients present higher levels of low-density granulocytes (LDGs), which are one subset of neutrophils with enhanced NET formation capacity (43). The increased LDG levels are found to be associated with the impaired cholesterol efflux capacity of HDL isolated from lupus patients (43). It has been proposed that enhanced levels of NETs enhances the oxidant potential in SLE and leads to the externalization to the extracellular space of oxidant enzymes such as MPO, nitric oxide synthase (NOS), and NADPH oxidase (NOX), ultimately promoting oxidation of HDL (Figure 3) (43,44). Data from SLE patients showed that MPO and NOX from NETs promoted 3-chlorotyrosine modification, and NOS and NOX promoted 3-nitrotyrosine modification on HDL, while inhibition of NETs decreased the oxidation

of HDL. These observations support the notion that NETs play a major role in the oxidation of HDL in SLE (39).

In addition to MPO, lipid peroxidation products also mediate the oxidation of HDL. Studies showed that oxidized phospholipids could covalently react with Apo A-I at various sites, forming lipid–protein adducts (45). It was also found that lipid hydroperoxide could chemically react with Apo A-I and Apo A-II, leading to the oxidation of Met residues to methionine sulfoxide (46). Since clinical studies have shown that lipid peroxidation is enhanced in SLE patients, this may also contribute to the increased oxidation of Apo A-I and HDL in this disease (47).

Functional changes in HDL in SLE patients

Impaired cholesterol efflux capacity. Removal of excess cholesterol from macrophages in the artery wall is recognized to be the key process of HDL for protection against atherosclerosis and improvement of cardiovascular outcomes. This process, known as reverse cholesterol transport, allows translocating excess cholesterol and other lipids from lipid-laden macrophages in atherosclerotic lesions to the liver for elimination. The first and most crucial step in reverse cholesterol transport is to efflux cholesterol from macrophages to HDL. HDL isolated from SLE patients displays a 15% decrease in cholesterol efflux ability compared to healthy control HDL (39). The decreased cholesterol efflux capacity of HDL purified from SLE patients has been found to significantly correlate with increased noncalcified coronary plaque burden (43). Multiple studies have proposed that the reason for decreased cholesterol efflux ability of HDL in SLE is increased levels of SAA. As mentioned earlier, increased levels of SAA promote dysfunctional proinflammatory HDL with diminished ability to remove cholesterol from macrophages and traffic cholesteryl ester to the liver (48).

Oxidation of HDL can also contribute to its reduced cholesterol efflux capacity in SLE. HDL containing oxidized Apo A-I has a reduced ability to efflux cholesterol (49,50). Furthermore, when Met-148 is oxidized in Apo A-I, HDL loses the ability to interact with lecithin-cholesterol acyltransferase, an enzyme responsible for the conversion to cholesterol ester, which is a key step in reverse cholesterol transport (51). Thus, the oxidation of Apo A-I could be a key reason for the impaired process of cholesterol efflux in SLE.

Reduced antiinflammatory function. In recent years, it has become widely accepted that HDL can directly inhibit the inflammation processes that lead to the development of atherosclerosis (52). Although the complex antiinflammatory mechanisms of HDL have not been fully elucidated, it has been suggested that several signaling pathways play a role in this process. First, HDL can inhibit Toll-like receptor (TLR) pathways through activation of the transcriptional repressor activating transcription factor 3 (ATF-3). Activated ATF-3 is translocated into the nucleus and inhibits
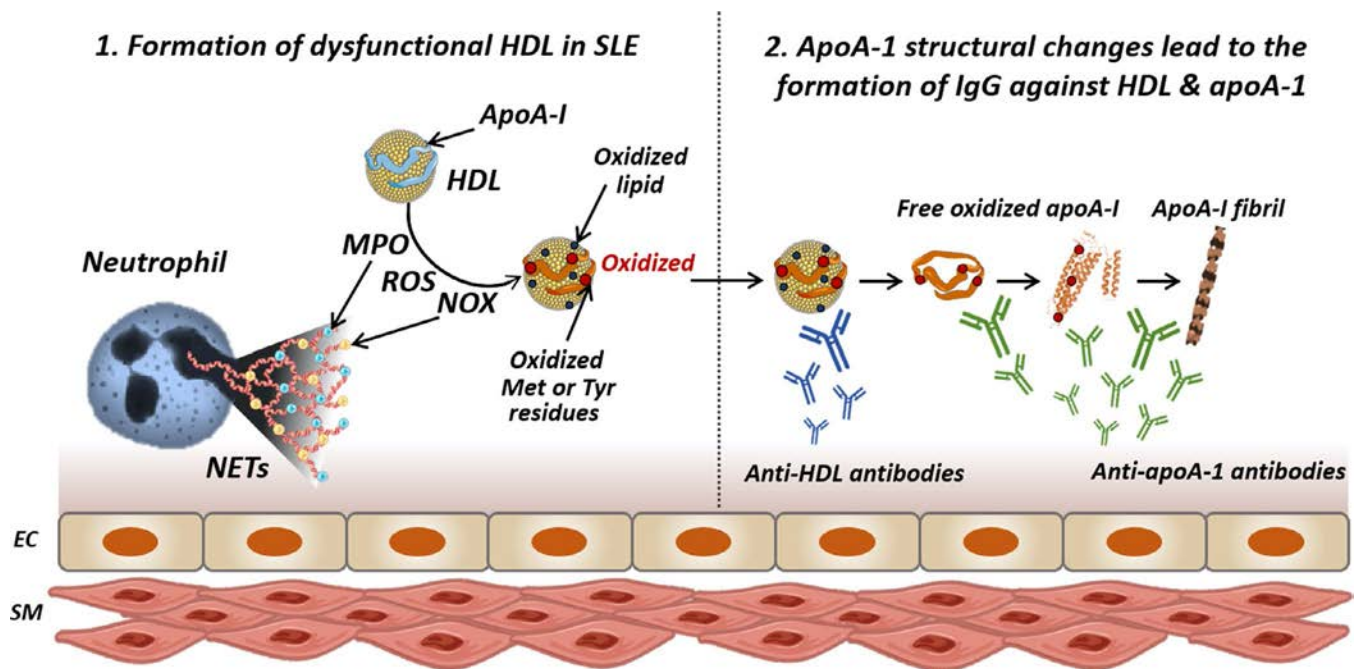
Figure 3. Formation of dysfunctional high-density lipoprotein (HDL) and autoantibodies against HDL and apolipoprotein A-I (Apo A-I) in systemic lupus erythematosus (SLE). In SLE, abnormal elevation of neutrophil extracellular traps (NETs) is observed, leading to endothelial cell (EC) damage. In the presence of NETs, increased levels of myeloperoxidase (MPO), nitric oxide synthase (NOS), NADPH oxidase (NOX), and reactive oxygen species (ROS) are observed, causing oxidation of HDL and Apo A-I. Oxidation of Apo A-I and HDL induces the formation of anti-HDL and anti–Apo A-I autoantibodies. Furthermore, oxidation of Apo A-I at Met-148 leads to conformational changes in Apo A-I, promoting protein misfolding, dissociation of misfolded Apo A-I from HDL, and formation of Apo A-I amyloid fibrils. This aggregated Apo A-I is more immunogenic, leading to a further increase in anti–Apo A-I autoantibody titers. SM = smooth muscle cell.

the promotion of TLR-induced inflammatory cytokines (53). HDL can also inhibit NF-κB–activated cell adhesion molecule expression, thus preventing vascular inflammation (54).

In contrast to the antiinflammatory response promoted by healthy HDL, HDL purified from SLE patients induces a proinflammatory response. Smith et al reported that HDL in SLE fails to inhibit cytokine induction driven by TLR pathways (55). In comparison to macrophages exposed to healthy HDL, macrophages treated with SLE HDL induced activation of NF-κB and increased expression of tumor necrosis factor (TNF) and interleukin-6 (IL-6). In addition, macrophages treated with SLE HDL had significantly repressed ATF-3 activation compared to control HDL or an untreated group, suggesting that HDL from SLE patients cannot inhibit TLR pathways via ATF-3 activation.

The oxidation of HDL in SLE promotes the binding of HDL to the lectin-like oxidized low-density lipoprotein receptor 1, preventing ATF-3 nuclear translocation and leading to increased synthesis of inflammatory cytokines (55). HDL from SLE patients was also found to be able to directly up-regulate monocyte platelet-derived growth factor receptor β and increase chemotaxis and TNF release (56). Another study associated the loss of antiinflammatory function of HDL in SLE with the increased SAA content in HDL particles. Under normal conditions, HDL can inhibit inflammatory responses by disrupting lipid rafts and sequestering

plasma membrane cholesterol; however, it has been suggested that the SAA binding on the surface of HDL impedes the interaction between HDL and cell membrane, decreasing the antiinflammatory role of HDL (33).

Reduced antioxidant capacity. In both the general population and in individuals with SLE, increased oxidized LDL level is a well-recognized risk factor for CVD (57). Under normal conditions, HDL prevents LDL oxidation by scavenging reactive oxygen species (ROS). The increased levels of oxidized HDL and oxidized Apo A-I in SLE reduce the ability of HDL particles to scavenge ROS. In addition, proinflammatory HDL in SLE may promote LDL oxidation. Elevated levels of oxidized LDL increase recruitment and adherence of monocytes to activated endothelial cells by increasing the expression of adhesion molecules and proinflammatory cytokines (58). These monocytes then transmigrate to the arterial intima, taking up oxidized LDL and eventually maturing to form foam cells.

PON enzymes also play a critical role in the antioxidant functions of HDL. Among the PON enzymes, PON-1 is the major antioxidant in HDL and prevents LDL from oxidation, thereby eliminating biologically active oxidized LDL (46). SLE patients have reduced PON-1 activity (7,16,34,35,59) and this correlates with the loss in antioxidative function of HDL (16). While the reasons for the loss in PON-1 activity are not fully understood, levels of

various autoantibodies inversely correlate with PON-1 activity. These include IgG against Apo A-I (8,16,34), HDL (34,35), and β_2-glycoprotein I (35), suggesting that autoantibodies may contribute to the decreased activity of PON-1. In addition to PON-1, PON-3, another member of the PON enzyme family, is decreased in SLE patients with subclinical atherosclerosis, potentially promoting the loss of the antioxidant ability of HDL in SLE (60) (Figure 2).

Formation of autoantibodies in SLE

The production of autoantibodies is the key manifestation of SLE. In patients affected by autoimmune disorders, highly reactive IgG antibodies against human Apo A-I are detected and can bind to both lipid-free Apo A-I as well as Apo A-I on HDL particles (34). It has been reported that 32.5% of patients with SLE tested positively for the presence of anti–Apo A-I autoantibodies in association with decreased levels of HDL (61). Similar studies have confirmed the presence of anti–Apo A-I and its association with higher disease activity in SLE patients (34,62,63). In comparison, only 1% of healthy individuals and 20% of patients with acute coronary syndrome without an autoimmune disorder have detectable levels of anti–Apo A-I (64). The presence of anti–Apo A-I has been reported to reduce the activity of PON, leading to increased LDL oxidation (34,35). Likewise, in lupus-prone murine models, anti–Apo A-I was associated with decreased levels of HDL cholesterol and PON-1 activity (8).

We hypothesize that increased levels of anti–Apo A-I in SLE patients correlates with increased lipid-free Apo A-I and oxidized free Apo A-I. Lipid-free Apo A-I can exist in plasma via several pathways, either due to de novo synthesis or dissociation from HDL due to displacement by elevated levels of SAA. In addition, oxidation of Apo A-I at the Met-148 position leads to conformational changes in the protein (65). Oxidation of Apo A-I favors protein misfolding from the native α-helical structure to β-sheets, facilitating dissociation of Apo A-I from HDL particles and initiating Apo A-I amyloid fibril formation (41). Thus, in SLE plasma and in the oxidative microenvironment associated with NETs and atherosclerosis, the levels of structurally modified Apo A-I are likely to be elevated, leading to higher levels of lipid-free misfolded protein (Figure 3). Indeed, in HDL isolated from SLE patients, the median levels of 3-nitrotyrosine and 3-chlorotyrosine were 1.9- and 120.9-fold higher than in HDL isolated from healthy controls (39). The misfolded and oxidized Apo A-I protein is likely more immunogenic, thus leading to higher titers of anti–Apo A-I in SLE.

Anti-HDL antibodies have recently been identified in SLE patients. The differences between anti-HDL antibodies and anti–Apo A-I antibodies remain unclear (34,61). Lipid-free Apo A-I–coated enzyme-linked immunosorbent assay is most commonly used to measure antibody titers in serum. However, in some instances, the entire HDL particle is used in the assay. It is possible that HDL used in the assay is partially oxidized and antibodies present in SLE patient serum recognize either oxidized or partially misfolded Apo A-I that remains to be lipid-bound in HDL particles (66). A few studies have reported significantly elevated levels of anti-HDL in SLE compared to either healthy subjects or patients with primary antiphospholipid syndrome (67,68). High anti-HDL titers were associated with increased SLE disease activity markers and decreased PON activity, which could lead to loss of antioxidant and atheroprotective functions of HDL and promotion of atherosclerosis development (7,34,60).

Applications of HDL therapeutics

The impact of statin use to control CVD development in SLE patients has been examined in several clinical studies. The Lupus Atherosclerosis Prevention Study showed no significant difference in carotid intima-media thickness of carotid plaque between SLE patients treated with atorvastatin and those treated with placebo (27). However, a recent nationwide population-based cohort study utilizing statin therapy showed promising results, with a significant reduction of risk of CVD mortality by 30% in SLE patients with hyperlipidemia (69). In addition, short-term atorvastatin therapy improved endothelium-dependent vasodilation in SLE patients (70). Therefore, sufficiently powered long-term prospective clinical trials are necessary to definitively conclude whether the use of statins is beneficial in SLE patients.

Reconstituted HDL, nanoparticles prepared from Apo A-I or Apo A-I mimetic peptides following reconstitution with phospholipids, have been extensively studied as an antiatherosclerosis therapeutic since 1984 (71). Infusions of reconstituted HDL have been shown to increase levels of circulating HDL, improve plasma cholesterol efflux capacity, inhibit the synthesis of proinflammatory mediators, and improve endothelial function, leading to increased overall atheroprotection in animal models and in clinical trials (72). As of today, 6 different reconstituted HDL products have been tested in clinical trials, including SRC-rHDL, CSL-111, ETC-216, ETC-642, CER-001, and CSL-112. Two products, ETC-216 and CSL-111, were shown to reduce plaque burden in CVD patients as assessed by intravascular ultrasound (73,74). CSL-112, a newer formulation of CSL-111, exhibited improved clinical safety and cholesterol efflux capacity in healthy volunteers compared to CSL-111 (75). A phase III study of 17,400 patients to explore the ability of CSL-112 to reduce major adverse cardiovascular events in CVD patients is currently ongoing (76).

HDL therapy has also presented beneficial effects on inflammatory disorders such as sepsis. It can neutralize endotoxin from bacteria, regulate the inflammatory response in macrophages, and inhibit endothelial cell activation in sepsis (77). As a result, the infusion of CSL-111 suppressed proinflammatory cytokine production, sepsis-induced hypotension, and reduced the severity of clinical symptoms (78). Similarly, L-4F, an Apo A-I mimetic peptide, demonstrated a beneficial effect in studies of various animal sepsis models by inhibiting proinflammatory cytokine production, reducing sepsis-induced hypotension, protecting
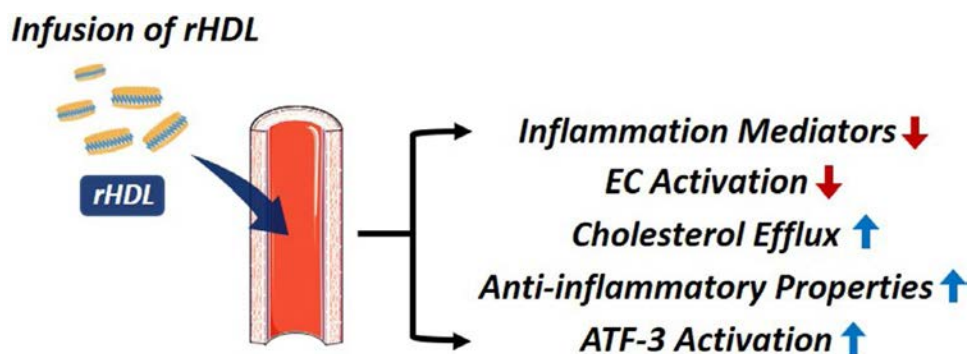
Figure 4. Reconstituted HDL (rHDL) as a putative therapeutic strategy in patients with systemic lupus erythematosus (SLE) at risk of cardiovascular disease (CVD). Infusion of reconstituted HDL in SLE patients may increase the level of pre–β-HDL, reduce the presence of inflammatory mediators and activation of endothelial cells, enhance antiinflammatory properties and activating transcription factor 3 (ATF-3) activation, and facilitate cholesterol efflux capacity.

against organ damage, and increasing the survival rate (79,80). Charles-Schoeman et al have proposed a possible therapy with Apo A-I mimetic peptides in collagen-induced arthritis, a rodent model of rheumatoid arthritis (81). Rats treated with combination therapy of Apo A-I mimetic peptides, D-4F, and pravastatin had a significantly improved clinical severity score and less erosive disease compared to both rats that received noncombination treatment and control groups. Levels of inflammatory cytokines and chemokines were notably reduced with combination therapy and the antiinflammatory properties of HDL were improved.

Use of Apo A-I mimetic peptides and reconstituted HDL in animal models of SLE. To date, very few studies have tested the putative benefit of HDL treatment in animal models of SLE. A study by Woo et al showed significant improvements in SLE manifestations in a murine lupus model associated with accelerated atherosclerosis via treatment with the Apo A-I mimetic peptide, L-4F, alone or with pravastatin (82). Notably, treatment with L-4F alone or with pravastatin significantly reduced IgG anti–double-stranded DNA (anti-dsDNA), IgG antioxidized phospholipids, proteinuria, glomerulonephritis, and osteopenia. L-4F also improved the antiinflammatory functions of plasma HDL while reducing the proinflammatory effects of LDL. In a more recent study by Black et al, increased levels of Apo A-I resulted in suppression of lymphocyte activation, IgG anti-dsDNA autoantibodies, interferon-γ–secreting CD4+ Th1 cells, and follicular T helper cells, along with improved glomerulonephritis in a normocholesterolemic murine model of SLE (83). Smith et al investigated whether reconstituted HDL can reverse the proinflammatory effects of lupus HDL by administering ETC-642, an HDL mimetic composed of the Apo A-I mimetic peptide (ESP24218) and phospholipid complex, in vivo to NZM2328 mice, a mouse model of lupus (55). Indeed, macrophages exposed to a 1:4 ratio of SLE HDL to ETC-642 significantly suppressed TNF, IL-6, and NF-κB activation while promoting ATF-3 nuclear translocation, suggesting that reconstituted HDL can successfully mimic the effects of healthy HDL. The therapy led to significant increases in ATF-3

expression and lowered IL-6 levels in serum, indicating that reconsituted HDL can also decrease cytokine synthesis.

Future directions for reconstituted HDL therapy in SLE patients with CVD. Underscoring the fact that dysfunctional HDL may promote CVD in SLE, HDL therapy may serve as a potential and alternative therapeutic because it can restore both the quantity and quality of HDL. It is worth noting that reconstituted HDL and naked Apo A-I mimetic peptides used in previous studies have not been optimized for CVD prevention and treatment trials in SLE, as they primarily focused on maximizing the efficacy of cholesterol efflux. Therefore, the potential benefit of reconstituted HDL therapy for CVD prevention and treatment in SLE patients remains unclear. An advantage of reconstituted HDL therapy is that it can be further customized to be more disease specific. We have recently discovered that the lipid component of HDL can significantly alter the cholesterol efflux capacity and antiinflammatory properties of HDL (84). Therefore, further investigations to understand the protective roles of reconstituted HDL in SLE with CVD are needed and will inform the optimization of the reconstituted HDL composition. Administration of optimized reconstituted HDL in SLE models would likely increase the level of pre–β-HDL and may restore the antiinflammatory functions of HDL, and reduce proinflammatory HDL and oxidized LDL. Improved and restored HDL may then exert its diverse protective mechanisms, including the reduction of inflammatory mediators and activation of endothelial cells, all while improving cholesterol efflux capacity (Figure 4). In addition, prevention of autoantibody recognition may be possible in reconstituted HDL therapy via altering protein/peptide composition. These observations suggest that HDL mimetics may serve as an effective therapeutic strategy for reducing CVD risk and, potentially, disease activity in SLE.

AUTHOR CONTRIBUTIONS

All authors drafted the article, revised it critically for important intellectual content, and approved the final version to be published.

REFERENCES

1. Urowitz MB, Gladman DD, Tom BD, Ibañez D, Farewell VT. Changing patterns in mortality and disease outcomes for patients with systemic lupus erythematosus. J Rheumatol 2008;35:2152–8.

2. Bernatsky S, Boivin JF, Joseph L, Manzi S, Ginzler E, Gladman DD, et al. Mortality in systemic lupus erythematosus. Arthritis Rheum 2006;54:2550–7.

3. Agarwal S, Elliott JR, Manzi S. Atherosclerosis risk factors in systemic lupus erythematosus. Curr Rheumatol Rep 2009;11:241–7.

4. Lerang K, Gilboe IM, Steinar Thelle D, Gran JT. Mortality and years of potential life loss in systemic lupus erythematosus: a population-based cohort study. Lupus 2014;23:1546–52.

5. Besler C, Lüscher TF, Landmesser U. Molecular mechanisms of vascular effects of high-density lipoprotein: alterations in cardiovascular disease. EMBO Mol Med 2012;4:251–68.

6. McMahon M, Grossman J, Skaggs B, FitzGerald J, Sahakian L, Ragavendra N, et al. Dysfunctional proinflammatory high-density lipoproteins confer increased risk of atherosclerosis in women with systemic lupus erythematosus. Arthritis Rheum 2009;60:2428–37.

7. Kiss E, Seres I, Tarr T, Kocsis Z, Szegedi G, Paragh G. Reduced paraoxonase1 activity is a risk for atherosclerosis in patients with systemic lupus erythematosus. Ann N Y Acad Sci 2007;1108:83–91.

8. Srivastava R, Yu S, Parks BW, Black LL, Kabarowski JH. Autoimmune-mediated reduction of high-density lipoprotein–cholesterol and paraoxonase 1 activity in systemic lupus erythematosus–prone gld mice. Arthritis Rheum 2011;63:201–11.

9. Kontush A, Lindahl M, Lhomme M, Calabresi L, Chapman MJ, Davidson WS. Structure of HDL: particle subclasses and molecular components. Handb Exp Pharmacol 2015;224:3–51.

10. Kontush A, Lhomme M, Chapman MJ. Unraveling the complexities of the HDL lipidome. J Lipid Res 2013;54:2950–63.

11. Rosenson RS, Brewer HB, Chapman MJ, Fazio S, Hussain MM, Kontush A, et al. HDL measures, particle heterogeneity, proposed nomenclature, and relation to atherosclerotic cardiovascular events. Clin Chem 2011;57:392–410.

12. Matyus SP, Braun PJ, Wolak-Dinsmore J, Saenger AK, Jeyarajah EJ, Shalaurova I, et al. HDL particle number measured on the Vantera®, the first clinical NMR analyzer. Clin Biochem 2015;48:148–55.

13. Lilleby V, Haugen M, Mørkrid L, Frøslie FK, Holven KB, Førre Ø. Body composition, lipid and lipoprotein levels in childhood-onset systemic lupus erythematosus. Scand J Rheumatol 2007;36:40–7.

14. Soep JB, Mietus-Snyder M, Malloy MJ, Witztum JL, von Scheven E. Assessment of atherosclerotic risk factors and endothelial function in children and young adults with pediatric-onset systemic lupus erythematosus. Arthritis Rheum 2004;51:451–7.

15. Yuan J, Li LI, Wang Z, Song W, Zhang Z. Dyslipidemia in patients with systemic lupus erythematosus: association with disease activity and B-type natriuretic peptide levels. Biomed Rep 2016;4:68–72.

16. Gaál K, Tarr T, Lőrincz H, Borbás V, Seres I, Harangi M, et al. High-density lipopoprotein antioxidant capacity, subpopulation distribution and paraoxonase-1 activity in patients with systemic lupus erythematosus. Lipids Health Dis 2016;15:60.

17. Toloza SM, Uribe AG, McGwin G Jr, Alarcón GS, Fessler BJ, Bastian HM, et al. Systemic lupus erythematosus in a multiethnic US cohort (LUMINA). XXIII. Baseline predictors of vascular events. Arthritis Rheum 2004;3947–57.

18. Gamal SM, Fawzy SM, Abdo M, Elgengehy FT, Ghoniem S, Alkemry A. Immunological profile and dyslipidemia in Egyptian systemic lupus erythematosus patients. Egypt Rheumatol 2017;39:89–92.

19. Heinecke JW. The not-so-simple HDL story: a new era for quantifying HDL and cardiovascular risk? Nat Med 2012;18:1346–7.

20. Chung CP, Oeser A, Raggi P, Solus JF, Avalos I, Linton MF, et al. Lipoprotein subclasses and particle size determined by nuclear magnetic resonance spectroscopy in systemic lupus erythematosus. Clin Rheumatol 2008;27:1227–33.

21. Wijaya LK, Kasjmir YI, Sukmana N, Subekti I, Prihartono J. The proportion of dyslipidemia in systemic lupus erythematosus patient and distribution of correlated factors. Acta Med Indones 2005;37:132–44.

22. Kashef S, Ghaedian MM, Rajaee A, Ghaderi A. Dyslipoproteinemia during the active course of systemic lupus erythematosus in association with anti-double-stranded DNA (anti-dsDNA) antibodies. Rheumatol Int 2007;27:235–41.

23. Sarkissian T, Beyenne J, Feldman B, Adeli K, Silverman E. The complex nature of the interaction between disease activity and therapy on the lipid profile in patients with pediatric systemic lupus erythematosus. Arthritis Rheum 2006;54:1283–90.

24. Cardoso CR, Signorelli FV, Papi JA, Salles GF. Prevalence and factors associated with dyslipoproteinemias in Brazilian systemic lupus erythematosus patients. Rheumatol Int 2008;28:323–7.

25. Durcan L, Winegar DA, Connelly MA, Otvos JD, Magder LS, Petri M. Longitudinal evaluation of lipoprotein variables in systemic lupus erythematosus reveals adverse changes with disease activity and prednisone and more favorable profiles with hydroxychloroquine therapy. J Rheumatol 2016;43:745–50.

26. Schanberg LE, Sandborg C, Barnhart HX, Ardoin SP, Yow E, Evans GW, et al. Use of atorvastatin in systemic lupus erythematosus in children and adolescents. Arthritis Rheum 2012;64:285–96.

27. Petri MA, Kiani AN, Post W, Christopher-Stine L, Magder LS. Lupus Atherosclerosis Prevention Study (LAPS). Ann Rheum Dis 2011;70:760–5.

28. Hua X, Su J, Svenungsson E, Hurt-Camejo E, Jensen-Urstad K, Angelin B, et al. Dyslipidaemia and lipoprotein pattern in systemic lupus erythematosus (SLE) and SLE-related cardiovascular disease. Scand J Rheumatol 2009;38:184–9.

29. Juárez-Rojas J, Medina-Urrutia A, Posadas-Sánchez R, Jorge-Galarza E, Mendoza-Pérez E, Caracas-Portilla N, et al. High-density lipoproteins are abnormal in young women with uncomplicated systemic lupus erythematosus. Lupus 2008;17:981–7.

30. Formiga F, Meco JF, Pinto X, Jacob J, Moga I, Pujol R. Lipid and lipoprotein levels in premenopausal systemic lupus erythematosus patients. Lupus 2001;10:359–63.

31. Machado D, Sarni RO, Abad TT, Silva SG, Khazaal EJ, Hix S, et al. Lipid profile among girls with systemic lupus erythematosus. Rheumatol Int 2017;37:43–8.

32. Shah D, Mahajan N, Sah S, Nath SK, Paudyal B. Oxidative stress and its biomarkers in systemic lupus erythematosus [review]. J Biomed Sci 2014;21:23.

33. Han CY, Tang C, Guevara ME, Wei H, Wietecha T, Shao B, et al. Serum amyloid A impairs the antiinflammatory properties of HDL. J Clin Invest 2016;126:266–81.

34. Batuca JR, Ames PR, Amaral M, Favas C, Isenberg DA, Delgado Alves J. Anti-atherogenic and anti-inflammatory properties of high-density lipoprotein are affected by specific antibodies in systemic lupus erythematosus. Rheumatology (Oxford) 2009;48:26–31.

35. Delgado Alves J, Ames PR, Donohue S, Stanyer L, Nourooz-Zadeh J, Ravirajan C, et al. Antibodies to high-density lipoprotein and β$_2$-glycoprotein I are inversely correlated with paraoxonase activity in systemic lupus erythematosus and primary antiphospholipid syndrome. Arthritis Rheum 2002;46:2686–94.

36. Hb G, Rao VS, Kakkar VV. Friend turns foe: transformation of anti-inflammatory HDL to proinflammatory HDL during acute-phase response. Cholesterol 2011;2011:274629.

37. Van Lenten BJ, Wagner AC, Nayak DP, Hama S, Navab M, Fogelman AM. High-density lipoprotein loses its anti-inflammatory properties during acute influenza A infection. Circulation 2001;103:2283–8.

38. McMahon M, Grossman J, FitzGerald J, Dahlin-Lee E, Wallace DJ, Thong BY, et al. Proinflammatory high-density lipoprotein as a biomarker for atherosclerosis in patients with systemic lupus erythematosus and rheumatoid arthritis. Arthritis Rheum 2006;54:2541–9.

39. Smith CK, Vivekanandan-Giri A, Tang C, Knight JS, Mathew A, Padilla RL, et al. Neutrophil extracellular trap–derived enzymes oxidize high-density lipoprotein: an additional proatherogenic mechanism in systemic lupus erythematosus. Arthritis Rheumatol 2014;66:2532–44.

40. Heinecke JW. The role of myeloperoxidase in HDL oxidation and atherogenesis. Curr Atheroscler Rep 2007;9:249–51.

41. Chan GK, Witkowski A, Gantz DL, Zhang TO, Zanni MT, Jayaraman S, et al. Myeloperoxidase-mediated methionine oxidation promotes an amyloidogenic outcome for apolipoprotein A-I. J Biol Chem 2015;290:10958–71.

42. Leffler J, Martin M, Gullstrand B, Tydén H, Lood C, Truedsson L, et al. Neutrophil extracellular traps that are not degraded in systemic lupus erythematosus activate complement exacerbating the disease. J Immunol 2012;188:3522–31.

43. Carlucci PM, Purmalek MM, Dey AK, Temesgen-Oyelakin Y, Sakhardande S, Joshi AA, et al. Neutrophil subsets and their gene signature associate with vascular inflammation and coronary atherosclerosis in lupus. JCI Insight 2018;3:99276.

44. Vivekanandan-Giri A, Slocum JL, Byun J, Tang C, Sands RL, Gillespie BW, et al. High density lipoprotein is targeted for oxidation by myeloperoxidase in rheumatoid arthritis. Ann Rheum Dis 2013;72:1725–31.

45. Szapacs ME, Kim HY, Porter NA, Liebler DC. Identification of proteins adducted by lipid peroxidation products in plasma and modifications of apolipoprotein A1 with a novel biotinylated phospholipid probe. J Proteome Res 2008;7:4237–46.

46. Hahn BH, Grossman J, Ansell BJ, Skaggs BJ, McMahon M. Altered lipoprotein metabolism in chronic inflammatory states: proinflammatory high-density lipoprotein and accelerated atherosclerosis in systemic lupus erythematosus and rheumatoid arthritis [review]. Arthritis Res Ther 2008;10:213.

47. Jiang X, Chen F. The effect of lipid peroxides and superoxide dismutase on systemic lupus erythematosus: a preliminary study. Clin Immunol Immunopathol 1992;63:39–44.

48. Artl A, Marsche G, Pussinen P, Knipping G, Sattler W, Malle E. Impaired capacity of acute-phase high density lipoprotein particles to deliver cholesteryl ester to the human HUH-7 hepatoma cell line. Int J Biochem Cell Biol 2002;34:370–81.

49. Bergt C, Pennathur S, Fu X, Byun J, O'Brien K, McDonald TO, et al. The myeloperoxidase product hypochlorous acid oxidizes HDL in the human artery wall and impairs ABCA1-dependent cholesterol transport. Proc Natl Acad Sci U S A 2004;101:13032–7.

50. Shao B, Oda MN, Bergt C, Fu X, Green PS, Brot N, et al. Myeloperoxidase impairs ABCA1-dependent cholesterol efflux through methionine oxidation and site-specific tyrosine chlorination of apolipoprotein A-I. J Biol Chem 2006;281:9001–4.

51. Shao B, Cavigiolio G, Brot N, Oda MN, Heinecke JW. Methionine oxidation impairs reverse cholesterol transport by apolipoprotein A-I. Proc Natl Acad Sci U S A 2008;105:12224–9.

52. Säemann MD, Poglitsch M, Kopecky C, Haidinger M, Hörl WH, Weichhart T. The versatility of HDL: a crucial anti-inflammatory regulator. Eur J Clin Invest 2010;40:1131–43.

53. De Nardo D, Labzin LI, Kono H, Seki R, Schmidt SV, Beyer M, et al. High-density lipoprotein mediates anti-inflammatory reprogramming of macrophages via the transcriptional regulator ATF3. Nat Immunol 2014;15:152–60.

54. Park SH, Park JH, Kang JS, Kang YH. Involvement of transcription factors in plasma HDL protection against TNF-α-induced vascular cell adhesion molecule-1 expression. Int J Biochem Cell Biol 2003;35:168–82.

55. Smith CK, Seto NL, Vivekanandan-Giri A, Yuan W, Playford MP, Manna Z, et al. Lupus high-density lipoprotein induces proinflammatory responses in macrophages by binding lectin-like oxidised low-density lipoprotein receptor 1 and failing to promote activating transcription factor 3 activity. Ann Rheum Dis 2017;76:602–11.

56. Skaggs BJ, Hahn BH, Sahakian L, Grossman J, McMahon M. Dysfunctional, pro-inflammatory HDL directly upregulates monocyte PDGFRβ, chemotaxis and TNFα production. Clin Immunol 2010;137:147–56.

57. Frostegård J, Svenungsson E, Wu R, Gunnarsson I, Lundberg IE, Klareskog L, et al. Lipid peroxidation is enhanced in patients with systemic lupus erythematosus and is associated with arterial and renal disease manifestations. Arthritis Rheum 2005;52:192–200.

58. Hansson GK, Libby P. The immune response in atherosclerosis: a double-edged sword. Nat Rev Immunol 2006;6:508–19.

59. Tripi LM, Manzi S, Chen Q, Kenney M, Shaw P, Kao A, et al. Relationship of serum paraoxonase 1 activity and paraoxonase 1 genotype to risk of systemic lupus erythematosus. Arthritis Rheum 2006;54:1928–39.

60. Marsillach J, Becker JO, Vaisar T, Hahn BH, Brunzell JD, Furlong CE, et al. Paraoxonase-3 is depleted from the high-density lipoproteins of autoimmune disease patients with subclinical atherosclerosis. J Proteome Res 2015;14:2046–54.

61. Dinu AR, Merrill JT, Shen C, Antonov IV, Myones BL, Lahita RG. Frequency of antibodies to the cholesterol transport protein apolipoprotein A1 in patients with SLE. Lupus 1998;7:355–60.

62. O'Neill SG, Giles I, Lambrianides A, Manson J, D'Cruz D, Schrieber L, et al. Antibodies to apolipoprotein A-I, high-density lipoprotein, and C-reactive protein are associated with disease activity in patients with systemic lupus erythematosus. Arthritis Rheum 2010;62:845–54.

63. Shoenfeld Y, Szyper-Kravitz M, Witte T, Doria A, Tsutsumi A, Tatsuya A, et al. Autoantibodies against protective molecules—C1q, C-reactive protein, serum amyloid P, mannose-binding lectin, and apolipoprotein A1: prevalence in systemic lupus erythematosus. Ann N Y Acad Sci 2007;1108:227–39.

64. Vuilleumier N, Reber G, James R, Burger D, de Moerloose P, Dayer JM, et al. Presence of autoantibodies to apolipoprotein A-1 in patients with acute coronary syndrome further links autoimmunity to cardiovascular disease. J Autoimmun 2004;23:353–60.

65. Townsend D, Hughes E, Hussain R, Siligardi G, Baldock S, Madine J, et al. Heparin and methionine oxidation promote the formation of apolipoprotein A-I amyloid comprising α-helical and β-sheet structures. Biochemistry 2017;56:1632–44.

66. Chistiakov DA, Orekhov AN, Bobryshev YV. ApoA1 and ApoA1-specific self-antibodies in cardiovascular disease. Lab Invest 2016;96:708–18.

67. Delgado Alves J, Kumar S, Isenberg DA. Cross-reactivity between anti-cardiolipin, anti-high-density lipoprotein and anti-apolipoprotein A-I IgG antibodies in patients with systemic lupus erythematosus and primary antiphospholipid syndrome. Rheumatology (Oxford) 2003;42:893–9.

68. Batuca JR, Ames PR, Isenberg DA, Alves JD. Antibodies toward high-density lipoprotein components inhibit paraoxonase activity in patients with systemic lupus erythematosus. Ann N Y Acad Sci 2007;1108:137–46.

69. Yu HH, Chen PC, Yang YH, Wang LC, Lee JH, Lin YT, et al. Statin reduces mortality and morbidity in systemic lupus erythematosus patients with hyperlipidemia: a nationwide population-based cohort study. Atherosclerosis 2015;243:11–8.

70. Castejon R, Castañeda A, Sollet A, Mellor-Pita S, Tutor-Ureta P, Jimenez-Ortiz C, et al. Short-term atorvastatin therapy improves arterial stiffness of middle-aged systemic lupus erythematosus patients with pathological pulse wave velocity. Lupus 2017;26:355–64.

71. Orekhov AN, Misharin AY, Tertov VV, Khashimov K, Pokrovsky SN, Repin VS, et al. Artificial HDL as an anti-atherosclerotic drug. Lancet 1984;2:1149–50.

72. Krause BR, Remaley AT. Reconstituted HDL for the acute treatment of acute coronary syndrome. Curr Opin Lipidol 2013;24:480–6.

73. Tardif JC, Grégoire J, L'Allier PL, Ibrahim R, Lespérance J, Heinonen TM, et al. Effects of reconstituted high-density lipoprotein infusions on coronary atherosclerosis: a randomized controlled trial. JAMA 2007;297:1675–82.

74. Tardif JC, Grégoire J, L'Allier PL, Ibrahim R, Lespérance J, Heinonen TM, et al. Effects of reconstituted high-density lipoprotein infusions on coronary atherosclerosis: a randomized controlled trial. JAMA 2007;297:1675–82.

75. Tricoci P, D'Andrea DM, Gurbel PA, Yao Z, Cuchel M, Winston B, et al. Infusion of reconstituted high-density lipoprotein, CSL112, in patients with atherosclerosis: safety and pharmacokinetic results from a phase 2a randomized clinical trial. J Am Heart Assoc 2015;4:e002171.

76. CSL Behring, sponsor. Study to investigate CSL112 in subjects with acute coronary syndrome (AEGIS-II). Clinicaltrails.gov identifier: NCT03473223; 2018.

77. Morin EE, Guo L, Schwendeman A, Li XA. HDL in sepsis: risk factor and therapeutic approach. Front Pharmacol 2015;6:244.

78. Pajkrt D, Doran JE, Koster F, Lerch PG, Arnet B, van der Poll T, et al. Antiinflammatory effects of reconstituted high-density lipoprotein during human endotoxemia. J Exp Med 1996;184:1601–8.

79. Zhang Z, Datta G, Zhang Y, Miller AP, Mochon P, Chen YF, et al. Apolipoprotein A-I mimetic peptide treatment inhibits inflammatory responses and improves survival in septic rats. Am J Physiol Heart Circ Physiol 2009;297:H866–73.

80. Moreira RS, Irigoyen M, Sanches TR, Volpini RA, Camara NO, Malheiros DM, et al. Apolipoprotein A-I mimetic peptide 4F attenuates kidney injury, heart injury, and endothelial dysfunction in sepsis. Am J Physiol Regul Integr Comp Physiol 2014;307:R514–24.

81. Charles-Schoeman C, Banquerigo ML, Hama S, Navab M, Park GS, Van Lenten BJ, et al. Treatment with an apolipoprotein A-1 mimetic peptide in combination with pravastatin inhibits collagen-induced arthritis. Clin Immunol 2008;127:234–44.

82. Woo JM, Lin Z, Navab M, Van Dyck C, Trejo-Lopez Y, Woo KM, et al. Treatment with apolipoprotein A-1 mimetic peptide reduces lupus-like manifestations in a murine lupus model of accelerated atherosclerosis. Arthritis Res Ther 2010;12:R93.

83. Black LL, Srivastava R, Schoeb TR, Moore RD, Barnes S, Kabarowski JH. Cholesterol-independent suppression of lymphocyte activation, autoimmunity, and glomerulonephritis by apolipoprotein A-I in normocholesterolemic lupus-prone mice. J Immunol 2015;195:4685–98.

84. Schwendeman A, Sviridov DO, Yuan W, Guo Y, Morin EE, Yuan Y, et al. The effect of phospholipid composition of reconstituted HDL on its cholesterol efflux and anti-inflammatory properties. J Lipid Res 2015;56:1727–37.

Cardiovascular Safety of Tocilizumab Versus Etanercept in Rheumatoid Arthritis: A Randomized Controlled Trial

Jon T. Giles,[1] [ID] Naveed Sattar,[2] Sherine Gabriel,[3] Paul M. Ridker,[4] Steffen Gay,[5] Charles Warne,[6] David Musselman,[7] Laura Brockwell,[6] Emma Shittu,[6] Micki Klearman,[7] and Thomas R. Fleming[8]

Objective. To assess the risk of major adverse cardiovascular events (MACE) in patients with rheumatoid arthritis (RA) treated with tocilizumab compared to those treated with the tumor necrosis factor inhibitor etanercept.

Methods. This randomized, open-label, parallel-group trial enrolled patients with active seropositive RA (n = 3,080) who had an inadequate response to conventional synthetic disease-modifying antirheumatic drugs and who had at least 1 cardiovascular (CV) risk factor. Patients were randomly assigned 1:1 to receive open-label tocilizumab at 8 mg/kg/month or etanercept at 50 mg/week. All patients were followed up for a mean of 3.2 years. The primary end point was comparison of time to first occurrence of MACE. The trial was powered to exclude a relative hazard ratio for MACE of 1.8 or higher in the tocilizumab group compared to the etanercept group.

Results. By week 4 of treatment, the serum low-density lipoprotein cholesterol, high-density lipoprotein cholesterol, and triglyceride levels were a median 11.1%, 5.7%, and 13.6% higher, respectively, in patients receiving tocilizumab compared to those receiving etanercept (each $P < 0.001$). During follow-up, 83 MACE occurred in the tocilizumab group compared to 78 MACE in the etanercept group. The estimated hazard ratio for occurrence of MACE in the tocilizumab group relative to the etanercept group was 1.05 (95% confidence interval 0.77–1.43). Results were similar in sensitivity analyses and in the on-treatment population analysis. Adverse events occurred more frequently in the tocilizumab group, including serious infection and gastrointestinal perforation.

Conclusion. The results of this trial, which provide insights into the CV safety of tocilizumab as compared to etanercept, ruled out a risk for occurrence of MACE of 1.43 or higher in patients treated with tocilizumab. This result should be interpreted in the context of the clinical efficacy and non-CV safety of tocilizumab.

INTRODUCTION

Treatment with tocilizumab, a fully humanized monoclonal antibody targeting interleukin-6 receptor α (IL-6α), reduces the signs and symptoms of rheumatoid arthritis (RA) and confers a marked reduction in the levels of circulating inflammatory markers (1,2). In parallel, treatment-associated increases in circulating lipid concentrations have been observed, with average increases in the low-density lipoprotein (LDL) cholesterol level of 12–20% noted across pivotal clinical trials (3). In a recent meta-analysis (4), the odds of having elevated LDL cholesterol levels, defined as >130 mg/dl, was 4.8-fold higher in tocilizumab-treated patients with RA than in those treated with placebo. High-density lipoprotein (HDL) cholesterol levels also tended to increase with tocilizumab treatment, with the odds of having a high HDL cholesterol level, defined as >60 mg/dl, being more than 2-fold higher in

tocilizumab-treated patients than in placebo-treated patients in the same meta-analysis. Considering that RA is associated with a greater burden of atherosclerosis (5,6) and that deaths from atherosclerotic events and cardiovascular disease (CVD) are higher in RA patients than in subjects without RA (7,8), treatment-associated increased concentrations of lipids with atherogenic potential have called into question the CVD risk-to-benefit ratio of tocilizumab in RA.

In the MEASURE trial, a study designed to evaluate the effects of tocilizumab therapy on CVD biomarkers in patients with RA, concentrations of the more atherogenic circulating small LDL particles and oxidized LDL did not increase with tocilizumab treatment and were similar to those observed with placebo, despite an increase in the overall LDL cholesterol level (9). At the same time, tocilizumab was associated with greater reductions, relative to placebo, in the levels of potentially proatherogenic factors, such as HDL-associated serum amyloid A, secretory phospholipase A_2, and lipoprotein(a). However, whether such changes affect CVD event risk has not been evaluated in a clinical trial.

Given the increased levels of circulating total cholesterol, LDL cholesterol, and triglycerides observed in patients following treatment with tocilizumab, the present study (designated the ENTRACTE trial) was designed to compare the risk of major adverse cardiovascular events (MACE) in patients with RA treated with tocilizumab to the risk in those treated with the tumor necrosis factor (TNF) inhibitor etanercept, a biologic standard-of-care treatment for RA with a mechanism of action different from that of tocilizumab and having minimal effects on atherogenic lipids. Patients with high RA disease activity and CVD risk factors at baseline were targeted.

PATIENTS AND METHODS

Trial oversight and design. ENTRACTE (ClinicalTrials. gov identifier: NCT01331837) was a multicenter 2-arm, parallel-group, randomized, open-label trial designed to address the CV safety of tocilizumab compared to that of etanercept in patients with RA. The trial was designed and executed as a postmarketing requirement of the US Food and Drug Administration (for a list of the trial sites and investigators, see Supplementary Table 1, available on the *Arthritis & Rheumatology* web site at http://online library.wiley.com/doi/10.1002/art.41095/abstract). The trial was approved by local institutional review boards/ethics committees. All patients provided written informed consent, in accordance with the Declaration of Helsinki.

Patient population. Eligible study subjects were patients with a diagnosis of RA based on the American College of Rheumatology 1987 revised classification criteria (10) who had a disease duration of ≥6 months and an inadequate response to a previous conventional synthetic disease-modifying antirheumatic drug (csDMARD) or anti-TNF treatment. In addition, eligible patients were required to have seropositivity for rheumatoid fac-

tor (RF) or anti–cyclic citrullinated peptide (anti-CCP) antibodies, ≥8 swollen joints (66 joint count) and ≥8 tender joints (68 joint count) at screening, and a C-reactive protein (CRP) level of >0.3 mg/liter. Additionally, patients were required to be age ≥50 years and to have ≥1 traditional CVD risk factor, extraarticular RA manifestations (including subcutaneous rheumatoid nodules, secondary Sjögren's syndrome, serositis, rheumatoid lung disease/interstitial lung disease, vasculitis, inflammatory peripheral neuropathy, or scleritis/episcleritis), or history of a CVD event, which included prior myocardial infarction (MI), cerebrovascular accident, coronary revascularization procedure, hospitalization for unstable angina, symptomatic carotid artery disease, peripheral arterial disease, or abdominal aortic aneurysm.

Patients with moderate or severe heart failure were excluded from the study due to the contraindication of being randomized to receive a TNF inhibitor. Furthermore, those who had previously received treatment with a non-TNF biologic agent or etanercept were excluded, and enrollment of those who had previously received treatment with non-etanercept TNF inhibitors was restricted to 20% of patients. Individuals with a history of diverticulitis, diverticulosis requiring antibiotic treatment, or chronic ulcerative lower gastrointestinal disease such as Crohn's disease, ulcerative colitis, or other symptomatic lower gastrointestinal conditions that might predispose to perforations were excluded. Additional inclusion and exclusion criteria are listed in Supplementary Table 2 (available on the *Arthritis & Rheumatology* web site at http://onlinelibrary. wiley.com/doi/10.1002/art.41095/abstract).

Intervention, randomization, and blinding. Patients were randomly assigned 1:1 to a treatment group using an interactive voice recording system (IVRS). Patients were randomized to receive either intravenous tocilizumab (8 mg/kg every 4 weeks) or subcutaneous etanercept (50 mg weekly), with or without background csDMARDs. A preallocated blocked randomization schedule was implemented using a block size of 4, with stratification according to previous exposure to anti-TNF therapy and history of CVD events. The random allocation sequence was generated by an independent vendor who managed the IVRS. Patients were enrolled by study site personnel and randomly assigned using the IVRS.

Tocilizumab was administered at the study site, whereas etanercept was self-administered at home. The trial was open-label at the study site, but the sponsor was blinded with regard to the treatment assignments. Site monitoring was carried out independent of the sponsor, and data on treatment allocation were not divulged to the sponsor by monitors. An independent data monitoring committee reviewed the unblinded data and monitored safety.

Study visits. On-site study visits occurred monthly for tocilizumab-treated patients and every 3 months for etanercept-treated patients, during years 1–3 and every 6 months during years 4 and 5. Enrollees could withdraw from active treatment

at any time; crossover was discouraged, however, and patients who withdrew from treatment were encouraged to continue to be monitored for ongoing CVD and safety assessments. The trial commenced on August 2, 2011 and concluded on March 25, 2016.

End points and safety assessments. The prespecified primary end point was time to first occurrence of MACE, consisting of CV-related death, nonfatal MI, and nonfatal stroke (of any type). Undetermined causes of death were classified as MACE according to the Standardized Definitions of End Points in Clinical Trials (11). A secondary end point was time to first occurrence of an expanded composite end point, consisting of MACE in conjunction with nonelective coronary revascularization procedures and hospitalization for unstable angina. Other secondary end points were all-cause mortality and time to first occurrence of each of the individual components of MACE. Exploratory end points included hospitalized heart failure (HHF), and the composite end point of MACE in conjunction with HHF.

CVD events and serious adverse events (SAEs) were assessed monthly throughout the trial, either on site or through a telephone call using an IVRS. Any affirmative responses resulted in an alert for the site to contact the patient for additional detail on the possible AE or SAE. All potential end point events were adjudicated by an independent CVD Events Adjudication Committee whose members were blinded with regard to the treatment assignments. In the circumstance that the event was adjudicated as "not a confirmed event," the patient was still considered at risk for a first event. No efficacy data were assessed.

Laboratory assessments. Peripheral blood was collected at 1 month and 3 months following randomization, every 3 months until year 3, and every 6 months from year 4 onward. Nonfasting total cholesterol, triglyceride, HDL cholesterol, and LDL cholesterol levels were measured using BMD methodology (Roche), RF was measured by a Tina-quant immunoturbidimetric assay (Roche), anti-CCP was measured by enzyme-linked immunosorbent assay, hemoglobin A1c was measured by high-performance liquid chromatography (Bio-Rad), and CRP was measured using a Tina-quant immunoturbidimetric assay (Roche).

Statistical analysis. The primary objective of this trial was to provide a screening evaluation of CV safety by addressing whether a hazard ratio (HR) for MACE of 1.8 or higher could be ruled out in patients who received tocilizumab compared to those who received etanercept. This objective would be achieved in a 131-event trial in which the estimated HR would be ≤1.278, which would occur with 92% probability if the true HR were 1. The primary analysis of the MACE primary end point and of all secondary and exploratory time-to-event end points was based on a stratified Cox proportional hazards

model using the intent-to-treat (ITT) population. Treatment arm was included as a covariate in the model, and the analysis was stratified by previous exposure to anti-TNF therapy and history of CVD events. For the on-treatment analyses, exposure time was truncated at 28 days after the last dose of randomized treatment, unless a new biologic agent was started during that period, in which case exposure time was truncated at the date of the initiation of the new biologic.

In many previous CV safety trials conducted in settings such as the evaluation of antidiabetes agents, obesity therapies, and cyclooxygenase 2 inhibitors and other nonsteroidal antiinflammatory drugs in osteoarthritis and RA, a definitive evaluation of CV safety typically has required ruling out a noninferiority margin for the HR of MACE in the range of 1.30–1.33. In those settings, ruling out much larger increases in the HR, in the range of 1.8–2.0, has provided a screening evaluation for CV safety (12,13). The design of the ENTRACTE trial was consistent with this screening evaluation. Its primary objective, as stated above, was to address whether a possible true HR of 1.8 could be ruled out (achieved when the upper limit of the 95% confidence interval [95% CI] is <1.8). Thus, if that were to be achieved, in a nested manner preserving the experimental alpha level of a traditional false positive error rate of 2.5%, a conclusion of "noninferiority of tocilizumab to etanercept" could be formally established if a possible true HR of 1.3 could be ruled out (achieved when the upper limit of the 95% CI is <1.3); this would be achieved in a 131-event trial in which the estimated HR would be ≤0.923 (or in a 161-event trial with an estimated HR of ≤0.954). The corresponding sample size was 1,540 patients per treatment arm. Non-CVD safety events were assessed in the on-treatment safety population.

RESULTS

A total of 3,080 patients with RA were enrolled; 1,538 were randomly assigned to the tocilizumab arm and 1,542 were randomly assigned to the etanercept arm. The tocilizumab and etanercept arms contributed 4,900 and 4,891 ITT patient-years, respectively. The allocation of patients in the trial is depicted in Figure 1. Over a mean follow-up time of 3.2 years, 2,957 patients (96%) completed the trial with a full assessment of CVD events. After exclusion of patients who died during the follow-up, there were 26 patients in the tocilizumab group and 33 patients in the etanercept group without a full assessment of CVD events. Early discontinuation of randomized treatment occurred in 361 (23%) of 1,542 etanercept-treated patients and 401 (26%) of 1,538 tocilizumab-treated patients, representing 518.5 and 655.2 patient-years, respectively. Etanercept-to-tocilizumab and tocilizumab-to-etanercept crossover occurred equally in 1% of enrollees in each arm.

The baseline characteristics of the patients according to randomized treatment assignment are summarized in Table 1.
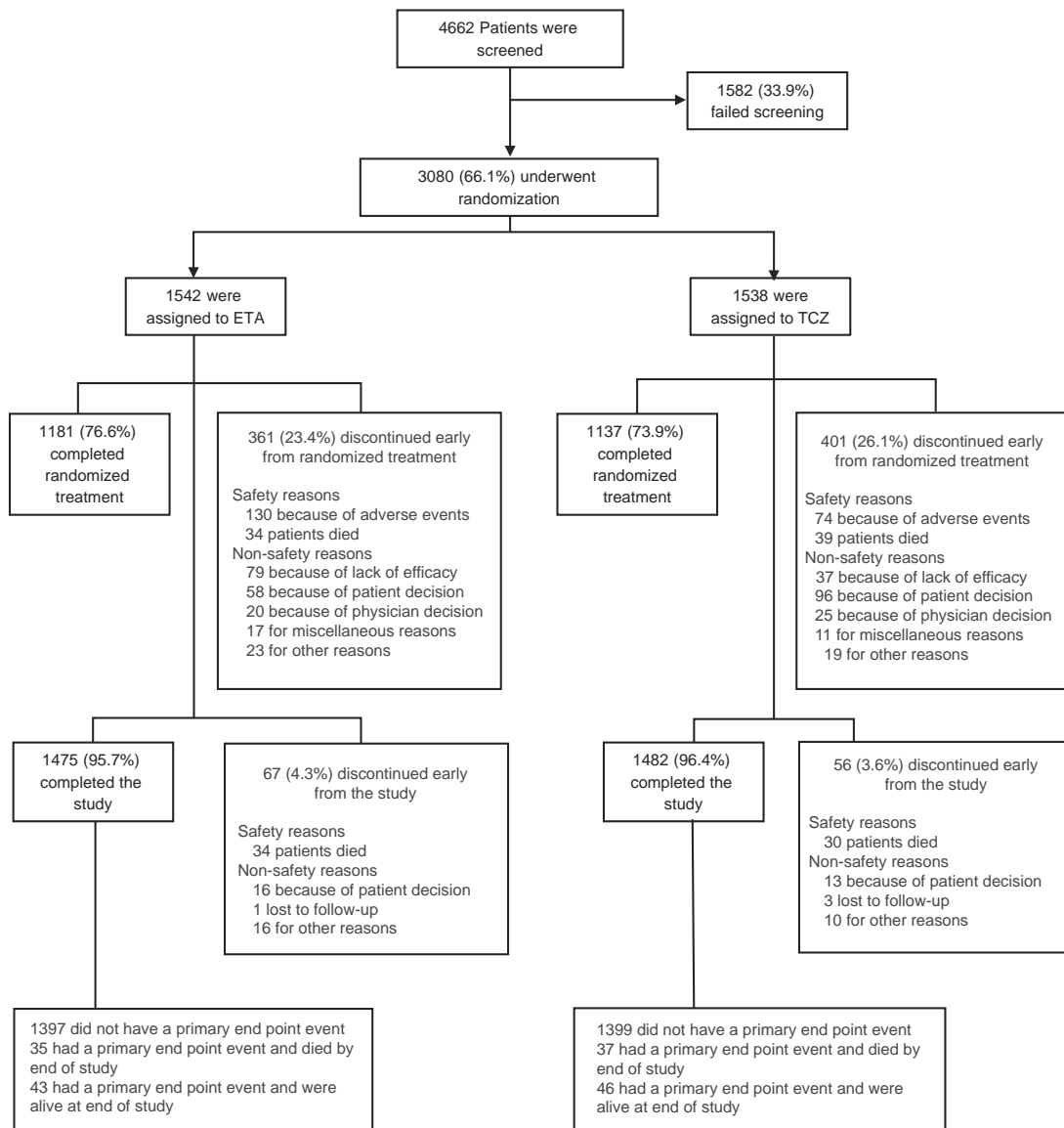
Figure 1. Distribution of trial participants. The primary end point was time to first cardiovascular (CV) event (CV-related death, nonfatal myocardial infarction, or nonfatal stroke, determined by the CV Disease Events Adjudication Committee) in the intent-to-treat population of rheumatoid arthritis patients randomized to receive either etanercept (ETA) or tocilizumab (TCZ). Treatment completers were defined as patients who were not marked as discontinuing from randomized treatment before the common study end date (CSED) 30-/90-day window. The early discontinuation from randomized treatment count does not include patients who were incorrectly marked as discontinuing treatment within the CSED 30-/90-day window (10 patients). Reasons for inclusion in the "miscellaneous" groups were the following: lost to follow-up, protocol violation, noncompliance with study drug, and noncompliance with protocol. Study completers were defined as patients who experienced a primary end point or completed their final study contact by direct telephone contact or site visit within the CSED 30-/90-day window. Only patients who died of non-CV–related causes or who died of CV-related causes >365 days after the last direct contact (therefore not classified as a primary end point) are reported as having discontinued from the study because of death.

Characteristics were balanced across the treatment arms and reflected a population selected for having severe/active RA and for being at high risk for CVD events.

Following initiation of study treatment, the tocilizumab group had a median 11.1% greater increase in LDL cholesterol levels, a median 5.4% greater increase in HDL cholesterol levels, and a median 13.6% greater increase in triglyceride levels compared to the etanercept group at 4 weeks (each $P < 0.001$). These effects persisted over time (Figure 2).

One hundred sixty-one patients experienced primary MACE events, 78 in the etanercept arm and 83 in the tocilizumab arm. Although the trial was designed to assess for 131 events, 30 additional events accrued because of inherent imprecision in identifying the proper timing of the data lock; this

Table 1. Baseline demographic and clinical characteristics of the RA patients according to randomized treatment allocation (intent-to-treat population)*

Baseline characteristic	Etanercept (n = 1,542)	Tocilizumab (n = 1,538)
Age, mean ± SD years	61 ± 8	61 ± 7
Male sex	340 (22)	345 (22)
White race	1,187 (77)	1,160 (75)
Body mass index, mean ± SD kg/m^2	29.0 ± 6.0	28.7 ± 5.9
CVD risk factors		
Current smoking	419 (27)	460 (30)
Hypertension	1,090 (71)	1,098 (71)
Diabetes	284 (18)	259 (17)
Family history of CVD	239 (16)	251 (16)
Total cholesterol, mean ± SD mg/dl	198 ± 42	199 ± 41
LDL cholesterol, mean ± SD mg/dl	113 ± 35	113 ± 35
HDL cholesterol, mean ± SD mg/dl	57 ± 16	57 ± 16
Triglycerides, median (IQR) mg/dl	123 (92–168)	123 (94–169)
Hemoglobin A1c, mean ± SD %	5.9 ± 1.1	5.9 ± 1.1
Current statin use	343 (22)	333 (22)
Previous CVD diagnoses, events, and procedures		
Any	184 (11.9)	163 (10.6)
MI	79 (5)	67 (4)
Stroke	35 (2)	39 (3)
Coronary revascularization	72 (5)	54 (4)
Hospitalized for unstable angina	44 (3)	50 (3)
Symptomatic carotid artery disease	14 (1)	7 (1)
Peripheral arterial disease	29 (2)	15 (1)
RA characteristics		
Duration, median (IQR) years	7.2 (3.1–4.6)	7.9 (3.1–14.7)
Rheumatoid factor seropositive	1,485 (97)	1,475 (97)
Anti-CCP seropositive†	1,139 (90)	1,149 (91)
CRP, median (IQR) mg/liter	10.5 (4.9–23.4)	10.4 (4.8–23.0)
Any extraarticular RA features	465 (30)	462 (30)
Prior TNF inhibitor use	41 (2.7)	33 (2.1)
Concurrent RA therapies		
Methotrexate	1,098 (71)	1,111 (72)
Antimalarials	193 (13)	213 (14)
Sulfasalazine	153 (10)	167 (11)
Leflunomide	168 (11)	161 (11)
Glucocorticoids	400 (26)	445 (29)
NSAIDs	814 (53)	828 (54)

* Except where indicated otherwise, values are the number (%) of rheumatoid arthritis (RA) patients. CVD = cardiovascular disease; LDL = low-density lipoprotein; HDL = high-density lipoprotein; IQR = interquartile range; MI = myocardial infarction; anti-CCP = anti–cyclic citrullinated peptide; CRP = C-reactive protein; TNF = tumor necrosis factor; NSAIDs = nonsteroidal antiinflammatory drugs.
† Tested in 1,269 patients in the etanercept group and 1,263 patients in the tocilizumab group.

was further complicated by the lag time between identification and adjudication of possible events. In the comparison between tocilizumab and etanercept, the HR for the primary end point of MACE, which included undetermined cause of death, in the ITT population was 1.05 (95% CI 0.77–1.43) (Table 2; for Kaplan-Meier plots of the primary end point, see Supplementary Figure 1, available on the *Arthritis & Rheumatology* web site at http://onlinelibrary.wiley.com/doi/10.1002/art.41095/abstract).

The estimated HR was similar in sensitivity analyses in which alternative classifications of MACE were used, and in the analysis restricted to the period when patients were actually receiving the treatment to which they were assigned (on-treatment). The

estimated HRs for the secondary end points for tocilizumab compared to etanercept (Table 2) ranged from an HR of 0.89 (95% CI 0.54–1.49) for non-fatal MI to an HR of 1.55 (95% CI 0.83–2.90) for all stroke types. For fatal and nonfatal stroke, 26 events occurred in the tocilizumab group compared to 16 events in the etanercept group. The HRs for CV-related death and death from any cause for the tocilizumab group compared to the etanercept group were 1.03 and 0.99, respectively.

Non-CVD AEs were common in both groups, but the rate was higher in the tocilizumab arm than in the etanercept arm (Table 3). However, neither the frequency of AEs leading to discontinuation of study drug nor the frequency of SAEs were

A

C

B

D
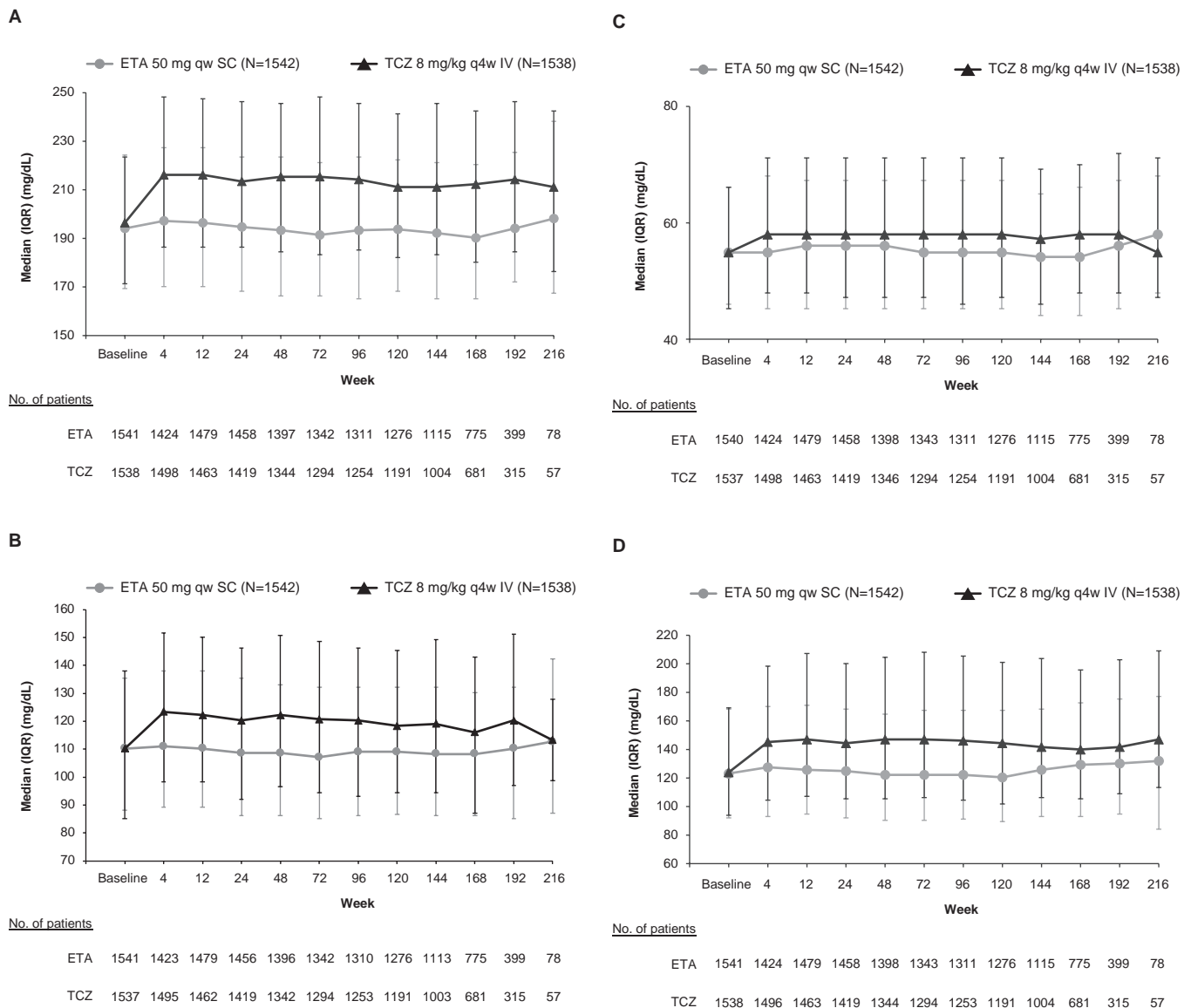
Figure 2. Baseline values and change in circulating levels of total cholesterol (**A**), low-density lipoprotein (LDL) cholesterol (**B**), high-density lipoprotein (HDL) cholesterol (**C**), and triglycerides (**D**) over 216 weeks in the etanercept (ETA) group compared to the tocilizumab (TCZ) group. Bars show the median with interquartile range (IQR). qw = every week; SC = subcutaneous; q4w = every 4 weeks; IV = intravenous.

meaningfully higher in the tocilizumab arm compared to the etanercept arm. Infections (any infections and serious infections) were higher in the tocilizumab arm than in the etanercept arm. Eight confirmed gastrointestinal perforation events occurred in the tocilizumab arm, compared to 1 event in the etanercept arm. Rates of malignancy, hypersensitivity events, serious bleeding events, and serious hepatic events were not meaningfully higher in the tocilizumab arm than in the etanercept arm, and no demyelinating events occurred.

DISCUSSION

The primary aim of the ENTRACTE trial was to determine whether a relative hazard for MACE of 1.8 or higher in the tocili-

zumab group compared to the etanercept group could be ruled out. The results of this trial, which provide screening insights into the CVD safety of tocilizumab compared to etanercept, ruled out a relative hazard for MACE of 1.43 or higher in tocilizumab-treated patients in the ITT population. Similar estimates regarding CVD safety were obtained when the analysis was restricted to events that occurred while patients were still receiving randomized treatment and when we assessed multiple secondary and exploratory outcomes, with the exception of stroke and HHF.

Macrophage-derived inflammatory cytokines, including IL-6, TNF, and IL-1β, are up-regulated in RA and are targets for effective treatment of the signs and symptoms of the disease (14). Multiple studies have shown that IL-6 is a key contributor to atherogenesis, plaque destabilization, and atherothrombosis

Table 2. Frequency of first-occurrence events and relative hazards (tocilizumab relative to etanercept) for the primary, secondary, and exploratory end points, and sensitivity analyses of the primary end point*

| | First event | | | | | |
| | Etanercept | | Tocilizumab | | | |
End point	No. (%) first events	No. first events/ 100 person-years (95% CI)	No. (%) first events	No. first events/ 100 person-years (95% CI)	HR†	95% CI†
Primary end point of MACE, including undetermined cause of death						
ITT population‡	78 (5)	1.70 (1.35–2.10)	83 (5)	1.82 (1.46–2.24)	1.05	0.77–1.43
On-treatment population§	52 (3)	1.28 (0.97–1.66)	57 (4)	1.44 (1.10–1.85)	1.11	0.76–1.62
Sensitivity analysis of primary end point (ITT population)						
MACE, excluding undetermined cause of death	72 (5)	1.57 (1.24–1.97)	74 (5)	1.63 (1.29–2.03)	1.01	0.73–1.40
MACE, before last direct contact	46 (3)	1.00 (0.74–1.33)	49 (3)	1.06 (0.79–1.40)	1.04	0.70–1.56
Secondary end points (ITT population)						
Nonfatal MI	31 (2)	0.65 (0.45–0.92)	28 (2)	0.59 (0.40–0.85)	0.89	0.54–1.49
Nonfatal and fatal MI	32 (2)	0.67 (0.46–0.95)	29 (2)	0.61 (0.41–0.87)	0.90	0.54–1.48
Nonfatal stroke, all types	15 (1)	0.33 (0.19–0.53)	24 (2)	0.49 (0.31–0.73)	1.53	0.80–2.92
Nonfatal and fatal stroke, all types	16 (1)	0.35 (0.20–0.56)	26 (2)	0.53 (0.35–0.78)	1.55	0.83–2.90
Cardiovascular-related death	35 (2)	0.72 (0.50–1.00)	36 (2)	0.73 (0.51–1.02)	1.03	0.64–1.63
Death from any cause	64 (4)	1.31 (1.01–1.67)	64 (4)	1.31 (1.01–1.67)	0.99	0.70–1.41
Expanded composite end point¶	84 (5)	1.98 (1.61–2.42)	84 (6)	1.90 (1.53–2.33)	0.99	0.73–1.34
Exploratory end points (ITT population)						
MACE and HHF	85 (6)	1.90 (1.53–2.33)	90 (6)	2.12 (1.73–2.57)	1.05	0.78–1.41
HHF	8 (1)	0.20 (0.10–0.38)	12 (1)	0.31 (0.17–0.50)	1.50	0.61–3.67

* Etanercept was administered at 50 mg weekly by subcutaneous injection. Tocilizumab was administered at 8 mg/kg monthly by intravenous infusion. HHF = hospitalized heart failure.
† The hazard ratios (HRs) with 95% confidence intervals (95% CIs) were estimated using Cox regression models that included treatment (tocilizumab or etanercept) as the only covariate, stratified by previous exposure to anti–tumor necrosis factor therapy and history of cardiovascular (CV) events. Time to first event was calculated as (randomization to first event or censoring date + 1)/365.25. The 95% CIs for secondary end points should be viewed only in a descriptive manner, because they have not been adjusted for multiplicity.
‡ The primary end point of time to first occurrence of major adverse cardiovascular events (MACE) is a composite of CV death (including events adjudicated as undetermined cause of death), nonfatal myocardial infarction (MI), and nonfatal stroke. Patients in the intent-to-treat (ITT) population who did not experience an event were censored at the latest of last date known to be alive, last direct contact, and last indirect contact, capped at the date of last direct contact + 365 days.
§ Censoring date in the on-treatment population was the latest of last date known to be alive, last direct contact, and last indirect contact, capped at the date of randomized treatment discontinuation or the common study end date, whichever was earlier.
¶ Defined as the CV composite measure of the primary end point with the addition of nonelective coronary revascularization procedures and hospitalization for unstable angina.

(15–18). Similar to IL-6 levels, higher TNF levels have been linked to future CVD events (19), and TNF knockout or treatment with TNF inhibitors was associated with a reduction in the burden of atherosclerosis in atherosclerosis-prone mice (20,21). Moreover, a growing body of evidence from observational registries of TNF inhibitor–treated patients with RA suggests that CVD events are lower with TNF inhibitor treatment (22), an effect that may depend on clinical response (23). However, whether this effect is unique to TNF inhibitors as a class or extends to targeted immunomodulators with different mechanisms of action is unknown.

In a recent analysis of Medicare and insurance claims beneficiaries (24), Xie et al reported a relative hazard of MACE in patients treated with etanercept compared to those treated with tocilizumab of 1.10 (95% CI 0.80–1.51). In a separate analysis of Medicare and private insurance claims (25), Kim et al also reported a lower, but nonsignificant, hazard of hospitalization for MI or stroke for those receiving tocilizumab compared to a combined

TNF inhibitor group (HR 0.84 [95% CI 0.56–1.26]). However, given the nonrandomized treatment allocation and retrospective design, a randomized clinical trial, such as ENTRACTE, is needed to more accurately estimate the true relative risk between the treatments. Furthermore, the concept that cytokine inhibition may have antiatherogenic or antithrombotic effects, or both, on conditions other than RA is supported by the recently published Canakinumab Anti-inflammatory Thrombosis Outcomes Study, in which anti–IL-1β treatment of patients who previously experienced MI and who had elevated CRP levels was associated with a 15% reduction, compared to placebo, in the risk of MACE over 48 months (26).

On a molecular level, IL-6 inhibition differs from TNF inhibition in several pathways involved in lipid metabolism. RA is associated with LDL hypercatabolism, an effect that, in 1 study, diminished with tocilizumab treatment, resulting in higher LDL cholesterol levels (27). In addition, tocilizumab was found to decrease IL-6–induced expression of the LDL

Table 3. Occurrence of AEs in the on-treatment safety population*

	Etanercept			Tocilizumab				
	No. (%) with event	No. of events	Rate per 100 patient-years	No. (%) with event	No. of events	Rate per 100 patient-years	HR†	95% CI†
General AEs								
AEs leading to withdrawal of study drug	105 (7)	105	2.4	120 (8)	120	2.8	1.15	0.89–1.49
All SAEs	356 (23)	631	14.4	421 (27)	666	15.7	1.10	0.94–1.28
AEs of special interest								
Serious infection	111 (7)	139	3.2	159 (10)	190	4.5	1.39	1.08–1.79
Fatal infection	8 (0.5)	8	0.18	6 (0.4)	6	0.14	0.76	0.26–2.21
Confirmed gastrointestinal perforation	1 (0.06)	1	0.02	8 (0.5)	8	0.19	8.43	1.06–67.26
Malignancies (including NMSC)	38 (3)	40	0.9	38 (3)	41	1.0	1.00	0.64–1.58
Malignancies (excluding NMSC)	27 (2)	28	0.6	29 (2)	30	0.7	1.09	0.64–1.84
Significant hypersensitivity‡	17 (1)	17	0.4	10 (1)	14	0.3	0.66	0.30–1.46
Serious hypersensitivity§	7 (0.5)	7	0.2	4 (0.3)	4	0.1	0.61	0.18–2.05
Serious demyelinating disorders	0	0	0	0	0	0	–	–
Serious bleeding events	13 (1)	17	0.4	19 (1)	20	0.5	1.26	0.61–2.62
Serious hepatic events	1 (0.06)	1	0	3 (0.2)	3	0.1	2.70	0.31–23.43
Deep vein thrombosis¶	12 (0.8)	12	0.3	9 (0.6)	10	0.2	0.83	0.34–2.03
Pulmonary embolism¶	8 (0.5)	8	0.2	1 (0.1)	1	(0.06)	0.13	0.02–1.04

* Adverse events (AEs) listed are from 4,373 patient-years of follow-up in 1,542 etanercept-treated patients and 4,245 patient-years of follow-up in 1,538 tocilizumab-treated patients. NMSC = nonmelanomatous skin cancer.
† Hazard ratios (HRs) with 95% confidence intervals (95% CIs) were calculated using the Andersen-Gill Cox regression model for repeated events, including treatment (tocilizumab or etanercept) as the only covariate and using the robust sandwich-type estimate of variance. Stratification factors are previous exposure to anti–tumor necrosis factor therapy (yes versus no) and history of cardiovascular events (yes versus no). Patients not experiencing an event were censored at the last direct contact, capped at the date of treatment discontinuation or the common study end date + 28 days, whichever was earlier.
‡ Significant hypersensitivity was defined as all AEs that occurred during or within 24 hours of an infusion or injection and which were not deemed unrelated to treatment by the investigator, regardless of whether or not they were clinically consistent with hypersensitivity, and led to study treatment discontinuation.
§ Serious hypersensitivity was defined as all AEs that occurred during or within 24 hours of an infusion or injection and which were not deemed unrelated to treatment by the investigator, regardless of whether or not they were consistent with the signs of hypersensitivity, and that were reported as a serious AE (SAE).
¶ Deep vein thrombosis and pulmonary embolism were not predefined AEs of special interest in the protocol.

receptor on cultured hepatocytes, an effect not observed with the TNF inhibitor adalimumab (28). Such down-regulation of the LDL receptor on hepatocytes and on other LDL receptor–expressing cells would be expected to result in higher circulating LDL levels. In the same study, tocilizumab treatment was associated with higher postprandial triglyceride levels and a delayed triglyceride peak after oral fat loading, suggesting that IL-6–induced lipolysis was attenuated (28).

The exact mechanism of tocilizumab-associated increases in levels of circulating triglycerides is, however, unclear. Perhaps more important is whether these tocilizumab-associated changes in lipid metabolism translate to actual CVD risk over time. Based on the findings in the ENTRACTE trial, CVD risk following treatment with tocilizumab does not appear to be markedly increased compared to CVD risk with etanercept, at least within the first several years after therapy initiation. Yet, we cannot rule out the possibility that there is a difference in relative hazard smaller than 1.43, given the width of the resulting CI for MACE. The certainty around the relative differences between tocilizumab and etanercept for the secondary and exploratory outcomes, particularly for stroke and HHF, was lower, largely driven by the overall infrequency of these outcomes. Given this infrequency, an even larger

trial than ENTRACTE would be needed to stringently explore comparative differences on any one of the secondary outcomes.

The ENTRACTE trial has a number of notable strengths and limitations. Among the strengths, the retention rate for assessment of CVD events was very high (96%), and the unintended crossover rate was low (1%), both of which are indicators of a well-executed safety trial designed to assess whether differences could be ruled out. The use of an external adjudication committee for blinded determination of CVD events eliminated the possibility of bias in the attribution of CVD events, and an automated call-in reporting system reduced the likelihood of reporting bias for CVD events and SAEs. However, more face-to-face opportunities for tocilizumab-treated patients to report AEs directly to study personnel provided an imbalance between the 2 treatment arms in the sensitivity for detection of AEs, which might have contributed to more nonserious safety events being reported for patients receiving tocilizumab therapy. The tocilizumab group experienced a higher infection rate and a significantly higher rate of gastrointestinal perforations. Although both these rates were consistent with the rates observed in previous tocilizumab clinical trials (29), they do provide additional insight into the comparative safety of tocilizumab relative to etanercept for RA therapy.

The limitations of this study include the fact that although the sample size of the ENTRACTE trial was larger than in a typical RA trial with a clinical efficacy end point, it was relatively small for a trial with a CVD event end point, in part because the eligible RA population is much smaller than the diabetes and obesity populations. As such, though it is estimated that the risk of MACE in patients treated with tocilizumab is 5% higher than in patients treated with etanercept, the uncertainty around this estimate was wide enough that the true risk of MACE in the tocilizumab arm could have been anywhere from 43% higher to 23% lower than in the etanercept arm. Although the trial did not rule out traditional noninferiority margins in the range of 1.30 to 1.33, it did succeed in ruling out the larger relative hazard of 1.8 for occurrence of MACE in patients receiving tocilizumab compared to those receiving etanercept, since, as a CV safety screening trial, the study was designed to address this.

In addition, the ENTRACTE trial enrolled an RA population remarkable for having both high RA disease activity and elevated CVD risk, which may not reflect the characteristics of the average patient with RA in clinical practice. Nevertheless, there is biologic reason to believe that the CVD safety of tocilizumab compared to that of etanercept can be extrapolated to patients with RA who have lower baseline disease activity or lower CVD risk.

Furthermore, although the dropout rate for the trial was very low (4%), this rate was similar to the overall rate of MACE. Thus, while unlikely, there is potential for even this small amount of dropout to bias the comparison of MACE between the 2 treatment groups.

Finally, since the trial was powered to assess CV safety, measures of RA disease activity were not collected after baseline. Powering the trial on the basis of both CV safety and clinical efficacy would have required the enrollment of a much larger sample size than what was feasible.

In summary, the primary results of the current ENTRACTE trial provide a framework for assessing the comparative CVD safety of tocilizumab to that of etanercept in the setting of treatment-associated increases in lipid parameters and in the context of its known clinical efficacy and non-CVD safety.

AUTHOR CONTRIBUTIONS

All authors were involved in drafting the article or revising it critically for important intellectual content, and all authors approved the final version to be published. Dr. Giles had full access to all of the data in the study and takes responsibility for the integrity of the data and the accuracy of the data analysis.
Study conception and design. Giles, Sattar, Gabriel, Ridker, Gay, Musselman, Klearman, Fleming.
Acquisition of data. Giles, Sattar, Gabriel, Ridker, Gay, Warne, Musselman, Brockwell, Shittu, Klearman, Fleming.
Analysis and interpretation of data. Giles, Sattar, Gabriel, Ridker, Gay, Warne, Musselman, Brockwell, Shittu, Klearman, Fleming.

ROLE OF THE STUDY SPONSOR

F. Hoffmann-La Roche Ltd. was involved in the design and conduct of the study, the collection, management, analysis, and interpretation of

ADDITIONAL DISCLOSURES

Dr. Musselman is an employee of Genentech, Inc., and Dr. Klearman was an employee of Genentech at the time of the study.

REFERENCES

1. Genovese MC, McKay JD, Nasonov EL, Mysler EF, da Silva NA, Alecock E, et al. Interleukin-6 receptor inhibition with tocilizumab reduces disease activity in rheumatoid arthritis with inadequate response to disease-modifying antirheumatic drugs: the Tocilizumab in Combination With Traditional Disease-Modifying Antirheumatic Drug Therapy Study. Arthritis Rheum 2008;58:2968–80.

2. Smolen JS, Beaulieu A, Rubbert-Roth A, Ramos-Remus C, Rovensky J, Alecock E, et al. Effect of interleukin-6 receptor inhibition with tocilizumab in patients with rheumatoid arthritis (OPTION study): a double-blind, placebo-controlled, randomised trial. Lancet 2008;371:987–97.

3. Schiff MH, Kremer JM, Jahreis A, Vernon E, Isaacs JD, van Vollenhoven RF. Integrated safety in tocilizumab clinical trials. Arthritis Res Ther 2011;13:R141.

4. Souto A, Salgado E, Maneiro JR, Mera A, Carmona L, Gómez-Reino JJ. Lipid profile changes in patients with chronic inflammatory arthritis treated with biologic agents and tofacitinib in randomized clinical trials: a systematic review and meta-analysis. Arthritis Rheumatol 2015;67:117–27.

5. Giles JT, Szklo M, Post W, Petri M, Blumenthal RS, Lam G, et al. Coronary arterial calcification in rheumatoid arthritis: comparison to the multi-ethnic study of atherosclerosis. Arthritis Res Ther 2009;11:R36.

6. Karpouzas GA, Malpeso J, Choi TY, Li D, Munoz S, Budoff MJ. Prevalence, extent and composition of coronary plaque in patients with rheumatoid arthritis without symptoms or prior diagnosis of coronary artery disease. Ann Rheum Dis 2014;73:1797–804.

7. Aviña-Zubieta JA, Choi HK, Sadatsafavi M, Etminan M, Esdaile JM, Lacaille D. Risk of cardiovascular mortality in patients with rheumatoid arthritis: a meta-analysis of observational studies. Arthritis Rheum 2008;59:1690–7.

8. Avina-Zubieta JA, Thomas J, Sadatsafavi M, Lehman AJ, Lacaille D. Risk of incident cardiovascular events in patients with rheumatoid arthritis: a meta-analysis of observational studies. Ann Rheum Dis 2012;71:1524–9.

9. McInnes IB, Thompson L, Giles JT, Bathon JM, Salmon JE, Beaulieu AD, et al. Effect of interleukin-6 receptor blockade on surrogates of vascular risk in rheumatoid arthritis: MEASURE, a randomised, placebo-controlled study. Ann Rheum Dis 2015;74:694–702.

10. Arnett FC, Edworthy SM, Bloch DA, McShane DJ, Fries JF, Cooper NS, et al. The American Rheumatism Association 1987 revised criteria for the classification of rheumatoid arthritis. Arthritis Rheum 1988;31:315–24.

11. Hicks KA, Tcheng JE, Bozkurt B, Chaitman BR, Cutlip DE, Farb A, et al. 2014 ACC/AHA key data elements and definitions for cardiovascular endpoint events in clinical trials: a report of the American College of Cardiology/American Heart Association Task Force on

Clinical Data Standards (Writing Committee to Develop Cardiovascular Endpoints Data Standards). Circulation 2015;132:302–61.

12. US Food and Drug Administration. Guidance for industry: diabetes mellitus—evaluating cardiovascular risk in new antidiabetic therapies to treat type 2 diabetes. 2008. URL: www.fda.gov/downloads/Drugs/GuidanceComplianceRegulatoryInformation/Guidances/ucm071627.pdf.

13. Fleming TR. Identifying and addressing safety signals in clinical trials: some issues and challenges. In: Fleming TR, Weir BS, editors. Proceedings of the fourth Seattle Symposium in Biostatistics: Clinical Trials. New York: Springer; 2013. p. 137–56.

14. Li J, Hsu HC, Mountz JD. Managing macrophages in rheumatoid arthritis by reform or removal. Curr Rheumatol Rep 2012;14:445–54.

15. Kaptoge S, Seshasai SR, Gao P, Freitag DF, Butterworth AS, Borglykke A, et al. Inflammatory cytokines and risk of coronary heart disease: new prospective study and updated meta-analysis. Eur Heart J 2014;35:578–89.

16. The Interleukin-6 Receptor Mendelian Randomisation Analysis (IL6R MR) Consortium. The interleukin-6 receptor as a target for prevention of coronary heart disease: a Mendelian randomisation analysis. Lancet 2012;379:1214–24.

17. IL6R Genetics Consortium Emerging Risk Factors Collaboration. Interleukin-6 receptor pathways in coronary heart disease: a collaborative meta-analysis of 82 studies. Lancet 2012;379:1205–13.

18. Maier W, Altwegg LA, Corti R, Gay S, Hersberger M, Maly FE, et al. Inflammatory markers at the site of ruptured plaque in acute myocardial infarction: locally increased interleukin-6 and serum amyloid A but decreased C-reactive protein. Circulation 2005;111:1355–61.

19. Cesari M, Penninx BW, Newman AB, Kritchevsky SB, Nicklas BJ, Sutton-Tyrrell K, et al. Inflammatory markers and onset of cardiovascular events: results from the Health ABC study. Circulation 2003;108:2317–22.

20. Ohta H, Wada H, Niwa T, Kirii H, Iwamoto N, Fujii H, et al. Disruption of tumor necrosis factor-α gene diminishes the development of atherosclerosis in ApoE-deficient mice. Atherosclerosis 2005;180:11–7.

21. Brånén L, Hovgaard L, Nitulescu M, Bengtsson E, Nilsson J, Jovinge S. Inhibition of tumor necrosis factor-α reduces atherosclerosis in apolipoprotein E knockout mice. Arterioscler Thromb Vasc Biol 2004;24:2137–42.

22. Roubille C, Richer V, Starnino T, McCourt C, McFarlane A, Fleming P, et al. The effects of tumour necrosis factor inhibitors, methotrexate, non-steroidal anti-inflammatory drugs and corticosteroids on cardiovascular events in rheumatoid arthritis, psoriasis and psoriatic arthritis: a systematic review and meta-analysis. Ann Rheum Dis 2015;74:480–9.

23. Dixon WG, Watson KD, Lunt M, Hyrich KL, British Society for Rheumatology Biologics Register Control Centre Consortium, Silman AJ, et al. Reduction in the incidence of myocardial infarction in patients with rheumatoid arthritis who respond to anti–tumor necrosis factor α therapy: results from the British Society for Rheumatology Biologics Register. Arthritis Rheum 2007;56:2905–12.

24. Xie F, Yun H, Levitan EB, Muntner P, Curtis JR. Tocilizumab and the risk for cardiovascular disease: a direct comparison among biologic disease-modifying antirheumatic drugs for rheumatoid arthritis patients. Arthritis Care Res (Hoboken) 2019;71:1004–18.

25. Kim SC, Solomon DH, Rogers JR, Gale S, Klearman M, Sarsour K, et al. Cardiovascular safety of tocilizumab versus tumor necrosis factor inhibitors in patients with rheumatoid arthritis: a multi-database cohort study. Arthritis Rheumatol 2017;69:1154–64.

26. Ridker PM, Everett BM, Thuren T, MacFadyen JG, Chang WH, Ballantyne C, et al, for the CANTOS Trial Group. Antiinflammatory therapy with canakinumab for atherosclerotic disease. N Engl J Med 2017;377:1119–31.

27. Robertson J, Porter D, Sattar N, Packard CJ, Caslake M, McInnes I, et al. Interleukin-6 blockade raises LDL via reduced catabolism rather than via increased synthesis: a cytokine-specific mechanism for cholesterol changes in rheumatoid arthritis. Ann Rheum Dis 2017;76:1949–52.

28. Strang AC, Bisoendial RJ, Kootte RS, Schulte DM, Dallinga-Thie GM, Levels JH, et al. Pro-atherogenic lipid changes and decreased hepatic LDL receptor expression by tocilizumab in rheumatoid arthritis. Atherosclerosis 2013;229:174–81.

29. Xie F, Yun H, Bernatsky S, Curtis JR. Risk of gastrointestinal perforation among rheumatoid arthritis patients receiving tofacitinib, tocilizumab, or other biologic treatments. Arthritis Rheumatol 2016;68:2612–7.

AMERICAN COLLEGE
of RHEUMATOLOGY
Empowering Rheumatology Professionals

BRIEF REPORT

Association of Inflammation With Pronociceptive Brain Connections in Rheumatoid Arthritis Patients With Concomitant Fibromyalgia

Chelsea M. Kaplan,[1] Andrew Schrepf,[1] Eric Ichesco,[1] Tony Larkin,[1] Steven E. Harte,[1] Richard E. Harris,[1] Alison D. Murray,[2] Gordon D. Waiter,[2] Daniel J. Clauw,[1] and Neil Basu[3]

Objective. Rheumatoid arthritis (RA) patients with concomitant fibromyalgia (FM) exhibit alterations in brain connectivity synonymous with central sensitization. This study was undertaken to investigate how peripheral inflammation, the principal nociceptive stimulus in RA, interacts with brain connectivity in RA patients with FM.

Methods. RA patients with concomitant FM and those without FM (FM+ and FM−, respectively; n = 27 per group) underwent functional connectivity magnetic resonance imaging. Seed-to–whole-brain functional connectivity analyses were conducted using seeds from the left mid/posterior insula and left inferior parietal lobule (IPL), which are regions that have been previously linked to FM symptoms and inflammation, respectively. The association between functional connectivity and erythrocyte sedimentation rate (ESR) was assessed in each group separately, followed by post hoc analyses to test for interaction effects. Cluster-level, family-wise error (FWE) rates were considered significant if the P value was less than 0.05.

Results. The group of RA patients with FM and those without FM did not differ by age, sex, or ESR ($P > 0.2$). In FM+ RA patients, increased functional connectivity of the insula–left IPL, left IPL–dorsal anterior cingulate, and left IPL–medial prefrontal cortex regions correlated with higher levels of ESR (all FWE-corrected $P < 0.05$). Post hoc interaction analyses largely confirmed the relationship between ESR and connectivity changes as FM scores increased.

Conclusion. We report the first neurobiologic evidence that FM in RA may be linked to peripheral inflammation via pronociceptive patterns of brain connectivity. In patients with such "bottom-up" pain centralization, concomitant symptoms may partially respond to antiinflammatory treatments.

INTRODUCTION

Rheumatoid arthritis (RA) is known for its heterogeneous clinical presentation, with some patients reporting pain localized to affected joints and others reporting widespread hyperalgesia, fatigue, and cognitive difficulties. This latter phenotype has remarkable similarities to symptoms observed in fibromyalgia (FM), and indeed the reported prevalence of concomitant FM in RA patients ranges from 12% to 48%, compared to 2–8% in the general population (1). Moreover, we recently showed that one of the chief neurobiologic signatures of FM (increased default mode network [DMN] to insula functional connectivity) also occurs in RA patients in proportion to their FM symptoms (2).

In the context of RA, it has long been hypothesized that peripheral inflammatory nociceptive processes sensitize the central nervous system (CNS) via pronociceptive CNS pathways and drive

the occurrence of concomitant FM (3). This suggests that individual differences in how the brain responds to inflammation may be critical to understanding concomitant FM in RA.

We recently provided some of the first evidence that functional brain connections are substantially altered in RA patients with high levels of peripheral inflammation (4). In the present study, we expanded on that effort by exploring the effect of the interaction between functional brain connectivity and inflammation on FM symptoms in the same cohort of RA patients. These analyses were designed to identify patterns of brain connectivity in RA that promote core symptoms of FM in response to inflammation. We hypothesized that higher inflammation would be associated with distinct changes in connectivity from the insula (a pronociceptive brain region) and left inferior parietal lobule (IPL; a region associated with the neural response to peripheral inflammation in RA patients) to other brain regions in patients with a high level of FM symptoms.

PATIENTS AND METHODS

Patients. RA patients were approached through a UK regional rheumatology service. Patients were considered eligible if they met the American College of Rheumatology (ACR)/ European League Against Rheumatism 2010 classification criteria for RA (5). This study was designed to examine the neural correlates of fatigue in RA; therefore, patients had to have had a clinically significant level of fatigue for at least 3 months (defined as a score of >3 on the Chalder Fatigue Binary Scale [6]). The analyses presented in this report address alternate hypotheses regarding inflammation and centralized pain in RA. Exclusion criteria were contraindications to magnetic resonance imaging (MRI), left-handedness, or the presence of an alternative medical explanation for fatigue. A total of 73 RA patients fulfilled these criteria, and 54 patients (41 female) completed the entire study. Ethical approval for the study was obtained from the North of Scotland Research Ethics Committee. All participants provided written informed consent in accordance with the Declaration of Helsinki.

Clinical evaluation. All consenting patients underwent a clinical evaluation and a functional MRI (fMRI) brain scan. FM diagnosis was assessed using the ACR modified 2010 criteria (7), which combine a measure of widespread pain (number of painful sites [range 0–19]) with a symptom severity scale (e.g., fatigue, subjective cognitive problems, headache, poor mood; scores range from 0 to 12). A combined score of ≥13 was used as the diagnostic cutoff for FM (7). Twenty-seven RA patients met the criteria for FM (FM+), and 27 did not (FM–). Inflammation was measured using the erythrocyte sedimentation rate (ESR), a measure of systemic inflammation that is commonly used to diagnose and monitor chronic inflammatory diseases such as RA. A trained phlebotomist collected venous blood samples during standard clinic hours, and blood

samples were immediately processed and analyzed for the calculation of ESR (via the Westergren method).

Functional MRI data acquisition and preprocessing. Functional MRI data were collected using an Achieva 3.0T X-series MR system (Philips Medical) with an 8-channel phased-array head coil. Each patient underwent an 11-minute functional scan while performing the Paced Auditory Serial Attention Test (PASAT), a validated measure of cognitive function. The PASAT was administered in a block design with three 3-minute "on" periods, interspersed with four 30-second rest or "off" periods. During the "on" periods, a series of numbers were audibly presented, and patients were asked to sum consecutive numbers and to press a button every time 2 consecutive numbers summed to 10. Concurrently, patients were shown a distracting visual stimulus of random, rapidly changing numbers that were intended to increase task difficulty. The functional images were acquired using a 3-dimensional (3-D) T2*-weighted gradient-echo single-shot echo-planar imaging pulse sequence with the following parameters: repetition time (TR) 3,000 msec, echo time (TE) 30 msec, flip angle 90°, in-plane
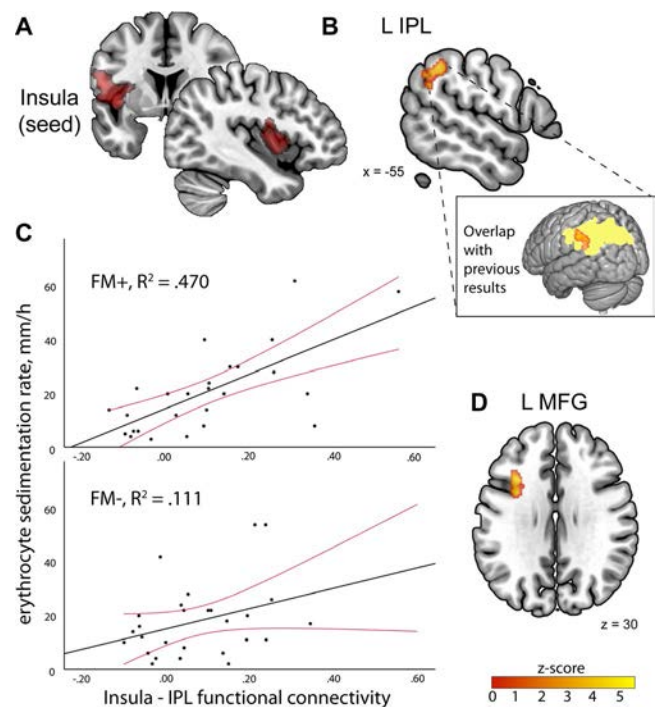
Figure 1. **A** and **B**, Correlation of higher levels of peripheral inflammation with increased brain connectivity between the left mid/ posterior insula (**A**) and the left inferior parietal lobule (L IPL) (**B**) in rheumatoid arthritis (RA) patients with concomitant fibromyalgia (FM). **Inset** in **B** shows overlap of the left IPL cluster with previous results (4), demonstrating that numerous brain networks were hyperconnected to the same region of the IPL in RA patients with high levels of inflammation. **C**, Scatterplots showing correlation between erythrocyte sedimentation rate and insula–IPL connectivity in RA patients with or without FM; 95% confidence intervals are displayed in red. **D**, Significant positive relationship between insula–left middle frontal gyrus (MFG) connectivity and peripheral inflammation in RA patients with FM.

Sensitivity Encoding (SENSE) acceleration 2, field of view (FOV) 240 mm, matrix size 128 × 128 pixels with 30 slices, voxel size 1.88 × 1.88 × 5 mm^3, and 226 volumes. A high-resolution structural T1-weighted fast field-echo 3-D structural scan was collected for normalization (TR 8.2 msec, TE 3.8 msec, inversion recovery time 1,018 msec, flip angle 8°, FOV 240 mm, matrix size 240 × 240 pixels with 160 slices, and voxel size 0.94 × 0.94 × 1 mm^3).

Functional MRI data were preprocessed using Statistical Parametric Mapping (SPM version 8; Wellcome Department of Cognitive Neurology, London, UK) running on MatLab R2014a (MathWorks), as previously described (2,4). Briefly, the first 4 volumes were discarded to avoid equilibration effects, and the remaining 222 functional images were realigned to the first image. The structural image was coregistered to a mean functional image and then segmented. The structural and functional scans were normalized to the standard SPM Montreal Neurological Institute template gray prior probability map via the individuals' segmented gray matter image. Functional scans were then smoothed with an 8-mm full-width half-maximum Gaussian kernel.

Seed-to–whole brain connectivity analysis. In these same RA patients, we have previously shown that DMN–left mid/posterior insula connectivity is associated with the FM survey criteria score (2) and that the left IPL is more connected to mul-

tiple brain networks in patients with high levels of inflammation (4). To determine how FM and inflammation interact in the brain, we used these same left insular and IPL clusters as seed regions (Figures 1A and 2A). The preprocessed functional data were entered into a Functional Connectivity Toolbox version 15 (CONN; Cognitive and Affective Neuroscience Laboratory, Massachusetts Institute of Technology, Cambridge [http://www.nitrc.org/projects/conn]). As previously described (2,4), a component-based method (CompCor) was performed to remove confounding effects. The confounds included 6 subject-specific motion parameters, and the signal from white matter and cerebrospinal fluid and their first-order derivatives. A band-pass filter (0.01–0.1 Hz) was applied to remove linear drifts and high-frequency noise in the data. Task and rest onset periods were modeled and concatenated in first-level analyses to generate beta maps representing connectivity between the insula and IPL and the rest of the brain during task and rest conditions. The resulting beta maps were passed onto second-level group analyses in SPM8. Rest periods were not analyzed at the group level because the summed resting condition (2 minutes) is too short for reliable connectivity estimates (8).

Using multiple regression models, the FM+ and FM− groups were assessed independently in SPM8. In each group we assessed the relationship between seed-to–whole brain connectivity and ESR, with age and sex considered covariates of no interest.
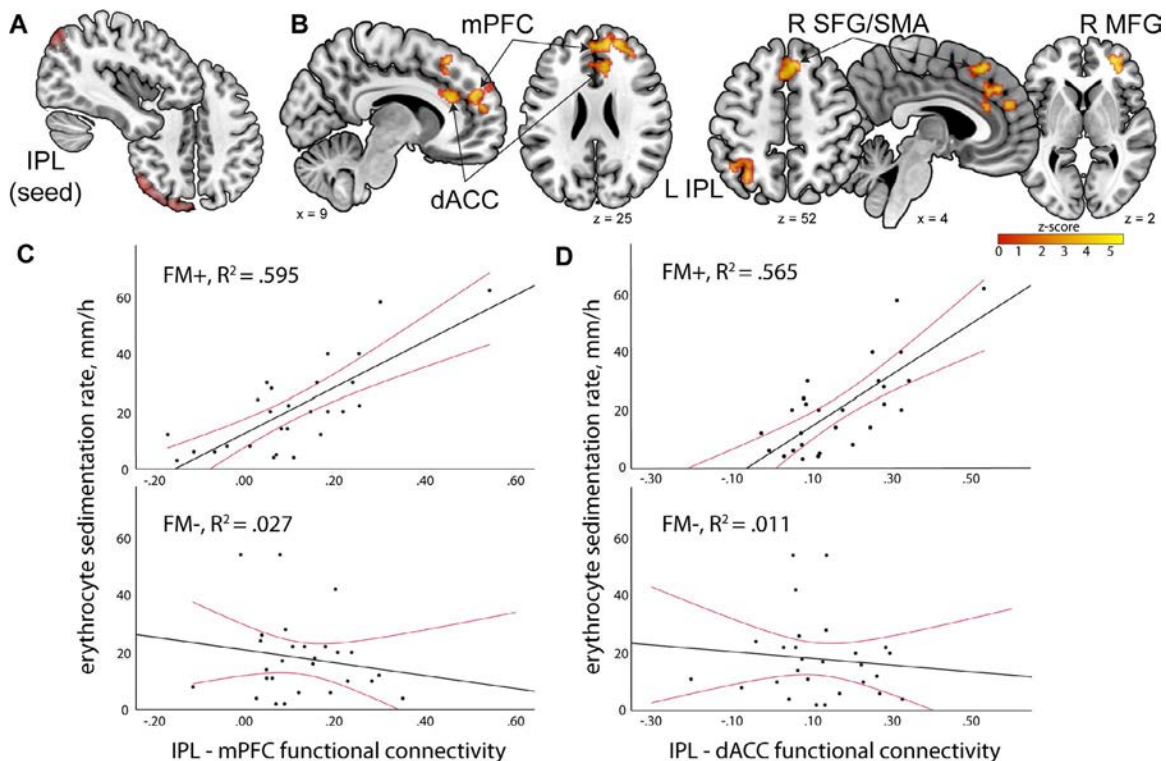
Figure 2. Association of inflammation with functional connectivity in RA patients with concomitant FM. **A** and **B**, In RA patients with FM, there was a significant relationship between peripheral inflammation and functional connectivity between the left IPL (**A**) and the dorsal anterior cingulate cortex (dACC), medial prefrontal cortex (mPFC), left IPL (adjacent to seed region), right superior frontal gyrus/supplementary motor area (R SFG/SMA), and right MFG (**B**). **C** and **D**, Scatterplots showing the correlation between erythrocyte sedimentation rate and IPL–mPFC connectivity (**C**) and IPL–dorsal ACC connectivity (**D**) in RA patients with or without FM; 95% confidence intervals are displayed in red. See Figure 1 for other definitions.

The resulting maps were thresholded at an uncorrected voxelwise level of $P < 0.001$, and cluster-level family-wise error rates were considered significant at $P < 0.05$ after correction for multiple comparisons. The average Fisher-transformed r values of significant clusters were extracted from the first-level beta maps for each patient for secondary analyses to test for interaction effects.

Post hoc interaction analyses. To formally test the possibility of interaction effects, we examined whether the relationship between connectivity values extracted from significant clusters (as described above) and ESR changes as a function of total FM scores. Total scores, rather than FM clinical cutoffs, were used as we have previously shown that this construct can be used continuously (2). ESR and FM survey scores were standardized and centered. These analyses were conducted with general linear models in R version 3.4.4. Post hoc Spearman's rank correlations between functional connectivity and C-reactive protein (CRP) level were calculated to confirm the relationships observed with ESR.

RESULTS

Clinical characteristics. The clinical characteristics of this cohort have been described previously (2,4) and are shown for FM+ and FM– groups separately (Supplementary Table 1, available on the *Arthritis & Rheumatology* web site at http://onlinelibrary.wiley.com/doi/10.1002/art.41069/abstract). Twenty-seven RA patients met criteria for FM. The mean ± SD FM score was 17.89 ± 4.77 in the FM+ RA group and 8.52 ± 3.19 in the FM– RA group. There was no significant difference in age, sex, or ESR between FM+ and FM– RA patients.

Seed-to–whole brain connectivity analyses. In FM+ RA patients, higher levels of peripheral inflammation were associated with increased functional connectivity between the insula and the left midfrontal gyrus (MFG) and the left IPL (Figures 1B–D and Table 1). Further, in FM+ RA patients, higher peripheral inflammation was associated with increased functional connectivity between the left IPL and multiple cortical regions, including the dorsal anterior cingulate cortex (ACC), medial prefrontal cortex (mPFC), right MFG, right superior frontal gyrus/supplementary motor area, and left IPL (adjacent to the seed IPL region) (Figures 2B–D and Table 1). Of the 7 connections associated with ESR in FM+ patients, 4 were significantly or close to significantly associated with CRP level (Supplementary Table 2, available on the *Arthritis & Rheumatology* web site at http://onlinelibrary.wiley.com/doi/10.1002/art.41069/abstract). In FM– RA patients, higher levels of peripheral inflammation were correlated with lower functional connectivity between the insula and right IPL and higher functional connectivity between the IPL and left superior temporal gyrus (Table 1).

It is possible that other aspects of disease activity, such as the swollen and tender joint counts that are incorporated into the Disease Activity Score in 28 joints (9), could have been affecting our results. We therefore conducted partial correlation analyses between the extracted connectivity values and ESR, while controlling for swollen and tender joint counts, separately in the FM + and FM– groups. There were no appreciable changes in the strength of the association between ESR and connectivity in these analyses (data not shown). Additionally, adjustment for body mass index did not alter the associations between ESR and connectivity in either group (data not shown).

Table 1. Associations between seed-to–whole brain functional connectivity and erythrocyte sedimentation rate*

Seed region cluster (direction of association)	MNI coordinates			Z score	Cluster size, no. of voxels	*P*, FWE-corrected	*P*, post hoc interaction
	X	Y	Z				
With fibromyalgia							
Left insula							
Left midfrontal gyrus (+)	−36	24	32	4.38	161	0.007	0.049
Left IPL (+)	−50	−50	40	3.98	132	0.019	0.015
Left IPL							
Bilateral dorsal ACC/mPFC (+)	2	38	36	4.43	239	0.001	0.016
Right midfrontal gyrus (+)	30	48	2	4.31	132	0.026	0.317
Bilateral SFG/SMA (+)	8	28	52	4.15	128	0.030	0.040
Right mPFC/right dorsal ACC (+)	12	60	30	3.88	349	0.000	0.002
Left IPL (+)†	−32	−48	46	3.76	135	0.023	0.016
Without fibromyalgia							
Left insula							
Right IPL/precuneus/angular (−)	28	−52	44	4.51	175	0.002	<0.001
Left IPL							
Left STG (+)	−50	−42	6	4.29	257	0.000	0.024

* MNI = Montreal Neurological Institute; FWE = family-wise error; ACC = anterior cingulate cortex; mPFC = medial prefrontal cortex; SFG = superior frontal gyrus; SMA = supplementary motor area; STG = superior temporal gyrus.
† Adjacent to the seed inferior parietal lobule (IPL) region.

Post hoc interaction analyses. There was a significant interaction effect between FM scores and ESR for each extracted connectivity value except for the left IPL–right MFG ($P = 0.317$) (Table 1). This suggests that the interaction between FM symptoms and inflammation is important irrespective of whether a patient meets epidemiologic criteria for FM.

DISCUSSION

In RA, peripheral inflammation appears to affect FM status as reflected on measures of brain functional connectivity. In our previous study (2), we demonstrated that a neurobiologic signature of pain centralization (enhanced insula–DMN connectivity) is also present in RA. Importantly, across the overall sample, this connectivity was not significantly associated with peripheral inflammation. In this study, we show for the first time that inflammation is neurobiologically associated with other more established patterns of pronociceptive connectivity in RA, but this is observed only in patients with more FM symptoms. These effects were apparent when FM was measured as a continuous construct, suggesting that FM symptoms may have important neurobiologic correlates irrespective of whether a patient meets clinical criteria for FM, as we have previously reported (2). This in turn suggests that there is an interaction between peripherally enhanced sensitization and centrally maintained sensitization that contributes to FM symptoms in RA. Put simply, how the brain responds to peripheral inflammation may be critical in understanding why some RA patients have high levels of concomitant FM symptoms while others do not.

The insula is a multimodal sensory processing region and is critically involved in pain perception (10). In FM+ RA patients, increased insula–left IPL connectivity was positively correlated with peripheral inflammation. The IPL is a key node of the DMN, and heightened DMN–insula connectivity is an established neurobiologic feature of FM (10), as well as of these same RA patients with high levels of FM symptoms (2). In FM+ RA patients, we would expect to see increased DMN–insula functional connectivity, but the relationship with peripheral inflammation observed in this study is novel. Interestingly, this left IPL region overlapped with the IPL cluster we previously identified as being more strongly connected to multiple brain networks in patients with high levels of peripheral inflammation (4).

Using the IPL cluster from our previous study (4) as a seed region, we found that IPL–dorsal ACC and IPL–mPFC functional connectivity was positively associated with inflammation only in FM+ RA patients. It has been previously shown that during the completion of a painful task, FM patients exhibit higher activity in the dorsal ACC compared to healthy participants (11). A previous study in RA patients demonstrated that the dorsal ACC, mPFC, and left IPL were activated during a provoked joint pain paradigm, and that the mPFC and left IPL regions were functionally connected during this painful task (12). In this context, our results may indicate preliminary evidence of the integration of inflammation-linked brain connectivity and classic pronociceptive brain connectivity.

In FM– patients, insula–right IPL functional connectivity was negatively correlated with peripheral inflammation, while insula–left IPL functional connectivity was positively correlated with peripheral inflammation in FM+ patients. There is evidence of hemispheric asymmetry in IPL function (13) and in the susceptibility to neurodegeneration. For instance, the left hemisphere is affected earlier and more severely in Alzheimer's disease, and the left IPL, compared to the right IPL, shows greater metabolic dysfunction in early dementia (13). The left IPL may be more susceptible to peripherally enhanced sensitization, which is why inflammation-associated connectivity changes in this region are predominantly observed in patients with concomitant FM.

This is the first study to examine patterns of inflammation-associated brain connectivity in the context of concomitant FM in RA. Although the evidence is limited, the coexistence of FM symptoms with another disorder is thought to constitute 2 broad processes: 1) a "bottom-up" form of central sensitization, driven primarily by ongoing nociceptive input and somewhat responsive to treatments that target peripheral nociceptive drivers and 2) a "top-down" central sensitization subtype, which is primarily central in origin and unaffected by manipulations of peripheral nociception (3). Consistent with this hypothesized distinction, a previous osteoarthritis study indicated that successful joint replacement surgery resulted in a substantial improvement of responses to experimental pain measures outside the surgical site and that patients whose surgery eliminated their pain exhibited a more normal inhibitory response to evoked pain than they did prior to surgery (14). In RA, an analogous phenomenon would involve improvement in concomitant FM symptoms following successful inhibition of inflammation. Future studies will focus on patterns of inflammation-associated brain connectivity that predict improvement in concomitant FM after inflammation-reducing therapy.

This study has some limitations. First, all of the RA patients in the study had significant levels of chronic fatigue, which may not necessarily be representative of all patients and could have biased the sample toward a centralized pain phenotype. Second, we examined functional connectivity during the performance of a cognitive task from 2 seed regions based on earlier results from the same cohort. Future studies should attempt a whole brain agnostic approach in an independent sample in which patients are at rest or performing other tasks. We do not know when patients developed FM symptoms relative to the onset of RA. Therefore, some patients may belong to a different phenotype wherein "top-down" central sensitization exists prior to RA diagnosis. We have made the reasonable assumption that our measure of systemic inflammation (ESR) is derived entirely from the well-established peripheral immune dysfunction that characterizes RA. However, considering the evolving evidence that supports a neural inflammatory reflex (15), it is also possible that altered brain connectivity drives peripheral inflammation, perhaps via endocrine pathways. It would be intriguing to evaluate

the responsiveness of identified pronociceptive connectivity in the context of a peripherally directed antiinflammatory treatment, as mentioned above.

In a small study on tumor necrosis factor inhibitors (TNFi) in RA, Rech et al demonstrated that pronociceptive brain connectivity decreased rapidly (i.e., 3 days) after commencement of TNFi treatment and before a positive clinical response was observed (16), providing some support for the concept of "bottom-up" sensitization. Ultimately, the great clinical value of distinguishing "bottom-up" mechanisms of central sensitization is the potential to identify RA patients whose FM symptoms may improve with an enhanced peripheral immunosuppressive approach. In contrast, "top-down" central sensitization would not be expected to respond to peripherally directed therapies. Instead, patients may receive benefit from centrally acting interventions. Until more definitive studies are conducted, these concepts remain as working hypotheses.

Our finding that peripheral inflammation enhances connectivity in established pronociceptive pathways provides preliminary neurobiologic evidence of a distinct FM-like subtype in RA. Identifying the neurobiologic patterns associated with different forms of central sensitization of FM in RA may help to refine therapeutic targets.

ACKNOWLEDGMENTS

AUTHOR CONTRIBUTIONS

All authors were involved in drafting the article or revising it critically for important intellectual content, and all authors approved the final version to be published. Dr. Kaplan had full access to all of the data in the study and takes responsibility for the integrity of the data and the accuracy of the data analysis.
Study conception and design. Kaplan, Schrepf, Ichesco, Larkin, Harte, Harris, Murray, Waiter, Clauw, Basu.
Acquisition of data. Murray, Waiter, Basu.
Analysis and interpretation of data. Kaplan, Schrepf, Ichesco, Larkin, Harte, Harris, Murray, Waiter, Clauw, Basu.

ROLE OF THE STUDY SPONSOR

REFERENCES

1. Boyden SD, Hossain IN, Wohlfahrt A, Lee YC. Non-inflammatory causes of pain in patients with rheumatoid arthritis. Curr Rheumatol Rep 2016;18:30.

2. Basu N, Kaplan CM, Ichesco E, Larkin T, Harris RE, Murray A, et al. Neurobiologic features of fibromyalgia are also present among rheumatoid arthritis patients. Arthritis Rheumatol 2018;70:1000–7.

3. Harte SE, Harris RE, Clauw DJ. The neurobiology of central sensitization. J Appl Biobehav Res 2018;23:e12137.

4. Schrepf A, Kaplan CM, Ichesco E, Larkin T, Harte SE, Harris RE, et al. A multi-modal MRI study of the central response to inflammation in rheumatoid arthritis. Nat Commun 2018;9:2243.

5. Aletaha D, Neogi T, Silman AJ, Funovits J, Felson DT, Bingham CO III, et al. 2010 rheumatoid arthritis classification criteria: an American College of Rheumatology/European League Against Rheumatism collaborative initiative. Arthritis Rheum 2010;62:2569–81.

6. Chalder T, Berelowitz G, Pawlikowska T, Watts L, Wessely S, Wright D, et al. Development of a fatigue scale. J Psychosom Res 1993;37:147–53.

7. Wolfe F, Clauw DJ, Fitzcharles MA, Goldenberg DL, Häuser W, Katz RS, et al. Fibromyalgia criteria and severity scales for clinical and epidemiological studies: a modification of the ACR Preliminary Diagnostic Criteria for Fibromyalgia. J Rheumatol 2011;38:1113–22.

8. Van Dijk KR, Hedden T, Venkataraman A, Evans KC, Lazar SW, Buckner RL. Intrinsic functional connectivity as a tool for human connectomics: theory, properties, and optimization. J Neurophysiol 2010;103:297–321.

9. Prevoo ML, van 't Hof MA, Kuper HH, van Leeuwen MA, van de Putte LB, van Riel PL. Modified disease activity scores that include twenty-eight–joint counts: development and validation in a prospective longitudinal study of patients with rheumatoid arthritis. Arthritis Rheum 1995;38:44–8.

10. Napadow V, LaCount L, Park K, As-Sanie S, Clauw DJ, Harris RE. Intrinsic brain connectivity in fibromyalgia is associated with chronic pain intensity. Arthritis Rheum 2010;62:2545–55.

11. Pujol J, López-Solà M, Ortiz H, Vilanova JC, Harrison BJ, Yücel M, et al. Mapping brain response to pain in fibromyalgia patients using temporal analysis of FMRI. PLoS One 2009;4:e5224.

12. Schweinhardt P, Kalk N, Wartolowska K, Chessell I, Wordsworth P, Tracey I. Investigation into the neural correlates of emotional augmentation of clinical pain. Neuroimage 2008;40:759–66.

13. Toga AW, Thompson PM. Mapping brain asymmetry. Nat Rev Neurosci 2003;4:37–48.

14. Kosek E, Ordeberg G. Lack of pressure pain modulation by heterotopic noxious conditioning stimulation in patients with painful osteoarthritis before, but not following, surgical pain relief. Pain 2000;88:69–78.

15. Pavlov VA, Tracey KJ. Neural regulation of immunity: molecular mechanisms and clinical translation. Nat Neurosci 2017;20:156–66.

16. Rech J, Hess A, Finzel S, Kreitz S, Sergeeva M, Englbrecht M, et al. Association of brain functional magnetic resonance activity with response to tumor necrosis factor inhibition in rheumatoid arthritis. Arthritis Rheum 2013;65:325–33.

AMERICAN COLLEGE
of RHEUMATOLOGY
Empowering Rheumatology Professionals

A Neutrophil Activation Biomarker Panel in Prognosis and Monitoring of Patients With Rheumatoid Arthritis

Mary Bach,[1] Jeonghun Moon,[2] Richard Moore,[1] Tiffany Pan,[3] J. Lee Nelson,[4] and Christian Lood[1] (ID)

Objective. Exaggerated neutrophil activation and formation of neutrophil extracellular traps (NETs) are linked to inflammation and autoimmunity, including rheumatoid arthritis (RA). However, whether NETs are present in the circulation of RA patients and contribute to inflammation and disease progression has not been carefully addressed. We undertook this study to assess markers of neutrophil activation and NET formation in plasma samples, investigating whether they add clinical value in improving the determination of prognosis and monitoring in RA patients.

Methods. Markers of neutrophil activation (calprotectin) and cell death (NETs) were analyzed, using enzyme-linked immunosorbent assay, in serum and plasma obtained from patients in 3 cross-sectional RA cohorts and sex-matched healthy controls. A longitudinal inception cohort (n = 247), seen for a median follow-up of 8 years, was used for predictive analyses.

Results. Markers of neutrophil activation and cell death were increased in RA patients compared to healthy individuals ($P < 0.0001$). Calprotectin levels correlated with the Clinical Disease Activity Index (r = 0.53, $P < 0.0001$) and could be used to distinguish between patients with disease in remission and those with active disease, an observation not seen when examining C-reactive protein levels. A biomarker panel consisting of anti–citrullinated protein antibody and calprotectin could predict erosive disease (odds ratio [OR] 7.5, $P < 0.0001$) and joint space narrowing (OR 4.9, $P = 0.001$). NET levels were associated with markers of inflammation ($P = 0.0002$). Furthermore, NETs and a "neutrophil activation signature" biomarker panel had good predictive value in identifying patients who were developing extraarticular nodules (OR 5.6, $P = 0.006$).

Conclusion. Neutrophils undergo marked activation and cell death in RA. Neutrophil biomarkers can provide added clinical value in the monitoring and prognosis of RA patients and may allow for early preventive treatment intervention.

INTRODUCTION

Neutrophils are the most abundant immune cells in the circulation, participating in host defense mechanisms through production of reactive oxygen species (ROS), phagocytosis, and formation of neutrophil extracellular traps (NETs). NET formation, also called NETosis, is a neutrophil cell death process in which DNA is extruded together with cytoplasmic and granular contents in a web-like structure to eliminate extracellular pathogens (1–6). Although beneficial from a host–pathogen perspective, exaggerated neutrophil activation has been linked to inflammation and autoimmunity including rheumatoid arthritis (RA) and

systemic lupus erythematosus (SLE) (2,3,7–9). In RA, neutrophils are well-known contributors to local inflammation and participate in tissue destruction and erosion (10). Furthermore, neutrophils express high levels of peptidylarginine deiminase 2 (PAD2) and PAD4, which are key proteins in the enzymatic conversion of arginine into citrulline, the autoantigen toward which anti–citrullinated protein antibodies (ACPAs) are targeted. Two main processes through which citrullination may occur have emerged: 1) pore formation leading to "hypercitrullination" of cytosolic molecules (11,12), and 2) NETosis, exposing citrullinated histones and vimentin, which are key targets of RA autoantibodies (9,13–15). The latter process may be of particular importance in

the synovium, where local B cells have been found to produce anti-NET antibodies (13).

RA neutrophils are prone to spontaneous NETosis when examined ex vivo, as well as when stimulated with inflammatory cytokines and autoantibodies (9,16). The released NETs induce local inflammation and presentation of citrullinated peptides to antigen-specific T cells by fibroblast-like synoviocytes (FLS) (9,17). Illustrating the important role of NETs in the disease setting of RA, Cl-amidine, a PAD4 inhibitor, ameliorated disease development in the collagen-induced arthritis (CIA) model (18). However, PAD4 inhibition did not affect arthritis phenotype in the K/BxN serum–transfer model (19). In RA patients, neutrophil activation markers, including calprotectin, are elevated and associated with active disease and may predict radiographic progression (20–22). Serum levels of NETs and NET-derived products, including cell-free DNA, are also elevated in RA patients and associated with disease activity (16,23,24). However, given that fragile neutrophils undergo spontaneous NET formation upon serum processing (e.g., coagulation) (16), serum levels may not reflect the "true" physiologic levels of NETs experienced by patients with RA. Thus, whether RA patients have NETs in the circulation and what the relation of NETs is to disease activity and inflammation are still not known.

In the current study, we investigated the true levels of neutrophil activation markers, including NETs, in large cross-sectional and longitudinal RA cohorts and investigated whether detection of these markers could add value to diagnosis, prognosis, and monitoring of RA patients. Briefly, we found that neutrophil activation markers were superior to C-reactive protein (CRP) in identifying patients with active disease. Finally, neutrophil biomarkers improved the prognostic capacity of ACPA in predicting radiographic changes and development of extraarticular nodules. Thus, neutrophils are clearly implicated in RA pathogenesis, contributing to inflammation, organ damage, and exposure of autoantigens. As such, we propose that neutrophil activation biomarkers may assist clinicians in diagnosis and prognosis. Furthermore, neutrophil activation biomarkers may help identify patients with active disease and allow for the implementation of early preventive treatment strategies, thus reducing disabling morbidities and improving the quality of life of these patients.

PATIENTS AND METHODS

Patient cohorts. Patients with RA (n = 101; cohort 1) and age- and sex-matched healthy controls were recruited to participate in research studies at the University of Washington Medical Center in Seattle. Disease activity was recorded using the Clinical Disease Activity Index (CDAI) for RA (25), taking into account tender and swollen joints, patient global assessment, and provider global assessment. In this cohort, the median CDAI was 11 (moderate activity), with a range of 0–46. One cross-sectional cohort with established RA (n = 93; cohort 2) and age- and sex-matched healthy individuals

(n = 100), as well as one RA inception cohort (n = 247; cohort 3) were seen for a median follow-up of 8.3 years (range 4.4–19.8 years) after being recruited in Washington state. For additional patient characteristics, see Supplementary Table 1, available on the *Arthritis & Rheumatology* web site at http://online library.wiley.com/doi/10.1002/art.41062/abstract. This study was approved by regional ethics boards (nos. 3100 and 810), and written informed consent was obtained from all participants in accordance with the Helsinki Declaration.

Neutrophil activation and cell death markers. Levels of calprotectin (S100A8/A9) were analyzed using a commercial enzyme-linked immunosorbent assay (ELISA) kit according to instructions of the manufacturer (R&D Systems). For the detection of NETs, a 96-well microtiter plate (Corning) was coated with antimyeloperoxidase (anti-MPO) antibody (4 µg/ml; Bio-Rad) overnight at 4°C, followed by blocking with 1% bovine serum albumin (BSA) in phosphate buffered saline (PBS) for 2 hours at room temperature. After blocking, plasma or serum samples (10% in PBS–BSA) were added and incubated overnight at 4°C. Horseradish peroxidase (HRP)–conjugated anti–double-stranded DNA antibody (diluted 1:100; Roche Diagnostics) was then added for 2 hours at room temperature. The reaction was developed with 3,3′,5,5′-tetramethylbenzidine (TMB; BD Biosciences) and ended by the addition of $2N$ sulfuric acid. Absorbance was measured at 450 nm with a Synergy plate reader (BioTek). For cohorts 1 and 2, plasma and serum samples were obtained and analyzed, and for cohort 3, serum samples were obtained and analyzed. Isolated NETs were used to construct a standard curve, with 1 IU/ml equaling the quantity of NETs released by 10,000 neutrophils.

NET and DNA degradation. NET degradation was assessed using a previously published protocol (26), with some modifications. Briefly, neutrophils were isolated through density gradient (PolymorphPrep; Axis-Shield) and seeded at 1 × 10^6 cells/ml in a poly-L-lysine–coated black 96-well microtiter plate. Neutrophils were induced to undergo NETosis by addition of 20 nM phorbol myristate acetate (PMA) for 4 hours. Upon washing, attached NETs were stained with Sytox green (1:5,000; Life Technologies) followed by subsequent wash steps. After recording of baseline fluorescence, sera (5%, diluted in nuclease buffer [10 mM Tris HCl, pH 7.5, 10 mM MgCl$_2$, 2 mM CaCl$_2$, 50 mM NaCl]) were added and incubated for 90 minutes at 37°C. Micrococcal nuclease was used as a positive control. After the incubation, the wells were washed and residual NETs analyzed by plate reader. NET degradation was calculated as the relative loss of NETs (Sytox green signal) in each well, using the standard curve as a reference value. For DNA degradation, Sytox green–labeled DNA (5 µg/ml) was bound to poly-L-lysine–coated plates, and the capacity to degrade the DNA was assessed in the presence of 10% sera in nuclease buffer.

Serum-mediated neutrophil activation. Neutrophils, isolated as described above, were incubated with 10% serum for 3 hours and analyzed for cell surface expression of CD11b and CD66b (BioLegend) by flow cytometry. The CD11b antibody recognizes all forms of CD11b, including the nonactivated. The results are presented as the relative mean fluorescence intensity signal compared to nonactivated neutrophils.

Interleukin-6 and CRP ELISA. Interleukin-6 (IL-6) levels were measured using a sandwich ELISA. Briefly, a 96-well microtiter plate (Cornin Clear Polystyrene flat-bottomed, medium binding) was coated with 100 μl of capture antibody (4 μg/ml anti-human IL-6; BioLegend), diluted in PBS, and incubated overnight at 4°C. After blocking with 1% BSA in PBS for 2 hours at room temperature, samples were added and incubated overnight at 4°C. Plates were then incubated with biotinylated detection antibody

(1 μg/ml in blocking buffer [biotin/anti-human IL-6]) for 2 hours at room temperature, followed by addition of HRP–streptavidin (BioLegend) for an additional 2 hours at room temperature. The reaction was visualized by the addition of TMB; it was stopped by the addition of 2*N* sulfuric acid, and the absorbance at 450 nm was measured by plate reader. Wells were washed thoroughly 3 times in PBS–Tween between every step. CRP was analyzed by ELISA according to the manufacturer's protocol (Enzo Life Sciences).

Statistical analysis. For sample sets with a non-Gaussian distribution, the Mann-Whitney U test and Spearman's correlation test were used, as applicable. In some analyses, logistic regression analyses were used. For neutrophil markers, the cutoff for positivity was determined by the 95th percentile of the healthy individuals. For outcome measures (erosive disease and joint space narrowing), the upper quartile of the RA cohort was used.
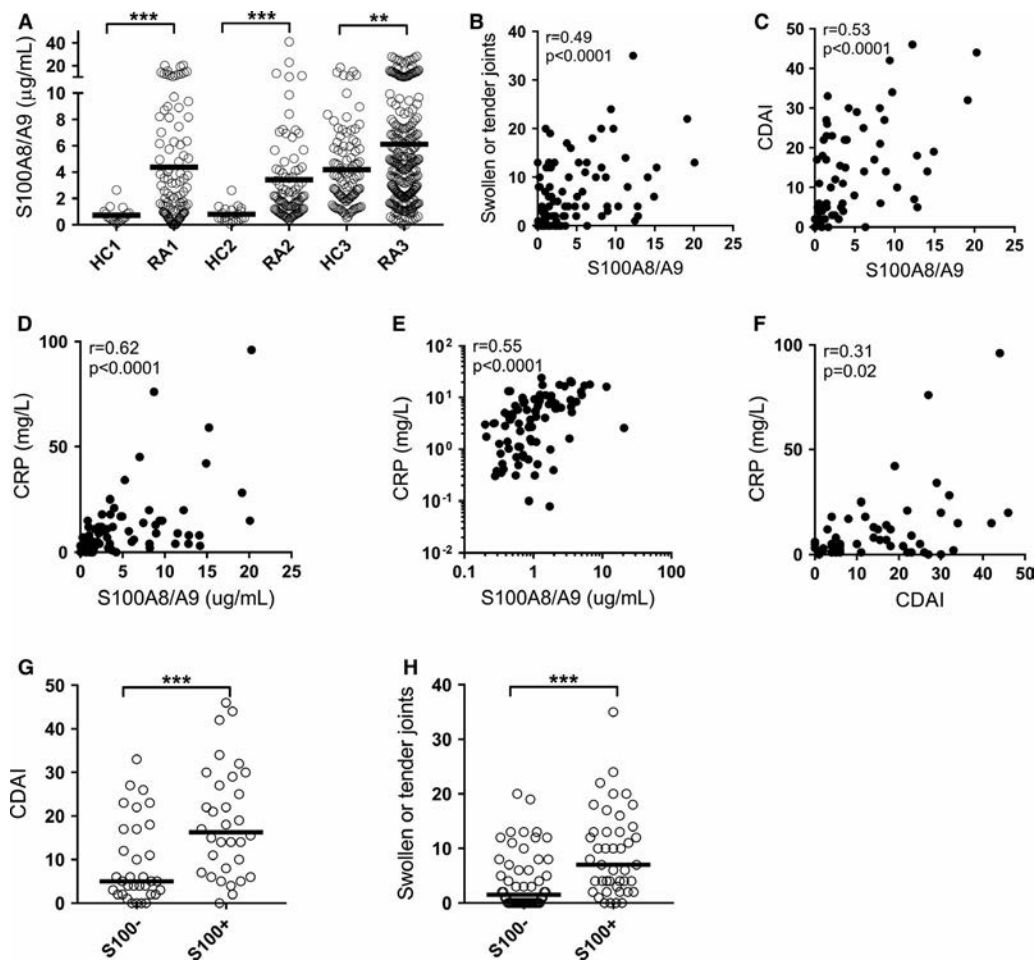
Figure 1. Association of calprotectin (S100A8/A9) levels with disease activity in rheumatoid arthritis (RA). **A**, Levels of calprotectin were analyzed in 3 cohorts of RA patients and 3 cohorts of healthy controls (HCs). Plasma samples were analyzed in the first and second cohorts, and serum samples were analyzed in the third cohorts. **B–E**, Calprotectin levels correlated with numbers of swollen or tender joints (**B**), disease activity as measured by the Clinical Disease Activity Index (CDAI) (**C**), and C-reactive protein (CRP) levels in cohort 1 (**D**) and in cohort 2 (**E**). **F**, CDAI scores correlated with CRP levels. **G** and **H**, Patients with elevated calprotectin levels (S100+) showed increased CDAI (**G**) and number of swollen or tender joints (**H**). In **A**, **G**, and **H**, each symbol represents a single subject. Bars show the median. ** = $P < 0.01$; *** = $P < 0.001$, by Mann-Whitney U test or Spearman's correlation test.

Odds ratios (ORs) were calculated. GraphPad Prism and SPSS software were used for the analyses. *P* values less than 0.05 were considered significant.

RESULTS

Elevated levels of calprotectin in RA patients and association with disease activity. Calprotectin is an acute-phase protein known to be elevated in several inflammatory conditions including RA (20,21). Consistent with prior findings, levels of calprotectin were elevated in our 3 RA cohorts compared to healthy subjects (*P* < 0.001) (Figure 1A). Notably, serum samples (cohort 3) exhibited higher baseline levels of calprotectin, compared to plasma samples (cohorts 1 and 2), which is consistent with findings of prior studies (27). Levels of calprotectin were not associated with any particular treatment strategy or with seropositivity (*P* = 0.10; data not shown), in contrast to previous findings (21,28). Furthermore, plasma levels of calprotectin were not associated with neutrophil count (*P* = 0.46; data not shown). Similar to findings in SLE (29), calprotectin levels have been shown to be associated with disease

activity in RA (21,30,31). Whether calprotectin would add clinical value and outperform gold standard serologic markers of disease activity, including CRP, is not known. In cohort 1, calprotectin was strongly correlated with markers of disease activity, including the number of swollen and tender joints (r = 0.49, *P* < 0.0001), CDAI (r = 0.53, *P* < 0.0001), and CRP (r = 0.62, *P* < 0.0001) (Figure 1). The correlation of calprotectin with CRP was validated in cohort 2 (r = 0.55, *P* < 0.0001) (Figure 1E).

Superiority of calprotectin to CRP in identifying patients with active disease. Next, we investigated whether calprotectin was superior to CRP in identifying patients with active disease in RA cohort 1. CRP only modestly correlated with CDAI (r = 0.31, *P* = 0.02) (Figure 1F), which was weaker compared to the correlation between calprotectin and CDAI (Figure 1C). Levels of calprotectin could be used to distinguish between patients with disease in remission versus those with active disease (*P* = 0.002) (Figure 2A), as well as between patients with low disease activity (CDAI ≤10) and those with moderate-to-high disease activity (CDAI ≥11) (*P* = 0.0005) (Figure 2B). Patients with disease in remission were indistinguishable from healthy controls
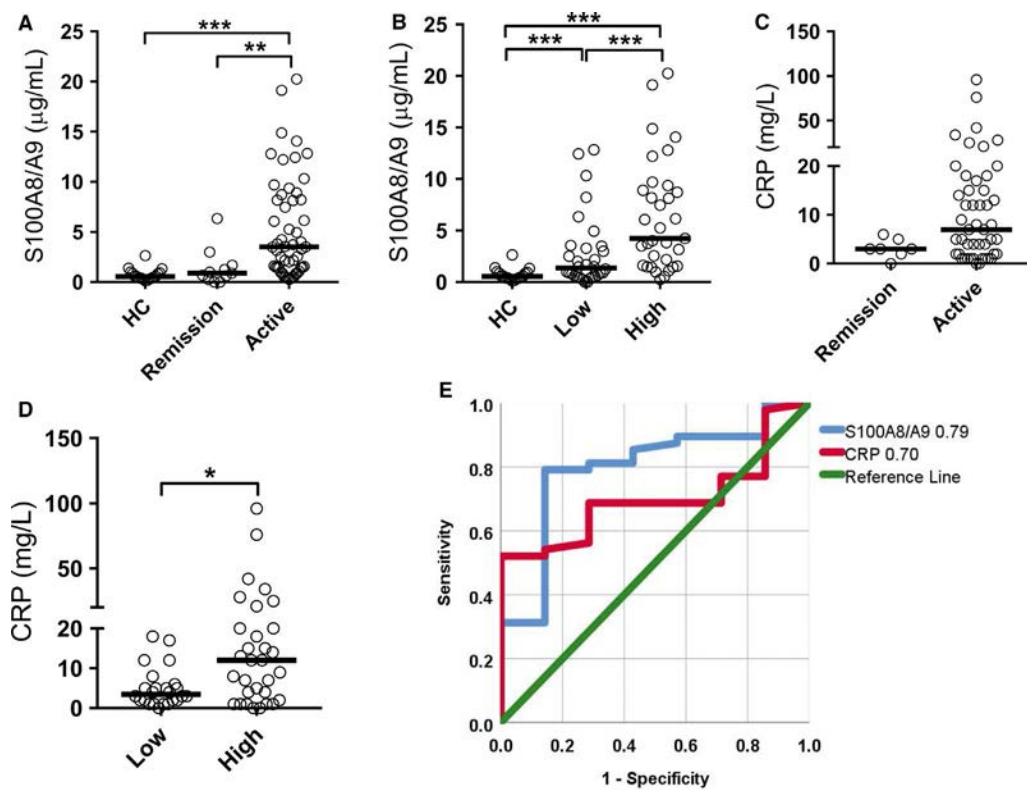
Figure 2. Superiority of calprotectin to CRP in monitoring RA disease activity. **A** and **B**, Levels of calprotectin were analyzed in plasma from healthy controls and RA patients during remission and active disease (**A**) and during low disease activity (CDAI ≤10) and high disease activity (CDAI ≥11) (**B**). **C** and **D**, Levels of CRP were analyzed in RA patients during remission and active disease (**C**) and during low disease activity and high disease activity (**D**). Each symbol represents a single subject. Bars show the median. **E**, A receiver operating characteristic curve was used to assess the capacity of calprotectin and CRP to distinguish patients with disease in remission from those with active disease. All analyses were performed using data on patients in cohort 1. * = *P* < 0.05; ** = *P* < 0.01; *** = *P* < 0.001, by Mann-Whitney U test. See Figure 1 for definitions.

(Figure 2A). CRP, on the other hand, could not be used to distinguish between patients with disease in remission and those with active disease ($P = 0.10$) (Figure 2C). However, CRP levels were elevated during high disease activity versus low disease activity ($P = 0.02$) (Figure 2D). In a receiver operating characteristic curve (ROC) analysis to identify active disease, levels of calprotectin performed better compared to CRP (ROC 0.79 and 0.70, respectively) (Figure 2E). Thus, calprotectin was found to be superior to CRP in assessing disease activity in RA.

Elevated NET levels in RA patients and association with disease activity. Neutrophils in RA patients are more prone to undergo NETosis than those in healthy controls, both spontaneously and upon activation (9,16). Serum levels of NETs and NET-derived products are elevated in RA patients and associated with disease activity (16,23,24). However, serum levels do not necessarily reflect physiologic levels of NETs in RA patients, as artificial NETs are formed upon serum processing, e.g., coagulation (16). In the current study, by using plasma samples (avoiding coagulation-mediated release of NETs) to assess true levels of NETs in patient circulation, we found that RA patients had markedly elevated NET levels compared to healthy controls ($P < 0.001$ in all 3 cohorts) (Figure 3A). In RA cohort 1, levels of

NETs were higher in seropositive patients ($P = 0.04$), including in ACPA-positive patients ($P = 0.04$) (Figure 3).

We next examined whether NET levels were associated with disease activity. In cohort 1, NET levels were elevated both in patients with disease in remission and in those with active disease ($P = 0.0003$ and $P < 0.0001$, respectively) (Figure 3D). However, there was not a statistically significant difference in NET levels between disease remission and disease flare ($P = 0.37$), nor did we find a direct correlation with CDAI ($r = 0.16$, $P = 0.19$). Given the heterogeneity in RA, and with seropositive patients showing elevated levels of NETs, we next stratified patients based on seropositivity. In seropositive patients, NET positivity could be used to distinguish between disease in remission and active disease, with a sensitivity and specificity of 68.6% and 75.0%, respectively ($P = 0.04$). In contrast, CRP levels could not be used to distinguish disease in remission from active disease (sensitivity 37.8% and specificity 100%; $P = 0.16$). Thus, NETs are increased in RA and associated with disease activity, particularly in seropositive disease.

Impaired capacity to degrade NETs in RA. The reason that elevated levels of NETs are present in RA is not known. Prior studies have shown evidence of NET-inducing
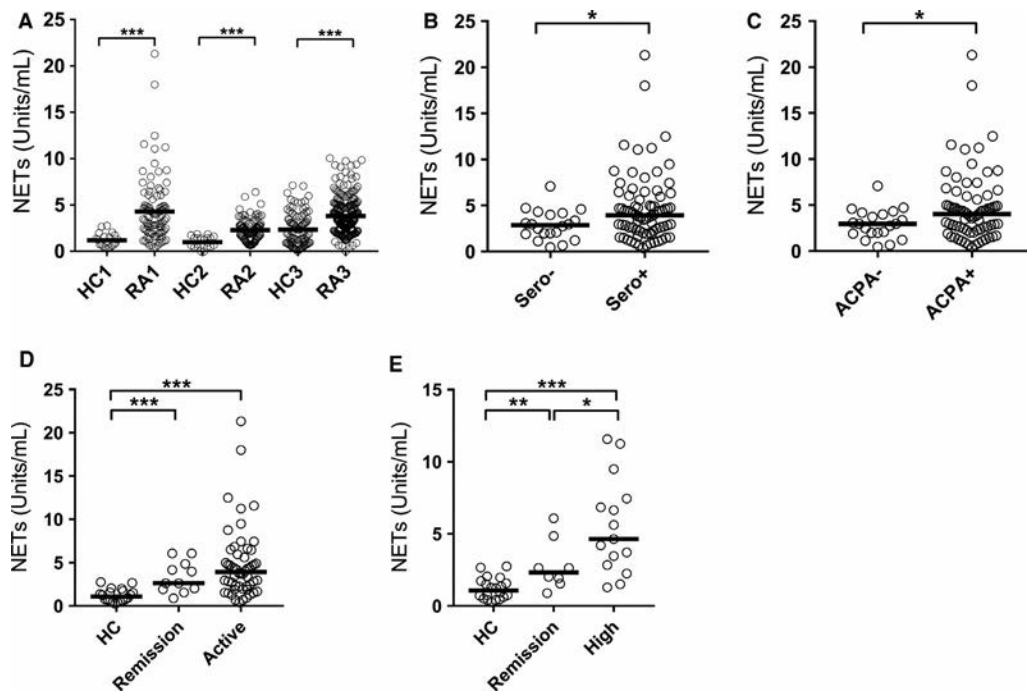
Figure 3. Increased levels of neutrophil extracellular traps (NETs) in RA. **A**, Levels of NETs (myeloperoxidase–DNA complexes) were analyzed in 3 cohorts of RA patients and 3 cohorts of healthy controls. Plasma samples were analyzed in the first and second cohorts, and serum samples were analyzed in the third cohort. **B** and **C**, RA patients were stratified according to seropositivity (Sero+ or Sero–) (**B**) and anti–citrullinated protein antibody (ACPA) positivity (**C**), and NET levels were assessed in these groups. **D**, NET levels were compared between healthy controls, RA patients with disease in remission (CDAI ≤3), and RA patients with active disease (CDAI >3). **E**, NET levels were compared between healthy controls, seropositive patients with disease in remission, and seropositive patients with high disease activity (CDAI >22). Each symbol represents a single subject. Bars show the median. All analyses were performed using data on patients in cohort 1. * = $P < 0.05$; ** = $P < 0.01$; *** = $P < 0.001$, by Mann-Whitney U test. See Figure 1 for other definitions.

stimuli (e.g., autoantibodies and inflammatory cytokines) in RA (9), as well as enhanced NET-forming capacity of neutrophils (9,16). However, impaired clearance may also promote accumulation of NETs in the circulation. It has been shown that NET degradation is impaired in SLE and is associated with disease activity and interferon induction (26,32). To determine whether NET degradation is also impaired in RA patients, the capacity of patient sera to degrade NETs was assessed using an in-house assay. As illustrated in Figure 4A, RA sera showed an overall reduced ability to degrade NETs ($P < 0.0001$ in cohort 3). Notably, plasma from RA patients did not have a reduced capacity to degrade DNA (Figure 4B). These data suggest that a NET-specific factor such as anti-NET antibodies, rather than reduced DNase I levels, contributes to the impaired degradation of NETs. Patients with a low capacity to degrade NETs showed increased disease activity ($P = 0.04$ in cohort 1) (Figure 4C). Furthermore, in cohort 1, reduced capacity to degrade NETs and/or elevated levels of circulating NETs were associated with increased inflammation, in particular IL-6 levels ($P = 0.03$ and $P = 0.0002$, respectively) (Figures 4D and E). Unexpectedly, the ability to degrade NETs did not correlate with levels of circulating NETs (r = 0.02, $P = 0.87$). Moreover, even patients with sufficient NET degradation capability had elevated levels of NETs compared to healthy controls ($P < 0.0001$) (Figure 4F),

suggesting that reduced NET degradation is not responsible for the accumulation of NETs in RA patients.

Circulating neutrophil-activating factors in RA. Considering the elevated levels of neutrophil-derived activation markers in peripheral blood from RA patients, we next investigated whether RA patients had circulating factors acting to induce neutrophil activation. Using a functional in vitro assay to assess serum-mediated neutrophil activation, RA sera from patients in cohort 1 were found to induce marked neutrophil activation, as illustrated by CD11b and CD66b up-regulation, compared to sera from healthy controls ($P < 0.0001$) (Figures 5A and B). Serum-mediated neutrophil activation was further increased in seropositive individuals ($P = 0.02$) (Figures 5C and D) and was related to disease severity, e.g., erosive disease (Figures 5E and F). Consistent with our hypothesis, serum-mediated neutrophil activation was found to be associated with elevated levels of circulating calprotectin (r = 0.40, $P < 0.0001$). Additionally, serum-mediated neutrophil activation was associated with elevated levels of circulating NETs in RA patients ($P = 0.04$) (Figure 5G). Given the findings of prior studies in SLE (2,33), we anticipated that immune complexes would participate in the observed serum-mediated neutrophil activation. Supporting this hypothesis was the finding that blocking of neutrophil
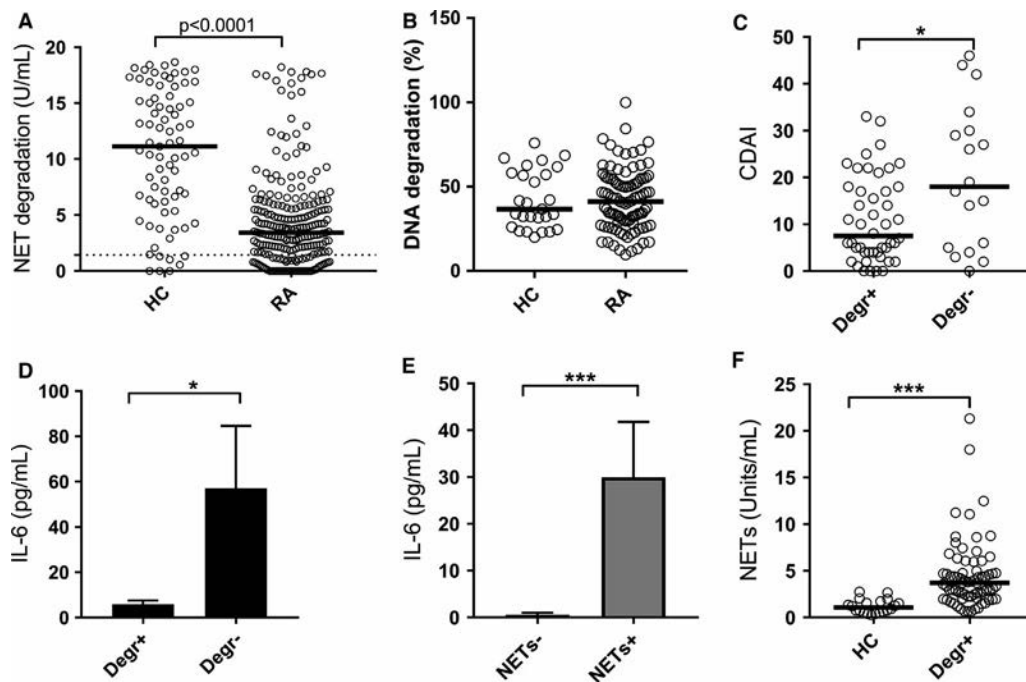
Figure 4. Impaired neutrophil extracellular trap (NET) degradation in RA. **A**, The capacity to degrade NETs was analyzed in sera from healthy controls and RA patients in cohort 3. The dotted line shows the cutoff for impaired NET degradation. **B**, The ability to degrade isolated DNA was analyzed in sera from healthy controls and RA patients in cohort 1. **C**, CDAI scores were compared between patients in cohort 1 who were stratified according to capacity to degrade NETs (Degr+) or not (Degr–). **D** and **E**, Serum levels of interleukin-6 (IL-6) in relation to NET degradation (**D**) and circulating NET levels (**E**) in cohort 1 were assessed. Values are the mean ± SD. **F**, NET levels were compared between cohort 1 healthy controls and RA patients with normal NET-degrading capacity. In **A**, **B**, **C**, and **F**, each symbol represents a single subject. Bars show the median. * = $P < 0.05$; *** = $P < 0.001$, by Mann-Whitney U test. See Figure 1 for other definitions.
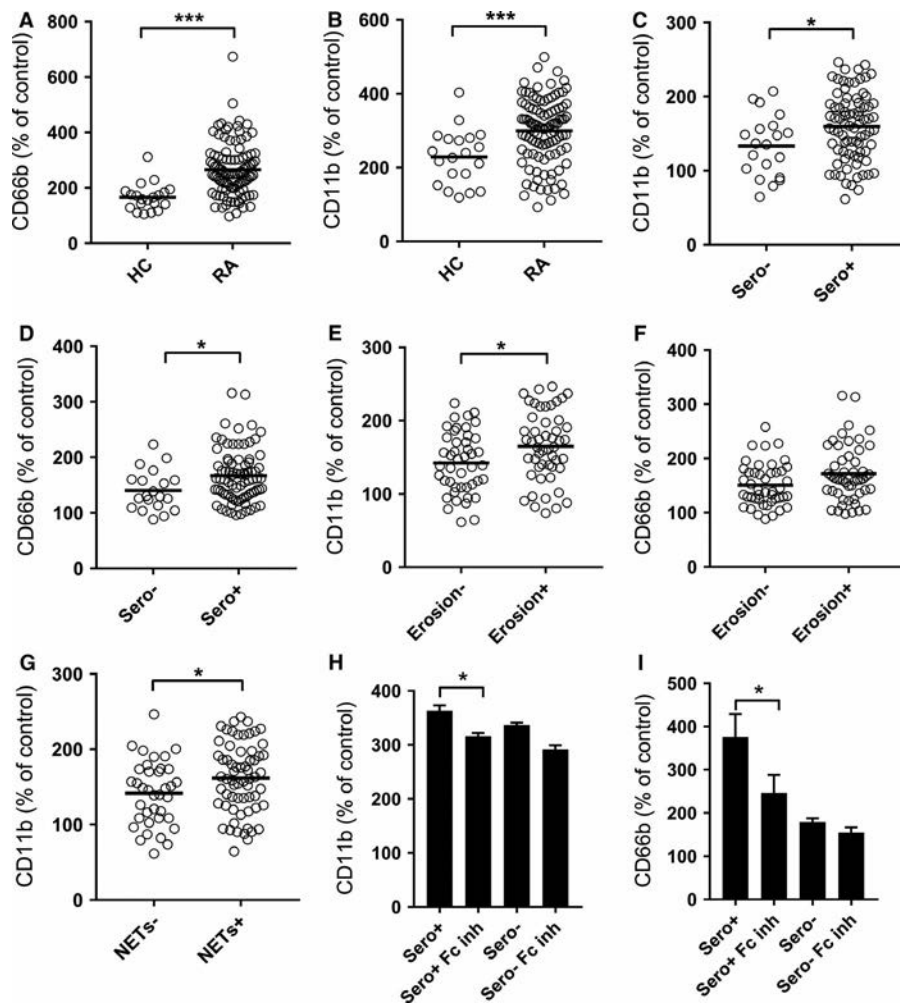
Figure 5. Serum-mediated neutrophil activation. **A** and **B**, Sera from healthy controls (HCs) and rheumatoid arthritis (RA) patients were incubated with normal neutrophils and assessed for the capacity to induce up-regulation of neutrophil activation markers CD66b (**A**) and CD11b (**B**). The values are related to unstimulated neutrophils (set at 100%). **C–F**, RA patients were stratified according to seropositivity (Sero+ or Sero–) (**C** and **D**) and erosion (**E** and **F**), and analyzed for CD11b up-regulation (**C** and **E**) and CD66b up-regulation (**D** and **F**). **G**, CD11b up-regulation was analyzed by stratifying RA patients according to presence of circulating neutrophil extracellular traps (NETs). **H** and **I**, Neutrophils were preincubated with anti–Fcγ receptor IIa (FcγRIIa) and anti-FcγRIIIb (Fc inh) prior to the addition of RA sera and assessed for CD11b up-regulation (**H**) and CD66b up-regulation (**I**). Patients were stratified according to seropositivity. Values are the mean ± SD. In **A–G**, each symbol represents a single subject. Bars show the median. All analyses were performed using data on patients in cohort 1. * = $P < 0.05$; *** = $P < 0.001$, by Mann-Whitney U test or Wilcoxon's paired test.

Fcγ receptor IIa (FcγRIIa) and FcγRIIIb, particularly in seropositive RA patients, reduced the capacity of RA sera to induce CD66b and CD11b up-regulation ($P = 0.02$) (Figures 5H and I). Notably, FcγR blockade only partially reduced the CD11b and CD66b levels, clearly suggesting that other factors, including inflammatory cytokines, may also contribute to neutrophil activation in RA.

Prediction of disease outcomes by neutrophil levels. Calprotectin is known as an independent predictor of radiographic changes in RA (21,22). However, whether NETs can also predict radiographic changes, the role of neutrophil biomarkers in the prediction of extraarticular disease, and whether there would be added value in using a biomarker panel rather than individual biomarkers have not yet been elucidated. To investigate these

questions, we analyzed levels of calprotectin in a longitudinal inception cohort of 250 RA patients (cohort 3) seen for a median of 8 years of follow-up after RA onset. Patients with evidence of erosive disease at inception (10%) were excluded from further analysis. As a comparator, we analyzed ACPA positivity, which is known to predict a severe erosive disease (34). Consistent with conclusions from previous literature, ACPA positivity and calprotectin were independent predictors of radiographic changes in RA (Table 1). As these 2 biomarkers were independently associated with radiographic change, we next explored whether combining the markers would improve the prognostic value. As illustrated in Table 1, a biomarker panel requiring positivity for both ACPA and calprotectin (ACPA–S100) was superior to the individual markers in detecting erosive disease and joint space narrowing. Patients

Table 1. Prognostic capacity of neutrophil biomarkers

	Erosion				Joint space narrowing				Extraarticular nodules			
	Sensitivity, %	Specificity, %	Odds ratio	P	Sensitivity, %	Specificity, %	Odds ratio	P	Sensitivity, %	Specificity, %	Odds ratio	P
ACPA	85.7	50.0	6.0	0.002	70.4	45.4	2.0	0.15	70.6	45.5	2.0	0.22
S100A8/A9	45.2	87.3	5.6	0.0002	37.5	85.3	3.5	0.006	42.1	82.0	3.3	0.02
NETs	32.3	74.5	1.4	0.45	31.3	74.3	1.3	0.53	52.6	76.3	3.6	0.01
CD66b	32.1	82.3	2.2	0.10	29.6	81.4	1.8	0.22	41.2	83.7	3.6	0.02
BioNeu*	64.5	58.2	2.5	0.03	59.4	56.9	1.9	0.11	78.9	57.6	5.1	0.006
ACPA–S100†	46.4	89.6	7.5	<0.0001	40.7	87.6	4.9	0.001	41.2	84.6	3.8	0.02

* Positivity for S100A8/A9 (calprotectin), neutrophil extracellular traps (NETs), or CD66b.
† Positivity for both anti–citrullinated protein antibody (ACPA) and S100A8/A9.

positive for ACPA–S100 had increased odds of developing erosive disease (OR 7.5, $P < 0.0001$) and joint space narrowing (OR 4.9, $P = 0.001$), compared to those positive for calprotectin alone (OR 5.6 [$P = 0.0002$] and OR 3.5 [$P = 0.006$], respectively) and to those positive for ACPA alone (OR 6.0 [$P = 0.002$] and OR 2.0 [$P = 0.15$], respectively). Thus, the combined ACPA–S100 biomarker demonstrated improved prognostic capacity.

Although it is considered to be an articular disease, ~50% of patients with RA develop extraarticular disease (with nodules), which is commonly associated with increased morbidity and mortality (35). However, whether neutrophil biomarkers are able to predict development of extraarticular nodules was not previously known. To determine this, we measured a broad range of neutrophil markers (NETs, calprotectin, and CD66b induction) in the longitudinal RA inception cohort, and investigated whether individual neutrophil biomarkers, and/or a "neutrophil activation signature" could predict future extraarticular disease. In cohort 3, 23 of 165 RA patients (14%) had developed extraarticular nodules at follow-up. All of the neutrophil markers were able to predict extraarticular nodules (Table 1). Creating a biomarker score, referred to here as BioNeu, that identified patients using a neutrophil activation signature (e.g., positivity for any of the neutrophil activation markers) improved the ability to predict extraarticular nodule development (OR 5.1, $P = 0.006$) (Table 1). Only 1 patient was recorded as having developed interstitial lung disease; therefore, no further analyses on this extraarticular disease could be performed. Our findings indicate that neutrophil activation at inception is an early sign of severe erosive disease and is predictive of development of extraarticular nodules.

DISCUSSION

Neutrophils are instrumental immune cells in RA pathogenesis, infiltrating the joint through immune complex– and complement-mediated mechanisms and participating in the release of proteolytic enzymes that cause tissue damage and inflammation (36). However, even though neutrophils are known to play a central role in the disease pathogenesis, neutrophil biomarkers are seldom used in a clinical setting, and their clinical value compared to that of current established markers, such as CRP and ACPA, had not previously

been evaluated. In the current study, we proposed that a neutrophil biomarker panel, either individually or when combined with currently established markers, may offer significant clinical value and improve the capacity to monitor disease activity, allowing for the ability to predict future morbidities such as erosion and extraarticular disease. Furthermore, our findings highlight the essential role of neutrophils in RA pathogenesis and support the development of therapies that target neutrophil-mediated inflammation in these patients.

Neutrophils have several effector functions enabling efficient disposal of invading pathogens, including release of inflammatory mediators such as calprotectin. Also known as S100A8/A9, calprotectin is a heterodimer that functions as an intracellular calcium-binding protein. When released into the extracellular environment, however, it acts as an efficient damage-associated molecular pattern (DAMP), signaling through Toll-like receptor 4 and the receptor for advanced glycation end products to induce inflammation. Additionally, calprotectin may facilitate extravasation of immune cells into tissue (37). Previous reports have described production of calprotectin by several immune cells, including plasmacytoid dendritic cells (38) and platelets (27), although the majority of calprotectin (comprising 40% of the cytosolic content) is derived from neutrophils (39). Elevated levels of calprotectin are found in many inflammatory diseases and are used clinically in the diagnosis of inflammatory bowel disease (40). In chronic inflammatory diseases such as RA, calprotectin levels have been described as early as 1988 and have been shown to be related to markers of inflammation, disease activity, and radiographic progression (20–22,30,31,41).

In the current study, we were able to validate and add to previous findings. For instance, calprotectin was shown to be superior to CRP in assessing disease activity, which is a novel observation that further strengthens the clinical potential of this neutrophil-derived marker. However, the main novelty and significant finding is not in the capacity to identify patients with active disease or the added diagnostic potential. Rather, it is that calprotectin, in combination with ACPA, may improve the ability to identify patients prone to developing erosive disabling disease, including joint space narrowing. This is an important finding that may allow for closer monitoring as well as expedited and aggressive treatment of these patients, in order to avoid disabling

(and potentially permanent) disease progression and to improve their quality of life.

Recently, neutrophil cell death, also known as NETosis, was proposed to be involved in RA pathogenesis. It has been observed that RA-associated autoantibodies and inflammatory cytokines activate neutrophils to undergo NET formation and subsequent induction of synovial inflammation, in addition to the presentation of NET-derived citrullinated peptides to antigen-specific T cells by FLS (9,17). Even though NETosis has been implicated in RA pathogenesis, the role of NETs in vivo, both in mice and humans, is controversial. In mouse models of RA, PAD4 inhibition, using the synthetic chemical Cl-amidine, ameliorated disease development in the CIA model (18). In stark contrast, PAD4 knockout (though dependent on neutrophils for disease progression [42]) did not rescue arthritis phenotype in the K/BxN serum–transfer mouse model (19). Whether the contrasting results are due to differences in the disease pathogenesis of the select mouse models and/or to potential off-target effects of Cl-amidine has not yet been determined.

In human RA, early observations demonstrated elevated levels of NET-derived fragments, including cell-free DNA or neutrophil-derived granular proteins (e.g., MPO), in the circulation of RA patients, with a few reports describing even MPO–DNA complexes as being associated with disease activity (16,23,24). However, given the marked effect of coagulation in promoting neutrophil activation and de novo NETosis (16), and the particular propensity of RA neutrophils to undergo NETosis ex vivo (9,16), these studies assessing NET levels in serum did not reflect true NET levels seen in patients. Our investigation is the first to demonstrate true NET levels in plasma from RA patients and their relation to disease activity. Our observation that NET levels are elevated even during clinical remission is of particular interest and suggests chronicity in the immunologic and inflammatory response, even when in the absence of overt disease. Whether this low-grade inflammation indicates a propensity to develop atherosclerosis or other comorbidities is not known. However, we did make the novel observation that levels of NETs predicted development of a common extraarticular disease, namely RA nodules. The underlying mechanisms for this association are not clear and further investigation is needed.

The elevated levels of circulating NETs observed in RA could be due to either increased formation of NETs and/or decreased clearance of NETs. Consistent with the first hypothesis, prior findings have demonstrated increased capacity of RA neutrophils to undergo NETosis (9,16), with RA-associated autoantibodies and inflammatory cytokines driving NET formation (9,43). Similarly, we found that RA patients had circulating factors (e.g., immune complexes) promoting neutrophil activation ex vivo. Thus, there are several potential triggers of NETosis operating in RA that may account for the increased levels of circulating NETs. However, we also observed select reduced NET degradation (but not DNA degradation) in these patients, similar to what has been described in SLE by us and others (32,44). Given the presence of anti-NET antibodies in RA, including the ones targeting citrullinated histones,

and previous findings suggesting normal levels of DNase1L3 (45), we anticipate that a similar mechanism as that described in SLE (32) also operates in RA (e.g., autoantibody-mediated blockade of DNase I). Regardless of the mechanism, NET clearance alone did not account for the overall increase in NETosis, as RA patients with sufficient NET degradation had elevated levels of circulating NETs. As such, targeting NET formation rather than clearance would likely be a more beneficial therapeutic approach.

In conclusion, neutrophils are instrumental in RA pathogenesis and reflect key processes that are not currently captured efficiently in clinical settings. Our data clearly demonstrate the clinical value of neutrophil-derived biomarkers and/or panels in monitoring disease activity and predicting disease severity. Future studies are needed to validate our findings in larger cohorts as well as to evaluate whether early identification of these patients would lead to effective preventative treatment strategies.

AUTHOR CONTRIBUTIONS

All authors were involved in drafting the article or revising it critically for important intellectual content, and all authors approved the final version to be published. Dr. Lood had full access to all of the data in the study and takes responsibility for the integrity of the data and the accuracy of the data analysis.
Study conception and design. Bach, Nelson, Lood.
Acquisition of data. Moon, Moore, Pan, Nelson, Lood.
Analysis and interpretation of data. Bach, Pan, Lood.

REFERENCES

1. Kaplan MJ, Radic M. Neutrophil extracellular traps: double-edged swords of innate immunity. J Immunol 2012;189:2689–95.

2. Lood C, Blanco LP, Purmalek MM, Carmona-Rivera C, De Ravin SS, Smith CK, et al. Neutrophil extracellular traps enriched in oxidized mitochondrial DNA are interferogenic and contribute to lupus-like disease. Nat Med 2016;22:146–53.

3. Lood C, Hughes GC. Neutrophil extracellular traps as a potential source of autoantigen in cocaine-associated autoimmunity. Rheumatology (Oxford) 2017;56:638–43.

4. Kolaczkowska E, Kubes P. Neutrophil recruitment and function in health and inflammation. Nat Rev Immunol 2013;13:159–75.

5. Nathan C. Neutrophils and immunity: challenges and opportunities. Nat Rev Immunol 2006;6:173–82.

6. Pham CT. Neutrophil serine proteases: specific regulators of inflammation. Nat Rev Immunol 2006;6:541–50.

7. Garcia-Romo GS, Caielli S, Vega B, Connolly J, Allantaz F, Xu Z, et al. Netting neutrophils are major inducers of type I IFN production in pediatric systemic lupus erythematosus. Sci Transl Med 2011;3:73ra20.

8. Villanueva E, Yalavarthi S, Berthier CC, Hodgin JB, Khandpur R, Lin AM, et al. Netting neutrophils induce endothelial damage, infiltrate tissues, and expose immunostimulatory molecules in systemic lupus erythematosus. J Immunol 2011;187:538–52.

9. Khandpur R, Carmona-Rivera C, Vivekanandan-Giri A, Gizinski A, Yalavarthi S, Knight JS, et al. NETs are a source of citrullinated autoantigens and stimulate inflammatory responses in rheumatoid arthritis. Sci Transl Med 2013;5:178ra140.

10. Wright HL, Moots RJ, Edwards SW. The multifactorial role of neutrophils in rheumatoid arthritis [review]. Nat Rev Rheumatol 2014;10:593–601.

11. Elkon KB. Poking holes in rheumatoid joints. Sci Transl Med 2013;5:209fs239.

12. Romero V, Fert-Bober J, Nigrovic PA, Darrah E, Haque UJ, Lee DM, et al. Immune-mediated pore-forming pathways induce cellular hypercitrullination and generate citrullinated autoantigens in rheumatoid arthritis. Sci Transl Med 2013;5:209ra150.

13. Corsiero E, Bombardieri M, Carlotti E, Pratesi F, Robinson W, Migliorini P, et al. Single cell cloning and recombinant monoclonal antibodies generation from RA synovial B cells reveal frequent targeting of citrullinated histones of NETs. Ann Rheum Dis 2016;75:1866–75.

14. Dwivedi N, Upadhyay J, Neeli I, Khan S, Pattanaik D, Myers L, et al. Felty's syndrome autoantibodies bind to deiminated histones and neutrophil extracellular chromatin traps. Arthritis Rheum 2012;64:982–92.

15. Pratesi F, Dioni I, Tommasi C, Alcaro MC, Paolini I, Barbetti F, et al. Antibodies from patients with rheumatoid arthritis target citrullinated histone 4 contained in neutrophils extracellular traps. Ann Rheum Dis 2014;73:1414–22.

16. Sur Chowdhury C, Giaglis S, Walker UA, Buser A, Hahn S, Hasler P. Enhanced neutrophil extracellular trap generation in rheumatoid arthritis: analysis of underlying signal transduction pathways and potential diagnostic utility. Arthritis Res Ther 2014;16:R122.

17. Carmona-Rivera C, Carlucci PM, Moore E, Lingampalli N, Uchtenhagen H, James E, et al. Synovial fibroblast-neutrophil interactions promote pathogenic adaptive immunity in rheumatoid arthritis. Sci Immunol 2017;2:eaag3358.

18. Papadaki G, Kambas K, Choulaki C, Vlachou K, Drakos E, Bertsias G, et al. Neutrophil extracellular traps exacerbate Th1-mediated autoimmune responses in rheumatoid arthritis by promoting DC maturation. Eur J Immunol 2016;46:2542–54.

19. Rohrbach AS, Hemmers S, Arandjelovic S, Corr M, Mowen KA. PAD4 is not essential for disease in the K/BxN murine autoantibody-mediated model of arthritis. Arthritis Res Ther 2012;14:R104.

20. Kuruto R, Nozawa R, Takeishi K, Arai K, Yokota T, Takasaki Y. Myeloid calcium binding proteins: expression in the differentiated HL-60 cells and detection in sera of patients with connective tissue diseases. J Biochem 1990;108:650–3.

21. Abildtrup M, Kingsley GH, Scott DL. Calprotectin as a biomarker for rheumatoid arthritis: a systematic review. J Rheumatol 2015;42:760–70.

22. Hammer HB, Ødegård S, Syversen SW, Landewé R, van der Heijde D, Uhlig T, et al. Calprotectin (a major S100 leucocyte protein) predicts 10-year radiographic progression in patients with rheumatoid arthritis. Ann Rheum Dis 2010;69:150–4.

23. Kaneko C, Kobayashi T, Ito S, Sugita N, Murasawa A, Nakazono K, et al. Circulating levels of carbamylated protein and neutrophil extracellular traps are associated with periodontitis severity in patients with rheumatoid arthritis: a pilot case-control study. PLoS One 2018;13:e0192365.

24. Pérez-Sánchez C, Ruiz-Limón P, Aguirre MA, Jiménez-Gómez Y, Arias-de la Rosa I, Ábalos-Aguilera MC, et al. Diagnostic potential of NETosis-derived products for disease activity, atherosclerosis and therapeutic effectiveness in rheumatoid arthritis patients. J Autoimmun 2017;82:31–40.

25. Aletaha D, Nell VP, Stamm T, Uffmann M, Pflugbeil S, Machold K, et al. Acute phase reactants add little to composite disease activity indices for rheumatoid arthritis: validation of a clinical activity score. Arthritis Res Ther 2005;7:R796–806.

26. Leffler J, Gullstrand B, Jönsen A, Nilsson JÅ, Martin M, Blom AM, et al. Degradation of neutrophil extracellular traps co-varies with disease activity in patients with systemic lupus erythematosus. Arthritis Res Ther 2013;15:R84.

27. Lood C, Tydén H, Gullstrand B, Jönsen A, Källberg E, Mörgelin M, et al. Platelet-derived S100A8/A9 and cardiovascular disease in systemic lupus erythematosus. Arthritis Rheumatol 2016;68:1970–80.

28. Hammer HB, Haavardsholm EA, Kvien TK. Calprotectin (a major leucocyte protein) is associated with the levels of anti-CCP and rheumatoid factor in a longitudinal study of patients with very early rheumatoid arthritis. Scand J Rheumatol 2008;37:179–82.

29. Tydén H, Lood C, Gullstrand B, Jönsen A, Ivars F, Leanderson T, et al. Pro-inflammatory S100 proteins are associated with glomerulonephritis and anti-dsDNA antibodies in systemic lupus erythematosus. Lupus 2017;26:139–49.

30. Hurnakova J, Zavada J, Hanova P, Hulejova H, Klein M, Mann H, et al. Serum calprotectin (S100A8/9): an independent predictor of ultrasound synovitis in patients with rheumatoid arthritis. Arthritis Res Ther 2015;17:252.

31. Hurnakova J, Hulejova H, Zavada J, Hanova P, Komarc M, Mann H, et al. Relationship between serum calprotectin (S100A8/9) and clinical, laboratory and ultrasound parameters of disease activity in rheumatoid arthritis: a large cohort study. PLoS One 2017;12:e0183420.

32. Leffler J, Martin M, Gullstrand B, Tydén H, Lood C, Truedsson L, et al. Neutrophil extracellular traps that are not degraded in systemic lupus erythematosus activate complement exacerbating the disease. J Immunol 2012;188:3522–31.

33. Lood C, Arve S, Ledbetter J, Elkon KB. TLR7/8 activation in neutrophils impairs immune complex phagocytosis through shedding of FcγRIIA. J Exp Med 2017;214:2103–19.

34. Jilani AA, Mackworth-Young CG. The role of citrullinated protein antibodies in predicting erosive disease in rheumatoid arthritis: a systematic literature review and meta-analysis. Int J Rheumatol 2015;2015:728610.

35. Das S, Padhan P. An overview of the extraarticular involvement in rheumatoid arthritis and its management. J Pharmacol Pharmacother 2017;8:81–6.

36. Paoliello-Paschoalato AB, Marchi LF, de Andrade MF, Kabeya LM, Donadi EA, Lucisano-Valim YM. Fcγ and complement receptors and complement proteins in neutrophil activation in rheumatoid arthritis: contribution to pathogenesis and progression and modulation by natural products [review]. Evid Based Complement Alternat Med 2015;2015:429878.

37. Schiopu A, Cotoi OS. S100A8 and S100A9: DAMPs at the crossroads between innate immunity, traditional risk factors, and cardiovascular disease [review]. Mediators Inflamm 2013;2013:828354.

38. Lood C, Stenström M, Tydén H, Gullstrand B, Källberg E, Leanderson T, et al. Protein synthesis of the pro-inflammatory S100A8/A9 complex in plasmacytoid dendritic cells and cell surface S100A8/A9 on leukocyte subpopulations in systemic lupus erythematosus. Arthritis Res Ther 2011;13:R60.

39. Teigelkamp S, Bhardwaj RS, Roth J, Meinardus-Hager G, Karas M, Sorg C. Calcium-dependent complex assembly of the myeloic differentiation proteins MRP-8 and MRP-14. J Biol Chem 1991;266:13462–7.

40. Walsham NE, Sherwood RA. Fecal calprotectin in inflammatory bowel disease. Clin Exp Gastroenterol 2016;9:21–9.

41. Berntzen HB, Munthe E, Fagerhol MK. The major leukocyte protein L1 as an indicator of inflammatory joint disease. Scand J Rheumatol Suppl 1988;76:251–6.

42. Wipke BT, Allen PM. Essential role of neutrophils in the initiation and progression of a murine model of rheumatoid arthritis. J Immunol 2001;167:1601–8.

43. Aleyd E, Al M, Tuk CW, van der Laken CJ, van Egmond M. IgA complexes in plasma and synovial fluid of patients with rheumatoid arthritis induce neutrophil extracellular traps via FcαRI. J Immunol 2016;197:4552–9.

44. Hakkim A, Fürnrohr BG, Amann K, Laube B, Abed UA, Brinkmann V, et al. Impairment of neutrophil extracellular trap degradation is associated with lupus nephritis. Proc Natl Acad Sci U S A 2010;107:9813–8.

45. Zhao Q, Yang C, Wang J, Li Y, Yang P. Serum level of DNase1l3 in patients with dermatomyositis/polymyositis, systemic lupus erythematosus and rheumatoid arthritis, and its association with disease activity. Clin Exp Med 2017;17:459–65.

AMERICAN COLLEGE
of RHEUMATOLOGY
Empowering Rheumatology Professionals

Sepiapterin Reductase Inhibition Leading to Selective Reduction of Inflammatory Joint Pain in Mice and Increased Urinary Sepiapterin Levels in Humans and Mice

Masahide Fujita,[1] Débora da Luz Scheffer,[1] Bruna Lenfers Turnes,[1] Shane J. F. Cronin,[2] Alban Latrémolière,[1] Michael Costigan,[1] Clifford J. Woolf,[1] Alexandra Latini,[1] and Nick A. Andrews[1] ID

Objective. To evaluate the antiinflammatory and analgesic effects of sepiapterin reductase (SPR) inhibition in a mouse model of inflammatory joint disease, and to determine whether urinary sepiapterin levels, as measured in mice and healthy human volunteers, could be useful as a noninvasive, translational biomarker of SPR inhibition/target engagement.

Methods. The collagen antibody–induced arthritis (CAIA) model was used to induce joint inflammation in mice. The effects of pharmacologic inhibition of SPR on thresholds of heat-, cold-, and mechanical-evoked pain sensitivity and on signs of inflammation were tested in mice with CAIA. In addition, mice and healthy human volunteers were treated with SPR inhibitors, and changes in urinary sepiapterin levels were analyzed by high-performance liquid chromatography.

Results. CAIA in mice was characterized by 2 phases: in the acute inflammation (early) phase, joint inflammation and heat-, mechanical-, and cold-induced pain hypersensitivity were present, while in the postinflammation (late) phase, no joint inflammation was observed but heat- and mechanical-induced hypersensitivity, but not cold hypersensitivity, were present. Inhibition of SPR in mice with CAIA significantly attenuated the heat-induced hyperalgesia in both phases, and the mechanical allodynia in the late phase. Signs of inflammation were unaffected by SPR inhibition. Urinary tetrahydrobiopterin levels, as a marker of inflammatory pain, were increased during inflammation in mice with CAIA (2-fold increase over controls; $P < 0.05$) and significantly reduced by SPR inhibition ($P < 0.05$ versus vehicle-treated mice). Increased urinary sepiapterin levels in the presence of SPR inhibition in both mice and healthy human volunteers were associated with high sensitivity (70–85%) and high specificity (82–88%) for the prediction of SPR inhibition/target engagement.

Conclusion. SPR inhibition reduces the pain associated with joint inflammation, thus showing its potential utility as an analgesic strategy for inflammatory joint pain. In addition, SPR inhibition increases urinary sepiapterin levels, indicating the potential of this measurement as a noninvasive biomarker of target engagement of SPR inhibitors, such as sulfasalazine, a disease-modifying antirheumatic drug that is currently used as a first-line treatment for rheumatoid arthritis.

INTRODUCTION

Tetrahydrobiopterin (BH4) has been traditionally described as a mandatory cofactor for aromatic amino acid hydroxylases, all

nitric oxide (NO) synthase isoforms, and alkylglycerol monooxygenase (for review, see refs. 1 and 2). The enzyme sepiapterin reductase (SPR) plays a dual role in the regulation of BH4 intracellular levels: SPR catalyzes the last step of the de novo BH4

synthetic pathway, which initiates from GTP, and also participates in the BH4 biosynthetic salvage pathway, using sepiapterin and 7,8-dihydrobiopterin (BH2) as metabolic intermediates (2,3).

Increased BH4 levels in injured sensory neurons and inflamed tissue are correlated with pain severity scores both in humans and in mice (4), and reducing BH4 production by treatment of mice with a small-molecule SPR inhibitor (SPRi3) reduces pain and inflammation in mice with granulomatous skin (complete Freund's adjuvant [CFA] granulomatous inflammation model) or in experimental mouse models of joint inflammation, and reduces the release of NO from macrophages in vitro (5). Recently, it was also discovered that SPR inhibition reduces T cell proliferation and decreases both autoimmune and type 2 allergic inflammation (6).

In the present study we investigated whether inhibition of SPR by treatment with 2 chemically distinct SPR inhibitors, SPRi3 and QM385, would reduce pain in the CAIA mouse model of inflammatory joint pain. The model differs from the granulomatous CFA model because it is induced by injection of a cocktail of 5 mouse monoclonal antibodies that recognize conserved individual epitopes on LyC1 and LyC2 of the CB11 fragment of various species of type II collagen (7). After a trigger injection of lipopolysaccharide (LPS), there is rapid onset of clinical signs of arthritis (swelling and redness, with a peak at 8–12 days and lasting for up to 28 days postinduction) accompanied by persistent mechanical and thermal hypersensitivity, lasting at least 55 days postinduction (7).

Biomarkers have many essential uses, including confirmation of target engagement, aiding dose selection for efficacy, and minimizing adverse effects (8). We have shown that sepiapterin levels in plasma and sensory neurons can reflect the degree of SPR inhibition in vitro and in vivo (5,6), suggesting that sepiapterin could be used as a biomarker for SPR inhibition. In this study we assessed the reliability of sepiapterin levels in the urine as a biomarker for SPR inhibition, both in mice and in humans. Additionally, in a human volunteer study we used sulfasalazine (SSZ), a small-molecule disease-modifying antirheumatic drug (DMARD) commonly recommended as a first-line treatment in patients with rheumatoid arthritis (RA) (9). SSZ inhibits SPR in vitro at high concentrations (10), and we have now extended these investigations to determine whether SSZ inhibits SPR in vivo.

MATERIALS AND METHODS

Animals. Male BALB/c mice (9–10 weeks old; Jackson Laboratory) were housed in groups of 5, with food and water available ad libitum, in a temperature-controlled room (mean ± SD 22 ± 1°C, 45–55% humidity) maintained on a 12-hour light/dark cycle (lights on from 7:00 AM to 7:00 PM); the mice were used after at least 1 week of acclimatization. All animal procedures were approved by the Boston Children's Hospital Institutional Animal Care and Use Committee.

Healthy human volunteers. A group of 10 pain-free human subjects (male n = 4, female n = 6; mean ± SD age 31.9 ± 6.7 years) from Florianópolis, Brazil were recruited. None of the subjects were taking any medication for pain symptoms, and none reported any symptoms of pain prior to or during the study. Each volunteer collected 1 sample of urine before initiating treatment with SSZ, and 3 days thereafter began taking a 500-mg tablet of SSZ approximately every 6 hours (total dosage 2 gm/day); each subsequent day post–SSZ initiation, the subjects collected a sample of the first voided urine each morning. After the third day of SSZ treatment, volunteers did not take any further doses of SSZ but continued to collect a sample of the first voided urine of the day for 4 more days. A total of 8 urine samples per volunteer were collected for analysis. All treatments and urine collections were completed between June 2017 and July 2017.

Studies in healthy human volunteers were performed in accordance with the principles of the Declaration of Helsinki. Written informed consent was received from all participants prior to inclusion (Ethical Committee for Research in Humans, Universidade Federal de Santa Catarina, Brazil; protocol no. CAAE 54297916.7.0000.0121).

CAIA model induction. Mice were randomly assigned to either the CAIA group or the control group, with both treatments represented in every cage. The control mice were injected with nonspecific IgG and tested together with the mice with experimental CAIA in a blinded manner. On day 0, mice assigned to the experimental CAIA group received an injection (1.5 mg intraperitoneally [IP]) of a cocktail of 5 monoclonal antibodies (clone A2-10 [IgG2a], F10-21 [IgG2a], D8-6 [IgG2a], D1-2G [IgG2b], and D2-112 [IgG2b]) recognizing the conserved epitopes on various species of type II collagen (Chondrex). On day 3, all control and experimental CAIA mice were injected IP with LPS (50 μg/mouse; Chondrex), since LPS is known to enhance arthritis induction (7).

Behavioral testing for responses to thermal, mechanical, and cold stimuli. To ensure the equivalency of baseline data prior to dosing of the test compound, treatments were allocated a letter (A or B) and mice were ranked from low to high in terms of heat-response latencies or mechanical-evoked pain sensitivity. Treatments were then allocated in order, resulting in random allocation across cages. All behavioral testing was performed by an individual who was blinded with regard to the model status (CAIA or control) and compound treatment. The individual who performed the treatments was different from the individual who performed the measurements of behavioral responses.

Overall, 2 separate experiments were performed in mice with CAIA. Experiment 1 tested the effects of SPRi3 on pain hypersensitivity in both the early and the late phases of the CAIA model. Experiment 2 focused on the early phase of the model, during which joint inflammation is the key characteristic, and we

tested the effect of a chemically distinct SPR inhibitor, QM385, which is a more potent inhibitor of SPR than SPRi3. The effects of pharmacologic treatments on urinary or plasma sepiapterin levels were measured in both experiments.

Testing with radiant heat. Mice were assessed for responses to radiant heat (IITC Life Science) (experiment 1, day 0 to day 60; experiment 2, day 0 and day 10) (5). Testing was performed at the same time of day as when baseline responses were measured. After habituation of the mice on a glass surface (temperature 30°C, 30–60 minutes), a radiant heat source was applied to 1 hind paw, and the latency time to withdraw the paw from the heat stimulus was recorded.

Testing with mechanical stimuli. Mice were assessed for responses to mechanical stimuli (experiment 1, day 0 to day 60; experiment 2, day 0 to day 9), as previously reported (5). Testing was performed at the same time of day as when baseline responses were measured. After habituation of the mice to the test cages (cage dimension 7.5 × 7.5 × 15 cm, 30–60 minutes), baseline mechanical sensitivity was determined with 8 von Frey filaments (bending forces of 0.02, 0.04, 0.07, 0.16, 0.4, 0.6, 1, and 2 grams) applied to the central part of the hind paw. Following an elicited response, filaments were applied ≥3 seconds after the mouse had returned the paw to the floor. For the threshold of mechanical response, the minimal force filament to which animals responded (at least 5 of the 10 stimulations) determined the response threshold.

Testing with a cold stimulus. Mice were assessed for nocifensive responses to cooling by acetone evaporation (experiment 1, day 0 to day 60; experiment 2, day 0 to day 14) (5). Testing was performed at the same time of day as when baseline responses were measured. After habituation of the mice to the test cages (cage dimension 7.5 x 7.5 × 15 cm, 30–60 minutes), a drop of acetone was applied to the hind paw and the duration of flinching, lifting, and licking was recorded for 1 minute.

Determination of clinical signs of inflammation. Over 60 days in experiment 1, body weight and clinical arthritis scores were assessed by a single observer (MF), who was blinded with regard to the treatments. For experiment 2, the measurements were performed by a single observer (BLT) from day 0 to day 13. For the clinical arthritis score, a 16-point scoring system was used, in which 0 = normal paw, 1 = 1 toe inflamed and swollen, 2 = mild swelling of the entire paw, 3 = entire paw inflamed and swollen, and 4 = very inflamed, swollen, and ankylosed paw (7). All pharmacologic treatments were randomized within the home cage.

Measurement of paw edema. Right and left hind paw edema was measured as paw volume (in ml) from day 0 to day 13 in experiment 2, using a Digital Water Plethysmometer (Bioseb). The mouse was gently restrained, and each hind paw was placed separately into a water bath. The increase in paw volume (mean of 2 measures) was calculated daily relative to the paw volume at baseline.

Joint histology. Mice were killed on day 13 and at 60 minutes after QM385 administration. The hind paws were removed, placed in 4% paraformaldehyde, and then decalcified, sectioned, and stained with hematoxylin and eosin. The hematoxylin and eosin–stained paw specimens were analyzed for the presence of inflammatory cells and proliferation of new bone and cartilage around and within the joint. All fields of the sections were examined and evaluated carefully by a pathologist who was blinded with regard to the treatment. The degree of histologic changes was graded semiquantitatively on a scale of 0–4, in which 0 = no visible inflammation, 1 = some inflammation, 2 = more inflammation, 3 = moderate inflammation, and 4 = extensive inflammation) (7).

Sample collections and high-performance liquid chromatography (HPLC) measurements. *Blood collection*. Mouse blood samples were collected 1 hour after SPR inhibitor administration (on day 13 in experiment 2) by cardiac puncture. Samples were collected into tubes containing anticoagulant (ethylenediaminetetraacetic acid) and centrifuged at 5,000g for 15 minutes at room temperature to isolate plasma. Plasma samples were precipitated by the addition of 1 volume (volume/volume) of 5% trichloroacetic acid (TCA) containing 6.5 mM dithioerythritol (DTE). Thereafter, samples were centrifuged at 10,000g for 10 minutes at 4°C, and 20 μl of each plasma sample was analyzed for sepiapterin levels.

Urine collection. In animals, urine was collected from unrestrained mice by placing the mice in the same device used for von Frey filament tests (a plastic cage on a wire grid floor). Urine was collected by pipette on a plastic sheet under the rack, on days 0 and 7, 13, 14, 21, 28, and 35 at 1 hour after SPRi3 administration, and on days 1 and 2 after SSZ administration, and stored at –80°C until analyzed.

In human subjects, each healthy human volunteer collected a urine sample from the first urination of the day; each sample was stored at –20°C until all 8 samples had been collected. All samples were then submitted to the laboratory and stored at –80°C until analyzed. Samples from human subjects were treated before sepiapterin measurements in the same manner as described above for mice.

BH4 measurements. Urine samples were precipitated by the addition of 1 volume of 5% TCA containing 6.5 mM DTE. Samples were centrifuged at 16,000g for 10 minutes at 4°C. Ten microliters of supernatant was transferred to an HPLC vial for analysis. The HPLC analysis of BH4 was carried out using a Waters Atlantis dC-18 5-μm reverse-phase column (4.6 × 250 mm), with a flow rate set at 0.60 ml/minute and an isocratic elution of 6.5 mM sodium phosphate buffer, 6 mM citric acid, 1 mM sodium octyl sulfate (OSA), 2.5 mM diethylenetriaminepentaacetic acid (DTPA), 160 μM DTE, and 12% acetonitrile, pH 3.0. The OSA was used in the mobile phase as an ion-pairing reagent, which acts as an anionic counter ion for the separation and

Table 1. Parameters to determine the usefulness of sepiapterin levels as a pharmacodynamic biomarker of SPR inhibition*

Parameter	Calculation	Definition
True-positive	Sepiapterin levels above the cutoff value†	Identified in samples treated with SPRi3 or SSZ
False-positive	Sepiapterin levels above the cutoff value†	Identified in samples treated with vehicle
True-negative	Sepiapterin levels below the cutoff value†	Identified in samples treated with vehicle
False-negative	Sepiapterin levels below the cutoff value†	Identified in samples treated with SPRi3 or SSZ
Sensitivity	True-positive/(true-positive + false-negative)	Probability of a positive test result in mice administered SPR inhibitor
Specificity	True-negative/(true-negative + false-positive)	Probability of a negative test result in mice administered SPR inhibitor
False-positive rate	False-positive/(true-negative + false-positive)	Probability of a positive test result in mice administered vehicle
False-negative rate	False-negative/(true-positive + false-negative)	Probability of a negative test result in mice administered vehicle
Accuracy	(True-positive + true-negative)/(true-positive + true-negative + false-positive + false-negative)	Probability of correct test results

* SPR = sepiapterin reductase; SSZ = sulfasalazine.
† The cutoff value was defined as 3.3 µmoles/mmoles creatinine (equivalent to the mean + 1SD level measured in the urine of all non–drug-treated mice).

resolution of positively charged analytes. The DTPA was added to chelate transition metals to prevent oxidation of the analytes, and the DTE was used as a reductant to further stabilize the reduced form of BH4.

The Beckman Coulter HPLC system included a Model 125 Solvent Delivery Module and a Model 508 Autosampler that was controlled via 32 Karat software version 8.0. The electrochemical detector (Thermo Scientific/Dionex Coulochem III) with 2-sensor electrochemical cells was routinely operated at +50 and +450 mV. The +450 mV channel provided the most sensitive response for measuring BH4. The results are expressed as µmoles of BH4 per mmoles creatinine (µmoles/mmoles creatinine).

Sepiapterin measurements. Blood samples were precipitated by the addition of 1 volume of 5% TCA containing 6.5 mM DTE. Samples were centrifuged at 16,000g for 10 minutes at 4°C. Ten microliters of supernatant was transferred to an HPLC vial for analysis. Urine samples were centrifuged at 16,000g for 10 minutes at 4°C. The supernatant was diluted in 10 volumes (volume/volume) of 15 mM phosphate buffer, and 20 µl of the sample was analyzed.

HPLC analysis of sepiapterin was done using an Alliance e2695 apparatus on a Waters Atlantis dC-18, 5-µm RP column (4.6 × 250 mm; temperature 35°C), with a flow rate of 0.7 ml/minute and isocratic elution of mobile phase (85% phosphate buffer [15 mM], 15% acetonitrile, pH 6.4). Identification and quantification of sepiapterin was done using a multi-wavelength fluorescence detector (excitation wavelength 425 nm, emission wavelength 530 nm) (module 2475; Waters), with results expressed as nmoles of sepiapterin per liter of plasma (nmoles/liter) or µmoles of sepiapterin per mmoles of creatinine (µmoles/mmoles creatinine).

Biomarker calculations. Assessment of sepiapterin levels as a pharmacodynamic biomarker of SPR inhibition was done by determining the number of true-positive, true-negative, false-positive, and false-negative values for urinary sepiapterin

levels after SPRi3 or SSZ treatment. The cutoff value for these calculations was defined as the mean + 1SD urinary sepiapterin level in all non–drug-treated mice (Table 1).

Compounds. Compounds for mouse studies were prepared fresh on the day of testing and administered by an individual other than the individual who performed the behavior testing. The collagen cocktail, IgG, and LPS (supplied frozen) were defrosted immediately prior to injection. Compounds for systemic injection were administered at a dose of 10 ml/kg.

SPRi3 (50% inhibitory concentration [IC_{50}] 5.2 µM in a cell-based assay) (5) was dissolved (30 mg/ml, IP) in 2-hydroxypropyl-β-cyclodextrin (50% weight/volume prepared in 0.9% sterile saline). SPRi3 is rapidly absorbed into the plasma (T_{max} 0.11 hours, $T_{1/2}$ 3.95 hours) after IP injection (6) and induces a maximum reduction of nociceptive hypersensitivity and plasma BH4 levels at 1 hour postadministration (5). We therefore administered SPRi3 1 hour before behavioral and biomarker measurements.

QM385 (IC_{50} 35 nM in a cell-based assay) was suspended (0.3 mg/ml, orally) in 1% Tween 80/0.5% carboxymethyl cellulose in 0.9% saline. QM385 is also rapidly adsorbed into the plasma (T_{max} 1 hour, $T_{1/2}$ 4 hours) after oral administration (6). QM385 was therefore administered twice per day for 3 days, and testing was performed at 1 hour after the final dose.

In mice, SSZ (10 mg/ml, orally; Sigma) was prepared in 5% dimethyl sulfoxide in 0.9% sterile saline. In human volunteers, SSZ (Azulfin; Apsen Farmaceutica) was administered orally as a tablet.

Of note, SPRi3, QM385, and SSZ are 3 structurally different SPR inhibitors (5,6).

Statistical analysis. Sample sizes for the mouse behaviorial tests were determined a priori based on our experience with models of pain in mice (5) and biomarkers from the literature (11). Dose-dependent experiments were analyzed by one-way analysis of variance (ANOVA) with Dunnett's post hoc test and linear

regression analysis. Differences between groups in time courses of response were analyzed by mixed ANOVA with Tukey's post hoc test. Paired and unpaired t-tests were used when only 2 dependent or independent groups were compared. P values less than 0.05 were considered significant.

RESULTS

Injection of a cocktail of collagen antibodies (Figure 1A) into mice induced, as reported before (7), a pain-related hypersensitivity syndrome consisting of 2 distinct phases: 1 phase with clinical signs of active joint inflammation (early phase) and 1 phase without clinical signs of active joint inflammation (late phase).

Both control mice and mice with CAIA initially lost weight following the injection of LPS. Mice with CAIA lost significantly more weight than the control group between day 8 and day 12 (mixed ANOVA for time, $F_{(7,224)} = 31.40$, $P < 0.01$); however, the rate of weight gain from day 12 onward was equivalent to that in control animals (Figure 1B).

The CAIA model resulted in marked disease activity (mixed ANOVA for time, $F_{(7, 224)} = 94.30$, $P < 0.01$; mixed ANOVA for group comparison, $F_{(2, 224)} = 416.5$, $P < 0.01$; mixed ANOVA for time by group interaction, $F_{(14, 224)} = 20.13$, $P < 0.01$) during the early, acute inflammation phase (days 3–28) (Figure 1C), as shown by physical signs of swelling and redness in the toe joints on both the front and rear paws of mice. The total clinical arthritis score in mice with CAIA peaked 3 days after LPS injection (mean ± SD score 13.1 ± 0.5) and persisted until day 15, and then gradually declined to the values in control mice by day 28.

Cold allodynia followed the same time course as the arthritis score (i.e., similar time course of pain response to cold stimuli in the early, acute inflammation phase) (Figure 1F), whereas heat- and mechanical-evoked hypersensitivity each started 6 days after the collagen antibody cocktail injection, and both persisted even when visible signs of inflammation had resolved (CAIA late phase, >28 days) (Figures 1D and E). Control mice did not show significant changes in arthritis scores, body weight, or evoked hypersensitivity to heat, cold, or mechanical stimuli as compared with pretreatment values ($P > 0.05$ for each measure).
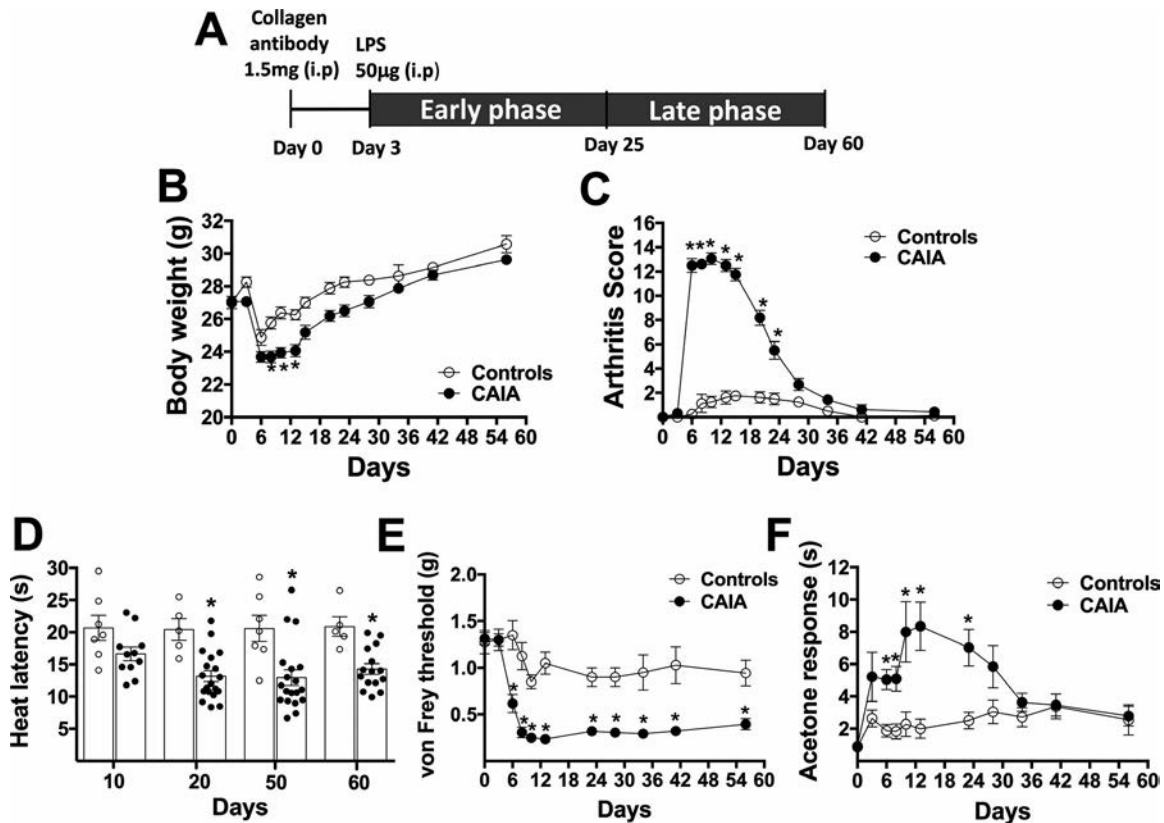
Figure 1. Changes in body weight, clinical arthritis scores, and pain-related responses following collagen antibody cocktail administration in mice. **A**, Timeline of experimental collagen antibody–induced arthritis (CAIA), with a booster injection of lipopolysaccharide (LPS) on day 3. **B**, Time course of body weight measurements in mice with CAIA and IgG-treated controls (each n = 13). **C**, Clinical arthritis scores (each n = 13). **D–F**, Thresholds of pain sensitivity in response to heat (controls n = 5, mice with CAIA n = 19) (**D**), a mechanical stimulus (von Frey filaments) (each n = 11) (**E**), and acetone cooling (each n = 11) (**F**). Measurements were performed every 3 days, starting on day 0 to day 56. In **B**, **C**, **E**, and **F**, results are the mean ± SEM. In **D**, symbols represent individual mice; bars show the mean ± SEM. * = $P < 0.05$ versus same time point in controls, by Tukey's post hoc test. IP = intraperitoneally.

Early phase

Late phase
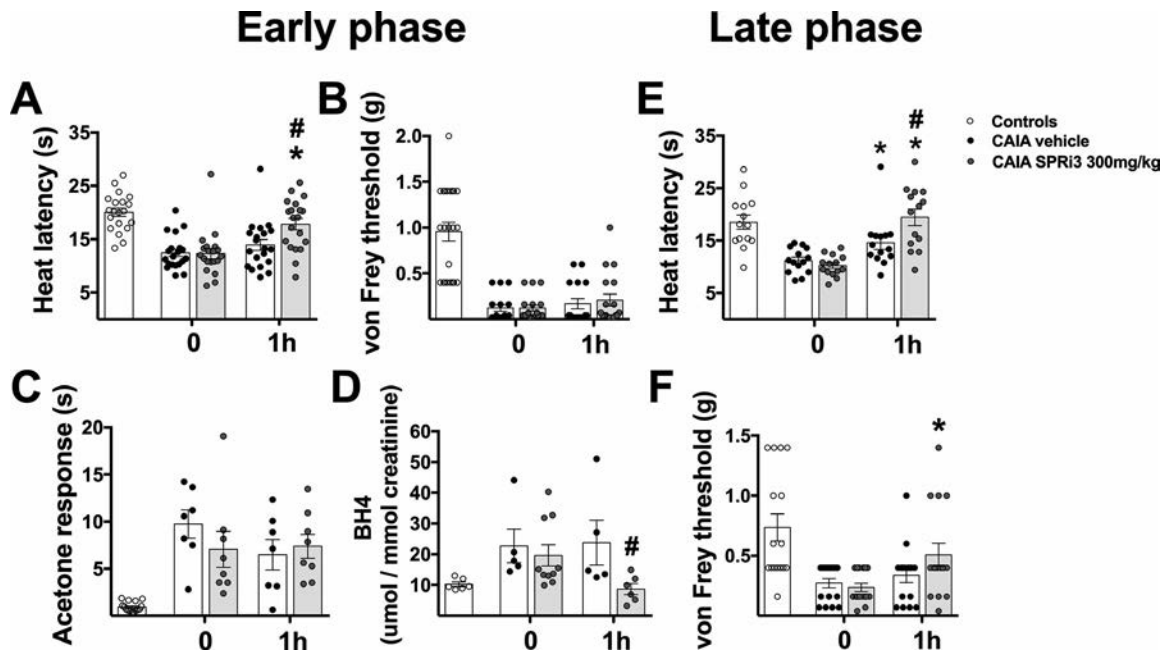
Figure 2. Effect of sepiapterin reductase (SPR) inhibition with SPRi3 on pain-related responses and urinary tetrahydrobiopterin (BH4) levels in the mouse collagen antibody–induced arthritis (CAIA) model. **A–D**, In the acute inflammatory (early) phase of CAIA, the effects of SPRi3 on pain sensitivity thresholds at 1 hour in response to heat (each n = 20) (**A**), a mechanical stimulus (von Frey filaments) (controls n = 24, vehicle-treated mice with CAIA n = 16, SPRi3-treated mice with CAIA n = 18) (**B**), and acetone cooling (controls n = 15, vehicle-treated mice with CAIA n = 7, SPRi3-treated mice with CAIA n = 8) (**C**) were examined, along with urinary BH4 levels on day 7 (controls n = 6, vehicle-treated mice with CAIA n = 5, SPRi3-treated mice with CAIA n = 6–10) (**D**). **E** and **F**, In the noninflammatory (late) phase of CAIA, most of these same mice were also tested for pain sensitivity in response to heat (each n = 14) (**E**) and a mechanical stimulus (each n = 16) (**F**). Symbols represent individual mice; bars show the mean ± SEM. # = $P < 0.05$ versus vehicle-treated mice with CAIA; * = $P < 0.05$ versus 0 hours, by Student's unpaired t-test.

In experiment 1 with the SPR inhibitor SPRi3, the treatment significantly reduced the heat-induced hyperalgesia both in the early phase ($t_{(19)}$ = 5.5, $P < 0.01$ by paired t-test) and in the late phase ($t_{(13)}$ = 6.0, $P < 0.01$ by paired t-test) of the CAIA model (Figures 2A and E), whereas mechanical hypersensitivity was reduced by SPR inhibition in only the late phase of CAIA ($t_{(15)}$ = 2.9, $P < 0.05$ by paired t-test) (Figures 2B and F). Cold hypersensitivity, analyzed in the early phase when physical signs of joint inflammation were present, was not modified by SPRi3 treatment ($P > 0.05$) (Figure 2C).

As a marker of inflammatory pain, the levels of BH4 were assessed on day 7 in the urine of mice 1 hour after SPR inhibition. SPRi3 significantly reduced urinary BH4 levels ($t_{(14)}$ = 2.3, $P < 0.05$ by unpaired t-test) (Figure 2D), a finding that correlates with the analgesic activity of the compound.

In experiment 2, we also studied the effect of SPR inhibition on the signs of inflammation evident during the early phase of the CAIA model, using a recently developed inhibitor of BH4 synthesis, QM385, which was recently shown to have immunosuppressive properties in experimental autoimmune models (6). Initially, the inhibitory effect of QM385 on SPR activity was confirmed by measuring the plasma levels of sepiapterin in response to QM385 administration in naive mice. As shown in Figure 3A, the effect of QM385 was dose-dependent, with a minimum effective dose

of 0.3 mg/kg ($F_{(5, 30)}$ = 42.70, $P < 0.01$) and a maximum effective dose of 3 mg/kg (β = 0.71, $P < 0.001$).

We then tested the effects of QM385 on the pain hypersensitivity and signs of inflammation present during the early phase of CAIA. QM385 (3 mg/kg, orally) inhibited SPR, as shown by the increased plasma levels of sepiapterin after QM385 administration in mice with CAIA ($F_{(2, 17)}$ = 53.22, $P < 0.01$ by one-way ANOVA) (Figure 3B). Similar to the effects of SPRi3, QM385 administration in the early phase of CAIA reduced the pain hypersensitivity induced by heat (degrees of freedom 5, $t_{(5)}$ = 2.9, $P < 0.05$ by paired t-test), but not the pain hypersensitivity induced by mechanical stimuli or cold allodynia (each $P > 0.05$) (Figures 3C–E).

The analgesic effect of QM385 could not be attributed to antiinflammatory properties of the compound, since QM385 had no effect on the clinical arthritis score (Figure 3F), the external appearance of the joints (redness or swelling) (Figures 3G and H), or the extent of inflammation scored histologically on paw sections (Figure 3I) (each $P > 0.05$ versus vehicle-treated mice).

Taken together, the results of experiment 2 confirmed that SPR inhibition induces a selective reduction in the pain hypersensitivity present at the time of heightened inflammation in this model of joint inflammation, without reducing the inflammation per se. The data acquired using 2 chemically unrelated SPR inhibitors extend the analgesic profile of SPR inhibition from that previously
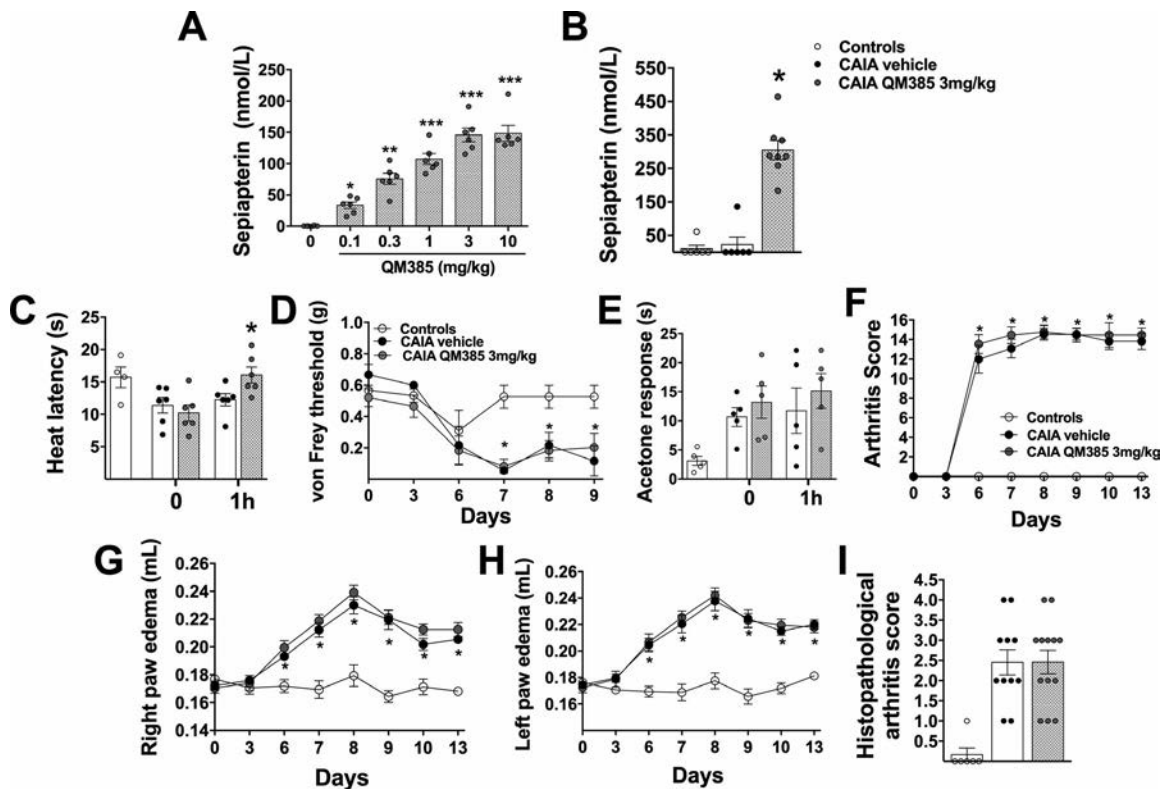
Figure 3. Effect of sepiapterin reductase (SPR) inhibition with QM385 on pain-related responses and clinical arthritis features in the acute inflammatory phase of mouse collagen antibody–induced arthritis (CAIA). The effects of SPR inhibition were assessed according to sepiapterin levels in the plasma of naive mice treated with different doses of QM385 (increasing concentrations, administered orally; n = 6) (**A**) and in the early inflammatory phase of CAIA (day 13; controls n = 6, vehicle-treated mice with CAIA n = 6, QM385-treated mice with CAIA n = 8) (**B**), pain sensitivity thresholds determined on day 14 in response to heat (controls n = 4, vehicle-treated mice with CAIA n = 6, QM385-treated mice with CAIA n = 6; performed on day 10) (**C**), a mechanical stimulus (controls n = 6, vehicle-treated mice with CAIA n = 8, QM385-treated mice with CAIA n = 6; performed on day 9) (**D**), and acetone cooling (each n = 5); (**E**), changes in clinical arthritis scores (**F**) and extent of edema in the right (**G**) and left (**H**) hind paws from day 0 to day 13 (each n = 7), and histopathologic arthritis scores on day 14 (controls n = 7, vehicle-treated mice with CAIA n = 11, QM385-treated mice with CAIA n = 13) (**I**). In **A**, **B**, **C**, **E**, and **I**, symbols represent individual mice; bars show the mean ± SEM. In **D**, **F**, **G**, and **H**, results are the mean ± SEM. In **A**, * = $P < 0.05$, ** = $P < 0.01$, *** = $P < 0.001$ versus 0 mg/kg, by one-way analysis of variance (ANOVA) with Dunnett's post hoc test. In **B**, * = $P < 0.05$ versus the other groups, by Student's unpaired *t*-test. In **D** and **F**, * = $P < 0.05$ versus controls at the same time point, by mixed-model repeated-measures ANOVA with Dunnett's post hoc test. In **C,** * = $P < 0.05$ versus 0 hours, by Student's unpaired *t*-test. In **G–I**, * = $P < 0.05$ versus controls at the same time point, by one-way ANOVA with Dunnett's post hoc test.

reported in studies of neuropathic and soft tissue inflammation (5,6), to include effects on joint inflammation. Based on its observed effects on evoked pain in an RA-like model of joint disease, we may conclude that SPR inhibition is sufficient to produce analgesia during joint inflammation, differentiating this mechanism of action from that of currently known DMARDs.

Sepiapterin levels have been previously shown to be increased in the cerebrospinal fluid, blood, and urine of patients affected by mutations in the SPR gene, leading to compromised SPR content or activity (11). The increased sepiapterin levels indicate that SPR function can be assessed noninvasively by measuring urinary sepiapterin levels. To test whether urinary sepiapterin levels could be used to reliably monitor pharmacologic inhibition of SPR, we measured the metabolite in mouse and human urine following administration of 3 structurally unrelated SPR inhibitors (SPRi3 and SSZ in rodents and SSZ in humans).

Sepiapterin levels were significantly increased in the urine of mice with CAIA at 1 hour after SPRi3 administration (300 mg/kg), on day 7 (mean 3.7 μmoles/mmoles creatinine [95% confidence interval 2.7–4.8] in control mice versus 6.7 μmoles/mmoles creatinine [95% confidence interval 4.8–8.6] in SPRi3-treated mice; $P < 0.05$) and on day 45 (mean 3.9 μmoles/mmoles creatinine [95% confidence interval 2.6–5.1] in control mice versus 8.9 μmoles/mmoles creatinine [95% confidence interval 4.6–13.1] in SPRi3-treated mice; $P < 0.05$) (Figure 4A). Sepiapterin levels returned to baseline levels in the absence of SPRi3 (measured on days 14, 21, 28, and 35), indicating the specificity of sepiapterin for SPR inhibition.

Parameters of the capacity of urinary sepiapterin levels to serve as a biomarker for predicting SPR inhibition were calculated on the basis of a cutoff value of 3.3 μmoles/mmoles creatinine (equivalent to the mean + 1SD urinary level of sepiapterin measured in mice not treated with SPRi3 [n = 78 samples])
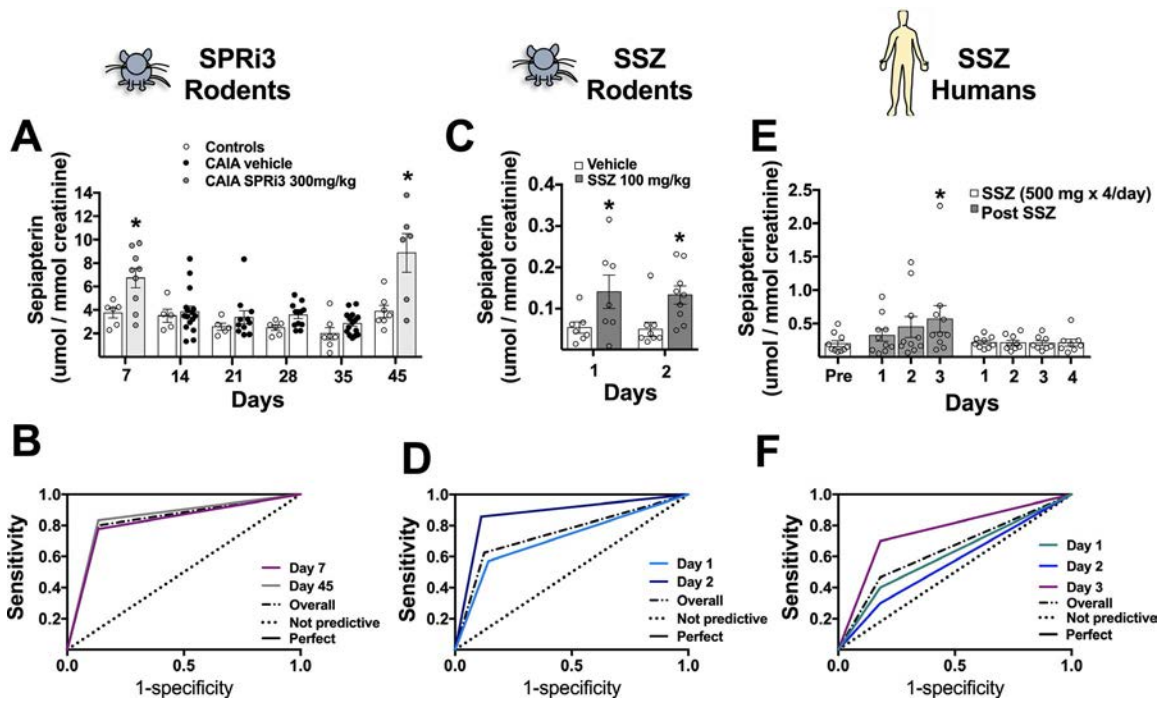
Figure 4. Levels of urinary sepiapterin following treatment with sepiapterin reductase (SPR) inhibitors. **A**, **C**, and **E**, Effects of SPRi3 administration in mice on days 7, 14, 21, 28, 35, and 45 (controls n = 4–7, vehicle-treated mice with collagen antibody–induced arthritis [CAIA] n = 7–16, SPRi3-treated mice with CAIA n = 6–9) (**A**), sulfasalazine (SSZ) administered for 2 consecutive days in mice (day 1, each n = 7; day 2, each n = 9) (**C**), and SSZ administered for 3 days in human volunteers (pre-SSZ up to day 7 post-SSZ; n = 10) (**E**) on urinary levels of sepiapterin. In **A** and **C**, * = $P < 0.05$ versus controls, by Student's unpaired t-test. In **E**, * = $P < 0.05$ by one-way analysis of variance with Tukey's post hoc test. **B**, **D**, and **F**, Area under the receiver operating characteristic curves for urinary sepiapterin levels as a biomarker of SPR inhibition with SPRi3 or SSZ. An ideal biomarker would have both sensitivity and specificity equal to 1, meaning all mice treated with SPRi3 would have urinary sepiapterin levels higher than the cutoff value, and all samples from mice not treated with an SPR inhibitor would have levels lower than the cutoff value. A biomarker with no predictive value (dotted line) would have equal sensitivity and a false-positive rate, because a mouse with or without SPR inhibitor treatment would be equally likely to have a positive test result.

(Table 2). As shown in Figure 4B, the area under the receiver operating characteristics curve plot depicts the clear effectiveness of the urinary sepiapterin level as a biomarker for inhibition with SPRi3 in mice. When samples from day 7 and day 45 were combined, urinary levels of sepiapterin were associated with an overall sensitivity of 80%, specificity of 86.7%, and accuracy of

85.7% for prediction of SPR inhibition with SPRi3; these values were similar to the day 7 or day 45 data examined separately (Table 2).

SSZ has been used for more than 6 decades as a first-line treatment for RA because of its disease-modifying properties (9) and, more recently, has been found to be an inhibitor of SPR

Table 2. Predictive capacity of urinary sepiapterin levels as a biomarker for SPR inhibition with SPRi3 or SSZ*

Experiment	Sensitivity	Specificity	False-negative rate	False-positive rate	Accuracy
SPRi3 in mice					
Day 7	77.7	86.7	13.3	22.2	85.8
Day 45	83.3	86.7	13.3	16.6	86.5
Overall	80	86.7	13.3	20	85.7
SSZ					
Mice					
Day 1	57.1	85.7	14.3	42.9	71.4
Day 2	85.7	88.8	11.1	33.3	77.7
Overall	62.5	87.5	16.7	12.5	75
Human volunteers					
Day 1	40	82.2	17.7	60	74.5
Day 2	30	82.2	17.7	70	72.7
Day 3	70	82.2	17.7	30	80
Overall	46.6	82.2	17.7	53.3	68

* Values are the percentage. SPR = sepiapterin reductase; SSZ = sulfasalazine.

(10,11). We have previously demonstrated that SSZ treatment elicited tissue and plasma accumulation of sepiapterin in mice (5). In the present study, we administered SSZ to mice as well as to healthy human volunteers. The dose of SSZ used for the mouse biomarker measurements was selected based on our observations of its analgesic effects in previous experiments with the intraplantar CFA model of inflammation (5). As shown in Figure 4C, within 1–3 hours after SSZ administration (100 mg/kg, orally) on each of 2 separate days, sepiapterin levels in the urine of mice increased (day 1, $t_{(12)} = 2.05$, $P = 0.065$ and day 2, $t_{(16)} = 3.0$, $P < 0.05$ by unpaired t-test) relative to that in vehicle-treated mice. Biomarker parameters (Figure 4D and Table 2) showed that the specificity, false-negative rates, and false-positive rates were consistent with those from the SPRi3 experiment (see Table 2 for the magnitude of effects). However, the accuracy and sensitivity were lower, which may reflect the lower potency of SSZ relative to that of SPRi3.

The standard initial dosage of SSZ in the clinic is 2 gm/day (given at a dose of 4 × 500 mg, every 6 hours) and takes several days to reach steady-state levels; we therefore selected this dosage for the treatment of healthy human volunteers. After administration of SSZ to healthy volunteers (2 gm/day for 3 consecutive days), sepiapterin levels increased in the urine each day, reaching a significant difference on day 3 of sampling following administration of SSZ ($t_{(18)} = 1.8$, $P < 0.05$ by unpaired t-test) (Figures 4E and F). Urinary sepiapterin levels immediately returned to pretreatment levels on cessation of treatment with SSZ. The timing of the change in sepiapterin levels in the urine is consistent with the clinical observation that SSZ is required to be administered for at least 3–5 days to achieve therapeutically relevant levels in the patient.

In addition, BH4 levels were measured in the urine from healthy human volunteers. The urinary BH4 levels did not change in response to SSZ treatment (data not shown). These findings underline the value of urinary sepiapterin specifically as a biomarker of SPR inhibition.

DISCUSSION

In this study, SPR inhibition reduced the heat- and mechanical-evoked pain hypersensitivity resulting from systemic inflammation in a mouse model of RA-like joint inflammation, extending earlier work on the analgesic effects of SPR inhibition in granulomatous inflammation (5). SPR inhibitors also increased sepiapterin levels in the urine and plasma of mice and in the urine of healthy human volunteers, revealing for the first time that sepiapterin is a specific and sensitive pharmacodynamic biomarker of SPR inhibition in humans. The data also confirm that SSZ inhibits SPR activity at a dose used therapeutically in the clinic as a DMARD. The biomarker findings were translated from mouse to healthy humans, implying the potential utility of this measure of target engagement for clinical monitoring and future studies of novel SPR inhibitors.

Our data are consistent with previous findings from other groups showing that injection of a cocktail of collagen antibodies induces a pain syndrome consisting of 2 distinct phases. The acute phase is characterized by marked inflammation and pain, whereas the late phase shows no joint inflammation but pain is present (12–14), supporting the notion that active inflammation per se is not necessarily the direct cause of the pain hypersensitivity in this model (15). Consequently, this may not be an accurate model of the pathophysiology of RA-like diseases. Furthermore, conventional and biologic DMARDs, e.g., SSZ and anti–interleukin-1β antibody, show limited analgesia (16), in contrast to that shown herein with the use of SPR inhibitors.

SPR inhibition, by administration of SPRi3, reduced heat-induced hyperalgesia in mice in both the early phase and late phase of CAIA, had no effect on cold-induced hypersensitivity, and reduced mechanical-induced hypersensitivity in the late phase of this model of arthritis. In a separate experiment, in which we focused on the effect of SPR inhibition on pain and signs of inflammation in the early phase, we found that QM385, an SPR inhibitor chemically unrelated to SPRi3, also inhibited heat-induced hypersensitivity during the period of heightened inflammation. Interestingly, QM385 did not reduce the signs of inflammation (physical appearance of the joints, histologic inflammation score, and extent of immune infiltrate), showing that SPR inhibition produces a selective effect on pain associated with inflammation. Since we have recently found that BH4 promotes T cell proliferation and that SPR inhibition decreases inflammation in mouse models of T cell transfer–induced colitis, the experimental autoimmune encephalomyelitis model of multiple sclerosis, and type 2 allergic inflammation in the lung and skin (6), we conclude that the mouse model of CAIA very likely does not include a T cell–proliferative component, and it is therefore unlikely to be a model of autoimmune, inflammatory polyarthritic disorders, as such disorders are T cell dependent (17). Moreover, the direct administration of anticollagen antibodies may only replicate the terminal steps of autoimmune joint inflammation. Nevertheless, the CAIA model generated pain, which was sensitive to SPR inhibition, and this may reflect changes in BH4 activity in sensory neurons innervating inflamed joints, though other cell types (e.g., macrophages, monocytes, mast cells) cannot be dismissed.

A biomarker is a quantifiable trait of normal or pathogenic biologic processes or of responses to an exposure or intervention, including therapeutic interventions. An ideal biomarker would be one that can be measured in a biologic fluid that can be obtained from the patient in a noninvasive manner, i.e., using urine or saliva samples or a skin wipe, and would be stable at room temperature (8). Our results indicate that measurement of sepiapterin in the urine fits these criteria for a biomarker that would be useful for monitoring target engagement (patient compliance) and/or treatment safety based on the premise that high exposure increases risk of on-target adverse effects.

Studies by other investigators have shown that DMARDs such as SSZ are able to bind to SPR and inhibit its activity in vitro, and this interaction was suggested to be responsible for some of the side effects of SSZ as a consequence of reduced BH4 levels in the central nervous system (18). Extrapolating from the mouse model results, our data suggest that SPR inhibition is also a likely mechanism for the analgesic action of SSZ. Further work in clinical populations evaluating the dose range of SSZ and other SPR inhibitors, and variance of therapeutic efficacy and biomarker response, could establish the relationship between sepiapterin levels in the urine and analgesic efficacy and side effects. Clinical use of this biomarker could assist in precision medicine by detecting ranges associated with efficacy for RA, ulcerative colitis, inflammatory bowel disease, and Crohn's disease, and perhaps also improve the management of the risk of adverse effects due to excessive inhibition of BH4. Polymorphisms in *N*-acetyltransferase 2 play a role in the differential response to SSZ (19), and therefore achieving an optimal combination of biomarkers and genetics to maximize efficacy and reduce side effects is now in reach.

In conclusion, we have shown that SPR inhibition reduces pain hypersensitivity in a mouse model of joint inflammation. Furthermore, we have demonstrated, using 3 chemically distinct SPR inhibitors, that urinary sepiapterin is a sensitive and specific biomarker of pharmacologic inhibition of SPR and could be used to improve the effectiveness of SSZ in the clinic when used as a biomarker of target engagement.

ACKNOWLEDGMENTS

AUTHOR CONTRIBUTIONS

All authors were involved in drafting the article or revising it critically for important intellectual content, and all authors approved the final version to be published. Dr. Andrews had full access to all of the data in the study and takes responsibility for the integrity of the data and the accuracy of the data analysis.
Study conception and design. Fujita, Scheffer, Turnes, Cronin, Latrémolière, Costigan, Woolf, Latini, Andrews.
Acquisition of data. Fujita, Scheffer, Turnes, Latini, Andrews.
Analysis and interpretation of data. Fujita, Scheffer, Turnes, Cronin, Latrémolière, Costigan, Woolf, Latini, Andrews.

REFERENCES

1. Ghisoni K, de Paula Martins R, Barbeito L, Latini A. Neopterin as a potential cytoprotective brain molecule [review]. J Psychiatr Res 2015;71:134–9.

2. Werner ER, Blau N, Thöny B. Tetrahydrobiopterin: biochemistry and pathophysiology [review]. Biochem J 2011;438:397–414.

3. Hirakawa H, Sawada H, Yamahama Y, Takikawa SI, Shintaku H, Hara A, et al. Expression analysis of the aldo-keto reductases involved in the novel biosynthetic pathway of tetrahydrobiopterin in human and mouse tissues. J Biochem 2009;146:51–60.

4. Costigan M, Latremoliere A, Woolf CJ. Analgesia by inhibiting tetrahydrobiopterin synthesis. Curr Opin Pharmacol 2012;12:92–9.

5. Latremoliere A, Latini A, Andrews N, Cronin SJ, Fujita M, Gorska K, et al. Reduction of neuropathic and inflammatory pain through inhibition of the tetrahydrobiopterin pathway. Neuron 2015;86:1393–406.

6. Cronin SJ, Seehus C, Weidinger A, Talbot S, Reissig S, Seifert M, et al. The metabolite BH4 controls T cell proliferation in autoimmunity and cancer [letter]. Nature 2018;563:564–8.

7. Khachigian LM. Collagen antibody-induced arthritis. Nat Protoc 2006;1:2512–6.

8. Amur S, for the US Food and Drug Administration Center for Drug Evaluation and Research. Biomarker terminology: speaking the same language. URL: https://www.fda.gov/files/BIOMARKER-TERMINOLOGY-SPEAKING-THE-SAME-LANGUAGE.

9. Smolen JS, Landewé R, Bijlsma J, Burmester G, Chatzidionysiou K, Dougados M, et al. EULAR recommendations for the management of rheumatoid arthritis with synthetic and biological disease-modifying antirheumatic drugs: 2016 update. Ann Rheum Dis 2017;76:960–77.

10. Chidley C, Haruki H, Pedersen MG, Muller E, Johnsson K. A yeast-based screen reveals that sulfasalazine inhibits tetrahydrobiopterin biosynthesis. Nat Chem Biol 2011;7:375–83.

11. Carducci C, Santagata S, Friedman J, Pasquini E, Carducci C, Tolve M, et al. Urine sepiapterin excretion as a new diagnostic marker for sepiapterin reductase deficiency. Mol Genet Metab 2015;115:157–60.

12. Nandakumar KS, Svensson L, Holmdahl R. Collagen type II-specific monoclonal antibody-induced arthritis in mice. Am J Pathol 2003;163:1827–37.

13. Bas DB, Su J, Sandor K, Agalave NM, Lundberg J, Codeluppi S, et al. Collagen antibody–induced arthritis evokes persistent pain with spinal glial involvement and transient prostaglandin dependency. Arthritis Rheum 2012;64:3886–96.

14. Nandakumar KS, Holmdahl R. Efficient promotion of collagen antibody induced arthritis (CAIA) using four monoclonal antibodies specific for the major epitopes recognized in both collagen induced arthritis and rheumatoid arthritis. J Immunol Methods 2005;304:126–36.

15. Chiu IM, Heesters BA, Ghasemlou N, Von Hehn CA, Zhao F, Tran J, et al. Bacteria activate sensory neurons that modulate pain and inflammation. Nature 2013;501:52–7.

16. Persson MS, Sarmanova A, Doherty M, Zhang W. Conventional and biologic disease-modifying anti-rheumatic drugs for osteoarthritis: a meta-analysis of randomized controlled trials. Rheumatology (Oxford) 2018;57:1830–7.

17. Dominguez-Villar M, Hafler DA. Regulatory T cells in autoimmune disease. Nat Immunol 2018;19:665–73.

18. Haruki H, Pedersen MG, Gorska KI, Pojer F, Johnsson K. Tetrahydrobiopterin biosynthesis as an off-target of sulfa drugs. Science 2013;340:987–91.

19. Kumagai S, Komada F, Kita T, Morinobu A, Ozaki S, Ishida H, et al. N-acetyltransferase 2 genotype-related efficacy of sulfasalazine in patients with rheumatoid arthritis. Pharm Res 2004;21:324–9.

AMERICAN COLLEGE
of RHEUMATOLOGY
Empowering Rheumatology Professionals

Peripheral Nervous System Disease in Systemic Lupus Erythematosus: Results From an International Inception Cohort Study

John G. Hanly,[1] [ID] Qiuju Li,[2] Li Su,[2] Murray B. Urowitz,[3] [ID] Caroline Gordon,[4] Sang-Cheol Bae,[5]
Juanita Romero-Diaz,[6] Jorge Sanchez-Guerrero,[3] Sasha Bernatsky,[7] Ann E. Clarke,[8] [ID] Daniel J. Wallace,[9]
David A. Isenberg,[10] [ID] Anisur Rahman,[10] Joan T. Merrill,[11] Paul R. Fortin,[12] Dafna D. Gladman,[3] Ian N. Bruce,[13]
Michelle Petri,[14] [ID] Ellen M. Ginzler,[15] M. A. Dooley,[16] Kristjan Steinsson,[17] Rosalind Ramsey-Goldman,[18]
Asad A. Zoma,[19] Susan Manzi,[20] Ola Nived,[21] Andreas Jonsen,[21] Munther A. Khamashta,[22] Graciela S. Alarcón,[23]
Elisabet Svenungsson,[24] [ID] Ronald F. van Vollenhoven,[25] Cynthia Aranow,[26] Meggan Mackay,[26]
Guillermo Ruiz-Irastorza,[27] Manuel Ramos-Casals,[28] S. Sam Lim,[29] Murat Inanc,[30] Kenneth C. Kalunian,[31]
Soren Jacobsen,[32] Christine A. Peschken,[33] Diane L. Kamen,[34] Anca Askanase,[35] Chris Theriault,[1] and
Vernon Farewell[2]

Objective. To determine the frequency, clinical characteristics, associations, and outcomes of different types of peripheral nervous system (PNS) disease in a multiethnic/multiracial, prospective inception cohort of systemic lupus erythematosus (SLE) patients.

Methods. Patients were evaluated annually for 19 neuropsychiatric (NP) events including 7 types of PNS disease. SLE disease activity, organ damage, autoantibodies, and patient and physician assessment of outcome were measured. Time to event and linear regressions were used as appropriate.

Results. Of 1,827 SLE patients, 88.8% were female, and 48.8% were white. The mean ± SD age was 35.1 ± 13.3 years, disease duration at enrollment was 5.6 ± 4.2 months, and follow-up was 7.6 ± 4.6 years. There were 161 PNS events in 139 (7.6%) of 1,827 patients. The predominant events were peripheral neuropathy (66 of 161 [41.0%]), mononeuropathy (44 of 161 [27.3%]), and cranial neuropathy (39 of 161 [24.2%]), and the majority were attributed to SLE. Multivariate Cox regressions suggested longer time to resolution in patients with a history of neuropathy, older age at SLE diagnosis, higher SLE Disease Activity Index 2000 scores, and for peripheral neuropathy versus other neuropathies. Neuropathy was associated with significantly lower Short Form 36 (SF-36) physical and mental component summary scores versus no NP events. According to physician assessment, the majority of neuropathies resolved or improved over time, which was associated with improvements in SF-36 summary scores for peripheral neuropathy and mononeuropathy.

Conclusion. PNS disease is an important component of total NPSLE and has a significant negative impact on health-related quality of life. The outcome is favorable for most patients, but our findings indicate that several factors are associated with longer time to resolution.

INTRODUCTION

Involvement of the nervous system in systemic lupus erythematosus (SLE) presents clinically as a variety of neurologic and psychiatric features, collectively referred to as neuropsychiatric SLE (NPSLE). Approximately one-third of NP events are directly attributable to SLE and occur in 21% of SLE patients in the first 6.6 years of their disease (1). Central nervous system (CNS) involvement accounts for >90% of events compared to involvement of the peripheral nervous system (PNS), which accounts for most of the other events (1). Although there is a large body of work on CNS disease in SLE patients, involvement of the PNS is less well established.

Of the 3 current classification criteria for SLE (2–4), only the Systemic Lupus International Collaborating Clinics (SLICC) criteria include PNS events as a variable. In the American College of Rheumatology (ACR) case definitions for NPSLE (5), 7 of 19 manifestations affect the PNS. The aim of the present study was to determine the frequency, clinical characteristics, autoantibody associations, and outcomes as assessed by physicians and patients of these 7 PNS manifestations in a large, multiethnic/multiracial, prospective, inception cohort of SLE patients.

PATIENTS AND METHODS

Research study network. The study was conducted by SLICC (6), a network of 52 investigators at 43 academic centers in 16 countries. From 1999 to 2011, a cohort of recently diagnosed SLE patients was recruited from 31 SLICC sites in Europe, Asia, and North America. Data were collected per protocol at enrollment and annually, submitted to the coordinating centers in Toronto, Ontario and Halifax, Nova Scotia, Canada, and entered into a centralized Access database. Appropriate procedures ensured data quality, management, and security. The Nova Scotia Health Authority Central Zone Research Ethics Board, Halifax, and each of the participating centers' institutional research ethics review boards approved the study.

Patients. Patients fulfilled the revised ACR classification criteria for SLE (2), the date of which was used as the date of diagnosis, and provided written informed consent. Enrollment was permitted up to 15 months following the diagnosis. Demographic variables, education, and medication history were collected. Lupus-related variables included the SLE Disease Activity Index 2000 (SLEDAI-2K) (7) and SLICC/ACR damage index (SDI) (8). Routine laboratory testing included hematologic, biochemical, and immunologic variables required to determine SLEDAI-2K and SDI scores.

Neuropsychiatric events. An enrollment window extended from 6 months prior to the diagnosis of SLE up to the actual enrollment date. NP events were characterized within this window using the ACR case definitions for 19 NP syndromes (5). These were diagnosed by clinical evaluation supported by investigations, if clinically warranted, as per existing guidelines. Patients were seen annually with a 6-month window around the anticipated assessment date. New NP events and the status of previous NP events since the last study visit were determined at each assessment.

The ACR case definitions (5) include 7 types of PNS disease: 1) peripheral neuropathy, 2) cranial neuropathy, 3) mononeuropathy, single or multiplex, 4) plexopathy, 5) autonomic neuropathy,

[5]Sang-Cheol Bae, MD, PhD: Hanyang University Hospital for Rheumatic Diseases, Seoul, Republic of Korea; [6]Juanita Romero-Diaz, MD, MSc: Instituto Nacional de Ciencias Medicas y Nutrición, Mexico City, Mexico; [7]Sasha Bernatsky, MD, PhD: McGill University, Montreal, Quebec, Canada; [8]Ann E. Clarke, MD, MSc: University of Calgary Cumming School of Medicine, Calgary, Alberta, Canada; [9]Daniel J. Wallace, MD: Cedars-Sinai and University of California, Los Angeles School of Medicine; [10]David A. Isenberg, MD, Anisur Rahman, MD, PhD: University College London, London, UK; [11]Joan T. Merrill, MD: Oklahoma Medical Research Foundation, Oklahoma City; [12]Paul R. Fortin, MD, MPH: CHU de Québec and Université Laval, Quebec City, Quebec, Canada; [13]Ian N. Bruce, MD: Arthritis Research UK Epidemiology Unit, University of Manchester, NIHR Manchester Musculoskeletal Biomedical Research Centre, and Manchester University NHS Foundation Trust, Manchester, UK; [14]Michelle Petri, MD, MPH: Johns Hopkins University School of Medicine, Baltimore, Maryland; [15]Ellen M. Ginzler, MD, MPH: SUNY Downstate Medical Center, Brooklyn, New York; [16]M. A. Dooley, MD, MPH: University of North Carolina, Chapel Hill; [17]Kristjan Steinsson, MD: Landspitali University Hospital, Reykjavík, Iceland; [18]Rosalind Ramsey-Goldman, MD, DrPH: Northwestern University and Feinberg School of Medicine, Chicago, Illinois; [19]Asad A. Zoma, MD: Hairmyres Hospital, East Kilbride, UK; [20]Susan Manzi, MD, MPH: Allegheny Health Network, Pittsburgh, Pennsylvania; [21]Ola Nived, MD, PhD, Andreas Jonsen, MD, PhD: Lund University, Lund, Sweden; [22]Munther A. Khamashta, MD: St. Thomas' Hospital and King's College London School of Medicine, London, UK; [23]Graciela S. Alarcón, MD, MPH: University of Alabama at Birmingham; [24]Elisabet Svenungsson, MD: Karolinska Institutet and Karolinska University Hospital, Stockholm, Sweden; [25]Ronald F. van Vollenhoven, MD: Amsterdam University Medical Centers, Amsterdam, The Netherlands; [26]Cynthia Aranow, MD, Meggan Mackay, MD: Feinstein Institute for Medical Research, Manhasset, New York;

[27]Guillermo Ruiz-Irastorza, MD: Hospital Universitario Cruces and University of the Basque Country, Barakaldo, Spain; [28]Manuel Ramos-Casals, MD: Institut d'Investigacions Biomèdiques August Pi i Sunyer and Hospital Clínic de Barcelona, Barcelona, Spain; [29]S. Sam Lim, MD, MPH: Emory University School of Medicine, Atlanta, Georgia; [30]Murat Inanc, MD: Istanbul University, Istanbul, Turkey; [31]Kenneth C. Kalunian, MD: University of California San Diego School of Medicine; [32]Soren Jacobsen, MD, DMSc: Rigshospitalet and Copenhagen University Hospital, Copenhagen, Denmark; [33]Christine A. Peschken, MD: University of Manitoba, Winnipeg, Manitoba, Canada; [34]Diane L. Kamen, MD: Medical University of South Carolina, Charleston; [35]Anca Askanase, MD, MPH: NYU Langone Orthopedic Hospital, New York, New York.

6) acute inflammatory demyelinating polyradiculoneuropathy (Guillain-Barré syndrome), and 7) myasthenia gravis. In view of the low frequency of the latter 4 types of PNS disease, they were not included in the detailed analyses, which were restricted to peripheral neuropathy, cranial neuropathy, and mononeuropathy. Recurring PNS and other NP events within the enrollment window or within each follow-up assessment period were recorded once. The date of the first such episode was taken as the onset of the event.

Attribution of NP events. To be consistent with other publications on NP events within the SLICC NPSLE inception cohort, the same decision rules were used to determine the attribution of all NP events (9,10). Factors considered in the decision rules included: 1) temporal onset of NP event(s) in relation to the diagnosis of SLE; 2) concurrent non-SLE factor(s), such as potential causes ("exclusions") or contributing factors ("associations") for each NP syndrome in the glossary for the ACR case definitions of NP events (5); and 3) common NP events, which are frequent in normal population controls as described by Ainiala et al (11). These include isolated headaches, anxiety, mild depression (mood disorders failing to meet criteria for "major depressive-like episodes"), mild cognitive impairment (deficits in <3 of the 8 specified cognitive domains), and peripheral neuropathy without electrophysiologic confirmation. Two attribution decision rules of different stringency (models A and B) were used (9,10).

Attribution model A. NP events that had their onset within the enrollment window or subsequently <u>and</u> had no "exclusions" or "associations" <u>and</u> were not one of the NP events identified by Ainiala et al (11) were attributed to SLE.

Attribution model B. NP events that had their onset within 10 years of the diagnosis of SLE and were still present within the enrollment window or had their onset at a later date <u>and</u> had no "exclusions" <u>and</u> were not one of the NP events identified by Ainiala et al (11) were attributed to SLE.

NP events that fulfilled the criteria for model A (most stringent) or for model B (least stringent) were attributed to SLE. By definition, all NP events attributed to SLE using model A were included in the NP events using model B. Those events that did not fulfill these criteria were classified as a non-SLE NP event.

Outcome of PNS events. At each follow-up assessment the change in PNS events between onset and follow-up was assessed by the physician using a 7-point Likert scale (where 1 = patient demise, 2 = much worse, 3 = worse, 4 = no change, 5 = improved, 6 = much improved, and 7 = resolved) (12). Patients completed a Short Form 36 (SF-36) questionnaire at each assessment that included 8 subscales and the mental component summary (MCS) and physical component summary (PCS) scores (12,13); these were not available to physicians at the time of their assessments.

Autoantibodies. Lupus anticoagulant, IgG anticardiolipin, anti–β_2-glycoprotein I, anti–ribosomal P, and anti–NR2 glutamate receptor antibodies were measured at the Oklahoma Medical Research Foundation (14–17).

Statistical analysis. The Kaplan-Meier method was used to estimate cumulative incidence for first and recurrent PNS events and the probability of neuropathy not resolving over time. We used Cox regression to examine the risk of first SLE

Table 1. Demographic and clinical features of the 1,827 SLE patients at enrollment*

Sex, no. (%) female/male	1,623 (88.8)/204 (11.2)
Age, mean ± SD years	35.1 ± 13.3
Race/ethnicity, no. (%)	
White	891 (48.8)
African	307 (16.8)
Hispanic	282 (15.4)
Asian	275 (15.1)
Other	72 (3.9)
Single/married/other, no. (%)	819 (44.9)/766 (42.0)/238 (13.1)
Postsecondary education, no. (%)†	1,065 (61.9)
Disease duration, mean ± SD months	5.6 ± 4.2
Number of ACR criteria met, mean ± SD	4.9 ± 1.1
ACR manifestations, no. (%)	
Malar rash	660 (36.1)
Discoid rash	227 (12.4)
Photosensitivity	653 (35.7)
Oral/nasal ulcers	678 (37.1)
Serositis	502 (27.5)
Arthritis	1368 (74.9)
Renal disorder	510 (27.9)
Neurologic disorder	88 (4.8)
Hematologic disorder	1130 (61.9)
Immunologic disorder	1393 (76.2)
Antinuclear antibodies	1732 (94.8)
SLEDAI-2K score, mean ± SD	5.3 ± 5.4
SDI, mean ± SD‡	0.32 ± 0.74
Medications, no. (%)	
Glucocorticoids	1285 (70.3)
Antimalarials	1231 (67.4)
Immunosuppressants	732 (40.1)
ASA	261 (14.3)
Antidepressants	184 (10.1)
Warfarin	99 (5.4)
Anticonvulsants	80 (4.4)
Antipsychotics	12 (0.7)
Autoantibody positivity, no. (%)§	
Lupus anticoagulant	241 (20.5)
Anticardiolipin	138 (12.1)
Anti–β_2-glycoprotein I	163 (14.3)
Anti–ribosomal P	112 (9.9)
Anti-NR2	130 (12.2)

* SLE = systemic lupus erythematosus; ACR = American College of Rheumatology; SLEDAI-2K = SLE Disease Activity Index 2000; ASA = acetylsalicylic acid.
† Data were not available for all patients.
‡ The Systemic Lupus International Collaborating Clinics/American College of Rheumatology damage index (SDI) was not available in 1,058 patients with a disease duration of <6 months at the enrollment visit.
§ Data were available for 1,174 patients for lupus anticoagulant, 1,142 patients for anticardiolipin and anti–β_2-glycoprotein I, 1,136 patients for anti–ribosomal P, and 1,064 patients for anti-NR2.

neuropathy (either peripheral neuropathy, mononeuropathy, or cranial neuropathy attributed to SLE in model B). Hazard ratios (HRs) and 95% confidence intervals (95% CIs) were calculated. Due to sparse data, logistic regression with generalized estimating equation (GEE) estimation was used to analyze grouped Likert scale outcomes (≥5 versus ≤4) for unresolved SLE neuropathies. Cox regression was also used for analyzing the time to resolution since it examines how quickly the neuropathy events resolved, while the analysis of the Likert scale outcome examines the probability of a neuropathy event being improved (if not resolved) at a specific time point. Covariates examined included sex, race/ethnicity, SLICC sites, postsecondary education, number of ACR criteria met at enrollment, age at SLE diagnosis, the presence or absence of autoantibodies at baseline and, as time-varying variables updated at each assessment, SDI (without NP variables), other concurrent NP events, age at SLE diagnosis, disease duration (in years), SLEDAI-2K (without NP variables, standardized by taking [x–4]/4), the presence or absence of autoantibodies at follow-up assessments, and medication use since last assessment (glucocorticoids, antimalarials, immunosuppressants, anticoagulants). For analyses of the physician-assessed outcomes of neuropathy, history of SLE neuropathy prior to the onset of the current event, SLE attribution, and subtypes of neuropathies were also examined. For analyses of longitudinal SF-36 summary scores, linear regression with GEE estimation allowed for correlation of observations within patients and adjustment for variables including time/visit, sex, age at SLE diagnosis, race/ethnicity/location, education, SLEDAI-2K and SDI scores (without NP variables), and glucocorticoid, antimalarial, and immunosuppressant use since last assessment.

RESULTS

Patient characteristics. A total of 1,827 patients were recruited between October 1999 and December 2011, from centers in the US (n = 540 [29.5%]), Europe (n = 477 [26.1%]), Canada (n = 418 [22.9%]), Mexico (n = 223 [12.2%]), and Asia (n = 169 [9.3%]). Patient characteristics are shown in Table 1. The number of patient assessments varied from 1 to 19, with a mean ± SD follow-up of 7.6 ± 4.6 years, and the final assessment took place in September 2017.

NP manifestations. NP events (≥1) occurred in 955 (52.3%) of 1,827 patients, and 493 (27.0%) of 1,827 patients experienced ≥2 events during the study period. There were 1,910 unique NP events, encompassing all 19 NP syndromes in the ACR case definitions (5). The proportion of NP events attributed to SLE varied from 17.9% (in attribution model A) to 31.0% (in attribution model B), and these events occurred in 13.5% of patients (in model A) to 21.2% of patients (in model B). Of the 1,910 unique NP events, 1,749 (91.6%) involved the CNS and 161 (8.4%) involved the PNS (5). Of the NP events, 1,479 (77.4%) were classified as diffuse and 431 (22.6%) were classified as focal (10).

PNS manifestations. There were 161 PNS events in 139 (7.6%) of 1,827 patients (Table 2). Fifty-four (33.5%) of the 161 PNS events were identified at the enrollment visit (13 preceded the diagnosis of SLE by up to 4 months), and the remainder presented over the ensuing follow-up period. The most frequent events were peripheral neuropathy (66 of 161 [41.0%]), mononeuropathy (44 of 161 [27.3%]), 17 of which (38.6%) were multiplex, and cranial neuropathy (39 of 161 [24.2%]); there were few patients in the remaining categories: autonomic neuropathy (4 of 161 [2.5%]), myasthenia gravis (3 of 161 [1.9%]), acute inflammatory demyelinating polyradiculoneuropathy (Guillain-Barré syndrome) (3 of 161 [1.9%]), and plexopathy (2 of 161 [1.2%]). For the patients with peripheral neuropathy or mononeuropathy who underwent electrophysiologic testing (60 of 110 [54.5%]), the predominant abnormality was axonal damage (25 of 60 [41.7%]) followed by demyelination (13 of 60 [21.7%]). Of the 31 patients with peripheral neuropathy who underwent electrophysiologic testing, 5 (16.1%) had isolated sensory neuropathy, 3 (9.7%) had isolated motor neuropathy, and 22 (71%) had sensorimotor neuropathy. The most frequent cranial neuropathies were II (32.6%), VIII (27.9%), VII (9.3%), V, VI, IX (all 7%), III (4.7%), I, and IV (both 2.3%).

Table 2. Characteristics and attribution of PNS disease events in SLE patients throughout the duration of the study*

PNS disease	Total no. of PNS events	PNS events attributed to SLE (model A)	PNS events attributed to SLE (model B)	PNS events attributed to non-SLE causes
Peripheral neuropathy	66	25 (37.9)	30 (45.5)	36 (54.5)
Mononeuropathy, single or multiplex	44	24 (54.5)	44 (100)	0 (0)
Cranial neuropathy	39	32 (82.1)	35 (89.7)	4 (10.3)
Plexopathy	2	0 (0)	0 (0)	2 (100)
Autonomic neuropathy	4	3 (75.0)	3 (75.0)	1 (25.0)
Acute inflammatory demyelinating polyradiculoneuropathy (Guillain-Barré syndrome)	3	3 (100)	3 (100)	0 (0)
Myasthenia gravis	3	1 (33.3)	3 (100)	0 (0)
Total no. of PNS events	161	88 (54.7)	118 (73.3)	43 (26.7)

* Two attribution models of different stringency (model A and model B) were used, as described in Patients and Methods. Except where indicated otherwise, values are the number (%). PNS = peripheral nervous system; SLE = systemic lupus erythematosus.

Eighty-eight (54.7%) of the 161 events in 80 (57.6%) of 139 patients were attributed to SLE using model A, and 118 (73.3%) of 161 events in 104 (74.8%) of 139 patients were attributed to SLE using model B attribution rules. Using model B, the majority of neuropathies were attributed to SLE, with the exception of peripheral neuropathies, of which 36 (54.5%) of 66 were attributed to the non-SLE category. In 34 (94.4%) of these 36 cases, electrophysiologic studies were not done, which precluded attributing the neuropathy to SLE as per the attribution rules. An alternative cause for the peripheral neuropathy was identified in only 8 cases (hypothyroidism in 6 and vitamin deficiency in 2).
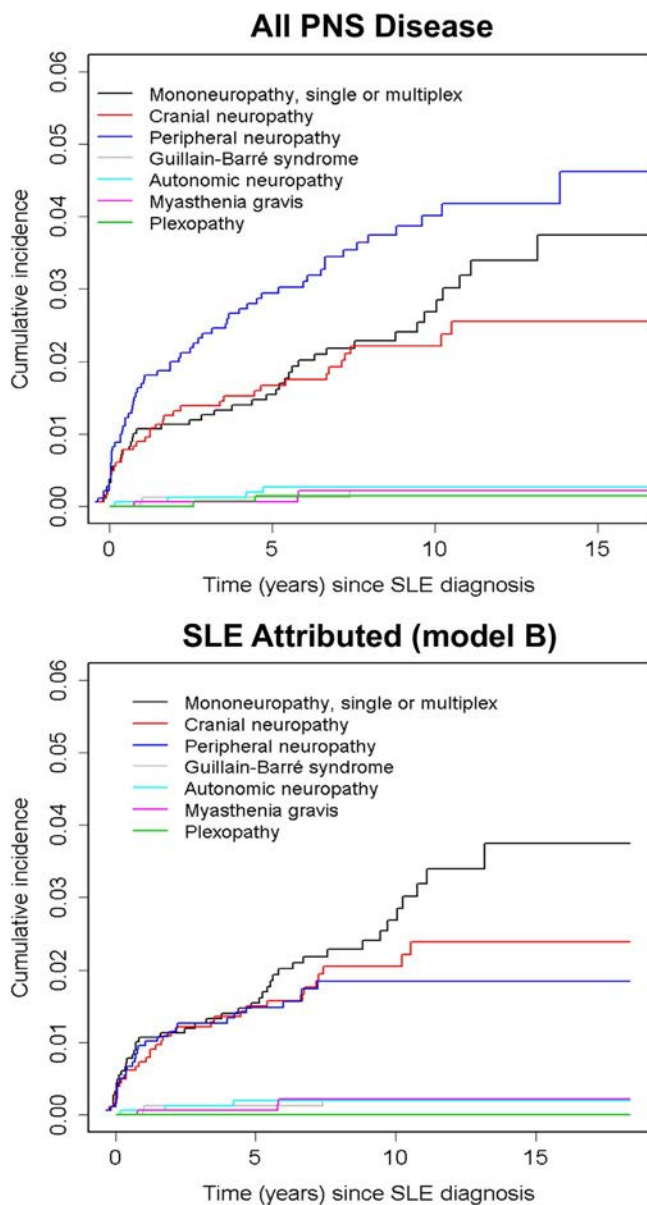
Figure 1. Estimated cumulative incidence of all peripheral nervous system (PNS) disease (top) and PNS attributed to systemic lupus erythematosus (SLE) using attribution model B (described in Patients and Methods) (bottom).

The estimated cumulative incidence of any PNS event regardless of attribution was 8.8% (95% CI 7.3–10.3%), and for events attributed to SLE (according to model B attribution rules) the estimated cumulative incidence was 6.5% (95% CI 5.2–7.8%) after 10 years (see Figure 1 for rates of specific neuropathy types). In patients with a previous PNS event attributed to SLE, the estimate of recurrence at 5 years after the initial PNS event was 11.7% (95% CI 4.6–18.4%). The incidence rate of first SLE PNS event was 7.4 per 1,000 person-years, and the incidence of recurrence was 18.2 per 1,000 person-years.

Clinical and laboratory associations with PNS disease attributed to SLE. Using Cox regression we looked for associations with the risk of the first episode of either peripheral neuropathy, mononeuropathy, or cranial neuropathy attributed to SLE using attribution model B. There were insufficient numbers of the other neuropathies to perform this and subsequent analyses. Univariate analysis revealed a negative association with Asian race/ethnicity (HR 0.40 [95% CI 0.18–0.88]) and postsecondary education (HR 0.65 [95% CI 0.43–0.98]) and a positive association with other concurrent central NP events (HR 2.96 [95% CI 1.66–5.26]) or diffuse NP events (HR 2.58 [95% CI 1.25–5.33]) (cerebrovascular disease, cognitive dysfunction, psychosis) attributed to SLE. There was no association between neuropathy and any of the autoantibodies examined. Multivariate analyses, which included these variables, indicated similar trends for Asian race/ethnicity (HR 0.42 [95% CI 0.19– 0.93]), post secondary education (HR 0.69 [0.45–1.04]), and other concurrent NP events attributed to SLE (HR 2.74 [95% CI 1.49–5.03]), but the effect of postsecondary education had a slightly wider confidence interval.

Clinical outcome of PNS events. Of 149 neuropathies (peripheral neuropathy, mononeuropathy, and cranial neuropathy) 76 (51.0%) were resolved by the end of study (27 peripheral neuropathies, 23 mononeuropathies, and 26 cranial neuropathies). Figure 2 illustrates the probability of these neuropathies not resolving over time. For the total group the estimated probability at 10 years was 37.2% (95% CI 27.6–50.0%), for peripheral neuropathy it was 42.6% (95% CI 25.4–71.6%), for mononeuropathy it was 28.6% (95% CI 14.1–58.0%), and for cranial neuropathy it was 30.4% (95% CI 18.5–49.8%). Although the probability of resolution was comparable for all 3 types of neuropathy, the time to reach resolution was most rapid for cranial neuropathy, followed by mononeuropathy and peripheral neuropathy.

In univariate Cox regression analyses, resolution times were negatively associated with history of neuropathy prior to the onset of the current neuropathy (HR 0.38 [95% CI 0.16–0.88]), older age at SLE diagnosis (HR 0.75 [95% CI 0.58–0.96]), and peripheral neuropathy versus cranial neuropathy (HR 0.44 [95% CI 0.24–0.80]) and mononeuropathy (HR 0.67 [95% CI 0.41–1.08]), (P = 0.027 [2 degrees of freedom]). These findings suggest that history of neuropathy, older age at SLE diagnosis, and peripheral versus
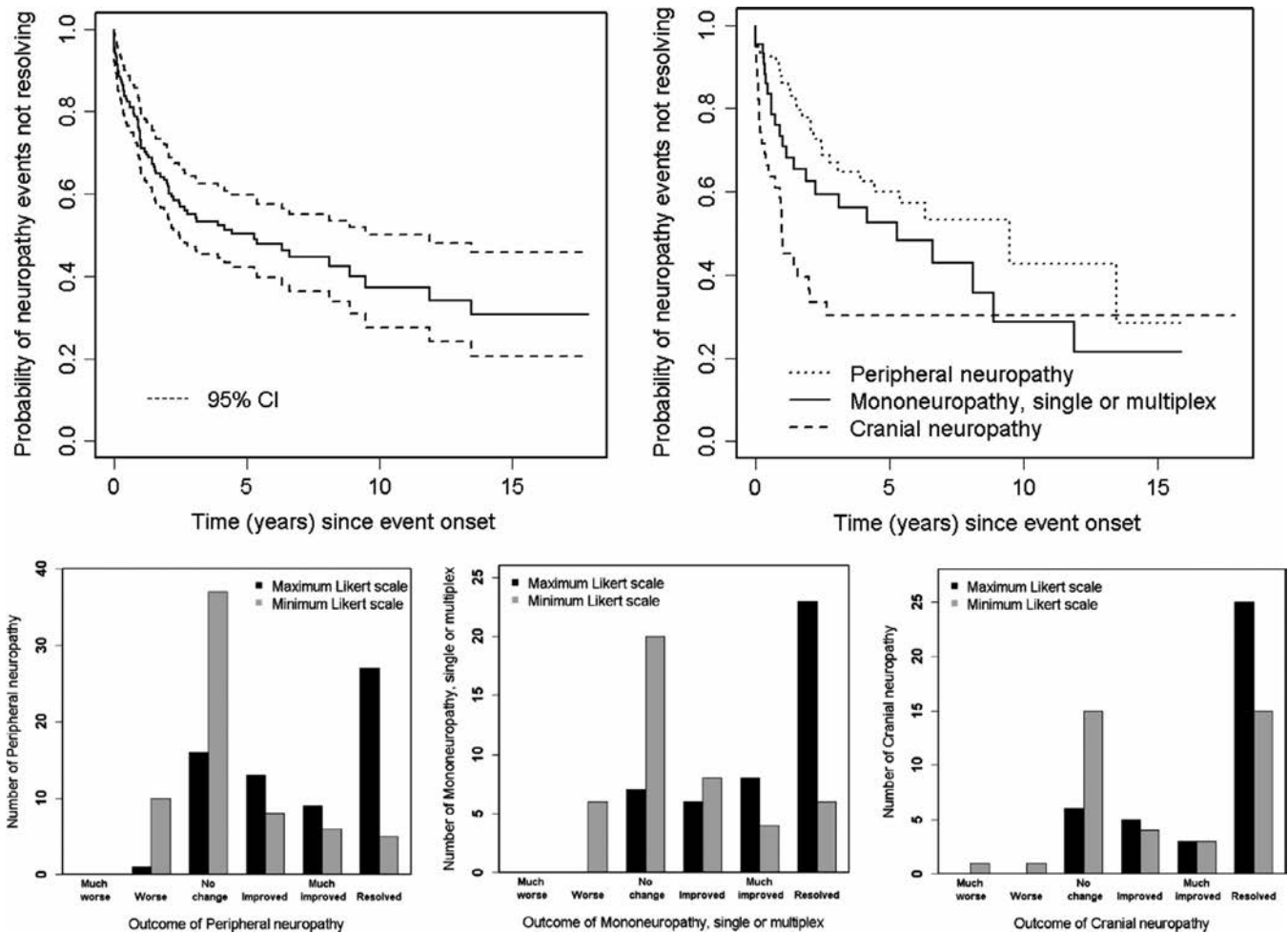
Figure 2. Physician-determined change in peripheral neuropathy, mononeuropathy, and cranial neuropathy (n = 149) attributed to systemic lupus erythematosus (SLE) or non-SLE using attribution model B (described in Patients and Methods). Top, Survival curves for resolution of all neuropathies (left) and individual neuropathies (right). 95% CI = 95% confidence interval. Bottom, Likert scale scores for physician assessment of outcome over the duration of followup. Scores are shifted to the right, indicating improvement. This improvement is most pronounced for cranial neuropathies (right).

cranial neuropathy and possibly mononeuropathy were all factors indicating longer time to resolution. In multivariate analyses, we noted persistent negative associations between time to resolution and history of neuropathy (HR 0.38 [95% CI 0.16–0.90]), older age at SLE diagnosis (HR 0.76 [95% CI 0.60–0.98]), and for peripheral neuropathy versus cranial neuropathy (HR 0.45 [95% CI 0.25–0.82]) and versus mononeuropathy (HR 0.74 [95% CI 0.44–1.22]) (P = 0.034 [2 degrees of freedom]). The multivariate analyses also suggested longer time to resolution with higher SLEDAI-2K score (excluding NP variables) (HR for an increase of 4 in SLEDAI 0.71 [95% CI 0.51–0.99]).

Figure 2 summarizes the distribution of maximum and minimum Likert scale scores indicating physician assessment of outcome of neuropathies during follow-up. The Likert scale scores over the duration of follow-up are shifted to the right, indicating improvement, and this is most pronounced for cranial neuropathies. In univariate analyses, lower probabilities of improvement in unresolved neuropathies at a specific time point since onset were

associated with history of neuropathy (odds ratio [OR] 0.45 [95% CI 0.29–0.69]), US sites versus European sites (OR 0.40 [95% CI 0.84–0.95]), longer disease duration prior to onset of neuropathy (OR –0.90 [95% CI 0.83–0.99]), and presence of anti-NR2 antibodies at enrollment [OR 0.18 [95% CI 0.03–0.91]). The associations with geographical region (P by global test 0.05), longer disease duration prior to onset of neuropathy (P = 0.011), and for those patients with antibody measurements available, the presence of anti-NR2 antibodies at enrollment (P = 0.008) remained in the multivariate analyses.

Health-related quality of life (HRQoL) and PNS events. The association between peripheral neuropathy, mononeuropathy, and cranial neuropathy grouped together and SF-36 summary and subscale scores is illustrated in Figure 3 using data in the following 3 groups of patients over time: 1) patients with any neuropathy event occurring at or prior to the study assessment, 2) patients with any NP event other than a neuropathy
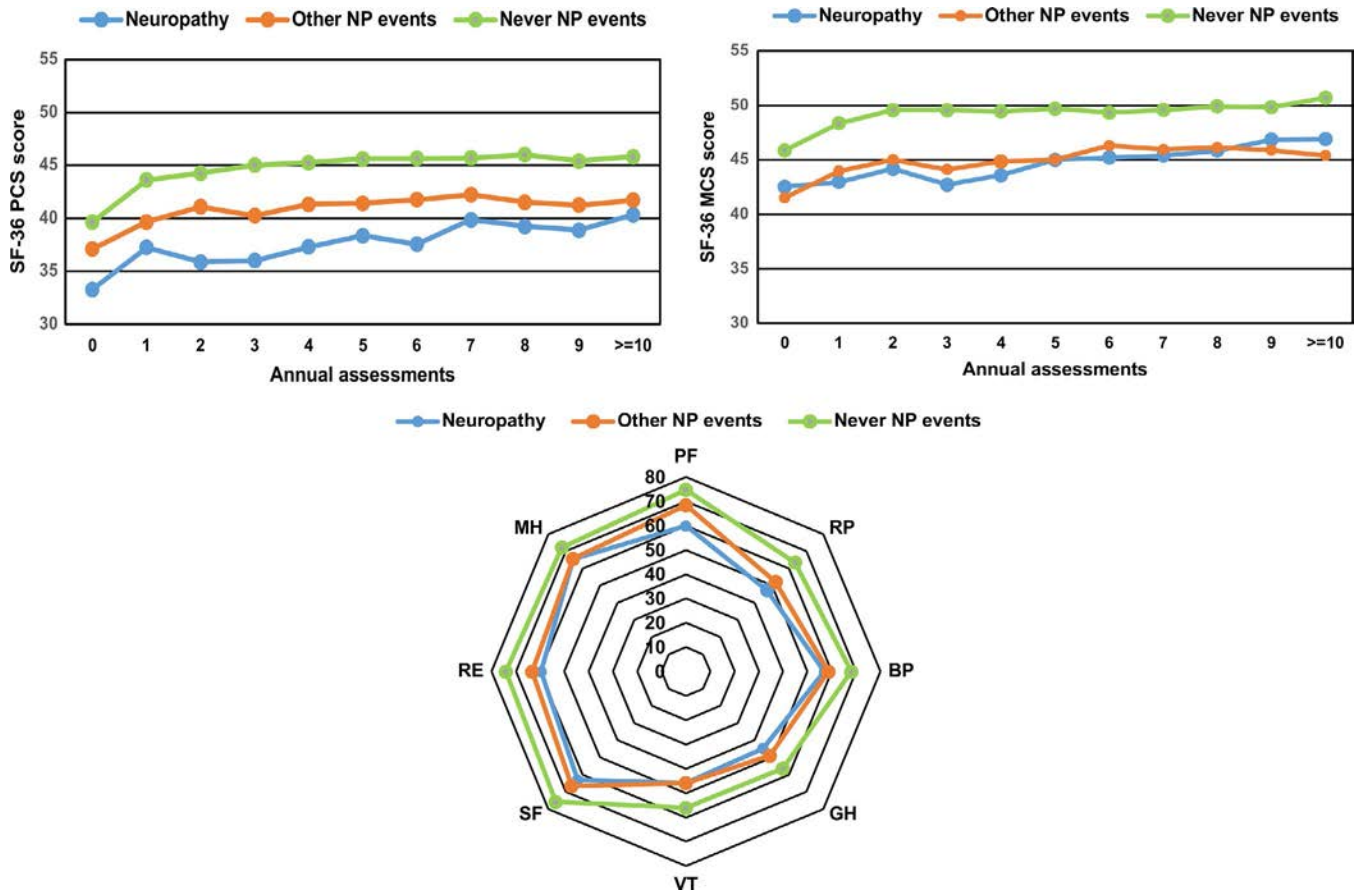
Figure 3. Association of Short Form 36 (SF-36) summary and subscale scores with neuropathy (peripheral neuropathy, mononeuropathy, and cranial neuropathy) attributed to systemic lupus erythematosus (SLE) or non-SLE using attribution model B (described in Patients and Methods) for the following 3 patient groups: 1) patients with neuropathy events occurring at or prior to the study assessment, 2) patients with any neuropsychiatric (NP) event other than a neuropathy event occurring at or prior to the study assessment, and 3) patients who never had any NP event up to the study assessment. Top, SF-36 physical component summary (PCS) scores (left) and mental component summary (MCS) scores (right) with neuropathy over time. Bottom, Comparison of individual SF-36 subscale scores in the 3 patient groups. The SF-36 subscales are vitality (VT), social function (SF), role-emotional (RE), mental health (MH), physical function (PF), role-physical (RP), bodily pain (BP), and general health (GH). Values are the mean.

event occurring at or prior to the study assessment, and 3) patients who never had any NP event up to the study assessment. Once assigned, each patient retained the same group membership throughout the follow-up period until they had a new or subsequent NP event, which could trigger a change in group assignment.

Using scores from all assessments, the lowest PCS score occurred in patients with neuropathies (mean ± SD 38.9 ± 12.3) compared to patients with other NP events (mean ± SD 40.8 ± 11.7) and patients without NP events (mean ± SD 44.1 ± 10.9) (overall $P < 0.001$ after adjustment for covariates). Similar but less marked differences in MCS scores were seen with the same group assignments (mean ± SD 46.0 ± 12.0 for patients with neuropathies versus 44.9 ± 12.2 for patients with other NP events versus 48.9 ± 10.7 for patients without NP events) (overall $P < 0.0001$ after adjustment). For both PCS and MCS scores there were significant differences between patients with neuropathy and patients without NP events ($P < 0.0001$ and $P = 0.0008$, respectively) but not between patients with neurop-

athy and patients with other NP events ($P > 0.05$) after adjustments. The group differences in PCS and MCS scores over time (Figure 3) persisted for 10 years of follow-up (global P for group effects <0.0001 after adjustments). Using scores from all assessments, the mean group differences in individual SF-36 subscale scores in the same 3 groups of patients (Figure 3) indicated that at least 6 of 8 self-reported health domains were lower in patients with SLE neuropathy compared to the other 2 groups.

The change in patient self-reported HRQoL following physician-determined resolution of peripheral neuropathy, mononeuropathy, or cranial neuropathy was examined by comparing SF-36 scores in the following groups of patients (Figure 4): 1) active peripheral neuropathy, 2) resolved peripheral neuropathy, 3) active mononeuropathy, 4) resolved mononeuropathy, 5) active cranial neuropathy, 6) resolved cranial neuropathy, 7) any active NP event other than peripheral neuropathy, mononeuropathy, or cranial neuropathy, 8) any resolved NP event other than peripheral neuropathy,
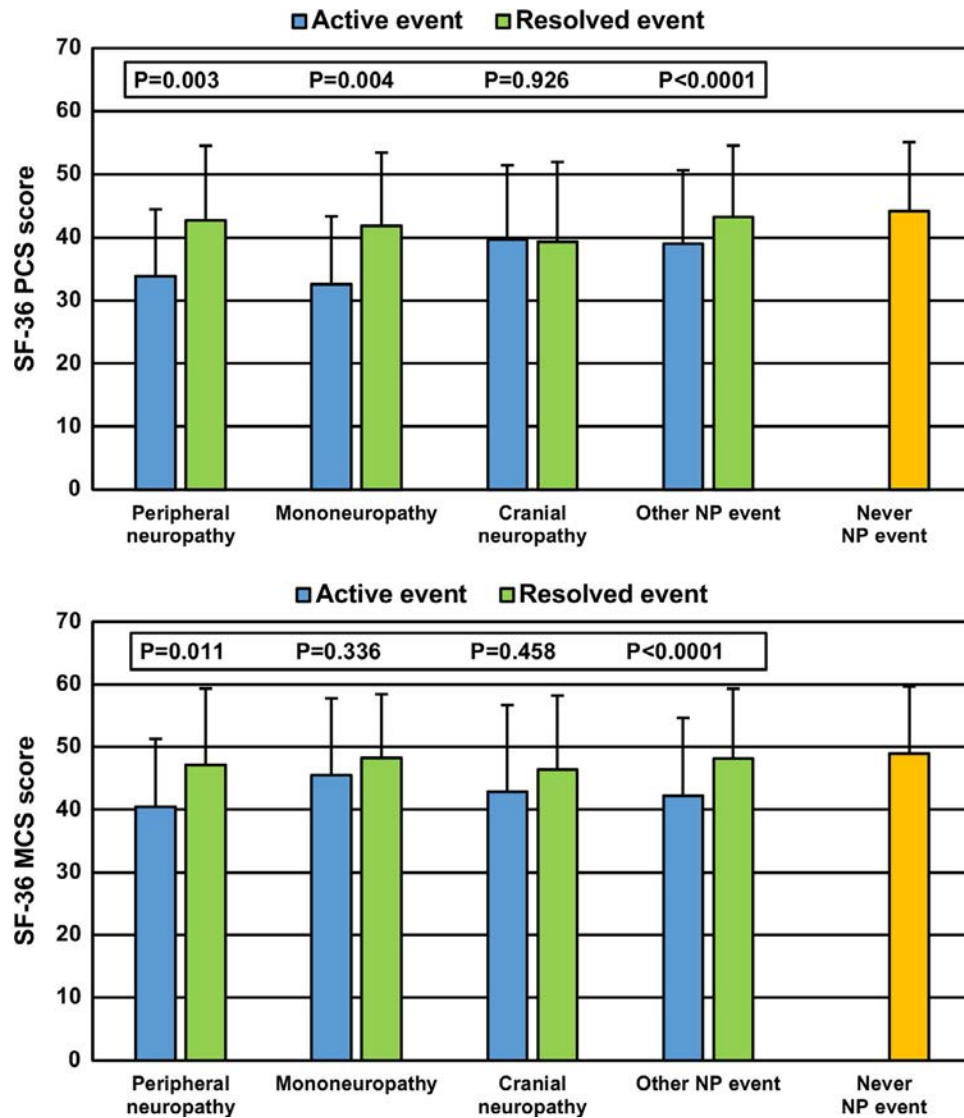
Figure 4. Change in Short Form 36 (SF-36) physical component summary (PCS) scores (top) and mental component summary (MCS) scores (bottom) following resolution of neuropathy (peripheral neuropathy, mononeuropathy, and cranial neuropathy) attributed to systemic lupus erythematosus (SLE) or non-SLE using attribution model B (described in Patients and Methods) for the following groups: 1) peripheral neuropathy events (n = 235) that occurred at or prior to the study assessment up to resolution, 2) resolved peripheral neuropathy events (n = 130) up to last follow-up or recurrence of peripheral neuropathy, 3) mononeuropathy events (n = 135) that occurred at or prior to the study assessment up to resolution, 4) resolved mononeuropathy events (n = 120) up to last follow-up or recurrence of mononeuropathy, 5) cranial neuropathy events (n = 89) that occurred at or prior to the study assessment up to resolution, 6) resolved cranial neuropathy events (n = 130) up to last follow-up or recurrence of cranial neuropathy, 7) any neuropsychiatric (NP) event (n = 2,718) other than peripheral neuropathy, mononeuropathy, or cranial neuropathy events that occurred at or prior to the study assessment, 8) any resolved NP event (n = 2,307) other than peripheral neuropathy, mononeuropathy, or cranial neuropathy up to last follow-up or recurrence, and 9) no NP event (n = 6,064) up to the study assessment. Bars show the mean ± SD.

mononeuropathy, or cranial neuropathy, and 9) patients who never had any NP event. Due to the small number of unique patients for some groups, adjustments for other variables were not performed in the linear regression with GEE estimation. In parallel with physician-determined resolution, there was a clinically and statistically significant improvement in PCS scores for peripheral and mononeuropathies and a similar improvement in MCS scores for peripheral neuropathies. These changes were similar to those seen in patients with other non-neuropathy

NP events, and the final PCS and MCS scores were similar to those reported by patients who never had an NP event.

DISCUSSION

The focus of the present study was PNS disease in a large international inception cohort of patients in the first decade following the diagnosis of SLE. PNS manifestations in SLE were confirmed to be uncommon (7.6% of patients), and of the 7 ACR

case definitions for PNS disease in NPSLE, only peripheral neuropathy (41.0% of PNS events), mononeuropathy (27.3% of PNS events), and cranial neuropathy (24.2% of PNS events) occurred with notable frequency. Although peripheral neuropathy was frequently attributed to non-SLE causes, this was because 35 (53%) of 66 of these patients did not undergo electrophysiologic testing, which precluded attributing the neuropathy to SLE. In only a minority of cases was an alternative cause for peripheral neuropathy identified, and thus we cannot exclude the possibility that many more of the peripheral neuropathies could have been due to SLE. Physician-determined outcomes were generally favorable, although the speed of resolution differed between the 3 types of neuropathy and was most rapid for cranial neuropathy. The occurrence of PNS disease was associated with a reduction in patient self-reported HRQoL. Following resolution this improved significantly for peripheral and mononeuropathy but not for cranial neuropathy.

Although PNS manifestations are well recognized in SLE patients, the literature consists largely of individual case reports and small case series. There have been 3 large, single-center, prevalent cohort studies of SLE patients (18–20) with longitudinal follow-up in one (18). Oomatia et al (19) reported peripheral neuropathy in 123 (5.9%) of 2,097 patients, which was attributed to SLE in 66.7% of cases and associated with lower SLE disease activity and cumulative organ damage. A cross-sectional study by Toledano et al (20) used the ACR case definitions to characterize PNS disease. Overall, 93 (17.7%) of 524 patients had disease attributed to SLE. The most frequent manifestation was peripheral neuropathy (36.6%), followed by mononeuropathy (23.7%), cranial neuropathy, myasthenia gravis (7.5% each), and Guillain-Barré syndrome (1.1%). In the most comprehensive study to date, by Florica et al (18), 207 (14%) of 1,533 patients had PNS disease, which was attributed to SLE in 60% of cases. Peripheral neuropathy was diagnosed in 56%, cranial neuropathy in 13%, mononeuropathy in 11%, and mononeuritis multiplex in 9% of patients with PNS disease. Electrophysiologic studies were available for 126 (60.8%) of 207 patients and indicated axonal neuropathy in 70% and demyelination in 20% of patients, regardless of attribution to SLE and non-SLE causes. In a nested case–control design, those with PNS events had significantly more CNS involvement, higher SLE disease activity, and lower patient self-reported HRQoL compared with patients without PNS events.

The present study supports and expands the findings of previous work (18–21). The overall frequency of PNS events in our study (7.6%) was higher than that reported by Oomatia et al (5.9%) (19) but lower than that in the other 2 large cohort studies (14% and 17.7%) (18,20). This is to be expected in view of the differences between inception and prevalent disease cohorts. Our findings regarding the relative frequency of different types of PNS events, as defined by the ACR case definitions, are consistent with the findings of Florica et al (18) and Toledano et al (20), as is the proportion of PNS events attributed to SLE (18,19). The pres-

ent study demonstrates that PNS disease increases over time, at least over the first 10 years. This is in contrast to some other NP manifestations (e.g., seizures [22], cerebrovascular events [1]) and non-NP manifestations of SLE (e.g., nephritis [23]) which have a strong predilection to present early in the disease course and frequently as part of the initial manifestations of SLE. The outcomes of the different PNS manifestations, as determined by physician assessment, indicated a similar degree of improvement and resolution across neuropathy type, although the rate of improvement was most rapid for cranial neuropathies. Factors associated with a slower improvement were older age at SLE diagnosis, longer disease duration at onset of neuropathy, active SLE outside of the nervous system, and recurrent PNS events. There was no association between the onset of PNS events and any of the selected panel of autoantibodies, including previously reported associations with anti–ribosomal P (24) and anticardiolipin antibodies (25). The presence of anti-NR2 antibodies was associated with a slower rate of improvement of PNS events, which has not previously been reported and requires further study to demonstrate the reproducibility and/or plausibility of this result.

One of the goals of our study was to determine the impact of PNS events on patient-reported HRQoL, as reflected by SF-36 summary and subscale scores, as this has only been examined in one previous study (18). Compared to no NP events, the occurrence of any of the 3 most frequent neuropathies was associated with a significant reduction in HRQoL, which was comparable to that seen with other NP events. As expected, the negative effect on HRQoL was most profound on patient-reported physical function, although mental function was also impacted. Florica et al (18) reported similar findings. We also examined the potential reversibility of low HRQoL by analyzing the change in SF-36 summary scores in patients who had a physician-determined resolution of neuropathy. There were statistically significant and clinically meaningful improvements in HRQoL scores reported by patients who had resolution of peripheral neuropathy and mononeuropathy but not those who had resolution of cranial neuropathy. Baseline PCS scores, generated at the first annual assessment following the onset of the NP event, were better for patients with cranial neuropathy than for the other neuropathies and thus had less potential to improve. Due to the rapid improvement in cranial neuropathies (Figure 2), the first SF-36 summary scores following their onset were not adversely affected as occurred in patients with peripheral neuropathy and mononeuropathy, both of which had a slower recovery (Figure 2). Discrepancy between physician-reported and patient-reported outcomes has been seen in other SLE manifestations (1,26). This finding emphasizes the importance of capturing both physician and patient perspectives on the potential benefit of an intervention, be it in the treatment of individual patients or in the context of clinical trials.

There are some limitations to the present study. First, specialized investigations such as nerve conduction studies and test

batteries for autonomic dysfunction (27) were not routinely performed on all patients but were left to the discretion of individual investigators. It is likely that the universal application of such investigations would have detected additional PNS abnormalities. However, our research protocol more accurately reflects what is done in clinical practice, which was a deliberate strategy of our study. Furthermore, these investigations would not have helped to determine causal attribution for neuropathies (18). Second, the unavailability of autoantibody data for some patients and restriction to a panel of autoantibodies more suited to CNS disease may have limited our ability to fully assess the role of autoantibodies in the pathogenesis of PNS events. For example, some studies have shown associations with anti-Sm (28) and anti-Ro (29) and with the more specialized anti-ganglioside antibodies (30). Third, since this was an observational cohort study, any association between immunosuppressive therapies and outcome of neuropathies was difficult to determine, and we could not reliably identify symptomatic neurotropic therapies or the specific indications for their use. Similarly, SLE disease activity and autoantibodies were measured at annual assessments, which usually did not coincide precisely with the onset of neuropathies. Finally, although the ACR classification of NPSLE is quite detailed and extensive, the reports of PNS events were not reviewed centrally by a neurologist and there are PNS disease manifestations described in SLE that are not captured. These include small-fiber neuropathy (19,31) and chronic inflammatory demyelinating polyradiculoneuropathy (32). The former could account for some of the peripheral sensory neuropathies in patients with normal findings on electrophysiologic testing, and both entities should be considered in any revision of the ACR case definitions.

There are also many strengths to our study. These include a large disease inception cohort of SLE patients, the long-term prospective study design using a standardized protocol for data collection, and the identification of all PNS events with application of decision rules for determination of attribution. Overall, the results of our study provide a comprehensive overview of the frequency and characteristics of PNS disease in SLE patients, the impact on HRQoL, and the outcome with current treatment modalities for SLE. The findings provide a benchmark for the assessment of future treatment modalities.

AUTHOR CONTRIBUTIONS

REFERENCES

1. Hanly JG, Li Q, Su L, Urowitz MB, Gordon C, Bae SC, et al. Cerebrovascular events in systemic lupus erythematosus: results from an international inception cohort study. Arthritis Care Res (Hoboken) 2018;70:1478–87.

2. Hochberg MC, for the Diagnostic and Therapeutic Criteria Committee of the American College of Rheumatology. Updating the American College of Rheumatology revised criteria for the classification of systemic lupus erythematosus [letter]. Arthritis Rheum 1997;40:1725.

3. Petri M, Orbai AM, Alarcon GS, Gordon C, Merrill JT, Fortin PR, et al. Derivation and validation of the Systemic Lupus International Collaborating Clinics classification criteria for systemic lupus erythematosus. Arthritis Rheum 2012;64:2677–86.

4. Schmajuk G, Hoyer BF, Aringer M, Johnson SR, Daikh DI, Dörner T, on behalf of the SLE Classification Criteria Steering Committee and the International SLE Expert Panel of the Initiative. Multicenter Delphi exercise to identify important key items for classifying systemic lupus erythematosus. Arthritis Care Res (Hoboken) 2018;70:1488–94.

5. ACR Ad Hoc Committee on Neuropsychiatric Lupus Nomenclature. The American College of Rheumatology nomenclature and case definitions for neuropsychiatric lupus syndromes. Arthritis Rheum 1999;42:599–608.

6. Isenberg D, Ramsey-Goldman R, SLICC Group. Systemic Lupus International Collaborating Group—onwards and upwards? [editorial]. Lupus 2006;15:606–7.

7. Gladman DD, Ibañez D, Urowitz MB. Systemic lupus erythematosus disease activity index 2000. J Rheumatol 2002;29:288–91.

8. Gladman D, Ginzler E, Goldsmith C, Fortin P, Liang M, Urowitz M, et al. The development and initial validation of the Systemic Lupus International Collaborating Clinics/American College of Rheumatology damage index for systemic lupus erythematosus. Arthritis Rheum 1996;39:363–9.

9. Hanly JG, Urowitz MB, Sanchez-Guerrero J, Bae SC, Gordon C, Wallace DJ, et al, for the Systemic Lupus International Collaborating Clinics. Neuropsychiatric events at the time of diagnosis of systemic lupus erythematosus: an international inception cohort study. Arthritis Rheum 2007;56:265–73.

10. Hanly JG, Urowitz MB, Su L, Sanchez-Guerrero J, Bae SC, Gordon C, et al, for the Systemic Lupus International Collaborating Clinics. Short-term outcome of neuropsychiatric events in systemic lupus erythematosus upon enrollment into an international inception cohort study. Arthritis Rheum 2008;59:721–9.

11. Ainiala H, Hietaharju A, Loukkola J, Peltola J, Korpela M, Metsänoja R, et al. Validity of the new American College of Rheumatology criteria for neuropsychiatric lupus syndromes: a population-based evaluation. Arthritis Rheum 2001;45:419–23.

12. Hanly JG, Urowitz MB, Jackson D, Bae SC, Gordon C, Wallace DJ, et al, for the Systemic Lupus International Collaborating Clinics (SLICC). SF-36 summary and subscale scores are reliable outcomes of neuropsychiatric events in systemic lupus erythematosus. Ann Rheum Dis 2011;70:961–7.

13. Thumboo J, Fong KY, Ng TP, Leong KH, Feng PH, Thio ST, et al. Validation of the MOS SF-36 for quality of life assessment of patients with systemic lupus erythematosus in Singapore. J Rheumatol 1999;26:97–102.

14. Merrill JT, Zhang HW, Shen C, Butman BT, Jeffries EP, Lahita RG, et al. Enhancement of protein S anticoagulant function by β2-glycoprotein I, a major target antigen of antiphospholipid antibodies: β2-glycoprotein I interferes with binding of protein S to its plasma inhibitor, C4b-binding protein. Thromb Haemost 1999;81:748–57.

15. Merrill JT, Shen C, Gugnani M, Lahita RG, Mongey AB. High prevalence of antiphospholipid antibodies in patients taking procainamide. J Rheumatol 1997;24:1083–8.

16. Erkan D, Zhang HW, Shriky RC, Merrill JT. Dual antibody reactivity to β2-glycoprotein I and protein S: increased association with thrombotic events in the antiphospholipid syndrome. Lupus 2002;11:215–20.

17. Hanly JG, Urowitz MB, Siannis F, Farewell V, Gordon C, Bae SC, et al. Autoantibodies and neuropsychiatric events at the time of systemic lupus erythematosus diagnosis: results from an international inception cohort study. Arthritis Rheum 2008;58:843–53.

18. Florica B, Aghdassi E, Su J, Gladman DD, Urowitz MB, Fortin PR. Peripheral neuropathy in patients with systemic lupus erythematosus. Semin Arthritis Rheum 2011;41:203–11.

19. Oomatia A, Fang H, Petri M, Birnbaum J. Peripheral neuropathies in systemic lupus erythematosus: clinical features, disease associations, and immunologic characteristics evaluated over a twenty-five–year study period. Arthritis Rheumatol 2014;66:1000–9.

20. Toledano P, Orueta R, Rodriguez-Pintó I, Valls-Solé J, Cervera R, Espinosa G. Peripheral nervous system involvement in systemic lupus erythematosus: prevalence, clinical and immunological characteristics, treatment and outcome of a large cohort from a single centre [review]. Autoimmun Rev 2017;16:750–5.

21. Bortoluzzi A, Piga M, Silvagni E, Chessa E, Mathieu A, Govoni M. Peripheral nervous system involvement in systemic lupus erythematosus: a retrospective study on prevalence, associated factors and outcome. Lupus 2019;28:465–74.

22. Hanly JG, Urowitz MB, Su L, Gordon C, Bae SC, Sanchez-Guerrero J, et al. Seizure disorders in systemic lupus erythematosus: results from an international, prospective, inception cohort study. Ann Rheum Dis 2012;71:1502–9.

23. Hanly JG, O'Keeffe AG, Su L, Urowitz MB, Romero-Diaz J, Gordon C, et al. The frequency and outcome of lupus nephritis: results from an international inception cohort study. Rheumatology (Oxford) 2016;55:252–62.

24. Gaber W, Ezzat Y, El Fayoumy NM, Helmy H, Mohey AM. Detection of asymptomatic cranial neuropathies in patients with systemic lupus erythematosus and their relation to antiribosomal P antibody levels and disease activity. Clin Rheumatol 2014;33:1459–66.

25. Ubogu EE, Zaidat OO, Suarez JI. Acute motor-sensory axonal neuropathy associated with active systemic lupus erythematosus and anticardiolipin antibodies. J Clin Rheumatol 2001;7:326–31.

26. Golder V, Ooi JJ, Antony AS, Ko T, Morton S, Kandane-Rathnayake R, et al. Discordance of patient and physician health status concerns in systemic lupus erythematosus. Lupus 2018;27:501–6.

27. Straub RH, Zeuner M, Lock G, Rath H, Hein R, Schölmerich J, et al. Autonomic and sensorimotor neuropathy in patients with systemic lupus erythematosus and systemic sclerosis. J Rheumatol 1996;23:87–92.

28. Huynh C, Ho SL, Fong KY, Cheung RT, Mok CC, Lau CS. Peripheral neuropathy in systemic lupus erythematosus. J Clin Neurophysiol 1999;16:164–8.

29. Su YJ, Huang CR, Chang WN, Tsai NW, Kung CT, Lin WC, et al. The association between autoantibodies and peripheral neuropathy in lupus nephritis. Biomed Res Int 2014;2014:524940.

30. Labrador-Horrillo M, Martinez-Valle F, Gallardo E, Rojas-Garcia R, Ordi-Ros J, Vilardell M. Anti-ganglioside antibodies in patients with systemic lupus erythematosus and neurological manifestations. Lupus 2012;21:611–5.

31. Gøransson LG, Tjensvoll AB, Herigstad A, Mellgren SI, Omdal R. Small-diameter nerve fiber neuropathy in systemic lupus erythematosus. Arch Neurol 2006;63:401–4.

32. Vina ER, Fang AJ, Wallace DJ, Weisman MH. Chronic inflammatory demyelinating polyneuropathy in patients with systemic lupus erythematosus: prognosis and outcome. Semin Arthritis Rheum 2005;35:175–84.

AMERICAN COLLEGE
of RHEUMATOLOGY
Empowering Rheumatology Professionals

Complement Activation in Patients With Probable Systemic Lupus Erythematosus and Ability to Predict Progression to American College of Rheumatology–Classified Systemic Lupus Erythematosus

Rosalind Ramsey-Goldman,[1] Roberta Vezza Alexander,[2] Elena M. Massarotti,[3] Daniel J. Wallace,[4] Sonali Narain,[5] Cristina Arriens,[6] (iD) Christopher E. Collins,[7] Amit Saxena,[8] Chaim Putterman,[9] Kenneth C. Kalunian,[10] Tyler O'Malley,[2] Thierry Dervieux,[2] and Arthur Weinstein[11] (iD)

Objective. To evaluate the frequency of cell-bound complement activation products (CB-CAPs) as a marker of complement activation in patients with suspected systemic lupus erythematosus (SLE) and the usefulness of this biomarker as a predictor of the evolution of probable SLE into SLE as classified by the American College of Rheumatology (ACR) criteria.

Methods. Patients in whom SLE was suspected by lupus experts and who fulfilled 3 ACR classification criteria for SLE (probable SLE) were enrolled, along with patients with established SLE as classified by both the ACR and the Systemic Lupus International Collaborating Clinics (SLICC) criteria, patients with primary Sjögren's syndrome (SS), and patients with other rheumatic diseases. Individual CB-CAPs were measured by flow cytometry, and positivity rates were compared to those of commonly assessed biomarkers, including serum complement proteins (C3 and C4) and autoantibodies. The frequency of a positive multianalyte assay panel (MAP), which includes CB-CAPs, was also evaluated. Probable SLE cases were followed up prospectively.

Results. The 92 patients with probable SLE were diagnosed more recently than the 53 patients with established SLE, and their use of antirheumatic medications was lower. At the enrollment visit, more patients with probable SLE were positive for CB-CAPs (28%) or MAP (40%) than had low complement levels (9%) ($P = 0.0001$ for each). In probable SLE, MAP scores of >0.8 at enrollment predicted fulfillment of a fourth ACR criterion within 18 months (hazard ratio 3.11, $P < 0.01$).

Conclusion. Complement activation occurs in some patients with probable SLE and can be detected with higher frequency by evaluating CB-CAPs and MAP than by assessing traditional serum complement protein levels. A MAP score above 0.8 predicts transition to classifiable SLE according to ACR criteria.

INTRODUCTION

Systemic lupus erythematosus (SLE) is a clinically heterogeneous autoimmune disease characterized by the presence of diverse autoantibodies and activation of the complement system (1). The classification criteria for SLE by the American College of Rheumatology (ACR) (2) and more recently by the Systemic Lupus International Collaborating Clinics (SLICC) (3)—both developed

for research purposes (3,4)—recognize this clinical and laboratory heterogeneity. Low levels of serum complement protein (C3 and C4) are included in the SLICC criteria as well as the classification criteria newly developed by the European League Against Rheumatism (EULAR) and the ACR (5), due to the relatively high specificity of complement activation leading to low serum complement in SLE (6).

Despite the specificity of hypocomplementemia, its frequency in SLE is low (1). We have previously shown that complement activation, measured reliably by assessing cell-bound complement activation products (CB-CAPs), especially C4d bound to erythrocytes (EC4d) and to B lymphocytes (BC4d), can be detected in SLE with greater frequency than by assessing high anti–double-stranded DNA (anti-dsDNA) and low serum complement proteins (7,8).

Many patients with suspected SLE who do not fulfill ACR criteria have been designated as having "probable, possible, latent, or incomplete" SLE (9–12). There is no consensus definition or nomenclature for these patients (13). However, some patients develop classifiable SLE over time (9–11). Currently, there are no biomarkers to reliably distinguish who, among patients with probable SLE, will develop SLE by classification criteria. However, early diagnosis and appropriate intervention may prevent lupus flares and more serious organ inflammation (9,14,15).

We hypothesized that probable SLE which ultimately develops into classifiable SLE may have detectable complement activation (1). Therefore, we conducted a cross-sectional and prospective study of patients with probable SLE to determine the frequency of elevated CB-CAPs in these patients and whether the presence of CB-CAPs, measured either directly or within a multianalyte assay panel (MAP), is predictive of development of classifiable SLE.

PATIENTS AND METHODS

Study populations. Adult patients were enrolled, in compliance with the Helsinki Declaration, from 2015 to 2017. Central or internal review boards at 7 academic institutions approved the study, and all subjects provided informed consent. Patients were recruited from lupus cohorts and faculty practices overseen by an experienced SLE investigator.

Patients with SLE fulfilled both the ACR classification criteria (2) and the SLICC classification criteria (3) for SLE at enrollment. Patients with probable SLE were enrolled if they fulfilled 3 ACR criteria, irrespective of whether they fulfilled the SLICC criteria, and if the investigator had a high suspicion of the diagnosis of lupus. Patients with probable SLE could not be enrolled if they had proteinuria of >200 mg or biopsy-proven lupus nephritis. Investigators were asked to examine the historic electronic records for clinical, hematologic, and immunologic features. The date of diagnosis for probable SLE was the date on which the third ACR criterion was confirmed.

Patients with probable SLE were followed up prospectively, and 69 patients had a first follow-up visit 9–18 months after enrollment. Investigators determined whether patients met a fourth ACR criteria at the follow-up visit and the approximate date that classifiable SLE occurred, either at or prior to evaluation.

Disease activity was measured in SLE and probable SLE using the Safety of Estrogens in Lupus Erythematosus National Assessment (SELENA) version of the SLE Disease Activity Index (SLEDAI) (16). Low complement and anti-dsDNA levels were scored if they were shown to be abnormal in the central clinical laboratory (Exagen, Vista, CA). Nonserologic SELENA–SLEDAI was calculated by excluding the anti-dsDNA and complement components from the score.

This study also included patients with primary Sjögren's syndrome (SS) and other well-defined rheumatic diseases, who served as controls. For the latter group (n = 51), clinical diagnosis was based on the expert opinion of the investigators, and the group included patients with rheumatoid arthritis (RA) (n = 31), psoriatic arthritis (n = 10), dermatomyositis (n = 4), juvenile idiopathic arthritis (n = 3), systemic sclerosis (n = 2), and ankylosing spondylitis (n = 1). Diagnosis of SS was based on a modification of the ACR criteria for SS (17), and patients were enrolled if positive for 2 of following 3 features: 1) current keratoconjunctivitis sicca in ≥1 eye with either an ocular staining score of ≥3 or a Schirmer's test result of ≤5 mm in 5 minutes; 2) labial or salivary biopsy with a positive focus score (≥1 focus/4 mm^2); 3) positive serum anti-SSA/Ro and/or anti-SSB/La and antinuclear antibody (ANA) titer of ≥1:80 determined by immunofluorescence assay (IFA).

Each of the 7 sites recruited patients with SLE, probable SLE, and other rheumatic diseases; patients with SS were recruited at 6 sites. Case report forms from the enrollment visit of all patients with probable SLE and 32 randomly selected patients with SLE were reviewed and adjudicated by a lupus expert clinician (KCK) not affiliated with any institution enrolling patients in the study. Case report forms from the probable SLE patient follow-up visits were adjudicated by 2 of the authors (KCK [n = 52] and AW [n = 17]) without knowledge of the results of the laboratory tests performed by Exagen (see below). The adjudicators assessed clinical features and routine laboratory tests, including complete blood cell counts and urinalyses, and the investigators were often asked to provide additional records as needed.

Patients provided venous blood samples that were collected in EDTA-containing tubes and serum separator tubes at all visits. Specimens were shipped overnight to Exagen for diagnostic immunology testing.

Biomarker analysis. ANA was measured using an enzyme-linked immunosorbent assay (ELISA) (QUANTA Lite; Inova Diagnostics) and indirect IFA (NOVA Lite; Inova Diagnostics) as described previously (8,18). Anti-dsDNA antibodies were also measured by ELISA and were confirmed using an IFA with *Crithidia luciliae* (8,18). Autoantibodies to extractable nuclear antigens

(anti-Sm, anti-SSB/La, anti-SSA/Ro, anti-CENP, anti–Jo-1, and anti–Scl-70), anti–cyclic citrullinated peptide (anti-CCP) antibodies, and rheumatoid factor (RF) were measured using the EliA test on the Phadia 250 platform (ThermoFisher Scientific) (19). The IgG, IgM, and IgA isotypes of anticardiolipin and anti–β$_2$-glycoprotein I, and the IgG isotype of anti-phosphatidylserine/prothrombin were measured using chemiluminescence immunoassay or ELISA.

Serum complement proteins C3 and C4 were measured by standard immunoturbidimetry assay (The Binding Site) (19) and were considered low if they were below the manufacturer's cutoff levels (81.1 mg/dl and 12.9 mg/dl, respectively). Individual CB-CAPs (EC4d and BC4d) were measured by quantitative flow cytometry and expressed as net mean fluorescence intensity (MFI), as previously described (8,19). CB-CAP positivity was determined by a net MFI of >14 for EC4d and/or a net MFI of >60 for BC4d. Assessment

of CB-CAPs was not available for 3 patients (2 SLE and 1 SS) at enrollment. These patients were included in all other analyses.

The MAP with algorithm, which included EC4d, BC4d, ANA, anti-dsDNA, anti-Sm, as well as other lupus and non-lupus autoantibodies, was evaluated as described in detail elsewhere (8,18,19). MAP assessment was not available for 3 patients (1 SLE, 1 probable SLE, and 1 SS) at enrollment; these subjects were included in all other analyses. For 1 of the follow-up visits, BC4d and MAP determination was not available; this visit was included in all other analyses.

Statistical analysis. Statistical comparisons were conducted using unpaired *t*-test, Mann-Whitney test, Fisher's exact test, chi-square test, or McNemar's test, as appropriate (Graph-Pad). Sensitivity, specificity, positive and negative likelihood
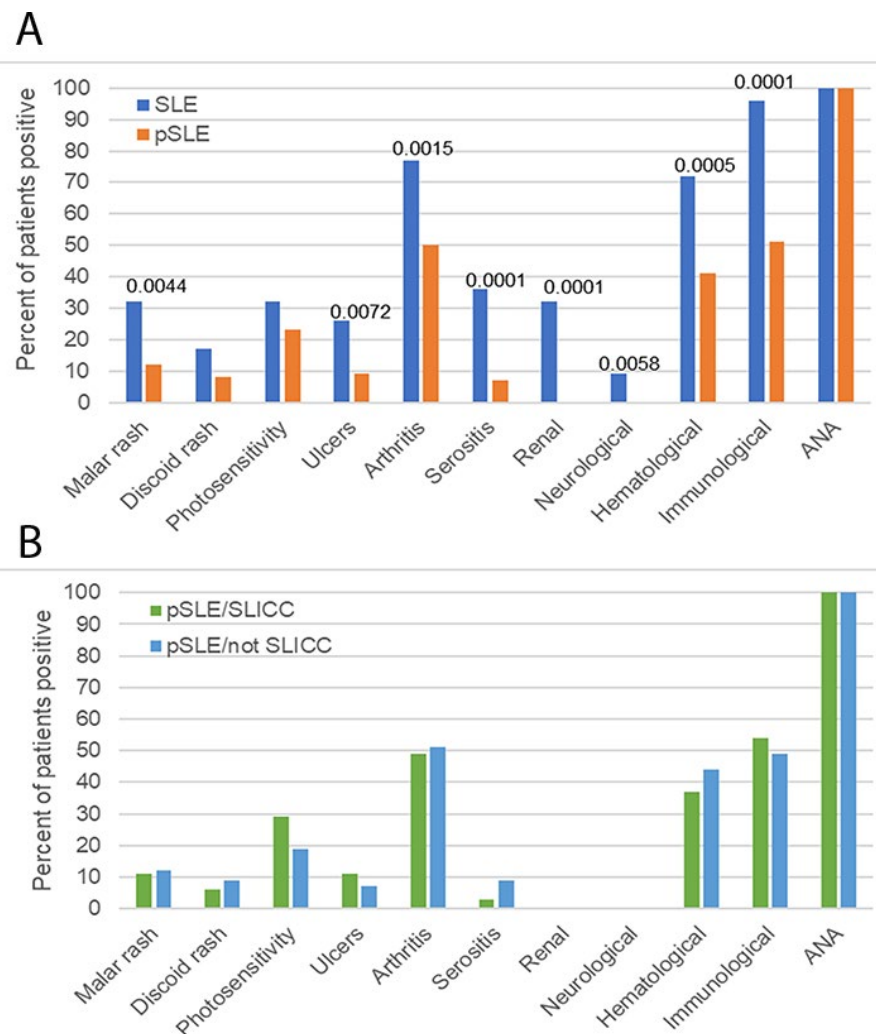
Figure 1. American College of Rheumatology (ACR) criteria for systemic lupus erythematosus (SLE) at enrollment. Clinical and immunologic 1997 ACR criteria were evaluated in the entire population of patients with SLE and patients with probable SLE (pSLE) (**A**) and in the probable SLE subgroups fulfilling or not fulfilling the 2012 Systemic Lupus International Collaborating Clinics (SLICC) criteria (**B**) at enrollment. All criteria, including antinuclear antibody (ANA) and immunologic criteria, refer to historical positivity. The average number of ACR criteria fulfilled by the patients with SLE was 5.3, while those with probable SLE fulfilled 3 ACR criteria (per study protocol). Statistically significant differences are indicated with *P* values, obtained by Fisher's exact test.

ratios (LRs) (8,18), and the Youden index (J = [sensitivity + specificity] − 1) (20,21), which is a measure of diagnostic accuracy of a test compared to other tests, were also calculated. Confidence intervals of the LRs were calculated using the Miettinen and Nurminen method (Analyse-it Software). For statistical analysis, MAP-indeterminate assessments (14 subjects) and equivocal assessments (8 subjects) at enrollment were considered positive or negative based on their actual MAP score value.

Follow-up data on the patients with probable SLE were analyzed using Fisher's exact test and a Kaplan-Meier curve with log rank test and Cox proportional hazards model (MedCalc Software), for time to fulfillment of the fourth ACR criterion. Analyse-it software was used for the receiver operating characteristics curve and decision plot analyses.

RESULTS

Study populations. *Baseline.* A total of 246 patients were included in this study: 53 patients with SLE, 92 with probable SLE, 50 with SS, and 51 with other rheumatic diseases. Of the 92 patients with probable SLE, 35 (38%) met the SLICC classification criteria at enrollment. Patients who did not meet the criteria for study enrollment or for whom the adjudicator could not make a definite determination were excluded from the study, and follow-up visits were not required (see Supplementary Table 1, on the *Arthritis & Rheumatology* web site at http://online library.wiley.com/doi/10.1002/art.41093/abstract).

The demographic characteristics at enrollment of all subjects are reported in Supplementary Table 2 (http://online library.wiley.com/doi/10.1002/art.41093/abstract). A higher percentage of patients with probable SLE were white compared to patients with SLE (*P* = 0.002). The mean number of years since diagnosis of probable SLE was lower than that of SLE (3.6 ± 4.9 years and 9.6 ± 9.4 years, respectively; *P* = 0.0001), which is consistent with the possibility that patients with probable SLE were enrolled early in their disease. The demographic characteristics of patients with probable SLE who fulfilled the SLICC criteria were similar to those of patients who did not.

The ACR criteria and the SLICC criteria fulfilled by the SLE and probable SLE patients at enrollment are reported in Figure 1 and Figure 2. According to study protocol, all subjects fulfilled the criterion of historical ANA positivity, and none of the patients with probable SLE had renal proteinuria.

Consistent with findings from other studies (12,22–24), the most common ACR clinical criteria fulfilled by patients with SLE and patients with probable SLE were arthritis (77% and 50%, respectively) and hematologic disorder (72% and 41%), while the most common SLICC clinical criterion was synovitis (75% and 47%). Patients with SLE had more mucosal ulceration, serositis, hematologic features, and immunologic features than patients with probable SLE.

Fulfillment rates of individual ACR criteria (Figure 1B) and SLICC criteria (Figure 2B) were similar among patients with probable SLE who did or did not satisfy SLICC classification criteria, apart from historical low complement levels and alopecia. The presence of historical anti-Sm antibodies approached significance (*P* = 0.052) (Figure 2B).

Disease activity in both patients with SLE and patients with probable SLE was mild at enrollment (see Supplementary Data and Supplementary Table 3, http://onlinelibrary.wiley.com/doi/10.1002/art.41093/abstract). Hydroxychloroquine (HCQ) and prednisone use were significantly lower in patients with probable SLE compared to patients with SLE, despite the physician's opinion that the patients with probable SLE likely had SLE (Supplementary Figures 1A and 1B, http://onlinelibrary.wiley.com/doi/10.1002/art.41093/abstract).

Follow-up. Sixty-nine patients with probable SLE completed a follow-up visit 9–18 months after enrollment. Follow-up visits were conducted at all sites, and there were no differences in age, sex, time since diagnosis, race/ethnicity, or fulfillment of SLICC criteria or individual ACR criteria between the group of patients who had a follow-up visit in this time frame (n = 69) and those who did not (n = 23) (data not shown). Disease activity was slightly higher in the group that did not attend a follow-up visit (nonserologic SELENA–SLEDAI 2.09 versus 1.09; *P* = 0.04).

Of the 69 patients who completed a follow-up visit, 20 (29%) fulfilled ≥1 additional ACR criterion. Hematologic disorder was the criterion fulfilled with highest frequency (50%), followed by oral ulcers (19%), immunologic disorder (8%), serositis (8%), arthritis (8%), photosensitivity (4%), and rash (4%). Of the 13 patients who fulfilled an additional hematologic criterion at follow-up, 10 had lymphopenia as their sole feature. Of these, 3 were receiving medications that might have affected lymphocyte counts: azathioprine 50 mg/day, methotrexate 15 mg/week, and/or mycophenolate 2,000 mg/day plus prednisone 2.5 mg/day. Investigators concluded that the lymphopenias were due to SLE.

Fulfillment of the SLICC criteria at enrollment did not predict fulfillment of the ACR criteria 18 months later. Of the 69 patients with probable SLE who completed a follow-up visit, 26 (38%) had fulfilled SLICC criteria at enrollment and 43 (62%) had not. Ten of the 26 patients with probable SLE who had fulfilled SLICC at enrollment (38.5%) acquired additional ACR classification criteria versus 10 of the 43 (23.3%) who had not fulfilled SLICC criteria at enrollment (*P* = 0.27). In addition, fulfillment of the SLICC criteria at baseline did not lead to faster fulfillment of the ACR criteria (*P* = 0.19 by Cox regression) (Supplementary Table 4, http://onlinelibrary.wiley.com/doi/10.1002/art.41093/abstract). Six patients converted from SLICC criteria–negative to SLICC criteria–positive at follow-up, 5 of whom also transitioned to ACR-classifiable SLE.

The number of organ manifestations at enrollment did not contribute to progression. Among the 69 patients with probable
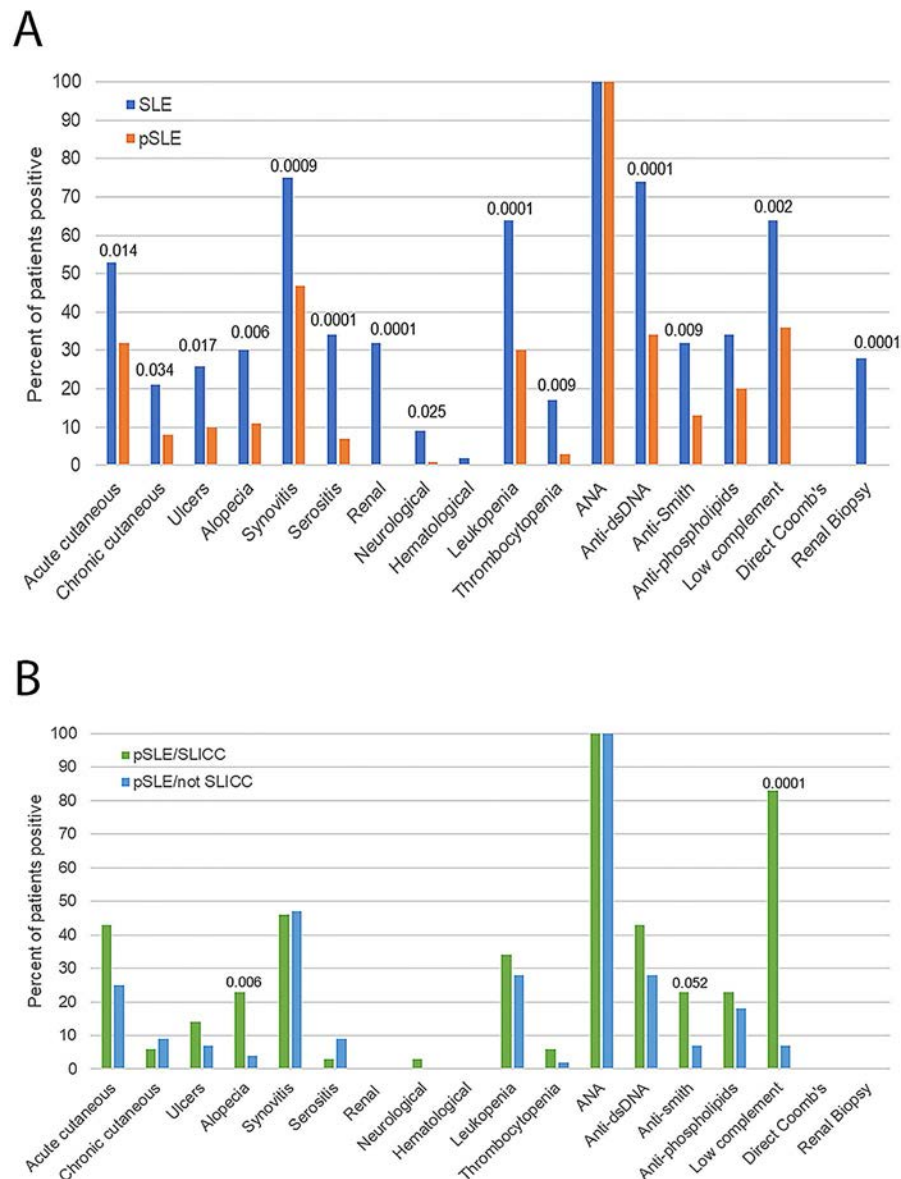
Figure 2. SLICC criteria for SLE at enrollment. Clinical and immunologic 2012 SLICC criteria were evaluated in the entire population of patients with SLE and patients with probable SLE (**A**) and in the probable SLE subgroups fulfilling or not fulfilling the SLICC criteria (**B**) at enrollment. All criteria, including ANA and immunologic criteria, refer to historical positivity. The average number of SLICC criteria fulfilled by the patients with SLE and the patients with probable SLE was 7.2 and 3.8, respectively. The average number of SLICC criteria was higher in the 35 patients with probable SLE who fulfilled these classification criteria, compared to the 57 patients who did not (4.8 versus 3.2, respectively). Statistically significant differences are indicated with *P* values, obtained by Fisher's exact test. Anti-dsDNA = anti–double-stranded DNA (see Figure 1 for other definitions).

SLE who had a follow-up visit, 41 (59%) had 1 organ manifestation (including hematologic, excluding immunologic), and 28 (41%) had 2. Of the 41 patients with 1 organ involved, 14 (34%) transitioned to classifiable SLE, whereas of the 28 patients with 2 organs involved, 6 (21%) transitioned. This difference was not significant (*P* = 0.29).

At follow-up, HCQ use increased from 63% to 74%. Among the 20 patients who converted to classifiable SLE, HCQ use increased from 75% to 80% (data not shown).

Biomarker analysis at baseline and follow-up. Most patients with SLE and probable SLE were ANA-positive on the day of the enrollment visit (Table 1). The ANA IFA assay used in this study was more sensitive than an ELISA in most cases, although ANA positivity is known to vary greatly depending on the assay platform or kit used (25,26). Specificity of ANA for SLE was low, while anti-dsDNA had a high specificity for SLE, as 2% of the patients with SS and none of the patients with other diseases were anti-dsDNA–positive.

Table 1. Diagnostic assay results for patients with SLE, probable SLE, SS, and other rheumatic diseases at enrollment*

Biomarker	SLE (n = 53)	Probable SLE (n = 92)	Probable SLE/ SLICC-positive (n = 35)	Probable SLE/ SLICC-negative (n = 57)	SS (n = 50)	Other rheumatic diseases (excluding RA) (n = 20)	RA only (n = 31)
Low complement levels†	23	9	20	2	2	0	3
CB-CAPs‡	61	28	46	18	10	10	16
MAP	77	40	49	34	27	5	3
ANA (IFA)	91	92	97	89	88	75	74
ANA (ELISA)	91	82	86	79	92	40	65
Anti-dsDNA§	38	11	20	5	2	0	0
Anti-Sm	19	4	9	2	0	0	0
Anti-SSA/Ro	47	30	26	33	76	0	0
Anti-SSB/La	9	9	6	11	34	0	0
RF (IgM)	11	16	20	14	36	10	68
RF (IgA)	8	9	3	12	34	0	42
Anti-CCP	4	1	0	2	6	0	71

* Values are percentages. SLE = systemic lupus erythematosus; SS = Sjögren's syndrome; SLICC = Systemic Lupus International Collaborating Clinics; RA = rheumatoid arthritis; CB-CAPs = positive cell-bound complement activation products; MAP = multianalyte assay panel; ANA = antinuclear antibody; anti-dsDNA = anti–double-stranded DNA; RF = rheumatoid factor; anti-CCP = anti–cyclic citrullinated peptide.
† C3 and/or C4.
‡ Elevated C4d bound to erythrocytes (EC4d) (mean fluorescence intensity [MFI] >14) and/or BC4d (MFI >60).
§ Measured by enzyme-linked immunosorbent assay (ELISA) and confirmed by immunofluorescence assay (IFA).

Anti-dsDNA sensitivity was low for SLE (38%) and even lower for probable SLE (11%), although among patients with probable SLE, positivity for anti-dsDNA was more frequent in those who fulfilled the SLICC criteria than in those who did not (20% versus 5%; $P = 0.039$). Unsurprisingly, anti-SSA and anti-SSB positivity rates were highest among SS patients (27), whereas RF and anti-CCP positivity was observed mainly in RA patients (28) (Table 1).

Although a high percentage of patients with SLE and probable SLE had historically low complement levels (64% and 36%, respectively) (Figure 2), complement protein levels were low on the day of enrollment in a minority of patients with SLE and probable SLE (23% and 9%), respectively) (Table 1), consistent with findings from previous studies (8,18). At baseline, anti-C1q antibodies were present in 34% of patients with SLE and 13% of patients with probable SLE. Other plasma complement-related markers were not measured. The positivity rate for antiphospholipid antibodies with isotypes was 25% in SLE, 17% in probable SLE, 10% in SS, and 8% in other diseases. None of these biomarkers individually or in combination were significantly associated with transition of probable SLE to classifiable SLE (Supplementary Table 4, http://online library.wiley.com/doi/10.1002/art.41093/abstract).

The frequency of CB-CAP positivity was higher than that of low complement levels in both SLE and probable SLE ($P = 0.0001$ for both) (Table 1). In probable SLE, this was true whether or not patients fulfilled the SLICC criteria. The difference between the rate of low complement levels and the rate of CB-CAP positivity in probable SLE was especially large in the subgroup not fulfilling the SLICC criteria (2% and 18% respectively; $P < 0.008$). In

addition, CB-CAP positivity demonstrated higher sensitivity than anti-dsDNA positivity in probable SLE ($P < 0.0005$).

MAP positivity, unlike CB-CAP positivity, was equally distributed between the subgroups fulfilling or not fulfilling the SLICC criteria (Table 1). The MAP algorithm includes biomarkers (in addition to CB-CAPs) that increase its diagnostic sensitivity for SLE, but may not correlate as closely with low serum complement levels as with CB-CAPs alone.

More patients with probable SLE were white than black (61% versus 16%), while patients with SLE were more racially diverse (34% white versus 38% black) (Supplementary Table 2, http:// onlinelibrary.wiley.com/doi/10.1002/art.41093/abstract). Positivity for CB-CAPs was more common in black patients with SLE and probable SLE (SLE: white 56%, black 68%; probable SLE: white 21%, black 33%), but this difference was not statistically significant.

The MAP demonstrated higher sensitivity at enrollment than low complement levels in SLE (77% versus 23%) and in probable SLE (40% versus 9%) ($P = 0.0001$ for both) and higher positive LRs for SLE and probable SLE (Tables 1 and 2). The MAP was also more sensitive ($P < 0.05$) and more specific than positive CB-CAPs in probable SLE (Tables 1 and 2). Specificity of the MAP versus all patients with other autoimmune rheumatic diseases (n = 101, including SS) was 85% (data not shown).

Since the specificity of anti-dsDNA for SLE compared to the group of patients with other diseases, excluding SS, was 100% (leading to infinite positive LRs for SLE and probable SLE), an adjusted specificity of 97.5% was used for the calculation of these LRs (18). Although, as expected, the positive LR of anti-dsDNA was strong for SLE (>15.1), it was moderate for probable SLE (>4.35), due to its low sensitivity (11%). The positive LR of the MAP

Table 2. Performance of biomarkers for SLE and probable SLE at enrollment*

	SLE (n = 53)				Probable SLE (n = 92)				
	Sensitivity, %	LR+ (95% CI)	LR− (95% CI)	J	Sensitivity, %	LR+ (95% CI)	LR− (95% CI)	J	Specificity, %
Anti-dsDNA†	38	>15.1 (5.34–∞)	0.64 (0.49–0.74)	0.38	11	>4.35 (1.52–∞)	0.91 (0.81–0.98)	0.11	100
Low complement levels‡	23	11.5 (2.06–68.2)	0.79 (0.66–0.90)	0.21	9	4.43 (0.76–27.05)	0.93 (0.85–1.02)	0.07	98
CB-CAPs§	61	4.43 (2.26–6.18)	0.45 (0.31–0.63)	0.47	28	2.06 (1.0–4.42)	0.83 (0.70–1.0)	0.15	86
MAP	77	19.6 (5.73–71.54)	0.24 (0.12–0.38)	0.73	40	10.1 (2.91–37.25)	0.63 (0.52–0.74)	0.36	96

* Specificity of biomarkers for SLE and probable SLE was calculated versus the group of patients with other rheumatic diseases (n = 51). Specificity of anti-dsDNA was estimated at 97.5% for calculation of likelihood ratios (LRs). The upper limit of the 95% confidence interval (95% CI) of anti-dsDNA (infinity) indicates 100% predictability. J = Youden index (see Table 1 for other definitions).
† Measured by ELISA and confirmed by IFA.
‡ C3 and/or C4.
§ Elevated EC4d (MFI >14) and/or BC4d (MFI >60).

was higher than that of low complement and anti-dsDNA for both SLE and probable SLE (Table 2), indicating that a positive MAP increases the posttest probability of lupus more than the positivity of any individual biomarker.

The MAP was associated with a moderate negative LR (0.24 in SLE and 0.63 in probable SLE), indicating that a negative test has moderate ability to reduce the likelihood of the diagnosis of SLE or probable SLE. Nonetheless, the MAP yielded a negative LR lower than that obtained with complement and anti-dsDNA levels in both SLE and probable SLE. Therefore, the MAP and positive CB-CAPs had greater diagnostic accuracy as demonstrated by a higher Youden index (J score) than did low complement levels and anti-dsDNA in SLE and probable SLE (Table 2).

At follow-up, positivity for CB-CAPs (n = 69) decreased from 30% to 17% ($P = 0.01$) and positivity for the MAP (n = 68) decreased from 41% to 32% ($P = 0.05$). Nonsignificant decreases in disease activity were seen in mean SELENA–SLEDAI scores (from 1.63 to 1.21; $P = 0.54$) and in mean nonserologic SELENA–SLEDAI scores (from 1.1 to 0.8; $P = 0.65$).

Only 2% of SS patients had low complement levels, while CB-CAPs were elevated in 10% of these patients, and 27% had a positive MAP score (Table 1). In patients with SS, positive and negative LRs for the MAP were 6.77 and 0.76, respectively, and the Youden index was 0.23 (data not shown).

We evaluated whether positivity for CB-CAPs, MAP, or other biomarkers at enrollment predicted fulfillment of the ACR classification criteria in the probable SLE population at
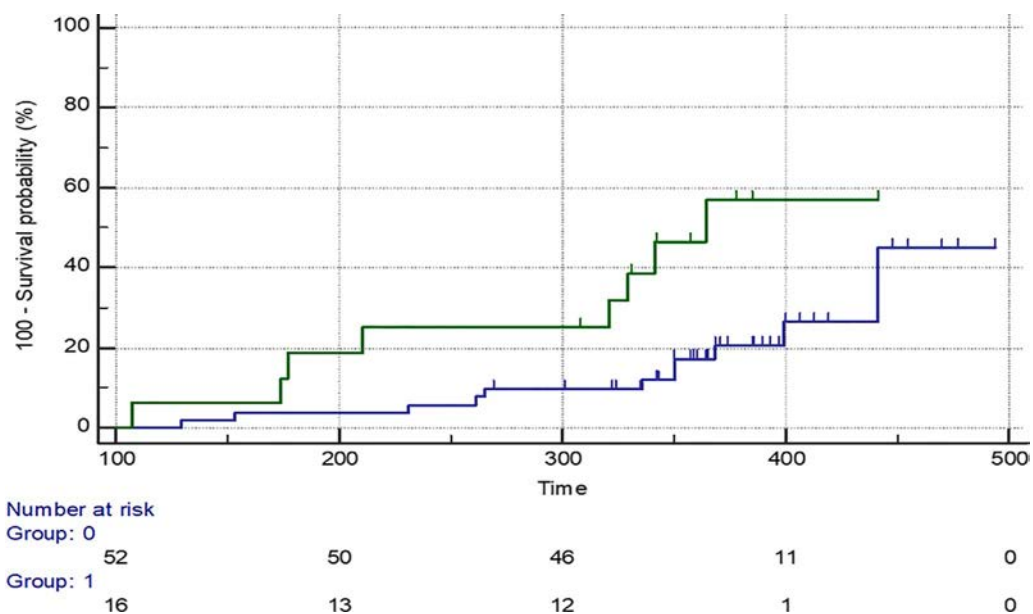
Figure 3. Kaplan-Meier survival estimates in the cohort of patients with probable systemic lupus erythematosus (SLE) who had a follow-up visit within 18 months of enrollment. Kaplan-Meier survival curves show the percentage of patients with probable SLE who fulfilled American College of Rheumatology classification criteria during the 18-month follow-up period (time in days). Data on the 68 patients with probable SLE who had a follow-up visit 9–18 months after enrollment and for whom a multianalyte assay panel (MAP) score could be calculated are plotted. Group 1 (green line) represents the 16 patients with probable SLE with a MAP score of >0.8 at enrollment; group 0 (blue line) represents the 52 patients with probable SLE with a MAP score of ≤0.8 at enrollment.

Table 3. HRs of biomarkers predicting fulfillment of ACR classification criteria by 18 months in patients with probable SLE*

	HR	95% CI	P
Anti-dsDNA†	2.97	0.98–8.99	0.043
Low complement levels‡	1.93	0.44–8.53	0.375
CB-CAPs§	1.66	0.67–4.09	0.275
EC4d >20 MFI	2.61	0.99–6.88	0.053
MAP >0.8	3.11	1.26–7.69	0.0097

* Hazard ratios (HRs) of the biomarkers were calculated by Cox regression. Data on 69 follow-up visits (n = 68 for MAP) that occurred 9–18 months after enrollment were analyzed. ACR = American College of Rheumatology (see Table 1 for other definitions).
† Measured by ELISA and confirmed by IFA.
‡ C3 and/or C4.
§ Elevated EC4d (MFI >14) and/or BC4d (MFI >60).

follow-up visits 9–18 months after enrollment. A decision plot indicated that the optimal cutoff for MAP score, based on the Youden index, was >0.8 (Supplementary Figure 2, http://online library.wiley.com/doi/10.1002/art.41093/abstract). A similar plot for EC4d showed an MFI cutoff of >20 (data not shown).

Of the 20 patients with probable SLE who fulfilled the ACR classification criteria within 18 months, 8 (40%) had a MAP score of >0.8 at enrollment. Of the 48 patients (71%) who continued to be identified as having probable SLE at follow-up visits, only 8 had a MAP score of >0.8 at enrollment (17%). The association between frequency of a MAP score of >0.8 at enrollment and fulfillment of the ACR criteria within 18 months approached statistical significance (P = 0.059).

We also evaluated time to fulfillment of ACR criteria in patients with probable SLE based on whether their MAP score at enrollment was above or below 0.8. Of the 69 visits, MAP scores could be analyzed for 68; at enrollment, 16 patients with probable SLE had a MAP score of >0.8, and 52 had a MAP score of ≤0.8. Figure 3 shows the Kaplan-Meier survival curves of the 2 groups (P < 0.010), with a hazard ratio of 3.11 (95% confidence interval 1.26–7.69). The hazard ratio of MAP scores was higher than that of other biomarkers (Table 3). Anti-dsDNA positivity and an EC4d MFI of >20 also showed higher hazard ratios (2.97 [P = 0.043] and 2.61 [P = 0.053], respectively) than that of low complement levels (Table 3). However, a MAP score of >0.8 outperformed all the other measured biomarkers, including anti-DNA plus anti-Sm, low complement levels, and antiphospholipid antibodies (Table 3 and Supplementary Table 4, http://online library.wiley.com/doi/10.1002/art.41093/abstract).

DISCUSSION

We assessed the frequency of positive CB-CAPs measured directly or within the MAP algorithm in patients with probable SLE compared to those with SLE and other autoimmune rheumatic diseases, and we evaluated the usefulness of these measures of complement activation as predictors of the evolution of probable SLE to classifiable SLE (according

to ACR criteria). Our data suggest that CB-CAPs, measured directly or within the MAP algorithm, perform well as a potential test to support the diagnosis of SLE in patients with probable SLE. In particular, CB-CAPs and the MAP performed better than standard testing, which includes assessing antibodies to dsDNA or low serum complement levels. In addition, a MAP score of >0.8 was the best predictor that a patient with probable SLE would acquire a fourth ACR criterion within 18 months postenrollment.

It is well recognized that diagnosis relates to the probability of an illness in a specific symptomatic individual, in contrast to classification criteria, which are based on performance characteristics, such as sensitivity and specificity (29,30). However, in the absence of diagnostic SLE guidelines, the classification criteria are often used to diagnose SLE (31). In a recent study of newly diagnosed lupus patients, with physician diagnosis as the gold standard, only 66.1% met ACR criteria and 83.5% met SLICC criteria; 89 patients (23%) fulfilled only 3 ACR criteria (32). Furthermore, while the SLICC criteria are more sensitive than the ACR criteria, they are somewhat less specific (33). This demonstrates a need for better diagnostic biomarkers.

Probable, incomplete, or latent lupus has been a diagnostic construct applied to patients who do not fulfill ACR classification criteria for SLE (34). Cohort studies have shown that in up to 20% of patients, probable SLE may progress to SLE that fulfills ACR classification criteria over a period of 2–5 years, and some may develop organ damage (9,10,35). If patients who are more likely to have true incipient SLE can be identified at an early stage, decision-making regarding therapeutic intervention may be improved For example, James et al demonstrated that HCQ therapy delayed the onset of complete SLE in patients who had not yet been diagnosed (36). The patients with probable SLE in the current study were less likely to be treated with HCQ or prednisone compared to patients with SLE, despite fulfilling 3 ACR criteria and the belief by a physician experienced in lupus that SLE was a likely diagnosis.

Since we recruited patients from academic sites where large lupus cohorts were being followed up, the likelihood of an SLE diagnosis was based on expert opinion. We surmised that a higher percentage of these selected patients with probable SLE would be more likely to develop a fourth ACR criterion over 2–3 years than those in a more loosely defined probable SLE group. This is supported by the observation that 35 of 92 patients with probable SLE (38%) who did not meet the ACR classification for SLE did meet the SLICC classification criteria at enrollment. This suggests that the investigators considered ≥1 SLICC feature in their evaluations to not be definitely related to SLE, since those patients could have been included in the SLE group instead of the probable SLE group. This also highlights an important difference between classification criteria and diagnosis. A similar percentage

of SLICC criteria fulfillment was found in a recently described cohort of patients who fulfilled 3 ACR criteria (37). Furthermore, in the present study, 29% of the 69 patients with a follow-up visit within 18 months acquired a fourth ACR criterion. This is a much higher rate in a shorter period of time than shown in prior studies (13,24).

We have confirmed findings of previous studies (7,8), demonstrating that positive CB-CAPs measured directly and within the MAP algorithm are more sensitive biomarkers than low serum complement levels or anti-dsDNA antibodies in SLE. We report positive CB-CAPs in a significant number (28%) of patients with probable SLE, whereas low serum complement levels were present in only 9% and anti-dsDNA in 11%. Furthermore, the MAP algorithm was positive in 77% of patients with SLE and in 40% of patients with probable SLE. This confirms our hypothesis and observations that complement activation is characteristic of SLE and can be detected more reliably by measuring activation products than serum complement component levels (1,8). We and others have shown that the presence of complement activation products closely correlates with active SLE (38,39).

The clinical and laboratory (immunologic) individual ACR and SLICC criteria in the probable SLE group versus the SLE group showed, as expected, a numerical and statistically significant lower incidence of many features, including arthritis, rashes, alopecia, serositis, and leukopenia. Conversely, there were few differences between the probable SLE subsets fulfilling SLICC criteria or not, except for alopecia and a history of low complement levels. However, C3 and C4 lack sensitivity as markers of complement activation in probable SLE, with only 9% showing hypocomplementemia at baseline. While 83% of the patients with probable SLE who fulfilled SLICC criteria had historically low complement levels, only 20% presented with low levels at the time of testing. Even within the SLICC-positive subset, positive CB-CAPs and MAP were significantly more frequent than low serum complement levels.

In this study, the presence of CB-CAPs (BC4d and/or EC4d) alone did not predict progression to classifiable SLE. However, a MAP score of >0.8 did predict progression, as did an EC4d MFI of >20 and anti-dsDNA positivity, although with lower hazard ratios. This may be related to the greater frequency of MAP positivity in probable SLE, since the cohort of patients followed up is relatively small. A higher cutoff for the MAP index (0.8 versus 0.1) was needed to show prediction of developing ACR-classifiable SLE. This may be related to the lack of specificity of a lower index in this small cohort of patients with probable SLE who converted. EC4d alone (at a higher cutoff than what is used routinely [MFI of 20 versus 14]) also showed a correlation with conversion, suggesting that complement activation is one key pathogenetic element in the evolution of SLE and is better detected by measurement of CB-CAPs directly or within the MAP than by low serum complement levels. We suggest that a longer follow-up, with potential evolution from probable SLE to SLE in more patients, might reveal that

EC4d alone and the MAP would correlate with conversion even more significantly.

We also studied patients with SS, since they can exhibit numerous autoantibodies and low serum complement levels (40). We observed an increased frequency of positive CB-CAPs compared to low serum complement levels (10% versus 2%) in SS patients, but these were not significantly different from frequencies in the control group with other rheumatic diseases. However, the MAP did show a higher positivity rate than in the control group (27% versus 4%), possibly because of the high titers of ANA found in our SS cohort (data not shown), which can influence the results of the algorithm. Since only 2% of the SS patients exhibited low serum C3 or C4 levels, it is possible that our group of 50 patients is not representative of the large cohorts that have been studied in the past (40).

A limitation of this study is the small cohort size of patients with probable SLE for whom we have follow-up data, as well as the relatively short follow-up period. However, 20 of the 69 patients (29%) who had a follow-up visit within 18 months fulfilled a fourth ACR criterion in this time frame, confirming our expectation that this cohort from academic lupus centers might be more likely to progress to classifiable SLE than prior studies have suggested. Another limitation is that retrospective determination of whether patients fulfill classification criteria is dependent on a comprehensive review of prior medical records and laboratory test results (including the presence of leukopenia or lymphopenia), and these may not have been available for all patients at every site. The adjudicators often requested and received additional records. However, the records we received may have been incomplete, as data on the lupus anticoagulant test, for example, were rarely reported. One strength of our study is that the probable SLE group is well defined and not classified by physician judgment alone.

In summary, our data show that positive CB-CAPs alone or in the MAP algorithm are present in a higher percentage of patients with SLE and patients with probable SLE compared to antibodies to dsDNA or low serum complement levels. The relatively high positivity rate of CB-CAPs and the MAP in the probable SLE group suggests that complement activation might occur early in the evolution of SLE and may be a feature in patients with suspected lupus. In addition, patients with probable SLE who had a MAP score of >0.8 or an EC4d MFI of >20 at enrollment were more likely to fulfill a fourth ACR criterion during a relatively brief follow-up; these biomarkers predicted the transition to SLE better than other clinical and laboratory parameters. The detection of complement activation in patients with probable lupus who do not fulfill ACR criteria or even SLICC criteria could have implications with regard to treatment, as early appropriate therapy in these patients may potentially slow the rate of disease progression (36,41).

ACKNOWLEDGMENTS

AUTHOR CONTRIBUTIONS

All authors were involved in drafting the article or revising it critically for important intellectual content, and all authors approved the final version to be published. Dr. Weinstein had full access to all of the data in the study and takes responsibility for the integrity of the data and the accuracy of the data analysis.

Study conception and design. Ramsey-Goldman, Alexander, Massarotti, Wallace, Kalunian, Dervieux, Weinstein.

Acquisition of data. Alexander, Massarotti, Wallace, Narain, Arriens, Collins, Saxena, Putterman, Kalunian, O'Malley, Dervieux, Weinstein.

Analysis and interpretation of data. Ramsey-Goldman, Alexander, Kalunian, O'Malley, Dervieux, Weinstein.

ROLE OF THE STUDY SPONSOR

REFERENCES

1. Ramsey-Goldman R, Li J, Dervieux T, Alexander RV. Cell-bound complement activation products in SLE. Lupus Sci Med 2017; 4:e000236.

2. Hochberg MC, for the Diagnostic and Therapeutic Criteria Committee of the American College of Rheumatology. Updating the American College of Rheumatology revised criteria for the classification of systemic lupus erythematosus [letter]. Arthritis Rheum 1997;40:1725.

3. Petri M, Orbai AM, Alarcón GS, Gordon C, Merrill JT, Fortin PR, et al. Derivation and validation of the Systemic Lupus International Collaborating Clinics classification criteria for systemic lupus erythematosus. Arthritis Rheum 2012;64:2677–86.

4. Tan EM, Cohen AS, Fries JF, Masi AT, McShane DJ, Rothfield NF, et al. The 1982 revised criteria for the classification of systemic lupus erythematosus. Arthritis Rheum 1982;25:1271–7.

5. Aringer M, Costenbader K, Daikh D, Brinks R, Mosca M, Ramsey-Goldman R, et al. 2019 European League Against Rheumatism/American College of Rheumatology classification criteria for systemic lupus erythematosus. Arthritis Rheumatol 2019;71:1400–12.

6. Weinstein A, Bordwell B, Stone B, Tibbetts C, Rothfield NF. Antibodies to native DNA and serum complement (C3) levels: application to diagnosis and classification of systemic lupus erythematosus. Am J Med 1983;74:206–16.

7. Kalunian KC, Chatham WW, Massarotti EM, Reyes-Thomas J, Harris C, Furie RA, et al. Measurement of cell-bound complement activation products enhances diagnostic performance in systemic lupus erythematosus. Arthritis Rheum 2012;64:4040–7.

8. Putterman C, Furie R, Ramsey-Goldman R, Askanase A, Buyon JP, Kalunian K, et al. Cell-bound complement activation products in systemic lupus erythematosus: comparison with anti-double-stranded DNA and standard complement measurements. Lupus Sci Med 2014;1:e000056.

9. Robertson JM, James JA. Preclinical systemic lupus erythematosus. Rheum Dis Clin North Am 2014;40:621–35.

10. Doria A, Mosca M, Gambari PF, Bombardieri S. Defining unclassifiable connective tissue diseases: incomplete, undifferentiated, or both? [editorial]. J Rheumatol 2005;32:213–5.

11. Doria A, Zen M, Canova M, Bettio S, Bassi N, Nalotto L, et al. SLE diagnosis and treatment: when early is early. Autoimmun Rev 2010;10:55–60.

12. Aberle T, Bourn RL, Munroe ME, Chen H, Roberts VC, Guthridge JM, et al. Clinical and serologic features in patients with incomplete lupus classification versus systemic lupus erythematosus patients and controls. Arthritis Care Res (Hoboken) 2017;69:1780–8.

13. Costenbader KH, Schur PH. We need better classification and terminology for "people at high risk of or in the process of developing lupus" [editorial]. Arthritis Care Res (Hoboken) 2015;67:593–6.

14. Bruce IN, O'Keeffe AG, Farewell V, Hanly JG, Manzi S, Su L, et al. Factors associated with damage accrual in patients with systemic lupus erythematosus: results from the Systemic Lupus International Collaborating Clinics (SLICC) Inception Cohort. Ann Rheum Dis 2015;74:1706–13.

15. Bruce IN, Urowitz M, van Vollenhoven R, Aranow C, Fettiplace J, Oldham M, et al. Long-term organ damage accrual and safety in patients with SLE treated with belimumab plus standard of care. Lupus 2016;25:699–709.

16. Petri M, Kim MY, Kalunian KC, Grossman J, Hahn BH, Sammaritano LR, et al. Combined oral contraceptives in women with systemic lupus erythematosus. N Engl J Med 2005;353:2550–8.

17. Shiboski SC, Shiboski CH, Criswell LA, Baer AN, Challacombe S, Lanfranchi H, et al, for the Sjögren's International Collaborative Clinical Alliance (SICCA) Research Groups. American College of Rheumatology classification criteria for Sjögren's syndrome: a data-driven, expert consensus approach in the Sjögren's International Collaborative Clinical Alliance Cohort. Arthritis Care Res (Hoboken) 2012;64:475–87.

18. Wallace DJ, Silverman SL, Conklin J, Barken D, Dervieux T. Systemic lupus erythematosus and primary fibromyalgia can be distinguished by testing for cell-bound complement activation products. Lupus Sci Med 2016;3:e000127.

19. Dervieux T, Conklin J, Ligayon JA, Wolover L, O'Malley T, Alexander RV, et al. Validation of a multi-analyte panel with cell-bound complement activation products for systemic lupus erythematosus. J Immunol Methods 2017;446:54–9.

20. Youden WJ. Index for rating diagnostic tests. Cancer 1950;3:32–5.

21. Tan L, Wang Q, Zeng T, Long T, Guan X, Wu S, et al. Clinical significance of detecting HLA-DR, 14-3-3η protein and d-dimer in the diagnosis of rheumatoid arthritis. Biomark Med 2018;12:697–705.

22. Lim SS, Bayakly AR, Helmick CG, Gordon C, Easley KA, Drenkard C. The incidence and prevalence of systemic lupus erythematosus, 2002–2004: the Georgia Lupus Registry. Arthritis Rheumatol 2014;66:357–68.

23. Alarcón GS, McGwin G Jr, Roseman JM, Uribe A, Fessler BJ, Bastian HM, et al. Systemic lupus erythematosus in three ethnic groups. XIX. Natural history of the accrual of the American College of Rheumatology criteria prior to the occurrence of criteria diagnosis. Arthritis Rheum 2004;51:609–15.

24. Bodolay E, Csiki Z, Szekanecz Z, Ben T, Kiss E, Zeher M, et al. Five-year follow-up of 665 Hungarian patients with undifferentiated connective tissue disease (UCTD). Clin Exp Rheumatol 2003;21:313–20.

25. Pisetsky DS, Spencer DM, Lipsky PE, Rovin BH. Assay variation in the detection of antinuclear antibodies in the sera of patients with established SLE. Ann Rheum Dis 2018;77:911–3.

26. Pisetsky DS. Antinuclear antibody testing—misunderstood or mis-begotten? Nat Rev Rheumatol 2017;13:495–502.

27. Trier NH, Nielsen IØ, Friis T, Houen G, Theander E. Comparison of antibody assays for detection of autoantibodies to Ro 52, Ro 60 and La associated with primary Sjögren's syndrome. J Immunol Methods 2016;433:44–50.

28. Puszczewicz M, Iwaszkiewicz C. Role of anti-citrullinated protein antibodies in diagnosis and prognosis of rheumatoid arthritis. Arch Med Sci 2011;7:189–94.

29. Aggarwal R, Ringold S, Khanna D, Neogi T, Johnson SR, Miller A, et al. Distinctions between diagnostic and classification criteria? [review]. Arthritis Care Res (Hoboken) 2015;67:891–7.

30. Bertsias GK, Pamfil C, Fanouriakis A, Boumpas DT. Diagnostic criteria for systemic lupus erythematosus: has the time come? Nat Rev Rheumatol 2013;9:687–94.

31. Bortoluzzi A, Furini F, Campanaro F, Govoni M. Application of SLICC classification criteria in undifferentiated connective tissue disease and evolution in systemic lupus erythematosus: analysis of a large mono-centric cohort with a long-term follow-up. Lupus 2017;26:616–22.

32. Mosca M, Costenbader KH, Johnson SR, Lorenzoni V, Sebastiani GD, Hoyer BF, et al. How do patients with newly diagnosed systemic lupus erythematosus present? A multicenter cohort of early systemic lupus erythematosus to inform the development of new classification criteria. Arthritis Rheumatol 2019;71:91–8.

33. Ighe A, Dahlström Ö, Skogh T, Sjöwall C. Application of the 2012 Systemic Lupus International Collaborating Clinics classification criteria to patients in a regional Swedish systemic lupus erythematosus register. Arthritis Res Ther 2015;17:3.

34. Daikh DI, Costenbader KH. How do we classify "incomplete lupus?" [editorial]. Arthritis Care Res (Hoboken) 2017;69:1777–9.

35. Vilá LM, Mayor AM, Valentín AH, García-Soberal M, Vilá S. Clinical outcome and predictors of disease evolution in patients with incomplete lupus erythematosus. Lupus 2000;9:110–5.

36. James JA, Kim-Howard XR, Bruner BF, Jonsson MK, McClain MT, Arbuckle MR, et al. Hydroxychloroquine sulfate treatment is associated with later onset of systemic lupus erythematosus. Lupus 2007;16:401–9.

37. Aberle T, Bourn RL, Chen H, Roberts VC, Guthridge JM, Bean K, et al. Use of SLICC criteria in a large, diverse lupus registry enables SLE classification of a subset of ACR-designated subjects with incomplete lupus. Lupus Sci Med 2017;4:e000176.

38. Merrill JT, Petri MA, Buyon J, Ramsey-Goldman R, Kalunian K, Putterman C, et al. Erythrocyte-bound C4d in combination with complement and autoantibody status for the monitoring of SLE. Lupus Sci Med 2018;5:e000263.

39. Kim AH, Strand V, Sen DP, Fu Q, Mathis NL, Schmidt MJ, et al. Association of blood concentrations of complement split product iC3b and serum C3 with systemic lupus erythematosus disease activity. Arthritis Rheumatol 2019;71:420–30.

40. García-Carrasco M, Mendoza-Pinto C, Jiménez-Hernández C, Jiménez-Hernández M, Nava-Zavala A, Riebeling C. Serologic features of primary Sjögren's syndrome: clinical and prognostic correlation. Int J Clin Rheumtol 2012;7:651–9.

41. Lamichhane D, Weinstein A. Probable systemic lupus erythematosus with cell-bound complement activation products (CB-CAPS). Lupus 2016;25:1050–3.

AMERICAN COLLEGE
of RHEUMATOLOGY
Empowering Rheumatology Professionals

High Prevalence and Disease Correlation of Autoantibodies Against p40 Encoded by Long Interspersed Nuclear Elements in Systemic Lupus Erythematosus

Victoria Carter,[1] John LaCava,[2] [iD] Martin S. Taylor,[3] Shu Ying Liang,[1] Cecilia Mustelin,[1] Kennedy C. Ukadike,[1] Anders Bengtsson,[4] Christian Lood,[1] and Tomas Mustelin[1] [iD]

Objective. Long interspersed nuclear element 1 (LINE-1) encodes 2 proteins, the RNA binding protein p40 and endonuclease and reverse transcriptase (open-reading frame 2p [ORF2p]), which are both required for LINE-1 to retrotranspose. In cells expressing LINE-1, these proteins assemble with LINE-1 RNA and additional RNA binding proteins, some of which are well-known autoantigens in patients with systemic lupus erythematosus (SLE). This study was undertaken to investigate whether SLE patients also produce autoantibodies against LINE-1 p40.

Methods. Highly purified p40 protein was used to quantitate IgG autoantibodies in serum from 172 SLE patients and from disease controls and age-matched healthy subjects by immunoblotting and enzyme-linked immunosorbent assay (ELISA). Preparations of p40 that also contained associated proteins were analyzed by immunoblotting with patient sera.

Results. Antibodies reactive with p40 were detected in the majority of patients and many healthy controls. Their levels were higher in patients with SLE, but not those with systemic sclerosis, compared to healthy subjects ($P = 0.01$). Anti-p40 reactivity was higher in patients during a flare than in patients with disease in remission ($P = 0.03$); correlated with the SLE Disease Activity Index score ($P = 0.0002$), type I interferon score ($P = 0.006$), decrease in complement C3 level ($P = 0.0001$), the presence of anti-DNA antibodies ($P < 0.0001$) and anti-C1q antibodies ($P = 0.004$), and current or past history of nephritis ($P = 0.02$ and $P = 0.003$, respectively); and correlated inversely with age ($r = -0.49$, $P < 0.0001$). SLE patient sera also reacted with p40-associated proteins.

Conclusion. Autoantibodies reacting with LINE-1 p40 characterize a population of SLE patients with severe and active disease. These autoantibodies may represent an early immune response against LINE-1 p40 that does not yet by itself imply clinically significant autoimmunity, but may represent an early, and still reversible, step toward SLE pathogenesis.

INTRODUCTION

Long interspersed nuclear element 1 (LINE-1; also known as L1) constitutes 17% of the human genome (1–4). While most of the ~500,000 LINE-1 copies are mutated and truncated, some ~180 are seemingly intact and a handful of them remain "hot" today (5), i.e., they continue to retrotranspose by a copy-and-paste mechanism, occasionally disrupting genes or regulatory regions by novel insertions (6). To counteract this threat, an elaborate set of defense mechanisms has evolved against retroelements and retroviruses (7–12), and it has been proposed that many human diseases, including cancer and immune-mediated diseases, are connected with LINE-1 biology (13,14).

Indeed, loss-of-function mutations in several genes for these defense mechanisms cause a severe developmental disease known as Aicardi-Goutières syndrome (15,16), which is characterized by constitutively high production of type I interferons (IFNs), neurologic deficits due to IFN toxicity, and autoimmunity with all

the hallmarks of systemic lupus erythematosus (SLE). In patients with Aicardi-Goutières syndrome with mutations in the cytosolic DNase *TREX1* gene (17,18), type I IFNs are produced in response to aberrantly present intracellular DNA (which TREX1 normally degrades). Further, in patients with Aicardi-Goutières syndrome with mutations in *RNASEH2* (17), which degrades DNA–RNA heteroduplexes, or *SAMHD1* (19,20), which removes deoxynucleotides required for reverse transcription, the IFN-driving aberrant DNA apparently results from reverse transcription of cellular RNAs. The cellular enzyme most likely responsible for this reverse transcription is the second open-reading frame (ORF2p) of LINE-1, which encodes a highly efficient reverse transcriptase (21,22) that can use many cellular RNA templates, including its own messenger RNA (mRNA) (3,4) or Alu transcripts, to generate DNA species that may trigger IFN production.

There are additional reasons to suspect that LINE-1 could potentially be involved in SLE development, perpetuation, and/or disease flares: 1) the first ORF of LINE-1 encodes a 40-kd RNA binding protein (p40), which is physically associated with Ro, La, small nuclear RNP 70, and other well-known SLE autoantigens (23–26) together with RNA in heterogenous macromolecular assemblies (possibly stress granules); and 2) while LINE-1 loci are largely silent in healthy subjects, LINE-1 transcripts and p40 protein have been detected in patients with SLE and Sjögren's syndrome (27–29). Furthermore, LINE-1 transcription can be induced by many conditions known to precipitate SLE flares, such as reduced genomic methylation (29), low DNA methyltransferase (DNMT) expression (30), DNMT1 polymorphisms, demethylating drugs (e.g., hydralazine and procainamide [31]), and ultraviolet light (32). LINE-1 loci are also transcriptionally active in patients with Aicardi-Goutières syndrome (33), suggesting that LINE-1 ORF2p is indeed the reverse transcriptase responsible for the aberrant DNA (34) that drives type I IFN production and the disease in patients with Aicardi-Goutières syndrome (35). Inhibitors of the reverse transcriptase can reduce the IFN gene signature in patients with Aicardi-Goutières syndrome (36).

In this study, we demonstrate that a majority of SLE patients have IgG autoantibodies against LINE-1 p40 protein and that the reactivity against this autoantigen correlates with disease activity and serologic measures of disease. We also show that patients have autoantibodies against some p40-associated proteins.

MATERIALS AND METHODS

SLE patients. A first cohort of patients with SLE (n = 10) was recruited through the University of Washington Division of Rheumatology Biorepository to participate in research studies at the University of Washington Medical Center. The study was approved by regional ethics boards (STUDY00006196), and written informed consent was obtained from all participants. A second cohort of SLE patients with disease in remission (n = 83),

SLE patients experiencing a flare (n = 79), disease controls (with systemic sclerosis; n = 20), and healthy individuals (n = 78) was recruited in the Department of Medicine, Skåne University Hospital (Lund, Sweden). The study was approved by the Lund University local ethics board (LU06014520 and LU 378-02). Written informed consent was obtained from all participants in accordance with the Declaration of Helsinki. The Swedish patient cohorts have been described in great detail previously (37–39).

Purification of LINE-1 ORF1p p40 protein. ORF1p was expressed in *Escherichia coli* LOBSTR pLysS pRare2 (DE3) (40) from plasmid pMT538, containing full-length synthetic human ORF1p (ORFeusHS) with an N-terminal HIS6-TEV sequence in a pETM11 backbone such that cleavage leaves only an N-glycine scar. Protein was purified using nickel–nitrilotriacetic acid affinity, cleaved from the column overnight using excess TEV protease and RNAse A, and then further purified by size exclusion in a buffer containing 50 mM HEPES pH 7.8, 500 mM NaCl, 10 mM MgCl$_2$, and 0.5 mM tris(2-carboxyethyl)phosphine. Peak fractions corresponding to monomeric ORF1p were pooled and concentrated at ~8 mg/ml. The purity of this preparation is illustrated in Figure 1A.

Separate p40 preparations were generated to include p40-associated proteins (26). Anti-FLAG affinity capture of C-terminal, FLAG-tagged ORF1p was conducted as previously described (41,42). Briefly, HEK 293T$_{LD}$ cells expressing either doxycycline-inducible, intact LINE-1 (*ORF1::FLAG*; pLD288); ORF1p alone (*ΔORF2*; pLD603); or, as a control, empty vector (pCEP-puro), were all subjected to anti-FLAG affinity capture. At the point of elution, ORF1p-containing macromolecules were released either by native elution in 3× FLAG peptide (1 mg/ml) or by the application of lithium dodecyl sulfate–containing NuPAGE sample buffer. For each sample type: 50 mg cell powder per experiment, extracted at 25% (weight/volume) in 20 mM HEPES, pH7.4, 1% (volume/volume) Triton X-100, 500 mM NaCl, supplemented with protease inhibitors. Centrifugally clarified extracts were combined with 50 µl of anti-FLAG magnetic medium.

Immunoblotting. One microgram of p40 protein per sodium dodecyl sulfate (SDS) gel was resolved by electrophoresis and transferred onto PVDF membranes, which were cut into 12–15 strips, and immunoblotted with patient or healthy control serum, each diluted 1:100, and developed by horseradish peroxidase–conjugated anti-human IgG and enhanced chemiluminescence. Anti–LINE-1 ORF1p antibody, clone 4H1, was from MilliporeSigma.

Enzyme-linked immunosorbent assays (ELISAs). Purified p40 protein was adsorbed onto 96-well polystyrene plates at 330 ng/well in 0.1M carbonate (pH 9.6) buffer overnight, washed in phosphate buffered saline (PBS)–Tween, and blocked in 1% bovine serum albumin in PBS for 2 hours. Patient or healthy control serum was added at 0.5%
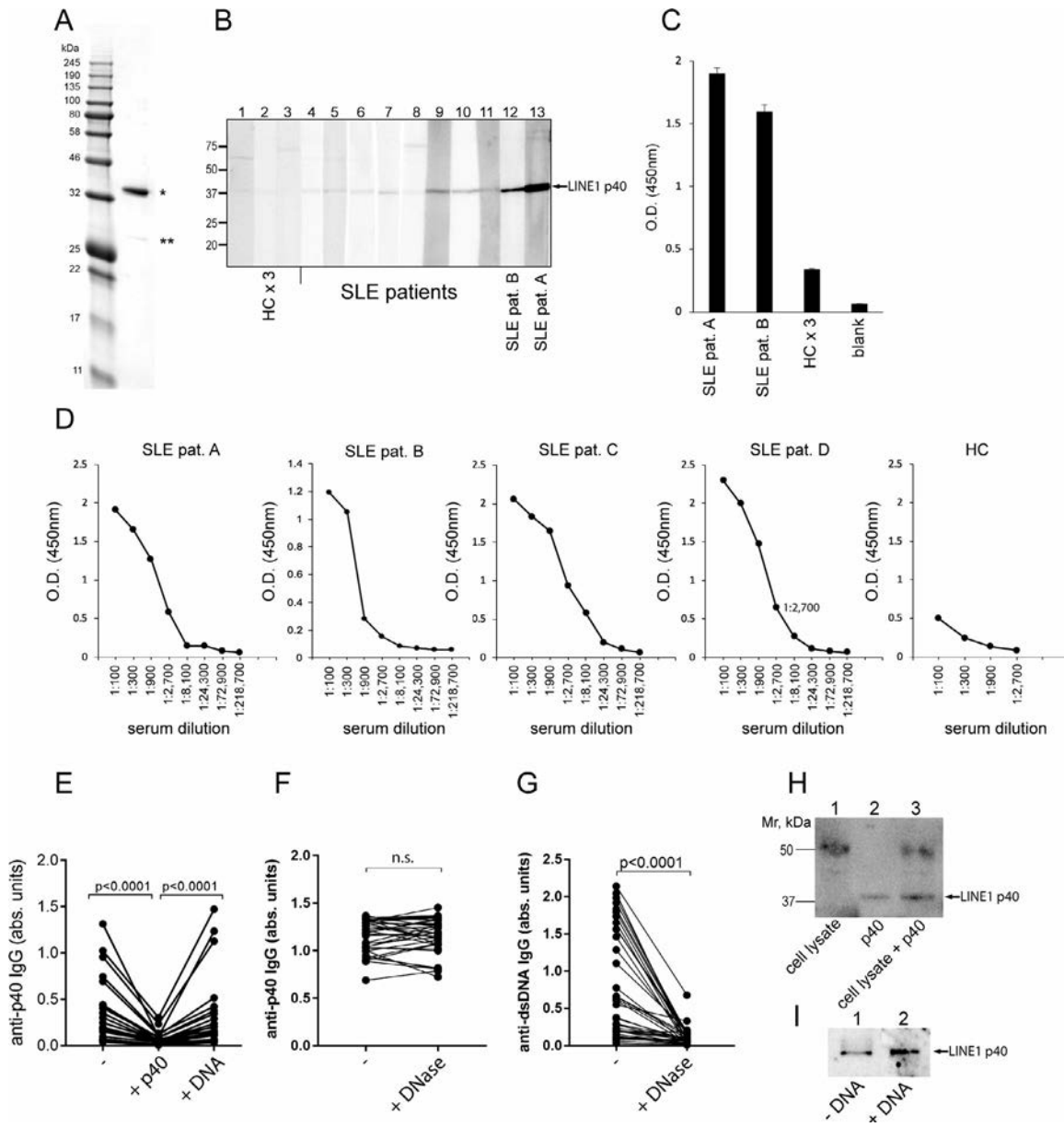
Figure 1. Systemic lupus erythematosus (SLE) sera recognize long interspersed nuclear element 1 (LINE-1) open-reading frame 1 p40 protein. **A,** Coomassie brilliant blue staining of the purified p40 preparation. The **asterisk** denotes p40 and the **double asterisks** indicate a minor amount of cleaved p40. **B,** Immunoblot showing levels of anti-p40 antibodies in sera from 3 healthy controls (HCs; lanes 1–3) and 10 patients with SLE (lanes 4–13). **C,** Enzyme-linked immunosorbent assay (ELISA) for anti-p40 antibodies in the samples from SLE patient A (SLE pat. A; lane 13 in **B**), SLE patient B (lane 12 in **B**), and the 3 healthy controls combined. Bars show the mean ± SD (n = 9 wells per group). **D,** ELISA for anti-p40 antibodies with the indicated dilutions of sera from 4 SLE patients and 1 healthy control, including the same patients (SLE patients A and B) as in **B**. **E,** ELISA for anti-p40 antibodies in SLE patient samples without additions to the assay (–), with a 10-fold excess of soluble p40, and with an equal amount of soluble DNA. **F,** ELISA for anti-p40 antibodies in SLE patient samples without additions to the assay and with DNase. **G,** ELISA for anti-double-stranded DNA (anti-dsDNA) antibodies in SLE patient samples without additions to the assay and with DNase. In **E–G**, lines represent individual patients. **H,** Immunoblot showing anti-p40 reactivity with a neutrophil lysate from SLE patient serum, 300 ng of p40, and a mixture of neutrophil lysate and p40. **I,** Immunoblot showing anti-p40 reactivity in SLE serum without additional treatment and in the presence of 1 μg soluble DNA. abs = absorbance; NS = not significant.

in blocking buffer for overnight incubation at 4°C, washed extensively, and then incubated with a 1:20,000 dilution of horseradish peroxidase–conjugated anti-human IgG. The reaction was then washed and developed with tetramethylb-enzidine, the color reaction was terminated with 2*N* sulfuric

acid, and absorbance was measured at 450 nm using a plate reader.

In competition ELISAs, 3 μg of soluble p40 or 3 μg of salmon sperm DNA was added to the wells at the same time as patient serum. DNase treatment (to prevent DNA from potentially associating
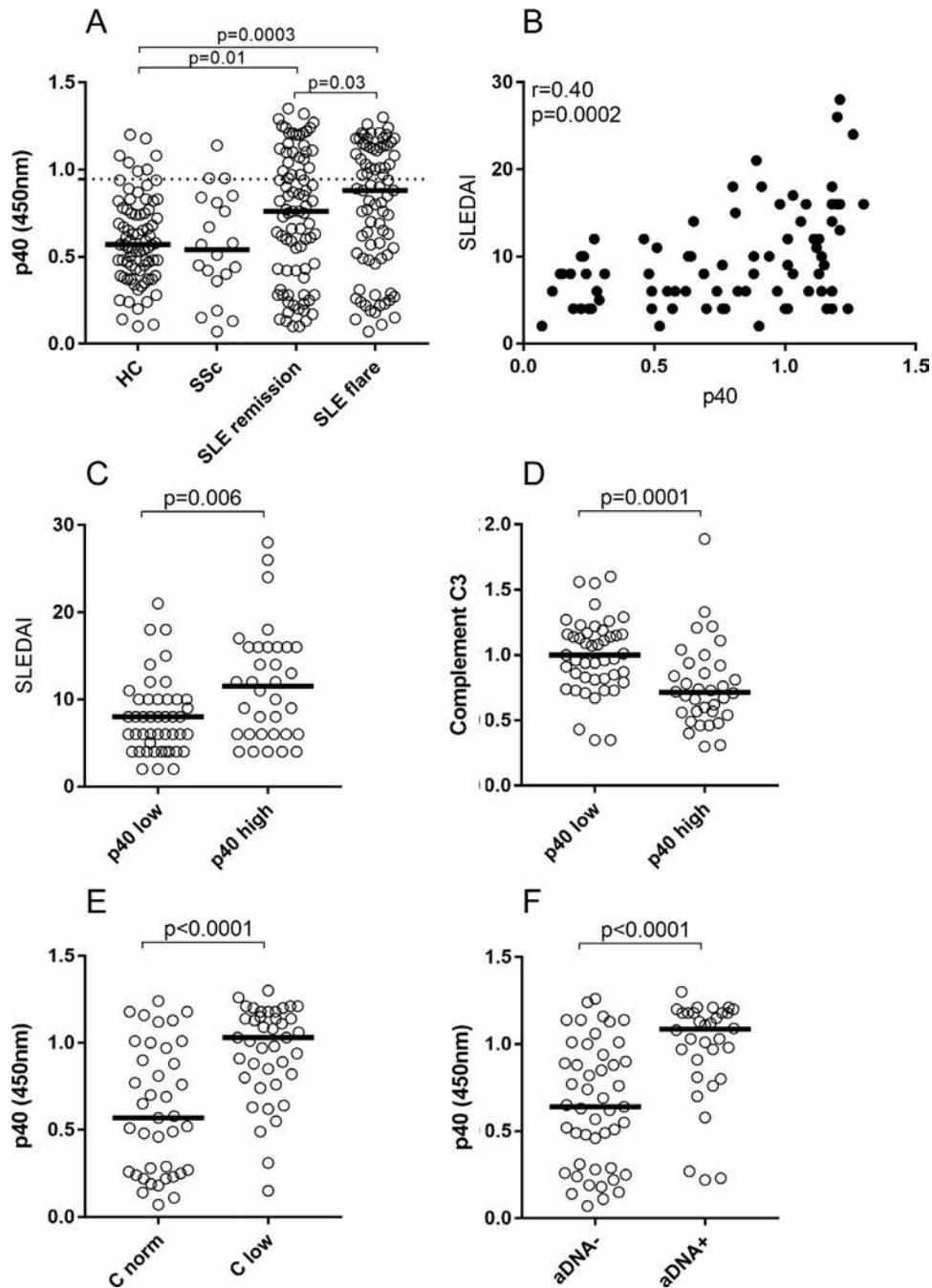
Figure 2. Correlation of levels of autoantibodies against LINE-1 p40 with SLE disease activity. **A**, Quantitation of autoantibodies reactive with LINE-1 p40 in serum from healthy control subjects (n = 78), patients with systemic sclerosis (SSc; n = 20), patients with SLE in remission (n = 83), and patients with SLE during a flare (n = 79). The broken line indicates the 90th percentile in healthy controls. **B**, Correlation between anti-p40 autoantibody levels and SLE Disease Activity Index (SLEDAI) score in the 79 SLE patients experiencing a flare. **C**, SLEDAI score in the SLE patients with anti-p40 reactivity below the 90th percentile in healthy controls (p40 low) and those with anti-p40 reactivity above the 90th percentile in healthy controls (p40 high). **D**, Levels of complement C3 in SLE patients categorized as in **C**. **E**, Anti-p40 reactivity in SLE patients with normal complement levels as defined by the SLEDAI and those with low complement levels as defined by the SLEDAI. **F**, Anti-p40 reactivity in SLE patients without anti-dsDNA antibodies and those with anti-dsDNA antibodies. Symbols represent individual subjects; horizontal lines show the median. *P* values were determined by Mann-Whitney U test in **A** and **C**–**F** and by Spearman's correlation test in **B**. See Figure 1 for other definitions.

with p40) was carried out by adding 1 μg/ml of DNase in buffer with Mg^{2+} and Ca^{2+} to wells with either adsorbed p40 or DNA at the same time patient serum was added.

Type I IFN assay. Type I IFN activity was measured as previously described (43–45). Briefly, endothelial WISH cells were cultured with patient serum and analyzed for the induction of 6

IFN-regulated genes and 3 housekeeping genes using a QuantiGene Plex 2.0 assay according to the recommendations of the manufacturer (Panomics).

Statistical analysis. For unpaired sample sets with non-Gaussian distribution, Mann-Whitney U test and Spearman's correlation test were used, as applicable. For paired sample sets, Wilcoxon matched pairs signed rank test was used. In some analyses, logistic regression analysis was used for dichotomized variables. As a cutoff for positivity, the 90th percentile in the healthy controls was used. GraphPad Prism and IBM SPSS software were used for statistical analyses. P values less than 0.05 were considered significant.

RESULTS

Autoantibodies against LINE-1 p40. To determine if SLE patients have autoantibodies of the IgG class against LINE-1 proteins, 1 μg purified p40 was resolved on SDS gels, transferred onto PVDF membranes, which were cut into 15–20 vertical strips, and immunoblotted with 1:100 diluted sera from SLE patients or healthy subjects. As shown in Figure 1B, all 10 SLE patients had antibodies against p40, some strong, some weaker, while healthy subjects showed a very faint band. The intensity of the p40 band was strongest in the 2 SLE patients with the highest SLE Disease Activity Index (SLEDAI) scores (46).

Quantitation of anti-p40 autoantibodies. To better quantitate the anti-p40 reactivity, and to be able to screen a larger

number of SLE patients, healthy controls, and other disease controls, we developed an ELISA using the highly purified p40 protein. Reactivity in these assays correlated closely with the intensity of the bands on the p40 immunoblots with sera from the same patients (Figure 1C). As shown in Figure 2A, autoantibodies reactive with p40 were detected in the majority of patients and healthy controls, but their levels were considerably higher in patients with SLE, but not those with systemic sclerosis, than in healthy subjects ($P = 0.01$). Reactivity was also higher in SLE patients experiencing a flare (n = 79) compared to those whose disease was in remission (n = 83) ($P = 0.03$). Using the sera at a higher dilution (1:1,000) resulted in similar data, but with significant loss of resolution for the lower and medium values, while gaining a somewhat better resolution for the highest values. Strongly reactive sera still gave a positive signal at dilutions down to 1:8,100 or 1:24,300 (Figure 1D).

Specificity of anti-p40 autoantibodies. Because p40 can bind nucleic acids, we wanted to exclude the possibility that patient autoantibodies may react with double-stranded DNA (dsDNA) in complex with p40. ELISAs performed in the presence of a 10-fold excess of soluble p40 resulted in a marked decrease in IgG binding to the plate-bound p40, while an equal amount of soluble DNA had no effect (Figure 1E). Similarly, when DNase was included in the ELISA, no change in p40 reactivity was observed (Figure 1F), while binding of autoantibodies to a DNA-coated plate was greatly reduced (Figure 1G). Furthermore, patient sera still recognized p40 when it was mixed with total cell lysates of blood neutrophils (Figure 1H), and the addition of DNA had no effect on anti-p40 reactivity in immunoblot analysis (Figure 1I). These
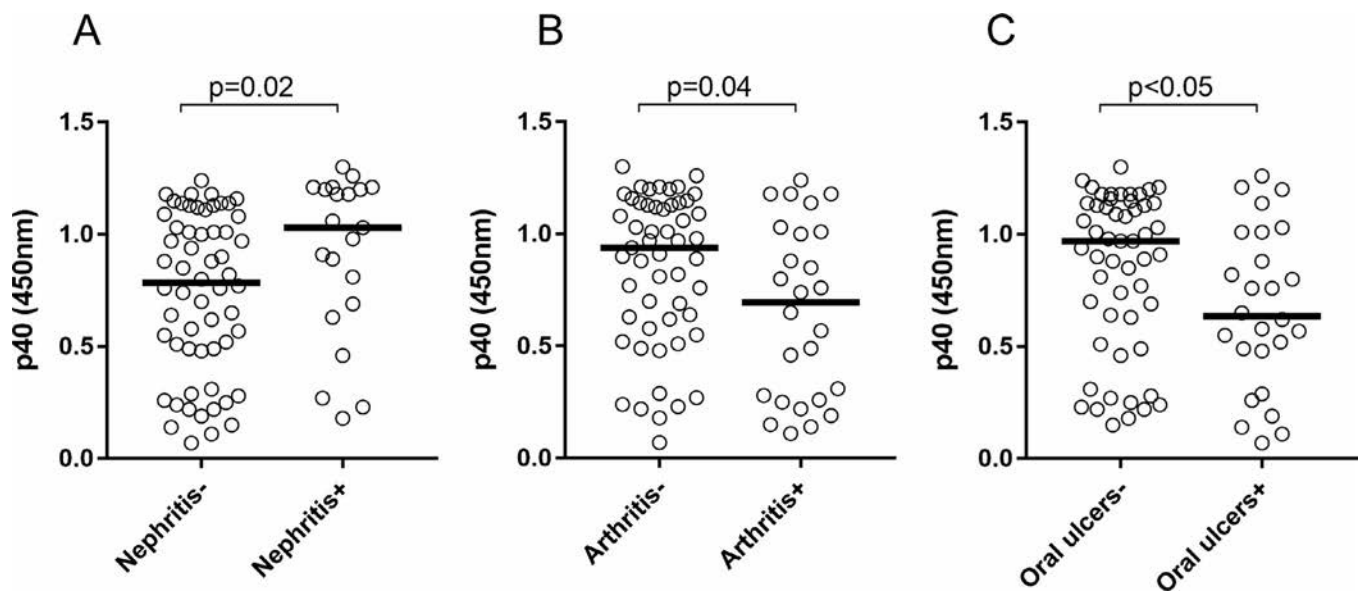
Figure 3. Correlation between anti-p40 autoantibody levels and systemic lupus erythematosus (SLE) organ manifestations. **A**, Reactivity with p40 in SLE patients without established kidney involvement and those with established kidney involvement. **B**, Reactivity with p40 in SLE patients without arthritis and those with arthritis. **C**, Reactivity with p40 in SLE patients without a history of oral ulcers and those with a history of oral ulcers. Symbols represent individual patients; horizontal lines show the median. P values were determined by Mann-Whitney U test. See Results for a discussion of the impact of Bonferroni correction on the P values.

experiments demonstrate that SLE patient autoantibodies directly recognize LINE-1 p40 protein.

Association of anti-p40 autoantibody levels with higher disease activity. As already suggested by the immunoblot in Figure 1B, anti-p40 reactivity correlated with the SLEDAI score ($P = 0.0002$) in the patients with an SLE flare (Figure 2B). Patients with high titers (above the 90th percentile in healthy controls) had higher SLEDAI scores than those with levels below this cutoff (Figure 2C). Anti-p40 antibody levels were also associated with complement consumption ($P = 0.0001$) (Figures 2D and E) and the presence of anti-dsDNA antibodies

($P < 0.0001$) (Figure 2F). Taken together, these data indicate that higher anti-p40 levels tend to accompany active disease.

Associations of anti-p40 antibody levels with organ manifestations and with other autoantibodies. Higher anti-p40 antibody levels also characterized SLE patients with active lupus nephritis ($P = 0.02$) (Figure 3A), and a history of nephritis ($P = 0.003$) but were inversely correlated with active arthritis ($P = 0.04$) (Figure 3B) and a history of oral ulcers ($P < 0.05$) (Figure 3C). While these correlations were significant, applying a Bonferroni correction for multiple correlates rendered the correlations with both arthritis and oral ulcers nonsignificant.
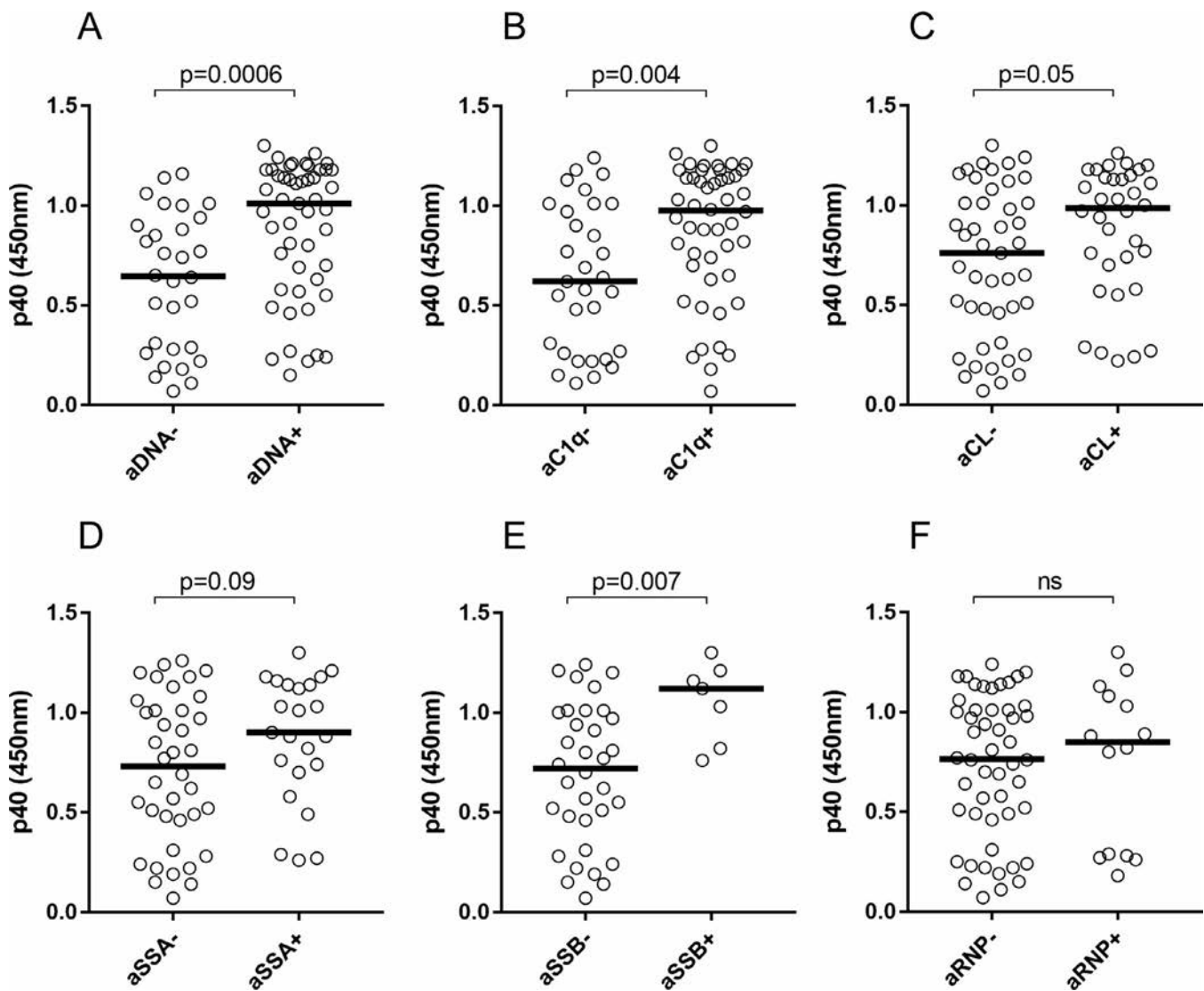
Figure 4. Correlation of levels of autoantibodies against LINE-1 p40 with the presence of other autoantibodies. **A**, Reactivity with p40 in SLE patients without a history of anti-dsDNA positivity and those with a history of anti-dsDNA positivity. **B**, Reactivity with p40 in SLE patients without anti-C1q antibodies and those with anti-C1q antibodies. **C**, Reactivity with p40 in SLE patients without anticardiolipin antibodies (aCLs) and those with aCLs. **D**, Reactivity with p40 in SLE patients without anti-Ro/SSA antibodies and those with anti-Ro/SSA antibodies. **E**, Reactivity with p40 in SLE patients without anti-La/SSB antibodies and those with anti-La/SSB antibodies. **F**, Reactivity with p40 in SLE patients without anti-RNP antibodies and those with anti-RNP antibodies. Symbols represent individual patients; horizontal lines show the median. *P* values were determined by Mann-Whitney U test. See Figure 1 for other definitions.

Whether significant or not, these inverse correlations were unexpected. Since SLE is a heterogenous disease that may include several molecularly distinct endotypes, it is possible that arthritis and oral ulcers arise by molecular mechanisms that do not include LINE-1 biology or p40 autoantibodies.

We next investigated whether anti-p40 antibodies are associated with other common lupus autoantibodies, including those against dsDNA, complement C1q, Sm, RNP, Ro/SSA, La/SSB, and cardiolipin. Briefly, anti-p40 antibody levels were strongly associated with anti-dsDNA levels ($P = 0.0006$) (Figure 4A) and anti-C1q antibodies ($P = 0.004$) (Figure 4B), consistent with their

association with nephritis, as well as anticardiolipin antibodies ($P = 0.05$) (Figure 4C). Further, anti-p40 antibodies were correlated with Ro/SSA positivity ($P = 0.09$) (Figure 4D) and La/SSB positivity ($P = 0.007$) (Figure 4E), although the correlation with Ro/SSA did not reach statistical significance. There was no significant association with Sm (not shown) or anti-RNP antibodies (Figure 4F).

Increased anti-p40 antibody levels in patients with elevated type I IFN levels. The sera from this cohort of SLE patients were previously analyzed for type I IFN levels using a
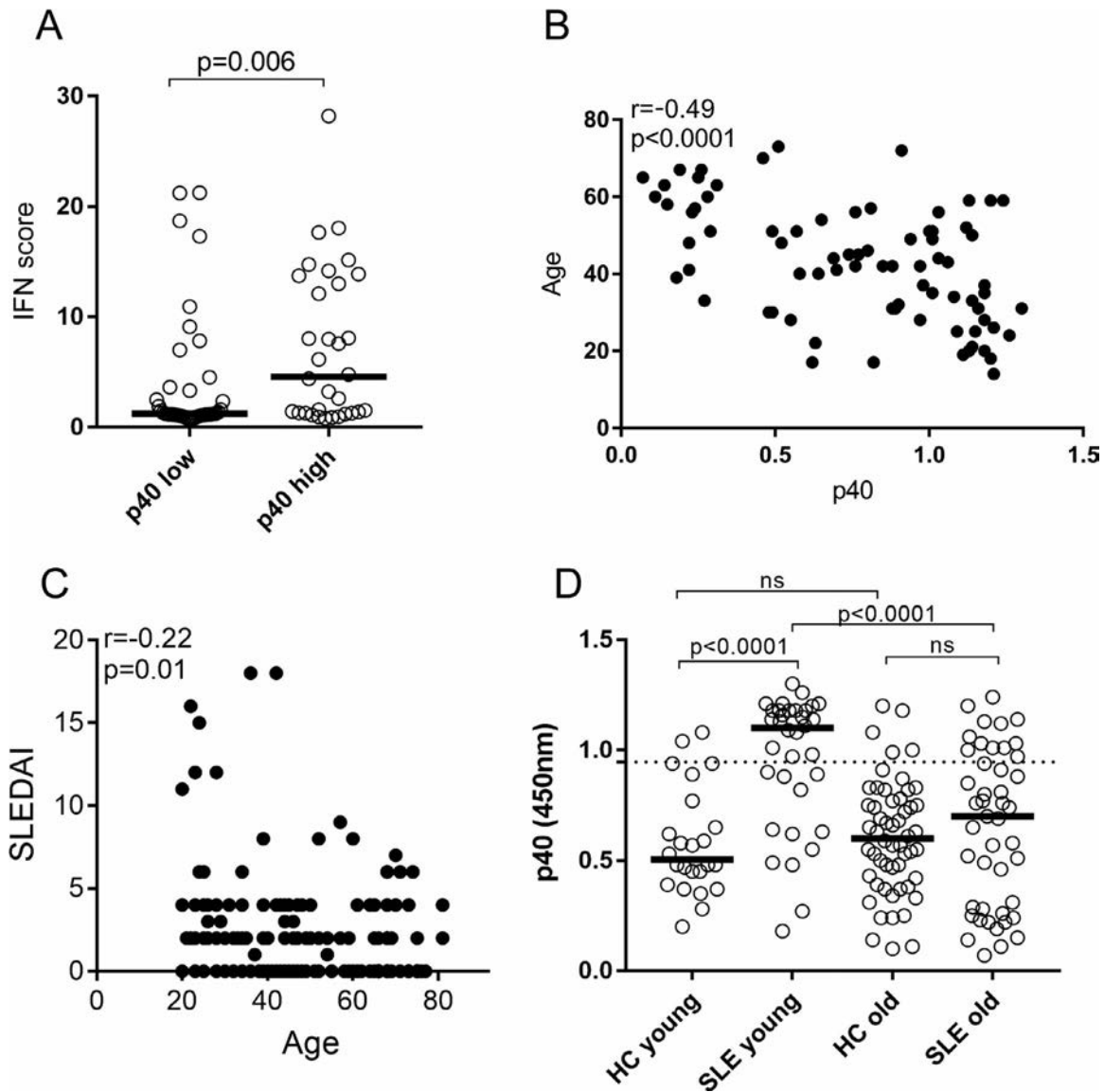
Figure 5. Correlation of type I interferon (IFN) score and of age with anti-p40 autoantibody levels. **A**, Induction of type I IFN–inducible genes by serum from SLE patients with anti-p40 reactivity below the 90th percentile in healthy controls (p40 low) and those with anti-p40 reactivity above the 90th percentile in healthy controls (p40 high). **B**, Inverse correlation between anti-p40 reactivity and age in the SLE patients. **C**, Inverse correlation between SLE Disease Activity Index (SLEDAI) score and age in the SLE patients. **D**, Anti-p40 reactivity in healthy controls and SLE patients grouped by age, where subjects <40 years old were classified as young and subjects ≥40 years old were classified as old. The broken line indicates the 90th percentile in healthy controls. In **A** and **D**, symbols represent individual subjects; horizontal lines show the median. P values were determined by Mann-Whitney U test and Spearman's correlation test. See Figure 1 for other definitions.

reporter cell, and measuring the induction of type I IFN–regulated genes (43–45). Patients with levels of anti-p40 antibodies above the 90th percentile in the healthy subjects also had elevated levels of type I IFNs ($P = 0.006$) (Figure 5A). There was also a direct correlation between autoantibody level and type I IFN activity ($r = 0.36$, $P < 0.0001$). In logistic regression analysis, patients with anti-p40 antibodies more often had high levels of type I IFNs (odds ratio 3.26 [1.25–8.53]; $P = 0.02$).

Inverse correlation of anti-p40 autoantibody levels with age. Unexpectedly, our data set also revealed a highly significant inverse correlation of anti-p40 reactivity with the age of the SLE patients ($r = -0.49$; $P < 0.0001$) (Figure 5B). This association may be, at least in part, explained by the higher SLEDAI in younger patients ($r = -0.22$; $P = 0.01$) (Figure 5C). Nevertheless, when the entire cohort of SLE patients and healthy controls was divided into 2 groups based on age with a cut-off at 40 years, the association of anti-p40 reactivity with SLE became even

more marked in the younger group ($P < 0.0001$) (Figure 5D) compared to the total cohort (Figure 2A), while it became statistically insignificant in the older patient group. There was a trend toward increased anti-p40 reactivity in the older group of healthy controls.

Autoantibodies against p40-associated proteins in SLE patients. Since LINE-1 p40, together with its cognate mRNA, is located in cellular stress granules in complex with several other RNA binding proteins, we wanted to see if any of these associated proteins are also targets of the immune response in SLE. To this end, epitope-tagged p40 was purified from overexpressing cells under conditions that allowed associated proteins to co-purify with p40. These preparations were immunoblotted with the sera of SLE patients who had strong reactivity with p40. As shown in Figure 6, weaker bands at ~23, 27, 34, 60, 100, 145, and a smear at ~200 kd were discernible in these blots. Although p40-associated proteins of these sizes have been reported (e.g.,
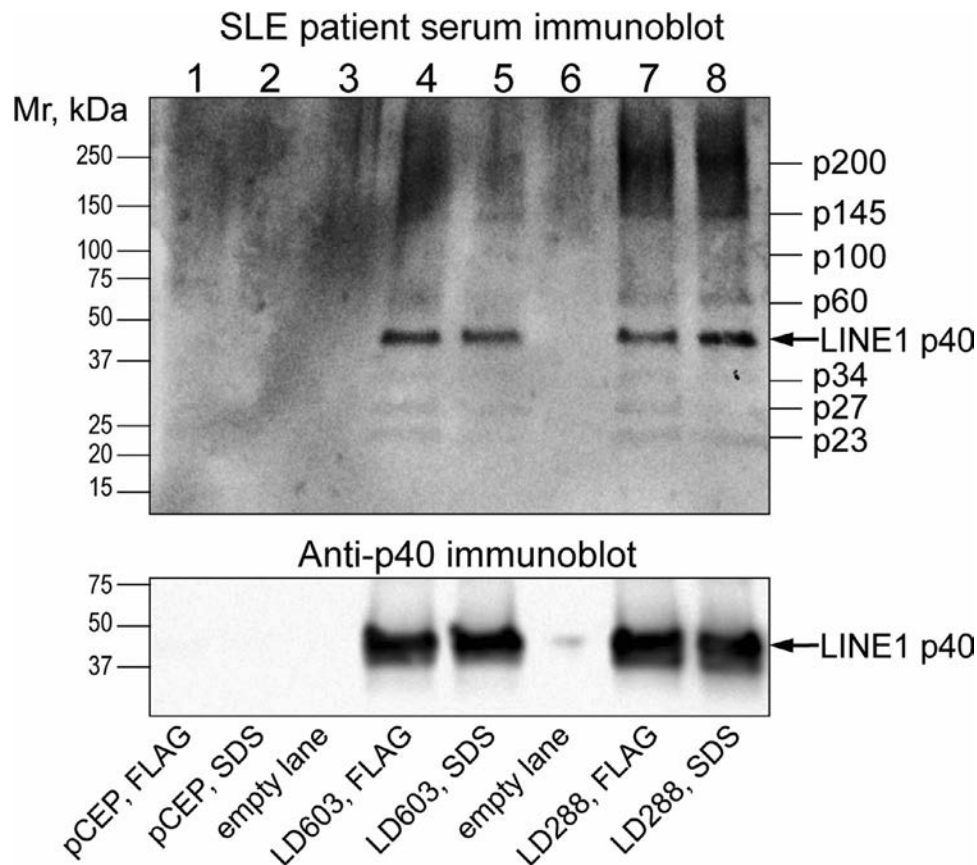
Figure 6. Sera from patients with systemic lupus erythematosus (SLE) contain autoantibodies against proteins that co-purify with p40. Top, Immunoblotting of p40 with sera from patients with SLE with strong reactivity with p40. Bottom, Immunoblotting of the same samples as in the top panel with anti-p40 monoclonal antibody. Similar results were obtained on 2 additional immunoblots. Lane 1, Anti-FLAG immunoprecipitate from cells transfected with empty vector (pCEP) and eluted with FLAG peptide. Lane 2, Anti-FLAG immunoprecipitate from cells transfected with empty vector (pCEP) and eluted with sodium dodecyl sulfate (SDS). Lane 3, Empty. Lane 4, Anti-FLAG immunoprecipitate from cells transfected with the p40 expression vector LD603 and eluted with FLAG peptide. Lane 5, Anti-FLAG immunoprecipitate from cells transfected with the p40 expression vector LD603 and eluted with SDS. Lane 6, Empty. Lane 7, Anti-FLAG immunoprecipitate from cells transfected with the p40 expression vector LD288 and eluted with FLAG peptide. Lane 8, Anti-FLAG immunoprecipitate from cells transfected with the p40 expression vector LD288 and eluted with SDS.

Ro/SSA at 60 kd), the identities of the proteins recognized by SLE sera in Figure 6 remain to be established in future studies.

DISCUSSION

Our findings reveal a previously unrecognized autoantigen in SLE, the LINE-1 ORF1-encoded p40 protein. Unlike most of the well-characterized autoantigens in this disease, p40 is recognized by IgG in a majority of SLE patients (depending on how one defines the threshold for positivity), as well as in many healthy control subjects, albeit mostly with much lower titers. In this respect, anti-p40 autoantibodies resemble anti-dsDNA antibodies, which are also present in a subset of healthy subjects, yet correlate with active SLE. Importantly, we excluded the possibility that anti-p40 autoantibodies represent anti-dsDNA antibodies recognizing p40-bound DNA.

Clearly, anti-p40 antibodies do not by themselves herald clinically relevant autoimmunity, but more likely represent an early phase of self-reactivity that may, or may not, progress toward SLE. In healthy individuals, LINE-1 transcription is typically undetectable, being largely suppressed by DNA methylation. However, expression can be induced by environmental or genetic factors that reduce this methylation, such as certain drugs, reduced expression of methyltransferases, ultraviolet light, and perhaps viral infections. LINE-1 expression is also elevated in malignant cells. Hence, it may be that healthy subjects occasionally express enough p40 to provoke a low level humoral immune response to it. Although we have not studied LINE-1 expression in the thymus, we surmise that these elements may remain transcriptionally silent during T cell selection in the thymus, as well as during B cell maturation in the bone marrow. If so, humans may have a weak, or even absent, central tolerance against LINE-1 p40.

Over the past 25 years, many investigators have suggested that endogenous retroviruses or retroelements may play a role in the pathogenesis of SLE (47–50), proposing various mechanisms for the induction of autoimmunity, such as molecular mimicry, superantigen properties of retroelement proteins, or the perturbation of the transcription of nearby genes. In comparison, only a few studies focused on LINE-1 and, to the best of our knowledge, never tested SLE patients for direct humoral immunity against LINE-1 proteins. Taken together, our findings that nearly all SLE patients have autoantibodies against the LINE-1 p40 protein and that these antibodies are associated with disease activity, specific disease manifestations, low complement levels, other autoantibodies, and type I IFNs, suggest that LINE-1 biology is coupled in some way to SLE pathogenesis.

First, it should be noted that LINE-1 may lack any causative role and perhaps is targeted by the immune response as an innocent bystander. The physical interaction of p40 with well-known SLE autoantigens would be compatible with such a role, at least if one assumes that Ro and La are the intended antigens for the immune response. However, it is equally plausible that the reverse is true, namely, that the LINE-1 proteins, by virtue of their biologic functions, are responsible for the immune attack on cells that express LINE-1 and that other associated proteins are the innocent bystanders. The recognition of p40-associated proteins by SLE autoantibodies (Figure 6) would support this notion. We speculate that individuals who express more LINE-1, either in an episodic or a chronic manner, boost their humoral and cellular immunity against p40 over time and eventually reach levels of response that may be pathogenic.

Cells that express the LINE-1–encoded proteins may display features of virally infected cells. In addition to the immunogenicity of p40, these cells may have sufficient amounts of the ORF2 protein, which has reverse transcriptase activity, to generate DNA copies of available RNA species, such as its own cognate mRNA, Alu element transcripts, and others. Such DNA copies can presumably trigger the cyclic GMP-AMP synthase (cGAS)/stimulator of IFN genes pathway to induce expression of IFNβ (35), which appears to play an important role in driving SLE (51–54). Indeed, transfection of LINE-1 into cells induces production of IFNβ (55). Also, a recent study (56) showed that blood mononuclear cells from ~17% of SLE patients have detectable cyclic GMP-AMP, the second messenger exclusively made by cGAS when it is activated by aberrant intracellular DNA (18,57). Given the minute quantities and rapid turnover of this second messenger, these data likely represent an underestimate. Further, cells that contain active LINE-1 proteins may also up-regulate major histocompatibility complex expression, and other surface markers induced either directly by cGAS through IRF3 activation, or indirectly by IFNβ signaling (58), resulting in a chronic, but perhaps episodic, (auto)immune response against such cells.

An unexpected feature of our data set was the inverse correlation of anti-p40 reactivity with the age of the SLE patients. This inverse correlation can be partly explained by the presence of many young patients with high SLEDAI scores. There was also a trend toward increasing anti-p40 reactivity in healthy controls with age, similar to how anti-dsDNA antibodies tend to increase slowly with age. The difference between younger SLE patients and age-matched controls was more striking than in the total population. Although this age correlation does not have any immediately obvious explanation, it may be related to the decline in general humoral immunity with age (59), the group of young SLE patients with very active disease, or the typical presentation of SLE earlier in life and its slow decline in activity over time. As anti-p40 reactivity was strongly increased in young SLE patients compared to young control subjects, this correlation is compatible with an early role of p40 immunogenicity in the pathogenesis of the disease.

ACKNOWLEDGMENTS

AUTHOR CONTRIBUTIONS

All authors were involved in drafting the article or revising it critically for important intellectual content, and all authors approved the final version to be published. Dr. T. Mustelin had full access to all of the data in the study and takes responsibility for the integrity of the data and the accuracy of the data analysis.

Study conception and design. LaCava, Ukadike, Lood, T. Mustelin.
Acquisition of data. Carter, LaCava, Taylor, Liang, C. Mustelin, Lood, T. Mustelin.
Analysis and interpretation of data. Carter, LaCava, Taylor, Bengtsson, Lood, T. Mustelin.

REFERENCES

1. Lander ES, Linton LM, Birren B, Nusbaum C, Zody MC, Baldwin J, et al. Initial sequencing and analysis of the human genome. Nature 2001;409:860–921.

2. Weiss RA, Stoye JP. Virology: our viral inheritance. Science 2013;340:820–1.

3. Esnault C, Maestre J, Heidmann T. Human LINE retrotransposons generate processed pseudogenes [letter]. Nat Genet 2000;24:363–7.

4. Ostertag EM, Kazazian HH Jr. Biology of mammalian L1 retrotransposons. Annu Rev Genet 2001;35:501–38.

5. Brouha B, Schustak J, Badge RM, Lutz-Prigge S, Farley AH, Moran JV, et al. Hot L1s account for the bulk of retrotransposition in the human population. Proc Natl Acad Sci U S A 2003;100:5280–5.

6. Kano H, Godoy I, Courtney C, Vetter MR, Gerton GL, Ostertag EM, et al. L1 retrotransposition occurs mainly in embryogenesis and creates somatic mosaicism. Genes Dev 2009;23:1303–12.

7. Duggal NK, Emerman M. Evolutionary conflicts between viruses and restriction factors shape immunity. Nat Rev Immunol 2012;12:687–95.

8. D'Urbano V, De Crignis E, Re MC. Host restriction factors and human immunodeficiency virus (HIV-1): a dynamic interplay involving all phases of the viral life cycle. Curr HIV Res 2018;16:184–207.

9. Goodier JL, Cheung LE, Kazazian HH Jr. MOV10 RNA helicase is a potent inhibitor of retrotransposition in cells. PLoS Genet 2012;8:e1002941.

10. Merindol N, Berthoux L. Restriction factors in HIV-1 disease progression. Curr HIV Res 2015;13:448–61.

11. Pyndiah N, Telenti A, Rausell A. Evolutionary genomics and HIV restriction factors. Curr Opin HIV AIDS 2015;10:79–83.

12. Ghimire D, Rai M, Gaur R. Novel host restriction factors implicated in HIV-1 replication. J Gen Virol 2018;99:435–46.

13. Volkman HE, Stetson DB. The enemy within: endogenous retroelements and autoimmune disease. Nat Immunol 2014;15:415–22.

14. Stetson DB, Ko JS, Heidmann T, Medzhitov R. Trex1 prevents cell-intrinsic initiation of autoimmunity. Cell 2008;134:587–98.

15. Aicardi J, Goutières F. A progressive familial encephalopathy in infancy with calcifications of the basal ganglia and chronic cerebrospinal fluid lymphocytosis. Ann Neurol 1984;15:49–54.

16. Crow YJ, Manel N. Aicardi-Goutières syndrome and the type I interferonopathies. Nat Rev Immunol 2015;15:429–40.

17. Crow YJ, Chase DS, Lowenstein Schmidt J, Szynkiewicz M, Forte GM, Gornall HL, et al. Characterization of human disease phenotypes associated with mutations in TREX1, RNASEH2A, RNASEH2B, RNASEH2C, SAMHD1, ADAR, and IFIH1. Am J Med Genet A 2015;167A:296–312.

18. Ablasser A, Hemmerling I, Schmid-Burgk JL, Behrendt R, Roers A, Hornung V. TREX1 deficiency triggers cell-autonomous immunity in a cGAS-dependent manner. J Immunol 2014;192:5993–7.

19. Rice GI, Bond J, Asipu A, Brunette RL, Manfield IW, Carr IM, et al. Mutations involved in Aicardi-Goutières syndrome implicate SAMHD1 as regulator of the innate immune response. Nat Genet 2009;41:829–32.

20. Zhao K, Du J, Han X, Goodier JL, Li P, Zhou X, et al. Modulation of LINE-1 and Alu/SVA retrotransposition by Aicardi-Goutières syndrome-related SAMHD1. Cell Rep 2013;4:1108–15.

21. Mathias SL, Scott AF, Kazazian HH Jr, Boeke JD, Gabriel A. Reverse transcriptase encoded by a human transposable element. Science 1991;254:1808–10.

22. Clements AP, Singer MF. The human LINE-1 reverse transcriptase: effect of deletions outside the common reverse transcriptase domain. Nucleic Acids Res 1998;26:3528–35.

23. Goodier JL, Zhang L, Vetter MR, Kazazian HH Jr. LINE-1 ORF1 protein localizes in stress granules with other RNA-binding proteins, including components of RNA interference RNA-induced silencing complex. Mol Cell Biol 2007;27:6469–83.

24. Goodier JL, Cheung LE, Kazazian HH Jr. Mapping the LINE1 ORF1 protein interactome reveals associated inhibitors of human retrotransposition. Nucleic Acids Res 2013;41:7401–19.

25. Hung T, Pratt GA, Sundararaman B, Townsend MJ, Chaivorapol C, Bhangale T, et al. The Ro60 autoantigen binds endogenous retroelements and regulates inflammatory gene expression. Science 2015;350:455–9.

26. Taylor MS, LaCava J, Mita P, Molloy KR, Huang CR, Li D, et al. Affinity proteomics reveals human host factors implicated in discrete stages of LINE-1 retrotransposition. Cell 2013;155:1034–48.

27. Mavragani CP, Nezos A, Sagalovskiy I, Seshan S, Kirou KA, Crow MK. Defective regulation of L1 endogenous retroelements in primary Sjögren's syndrome and systemic lupus erythematosus: role of methylating enzymes. J Autoimmun 2018;88:75–82.

28. Mavragani CP, Sagalovskiy I, Guo Q, Nezos A, Kapsogeorgou EK, Lu P, et al. Expression of long interspersed nuclear element 1 retroelements and induction of type I interferon in patients with systemic autoimmune disease. Arthritis Rheumatol 2016;68:2686–96.

29. Huang X, Su G, Wang Z, Shangguan S, Cui X, Zhu J, et al. Hypomethylation of long interspersed nucleotide element-1 in peripheral mononuclear cells of juvenile systemic lupus erythematosus patients in China. Int J Rheum Dis 2014;17:280–90.

30. Balada E, Ordi-Ros J, Serrano-Acedo S, Martinez-Lostao L, Rosa-Leyva M, Vilardell-Tarrés M. Transcript levels of DNA methyltransferases DNMT1, DNMT3A and DNMT3B in CD4+ T cells from patients with systemic lupus erythematosus. Immunology 2008;124:339–47.

31. Cornacchia E, Golbus J, Maybaum J, Strahler J, Hanash S, Richardson B. Hydralazine and procainamide inhibit T cell DNA methylation and induce autoreactivity. J Immunol 1988;140:2197–200.

32. Lieberman MW, Beach LR, Palmiter RD. Ultraviolet radiation-induced metallothionein-I gene activation is associated with extensive DNA demethylation. Cell 1983;35:207–14.

33. Li P, Du J, Goodier JL, Hou J, Kang J, Kazazian HH Jr, et al. Aicardi-Goutières syndrome protein TREX1 suppresses L1 and maintains genome integrity through exonuclease-independent ORF1p depletion. Nucleic Acids Res 2017;45:4619–31.

34. Lim YW, Sanz LA, Xu X, Hartono SR, Chédin F. Genome-wide DNA hypomethylation and RNA:DNA hybrid accumulation in Aicardi-Goutières syndrome. Elife 2015;4:e08007.

35. Keating SE, Baran M, Bowie AG. Cytosolic DNA sensors regulating type I interferon induction. Trends Immunol 2011;32:574–81.

36. Rice GI, Meyzer C, Bouazza N, Hully M, Boddaert N, Semeraro M, et al. Reverse-transcriptase inhibitors in the Aicardi-Goutières Syndrome [letter]. N Engl J Med 2018;379:2275–7.

37. Lood C, Eriksson S, Gullstrand B, Jönsen A, Sturfelt G, Truedsson L, et al. Increased C1q, C4 and C3 deposition on platelets in patients with systemic lupus erythematosus—a possible link to venous thrombosis? Lupus 2012;21:1423–32.

38. Lood C, Tydén H, Gullstrand B, Jönsen A, Källberg E, Mörgelin M, et al. Platelet-derived S100A8/A9 and cardiovascular disease in systemic lupus erythematosus. Arthritis Rheumatol 2016;68:1970–80.

39. Lood C, Tydén H, Gullstrand B, Nielsen CT, Heegaard NH, Linge P, et al. Decreased platelet size is associated with platelet activation and anti-phospholipid syndrome in systemic lupus erythematosus. Rheumatology (Oxford) 2017;56:408–16.

40. Andersen KR, Leksa NC, Schwartz TU. Optimized E. coli expression strain LOBSTR eliminates common contaminants from His-tag purification. Proteins 2013;81:1857–61.

41. Taylor MS, Altukhov I, Molloy KR, Mita P, Jiang H, Adney EM, et al. Dissection of affinity captured LINE-1 macromolecular complexes. Elife 2018;7:e30094.

42. Taylor MS, LaCava J, Dai L, Mita P, Burns KH, Rout MP, et al. Characterization of L1-ribonucleoprotein particles. Methods Mol Biol 2016;1400:311–38.

43. Bengtsson AA, Sturfelt G, Lood C, Rönnblom L, van Vollenhoven RF, Axelsson B, et al. Pharmacokinetics, tolerability, and preliminary efficacy of paquinimod (ABR-215757), a new quinoline-3-carboxamide derivative: studies in lupus-prone mice and a multicenter, randomized, double-blind, placebo-controlled, repeat-dose, dose-ranging study in patients with systemic lupus erythematosus. Arthritis Rheum 2012;64:1579–88.

44. Leffler J, Martin M, Gullstrand B, Tydén H, Lood C, Truedsson L, et al. Neutrophil extracellular traps that are not degraded in systemic lupus erythematosus activate complement exacerbating the disease. J Immunol 2012;188:3522–31.

45. Lood C, Tydén H, Gullstrand B, Klint C, Wenglén C, Nielsen CT, et al. Type I interferon-mediated skewing of the serotonin synthesis is associated with severe disease in systemic lupus erythematosus. PLoS One 2015;10:e0125109.

46. Bombardier C, Gladman DD, Urowitz MB, Caron D, Chang CH, and the Committee on Prognosis Studies in SLE. Derivation of the SLEDAI: a disease activity index for lupus patients. Arthritis Rheum 1992;35:630–40.

47. Krapf FE, Herrmann M, Leitmann W, Kalden JR. Are retroviruses involved in the pathogenesis of SLE? Evidence demonstrated by molecular analysis of nucleic acids from SLE patients' plasma. Rheumatol Int 1989;9:115–21.

48. Perl A, Nagy G, Koncz A, Gergely P, Fernandez D, Doherty E, et al. Molecular mimicry and immunomodulation by the HRES-1 endogenous retrovirus in SLE. Autoimmunity 2008;41:287–97.

49. Tugnet N, Rylance P, Roden D, Trela M, Nelson P. Human Endogenous Retroviruses (HERVs) and autoimmune rheumatic disease: is there a link? Open Rheumatol J 2013;7:13–21.

50. Talal N, Flescher E, Dang H. Are endogenous retroviruses involved in human autoimmune disease? J Autoimmun 1992;5 Suppl A:61–6.

51. Bennett L, Palucka AK, Arce E, Cantrell V, Borvak J, Banchereau J, et al. Interferon and granulopoiesis signatures in systemic lupus erythematosus blood. J Exp Med 2003;197:711–23.

52. Eloranta ML, Rönnblom L. Cause and consequences of the activated type I interferon system in SLE. J Mol Med (Berl) 2016;94:1103–10.

53. Bezalel S, Guri KM, Elbirt D, Asher I, Sthoeger ZM. Type I interferon signature in systemic lupus erythematosus [review]. Isr Med Assoc J 2014;16:246–9.

54. Furie R, Khamashta M, Merrill JT, Werth VP, Kalunian K, Brohawn P, et al. Anifrolumab, an anti–interferon-α receptor monoclonal antibody, in moderate-to-severe systemic lupus erythematosus. Arthritis Rheumatol 2017;69:376–86.

55. Kelly M, Lihua S, Zhe Z, Li S, Yoselin P, Michelle P, et al. Transposable element dysregulation in systemic lupus erythematosus and regulation by histone conformation and Hsp90. Clin Immunol 2018;197:6–18.

56. Bonandin L, Scavariello C, Mingazzini V, Luchetti A, Mantovani B. Obligatory parthenogenesis and TE load: Bacillus stick insects and the R2 non-LTR retrotransposon. Insect Sci 2017;24:409–17.

57. Gao D, Li T, Li XD, Chen X, Li QZ, Wight-Carter M, et al. Activation of cyclic GMP-AMP synthase by self-DNA causes autoimmune diseases. Proc Natl Acad Sci U S A 2015;112:E5699–705.

58. Schoggins JW, Wilson SJ, Panis M, Murphy MY, Jones CT, Bieniasz P, et al. A diverse range of gene products are effectors of the type I interferon antiviral response. Nature 2011;472:481–5.

59. Blanco E, Pérez-Andrés M, Arriba-Méndez S, Contreras-Sanfeliciano T, Criado I, Pelak O, et al. Age-associated distribution of normal B-cell and plasma cell subsets in peripheral blood. J Allergy Clin Immunol 2018;141:2208–19.

AMERICAN COLLEGE
of RHEUMATOLOGY
Empowering Rheumatology Professionals

Differential Responsiveness of Monocyte and Macrophage Subsets to Interferon

Shuhong Han,[1] 🔘 Haoyang Zhuang,[1] Pui Y. Lee,[2] Mingjia Li,[1] Lijun Yang,[1] Peter A. Nigrovic,[3] and Westley H. Reeves[1]

Objective. Peripheral blood mononuclear cells (PBMCs) in systemic lupus erythematosus (SLE) patients exhibit a gene expression program (interferon [IFN] signature) that is attributed to overproduction of type I IFNs by plasmacytoid dendritic cells. Type I IFNs have been thought to play a role in the pathogenesis of SLE. This study was undertaken to examine an unexpected influence of monocyte/macrophages on the IFN signature.

Methods. Proinflammatory (classic) and antiinflammatory (nonclassic) monocyte/macrophages were sorted from mice and analyzed by RNA sequencing and quantitative polymerase chain reaction (qPCR). Type I IFN-α/β/ω receptor (IFNAR-1) expression was determined by qPCR and flow cytometry. Macrophages were stimulated in vitro with IFNα, and pSTAT1 was measured.

Results. Transcriptional profiling of peritoneal macrophages from mice with pristane-induced SLE unexpectedly indicated a strong IFN signature in classic, but not nonclassic, monocyte/macrophages exposed to the same type I IFN concentrations. *Ifnar1* messenger RNA and IFNAR surface staining were higher in classic monocyte/macrophages versus nonclassic monocyte/macrophages ($P < 0.0001$ and $P < 0.05$, respectively, by Student's *t*-test). Nonclassic monocyte/macrophages were also relatively insensitive to IFNα-driven STAT1 phosphorylation. Humans exhibited a similar pattern: higher IFNAR expression ($P < 0.0001$ by Student's *t*-test) and IFNα-stimulated gene expression ($P < 0.01$ by paired Wilcoxon's rank sum test) in classic monocyte/macrophages and lower levels in nonclassic monocyte/macrophages.

Conclusion. This study revealed that the relative abundance of different monocyte/macrophage subsets helps determine the magnitude of the IFN signature. Responsiveness to IFNα signaling reflects differences in IFNAR expression in classic (high IFNAR) compared to nonclassic (low IFNAR) monocyte/macrophages. Thus, the IFN signature depends on both type I IFN production and the responsiveness of monocyte/macrophages to IFNAR signaling.

INTRODUCTION

Peripheral blood mononuclear cells (PBMCs) from systemic lupus erythematosus (SLE) patients exhibit high levels of gene transcripts regulated by type I interferons (IFNs), such as IFNα and IFNβ (1,2). In aggregate, this transcriptional program is termed the "IFN signature." Many of the IFN-stimulated genes overexpressed in SLE are involved in antiviral responses. A high IFN signature correlates with anti-Sm, anti-RNP, and anti–double-stranded DNA (anti-dsDNA) autoantibody production and lupus nephritis (3,4).

Mice with pristane-induced SLE also develop the IFN signature (5,6).

Several lines of evidence suggest that IFN responses play a role in disease pathogenesis. Patients treated with IFNα may develop antinuclear antibodies or clinical SLE (7,8), and anti-Sm, anti-RNP, and anti-dsDNA autoantibody production and lupus nephritis are greatly attenuated in mice with experimental lupus that lack the type I IFN-α/β/ω receptor (IFNAR-1) (9,10). This has prompted the search for SLE treatments that block the IFNAR, such as the anti-IFNAR monoclonal antibody anifrolumab (11).

High IFN signatures are associated with active SLE and constitute a risk factor for disease development (4,12). Measuring type I IFN in biologic samples is technically challenging (13). Consequently, type I IFN–regulated gene expression in PBMCs is a widely used surrogate marker for type I IFN (1,2,14). Although the IFN signature has been assumed to reflect type I IFN production, its magnitude could also reflect differences in signaling through the IFNAR, which activates the kinases JAK1 and Tyk-2, resulting in the phosphorylation of STAT1 and STAT2, or activation of Irf9, other Stat proteins, phosphatidylinositol 3-kinase (PI3K), and/or ERK-1/2 (15). Thus, the IFN signature could be influenced by expression of the IFNAR (*Ifnar1* and *Ifnar2* chains) or the expression/activity of key intermediates downstream of the receptor (16,17).

We recently found that CD138+ "nonclassic" monocyte/macrophages promoting the resolution of inflammation are deficient in mice with pristane-induced SLE (18). In the present study, transcriptional profiling of this novel monocyte/macrophage subset revealed a much lower IFN signature than is seen in "classic" Ly6C^{high} monocyte/macrophage (19) exposed to the same concentration of type I IFN. We showed that this is because nonclassic monocyte/macrophages are relatively insensitive to signaling through the IFNAR. Similarly, circulating human monocyte subsets exhibit differential responsiveness to type I IFN. Moreover, we demonstrated that the magnitude of the IFN signature in human PBMCs depends on the relative number of classic monocytes (equivalent to murine classic monocyte/macrophages). These data findings alter how we view the IFN signature, potentially with implications for understanding the pathogenesis of SLE.

MATERIALS AND METHODS

Mice. Female C57BL/6 (B6) mice (5–10 per group; The Jackson Laboratory) housed under specific pathogen–free conditions were injected intraperitoneally with 0.5 ml of either pristane (Sigma-Aldrich) or mineral oil (C. B. Fleet). Peritoneal exudate cells (PECs) were collected by lavage 3–14 days later (20). The study was conducted in accordance with the recommendations of the Animal Welfare Act and US Government Principles for the Utilization and Care of Vertebrate Animals and was approved by the University of Florida Institutional Animal Care and Use Committee.

Flow cytometry, cell sorting, and RNA isolation. Flow cytometry was performed using Fc Block anti-mouse CD16/32 (BD Biosciences) before staining with primary antibody or isotype controls. Cells were surface-stained and fixed/permeabilized using a Fix-Perm buffer (eBioscience), and then stained intracellularly. Monoclonal antibodies used for flow cytometry are listed in Supplementary Table 1, available on *Arthritis & Rheumatology* web site at http://onlinelibrary.wiley.com/doi/10.1002/art.41072/abstract. For cell purification, PECs were incubated with anti-CD11b–BV421, allophycocyanin (APC)–conjugated CD138, Alexa Fluor 488–conjugated Ly6C, and APC-Cy7–conjugated Ly6G

antibodies (20). Peritoneal nonclassic monocyte/macrophages (CD11b+CD138+Ly6C–Ly6G–), which we previously termed CD138+ macrophages, and classic monocyte/macrophages (CD11b+CD138–Ly6C^{high}Ly6G–), which we previously termed Ly6C^{high} monocyte/macrophages (18), were flow-sorted using a FACSAria cell sorter (3 mice/group; 30,000 cells/mouse). The gating strategy is shown in Figure 1A. Cells were lysed immediately, and RNA was isolated using an RNeasy Micro Kit (Qiagen).

Gene expression profiling. RNA sequencing (RNA-Seq) was performed at Broad Institute using the Smart-Seq2 platform (21–23). Smart-Seq2 libraries were prepared by the Broad Institute Technology Laboratories and sequenced using the Broad Genomics Platform. Transcripts were quantified using the Broad Technology Laboratories computational pipeline with Cuffquant version 2.2.1 (24). Preliminary data analysis confirmed that purity of the sorted cells was high: *Ly6c2* was more highly expressed in classic monocyte/macrophages and *Sdc1* (encoding syndecan-1/CD138) in nonclassic monocyte/macrophages. Reproducibility between mice was also high (data not shown). Gene set enrichment analysis (GSEA) was performed using Broad Institute GSEA Desktop version 2.2.4 and hallmark gene sets from the Molecular Signature Database version 6.2 (25,26). A false discovery rate (FDR) of q < 0.25 was considered significant (25). Heatmaps were constructed using Java Treeview (27). The RNA-Seq data discussed in this publication are available from the corresponding author upon request.

Quantitative polymerase chain reaction. Quantitative polymerase chain reaction (qPCR) was performed using RNA from 10^6 mouse PECs (TRIzol; Invitrogen). Complementary DNA (cDNA) was synthesized using a SuperScript II First-Strand Synthesis kit (Invitrogen). SYBR Green qPCR analysis was performed using the CFX Connect Real-Time system (Bio-Rad). Gene expression was normalized to 18S RNA, and the expression level was calculated using the $2^{-\Delta\Delta C_t}$ method. Primer sequences were as follows: mouse *Mx1*: forward 5′-GATCCGACTTCACTTCCAGATGG-3′, reverse 5′-CATCTCA GTGGTAGTCCAACCC-3′; mouse 18S: forward 5′-CGGCTAC CACATCCAAGGAA-3′, reverse 5′-GCTGGAATTACCGCGG CT-3′; human LY6E: forward 5′-CAGCTCGCTGATGTG CTT CT-3′, reverse 5′-CAGACACAGTCACGCAGTAGT-3′; human CXCL10: forward 5′-GTGGCATTCAAGGAGTACCTC-3′, reverse 5′-TGATGGCCTTCGATTCTGGATT-3; human ISG15: forward 5′-CGCAGATCACCCAGAAGATCG-3′, reverse 5′-TTCGTCGC ATTTGTCCACCA-3; human MX1: forward 5′-GGTGGTCCCC AGTAATGTGG-3′, reverse 5′-CGTCAAGATTCCGATGGTCCT-3.

In vitro IFNα-stimulated STAT1 phosphorylation. On day 15 after pristane treatment, PECs were cultured for up to 15 minutes in AIM-V medium in the presence or absence of IFNα4 (100 units/ml; R & D Systems). Cells were fixed/permeabilized for flow cytometry and stained with anti-CD11b, Ly6G, Ly6C, CD138,
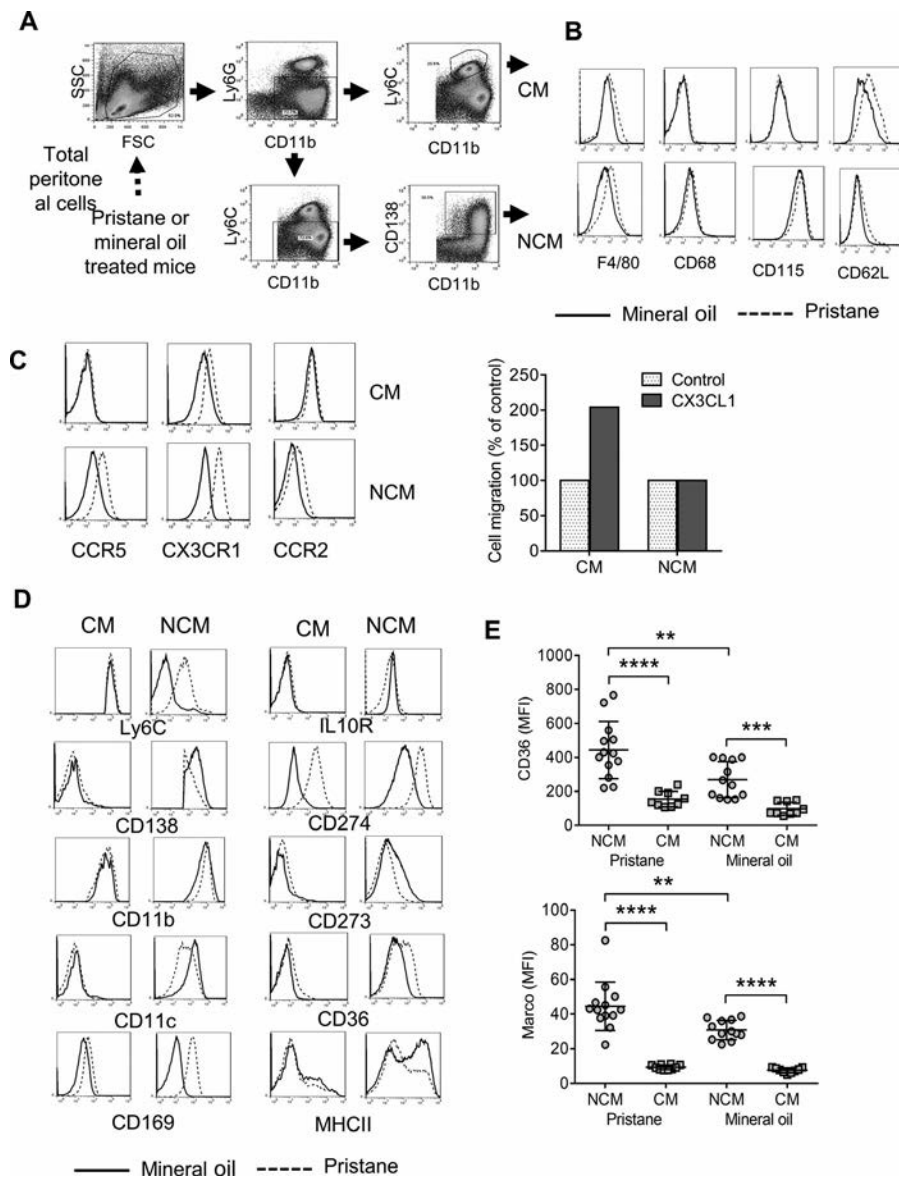
Figure 1. Surface staining phenotypes of macrophage subsets. **A**, Gating strategy for flow sorting of classic monocyte/macrophages (CMs) and nonclassic monocyte/macrophages (NCMs) from peritoneal exudate cells (PECs) from pristane- or mineral oil–treated mice. Cells were purified based on forward scatter, side scatter, and surface staining with monoclonal antibodies specific for CD11b, Ly6G, Ly6C, and CD138. **B**, Macrophage marker expression in flow-sorted classic monocyte/macrophages and nonclassic monocyte/macrophages from mineral oil– versus pristane-treated mice. Cells were stained with monoclonal antibodies specific for F4/80 (*Emr1*), CD68, CD115 (*Csf1r*), and CD62L (*Sell*). **C**, Left, Chemokine receptor expression on classic monocyte/macrophages and nonclassic monocyte/macrophages from mineral oil–treated mice versus pristane-treated mice. Cells were stained with monoclonal antibodies specific for CCR5, CX3CR1, and CCR2. Right, Transwell assay showing the migration of PECs from pristane-treated mice toward CX3CL1 (200 ng/ml). Results shown are representative of 3 separate experiments. **D**, Surface staining of cells with monoclonal antibodies specific for Ly6C, interleukin-10 receptor (IL-10R), CD138, CD274, CD11b, CD273, CD11c, CD36, CD169, and major histocompatibility complex class II (MHCII). **E**, Flow cytometry analysis of CD36 (top) and Marco (bottom) on the surface of nonclassic monocyte/macrophages and classic monocyte/macrophages from 14-day pristane-treated mice and mineral oil–treated mice. Each symbol represents an individual mouse. Bars show the mean ± SD. ** = $P < 0.01$; *** = $P < 0.001$; **** = $P < 0.0001$, by Student's *t*-test. MFI = mean fluorescence intensity.

and pSTAT1 antibodies (see Supplementary Table 1, available on *Arthritis & Rheumatology* web site at http://onlinelibrary.wiley.com/doi/10.1002/art.41072/abstract). The mean fluorescence intensity (MFI) of pSTAT1 staining in the CD11b+Ly6G–Ly6C^{high}CD138– and CD11b+Ly6G–Ly6C^{low}CD138+ cells was determined.

Transwell assays. Total PECs were isolated 14 days after pristane treatment, resuspended in RPMI culture medium containing 10% fetal bovine serum, and placed in the top well of an 8-μm Falcon Fluoroblock multiwall insert (Becton Dickinson). The lower chamber was filled with culture medium containing CX3CL1

(200 ng/ml; R & D Systems) or with culture medium alone. After 4 hours, cells in the upper and lower chambers were analyzed by flow cytometry (CD11b, Ly6C, CD138, Ly6G staining). Cell migration in response to CX3CL1 (classic monocyte/macrophage and nonclassic monocyte/macrophage subsets) was calculated as a percentage of migration with medium alone.

Flow cytometry of human blood cells. Heparinized whole blood was obtained from SLE patients (n = 10) who met the American College of Rheumatology criteria (28) and healthy donors who had no autoimmune disease (n = 11). Monoclonal antibodies were added to 100 μl of blood as follows: PerCP-conjugated anti-CD14, fluorescein isothio-cyanate–conjugated anti-CD16, phycoerythrin-conjugated anti-CD64, BV421-conjugated anti-CD45, and APC-conjugated anti–IFNAR-1 (see Supplementary Table 1, available on *Arthritis & Rheumatology* web site at http://onlinelibrary.wiley.com/doi/10.1002/art.41072/abstract) and incubated for 20 minutes in the dark. Lysis/Fix buffer was added for 5 minutes, and the cells were washed and resuspended in phosphate buffered saline (PBS) for flow cytometry. Neutrophils, monocytes, and lymphocytes were identified as CD45+ cells with high (neutrophils), low (lymphocytes), or intermediate (monocytes) side scatter. The monocyte population was gated for further analysis of CD14++CD16– cells (classic monocyte/macrophages), CD14++CD16+ cells (intermediate monocytes), and CD14+CD16++ cells (nonclassic monocyte/macrophages). CD14++CD16– monocytes are the human equivalent of murine classic monocyte/macrophages, whereas CD14+CD16++ monocytes are the equivalent of murine non-classic monocyte/macrophages (29). In some experiments, classic monocyte/macrophages and nonclassic monocyte/macrophages were stained with CD169 and CD64.

The study was conducted in accordance with recommendations from the International Committee of Medical Journal Editors and was approved by the University of Florida Institutional Review Board. All subjects provided written informed consent in accordance with the Declaration of Helsinki.

Expression of IFN-stimulated genes in human PBMC subsets. PBMCs were isolated from 8 healthy controls (30 ml heparinized peripheral blood) by Ficoll-Hypaque density gradient centrifugation and cultured for 11 hours in the presence of either IFNα2b (1,000 units/ml; R & D Systems) or vehicle (PBS). Cells were stained with anti-CD3, CD19, CD14, and CD16 antibodies and flow-sorted using a FACSAria cell sorter. T cells (CD3+CD19–CD14–CD16–), B cells (CD3–CD19+CD14–CD16–), classic macrophages (CD3–CD19–CD14++CD16–), and nonclassic macrophages (CD3–CD19–CD14+CD16++) were collected and lysed immediately. RNA was isolated using an RNeasy Micro Kit, and expression of IFN-stimulated genes (ISGs) (*LY6E*, *CXCL10*, *ISG15*, and *MX1*) was determined by qPCR as described above.

Responsiveness of human monocytes to type I IFN in vitro. PBMCs from SLE patients (n = 9) and healthy controls (n = 8) were isolated by Ficoll-Hypaque density gradient centrifugation as described above and cultured for 24 hours with IFNα2b (1,000 units/ml) or PBS, followed by incubation with fluorescently labeled monoclonal antibodies and flow cytometry. After gating on classic macrophage (CD14++CD16–), IFNAR-1, and CD64 staining intensity (mean fluorescence intensity) was determined.

Statistical analysis. Analyses were performed using GraphPadPrism 6.0. Differences between groups were analyzed by Student's unpaired 2-tailed *t*-test, unless otherwise indicated. Data were expressed as the mean ± SD. *P* values less than 0.05 were considered significant. Experiments were performed at least twice.

RESULTS

PECs from mice treated with pristane or mineral oil contain several myeloid populations, including CD11b+Ly6G–Ly6C^{high} classic macrophages, CD11b+Ly6C^{low}Ly6G–CD138+ nonclassic macrophages, and CD11b+Ly6G+ neutrophils (Figure 1A). Classic monocyte/macrophages and nonclassic monocyte/macrophages both expressed surface markers characteristic of monocyte/macrophages (F4/80, CD68, and CD115). F4/80 staining was higher in monocyte/macrophages from pristane-treated versus mineral oil–treated mice. As expected, classic monocyte/macrophages expressed higher levels of CD62L than nonclassic monocyte/macrophages (30) (Figure 1B). Both subsets expressed chemokine receptors involved in monocyte/macrophage migration (Figure 1C). As expected, classic monocyte/macrophages expressed more CCR2 than nonclassic monocyte/macrophages (18). Pristane treatment increased the expression of CCR5, CX3CR1, and CCR2 in nonclassic monocyte/macrophages and increased CX3CR1 expression in classic monocyte/macrophages, suggesting that it may promote monocyte/macrophage recruitment to the inflamed peritoneum more potently than monocytes. We previously showed that the recruitment of classic monocyte/macrophages to the peritoneum is dependent on CCR2/CCL2 in pristane-treated mice (31). Classic monocyte/macrophages from pristane-treated mice also migrated toward CX3CL1 (the ligand for CX3CR1) more efficiently than nonclassic monocyte/macrophages (Figure 1C).

Classic monocyte/macrophages from pristane-treated and mineral oil–treated mice expressed similar levels of most surface markers, although the M1 monocyte/macrophage marker CD274 was higher in classic monocyte/macrophages from pristane-treated mice (Figure 1D). In contrast, surface staining of nonclassic monocyte/macrophages from pristane-treated and mineral oil–treated mice differed somewhat, with higher Ly6C and CD274 and lower CD11c, CD273, and CD36 surface staining on
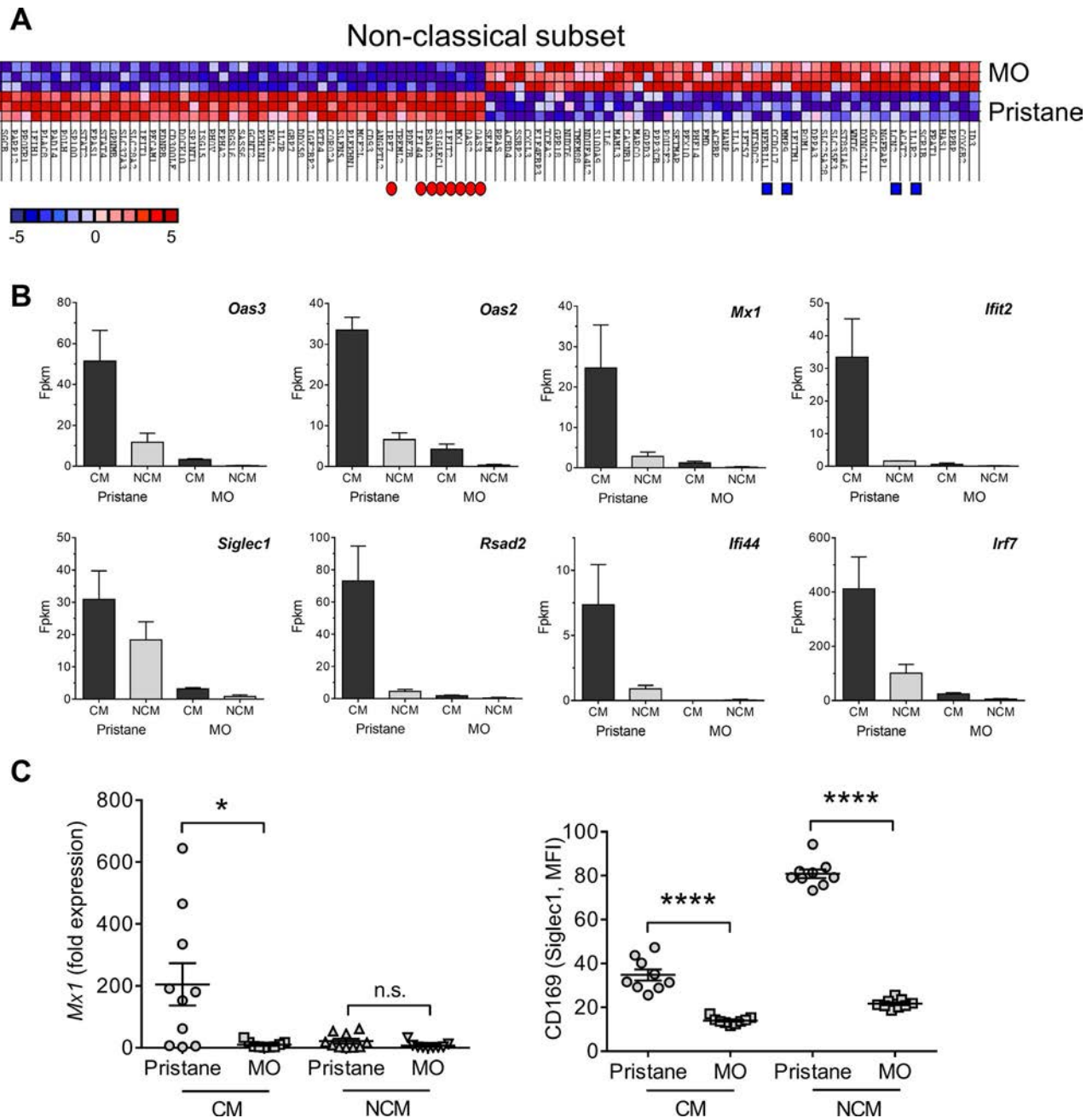
Figure 2. Transcriptional profiling of nonclassic monocyte/macrophages (NCMs) from pristane-treated mice versus mineral oil (MO)–treated mice. **A**, Heatmap of the top 50 features in nonclassic monocyte/macrophages from mineral oil–treated mice versus pristane-treated mice. Of the top 10 genes overexpressed in pristane-treated mice, 8 were interferon-stimulated genes (ISGs) associated with antiviral responses. Genes reported to have an inhibitory or immunomodulatory function overrepresented in nonclassic monocyte/macrophages from mineral oil–treated mice are indicated by blue squares. **B**, Expression of the 8 ISGs in the classic monocyte/macrophages (CMs) and nonclassic monocyte/macrophages from pristane-treated mice versus mineral oil–treated mice. Values are the mean ± SD. Fpkm = fragment per kilobase million. **C**, Left, *Mx1* expression levels relative to 18S ribosomal RNA (by quantitative polymerase chain reaction) in classic monocyte/macrophages versus nonclassic monocyte/macrophages from pristane-treated mice and mineral oil–treated mice. Right, Flow cytometry of CD169 (*Siglec1*) surface staining on classic monocyte/macrophages and nonclassic monocyte/macrophages from pristane-treated mice versus mineral oil–treated mice. Each symbol represents an individual mouse. Bars show the mean ± SD. * = $P = 0.016$; **** = $P < 0.0001$, by Student's *t*-test. NS = not significant.

nonclassic monocyte/macrophages from pristane-treated mice (Figure 1D). However, in both pristane-treated and mineral oil–treated mice, surface staining for the scavenger receptor CD36,

which promotes the phagocytosis of apoptotic cells (32), was considerably higher in nonclassic monocyte/macrophages versus classic monocyte/macrophages (Figure 1E). A similar staining pattern

was observed for Marco, another scavenger receptor involved in the phagocytosis of apoptotic cells (18,33), with increased staining intensity in nonclassic monocyte/macrophages versus classic monocyte/macrophages, and with higher expression in nonclassic monocyte/macrophages from pristane-treated mice compared to mineral oil–treated mice (Figure 1E).

We previously showed that nonclassic monocyte/macrophages from pristane-treated mice produce more tumor necrosis factor (TNF) and that TNF production and the surface phenotype become more "monocyte-like" after liver X receptor (LXR) agonist treatment (20). Thus, there may be more than one subset of nonclassic monocyte/macrophages or these cells may exhibit a greater degree of phenotypic/functional plasticity than classic monocyte/macrophages, potentially influencing whether peritoneal inflammation resolves or becomes chronic, resulting in autoimmune disease.

High expression of ISGs in nonclassic monocyte/macrophages from pristane-treated mice. To further explore peritoneal monocyte/macrophage heterogeneity, we performed transcriptional profiling of flow-sorted peritoneal monocyte/macrophages from pristane-treated and mineral oil–treated mice (Figure 2). Examination of the top 50 features differentially expressed by peritoneal nonclassic monocyte/macrophages from pristane-treated versus mineral oil–treated mice revealed that 8 of the top 10 genes overexpressed in pristane-treated mice were ISGs associated with antiviral responses (Figure 2A). Although expression of these 8 transcripts was substantially higher in nonclassic monocyte/macrophages from pristane-treated versus mineral oil–treated mice, they also were differentially expressed in classic monocyte/macrophages from pristane-treated versus mineral oil–treated mice (Figure 2B). The highest expression levels were in classic monocyte/macrophages from pristane-treated mice. Transcripts overrepresented in nonclassic monocyte/macrophages from mineral oil–treated mice included genes reported to have an inhibitory/immunomodulatory function, including *Il1r2*, *Lcn2*, *Mmp9*, and *Nfkbil1* (Figure 2A).

Weak expression of the ISG *Mx1* in peritoneal nonclassic monocyte/macrophages relative to classic monocyte/macrophages from pristane-treated mice (Figure 2B) was confirmed by qPCR (Figure 2C). Similarly, surface staining for the type I IFN–regulated protein CD169 (Siglec1) was higher on both classic monocyte/macrophages and nonclassic monocyte/macrophages from pristane-treated versus mineral oil–treated mice (Figure 2C). Interestingly, *Siglec1* messenger RNA (mRNA) appeared to be expressed at relatively higher levels in nonclassic monocyte/macrophages from pristane-treated mice than other ISGs (Figure 2B). This was reflected in high levels of Siglec-1 (CD169) surface staining on nonclassic monocyte/macrophages from pristane-treated mice (Figure 2C).

Increased type I IFN sensitivity of classic monocyte/macrophages versus nonclassic monocyte/macrophages. Peritoneal injection of pristane, but not mineral oil, induces a strong IFN signature (31). Transcriptional profiling of classic monocyte/macrophages versus nonclassic monocyte/macrophages from pristane-treated mice revealed that many of the top 50 genes overexpressed by classic monocyte/macrophages from pristane-treated mice were ISGs (Figure 3A). GSEA confirmed that classic monocyte/macrophages overexpressed members of the hallmark IFNα response gene set (25,26) (Figures 3B and C and Supplementary Table 2, available on *Arthritis & Rheumatology* web site at http://onlinelibrary.wiley.com/doi/10.1002/art.41072/abstract). Classic monocyte/macrophages also up-regulated transcripts in the IFNγ response and inflammatory response gene sets (Supplementary Table 2). Expression of the top 10 ISGs (Figure 3B) was markedly lower in classic monocyte/macrophages from mineral oil–treated mice versus those from pristane-treated mice (Figures 2B and 3D). The only exception was *Ifitm1*, which was expressed at high levels in classic monocyte/macrophages from both pristane-treated and mineral oil–treated mice (Figure 3D). However, like most other ISGs, *Ifitm1* was expressed only at low levels in nonclassic macrophages. The peritoneal nonclassic monocyte/macrophages and classic monocyte/macrophages were flow-sorted from the same mice and therefore were exposed to the same concentration of type I IFN prior to isolation, suggesting that nonclassic monocyte/macrophages from pristane-treated mice might be less sensitive to type I IFN than classic monocyte/macrophages.

ISG expression is related to *Ifnar1* levels. RNA sequencing suggested that *Ifnar1* transcripts were less abundant in nonclassic monocyte/macrophages versus classic monocyte/macrophages from both pristane-treated and mineral oil–treated mice (Figure 4A). The expression of *Ifnar2* and other intermediates in the IFNAR signaling pathway (*Tyk2* and *Jak1*) also appeared lower in nonclassic monocyte/macrophages. In pristane-treated mice, expression of downstream genes encoding subunits of the transcription factor IFN-stimulated transcription factor 3 (*Stat1*, *Stat2*, and *Irf9*) was lower in nonclassic monocyte/macrophages than in classic monocyte/macrophages, but these genes are type I IFN regulated (34). We confirmed by flow cytometry that nonclassic monocyte/macrophages from pristane-treated mice had substantially lower *Ifnar1* surface staining than classic monocyte/macrophages (Figure 4B). CD11b+Ly6G+ neutrophils and "other cells" (mainly lymphocytes) from the peritoneal exudates exhibited little or no *Ifnar1* staining. Thus, classic monocyte/macrophages may be poised to express an IFN-regulated transcriptional program when stimulated by type I IFN. To test that possibility, PECs were isolated 15 days after pristane treatment and incubated with IFNα4 (100 units/ml) for up to 15 minutes, followed by measurement of pSTAT1 in monocyte/macrophage subsets by flow cytometry (Figure 4C). At baseline (before IFNα treatment), pSTAT1 levels in classic monocyte/macrophages
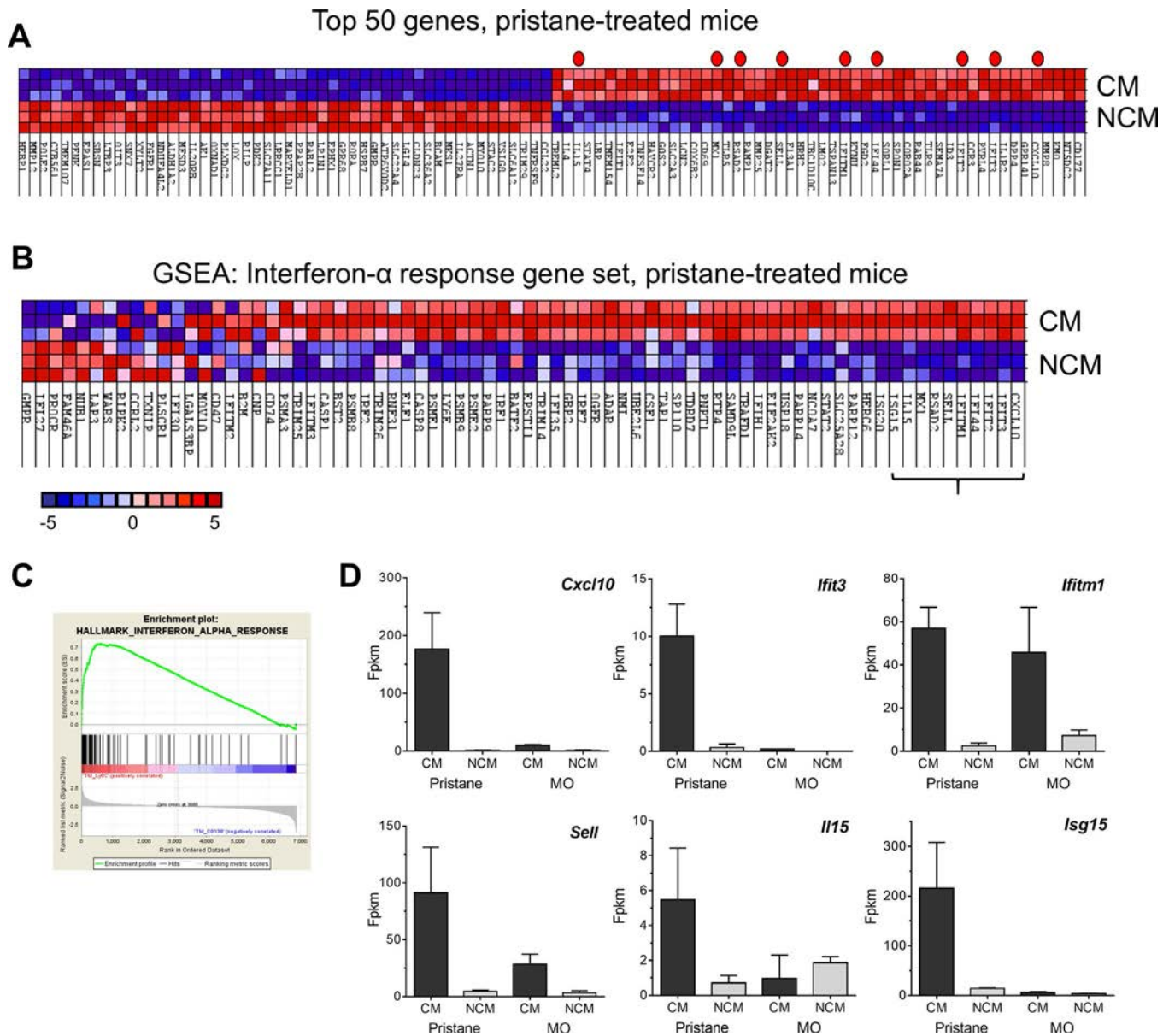
Figure 3. Gene expression in macrophage subsets from pristane-treated mice or mineral oil (MO)–treated mice. Classic monocyte/macrophages (CMs) and nonclassic monocyte/macrophages (NCMs) from pristane-treated mice were flow-sorted as in Figure 1 and analyzed by RNA-Seq. **A**, Heatmap of the top 50 features in classic monocyte/macrophages versus nonclassic monocyte/macrophages from pristane-treated mice. Genes represented in the hallmark interferon-α (IFNα) gene set are indicated by red dots. **B**, Gene set enrichment analysis (GSEA) of the hallmark IFNα response gene pathway in classic monocyte/macrophages versus nonclassic monocyte/macrophages from pristane-treated mice. Bracket indicates the top 10 genes in classic monocyte/macrophages and nonclassic monocyte/macrophages. **C**, GSEA enrichment plot of the hallmark IFNα response gene pathway. **D**, Expression of *Cxcl10*, *Ifit3*, *Ifitm1*, *Sell*, *Il15*, and *Isg15* in classic monocyte/macrophages versus nonclassic monocyte/macrophages from pristane-treated mice and mineral oil–treated mice. Values are the mean ± SD. Fpkm = fragment per kilobase million.

were significantly higher than in nonclassic monocyte/macrophages from the same mice (*P* < 0.01 by Student's *t*-test) and this pattern persisted after incubation with IFNα4.

In classic monocyte/macrophages, IFNα4 treatment enhanced the phosphorylation of STAT1 (*P* = 0.01 by Student's *t*-test), although the effect was not dramatic. This may suggest that STAT1 phosphorylation already was near-maximal in freshly isolated peritoneal classic monocyte/macrophages from pristane-treated

mice. Although signaling through the IFNγ receptor also results in STAT1 phosphorylation, nonclassic monocyte/macrophages and classic monocyte/macrophages expressed similar levels of *Ifngr1*; expression of *Ifngr2* mRNA may have been slightly lower in nonclassic monocyte/macrophages (Figure 4D). Thus, low STAT1 phosphorylation in nonclassic monocyte/macrophages correlated with the low level of *Ifnar1* mRNA and protein expressed by these cells.
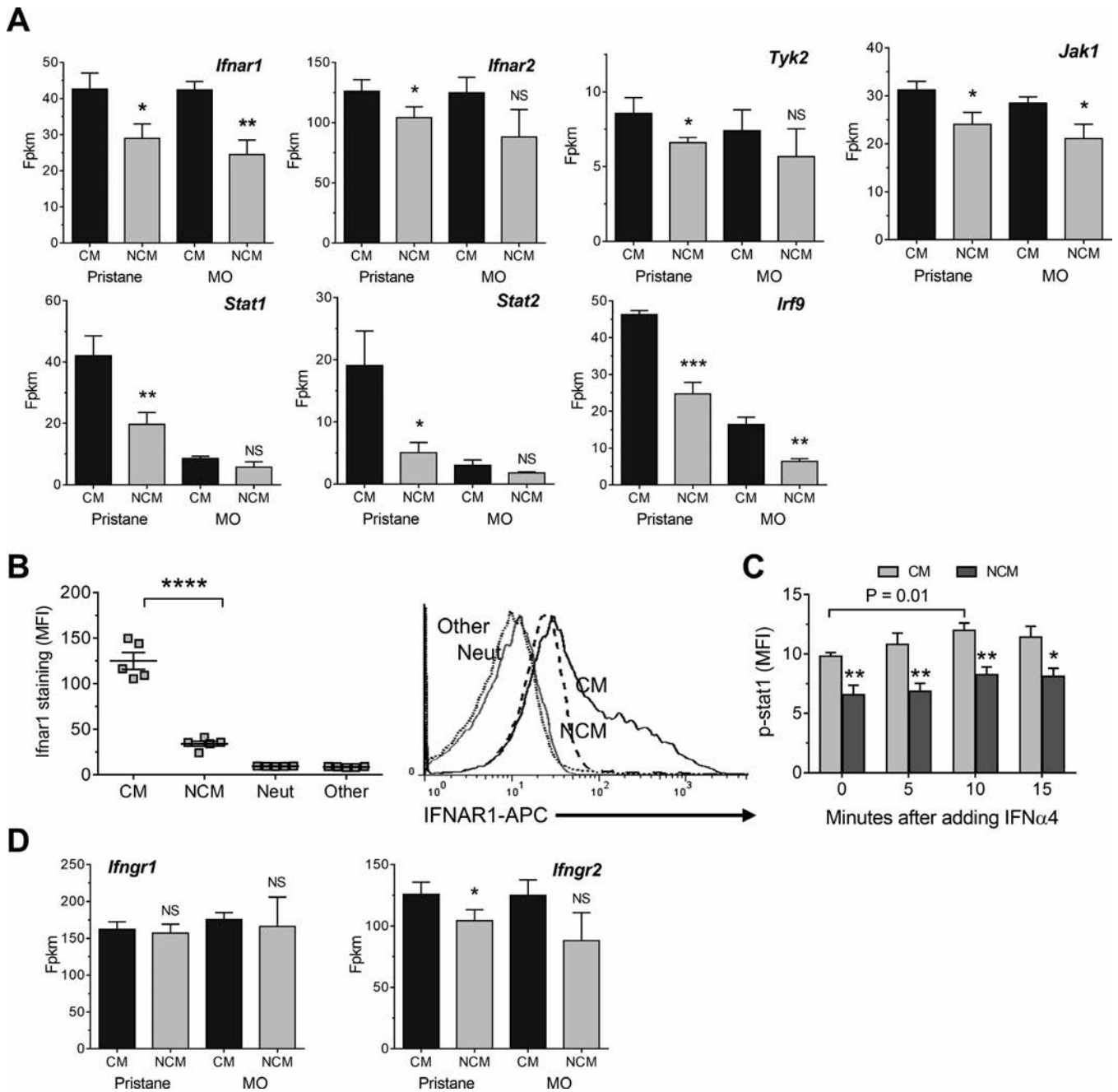
Figure 4. Nonclassic monocyte/macrophages (NCMs) express lower levels of interferon-α/β/ω receptor (IFNAR) surface staining than classic monocyte/macrophages (CMs). **A**, Expression of genes involved in IFNAR signaling (*Ifnar1*, *Ifnar2*, *Tyk2*, *Jak1*, *Stat1*, *Stat2,* and *Irf9*) in classic monocyte/macrophages versus nonclassic monocyte/macrophages from pristane-treated mice and mineral oil (MO)–treated mice. Values are the mean ± SD. **B**, Left, IFNAR surface staining of peritoneal exudate cell subsets (classic monocyte/macrophages, nonclassic monocyte/macrophages, Ly6G+ neutrophils [Neut], and CD11b–Ly6C–CD138–Ly6G– cells [Other]), primarily lymphocytes. MFI = mean fluorescence intensity. Each symbol represents an individual mouse. Bars show the mean ± SD. Right, Representative flow cytometry plot showing IFNAR staining of classic monocyte/macrophages, nonclassic monocyte/macrophages, neutrophils, and other cells. **C**, Intracellular pSTAT staining in peritoneal classic monocyte/macrophages versus nonclassic monocyte/macrophages from pristane-treated mice up to 15 minutes after addition of IFNα4. Values are the mean ± SD. **D**, Expression of mRNA encoding IFNγ receptor chains *Ifngr1* and *Ifngr2* in classic monocyte/macrophages versus nonclassic monocyte/macrophages from pristane-treated mice and mineral oil–treated mice. Values are the mean ± SD. * = $P < 0.05$; ** = $P < 0.01$; *** = $P < 0.001$; **** = $P < 0.0001$ versus classic monocyte/macrophages, by Student's *t*-test. Fpkm = fragment per kilobase million; NS = not significant.
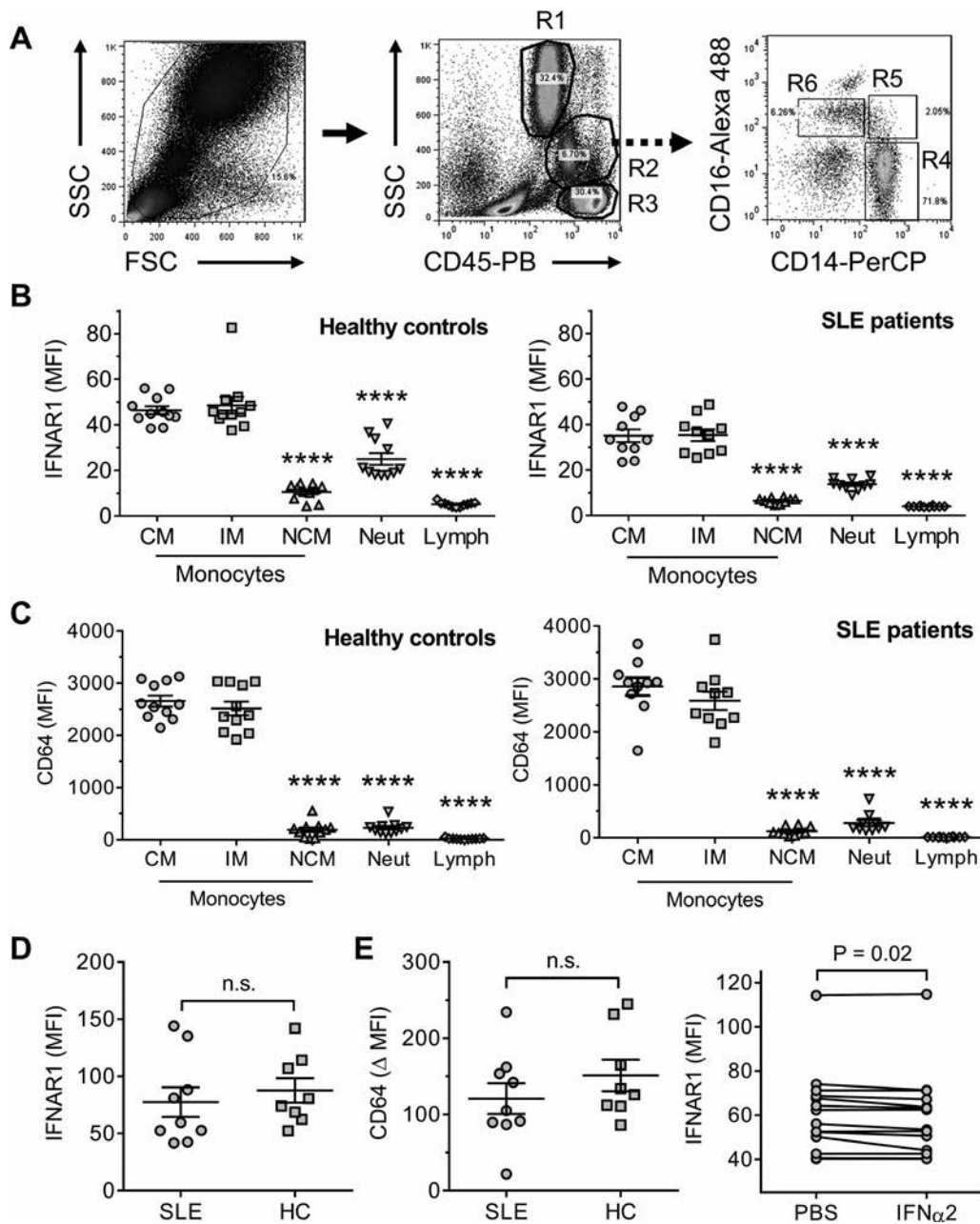
Figure 5. Flow cytometry of interferon-α/β/ω receptor (IFNAR) and CD64 in human peripheral blood mononuclear cells (PBMCs). PBMCs were isolated from systemic lupus erythematosus (SLE) patients (n = 10) and healthy controls (HCs) (n = 11), and analyzed by forward scatter, side scatter, and staining with anti-CD14, CD16, CD45, CD64, and IFNAR antibodies, showing neutrophils (R1), monocytes (R2), and lymphocytes (R3). Surface staining of IFNAR and CD64 (mean fluorescence intensity [MFI]) on CD14++CD16– cells (classic monocyte/macrophages [CMs], R4), CD14++CD16+ cells (intermediate monocytes [IMs], R5), and CD14+CD16++ cells (nonclassic monocyte/macrophages, R6) was quantified by flow cytometry. **A**, Gating strategy. **B**, IFNAR1 staining on monocyte subsets, neutrophils (Neut), and lymphocytes (Lymph) from peripheral blood of healthy controls and SLE patients. **** = $P < 0.0001$ versus classic monocyte/macrophages, by Student's t-test. **C**, CD64 staining on monocyte subsets, neutrophils, and lymphocytes from peripheral blood of healthy controls and SLE patients. **** = $P < 0.0001$ versus classic monocyte/macrophages, by Student's t-test. **D**, IFNAR staining on classic monocyte/macrophages from peripheral blood of healthy controls and SLE patients. **E**, Left, Change in CD64 surface staining on classic monocyte/macrophages from SLE patients and healthy controls after 24-hour culture with IFNα2 (1,000 units/ml). Right, type I IFNAR expression (MFI) on classic monocyte/macrophages after culture in vitro with phosphate buffered saline (PBS) or IFNα2 (1,000 units/ml) for 24 hours ($P < 0.02$, by paired Student's t-test). In **B–E** (left panel), each symbol represents an individual subject. Bars show the mean ± SD. NS = not significant.

IFNAR expression and type I IFN responsiveness of human monocyte subsets. We examined PBMCs from SLE patients and healthy controls to investigate whether the variable type I IFN responsiveness is also seen in human monocytes. Three human monocyte subsets have been described, CD14++CD16– (classic monocyte/macrophages), CD14++CD16+ (intermediate monocytes), and CD14+CD16++ (nonclassic monocyte/macrophages) (35,36) (Figure 5A). Classic monocyte/macrophages and intermediate monocytes from peripheral blood of both healthy controls and SLE patients exhibited IFNAR1 surface staining, whereas nonclassic monocyte/macrophages had minimal staining (Figure 5B). Classic monocyte/macrophages express higher levels of the type I IFN–regulated gene CD64 than nonclassic monocyte/macrophages (37), and CD64 staining (by flow cytometry) on total CD14+ cells correlates strongly with the IFN signature (38). Consistent with the IFNAR-1 staining pattern, classic monocyte/macrophages and intermediate monocytes, but not nonclassic monocyte/macrophages, from healthy controls and SLE patients stained strongly for CD64 (Figure 5C). Neutrophils and lymphocytes had only weak IFNAR-1 expression (Figure 5B). Thus, as in mouse monocyte/macrophages,
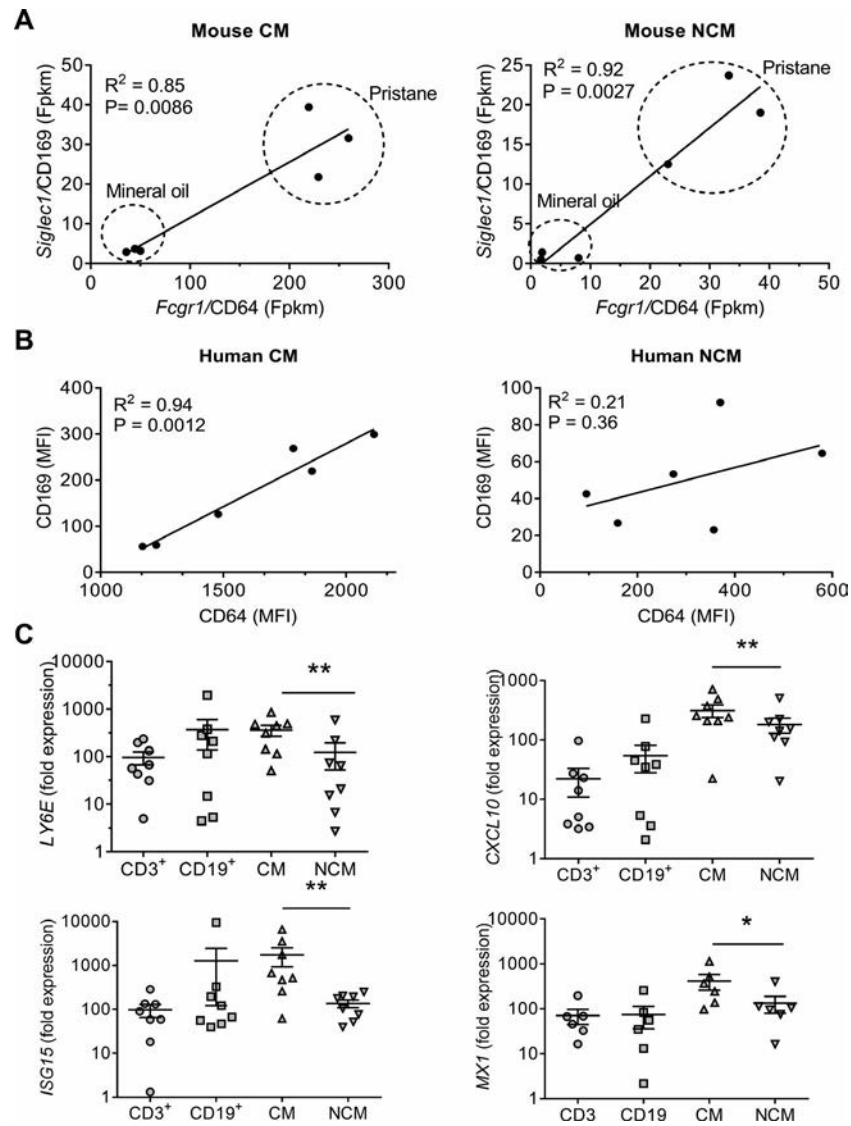
Figure 6. Expression of interferon-stimulated genes (ISGs) in human peripheral blood mononuclear cell (PBMC) subsets. **A**, Spearman's rank correlation of *Siglec1* (CD169) and *Fcgr1* (CD64) mRNA levels in murine classic monocyte/macrophages (CMs) versus nonclassic monocyte/macrophages (NCMs) from pristane-treated mice and mineral oil–treated mice. Fpkm = fragment per kilobase million. **B**, Spearman's rank correlation of CD169 and CD64 surface-staining levels on human classic monocyte/macrophages and nonclassic monocyte/macrophages, determined by flow cytometry. MFI = mean fluorescence intensity. **C**, Expression of ISGs (*LY6E, CXCL10, ISG15, and MX1*) as determined by quantitative polymerase chain reaction in flow-sorted human PBMC subsets 11 hours after treatment with interferon-α2b (1,000 units/ml) (T cells [CD3+], B cells [CD19+], classic monocyte/macrophages, and nonclassic monocyte/macrophages). Each symbol represents an individual subject. Bars show the mean ± SD. * = $P < 0.05$; ** = $P < 0.01$ by paired Wilcoxon's rank sum test.

the IFNAR was expressed differentially on human classic monocyte/macrophages/intermediate monocytes versus non-classic monocyte/macrophages.

Interestingly, IFNAR-1 protein expression was lower in peripheral blood classic macrophages/intermediate monocytes, as well as nonclassic monocyte/macrophages and neutrophils, from SLE patients versus healthy controls (Figure 5B). This difference also was seen in a second cohort of SLE patients and healthy controls, although it was not statistically significant (Figure 5D). To determine if classic monocyte/macrophages from SLE patients were more responsive to type I IFN, we cultured PBMCs from SLE patients and healthy controls for 24 hours with IFNα2b and then measured surface staining of the type I IFN–regulated protein CD64. The increase of CD64 staining (Δ MFI) was similar in CD14++CD16– classic monocyte/macrophages from SLE patients and healthy controls (Figure 5E), suggesting that monocytes from SLE patients were not hypersensitive to signaling through the IFNAR. However, IFNAR-1 surface staining was lower in classic monocyte/macrophages cultured for 24 hours with IFNα2b than in controls cultured with PBS (Figure 5E). In contrast, classic monocyte/macrophages cultured for 1.5 hours with IFNα2b exhibited similar IFNAR-1 staining to PBS controls (data not shown).

Based on their differential IFNAR-1 expression, we hypothesized that ISG expression would be higher in human classic monocyte/macrophages versus nonclassic monocyte/macrophages, as seen in mice. CD64 and CD169 are surface markers used to assess the IFN signature in human cells by flow cytometry (38,39). In murine monocyte/macrophages, levels of *Fcgr1* (CD64) and *Siglec1* (CD169) transcripts correlated and were higher in classic macrophages than nonclassic monocyte/macrophages (Figure 6A), consistent with findings with other ISGs (Figures 2 and 3). By flow cytometry, a similar pattern was seen in human classic monocyte/macrophages, although the 2 markers were not significantly correlated in nonclassic monocyte/macrophages (Figure 6B). Analysis of levels of mRNA for *LY6E*, *CXCL10* (IP-10), *ISG15, and MX1* in flow-sorted classic monocyte/macrophages, nonclassic monocyte/macrophages, CD3+ T cells, and CD19+ B cells by qPCR confirmed that ISG expression was higher in classic monocyte/macrophages than in nonclassic monocyte/macrophages after IFNα2b stimulation (Figure 6C).

DISCUSSION

The hydrocarbon oil pristane causes nonremitting peritoneal inflammation, a strong IFN signature, and clinical features of SLE in non–autoimmune-prone mice (6). Other hydrocarbon oils, such as mineral oil, cause acute inflammation without inducing overexpression of ISGs or SLE. Resolution of peritoneal inflammation in mineral oil–treated mice is associated with the disappearance of classic monocyte/macrophages and with increasing numbers of nonclassic monocyte/macrophages (18). Diverse mechanisms regulate the resolution of inflammation (40,41). We

show here that differential expression of the IFNAR on monocyte/macrophages may influence whether inflammation resolves or becomes chronic. We also show that classic monocyte/macrophages are the primary type I IFN–responsive cell type in mouse PECs and in human PBMCs. The balance between classic monocyte/macrophages and nonclassic monocyte/macrophages plays a previously unrecognized role in determining the magnitude of the IFN signature.

Unexpectedly, we found that in mouse PECs, ISG expression was lower in nonclassic monocyte/macrophages than in classic monocyte/macrophages exposed to the same concentration of type I IFN (Figure 3). The data suggest that the explanation lies in the level of IFNAR expression. *Ifnar1* transcripts and IFNAR surface staining were both lower in nonclassic monocyte/macrophages versus classic monocyte/macrophages (Figure 4). Peritoneal lymphocytes and neutrophils also had little or no *Ifnar1* surface staining. The low level of *Ifnar1* may be functionally significant, as it correlated with lower STAT1 activation in nonclassic monocyte/macrophages (Figure 4C).

Similarly, IFNAR expression was lower in human nonclassic monocyte/macrophages versus classic monocyte/macrophages and intermediate monocytes (Figure 5). Consistent with the mouse data, there was relatively little IFNAR expression in human neutrophils and lymphocytes, suggesting that classic monocyte/macrophages are major determinants of the IFN signature in human PBMCs. The relative expression of ISGs (*LY6E*, *CXCL10*, *ISG15*, and *MX1*) in flow-sorted PBMC subsets (Figure 6C) supports that conclusion. Thus, signaling through the IFNAR of classic monocyte/macrophages may be a significant determinant of the IFN signature in human PBMCs isolated by density-gradient centrifugation (containing monocytes and lymphocytes, but few neutrophils). A predominance of classic monocyte/macrophages/intermediate monocytes over nonclassic monocyte/macrophages may favor a strong IFN signature. Although IFNAR expression in neutrophils was lower than in classic monocyte/macrophages, neutrophils are more numerous than monocytes and could influence the IFN signature in blood samples collected in PAXgene tubes.

Although the overall pattern of IFNAR1 expression was similar in murine peritoneal monocyte/macrophages and human circulating monocyte subsets (i.e., higher in classic monocyte/macrophages than nonclassic monocyte/macrophages), there was a trend toward lower IFNAR1 expression in classic monocyte/macrophages from SLE patients versus healthy controls (Figure 5B). Several factors may influence IFNAR expression in human monocytes. As in mice with pristane-induced SLE (31), CCR2/CCL2-mediated recruitment of classic monocyte/macrophages to inflamed tissues may alter the proportions of classic monocyte/macrophages and nonclassic monocyte/macrophages in the blood of SLE patients. In addition, circulating classic monocyte/macrophages in most SLE patients are exposed to

higher concentrations of type I IFN than those from healthy controls. Although the lower IFNAR staining on SLE versus control classic monocyte/macrophages was not statistically significant, it was reproducible in 2 independent cohorts (Figures 5B and D). Classic monocyte/macrophages from SLE patients and healthy controls displayed similar induction of ISG expression in vitro (Figure 5E), suggesting that SLE monocytes were not hyperresponsive to IFNα. However, when classic monocyte/macrophages from both SLE patients and healthy controls were cultured with IFNα2b, IFNAR1 surface staining was reduced (Figure 5E). There are 2 potential explanations for this. The anti-IFNAR monoclonal antibody might compete with IFNα2 for binding to IFNAR-1, as is true of other anti–IFNAR-1 monoclonal antibodies (42,43). Alternatively, since type I IFN binding induces IFNAR-1 internalization (44), receptor expression could be modulated by endogenous type I IFN (SLE patients) or exogenous IFNα2b (in vitro). The latter explanation may be more likely, since a 1-hour preincubation with IFNα2b prior to staining with anti-IFNAR antibodies did not cause a dose-dependent reduction in IFNAR staining (data not shown).

The differential expression of *Ifnar1* mRNA in murine peritoneal classic monocyte/macrophages is under investigation. Although enhanced degradation of the IFNAR-1 chain is reported in colorectal cancer and influenza infection (45,46), the low level of *Ifnar1* transcripts in nonclassic macrophages in murine SLE is more consistent with transcriptional regulation. However, further studies are necessary to determine the mechanisms that regulate IFNAR1 expression in SLE monocyte/macrophages.

ISGs are expressed at high levels by PBMCs from patients with SLE (1,2) or genetic interferonopathies (13). Although it is assumed that the IFN signature results from overproduction of type I IFN, our data suggest the situation is more complex than that. First, the IFN signature critically depends on the responsiveness of monocyte/macrophages to signaling through the IFNAR. Second, classic monocyte/macrophages express high levels of the IFNAR-1 and exhibit a strong IFN signature, whereas nonclassic monocyte/macrophages and other blood cells have little IFNAR-1 expression and only a weak IFN signature. Finally, even in classic monocyte/macrophages, there would be no IFN signature without type I IFN production. This probably explains the low type I IFN–regulated gene expression in classic monocyte/macrophages from mineral oil–treated versus pristane-treated mice (Figures 2 and 3) despite their comparable levels of *Ifnar1*, *Ifnar2*, *Tyk2*, and *Jak1* mRNAs (Figure 4). Thus, the IFN signature, which is used increasingly to monitor disease activity and/or response to therapy, is a composite measure of both type I IFN production and IFNAR expression in monocyte/macrophages. Consequently, therapeutic intervention could abolish the IFN signature by driving monocyte/macrophage differentiation toward an antiinflammatory phenotype without substantially affecting the production of IFN. Recent studies suggest it may be feasible in principle to accomplish this using LXR agonists (20).

The balance between classic monocyte/macrophages and nonclassic monocyte/macrophages also could influence disease severity. Infiltration of target organs by monocyte/macrophages is seen in glomerulonephritis and atherosclerosis (47,48), both of which are associated with type I IFN production in SLE (4,49). Lupus monocyte/macrophages secrete higher than normal levels of proinflammatory cytokines and have an impaired capacity to take up apoptotic cells (18,50,51), possibly reflecting an imbalance between classic monocyte/macrophages and nonclassic monocyte/macrophages (18). In comparison with classic monocyte/macrophages, nonclassic monocyte/macrophages exhibited higher surface expression of the scavenger receptors CD36 and Marco (Figure 1E). We showed previously that treatment with anti-Marco neutralizing antibodies or the class A scavenger receptor antagonist poly(I) reduces in vivo phagocytosis of apoptotic cells by ~30% (18). Like Marco, the class B scavenger receptor CD36 promotes clearance of apoptotic cells (52). Increased nonclassic monocyte/macrophage expression of CD36 and Marco may help prevent the IFN signature by reducing the generation and release of Toll-like receptor 7/8/9 ligands from uncleared apoptotic cells undergoing secondary necrosis (53). Thus, nonclassic monocyte/macrophages may help limit the IFN signature in 2 ways: 1) by their insensitivity to signaling through the IFNAR and 2) by removing dead cells and preventing Toll-like receptor–mediated type I IFN production. It will be of interest in the future to examine the relationship of IFNAR expression in tissue-infiltrating monocyte/macrophages to disease severity (lupus nephritis, accelerated atherosclerosis).

ACKNOWLEDGMENTS

AUTHOR CONTRIBUTIONS

All authors were involved in drafting the article or revising it critically for important intellectual content, and all authors approved the final version to be published. Dr. Han had full access to all of the data in the study and takes responsibility for the integrity of the data and the accuracy of the data analysis.
Study conception and design. Han, Zhuang, Lee, Li, Yang, Nigrovic, Reeves.
Acquisition of data. Han, Zhuang, Lee, Li, Yang, Nigrovic, Reeves.
Analysis and interpretation of data. Han, Zhuang, Lee, Yang, Nigrovic, Reeves.

REFERENCES

1. Baechler EC, Batliwalla FM, Karypis G, Gaffney PM, Ortmann WA, Espe KJ, et al. Interferon-inducible gene expression signature in

peripheral blood cells of patients with severe lupus. Proc Natl Acad Sci U S A 2003;100:2610–5.

2. Bennett L, Palucka AK, Arce E, Cantrell V, Borvak J, Banchereau J, et al. Interferon and granulopoiesis signatures in systemic lupus erythematosus blood. J Exp Med 2003;197:711–23.

3. Zhuang H, Narain S, Sobel E, Lee PY, Nacionales DC, Kelly KM, et al. Association of anti-nucleoprotein autoantibodies with upregulation of Type I interferon-inducible gene transcripts and dendritic cell maturation in systemic lupus erythematosus. Clin Immunol 2005;117:238–50.

4. Kirou KA, Lee C, George S, Louca K, Peterson MG, Crow MK. Activation of the interferon-α pathway identifies a subgroup of systemic lupus erythematosus patients with distinct serologic features and active disease. Arthritis Rheum 2005;52:1491–503.

5. Nacionales DC, Kelly KM, Lee PY, Zhuang H, Weinstein JS, Sobel E, et al. Type I interferon production by tertiary lymphoid tissue developing in response to 2, 6, 10, 14 tetramethyl-pentadecane (pristane). Am J Pathol 2006;168:1227–40.

6. Reeves WH, Lee PY, Weinstein JS, Satoh M, Lu L. Induction of autoimmunity by pristane and other naturally occurring hydrocarbons. Trends Immunol 2009;30:455–64.

7. Rönnblom LE, Alm GV, Öberg KE. Autoimmunity after α-interferon therapy for malignant carcinoid tumors. Ann Intern Med 1991;115:178–83.

8. Wilson LE, Widman D, Dikman SH, Gorevic PD. Autoimmune disease complicating antiviral therapy for hepatitis C virus infection. Semin Arthritis Rheum 2002;32:163–73.

9. Santiago-Raber ML, Baccala R, Haraldsson KM, Choubey D, Stewart TA, Kono DH, et al. Type-I interferon receptor deficiency reduces lupus-like disease in NZB mice. J Exp Med 2003;197:777–88.

10. Nacionales DC, Kelly-Scumpia KM, Lee PY, Weinstein JS, Lyons R, Sobel E, et al. Deficiency of the type I interferon receptor protects mice from experimental lupus. Arthritis Rheum 2007;56:3770–83.

11. Furie R, Khamashta M, Merrill JT, Werth VP, Kalunian K, Brohawn P, et al. Anifrolumab, an anti–interferon-α receptor monoclonal antibody, in moderate-to-severe systemic lupus erythematosus. Arthritis Rheumatol 2017;69:376–86.

12. Niewold TB, Hua J, Lehman TJ, Harley JB, Crow MK. High serum IFN-α activity is a heritable risk factor for systemic lupus erythematosus. Genes Immun 2007;8:492–502.

13. Rodero MP, Crow YJ. Type I interferon-mediated monogenic autoinflammation: the type I interferonopathies, a conceptual overview. J Exp Med 2016;213:2527–38.

14. Rice GI, Forte GM, Szynkiewicz M, Chase DS, Aeby A, Abdel-Hamid MS, et al. Assessment of interferon-related biomarkers in Aicardi-Goutieres syndrome associated with mutations in TREX1, RNASEH2A, RNASEH2B, RNASEH2C, SAMHD1, and ADAR: a case-control study. Lancet Neurol 2013;12:1159–69.

15. Snell LM, McGaha TL, Brooks DG. Type I interferon in chronic virus infection and cancer. Trends Immunol 2017;38:542–57.

16. Platanias LC. Mechanisms of type-I- and type-II-interferon-mediated signalling. Nat Rev Immunol 2005;5:375–86.

17. Wang Y, Nan J, Willard B, Wang X, Yang J, Stark GR. Negative regulation of type I IFN signaling by phosphorylation of STAT2 on T387. EMBO J 2017;36:202–12.

18. Han S, Zhuang H, Shumyak S, Wu J, Li H, Yang LJ, et al. A novel subset of anti-inflammatory CD138⁺ macrophages is deficient in mice with experimental lupus. J Immunol 2017;199:1261–74.

19. Yáñez A, Coetzee SG, Olsson A, Muench DE, Berman BP, Hazelett DJ, et al. Granulocyte-monocyte progenitors and monocyte-dendritic cell progenitors independently produce functionally distinct monocytes. Immunity 2017;47:890–902.

20. Han S, Zhuang H, Shumyak S, Wu J, Xie C, Li H, et al. Liver X receptor agonist therapy prevents diffuse alveolar hemorrhage in murine lupus by repolarizing macrophages. Front Immunol 2018;9:135.

21. Lee PY, Sykes DB, Ameri S, Kalaitzidis D, Charles JF, Nelson-Maney N, et al. The metabolic regulator mTORC1 controls terminal myeloid differentiation. Sci Immunol 2017;2:eaam6641.

22. Picelli S, Björklund ÅK, Faridani OR, Sagasser S, Winberg G, Sandberg R. Smart-seq2 for sensitive full-length transcriptome profiling in single cells. Nat Methods 2013;10:1096–8.

23. Trombetta JJ, Gennert D, Lu D, Satija R, Shalek AK, Regev A. Preparation of single-cell RNA-Seq libraries for next generation sequencing. Curr Protoc Mol Biol 2014;107:4.22.1–17.

24. Trapnell C, Roberts A, Goff L, Pertea G, Kim D, Kelley DR, et al. Differential gene and transcript expression analysis of RNA-Seq experiments with TopHat and Cufflinks. Nat Protoc 2012;7:562–78.

25. Subramanian A, Tamayo P, Mootha VK, Mukherjee S, Ebert BL, Gillette MA, et al. Gene set enrichment analysis: a knowledge-based approach for interpreting genome-wide expression profiles. Proc Natl Acad Sci U S A 2005;102:15545–50.

26. Liberzon A, Birger C, Thorvaldsdóttir H, Ghandi M, Mesirov JP, Tamayo P. The Molecular Signatures Database (MSigDB) hallmark gene set collection. Cell Syst 2015;1:417–25.

27. Saldanha AJ. Java Treeview—extensible visualization of microarray data. Bioinformatics 2004;20:3246–8.

28. Tan EM, Cohen AS, Fries JF, Masi AT, McShane DJ, Rothfield NF, et al. The 1982 revised criteria for the classification of systemic lupus erythematosus. Arthritis Rheum 1982;25:1271–7.

29. Gordon S, Taylor PR. Monocyte and macrophage heterogeneity. Nat Rev Immunol 2005;5:953–64.

30. Sunderkötter C, Nikolic T, Dillon MJ, Van Rooijen N, Stehling M, Drevets DA, et al. Subpopulations of mouse blood monocytes differ in maturation stage and inflammatory response. J Immunol 2004;172:4410–7.

31. Lee PY, Li Y, Kumagai Y, Xu Y, Weinstein JS, Kellner ES, et al. Type-I interferon modulates monocyte recruitment and maturation in chronic inflammation. Am J Pathol 2009;175:2023–33.

32. Fadok VA, Warner ML, Bratton DL, Henson PM. CD36 is required for phagocytosis of apoptotic cells by human macrophages that use either a phosphatidylserine receptor or the vitronectin receptor (αᵥβ₃). J Immunol 1998;161:6250–7.

33. Wermeling F, Chen Y, Pikkarainen T, Scheynius A, Winqvist O, Izui S, et al. Class A scavenger receptors regulate tolerance against apoptotic cells, and autoantibodies against these receptors are predictive of systemic lupus. J Exp Med 2007;204:2259–65.

34. Rusinova I, Forster S, Yu S, Kannan A, Masse M, Cumming H, et al. Interferome v2.0: an updated database of annotated interferon-regulated genes. Nucleic Acids Res 2013;41:D1040–6.

35. Ziegler-Heitbrock L, Ancuta P, Crowe S, Dalod M, Grau V, Hart DN, et al. Nomenclature of monocytes and dendritic cells in blood. Blood 2010;116:e74–80.

36. Wong KL, Tai JJ, Wong WC, Han H, Sem X, Yeap WH, et al. Gene expression profiling reveals the defining features of the classical, intermediate and nonclassical human monocyte subsets. Blood 2011;118:e16–31.

37. Tacke F, Randolph GJ. Migratory fate and differentiation of blood monocyte subsets. Immunobiology 2006;211:609–18.

38. Li Y, Lee PY, Kellner ES, Paulus M, Switanek J, Xu Y, et al. Monocyte surface expression of Fcγ receptor RI (CD64), a biomarker reflecting type-I interferon levels in systemic lupus erythematosus. Arthritis Res Ther 2010;12:R90.

39. Rose T, Grützkau A, Hirseland H, Huscher D, Dähnrich C, Dzionek A, et al. IFNα and its response proteins, IP-10 and SIGLEC-1, are biomarkers of disease activity in systemic lupus erythematosus. Ann Rheum Dis 2013;72:1639–45.

40. Nathan C, Ding A. Nonresolving inflammation. Cell 2010;140:871–82.

41. Serhan CN. Pro-resolving lipid mediators are leads for resolution physiology. Nature 2014;510:92–101.

42. Benoit P, Maguire D, Plavec I, Kocher H, Tovey M, Meyer F. A monoclonal antibody to recombinant human IFN-α receptor inhibits biologic activity of several species of human IFN-α, IFN-β, and IFN-ω: detection of heterogeneity of the cellular type I IFN receptor. J Immunol 1993;150:707–16.

43. Peng L, Oganesyan V, Wu H, Dall'Acqua WF, Damschroder MM. Molecular basis for antagonistic activity of anifrolumab, an anti-interferon-α receptor 1 antibody. MAbs 2015;7:428–39.

44. Hurtado-Guerrero I, Pinto-Medel MJ, Urbaneja P, Rodriguez-Bada JL, León A, Guerrero M, et al. Activation of the JAK-STAT signaling pathway after in vitro stimulation with IFNß in multiple sclerosis patients according to the therapeutic response to IFNß. PloS One 2017;12:e0170031.

45. Araya RE, Goldszmid RS. IFNAR1 degradation: a new mechanism for tumor immune evasion? Cancer Cell 2017;31:161–3.

46. Xia C, Vijayan M, Pritzl CJ, Fuchs SY, McDermott AB, Hahm B. Hemagglutinin of influenza A virus antagonizes type I interferon (IFN) responses by inducing degradation of type I IFN receptor 1. J Virol 2015;90:2403–17.

47. Bethunaickan R, Berthier CC, Ramanujam M, Sahu R, Zhang W, Sun Y, et al. A unique hybrid renal mononuclear phagocyte activation phenotype in murine systemic lupus erythematosus nephritis. J Immunol 2011;186:4994–5003.

48. Moore KJ, Tabas I. Macrophages in the pathogenesis of atherosclerosis. Cell 2011;145:341–55.

49. Knight JS, Kaplan MJ. Lupus neutrophils: 'NET' gain in understanding lupus pathogenesis. Curr Opin Rheumatol 2012;24:441–50.

50. Steinbach F, Henke F, Krause B, Thiele B, Burmester GR, Hiepe F. Monocytes from systemic lupus erythematous patients are severely altered in phenotype and lineage flexibility. Ann Rheum Dis 2000;59:283–8.

51. Perez-Sanchez C, Barbarroja N, Messineo S, Ruiz-Limon P, Rodriguez-Ariza A, Jimenez-Gomez Y, et al. Gene profiling reveals specific molecular pathways in the pathogenesis of atherosclerosis and cardiovascular disease in antiphospholipid syndrome, systemic lupus erythematosus and antiphospholipid syndrome with lupus. Ann Rheum Dis 2015;74:1441–9.

52. Greenberg ME, Sun M, Zhang R, Febbraio M, Silverstein R, Hazen SL. Oxidized phosphatidylserine-CD36 interactions play an essential role in macrophage-dependent phagocytosis of apoptotic cells. J Exp Med 2006;203:2613–25.

53. Nagata S, Hanayama R, Kawane K. Autoimmunity and the clearance of dead cells [review]. Cell 2010;140:619–30.

American College
of Rheumatology
Empowering Rheumatology Professionals

Increased Adhesive Potential of Antiphospholipid Syndrome Neutrophils Mediated by β2 Integrin Mac-1

Gautam Sule, William J. Kelley, Kelsey Gockman, Srilakshmi Yalavarthi, Andrew P. Vreede, Alison L. Banka, Paula L. Bockenstedt, Omolola Eniola-Adefeso, and Jason S. Knight (ID)

Objective. While the role of antiphospholipid antibodies in activating endothelial cells has been extensively studied, the impact of these antibodies on the adhesive potential of leukocytes has received less attention. This study was undertaken to investigate the extent to which antiphospholipid syndrome (APS) neutrophils adhere to resting endothelial cells under physiologic flow conditions and the surface molecules required for that adhesion.

Methods. Patients with primary APS (n = 43), patients with a history of venous thrombosis but negative test results for antiphospholipid antibodies (n = 11), and healthy controls (n = 38) were studied. Cells were introduced into a flow chamber and perfused across resting human umbilical vein endothelial cells (HUVECs). Surface adhesion molecules were quantified by flow cytometry. Neutrophil extracellular trap release (NETosis) was assessed in neutrophil–HUVEC cocultures.

Results. Upon perfusion of anticoagulated blood through the flow chamber, APS neutrophils demonstrated increased adhesion as compared to control neutrophils under conditions representative of either venous (n = 8; $P < 0.05$) or arterial (n = 15; $P < 0.0001$) flow. At the same time, APS neutrophils were characterized by up-regulation of CD64, CEACAM1, β_2-glycoprotein I, and activated Mac-1 on their surface (n = 12–18; $P < 0.05$ for all markers). Exposing control neutrophils to APS plasma or APS IgG resulted in increased neutrophil adhesion (n = 10–11; $P < 0.0001$) and surface marker up-regulation as compared to controls. A monoclonal antibody specific for activated Mac-1 reduced the adhesion of APS neutrophils in the flow-chamber assay ($P < 0.01$). The same monoclonal antibody reduced NETosis in neutrophil–HUVEC cocultures ($P < 0.01$).

Conclusion. APS neutrophils demonstrate increased adhesive potential, which is dependent upon the activated form of Mac-1. In patients, this could lower the threshold for neutrophil–endothelium interactions, NETosis, and possibly thrombotic events.

INTRODUCTION

Antiphospholipid syndrome (APS) is an autoimmune condition of unknown cause and is defined by the presence of circulating antiphospholipid antibodies (aPLs; anticardiolipin, anti–β_2-glycoprotein I [anti-β_2GPI], or lupus anticoagulant [LAC]) (1). The morbidity and mortality of APS are significant, as patients carry a markedly increased risk of thrombotic events (especially stroke and deep vein thrombosis) and pregnancy loss (2).

Beyond these disease-defining events, patients with APS may also develop cytopenias, heart valve damage, nephropathy, and cognitive dysfunction, among other complications (3). While it has long been recognized that circulating leukocytes play some role in the pathophysiology of APS, the impact of neutrophils has only come to light in the past few years (4). Our group and others have shown that APS neutrophils are prone to the exaggerated release of neutrophil extracellular traps (NETs), prothrombotic tangles of DNA, and microbicidal proteins released from dying neutrophils

(5). At the same time, at least some APS blood does not degrade NETs normally (6). Indeed, dismantling NETs with deoxyribonuclease (7) and preventing NET release (NETosis) via activation of adenosine receptors (8) has proven effective in murine models of APS. In further support of neutrophil hyperactivity in APS, our group has demonstrated that the APS neutrophil transcriptome is characterized by the up-regulation of a number of meta-groups, including a cellular defense node that includes L-selectin and P-selectin glycoprotein I among other adhesion molecules (9).

Beyond neutrophils, both animal models and descriptive studies of patients have demonstrated signs of smoldering endothelial activation in APS. For example, tissue factor activity is increased in carotid homogenates from mice treated with antiphospholipid antibody (10), which correlates with increased leukocyte–endothelium interplay (11). In keeping with the latter concept, antagonizing either E-selectin or P-selectin (the key selectins expressed on the endothelium) is protective against thrombosis in mice; the same is true for strategies blocking the endothelial integrin ligands vascular cell adhesion molecule 1 and intercellular adhesion molecule 1 (ICAM-1) (12,13). One study has suggested that down-regulation of endothelial nitric oxide synthase by aPLs may be another important factor in increased leukocyte–endothelium interplay (14). Beyond these in vivo data, there is robust evidence in vitro that aPLs can activate endothelial cells to express tissue factor and adhesion molecules (15,16). Mechanistically, NF-κB, p38 MAPK, and Krüppel-like factors have all been implicated in antiphospholipid antibody–mediated activation of endothelial cells (17–19), demonstrating how aPLs may co-opt pathways normally associated with more "authentic" activating stimuli.

Mac-1 is a heterodimeric β2 integrin especially expressed by myeloid-lineage cells. In its activated state, Mac-1 mediates cell–cell interactions by engaging a variety of surface molecules, including the endothelium-expressed glycoprotein ICAM-1. In this study, we focused on leukocytes and especially neutrophils (rather than on the endothelium) and how they contribute to heterotypic adhesive interactions relevant to APS. We studied blood samples from APS patients as well as control leukocytes conditioned with either APS plasma or APS IgG. We characterized leukocyte adhesion to resting endothelial cells under physiologic flow conditions. We also considered key adhesion molecules, including Mac-1, on the surface of APS neutrophils and explored their role in not just adhesion, but also in NETosis.

MATERIALS AND METHODS

Human subjects. Patients were recruited from rheumatology and hematology clinics at the University of Michigan (Supplementary Tables 1–3, available on the *Arthritis & Rheumatology* web site at http://onlinelibrary.wiley.com/doi/10.1002/art.41057/abstract). All 43 patients diagnosed as having APS fulfilled the clinical and laboratory criteria for APS according to the updated international consensus (Sydney) classification criteria (1). None of the patients

met American College of Rheumatology revised criteria for systemic lupus erythematosus (20). Of the patients with APS, some were classified as having "obstetric APS" if they had no prior history of vascular thrombosis but did have APS-associated obstetric complications as defined by the Sydney classification criteria (i.e., ≥3 unexplained, consecutive spontaneous pregnancy losses; or ≥1 unexplained fetal deaths at ≥10 weeks of gestation; or ≥1 preterm deliveries of a morphologically normal infant before 34 weeks of gestation due to severe preeclampsia, eclampsia, or features consistent with placental insufficiency) (1). Eleven patients with a history of unprovoked venous thrombosis (VT) but with negative test results for aPLs, were also recruited (Supplementary Table 4, available at http://onlinelibrary.wiley.com/doi/10.1002/art.41057/abstract); many of these patients had genetic risk factors for VT, such as factor V Leiden heterozygosity as detailed in Supplementary Table 4.

Thirty-eight healthy controls were recruited through a posted flyer; exclusion criteria included history of a systemic autoimmune disease, active infection, and pregnancy. All 38 controls were screened for IgG anti-β_2GPI and all had negative test results. Blood samples were collected by phlebotomist-performed venipuncture, and serum was prepared by standard methods and stored at –80°C until used. IgG, IgM, and IgA anti-β_2GPI, as well as IgG and IgM anticardiolipin antibodies, were determined by multiplex assay on a BioPlex 2200 System (Bio-Rad). LAC was tested according to published guidelines (21). This study was reviewed and approved by the University of Michigan Institutional Review Board. Written informed consent was obtained from all participants prior to inclusion.

Preparation of human IgG. IgG was purified from human serum samples with a Protein G–Agarose kit according to the instructions of the manufacturer (Pierce). Briefly, serum was diluted in IgG binding buffer and passed through a protein G–agarose column at least 5 times. IgG was eluted with 0.1M glycine. This solution was neutralized with 1M Tris followed by overnight dialysis against phosphate buffered saline (PBS) at 4°C. After passage through a 0.2μ filter, IgG purity was verified by sodium dodecyl sulfate–polyacrylamide gel electrophoresis. IgG concentrations were quantified by bicinchoninic acid protein assay (Pierce). IgG preparations were confirmed to be free of endotoxin contamination as determined by a chromogenic endotoxin quantification kit (Pierce).

Human neutrophil purification. For neutrophil preparation, blood samples were collected into sodium citrate tubes by standard phlebotomy techniques. The anticoagulated blood was then fractionated by density-gradient centrifugation using Ficoll-Paque Plus (GE Healthcare). Neutrophils were further purified by dextran sedimentation of the red blood cell (RBC) layer before lysing residual RBCs with 0.2% sodium chloride. Neutrophil preparations were >98% pure as confirmed by both flow cytometry and nuclear morphology.

In vitro flow adhesion assays. For all flow chamber experiments, blood was collected into citrate tubes. A parallel-plate flow chamber (PPFC) with straight gaskets forming the flow channel (GlycoTech) was then used for in vitro flow adhesion assays. Briefly, a single straight gasket was placed over a human umbilical vein endothelial cell (HUVEC) monolayer cultured on a glass coverslip (22) and vacuum-sealed to the flow deck to form the bottom adhesion substrate of the chamber.

For some experiments, "leukocytes" were prepared by mixing together the buffy coat and RBCs (after discarding plasma). In other cases, "neutrophils" were prepared by retrieving the neutrophil–RBC pellet that remained after Ficoll gradient separation. For these leukocyte and neutrophil experiments, cells were always brought back to their original blood volume with flow buffer (PBS with calcium and magnesium with 1% bovine serum albumin [BSA]). A total of 2 ml of whole blood, leukocytes, or neutrophils was introduced into the chamber from an inlet reservoir via a programmable syringe pump (KD Scientific). For low-shear experiments, samples were perfused across the HUVEC monolayer using a laminar flow profile. The wall shear rate (WSR; γw) was fixed by adjusting the volumetric flow rate (Q) through the channel according to the following equation:

$$Q = \frac{\gamma h^2 w}{6}$$

where h is the channel height (127 μm) and w is the channel width (0.25 cm). The height of 127 μm and WSR of 200 seconds^{-1} were chosen to approximate the flow profile within veins and venules. Low-shear samples were perfused over HUVECs for 5 minutes. For high-shear experiments, pulsatile flow was used in the horizontal PPFC as described previously (22). Specifically, samples were perfused over HUVEC monolayers in pulsatile flow at a WSR of 1,000 seconds^{-1} for 15 minutes (23–25). The flow time was chosen to ensure the same volume of blood passed through the chamber as for laminar/low-shear experiments (22). At the end of the prescribed flow time, flow buffer was added to the PPFC to flush out nonadherent cells.

Ten images per sample were collected along the length of the flow chamber using a Nikon TE2000S inverted microscope with a digital camera (Photometrics CoolSNAP EZ with a Sony CCD sensor). Results were imaged and analyzed using NIS-elements analysis software and ImageJ. The adherent cells were normalized to the control cells examined on the same day so as to minimize variation attributable to different batches of HUVECs.

For experiments involving the pretreatment or conditioning of control leukocytes, the buffy coat/RBC sample was incubated at 37°C for 1 hour with plasma before washing again with flow buffer. For blocking experiments, anti–Mac-1 (20 μg/ml, clone CBRM1/5) antibody or isotype control was also included during the incubation.

Flow cytometry studies. For all flow cytometry experiments, blood samples were collected into citrate tubes and imme-

diately processed. Fc blocking of cells (in whole blood) was carried out using Human TruStain FcX (BioLegend), according to the instructions of the manufacturer. Subsequently, cells (still in whole blood) were stained with specific antibodies for 30 minutes on ice, followed by immediate lysis of RBCs and fixation of leukocytes using eBioscience 1-step Fix/Lyse Solution. Samples were analyzed on an LSRFortessa cell analyzer (BD Biosciences) and ZE5 cell analyzer (Bio-Rad). Further data were analyzed with FlowJo software (Tree Star). Specific primary antibodies were against apolipoprotein H (ABS162; EMD Millipore), CD15 (W6D3; BioLegend), CD16 (3G8; BioLegend), CEACAM1 (283340; R&D Systems), CD64 (10.1; BioLegend), activated lymphocyte function–associated antigen 1 (LFA-1) (m24; BioLegend), activated Mac-1 (CBRM1/5; BioLegend), and CD62L (DREG-56; BioLegend). We also used eBioscience Fixable Viability Dye eFluor 506 and secondary antibody Alexa Fluor 680 AffiniPure donkey anti-rabbit IgG (heavy and light chains) (711-625-152; Jackson ImmunoResearch). For leukocyte conditioning experiments, the sample was spiked with increasing concentrations of either APS or control IgG (10 μg/ml or 100 μg/ml), or the citrated plasma of the sample was discarded and replaced with heterologous control or APS plasma and incubated for 1 hour at 37°C before staining and flow analysis.

Toll-like receptor 4 (TLR-4) and complement inhibition. Anticoagulated control blood was preincubated with 20 μ*M* TLR-4 inhibitor (TAK-242) or 10 μ*M* C5a receptor antagonist (W-54011) (both from Cayman Chemical) for 30 minutes. The sample was then spiked with IgG as described above and incubated for 1 hour at 37°C.

Quantification of NETosis. Neutrophils were labeled with CytoTrace Red CMTPX (5 μ*M*; AAT Bioquest) according to the instructions of the manufacturer and resuspended in RPMI medium supplemented with 0.5% BSA and 0.5% fetal bovine serum (all from Gibco). Neutrophils (1.5×10^5 cells/well) were then incubated in 48-well plates with a preestablished monolayer of HUVECs at 37°C. Samples were additionally treated with 100 μg/ml APS IgG or control IgG in the presence of anti–Mac-1 (20 μg/ml; clone CBRM1/5) or isotype control. After 3 hours, Sytox green (ThermoFisher Scientific) was added to a final concentration of 0.2 μ*M* and incubated for an additional 10 minutes. Fluorescence was quantified at excitation and at emission wavelengths of 485 nm and 520 nm, respectively, using a BioTek Cytation 5 Cell Imaging Multi-Mode Reader. Representative images were captured by the BioTek Cytation 5 reader's 20× objective lens.

Statistical analysis. Data analysis was conducted using GraphPad Prism software, version 7. Normally distributed data were analyzed by *t*-tests, while skewed data were assessed by the Mann-Whitney test. Analysis of variance (ANOVA) with appropriate correction for multiple comparisons was also used where appropriate. For each panel of data, the specific statistical test is

indicated in the figure legend. *P* values less than 0.05 were considered significant.

RESULTS

Demonstration of increased adhesion under flow by APS neutrophils. Utilizing anticoagulated whole blood collected from patients with primary APS or matched healthy volunteers (Supplementary Tables 1–3, available at http://onlinelibrary.wiley.com/doi/10.1002/art.41057/abstract), we tested leukocyte adhesion to unactivated/resting early-passage HUVECs in a PPFC assay. Representative images of leukocyte adhesion in the PPFC assay are shown in Figure 1A. Compared to control blood, we observed increased adhesion of APS leukocytes under high-shear (1,000 seconds^{-1}) pulsatile flow conditions, as might be found in arteries or the arterioles (Figure 1B). Similar results were observed when blood was passed through the chamber under lower-shear (200 seconds^{-1}) laminar flow, as would be found in the venous system (Figure 1B). If the increased adhesion were being driven by factors inherent to the leukocytes themselves, we reasoned that a similar phenotype would be observed if plasma (along with the cytokines and autoantibodies that might activate the HUVECs) were discarded. Indeed, isolated APS leukocytes, in the absence of plasma, still adhered in exaggerated manner to HUVECs (under both high- and low-shear flow conditions) (Figure 1C). Finally, we removed not just plasma, but also peripheral blood mononuclear cells by spinning the blood through a density gradient. Again, we observed increased adhesion of neutrophils to HUVECs as compared to controls (Figure 1D). In summary, these data reveal that leukocytes, and specifically neutrophils, demonstrate increased adhesion to unstimulated HUVECs in the context of various flow profiles. The phenotype persisted even after plasma was discarded, which is consistent with an inherent role for neutrophils in the adhesive interaction.

Up-regulation of adhesion molecules on the surface of APS neutrophils. In an effort to understand what seemed to be an inherent increase in APS neutrophil adhesion, we evaluated
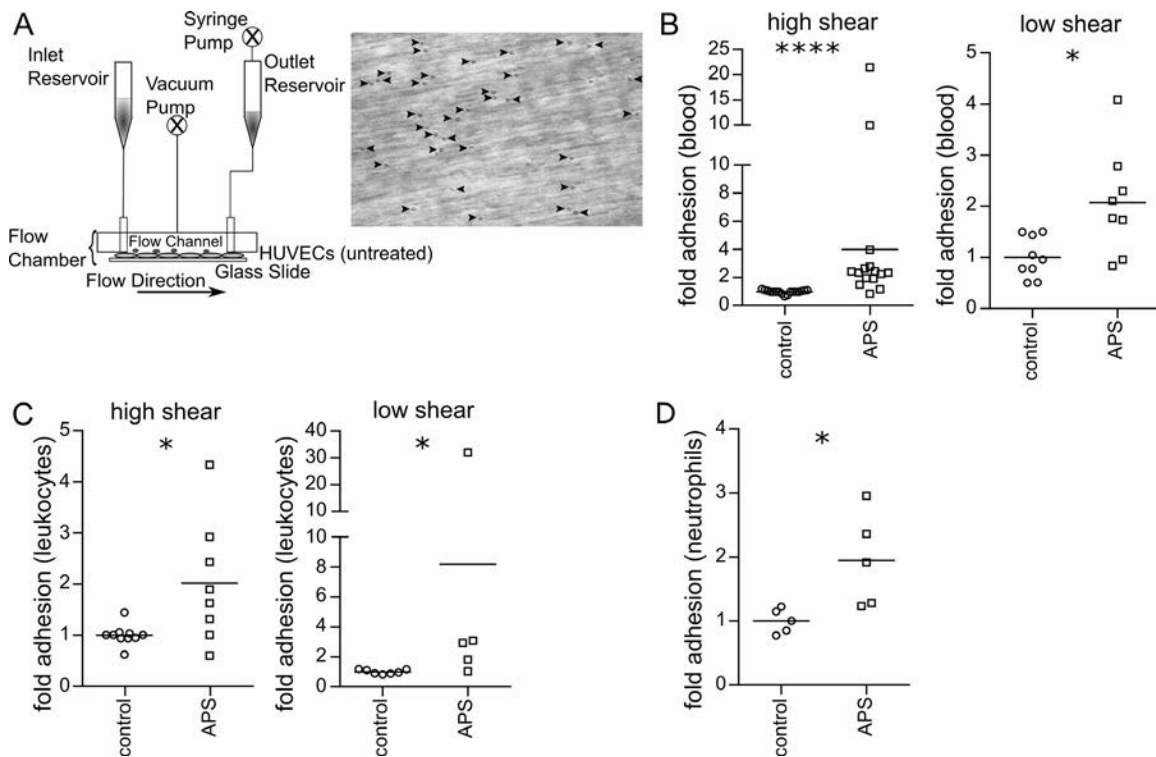
Figure 1. Antiphospholipid syndrome (APS) neutrophils showing increased adhesion in multiple flow profiles. Adhesion was measured under either pulsatile high-shear (1,000 seconds^{-1}) conditions or laminar low-shear (200 seconds^{-1}) conditions. **A**, Schematic illustration of the parallel-plate flow chamber (left) and a representative image (right) showing adhesion of APS leukocytes (**arrowheads**). Original magnification × 20. **B**, Perfusion of anticoagulated whole blood samples from healthy controls (n = 18 for high shear and n = 9 for low shear) or patients with APS (n = 15 for high shear and n = 8 for low shear) through the flow chamber and quantification of adherent cells. **** = *P* < 0.0001 versus controls, by Mann-Whitney test; * = *P* < 0.05 versus controls, by *t*-test. **C**, Perfusion of isolated and resuspended (in flow buffer; plasma discarded) control leukocytes (n = 10 for high shear and n = 7 for low shear) or APS leukocytes (n = 8 for high shear and n = 5 for low shear) through the flow chamber and quantification of adherent cells. * = *P* < 0.05 versus controls, by Mann-Whitney test. **D**, Perfusion of isolated and resuspended (in flow buffer) control neutrophils (n = 5) or APS neutrophils (n = 5) through the flow chamber and quantification of adherent cells. * = *P* < 0.05 versus controls, by *t*-test. In **B**–**D**, symbols represent individual samples; horizontal lines show the mean. HUVECs = human umbilical vein endothelial cells.

the surface expression of various adhesion molecules on the neutrophil surface (Figure 2A). As ICAM-1 is known to be expressed even by resting HUVECs, we reasoned that β2 integrin family members (which are well known to interact with ICAM-1) might be up-regulated on APS neutrophils, thus mediating the increased adhesion. While we observed no difference in the activated form of β2 integrin LFA-1 (Figure 2B), the activated form of another β_2 integrin, Mac-1, was robustly up-regulated on the surface of APS neutrophils (Figure 2C). An evaluation of other potential markers of neutrophil activation revealed no significant difference in CD62L (L-selectin), but did reveal up-regulation of both CD64 and CEACAM1 (Figures 2D–F). Interestingly, autoantigen β_2GPI was also present at increased levels on the surface of APS neutrophils (Figure 2G). In summary, these data demonstrate increased expression of activated Mac-1, but not activated LFA-1, on the neutrophil surface, which correlates with the up-regulation of other neutrophil activation markers such as CD64 and CEACAM1.

Dependence of APS IgG–mediated up-regulation of Mac-1 on neutrophils on TLR-4 and complement anaphylatoxin receptors. Previous work by our group has demonstrated that NETosis can be triggered from control neutrophils by

incubation with either APS serum or APS IgG (5). In the present study we explored whether adhesion molecules were also up-regulated by similar treatment (Figure 3A). When we "conditioned" control blood cells with APS plasma, we did not find increased expression of activated LFA-1 on the surface of neutrophils (Figure 3B). In contrast, there was a striking increase in surface expression of activated Mac-1 (Figure 3C). We also found evidence of shedding of CD62L from neutrophils and up-regulation of both CD64 and CEACAM1 (Figures 3D–F). β_2GPI was measured, but was not significantly up-regulated (Figure 3G). We then conditioned control blood with IgG purified from patients with primary APS; under these conditions we observed up-regulation of activated Mac-1 on neutrophils (Figure 4A), along with shedding of CD62L (Figure 4B). Having previously observed that APS IgG–mediated NETosis is dependent on TLR-4, we assessed that same pathway in the context of Mac-1 activation. Indeed, the TLR-4 signaling inhibitor TAK-242 prevented APS IgG from up-regulating activated Mac-1 on neutrophils (Figure 4C). We reasoned that we might also find a role for the complement cascade in neutrophil activation. When blood was treated with a C5a receptor inhibitory antibody, up-regulation of activated Mac-1 on neutrophils was blunted (Figure 4D). In summary, these data together indicate
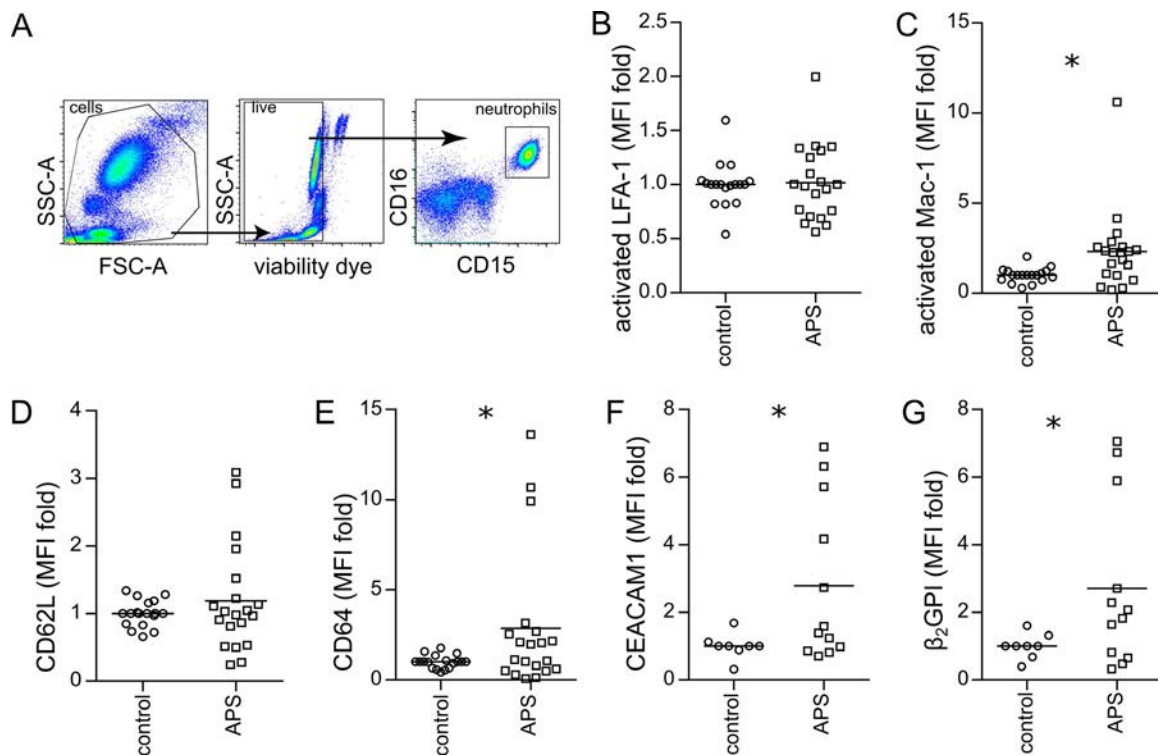
Figure 2. Increased expression of activated Mac-1 and other adhesion molecules on antiphospholipid syndrome (APS) neutrophils. Flow cytometry was performed after treating anticoagulated whole blood samples with fluorescently labeled antibodies. Mean fluorescence intensity (MFI) was normalized to controls run in the same batch. **A**, Cell sorting plots showing gating strategy for identification of neutrophils in whole blood. **B–G**, Up-regulation of activated lymphocyte function–associated antigen 1 (LFA-1) (**B**), activated Mac-1 (**C**), CD62L (**D**), CD64 (**E**), CEACAM1 (**F**), and β_2-glycoprotein I (β_2GPI). (**G**). In **B–E**, n = 18 for control samples and n = 20 for APS samples. In **F** and **G**, n = 8 for control samples and n = 12 for APS samples. In **B–G**, symbols represent individual samples; horizontal lines show the mean. * = $P < 0.05$ versus controls, by t-test. Differences in **B** and **D** were not significant.
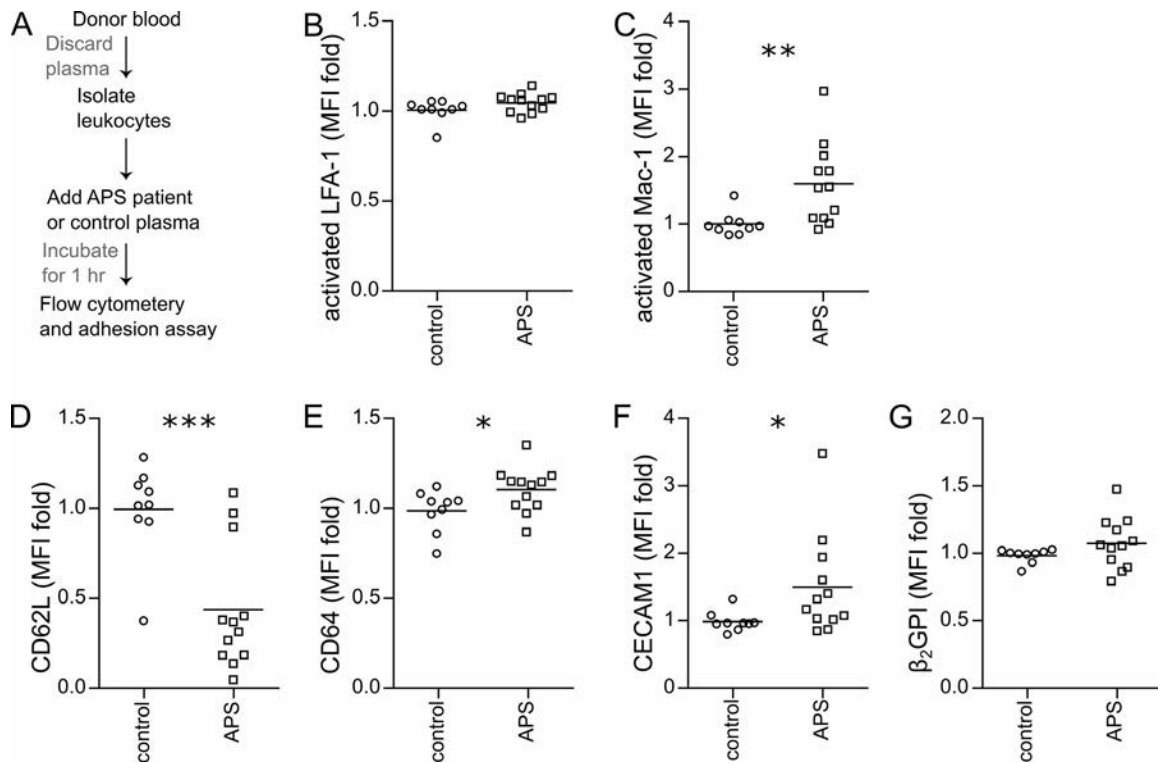
Figure 3. Increased expression of activated Mac-1 and other adhesion molecules when control neutrophils are conditioned with APS plasma. **A**, Conditioning of control leukocytes with heterologous control plasma or APS plasma and incubation with fluorescently labeled antibodies. MFI was normalized to controls run in the same batch. **B**, No increased expression of activated LFA-1 on the neutrophil surface (differences not significant, by t-test). **C**, Increase in surface expression of activated Mac-1. ** = $P < 0.01$ versus controls, by t-test. **D**, Shedding of CD62L from neutrophils. *** = $P < 0.001$ versus controls, by t-test. **E**, Up-regulation of CD64. * = $P < 0.05$ versus controls, by t-test. **F**, Up-regulation of CEACAM1. * = $P < 0.05$ versus controls, by Mann-Whitney test. **G**, Up-regulation of β_2GPI (differences not significant, by t-test). In **B**–**G**, symbols represent individual samples (n = 9 for controls and n = 12 for APS); horizontal lines show the mean. See Figure 2 for definitions.

that control neutrophils up-regulate activated Mac-1 in response to conditioning with either APS plasma or APS IgG and that this up-regulation requires TLR-4 and the C5a receptor.

Requirement of activated Mac-1 for increased adhesion of APS neutrophils. Having found that APS plasma up-regulates Mac-1 on the surface of control neutrophils, we reasoned that this up-regulation might be directly responsible for increased neutrophil adhesion. Indeed, APS plasma–treated cells, but not control plasma–treated cells, demonstrated increased adhesion under both high-shear and low-shear flow conditions (Figure 5A). Furthermore, a monoclonal antibody specific for the activated form of Mac-1 effectively neutralized adhesion in the context of conditioning with APS plasma, but had no effect in the setting of control plasma (Figure 5B). To determine whether the ability of plasma to stimulate cell adhesion was unique to patients with APS or whether the phenotype might extend to any patient with a history of thrombosis, we recruited 11 patients with a history of unprovoked VT but with test results negative for aPLs (Supplementary Table 4, available at http://onlinelibrary.wiley.com/doi/10.1002/art.41057/abstract).

When compared to plasma samples from healthy controls, plasma samples from the VT cohort triggered no increase in cell adhesion (Figure 5C). Similar to this finding, conditioning neutrophils with plasma from the VT cohort did not alter levels of activated Mac-1, CD62L, or CD64 (Figures 5D–F) on the neutrophil surface. Finally, we asked whether the increased cell adhesion triggered by APS plasma might be limited to patients with a history of "thrombotic APS" (i.e., at least 1 documented arterial, venous, or small vessel thrombotic event). Interestingly, we observed increased adhesion whether the plasma was collected from patients with "thrombotic APS" or patients with purely "obstetric APS" (Supplementary Figure 1, available on the *Arthritis & Rheumatology* web site at http://onlinelibrary.wiley.com/doi/10.1002/art.41057/abstract). In summary, these data demonstrate that antagonizing the activated form of Mac-1 is sufficient to reduce APS-relevant adhesion to levels seen in controls.

Requirement of activated Mac-1 for NETosis by APS neutrophils bound to endothelial cells. Given evidence by our group and others (5,26) that NETosis proceeds most efficiently upon cell adhesion, we investigated whether the aforementioned antibody targeting activated Mac-1 might mitigate NETosis.
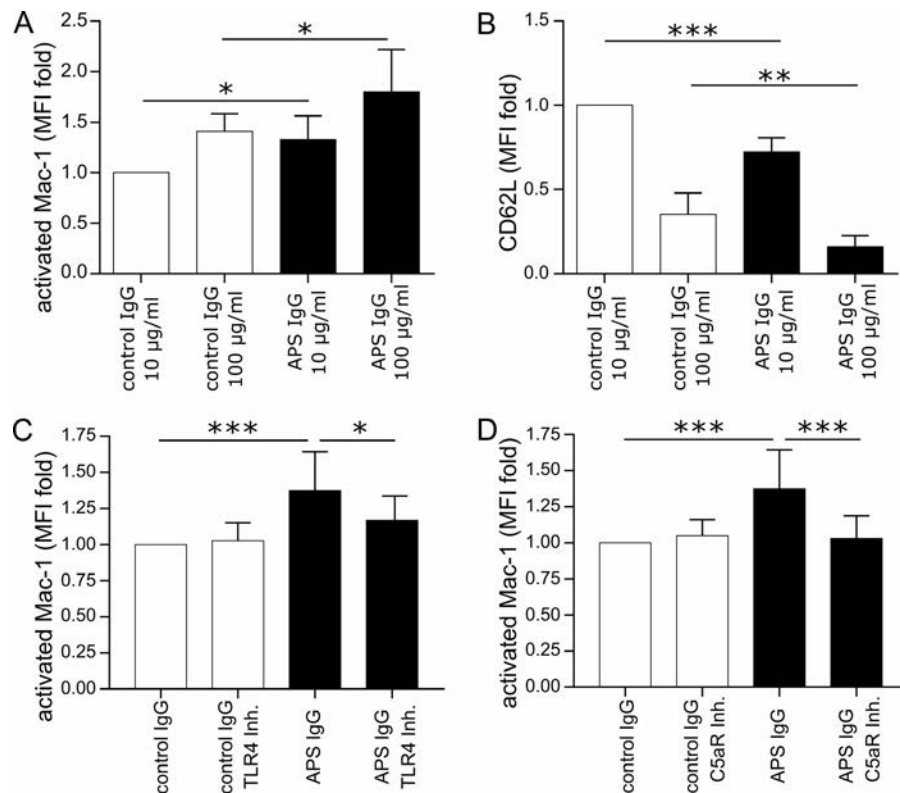
Figure 4. Increased expression of activated Mac-1 on control neutrophils occurring in a Toll-like receptor 4 (TLR-4)– and complement-dependent manner through exposure to purified APS IgG. Control leukocytes were treated with control or APS IgG as indicated. Activated Mac-1 and CD62L were quantified by flow cytometry. **A,** Up-regulation of activated Mac-1. * = $P < 0.05$ by one-way analysis of variance (ANOVA) with correction for multiple comparisons by the Holm-Sidak method (n = 4 independent experiments). **B,** Shedding of CD62L. ** = $P < 0.01$; *** = $P < 0.0001$ by one-way ANOVA with correction for multiple comparisons by the Holm-Sidak method (n = 4 independent experiments). **C,** Control leukocytes treated with control or APS IgG (100 μg/ml) in the presence or absence of TLR-4 inhibitor (Inh.). Activated Mac-1 was quantified by flow cytometry. * = $P < 0.05$; *** = $P < 0.001$ by one-way ANOVA with correction for multiple comparisons by the Holm-Sidak method (n = 8 independent experiments). **D,** Control leukocytes treated with control or APS IgG (100 μg/ml) in the presence or absence of C5a receptor (C5aR) inhibitor. Activated Mac-1 was quantified by flow cytometry. *** = $P < 0.001$ by one-way ANOVA with correction for multiple comparisons by the Holm-Sidak method (n = 7 independent experiments). Values are the mean ± SEM. See Figure 2 for other definitions.

To test this, we adhered vital dye–labeled neutrophils to resting HUVECs and then tracked NETosis in real time via the loss of vital dye and the local release of decondensed DNA (Figure 6A). As compared to isotype treatment, the Mac-1 monoclonal antibody significantly neutralized NETosis in response to APS IgG, but not phorbol myristate acetate (Figure 6B). In summary, these data demonstrate that inhibition of the activated form of Mac-1 can neutralize NETosis, at least in the context of APS.

DISCUSSION

While there are many studies characterizing the activated endothelium in APS (11,15), comparatively little is known about the adhesive nature of circulating cells (27). In this study we examined the adhesive potential of APS leukocytes and, particularly, neutrophils. We found enhanced adhesion of APS neutrophils to resting HUVECs irrespective of the flow conditions (Figures 1B and C). Notably, this functional increase in adhesion was observed in the

context of up-regulated adhesion molecules on the neutrophil surface, including CD64, CEACAM1, and the activated form of Mac-1 (Figure 2). These findings did not extend to patients with a history of unprovoked VT and negative test results for aPLs (Figures 5C–F), suggesting that these results may represent relatively unique features of APS. Of note, all flow experiments were performed in the presence of RBCs, which are known to stabilize leukocyte adhesion, thereby more closely modeling conditions observed in vivo (28).

In addition to thrombosis of arteries, veins, and small vessels, another hallmark of APS is pregnancy-related morbidity. There is evidence that obstetric complications of APS have distinct pathophysiology as compared to thrombotic APS (29); however, recent data have suggested that up to 60% of patients who begin with a diagnosis of "obstetric APS" will eventually develop a thrombotic event (30). While the cohort tested here was relatively enriched for patients with thrombotic complications, we identified and tested 8 patients with a history of only obstetric morbidity (see definition in Methods). Interestingly, these patients with obstetric APS
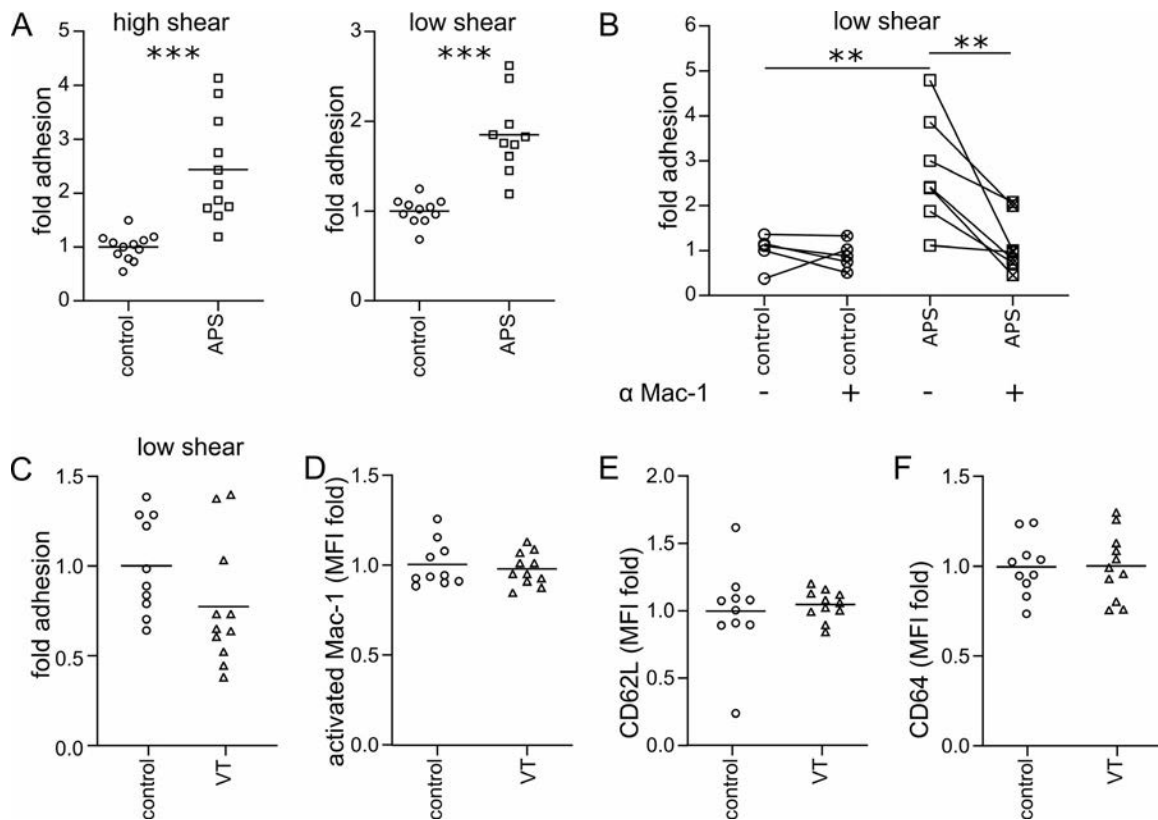
Figure 5. Increased adhesion of APS leukocytes mediated by activated Mac-1. Control leukocytes were incubated with heterologous control or APS plasma, resuspended in flow buffer, and perfused through the flow chamber. Adherent cells were quantified. **A**, Increased adhesion of APS plasma–treated cells. *** = $P < 0.001$ versus controls, by t-test. **B**, Conditions similar to those in **A**, except with the addition of a blocking antibody for activated Mac-1 to some samples. ** = $P < 0.01$ by one-way analysis of variance (ANOVA) with correction for multiple comparisons by the Holm-Sidak method. **C**, Conditions similar to those in **A**, except that control leukocytes were incubated with heterologous control plasma or plasma from patients with a history of unprovoked venous thrombosis (VT) and negative test results for antiphospholipid antibody. The leukocytes were then resuspended in flow buffer and perfused through the flow chamber. Adherent cells were quantified. **D**–**F**, Conditions similar to those in Figure 3, except that control leukocytes were conditioned with heterologous control plasma or VT plasma and incubated with fluorescently labeled antibodies, followed by quantification of the MFI fold change in activated Mac-1 (**D**), CD62L (**E**), and CD64 (**F**) in VT plasma–conditioned cells relative to controls run in the same batch. Differences in **C**–**F** were not significant, by t-test. Symbols represent individual samples; horizontal lines indicate the control value (set as 1). See Figure 2 for other definitions.

were indistinguishable from patients with a history of thrombotic events in terms of neutrophil adhesion (Supplementary Figure 1, http://onlinelibrary.wiley.com/doi/10.1002/art.41057/abstract). We hope that further research of disease models will allow us to understand the extent to which activated Mac-1 may be a direct mediator of thrombotic (versus obstetric) pathophysiology.

In our previous study, we found that inhibition of TLR-4 signaling could mitigate APS IgG–mediated NETosis (5). This is in addition to other studies demonstrating that TLR-4 deficiency protected mice from APS in vivo, and that neutrophil TLR-4 supported phagocytosis and reactive oxygen species production by APS neutrophils (10,31). We demonstrated that the TLR-4 inhibitor TAK-242 prevented APS IgG from up-regulating activated Mac-1 on neutrophils (Figure 4C). These data support further investigation of TLR-4 signaling as a potential therapeutic target in APS. Similar to the TLR-4 pathway, complement contributes to neutrophil activation in many contexts. Here we demonstrated

that inhibition of C5a receptor attenuates the up-regulation of activated Mac-1 on APS IgG–stimulated neutrophils (Figure 4D). These data are consistent with previous studies demonstrating that C5a receptor contributes to up-regulation of Mac-1 (32,33).

Despite extensive CD62L shedding in control neutrophils conditioned with APS plasma (Figure 3D), CD62L shedding was not detected at a significant level in neutrophils freshly isolated from patients with APS (Figure 2D). One possibility is that the patient neutrophils have had time to up-regulate CD62L expression, thereby effectively compensating for shedding. In support of this idea, CD62L was up-regulated at the gene level in our recent transcriptomic profiling of APS neutrophils (9). Alternatively, it is possible that neutrophils that have shed CD62L in vivo are strongly activated to the point that they have preferentially left circulation, thereby being unavailable for our analysis. Interestingly, we also detected increased surface expression of the APS autoantigen β_2GPI on the surface of APS neutrophils by flow cytometry
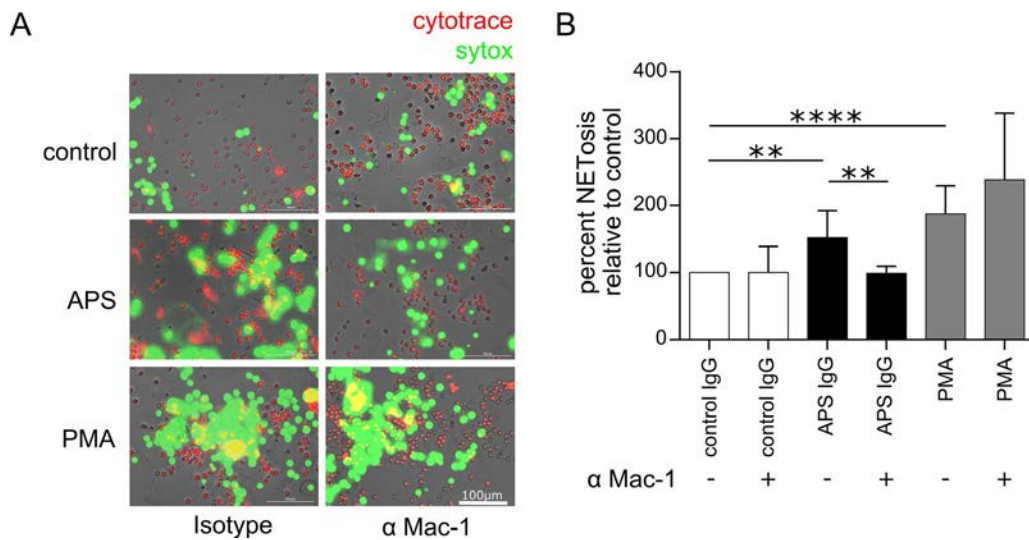
Figure 6. Necessary activation of Mac-1 for regulation of antiphospholipid syndrome (APS) IgG–mediated neutrophil extracellular trap release (NETosis). **A**, Fluorescence intensity showing live cells (stained with CytoTrace Red) and extracellular DNA (stained with Sytox green) in samples stimulated with control IgG (top), APS IgG (middle), or phorbol myristate acetate (PMA; bottom). Bars = 100 μm. **B**, Quantification of NETosis as measured by fluorescence intensity of Sytox green in cells stimulated as indicated in the presence or absence of antibodies to Mac-1. Bars show the mean ± SEM. ** = $P < 0.01$; **** = $P < 0.0001$ by one-way analysis of variance with correction for multiple comparisons by the Holm-Sidak method (n = 4 independent experiments).

(Figure 2G), which is in line with our 2017 study demonstrating a 4.5-fold increase in $β_2$GPI gene expression in APS neutrophils (9). It should be noted that at least one other group has demonstrated similar $β_2$GPI surface and expression phenotypes in circulating APS monocytes (34,35).

Blocking experiments demonstrated that the adhesion of APS neutrophils is at least partially mediated by activated Mac-1 (Figure 5B). Interestingly, we also showed that APS IgG–mediated NETosis was Mac-1 dependent (Figure 6). This latter finding is similar to a study by Neeli et al, who showed that Mac-1 was required for both hypercitrullination of histones and NETosis in response to lipopolysaccharide (LPS) stimulation (26). Of note, both LPS and APS IgG activate neutrophils via TLR-4 (5). Taken together, the data presented in this study reveal a previously unknown role for activated Mac-1 in the adhesion and NETosis of APS neutrophils.

In the general population, numerous study findings have suggested a link between Mac-1, neutrophils, and endothelium in thrombotic vascular diseases (36–38). For example, significant up-regulation of Mac-1 by neutrophils has been detected at the time of myocardial infarction and for up to 1 week after the event (39). In another study, neutrophils from myocardial infarction patients displayed enhanced adhesion to endothelial cells ex vivo, which could be reduced by blocking Mac-1 (40). In patients with acute ischemic stroke, there was significant up-regulation of neutrophil Mac-1 immediately after the event, and persisting into the subacute phase of the stroke (41). In patients with venous thromboembolism, increased adhesive potential of neutrophils was associated with a higher rate of recurrence (42). As indicated in Supplementary Table 1 (http://onlinelibrary.wiley.com/doi/10.1002/art.41057/abstract), the average time from last thrombotic event to blood collection

for patients with APS included in this study was approximately 4.5 years. One might hypothesize that up-regulation of activated Mac-1 is detected only acutely (i.e., at the time of thrombosis) for persons in the general population, but remains undetected in patients with APS, which is potentially consistent with the life-long anticoagulation that such patients require. To further explore this question, it will be necessary to build longitudinal APS cohorts and study them alongside cohorts from the general population.

Beyond activated Mac-1, we also observed consistent up-regulation of CD64 on the surface of APS neutrophils (Figure 2E). This is somewhat reminiscent of studies of patients with sickle cell disease. Sickle cell neutrophils demonstrate increased levels of CD64 and increased adhesion to endothelial cells, with some evidence that CD64 directly contributes to the adhesion (43,44). Future studies should investigate whether this surface molecule, typically thought of as an IgG receptor, might also play a role in APS neutrophil adhesion. CEACAM1 (CD66a) expression was also consistently up-regulated on APS neutrophils (Figure 2F). Interestingly, there are studies to suggest that signaling through CEACAM1 (and potentially other CEACAM family members) results in activation of Mac-1 and increased adhesion to endothelial cells (45–48). At the same time, recent reports (predominantly in mice) have suggested that CEACAM1 may have inhibitory functions, protecting against neutrophil hyperactivity and neutrophil-mediated tissue damage. For example, CEACAM1 protected against ischemic stroke by inhibiting matrix metalloproteinase 9 (49,50). CEACAM1-deficient mice also formed larger carotid thrombi in a ferric chloride injury model, suggesting that CEACAM1 may inhibit arterial thrombus (51). Thus, this very interesting molecule seems to warrant further study in APS.

In conclusion, our study has revealed a novel role for activated Mac-1 in regulating APS neutrophils and NETosis, and hints at a role for Mac-1 in APS pathophysiology. While Mac-1 can be considered as a therapeutic target in APS, mutations in CD11b are a well-recognized risk factor for lupus (52), and many, but not all, mouse studies have suggested that CD11b deficiency has the potential to exacerbate autoimmunity (52–55). Also, since Mac-1 binds to a variety of ligands, selective inhibition of specific Mac-1 adhesive interactions could emerge as a potential therapeutic strategy. For example, one proof-of-concept study has demonstrated that targeted inhibition of the Mac-1–CD40L interaction improved bacterial clearance and survival in a polymicrobial model of sepsis (56). Another innovative approach has involved the utilization of small-molecule Mac-1 agonists. These agonists tend to induce an intermediate-affinity conformation in Mac-1 (57), which may permit neutrophil adhesion, with less potential for endothelial damage. Indeed, a partial Mac-1 agonist not only protected MRL/lpr mice from end-organ injury, but also enhanced endothelium-dependent vasorelaxation and thereby demonstrated an overall vasoprotective effect (58). Taken together, these study findings indicate that targeting Mac-1 might indeed be feasible and emphasize the need for future research in patients with APS.

AUTHOR CONTRIBUTIONS

All authors were involved in drafting the article or revising it critically for important intellectual content, and all authors approved the final version to be submitted for publication. Dr. Knight had full access to all of the data in the study and takes responsibility for the integrity of the data and the accuracy of the data analysis.

Study conception and design. Sule, Kelley, Bockenstedt, Eniola-Adefeso, Knight.

Acquisition of data. Sule, Kelley, Gockman, Yalavarthi, Vreede, Banka.

Analysis and interpretation of data. Sule, Kelley, Gockman, Yalavarthi, Vreede, Banka, Eniola-Adefeso, Knight.

REFERENCES

1. Miyakis S, Lockshin MD, Atsumi T, Branch DW, Brey RL, Cervera R, et al. International consensus statement on an update of the classification criteria for definite antiphospholipid syndrome (APS). J Thromb Haemost 2006;4:295–306.

2. Garcia D, Erkan D. Diagnosis and management of the antiphospholipid syndrome. N Engl J Med 2018;378:2010–21.

3. Abreu MM, Danowski A, Wahl DG, Amigo MC, Tektonidou M, Pacheco MS, et al. The relevance of "non-criteria" clinical manifestations of antiphospholipid syndrome: 14th International Congress on Antiphospholipid Antibodies Technical Task Force report on antiphospholipid syndrome clinical features. Autoimmun Rev 2015;14:401–14.

4. Rao AN, Kazzaz NM, Knight JS. Do neutrophil extracellular traps contribute to the heightened risk of thrombosis in inflammatory diseases? World J Cardiol 2015;7:829–42.

5. Yalavarthi S, Gould TJ, Rao AN, Mazza LF, Morris AE, Núñez-Álvarez C, et al. Release of neutrophil extracellular traps by neutrophils stimulated with antiphospholipid antibodies: a newly identified mechanism of thrombosis in the antiphospholipid syndrome. Arthritis Rheumatol 2015;67:2990–3003.

6. Leffler J, Stojanovich L, Shoenfeld Y, Bogdanovic G, Hesselstrand R, Blom AM. Degradation of neutrophil extracellular traps is decreased in patients with antiphospholipid syndrome. Clin Exp Rheumatol 2014;32:66–70.

7. Meng H, Yalavarthi S, Kanthi Y, Mazza LF, Elfline MA, Luke CE, et al. In vivo role of neutrophil extracellular traps in antiphospholipid antibody–mediated venous thrombosis. Arthritis Rheumatol 2017;69:655–67.

8. Ali RA, Gandhi AA, Meng H, Yalavarthi S, Vreede AP, Estes SK, et al. Adenosine receptor agonism protects against NETosis and thrombosis in antiphospholipid syndrome. Nat Commun 2019;10:1916.

9. Knight JS, Meng H, Coit P, Yalavarthi S, Sule G, Gandhi AA, et al. Activated signature of antiphospholipid syndrome neutrophils reveals potential therapeutic target. JCI Insight 2017;2:93897.

10. Pierangeli SS, Vega-Ostertag ME, Raschi E, Liu X, Romay-Penabad Z, De Micheli V, et al. Toll-like receptor and antiphospholipid mediated thrombosis: in vivo studies. Ann Rheum Dis 2007;66:1327–33.

11. Pierangeli SS, Colden-Stanfield M, Liu X, Barker JH, Anderson GL, Harris EN. Antiphospholipid antibodies from antiphospholipid syndrome patients activate endothelial cells in vitro and in vivo. Circulation 1999;99:1997–2002.

12. Pierangeli SS, Espinola RG, Liu X, Harris EN. Thrombogenic effects of antiphospholipid antibodies are mediated by intercellular cell adhesion molecule-1, vascular cell adhesion molecule-1, and P-selectin. Circ Res 2001;88:245–50.

13. Espinola RG, Liu X, Colden-Stanfield M, Hall J, Harris EN, Pierangeli SS. E-selectin mediates pathogenic effects of antiphospholipid antibodies. J Thromb Haemost 2003;1:843–8.

14. Ramesh S, Morrell CN, Tarango C, Thomas GD, Yuhanna IS, Girardi G, et al. Antiphospholipid antibodies promote leukocyte-endothelial cell adhesion and thrombosis in mice by antagonizing eNOS via β2GPI and apoER2. J Clin Invest 2011;121:120–31.

15. Simantov R, LaSala JM, Lo SK, Gharavi AE, Sammaritano LR, Salmon JE, et al. Activation of cultured vascular endothelial cells by antiphospholipid antibodies. J Clin Invest 1995;96:2211–9.

16. Del Papa N, Guidali L, Sala A, Buccellati C, Khamashta MA, Ichikawa K, et al. Endothelial cells as target for antiphospholipid antibodies. Human polyclonal and monoclonal anti–β₂-glycoprotein I antibodies react in vitro with endothelial cells through adherent β₂-glycoprotein I and induce endothelial activation. Arthritis Rheum 1997;40:551–61.

17. Dunoyer-Geindre S, de Moerloose P, Galve-de Rochemonteix B, Reber G, Kruithof EK. NF kB is an essential intermediate in the activation of endothelial cells by anti-β(2)–glycoprotein 1 antibodies. Thromb Haemost 2002;88:851–7.

18. Vega-Ostertag M, Casper K, Swerlick R, Ferrara D, Harris EN, Pierangeli SS. Involvement of p38 MAPK in the up-regulation of tissue factor on endothelial cells by antiphospholipid antibodies. Arthritis Rheum 2005;52:1545–54.

19. Allen KL, Hamik A, Jain MK, McCrae KR. Endothelial cell activation by antiphospholipid antibodies is modulated by Kruppel-like transcription factors. Blood 2011;117:6383–91.

20. Hochberg MC, for the Diagnostic and Therapeutic Criteria Committee of the American College of Rheumatology. Updating the American College of Rheumatology revised criteria for the classification of systemic lupus erythematosus [letter]. Arthritis Rheum 1997;40:1725.

21. Pengo V, Tripodi A, Reber G, Rand JH, Ortel TL, Galli M, et al, for the Subcommittee on Lupus Anticoagulant/Antiphospholipid Antibody of the Scientific and Standardisation Committee of the International Society on Thrombosis and Haemostasis. Update of the guidelines for lupus anticoagulant detection. J Thromb Haemost 2009;7:1737–40.

22. Charoenphol P, Huang RB, Eniola-Adefeso O. Potential role of size and hemodynamics in the efficacy of vascular-targeted spherical drug carriers. Biomaterials 2010;31:1392–402.

23. Seki J. Flow pulsation and network structure in mesenteric micro-vasculature of rats. Am J Physiol 1994;266:H811–21.

24. Papaioannou TG, Stefanadis C. Vascular wall shear stress: basic principles and methods. Hellenic J Cardiol 2005;46:9–15.

25. Mahler F, Muheim MH, Intaglietta M, Bollinger A, Anliker M. Blood pressure fluctuations in human nailfold capillaries. Am J Physiol 1979;236:H888–93.

26. Neeli I, Dwivedi N, Khan S, Radic M. Regulation of extracellular chromatin release from neutrophils. J Innate Immun 2009;1:194–201.

27. Corban MT, Duarte-Garcia A, McBane RD, Matteson EL, Lerman LO, Lerman A. Antiphospholipid syndrome: role of vascular endothelial cells and implications for risk stratification and targeted therapeutics. J Am Coll Cardiol 2017;69:2317–30.

28. Abbitt KB, Nash GB. Characteristics of leucocyte adhesion directly observed in flowing whole blood in vitro. Br J Haematol 2001;112:55–63.

29. Meroni PL, Borghi MO, Grossi C, Chighizola CB, Durigutto P, Tedesco F. Obstetric and vascular antiphospholipid syndrome: same antibodies but different diseases? Nat Rev Rheumatol 2018;14:433–40.

30. De Jesús GR, Sciascia S, Andrade D, Barbhaiya M, Tektonidou M, Banzato A, et al. Factors associated with first thrombosis in patients presenting with obstetric antiphospholipid syndrome (APS) in the APS Alliance for Clinical Trials and International Networking Clinical Database and Repository: a retrospective study. BJOG 2019;126:656–61.

31. Gladigau G, Haselmayer P, Scharrer I, Munder M, Prinz N, Lackner K, et al. A role for Toll-like receptor mediated signals in neutrophils in the pathogenesis of the anti-phospholipid syndrome. PLoS One 2012;7:e42176.

32. Miyabe Y, Miyabe C, Murooka TT, Kim EY, Newton GA, Kim ND, et al. Complement C5a receptor is the key initiator of neutrophil adhesion igniting immune complex-induced arthritis. Sci Immunol 2017;2:eaaj2195.

33. Bekker P, Dairaghi D, Seitz L, Leleti M, Wang Y, Ertl L, et al. Characterization of pharmacologic and pharmacokinetic properties of CCX168, a potent and selective orally administered complement 5a receptor inhibitor, based on preclinical evaluation and randomized phase 1 clinical study. PLoS One 2016;11:e0164646.

34. Caronti B, Calderaro C, Alessandri C, Conti F, Tinghino R, Palladini G, et al. β2-glycoprotein I (β2-GPI) mRNA is expressed by several cell types involved in anti-phospholipid syndrome-related tissue damage. Clin Exp Immunol 1999;115:214–9.

35. Conti F, Sorice M, Circella A, Alessandri C, Pittoni V, Caronti B, et al. β-2-glycoprotein I expression on monocytes is increased in anti-phospholipid antibody syndrome and correlates with tissue factor expression. Clin Exp Immunol 2003;132:509–16.

36. Libby P, Lichtman AH, Hansson GK. Immune effector mechanisms implicated in atherosclerosis: from mice to humans. Immunity 2013;38:1092–104.

37. Doring Y, Drechsler M, Soehnlein O, Weber C. Neutrophils in atherosclerosis: from mice to man. Arterioscler Thromb Vasc Biol 2015;35:288–95.

38. Jickling GC, Liu D, Ander BP, Stamova B, Zhan X, Sharp FR. Targeting neutrophils in ischemic stroke: translational insights from experimental studies. J Cereb Blood Flow Metab 2015;35:888–901.

39. Meisel SR, Shapiro H, Radnay J, Neuman Y, Khaskia AR, Gruener N, et al. Increased expression of neutrophil and monocyte adhesion molecules LFA-1 and Mac-1 and their ligand ICAM-1 and VLA-4 throughout the acute phase of myocardial infarction: possible implications for leukocyte aggregation and microvascular plugging. J Am Coll Cardiol 1998;31:120–5.

40. Han L, Shen X, Pan L, Lin S, Liu X, Deng Y, et al. Aminobenzoic acid hydrazide, a myeloperoxidase inhibitor, alters the adhesive properties of neutrophils isolated from acute myocardial infarction patients. Heart Vessels 2012;27:468–74.

41. Tsai NW, Chang WN, Shaw CF, Jan CR, Huang CR, Chen SD, et al. The value of leukocyte adhesion molecules in patients after ischemic stroke. J Neurol 2009;256:1296–302.

42. Zapponi KC, Mazetto BM, Bittar LF, Barnabé A, Santiago-Bassora FD, De Paula EV, et al. Increased adhesive properties of neutrophils and inflammatory markers in venous thromboembolism patients with residual vein occlusion and high D-dimer levels. Thromb Res 2014;133:736–42.

43. Fadlon E, Vordermeier S, Pearson TC, Mire-Sluis AR, Dumonde DC, Phillips J, et al. Blood polymorphonuclear leukocytes from the majority of sickle cell patients in the crisis phase of the disease show enhanced adhesion to vascular endothelium and increased expression of CD64. Blood 1998;91:266–74.

44. Lard LR, Mul FP, de Haas M, Roos D, Duits AJ. Neutrophil activation in sickle cell disease. J Leukoc Biol 1999;66:411–5.

45. Stocks SC, Ruchaud-Sparagano MH, Kerr MA, Grunert F, Haslett C, Dransfield I. CD66: role in the regulation of neutrophil effector function. Eur J Immunol 1996;26:2924–32.

46. Skubitz KM, Campbell KD, Skubitz AP. CD66a, CD66b, CD66c, and CD66d each independently stimulate neutrophils. J Leukoc Biol 1996;60:106–17.

47. Skubitz KM, Skubitz AP. Two new synthetic peptides from the N-domain of CEACAM1 (CD66a) stimulate neutrophil adhesion to endothelial cells. Biopolymers 2011;96:25–31.

48. Skubitz KM, Skubitz AP. Interdependency of CEACAM-1, -3, -6, and -8 induced human neutrophil adhesion to endothelial cells. J Transl Med 2008;6:78.

49. Ludewig P, Sedlacik J, Gelderblom M, Bernreuther C, Korkusuz Y, Wagener C, et al. Carcinoembryonic antigen-related cell adhesion molecule 1 inhibits MMP-9-mediated blood-brain-barrier breakdown in a mouse model for ischemic stroke. Circ Res 2013;113:1013–22.

50. Sobey CG, Drummond GR. CEACAM1: an adhesion molecule that limits blood–brain barrier damage by neutrophils after stroke [editorial]. Circ Res 2013;113:952–3.

51. Wong C, Liu Y, Yip J, Chand R, Wee JL, Oates L, et al. CEACAM1 negatively regulates platelet-collagen interactions and thrombus growth in vitro and in vivo. Blood 2009;113:1818–28.

52. Khan SQ, Khan I, Gupta V. CD11b activity modulates pathogenesis of lupus nephritis. Front Med (Lausanne) 2018;5:52.

53. Rosetti F, Mayadas TN. The many faces of Mac-1 in autoimmune disease. Immunol Rev 2016;269:175–93.

54. Tang T, Rosenkranz A, Assmann KJ, Goodman MJ, Gutierrez-Ramos JC, Carroll MC, et al. A role for Mac-1 (CDIIb/CD18) in immune complex-stimulated neutrophil function in vivo: Mac-1 deficiency abrogates sustained Fcγ receptor-dependent neutrophil adhesion and complement-dependent proteinuria in acute glomerulonephritis. J Exp Med 1997;186:1853–63.

55. Kevil CG, Hicks MJ, He X, Zhang J, Ballantyne CM, Raman C, et al. Loss of LFA-1, but not Mac-1, protects MRL/MpJ-Fas(lpr) mice from autoimmune disease. Am J Pathol 2004;165:609–16.

56. Wolf D, Anto-Michel N, Blankenbach H, Wiedemann A, Buscher K, Hohmann JD, et al. A ligand-specific blockade of the integrin Mac-1 selectively targets pathologic inflammation while maintaining protective host-defense. Nat Commun 2018;9:525.

57. Maiguel D, Faridi MH, Wei C, Kuwano Y, Balla KM, Hernandez D, et al. Small molecule-mediated activation of the integrin CD11b/CD18 reduces inflammatory disease. Sci Signal 2011;4:ra57.

58. Faridi MH, Khan SQ, Zhao W, Lee HW, Altintas MM, Zhang K, et al. CD11b activation suppresses TLR-dependent inflammation and autoimmunity in systemic lupus erythematosus. J Clin Invest 2017;127:1271–83.

AMERICAN COLLEGE
of RHEUMATOLOGY
Empowering Rheumatology Professionals

Abatacept in Early Diffuse Cutaneous Systemic Sclerosis: Results of a Phase II Investigator-Initiated, Multicenter, Double-Blind, Randomized, Placebo-Controlled Trial

Dinesh Khanna,[1] Cathie Spino,[1] Sindhu Johnson,[2] Lorinda Chung,[3] Michael L. Whitfield,[4] Christopher P. Denton,[5] Veronica Berrocal,[1] Jennifer Franks,[4] Bhavan Mehta,[4] Jerry Molitor,[6] Virginia D. Steen,[7] Robert Lafyatis,[8] Robert W. Simms,[9] Anna Gill,[5] Suzanne Kafaja,[10] Tracy M. Frech,[11] Vivien Hsu,[12] Robyn T. Domsic,[13] Janet E. Pope,[14] Jessica K. Gordon,[15] Maureen D. Mayes,[16] Elena Schiopu,[1] Amber Young,[1] Nora Sandorfi,[17] Jane Park,[18] Faye N. Hant,[19] Elana J. Bernstein,[20] Soumya Chatterjee,[21] Flavia V. Castelino,[22] Ali Ajam,[23] Yue Wang,[4] Tammara Wood,[4] Yannick Allanore,[24] Marco Matucci-Cerinic,[25] Oliver Distler,[26] Ora Singer,[1] Erica Bush,[1] David A. Fox,[1] and Daniel E. Furst[27]

Objective. T cells play a key role in the pathogenesis of early systemic sclerosis. This study was undertaken to assess the safety and efficacy of abatacept in patients with diffuse cutaneous systemic sclerosis (dcSSc).

Methods. In this 12-month, randomized, double-blind, placebo-controlled trial, participants were randomized 1:1 to receive either subcutaneous abatacept 125 mg or matching placebo, stratified by duration of dcSSc. Escape therapy was allowed at 6 months for worsening disease. The coprimary end points were change in the modified Rodnan skin thickness score (MRSS) compared to baseline and safety over 12 months. Differences in longitudinal outcomes were assessed according to treatment using linear mixed models, with outcomes censored after initiation of escape therapy. Skin tissue obtained from participants at baseline was classified into intrinsic gene expression subsets.

Results. Among 88 participants, the adjusted mean change in the MRSS at 12 months was –6.24 units for those receiving abatacept and –4.49 units for those receiving placebo, with an adjusted mean treatment difference of –1.75 units ($P = 0.28$). Outcomes for 2 secondary measures (Health Assessment Questionnaire disability index and a composite measure) were clinically and statistically significantly better with abatacept. The proportion of subjects in whom escape therapy was needed was higher in the placebo group relative to the abatacept group (36% versus 16%). In the inflammatory and normal-like skin gene expression subsets, decline in the MRSS over 12 months was clinically and significantly greater in the abatacept group versus the placebo group ($P < 0.001$ and $P = 0.03$, respectively). In the abatacept group, adverse events occurred in 35 participants versus 40 participants in the placebo group, including 2 deaths and 1 death, respectively.

Conclusion. In this phase II trial, abatacept was well-tolerated, but change in the MRSS was not statistically significant. Secondary outcome measures, including gene expression subsets, showed evidence in support of abatacept. These data should be confirmed in a phase III trial.

Mehta, MS, Yue Wang, PhD, Tammara Wood, MS: Geisel School of Medicine at Dartmouth, Hanover, New Hampshire; [5]Christopher P. Denton, PhD, Anna Gill, MD: Royal Free Campus, London, UK; [6]Jerry Molitor, MD: University of Minnesota, Minneapolis; [7]Virginia D. Steen, MD: MedStar Georgetown University Hospital, Washington, DC; [8]Robert Lafyatis, MD: Pittsburgh University Medical Center, Pittsburgh, Pennsylvania; [9]Robert W. Simms, MD: Boston University School of Medicine, Boston, Massachusetts; [10]Suzanne Kafaja, MD: David Geffen School of Medicine at University of California, Los Angeles; [11]Tracy M. Frech, MD: University of Utah, Salt Lake City; [12]Vivien Hsu, MD: Robert Wood Johnson University, New Brunswick, New Jersey; [13]Robyn T. Domsic, MD: University of Pittsburgh, Pittsburgh, Pennsylvania; [14]Janet E. Pope, MD: University of Western Ontario, London, Ontario, Canada; [15]Jessica K. Gordon, MD: Hospital for Special Surgery, New York, New York; [16]Maureen D. Mayes, MD: University of Texas McGovern Medical School, Houston; [17]Nora Sandorfi, MD: Perelman School of Medicine at the University of Pennsylvania, Pittsburgh; [18]Jane Park, MD: Seattle Rheumatology Associates,

INTRODUCTION

Systemic sclerosis (SSc; scleroderma) is an immune-mediated rheumatic disease characterized by fibrosis of the skin and internal organs and by vasculopathy (1). It has the highest case fatality rate of any rheumatic disease. One subclassification of this disease, diffuse cutaneous SSc (dcSSc), has a 10-year mortality rate of 50% (1). There are no licensed treatments for SSc, and disease management is focused on organ-specific complications (2).

Several published studies support the concept that T cells play a key role in the pathogenesis of dcSSc, including cutaneous disease and at least some of its visceral complications (3–5). Skin biopsy samples obtained from patients with early dcSSc demonstrate a perivascular, mononuclear cell infiltrate comprising T cells and macrophages (3,4). The numbers of T cells have been found to correlate with the degree of skin thickening at the biopsy sites. T cells are the dominant population of lymphocytes in the skin and are activated in SSc. The adaptive immune system gene expression signature in the skin is higher in early dcSSc than in established dcSSc (6). Animal studies support the notion that abatacept (a CTLA4 immunoglobulin fusion protein) could be effective in the management of dcSSc, as it attenuates skin and lung fibrosis in models of scleroderma (7,8). Additionally, a 24-week, placebo-controlled pilot study consisting of 10 participants showed that abatacept was safe (9). When incorporating the molecular gene expression data in skin, 4 of 5 participants with the inflammatory subset of dcSSc showed improvement with abatacept (9).

Based on these observations, we conducted a phase II trial to evaluate weekly subcutaneous (SC) abatacept versus placebo in dcSSc. The primary objectives were to assess the safety of abatacept and its efficacy on skin thickening, as assessed by the modified Rodnan skin thickness score (MRSS), in a 12-month, double-blind study in patients with relatively early disease (≤36 months). We hypothesized that baseline MRSS scores might be lower in patients with early dcSSc (≤18 months) and higher among those with longer disease duration (>18 and ≤36 months) and that the impact of abatacept might differ by duration of disease. We therefore stratified by disease duration, which allowed us to control for disease duration in the overall analysis and also to explore the ability of abatacept to prevent or reverse disease progression in patients with early dcSSc and to reverse established disease in patients with longer disease duration. Our a priori hypothesis was that patients with an inflammatory gene signature would have a statistically significant decline in MRSS over 12 months.

PATIENTS AND METHODS

Study design. This was a phase II, investigator-initiated, randomized, double-blind, placebo-controlled trial of abatacept in patients with dcSSc. DcSSc was defined by the presence of skin thickening, proximal as well as distal, to the elbows or knees with

Seattle, Washington; [19]Faye N. Hant, MD: Medical University of South Carolina, Charleston; [20]Elana J. Bernstein, MD: Columbia University, New York, New York; [21]Soumya Chatterjee, MD: Cleveland Clinic, Cleveland, Ohio; [22]Flavia V. Castelino, MD: Harvard Medical School, Boston, Massachusetts; [23]Ali Ajam, MD: Ohio State University Wexner Medical Center, Columbus; [24]Yannick Allanore, MD, PhD: Hôpital Cochin, Paris, France; [25]Marco Matucci-Cerinic, MD, PhD: University of Florence, Florence, Italy; [26]Oliver Distler, MD: University Hospital Zurich, Zurich, Switzerland; [27]Daniel E. Furst, MD: University of California, Los Angeles.

or without involvement of the face and neck at the time of study entry. Patients were treated for 12 months with double-blind study medication and were offered an additional 6 months of open-label SC abatacept therapy. Patients were telephoned 30 days after the last dose of study drug to discuss any adverse events (AEs) that may have occurred.

The study received an Investigational New Drug Exemption from the Food and Drug Administration. The study protocol was approved by the institutional review board or ethics committee at each participating site (see the Protocol section of the Supplementary Text, available on the *Arthritis & Rheumatology* web site at http://onlinelibrary.wiley.com/doi/10.1002/art.41055/abstract) before research commenced. The study was conducted in accordance with the Declaration of Helsinki and Good Clinical Practice guideline. Written informed consent was obtained from each participant.

Study participation criteria. Key inclusion criteria were 1) age ≥18 years, 2) a diagnosis of SSc (defined by the 2013 American College of Rheumatology/European Union League Against Rheumatism criteria for SSc [10]) and dcSSc (defined by the Criteria for Early SSc [11]), and 3) disease duration of ≤36 months (defined as time from the first non–Raynaud's phenomenon manifestation). For individuals with a disease duration of ≤18 months, an MRSS of ≥10 and ≤35 units was required at the screening visit. For those with a disease duration of >18 to ≤36 months, an MRSS of ≥15 and ≤45 units was required along with one of the following conditions, which must have been observed at screening compared to the patient's last visit in the previous 1–6 months: 1) increase of ≥3 MRSS units, 2) involvement of 1 new body area with increase of ≥2 MRSS units, 3) involvement of 2 new body areas with increase of ≥1 MRSS unit, and/or 4) presence of ≥1 tendon friction rubs.

Oral glucocorticoids (≤10 mg/day of prednisone or equivalent) and nonsteroidal antiinflammatory drugs were permitted if the patient was on a stable dose regimen for ≥2 weeks prior to and at the baseline visit, but no background immunomodulatory therapies were allowed. More details are provided in the Protocol section of the Supplementary Text.

Randomization and blinding. Eligible participants were randomized at a 1:1 ratio to receive either SC abatacept 125 mg or matching placebo (provided by Bristol-Myers Squibb), stratified by duration of dcSSc disease (≤18 months versus >18 to ≤36 months). The first injection was given at the research office, and subsequent study medications were injected weekly at home. The Data Coordinating Center (DCC) at the University of Michigan prepared the randomization schedule, using computer-generated block randomization with random block sizes of 2 and 4 (known only by the DCC). The study staff (including the research pharmacists) and patients were blinded with regard to the treatment assigned.

Procedures. Patients were seen at regular intervals throughout the 12-month study period. Study assessments and their timing are summarized in the study protocol (see the Protocol section of the Supplementary Text, http://onlinelibrary.wiley.com/doi/10.1002/art.41055/abstract). Screening took place within 28 days before randomization. Eligible patients were assessed at baseline; months 1, 3, 6, 9, and 12 in clinic; and by telephone 30 days after the last dose (for those who did not continue into the open-label period).

Escape therapy with immunomodulatory agents was permitted as add-on therapy to study medications due to worsening of dcSSc starting at month 6 (Protocol section of the Supplementary Text). The decision to initiate escape therapy was based on investigator discretion. No biologic agents were allowed as escape therapy.

Outcome measures. The primary outcome measure was change in MRSS at 12 months. The same assessor performed the MRSS measurement at each time point during the trial. Live demonstration and standardization of the MRSS for the trial occurred during an investigator meeting prior to study initiation, at which it was agreed upon that the average score at each anatomic site would be used (12). Secondary outcome measures included 1) change in MRSS from baseline to months 1, 3, 6, and 9; 2) change from baseline to months 1, 3, 6, 9, and 12 in the swollen and tender joint counts in 28 joints; 3) change from baseline to months 3, 6, and 12 in the patient global assessment (PtGA) and physician global assessment (PhGA) for overall disease, the Patient-Reported Outcomes Measurement Information System 29-Item Profile, the Health Assessment Questionnaire disability index (HAQ DI), Scleroderma HAQ DI visual analog scale (VAS; which assesses pain, burden of digital ulcers, Raynaud's phenomenon, gastrointestinal involvement, breathing, and overall disease), and the University of California Los Angeles Gastrointestinal Tract 2.0 Questionnaire; and 4) change from baseline to months 6 and 12 in forced vital capacity percent predicted (FVC %), and the American College of Rheumatology Combined Response Index in diffuse cutaneous Systemic Sclerosis (ACR CRISS; a composite end point that captures cardiovascular/pulmonary/renal involvement and change in MRSS, HAQ DI, PtGA, PhGA, and FVC %).

The exploratory end points included 1) change from baseline to months 3, 6, and 12 in interference in the patient's physical functioning related to skin involvement and pain intensity due to SSc over the previous week on a 0–150 mm VAS; 2) proportion of patients with cardiac involvement, significant interstitial lung disease (ILD), and new renal crisis at 12 months; 3) change from baseline in body mass index and digital ulcer burden at 12 months; and 4) change from baseline to months 6 and 12 in % predicted diffusing capacity for carbon monoxide (corrected for hemoglobin) and FVC (ml).

Safety end points were 1) proportion of patients experiencing AEs; 2) incidence of AEs, serious AEs (SAEs), and AEs of special interest; 3) treatment discontinuation due to AEs; and 4) changes in clinical laboratory test results, vital signs, and physical examination results over time. The study was overseen by a Data and Safety Monitoring Committee that reviewed study conduct and safety outcomes approximately every 6 months.

RNA sequencing, read alignment, and gene expression calculation. Skin biopsy specimens measuring 3 mm were obtained from the involved forearm skin at each site, at baseline and at months 3 and 6. Biopsy specimens were stored in RNAlater and processed for RNA, as previously reported (13). Machine learning was used to classify biopsy specimens into intrinsic gene expression subsets. RNA-Seq data (reads per kilobase per million) were normalized, and baseline skin samples were classified into inflammatory, normal-like, or fibroproliferative intrinsic gene expression subsets (13). Details on the methodology are available in the Supplementary Methods at http://onlinelibrary.wiley.com/doi/10.1002/art.41055/abstract.

Statistical analysis. The size of the study population was based on practical considerations rather than a desired power for a prespecified difference. We planned to screen 121 patients and select 86 participants to randomize. With this sample size, we calculated that we could detect an effect size of at least 0.66 in the primary end point with 80% power, assuming a 5% 2-sided Type I error and a dropout rate of 15% (2-sample t-test; East software version 5.4). This effect size translates into a treatment difference in change in the MRSS from baseline to month 12 of 5.3, with an SD of 8 points (14). Sample sizes that were used in the detection of minimally important clinical differences of end points in previously published studies on dcSSc are detailed in the Supplementary Methods, available on the *Arthritis & Rheumatology* web site at http://onlinelibrary.wiley.com/doi/10.1002/art.41055/abstract, and provide context on the sample size needed for a confirmatory study.

The main analysis set for efficacy was the modified intent-to-treat (mITT) population, defined as all participants who were randomized to receive at least 1 dose of study medication. We analyzed the primary end point using a linear mixed model as described in Supplementary Methods. Escape therapy after 6 months was an indication of treatment failure; therefore, we censored primary end point data after initiation of escape therapy. In an additional sensitivity analysis, we applied the same model using all MRSS values (i.e., no censoring after escape therapy). Adjusted least squares means (LSMs), SEMs, 95% confidence intervals (95% CIs), and 2-sided P values for between-treatment comparisons are provided. Safety outcomes are summarized by treatment group using descriptive statistics (no tests were performed).

Analyses of all secondary end points utilized the same approach used for the primary end point, except for the ACR CRISS, for which a nonparametric approach was used (detailed in Supplementary Methods, available at http://onlinelibrary.wiley.com/doi/10.1002/art.41055/abstract). No adjustments for multiplicity were made; thus, P values for secondary and exploratory outcomes should be interpreted with caution. The Supplementary Methods also provide the analysis approach for gene signature data. The full statistical analysis plan was finalized before unblinding. All statistical analyses were performed using SAS software version 9.4.
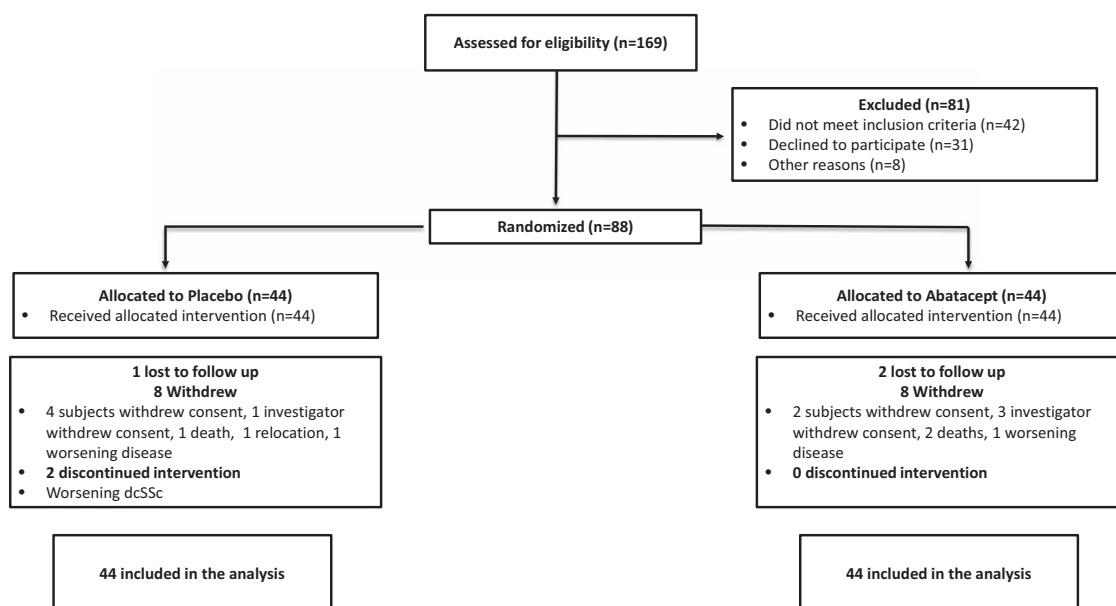
Figure 1. Flow chart showing the disposition of study participants.

Table 1. Demographic and baseline disease characteristics of the study patients*

	Overall (n = 88)	Placebo (n = 44)	Abatacept (n = 44)
Age, years	49 ± 13	49 ± 13	50 ± 12
Women, no. (%)	66 (75)	35 (80)	31 (70)
White, no. (%)	72 (82)	37 (84)	35 (80)
Not Hispanic or Latino, no. (%)	76 (86)	36 (82)	40 (91)
Disease duration, years†	1.59 ± 0.81	1.52 ± 0.79	1.66 ± 0.84
Disease duration ≤18 months, no. (%)	53 (60)	27 (61)	26 (59)
MRSS	22.45 ± 7.65	21.57 ± 7.33	23.34 ± 7.95
FVC % predicted	85.4 ± 15.10	86.5 ± 16.60	84.2 ± 13.50
Predicted DLco, corrected for Hgb	78.0 ± 18.24	76.5 ± 18.44	79.6 ± 18.12
PtGA, theoretical range 0–10	4.09 ± 2.38	4.31 ± 2.56	3.88 ± 2.21
HAQ DI, theoretical range 0–3	1.05 ± 0.71	0.97 (0.70)	1.14 (0.72)
PhGA, theoretical range 0–10	4.77 ± 1.67	4.76 ± 1.67	4.77 ± 1.67
Tendon friction rubs, no. (%)	32 (36)	13 (30)	19 (43)
Large joint contractures, no. (%)	63 (72)	32 (73)	31 (70)
Swollen joints, theoretical range 0–28	3.75 ± 5.70	3.86 ± 5.85	3.64 ± 5.62
Proportion of participants with ≥1 swollen joints, no. (%)	42 (48)	21 (48)	21 (48)
Use of prednisone, no. (%)	12 (14)	5 (11)	7 (16)
Prednisone dose, mg/day	7.9 ± 2.6	7.0 ± 2.7	8.6 ± 2.4

* Except where indicated otherwise, values are the mean ± SD. MRSS = modified Rodnan skin thickness score; FVC % predicted = forced vital capacity percent predicted; DLco = diffusing capacity for carbon monoxide; Hgb = hemoglobin; PtGA = patient global assessment; HAQ DI = Health Assessment Questionnaire disability index; PhGA = physician global assessment.
† Disease onset was defined as first non–Raynaud's sign or symptom.

RESULTS

Patient screening, enrollment, and continuation in the study. A total of 169 patients were screened for eligibility, and 88 were randomized to receive abatacept or placebo (44 in each treatment group) at 22 centers in the US, Canada, and the UK between September 22, 2014 and March 15, 2017 (Figure 1). Thirty-four patients in the abatacept group (77%) and 35 in the placebo group (80%) completed the 12-month trial. At 12 months, 7 patients in the abatacept group (16%) and 16 patients in the placebo group (36%) received escape therapy for worsening dcSSc (Supplementary Table 1, available on the *Arthritis & Rheumatology* web site at http://online library.wiley.com/doi/10.1002/art.41055/abstract). Eighty-eight patients were included in the mITT and safety analyses and 85 in the per-protocol analysis (43 in the abatacept group and 42 in the placebo group). A similar number of patients withdrew in each group. In the abatacept group, 10 patients withdrew due to the following reasons: investigator withdrew consent (n = 3), patient withdrew consent (n = 2), lost to follow-up (n = 2), death (n = 2), and worsening dcSSc (n = 1). In the placebo group, 9 patients withdrew due to the following reasons: investigator withdrew consent (n = 1), patient withdrew consent (n = 4), lost to follow-up (n = 1), death (n = 1), relocation (n = 1), and worsening dcSSc (n = 1). Compliance with the study drug was >98% (1 patient in the placebo group had a compliance of <80%). The median estimated duration of study medication exposure was 10.7 months (interquartile range [IQR] 5.2–11.1 months) in the abatacept group and 10.6 months (IQR 9.1–10.8 months) in the placebo group. The demographic and baseline disease characteristics were similar between treatment groups (Table 1).

Efficacy. Findings for the primary outcome measure did not differ significantly between the abatacept and placebo groups (LSM ± SEM change in MRSS –6.24 ± 1.14 and –4.49 ± 1.14, respectively with a treatment difference of –1.75 [95% CI –4.93, 1.43]) (Table 2 and Figure 2). Sensitivity analyses using the per-protocol population and incorporating all values after escape therapy in the mITT population showed comparable results (Table 2). There were also no statistically significant differences in MRSS change at months 1, 3, 6, and 9 (Supplementary Table 2, available on the *Arthritis & Rheumatology* web site at http://onlinelibrary.wiley.com/doi/10.1002/art.41055/abstract).

There were statistically significant and clinically meaningful treatment differences in LSM improvements in the HAQ DI at 12 months (–0.28; *P* = 0.005) (Table 2). There were no significant differences between the abatacept and placebo groups at 12 months in the swollen joint counts (LSM ± SEM 0.75 ± 0.84; *P* = 0.37) and tender joint counts (LSM ± SEM 0.76 ± 1.28; *P* = 0.55). There was statistically significant and clinically meaningful improvement in a new composite index, the ACR CRISS, that showed evidence in support of abatacept. The median change at 12 months in the ACR CRISS score was 0.72 (IQR 0.99) versus 0.02 (IQR 0.75) (*P* = 0.03) with the proportion of patients whose score improved by ≥0.60 (the clinically meaningful cutoff point [15]) significantly higher in the abatacept group compared to the placebo group (62.8%

Table 2. Changes from baseline to month 12 in primary and secondary efficacy end points in patients with diffuse cutaneous systemic sclerosis*

Efficacy end points	Placebo (n = 44)†	Abatacept (n = 44)†	Abatacept − placebo, LSM (95% CI)
Primary analysis of the mITT population with values censored after escape therapy	−4.49 ± 1.14	−6.24 ± 1.14	−1.75 (−4.93, 1.43)
Sensitivity analysis 1 of the per-protocol population with values censored after escape therapy	−4.63 ± 1.15	−6.25 ± 1.13	−1.62 (−4.79, 1.55)
Sensitivity analysis 2 of the mITT population with values not censored after escape therapy	−4.22 ± 1.04	−6.64 ± 1.10	−2.42 (−5.38, 0.54)
Secondary end point			
PtGA (0–10)‡	−0.09 ± 0.46	−0.31 ± 0.42	−0.22 (−1.45, 1.01)
PhGA (0–10)‡	−0.35 ± 0.32	−1.30 ± 0.29	−0.95 (−1.80, −0.10)§
FVC %	−4.13 ± 1.22	−1.34 ± 1.24	2.79 (−0.69, 6.27)
FVC (ml)	−121.6 ± 46.39	−36.39 ± 43.82	85.21 (−42.75, 213.16)
HAQ DI (0–3)‡	0.11 ± 0.07	−0.17 ± 0.07	−0.28 (−0.47, −0.09)¶
Scleroderma HAQ‡			
Overall VAS (0–150)	3.52 ± 6.05	−7.42 ± 5.64	−10.94 (−27.27, 5.38)
Breathing VAS (0–150)	16.95 ± 5.85	9.30 ± 5.51	−7.65 (−23.60, 8.30)
Raynaud's VAS (0–150)	−3.64 ± 7.17	7.58 ± 6.60	11.22 (−8.04, 30.47)
Digital ulcers VAS (0–150)	8.67 ± 5.52	−3.18 ± 5.13	−11.85 (−26.70, 3.01)
Gastrointestinal VAS (0–150)	8.01 ± 6.42	9.98 ± 6.00	1.96 (−15.40, 19.33)
Swollen joint count (0–28)‡	−0.86 ± 0.60	−0.11 ± 0.60	0.75 (−0.91, 2.41)
Tender joint count (0–28)‡	−1.47 ± 0.91	−0.71 ± 0.90	0.76 (−1.75, 3.27)
PROMIS-29			
Physical function	−0.17 ± 0.69	−1.54 ± 0.65	−1.36 (−3.23, 0.50)
Anxiety‡	−1.09 ± 1.37	−3.50 ± 1.31	−2.41 (−6.15, 1.32)
Depression‡	−0.41 ± 1.20	−0.02 ± 1.13	0.39 (−2.86, 3.64)
Fatigue‡	−0.98 ± 1.36	−0.65 ± 1.29	0.33 (−3.37, 4.03)
Sleep disturbance‡	−0.21 ± 0.62	−0.31 ± 0.57	−0.10 (−1.76, 1.57)
Pain interference‡	−1.56 ± 1.22	−4.10 ± 1.13	−2.53 (−5.81, 0.74)
Social roles‡	−1.26 ± 1.14	−1.11 ± 1.07	0.15 (−2.93, 3.24)
Pain intensity (0–10)‡	−0.18 ± 0.33	−0.72 ± 0.32	−0.54 (−1.44, 0.37)
UCLA GIT 2.0 total score (0.00–2.83)‡	0.05 ± 0.050	0.07 ± 0.047	0.12 (−0.01, 0.26)
ACR CRISS at 12 months, median (IQR)	0.02 (0.75)	0.72 (0.99)#	–

* For primary and sensitivity analyses, the estimates and *P* values are from a linear mixed model with treatment group, month (3, 6, 9, and 12), treatment group × month interaction, and baseline MRSS as fixed effects and study patient as a random effect. For secondary analyses, the estimates and *P* values are from a linear mixed model with treatment group, month, treatment group × month interaction, duration of dcSSc (≤18 versus >18–≤36 months), and baseline variable as fixed effects and study patient as a random effect. The modified intent-to-treat (mITT) population includes all of the randomized patients who received at least 1 dose of study medication. The per-protocol population includes mITT patients who did not experience a major protocol deviation, defined as eligibility criteria violations for which no exemption was granted, study drug compliance of <80% and >120%, and initiation of escape medication prior to month 3. LSM = least squares mean; 95% CI = 95% confidence interval; VAS = visual analog scale; PROMIS-29 = Patient-Reported Outcomes Measurement Information System 29-Item Profile; UCLA GIT 2.0 = University of California Los Angeles Gastrointestinal Tract 2.0 Questionnaire; IQR = interquartile range (see Table 1 for other definitions).
† Except where indicated otherwise, values are the LSM ± SEM.
‡ Higher score denotes worse symptoms.
§ *P* = 0.03 (not adjusted for multiplicity).
¶ *P* = 0.005 (not adjusted for multiplicity).
# *P* = 0.03 versus placebo, by Van Elteren test with adjustment for duration of diffuse cutaneous systemic sclerosis (dcSSc). Five participants in each group had cardiopulmonary-renal involvement and were given a probability score of 0.0. Multiple imputation was used to address missing follow-up data in MRSS, FVC % predicted, HAQ DI, PtGA, and PhGA, allowing calculation of American College of Rheumatology Combined Response Index in diffuse cutaneous Systemic Sclerosis (ACR CRISS) scores.

versus 37.2%; *P* = 0.01 by Cochran-Mantel-Haenszel test with adjustment for dcSSc duration). Other secondary outcomes are presented in Table 2 and Supplementary Table 2.

In analyses of exploratory end points, the proportion of patients with a decrease in MRSS of ≥5 units (a clinically important improvement [16]) was similar in both groups (Supplementary Table 3, available on the *Arthritis & Rheumatology* web site at http://onlinelibrary.wiley.com/doi/10.1002/art.41055/abstract). When the change in MRSS at 12 months was evaluated by disease duration (≤18 months versus >18–≤36 months) in an ad hoc analysis, numerically greater treatment effects were seen in early disease (n = 53) than in later disease (n = 35). LSM changes in
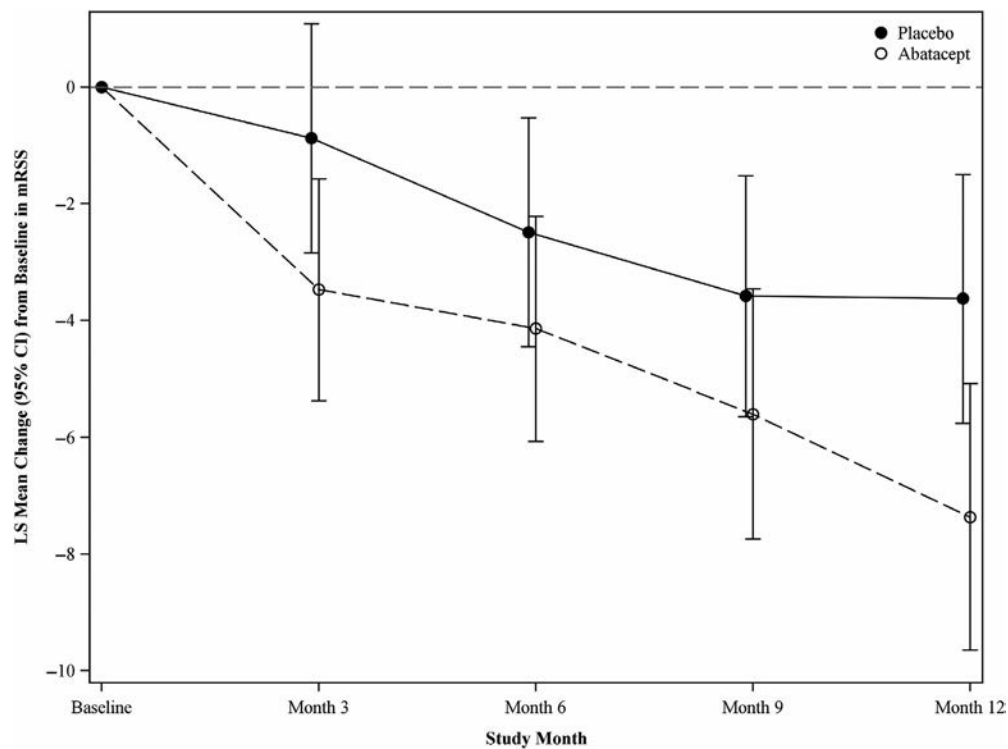
Figure 2. Change in modified Rodnan skin thickness score (MRSS) over a 12-month period in patients with diffuse cutaneous systemic sclerosis who received abatacept or placebo (modified intent-to-treat population). LS = least squares; 95% CI = 95% confidence interval.

MRSS in the abatacept group were –5.71 units and –6.62 units in the early and later disease groups, respectively, while in the placebo group, they were –2.98 units and –6.18 units. This resulted in an LSM treatment difference of –2.73 (95% CI –6.57, 1.11) in early disease and –0.44 (95% CI –6.10, 1.11) in later disease (*P* = 0.16 and *P* = 0.88, respectively).

A total of 23 patients (26%) needed escape therapy for worsening dcSSc, with a larger proportion needing escape therapy in the placebo group (16 [36%]) than in the abatacept group (7 [16%]). The reasons for escape therapy included worsening skin (8 in the placebo group and 4 in the abatacept group), worsening ILD (2 in placebo), polyarthritis (3 in placebo), and overall worsening disease (4 in placebo and 4 in abatacept). There was no increase in infections among those who received escape therapy and continued receiving abatacept (1 event; 0.4 person-year) versus those who did not receive escape therapy (27 events; 0.8 person-year). In comparison, patients who received placebo and started receiving escape therapy had 3 events (0.6; person-year) versus 40 events (1.2; person-year) among those who did not receive escape therapy.

Gene expression in skin biopsy specimens from 84 patients (43 in the abatacept group and 41 in the placebo group) was analyzed in 84 patients at baseline (43 in the abatacept group and 41 in the placebo group). No systemic biases were found related to collection site, time of biopsy, or the RNA-Seq analysis. Intrinsic gene expression subset (e.g., inflammatory, normal-like, fibroproliferative) was assigned using a machine learning classi-

fier before the unblinding of the study. At baseline, 33 patients (39%) were classified as having the inflammatory subtype, 33 (39%) as having the normal-like subtype, and 18 (21%) as having the fibroproliferative subtype. Patients with early disease were more likely to be in the inflammatory subset (21 of 33; 64%) or the normal-like subset (23 of 33; 70%) than the fibroproliferative subset (7 of 18; 39%). There were no significant differences between the distribution of intrinsic gene expression subsets at baseline in each treatment arm (Supplementary Table 4, available on the *Arthritis & Rheumatology* web site at http://onlinelibrary. wiley.com/doi/10.1002/art.41055/abstract). The LSM change in MRSS over 12 months was significantly different between the abatacept and placebo groups for the inflammatory and normal-like subsets (*P* < 0.001 and *P* = 0.03, respectively) (Figure 3 and Supplementary Table 5, available on the *Arthritis & Rheumatology* web site at http://onlinelibrary.wiley.com/doi/10.1002/art.41055/ abstract), but there was no difference in the fibroproliferative subset (*P* = 0.47). In the abatacept arm, the fibroproliferative subset showed a numerical increase in FVC % predicted (*P* = 0.19) while FVC % predicted decreased in the other 2 subsets. All gene expression subgroups showed numerical decreases in the HAQ DI in the abatacept arm that were not observed in the placebo arm.

Safety. Abatacept was found to be generally safe with no new safety signals and a lower number of patients experiencing AEs, infectious AEs, and SAEs compared to the placebo group
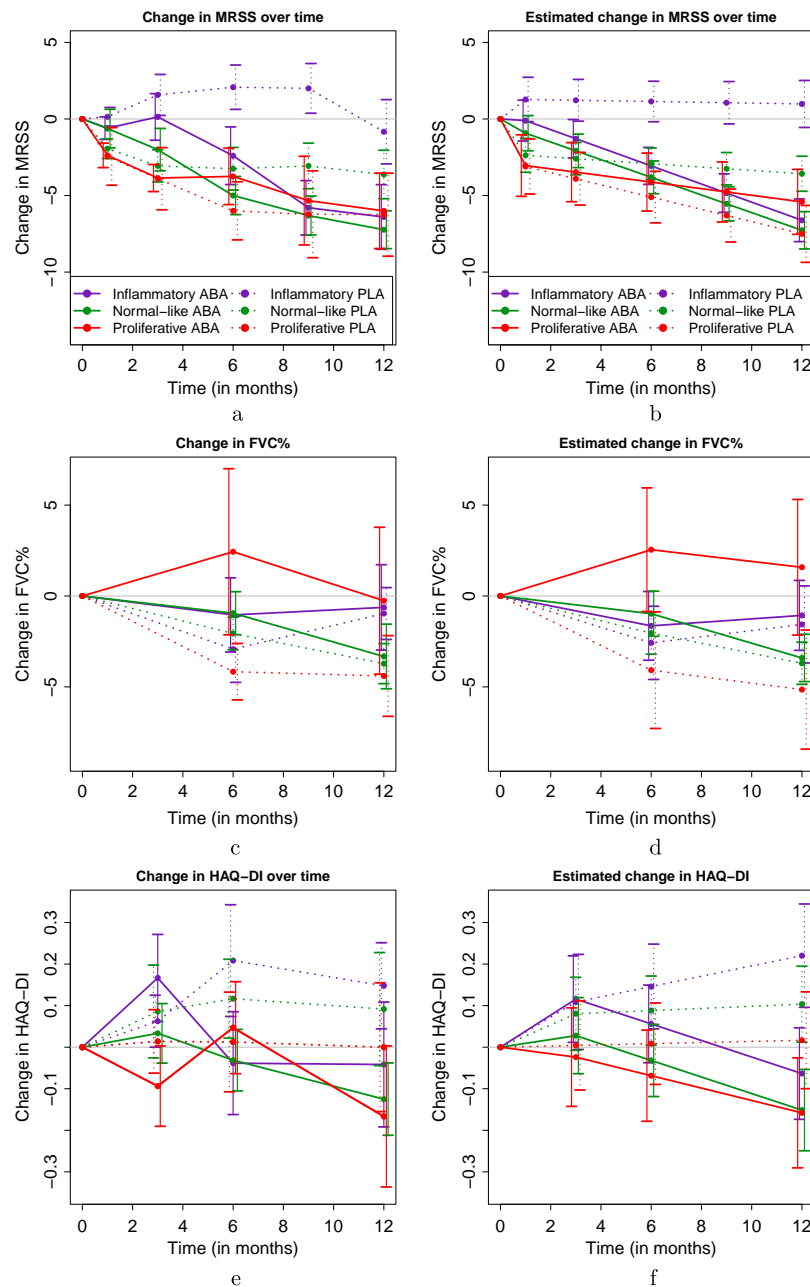
Figure 3. Observed average change from baseline in the modified Rodnan skin thickness score (MRSS) (**a**), forced vital capacity percent predicted (FVC %) (**c**), and Health Assessment Questionnaire disability index (HAQ DI) (**e**) and estimated average change from baseline in the MRSS (**b**), FVC % (**d**), and HAQ DI (**f**) in the placebo (PLA) and abatacept (ABA) groups and in the 3 intrinsic gene expression subsets (inflammatory, normal-like, and proliferative). Estimates were obtained from a linear mixed model fitted to the change from baseline in MRSS, FVC %, and HAQ DI, respectively, with the following predictors: MRSS, FVC %, and HAQ DI at baseline; month in the study; treatment group; interaction of treatment group and month; and a subject-specific random effect. Values are the mean ± 1 SEM.

(Table 3). In the placebo group, 27% of the patients experienced SAEs versus 20% in the abatacept group. These included more noninfectious SAEs in the placebo group compared to the abatacept group (23% versus 16%) and the same proportion of infectious SAEs in both groups (5%). Additionally, more patients in the placebo group withdrew from the study due to AEs (6 [14%]) compared to the abatacept group (5 [11%]). Renal crisis occurred in 3 patients in the abatacept group (days 11, 25, and 46 after

initiation of study medication) versus 1 patient in the placebo group (day 56 after initiation of study medication). The number of patients with treatment-emergent AEs by severity grade was similarly distributed between the 2 treatment groups, with a total of 36 (82%) in the abatacept group and 40 (91%) in the placebo group experiencing an AE (Supplementary Table 6, available on the *Arthritis & Rheumatology* web site at http://onlinelibrary.wiley.com/doi/10.1002/art.41055/abstract). There were no cases of

Table 3. Adverse events among study patients*

	Placebo (n = 44)	Abatacept (n = 44)
Participants with ≥1 AE, no. (%)	40 (91)	35 (80)
Participants with ≥1 infectious AE, no. (%)	25 (57)	19 (43)
Withdrawal because of an AE, no. (%)	6 (14)	5 (11)
Participants with ≥1 SAE, no. (%)	12 (27)	9 (20)
Participants with specific SAEs		
Infections and infestations		
Cellulitis	–	1
Mastoiditis	–	1
Paronychia	1	–
Pneumonia	1	–
Cardiac disorders		
Atrial flutter with conduction defects	1	–
Cardiac arrest	1	–
Congestive heart failure	1	–
Myocardial infarction/acute coronary syndrome	1	1
Pulmonary arterial hypertension	1	1
Pericardial effusion	–	1
Gastrointestinal disorders		
Anemia	1	–
Cholecystitis	1	–
Dysphagia	1	1
Erosive esophagitis	1	–
Gastric antral vascular ectasia	1	–
Gastric antral vascular ectasia with anemia	1	–
Melena	–	1
Pseudoobstruction	–	1
Neoplasm disorders		
Basal cell skin carcinoma	1	–
Squamous cell skin carcinoma	–	1
Respiratory disorders		
Respiratory failure	–	1
Renal disorders		
Scleroderma renal crisis	1	3
Vascular disorders		
Digital ischemia	1	–
Mental disorders		
Depression with suicidal ideation	1	–

* Some patients experienced ≥1 serious adverse event (SAE) during the course of the study.

tuberculosis during the trial. No significant laboratory abnormalities were noted; 1 patient in each group had a hemoglobin decline of >2 gm/dl related to dcSSc (among patients with baseline values ≥8 gm/dl). There were 20 AEs of special interest in the abatacept group and 26 in the placebo group, including 1 injection site reaction in the abatacept group (Supplementary Table 7, available on the *Arthritis & Rheumatology* web site at http://onlinelibrary.wiley.com/doi/10.1002/art.41055/abstract).

Three deaths occurred in the study. One patient died due to cardiac arrest 310 days after starting the study medication (placebo); this death was not considered to be related to the study medication. Two patients in the abatacept group experienced scleroderma renal crisis leading to death; of these 2 patients, 1 died on day 11 after randomization due to renal crisis (which was considered to not be related to the study medication), leading to respiratory failure (which was considered to be related to the study medication). The second patient was admitted to the hospital due to gastrointestinal dysmotility and myositis on day 25 and then experienced renal crisis on day 46; both were considered to be not related to the study medication.

DISCUSSION

In this phase II trial, we showed that abatacept is well-tolerated in early dcSSc. Although a statistically significant treatment difference in the primary efficacy end point (change from baseline in the MRSS at 12 months) was not achieved, there were clinically meaningful and statistically significant differences in HAQ DI (a measure of function) and ACR CRISS results. In addition, a larger proportion of patients who received placebo needed immunomodulatory escape therapy compared to those who received abatacept, further supporting the favorable impact of abatacept. In addition, this is the first prospective trial showing that intrinsic gene expression subsets can predict clinical outcome measures with greater precision.

Skin involvement was chosen as the primary outcome measure as it is an important concern for patients due to its relationship to disability caused by small and large joint contractures, pruritus, and allodynia (17). Skin thickness, as assessed by the MRSS, is a feasible, reliable, valid outcome measure and is sensitive to change (12). In addition, the MRSS is utilized by scleroderma physicians to assess for worsening and improvement of skin involvement (1). In early disease, skin involvement is a surrogate for internal organ involvement and mortality (18,19). Because of this, the MRSS has been incorporated as the primary end point in early SSc trials (20). However, the absence of a statistically significant result in the current trial is similar to recently published and presented data from studies on anti–interleukin-6 receptor in the treatment of SSc (20,21). The current results occurred despite recruitment of a study population with early disease (mean disease duration 1.59 years); 60% of patients were recruited within 18 months of diagnosis, and only a small proportion received background immunosuppressive therapy. There was a significant heterogeneity in MRSS trajectory over the 12-month study period (Supplementary Table 3, available on the *Arthritis & Rheumatology* web site at http://onlinelibrary.wiley.com/doi/10.1002/art.41055/abstract) (22,23), which is likely driven by autoantibodies (24) and skin gene expression profile (25).

The HAQ DI, which improved significantly with abatacept treatment, is a validated measure of function in SSc (26), and numerical improvements in other patient-reported outcome measures were seen as well (although many did not achieve clinically meaningful thresholds). These changes are important, as they directly address the Food and Drug Administration (FDA) mandate on assessing how a patient feels, functions, and survives (FDA Code of Federal Regulations, Title 21). The efficacy of abatacept

is also suggested by the lower proportion of the abatacept group who needed escape therapy for worsening dcSSc relative to the placebo group (16% versus 36%). These data should be interpreted with caution as no adjustments for multiplicity were made.

In addition, there were statistically significant and clinically meaningful improvements in a new composite index, the ACR CRISS (15), that showed evidence in support of abatacept. The ACR CRISS was designed to capture the global or holistic evaluation of the likelihood of improvement in early SSc. It is based on a probability score of 0.0 to 1.0 (no improvement to marked improvement, respectively, with an improvement of ≥0.60 considered clinically meaningful) and includes 2 steps. Step 1 assesses for worsening or incident cases of cardiopulmonary-renal involvement and assigns a score of 0.0. For those who do not meet the criteria for step 1, a probability score is calculated that incorporates changes in 5 physical or functional areas: MRSS (assessment of skin), FVC % predicted (assessment of lungs), HAQ DI (measure of patient function), PtGA, and PhGA. The median change in the ACR-CRISS score was 0.72 (IQR 0.99) with abatacept versus 0.02 (IQR 0.75) with placebo ($P = 0.03$), with the proportion of patients who improved by ≥0.60 significantly higher in the abatacept group. These results are similar to recent data from a phase III trial of tocilizumab (21) and highlight the importance of global assessment in a multisystem heterogeneous disease.

Study patients who received placebo experienced a greater number of AEs, AEs leading to discontinuation, and SAEs, which highlights the safety of abatacept in SSc when compared to those who received abatacept and other immunomodulatory therapies. These data are supported by findings from studies on other rheumatic diseases in which abatacept has been used with immunosuppressive therapy (27,28).

There were 3 deaths in the trial: 2 in the abatacept group and 1 in the placebo group. Both deaths in the abatacept group were related to scleroderma renal crisis, a challenging complication in early SSc. There was 1 additional case of scleroderma renal crisis in the abatacept group that did not result in death. All 3 cases occurred early in the disease (11–46 days after randomization), while the 1 case in the placebo group occurred 56 days after randomization. Inhibition of Treg cell function prior to reduction in the numbers and activity of pathogenic effector T cells in abatacept-treated patients could account for early flares but could also lead to eventual reduction in disease activity in SSc (29,30), though data are needed to validate this hypothesis.

In a prior pilot study of abatacept in SSc with molecular gene expression data obtained from skin (9), 4 of 5 patients who showed improvement with abatacept (as determined by change in MRSS) were in the inflammatory subset, and the remaining patient who showed improvement was in the normal-like subset. Improvement was accompanied by a decrease in gene expression for immune pathways, including the CD28 and CTLA-4 receptors targeted by abatacept. In this trial, we were able to test and support our a priori

hypothesis that patients in the inflammatory subset would show a significant decline in MRSS during abatacept therapy. The results are especially interesting and novel considering the likely mechanism of action of abatacept as a targeted immunomodulator. On this basis, it would be expected that patients showing the inflammatory gene signature would be the most likely to exhibit treatment effect in the skin (Figure 3). The most prominent difference in MRSS changes, as seen in both the actual and estimated plots in Figure 3, occurred among patients in the inflammatory subset. There was a marked (and statistically significant) divergence of trajectory of MRSS change among patients in the inflammatory subset compared to the other intrinsic subsets, and no apparent effect of abatacept on the fibroproliferative subgroup (Supplementary Table 5, available on the *Arthritis & Rheumatology* web site at http://onlinelibrary.wiley.com/doi/10.1002/art.41055/abstract).

In contrast, for FVC change, which may reflect lung fibrosis (31), only the fibroproliferative subset showed trends in support of abatacept. This provides evidence of differing potential molecular pathology between the skin and lung in SSc and is consistent with the impact of abatacept on different disease features at different sites. It is also notable that the MRSS is improved by abatacept, whereas for FVC the apparent impact in patients in the fibroproliferative subset is to prevent decline. These data are consistent with results from a pilot study of abatacept (9), and they extend these findings, for the first time, to a large placebo-controlled trial that shows intrinsic skin gene expression subsets may predict differential response to a targeted biologic therapy. This has implications for stratification of cases according to intrinsic gene expression subsets, which would in turn maximize the number of informative SSc cases in clinical trials as well as potentially for future clinical practice.

Our study has many strengths. First, it was conducted at centers with substantial experience in scleroderma, and we were able to recruit patients with early active disease. Second, despite a large proportion of patients who received escape therapy (26%), we made every effort to continue follow-up of these patients in the trial and capture actual data. Third, we continued to build a body of evidence on the potential utility of the ACR CRISS as a primary end point that can be used as an alternative to changes in skin thickness, given the number of SSc studies using MRSS as the primary end point that have yielded negative results. Use of the ACR CRISS is also supported by statistically significant results of the proof-of-concept trial on lenabasum, in which the ACR CRISS was the primary outcome measure (32) and post hoc and planned analyses performed using data from phase II and III trials on tocilizumab, in which study medication could not be differentiated from placebo when the MRSS was the primary outcome measure (21,33). Last, one of the novel aspects of this study was the ascertainment of intrinsic gene expression–based subsets (inflammatory, fibroproliferative, or normal-like) at baseline that could be integrated into a subgroup analysis for potential treatment effect.

Study limitations include the lack of trials in early dcSSc with positive results, which could have provided guidance for the sample size calculation, and missing data, which we addressed using mixed models and multiple imputation (both valid under the missing at random assumption). We did not adjust for multiple comparisons or control for Type I error with secondary and exploratory end points; thus, we cannot make definitive statements about these outcomes, which should be considered hypothesis-generating. In deriving conclusions for our study, we considered both the clinical importance of abatacept effects, the totality of the study data, and the literature on other biologics in SSc. We allowed background low-dose prednisone at study entry (as done universally in trials of early SSc), and 14% of study patients were taking low-dose prednisone at baseline visit. The impact of background prednisone on skin gene expression data is unknown and should be explored in future analyses. We have not reported data on autoantibodies and their relationship to outcome measures, but we plan to perform these analyses in a central laboratory in the near future. Finally, although the patients in our study are representative of other recent trials in early dcSSc, they may differ from patients seen in clinics (34).

In summary, abatacept was well-tolerated in the present study, but change in MRSS was not statistically significant. Secondary outcome measures showed some evidence in favor of abatacept. A phase III trial should be conducted before drawing definitive conclusions about the efficacy and safety of abatacept in dcSSc.

ACKNOWLEDGMENTS

We wish to thank the participants, study coordinators, statistical analysts (Haoyan Zhong and Richard McLain), and the Data Safety Monitoring Board (Donald Tashkin, MD, Chair, University of California at Los Angeles; Thomas Medsger, Jr., MD, University of Pittsburgh, Pittsburgh, Pennsylvania; and Robert Parker, ScD: Massachusetts General Hospital, Boston).

AUTHOR CONTRIBUTIONS

All authors were involved in drafting the article or revising it critically for important intellectual content, and all authors approved the final version to be published. Dr. Khanna had full access to all of the data in the study and takes responsibility for the integrity of the data and the accuracy of the data analysis.
Study conception and design. Khanna, Spino, Chung, Whitfield, Denton, Mehta, Molitor, Kafaja, Mayes, Hant, Matucci-Cerinic, Fox, Furst.
Acquisition of data. Khanna, Spino, Johnson, Chung, Whitfield, Denton, Mehta, Molitor, Steen, Lafyatis, Simms, Gill, Kafaja, Frech, Hsu, Domsic, Pope, Gordon, Mayes, Schiopu, Young, Sandorfi, Park, Hant, Bernstein, Chatterjee, Castelino, Ajam, Wang, Wood, Matucci-Cerinic, Distler, Bush, Fox, Furst.
Analysis and interpretation of data. Khanna, Spino, Chung, Whitfield, Denton, Berrocal, Franks, Mehta, Lafyatis, Kafaja, Pope, Schiopu, Hant, Castelino, Wang, Allanore, Matucci-Cerinic, Distler, Singer, Bush, Fox, Furst.

ROLE OF THE STUDY SPONSOR

REFERENCES

1. Denton CP, Khanna D. Systemic sclerosis. Lancet 2017;390:1685–99.

2. Kowal-Bielecka O, Fransen J, Avouac J, Becker M, Kulak A, Allanore Y, et al. Update of EULAR recommendations for the treatment of systemic sclerosis. Ann Rheum Dis 2017;76:1327–39.

3. Kalogerou A, Gelou E, Mountantonakis S, Settas L, Zafiriou E, Sakkas L. Early T cell activation in the skin from patients with systemic sclerosis. Ann Rheum Dis 2005;64:1233–5.

4. Roumm AD, Whiteside TL, Medsger TA Jr, Rodnan GP. Lymphocytes in the skin of patients with progressive systemic sclerosis: quantification, subtyping, and clinical correlations. Arthritis Rheum 1984;27:645–53.

5. Fleischmajer R, Perlish JS, Reeves JR. Cellular infiltrates in scleroderma skin. Arthritis Rheum 1977;20:975–84.

6. Assassi S, Khanna D, Hinchcliff M, Steen VD, Hant F, Gordon JK, et al. Cell type specific gene expression analysis of early systemic sclerosis skin shows a prominent activation pattern of innate and adaptive immune system in the Prospective Registry for Early Systemic Sclerosis (PRESS) cohort [abstract]. Arthritis Rheumatol 2017;69 Suppl 10. URL: https://acrabstracts.org/abstract/cell-type-specific-gene-expression-analysis-of-early-systemic-sclerosis-skin-shows-a-prominent-activation-pattern-of-innate-and-adaptive-immune-system-in-the-prospective-registry-for-early-system/.

7. Ponsoye M, Frantz C, Ruzehaji N, Nicco C, Elhai M, Ruiz B, et al. Treatment with abatacept prevents experimental dermal fibrosis and induces regression of established inflammation-driven fibrosis. Ann Rheum Dis 2016;75:2142–9.

8. Boleto G, Guignabert C, Pezet S, Cauvet A, Sadoine J, Tu L, et al. T-cell costimulation blockade is effective in experimental digestive and lung tissue fibrosis. Arthritis Res Ther 2018;20:197.

9. Chakravarty EF, Martyanov V, Fiorentino D, Wood TA, Haddon DJ, Jarrell JA, et al. Gene expression changes reflect clinical response in a placebo-controlled randomized trial of abatacept in patients with diffuse cutaneous systemic sclerosis. Arthritis Res Ther 2015;17:159.

10. Van den Hoogen F, Khanna D, Fransen J, Johnson SR, Baron M, Tyndall A, et al. 2013 classification criteria for systemic sclerosis: an American College of Rheumatology/European League Against Rheumatism collaborative initiative. Arthritis Rheum 2013;65:2737–47.

11. LeRoy EC, Medsger TA Jr. Criteria for the classification of early systemic sclerosis. J Rheumatol 2001;28:1573–6.

12. Khanna D, Furst DE, Clements PJ, Allanore Y, Baron M, Czirjak L, et al. Standardization of the modified Rodnan skin score for use in clinical trials of systemic sclerosis. J Scleroderma Relat Disord 2017;2:11–8.

13. Milano A, Pendergrass SA, Sargent JL, George LK, McCalmont TH, Connolly MK, et al. Molecular subsets in the gene expression signatures of scleroderma skin. PLoS One 2008;3:e2696.

14. Khanna D, Clements PJ, Furst DE, Korn JH, Ellman M, Rothfield N, et al, for the Relaxin Investigators and the Scleroderma Clinical Trials Consortium. Recombinant human relaxin in the treatment of systemic sclerosis with diffuse cutaneous involvement: a randomized, double-blind, placebo-controlled trial. Arthritis Rheum 2009;60:1102–11.

15. Khanna D, Berrocal VJ, Giannini EH, Seibold JR, Merkel PA, Mayes MD, et al. The American College of Rheumatology provisional Composite Response Index for clinical trials in early diffuse cutaneous Systemic Sclerosis. Arthritis Rheumatol 2016;68:299–311.

16. Khanna D, Clements PJ, Volkmann ER, Wilhalme H, Tseng CH, Furst DE, et al. Minimal clinically important differences for the modified Rodnan skin score: results from the Scleroderma Lung Studies (SLS-I and SLS-II). Arthritis Res Ther 2019;21:23.

17. Wiese AB, Berrocal VJ, Furst DE, Seibold JR, Merkel PA, Mayes MD, et al. Correlates and responsiveness to change of measures of skin and musculoskeletal disease in early diffuse systemic sclerosis. Arthritis Care Res (Hoboken) 2014;66:1731–9.

18. Clements PJ, Hurwitz EL, Wong WK, Seibold JR, Mayes M, White B, et al. Skin thickness score as a predictor and correlate of outcome in systemic sclerosis: high-dose versus low-dose penicillamine trial. Arthritis Rheum 2000;43:2445–54.

19. Domsic RT, Rodriguez-Reyna T, Lucas M, Fertig N, Medsger TA Jr. Skin thickness progression rate: a predictor of mortality and early internal organ involvement in diffuse scleroderma. Ann Rheum Dis 2011;70:104–9.

20. Khanna D, Denton CP, Jahreis A, van Laar JM, Frech TM, Anderson ME, et al. Safety and efficacy of subcutaneous tocilizumab in adults with systemic sclerosis (faSScinate): a phase 2, randomised, controlled trial. Lancet 2016;387:2630–40.

21. Khanna D, Lin CJ, Kuwana M, Allanore Y, Batalov A, Butrimiene I, et al. Efficacy and safety of tocilizumab for the treatment of systemic sclerosis: results from a phase 3 randomized controlled trial. Arthritis Rheumatol 2018, 70 Suppl 10. URL: https://acrabstracts.org/abstract/efficacy-and-safety-of-tocilizumab-for-the-treatment-of-systemic-sclerosis-results-from-a-phase-3-randomized-controlled-trial/.

22. Amjadi S, Maranian P, Furst DE, Clements PJ, Wong WK, Postlethwaite AE, et al, for the Investigators of the D-Penicillamine, Human RecombinantRelaxin, and Oral Bovine Type I Collagen Clinical Trials. Course of the modified Rodnan skin thickness score in systemic sclerosis clinical trials: analysis of three large multicenter, double-blind, randomized controlled trials. Arthritis Rheum 2009;60:2490–8.

23. Shand L, Lunt M, Nihtyanova S, Hoseini M, Silman A, Black CM, et al. Relationship between change in skin score and disease outcome in diffuse cutaneous systemic sclerosis: application of a latent linear trajectory model. Arthritis Rheum 2007;56:2422–31.

24. Herrick AL, Peytrignet S, Lunt M, Pan X, Hesselstrand R, Mouthon L, et al. Patterns and predictors of skin score change in early diffuse systemic sclerosis from the European Scleroderma Observational Study. Ann Rheum Dis 2018;77:563–70.

25. Stifano G, Sornasse T, Rice LM, Na L, Chen-Harris H, Khanna D, et al. Skin gene expression is prognostic for the trajectory of skin disease in patients with diffuse cutaneous systemic sclerosis. Arthritis Rheumatol 2018;70:912–9.

26. Khanna D, Furst DE, Hays RD, Park GS, Wong WK, Seibold JR, et al. Minimally important difference in diffuse systemic sclerosis: results from the D-penicillamine study. Ann Rheum Dis 2006;65:1325–9.

27. Langford CA, Monach PA, Specks U, Seo P, Cuthbertson D, McAlear CA, et al. An open-label trial of abatacept (CTLA4-IG) in non-severe relapsing granulomatosis with polyangiitis (Wegener's). Ann Rheum Dis 2014;73:1376–9.

28. Merrill JT, Burgos-Vargas R, Westhovens R, Chalmers A, D'Cruz D, Wallace DJ, et al. The efficacy and safety of abatacept in patients with non–life-threatening manifestations of systemic lupus erythematosus: results of a twelve-month, multicenter, exploratory, phase IIb, randomized, double-blind, placebo-controlled trial. Arthritis Rheum 2010;62:3077–87.

29. Langdon K, Haleagrahara N. Regulatory T-cell dynamics with abatacept treatment in rheumatoid arthritis. Int Rev Immunol 2018;37:206–14.

30. Frantz C, Auffray C, Avouac J, Allanore Y. Regulatory T cells in systemic sclerosis. Front Immunol 2018;9:2356.

31. Sargent JL, Milano A, Bhattacharyya S, Varga J, Connolly MK, Chang HY, et al. A TGFβ-responsive gene signature is associated with a subset of diffuse scleroderma with increased disease severity. J Invest Dermatol 2010;130:694–705.

32. Spiera R, Hummers L, Chung L, Frech T, Domsic R, Hsu V, et al. Safety and efficacy of lenabasum (JBT-101) in diffuse cutaneous systemic sclerosis subjects treated for one year in an open-label extension of trial JBT101-SSc-001 [abstract]. Ann Rheum Dis 2018;Suppl 2:52.

33. Khanna D, Lin CJ, Spotswood H, Siegel J, Jahreis A, Denton CP, et al. Evaluation of American College of Rheumatology provisional Composite Response Index in Systemic Sclerosis (ACR CRISS) in a phase 3 randomized controlled trial [abstract]. Arthritis Rheumatol 2018;70 Suppl 10. URL: https://acrabstracts.org/abstract/evaluation-of-american-college-of-rheumatology-provisional-composite-response-index-in-systemic-sclerosis-acr-criss-in-a-phase-3-randomized-controlled-trial/.

34. Villela R, Yuen SY, Pope JE, Baron M, and the Canadian Scleroderma Research Group. Assessment of unmet needs and the lack of generalizability in the design of randomized controlled trials for scleroderma treatment. Arthritis Rheum 2008;59:706–13.

AMERICAN COLLEGE
of RHEUMATOLOGY
Empowering Rheumatology Professionals

Dipeptidylpeptidase 4 as a Marker of Activated Fibroblasts and a Potential Target for the Treatment of Fibrosis in Systemic Sclerosis

Alina Soare,[1] 🆔 Hermina A. Györfi,[2] Alexandru E. Matei,[2] 🆔 Clara Dees,[2] Simon Rauber,[2] Thomas Wohlfahrt,[2] Chih-Wei Chen,[2] Ingo Ludolph,[2] Raymund E. Horch,[2] Tobias Bäuerle,[3] Stephan von Hörsten,[2] Carina Mihai,[4] Oliver Distler,[5] 🆔 Andreas Ramming,[2] Georg Schett,[2] 🆔 and Jörg H. W. Distler[2] 🆔

Objective. Expression of dipeptidylpeptidase 4 (DPP-4) identifies a dermal fibroblast lineage involved in scarring during wound healing. The role of DDP-4 in tissue fibrosis is, however, unknown. The aim of the present study was to evaluate DPP-4 as a potential target for the treatment of fibrosis in patients with systemic sclerosis (SSc).

Methods. Expression of DPP-4 in skin biopsy samples and dermal fibroblasts was analyzed by real-time polymerase chain reaction, immunofluorescence, and Western blot analyses. The activity of DPP-4 was modulated by overexpression, knockdown, and pharmacologic inhibition of DPP4 using sitagliptin and vildagliptin. The effects of DPP4 inhibition were analyzed in human dermal fibroblasts and in different mouse models of SSc (each n = 6).

Results. The expression of DPP-4 and the number of DPP-4–positive fibroblasts were increased in the fibrotic skin of SSc patients, in a transforming growth factor β (TGFβ)–dependent manner. DPP-4–positive fibroblasts expressed higher levels of myofibroblast markers and collagen (each $P < 0.001$ versus healthy controls). Overexpression of DPP4 promoted fibroblast activation, whereas pharmacologic inhibition or genetic inactivation of DPP4 reduced the proliferation, migration, and expression of contractile proteins and release of collagen (each $P < 0.001$ versus control mice) by interfering with TGFβ-induced ERK signaling. DPP4-knockout mice were less sensitive to bleomycin-induced dermal and pulmonary fibrosis ($P < 0.0001$ versus wild-type controls). Treatment with DPP4 inhibitors promoted regression of fibrosis in mice that had received bleomycin challenge and mice with chronic graft-versus-host disease, and ameliorated fibrosis in TSK1 mice (each $P < 0.001$ versus untreated controls). These antifibrotic effects were associated with a reduction in inflammation.

Conclusion. DPP-4 characterizes a population of activated fibroblasts and shows that DPP-4 regulates TGFβ-induced fibroblast activation in the fibrotic skin of SSc patients. Inhibition of DPP4 exerts potent antifibrotic effects when administered in well-tolerated doses. As DPP4 inhibitors are already in clinical use for diabetes, these results may have direct translational implications for the treatment of fibrosis in patients with SSc.

INTRODUCTION

Systemic sclerosis (SSc) is a chronic fibrotic disease that, of all the connective tissue diseases, is associated with the highest case-specific mortality (1). The central histopathologic hallmark of SSc is the uncontrolled and persistent activation of fibroblasts, which release excessive amounts of extracellular matrix (2). Fibroblasts are key effector cells in fibrotic diseases. However, fibroblasts are not a uniform population of cells, but rather are composed of functionally and phenotypically different subsets. Emerging evidence demonstrates that chronic inflammatory diseases, including rheumatoid arthritis, are associated with an imbalance in the ratio of different fibroblast subsets, and that those shifts may drive disease progression (3–7). The complexity of different fibroblast subsets in fibrotic diseases such as SSc is less well understood. However, it is well established that fibroblasts in fibrotic diseases can acquire an activated, so-called myofibroblast phenotype (8,9). Although transforming growth factor β (TGFβ) has emerged as a core pathway of fibroblast activation in SSc and in other fibrotic diseases, the molecular mechanisms underlying the persistent activation of fibroblasts remain incompletely understood (10).

Dipeptidylpeptidase 4 (DPP-4; also known as CD26) exists either as a type II transmembrane protein or in soluble form (11,12). DPP-4 functions as a serine protease that hydrolyzes proline or alanine from the N-terminus of a broad range of polypeptides (13,14). DPP-4 inactivates incretin hormones, such as glucagon-like peptides or glucose-dependent insulinotropic peptide, to inhibit insulin secretion and to promote diabetes mellitus. These findings have been successfully translated from bench to bedside, and DPP4 inhibitors are currently widely used for the treatment of diabetes mellitus (15). However, the substrates of DPP-4 are not restricted to incretin hormones, but also include a broad range of other soluble mediators, such as chemokines. Moreover, DPP-4 can modulate intracellular signaling not only via proteolytic cleavage of substrates, but also via direct interaction with key regulatory molecules, such as CD45 or adenosine deaminase, thereby exerting immunoregulatory functions (16,17).

DPP-4 is known to play a costimulatory role in T cells, by promoting both T and B cell activation (13,18). Treatment with DPP4 inhibitors lowered the incidence of autoimmune disorders in patients with diabetes mellitus (19). Of particular interest, Rinkevich and coworkers recently demonstrated that DPP-4 expression identifies an embryonic fibroblast lineage with unique functions in wound healing (20). They found that DPP-4–expressing fibroblasts accounted for the bulk of connective tissue deposition that occurred following surgical skin wounding. Inhibition of DPP4 reduced scarring without negatively affecting wound closure, suggesting that DPP4 inhibition may offer an avenue for selective targeting of a fibroblast population with a high capacity for matrix production, while not affecting other cell populations with more homeostatic functions (20). However, the concept of a DPP-4–expressing subpopulation of active, matrix-producing fibroblasts has not yet been translated and validated in the context of SSc.

In the present study, we aimed to characterize the role of DPP-4 in fibroblast activation and tissue fibrosis in SSc. Our findings demonstrate that 1) DPP-4 marks a population of activated fibroblasts whose levels are increased in a TGFβ-dependent manner in patients with SSc and in experimental murine models of fibrosis, 2) DPP-4 regulates fibroblast activation and collagen release in vitro and in vivo, 3) pharmacologic inhibition of DPP4 with approved drugs induces the regression of pre-established fibrosis when the inhibitors are administered in well-tolerated doses, and 4) despite the consistently observed antiinflammatory effects of DPP4 inhibition across different murine models, these effects were found to occur mainly through mediated DPP4 expression in tissue-resident cells such as fibroblasts.

MATERIALS AND METHODS

Patient skin biopsies and cell isolation. Skin biopsy samples were obtained and dermal fibroblasts were isolated from 23 patients with SSc and 21 healthy volunteers who were age- and sex-matched to the patients. All SSc patients fulfilled the American College of Rheumatology (ACR)/European League Against Rheumatism (EULAR) criteria for SSc (21). According to the LeRoy and Medsger classification of SSc (22), 15 patients (65.2%) had diffuse cutaneous SSc and 8 (34.7%) belonged to the limited cutaneous subset of SSc. Sixteen patients were female and 7 were male. The mean ± SD age of the patients with SSc was 52.7 ± 12.3 years, and the mean ± SD disease duration was 4.3 ± 2.2 years. In total, 5 patients (21.7%) were being treated with immunosuppressive drugs (low-dose steroids, methotrexate) at the time of biopsy or had previously received cyclophosphamide or rituximab. For additional, more detailed information on all of the study materials and procedures used, see Supplementary Materials and Methods (available on the *Arthritis & Rheumatology* web site at http://onlinelibrary.wiley.com/doi/10.1002/art.41058/abstract).

All patients and healthy volunteers signed an informed consent to participate. The study was approved by the local institutional review board.

Serum samples were collected from 50 patients with SSc fulfilling the ACR/EULAR classification criteria (53.8% with diffuse cutaneous SSc) and 30 healthy controls. The mean ± SD age of these patients with SSc was 55.6 ± 13.4 years, and the mean ± SD disease duration was 7.2 ± 3.4 years. In total, 11 patients (22.0%) were being treated with immunosuppressive drugs.

In addition to human fibroblasts, murine fibroblasts were isolated from DPP4-knockout (DPP4-KO) mice and wild-type (WT) littermates (23).

Western blot analysis. Proteins were separated by sodium dodecyl sulfate–polyacrylamide gel electrophoresis and transferred to a polyvinylidene difluoride membrane. The membranes were incubated with antibodies against Smad3 (Santa Cruz Technologies), phosphorylated p44/p42 MAPK (ERK1/2), p44/p42 MAPK (ERK1/2), SAPK/JNK, phosphorylated p38 MAPK, p38 MAPK, phosphorylated Akt, Akt (pan), phosphorylated NF-κB p65, NF-κB p65, phosphorylated SRC (Cell Signaling Technology), or DPP4, a primary antibody against phosphorylated JNK (Abcam), and horseradish peroxidase (HRP)–conjugated secondary antibodies (Dako). Blots were visualized using enhanced chemiluminescence. β-actin was used as a loading control (24).

Inhibition of canonical and non-canonical TGFβ pathways. To investigate the effect of the TGFβ non-canonical pathway on DPP-4 expression, dermal fibroblasts were incubated with the ERK inhibitor FR180204 (10 μM), the JNK inhibitor SP600125 (80 μM), the p38 inhibitor SP202190 (1 μM), the Akt inhibitor GSK690693 (0.1 μM), the SRC inhibitor SU6656 (500 nM), the NF-κB inhibitor bengamide B (0.1 μM) (all from Tocris Bioscience), the ABL inhibitor imatinib (1 μg/ml) (Novartis), or the JAK inhibitor ruxolitinib (5 μM) (LC Laboratories) for 4 hours before stimulation with TGFβ (10 ng/ml) (25,26). To block the canonical pathway, SIS3 (3 μM) (Sigma-Aldrich) was used. SD208 was used to inhibit the TGFβ receptor type I kinase activity (27,28).

Total RNA was isolated from dermal fibroblasts using a NucleoSpin RNA II extraction system (Machery-Nagel). The RNA was then reverse transcribed into complementary DNA with random hexamers.

Immunohistochemistry and immunofluorescence staining. Formalin-fixed, paraffin-embedded human or murine skin sections or fibroblasts were fixed in 4% paraformaldehyde and then stained with antibodies against α-smooth muscle actin (α-SMA) (Life Technologies), DPP-4, vimentin, prolyl-4-hydroxidase β (P4H), CD45, CD3, B220 (all from Abcam), and phosphorylated ERK (Cell Signaling). HRP-conjugated or Alexa Fluor 488– or Alexa Fluor 594–conjugated antibodies (Life Technologies) were used as secondary antibodies. Irrelevant isotype–matched antibodies served as controls (9). Nuclei were counterstained using DAPI (Santa Cruz Technologies). The staining was analyzed using a Nikon Eclipse 80i microscope.

Mouse models of SSc. *Bleomycin-induced skin fibrosis using preventive and therapeutic dosing.* DPP4-KO mice and WT littermates were injected subcutaneously with bleomycin or 0.9% sodium chloride for 4 weeks (29,30). Another group of mice was treated in parallel with the DPP4 inhibitor sitagliptin (10 mg/kg) (Selleckchem) throughout the 4 weeks of bleomycin challenge.

In the therapeutic dosing group, fibrosis was first induced by injection of bleomycin for 3 weeks (31). Thereafter, treatment with sitagliptin (3 mg/kg and 10 mg/kg) and vildagliptin (1.5 mg/kg and

15 mg/kg) (Biomol) was initiated for another 3 weeks, while mice were further challenged with bleomycin. The outcome was analyzed at 6 weeks after the first injection of bleomycin. Mice injected with 0.9% sodium chloride served as controls.

Sclerodermatous chronic graft-versus-host disease (GvHD). In the B10.D2→Balb/c (H-2^d) minor histocompatibility antigen–mismatched mouse model, chronic GvHD was induced by allogeneic transplantation of 5×10^6 splenocytes and 1×10^6 bone marrow cells from B10.D2 mice into sublethally irradiated BALB/c (H-2^d) mice. BALB/c (H-2^d) mice transplanted with splenocytes and bone marrow cells isolated from BALB/c (H-2^d) mice served as controls (32,33). Treatment was started after the appearance of the first clinical signs of chronic GvHD at day 21 posttransplantation, and the outcome was analyzed after 6 weeks.

Bleomycin-induced pulmonary fibrosis. DPP4-KO and WT mice were intratracheally injected with bleomycin or 0.9% sodium chloride (28). Mice were killed at 4 weeks after injection. A subgroup of mice was treated with sitagliptin at a dose of 10 mg/kg from day 1 to day 28.

Generation of bone marrow–chimeric mice. Mixed bone marrow chimeras were generated by transplanting bone marrow from DPP4-KO mice into WT mice or vice versa. Before transplantation, recipient mice (DPP4-KO or WT mice) were sublethally irradiated (34). Bone marrow cells were isolated from the tibial and femoral bones of DPP4-KO donor mice and injected into WT mice (KO→WT mice) or DPP4-KO (KO→KO). Similarly, bone marrow cells from WT mice were injected into DPP4-KO mice (WT→KO) and into WT mice (WT→WT). Fibrosis was induced by subcutaneous or intratracheal injections of bleomycin 10 days after the bone marrow transplantation.

Histologic, biochemical, and immunohistochemical analyses of the extent of fibrosis. The extent of fibrosis was analyzed using histologic, radiologic, biochemical, and immunohistochemical analyses. Histologic analyses included quantification of the dermal thickness on hematoxylin and eosin–stained skin tissue sections at 8 sites (viewed at 100-fold magnification) (35), evaluation of the fibrotic area as a percentage of the total lung area, in sirius red-stained skin tissue sections (36), quantification of pulmonary changes using the Ashcroft scale for evaluation of bleomycin-induced lung fibrosis (37), and direct visualization of collagen by trichrome staining (28). The total collagen content was analyzed biochemically using hydroxyproline assays. In addition, myofibroblasts were identified immunohistochemically as α-SMA–positive cells.

Statistical analysis. All data are presented as the median ± interquartile range, and differences between the groups were tested for their statistical significance using Student's paired t-tests for related samples and Mann-Whitney U nonparametric tests for nonrelated samples. P values less than 0.05 were considered significant.

RESULTS

Increased DPP-4 expression in SSc fibroblasts. We observed increased expression of DPP-4 gene and protein in the skin of SSc patients compared to the skin of age- and sex-matched healthy individuals (Figure 1A). Costaining with P4H demonstrated that SSc dermal fibroblasts expressed high levels of DDP-4. We found that DPP-4 was also expressed in B and T cells from patients with SSc, but that fibroblasts were the dominant cell type expressing DPP-4 in SSc skin (see Supplementary Figure 1, available on the *Arthritis & Rheumatology* web site at http://onlinelibrary.wiley.com/doi/10.1002/art.41058/abstract). In total, 75.8 ± 7.8% of P4H-positive fibroblasts were stained for DPP-4 in SSc skin, whereas only 29.1 ± 8.3% of fibroblasts in healthy skin expressed DPP-4 (Figure 1A). Moreover, significantly more DPP-4–positive fibroblasts coexpressed α-SMA as compared to DPP-4–negative fibroblasts (Figure 1B), indicating that DPP-4 marks a subpopulation of activated fibroblasts.

We also observed increased expression of DPP-4 gene and protein in murine models of SSc, such as in mice with bleomycin-induced skin fibrosis (Figure 1C) and in the B10.D2 (H-2^d)→BALB/c (H-2^d) mouse model of sclerodermatous chronic GvHD. In addition, both murine models of SSc showed prominent staining for DPP-4 in skin fibroblasts (Figure 1C).

The levels of soluble DPP-4 in the serum did not differ between patients with limited cutaneous SSc or with diffuse
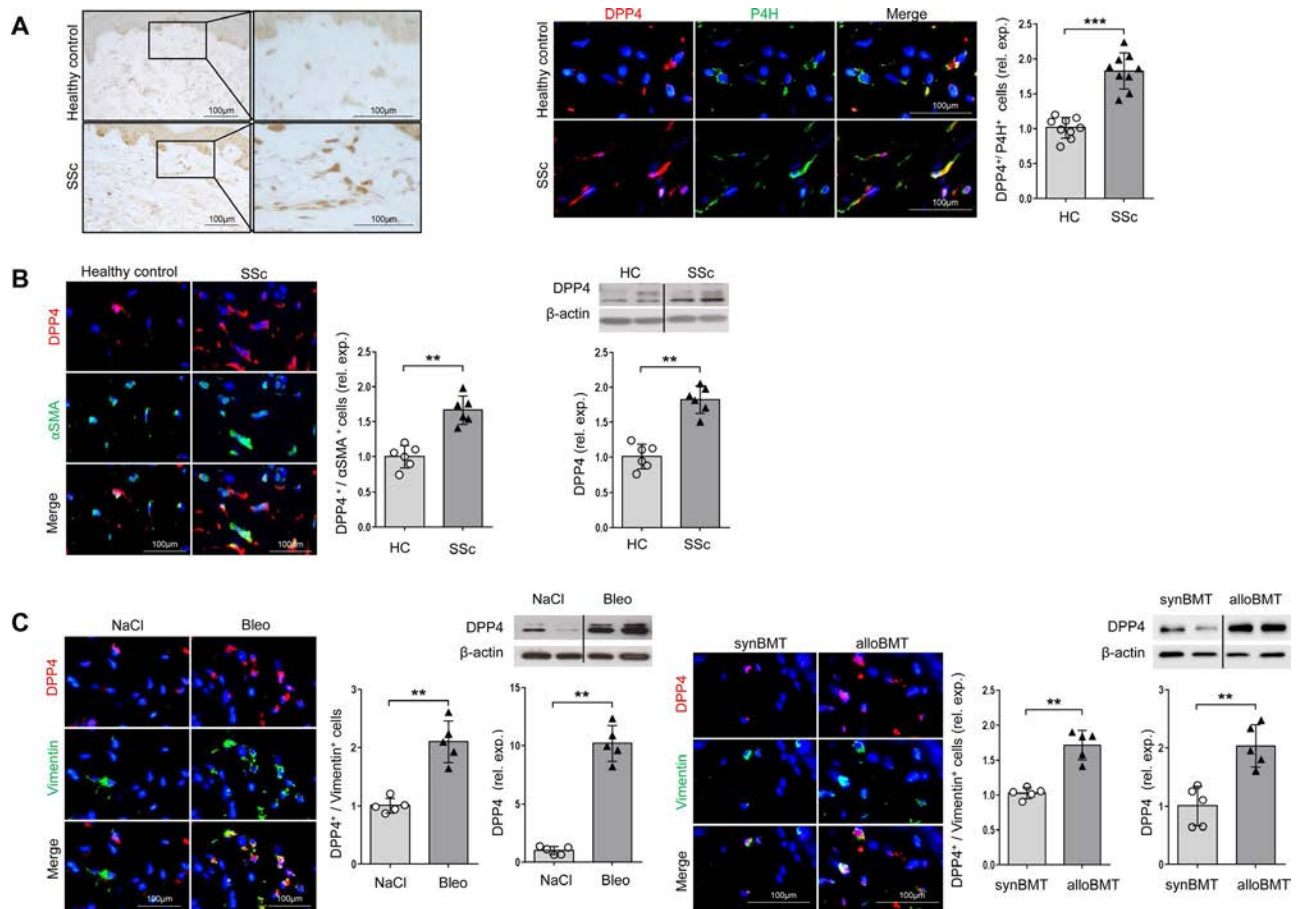
Figure 1. Dipeptidylpeptidase 4 (DPP-4) expression is increased in patients with systemic sclerosis (SSc) and murine models of SSc. **A**, Left, Immunohistochemical staining for DPP-4 in skin fibroblasts from a representative patient with SSc and healthy control (HC). Boxed areas on left are shown at higher magnification on right (original magnification × 200 [left]; × 600 [right]). Right, Immunofluorescence staining and quantification (relative expression [rel. exp.]) of DPP-4 and prolyl-4-hydroxidase β (P4H) in skin fibroblasts from SSc patients and controls (n = 9 per group). **B**, Left, Immunohistochemical staining for DPP-4 and α-smooth muscle actin (α-SMA) in skin fibroblasts from SSc patients and controls. Original magnification × 400. Right, Quantification of DPP-4+α-SMA+ cells and DPP-4 protein and gene expression in skin fibroblasts from SSc patients and controls (n = 6 per group). **C**, Analysis of DPP-4 and vimentin expression by immunofluorescence microscopy in mouse skin fibroblasts (nuclei stained with DAPI [blue]; original magnification × 400 in left panels and × 600 in middle panels), and quantification of DPP-4 protein and gene expression. Groups of mice (n = 5 each) comprised the bleomycin (bleo)–induced skin fibrosis model and sclerodermatous chronic graft-versus-host disease (GvHD) model (allogeneic bone marrow transplantation [alloBMT] of 5 × 10^6 splenocytes and 1 × 10^6 bone marrow cells from B10.D2 mice into BALB/c [H-2^d] mice). Their respective controls were NaCl-injected mice and mice receiving syngeneic bone marrow transplantation (synBMT) (5 × 10^6 splenocytes and 1 × 10^6 bone marrow cells from BALB/c [H-2^d] mice into BALB/c [H-2^d] mice). Symbols show individual samples; bars show the mean ± SEM. ** = $P \leq 0.001$; *** = $P \leq 0.0001$, by Mann-Whitney U test.

cutaneous SSc and healthy controls. Moreover, the enzymatic activity of DPP-4 in the serum also did not differ between SSc patients and healthy controls (see Supplementary Figures 2A and B, available on the *Arthritis & Rheumatology* web site at http://onlinelibrary.wiley.com/doi/10.1002/art.41058/abstract).

Induction of DPP-4 expression by TGFβ via ERK signaling in skin fibroblasts. Incubation of normal human dermal fibroblasts with recombinant TGFβ mimicked the pattern of DPP-4 expression observed in dermal fibroblasts from patients with SSc, with increased protein levels of DPP-4 evident after 24 and 48 hours (Figure 2A) but with normal levels of DPP4 messenger RNA (mRNA) (data not shown).

We next analyzed whether stimulation of human dermal fibroblasts with TGFβ would induce the enzymatic activity of DPP-4. Indeed, stimulation of human dermal SSc fibroblasts with recombinant TGFβ for 24 hours up-regulated DPP-4 activity, and this increase in activity correlated with the increase in DPP-4 protein

levels (see Supplementary Figure 2B [http://onlinelibrary.wiley.com/doi/10.1002/art.41058/abstract]).

Consistent with the results in vitro, we also observed increased expression of DPP-4 in skin fibroblasts from mice with fibroblast-specific overexpression of constitutively active TGFβ receptor type I (TBR[act]) compared to control mice (Figure 2A). Moreover, treatment of bleomycin-challenged mice with SD208, a specific inhibitor of TGFβ receptor type I kinase activity, prevented the bleomycin-induced up-regulation of DPP-4 protein (Figure 2A).

To identify which intracellular signaling cascades mediate the stabilization of DPP-4 protein by TGFβ, we knocked down Smad3 using small interfering RNA in normal human dermal fibroblasts. Knockdown of Smad3 did not inhibit the stimulatory effects of TGFβ on DPP-4 expression (Figure 2B). Comparable results were obtained when the dermal fibroblasts were incubated with the Smad inhibitor SIS3.

We thus tested the role of various noncanonical TGFβ pathways using specific inhibitors against various noncanonical intracellular mediators of TGFβ. Inhibition of ERK kinases ameliorated
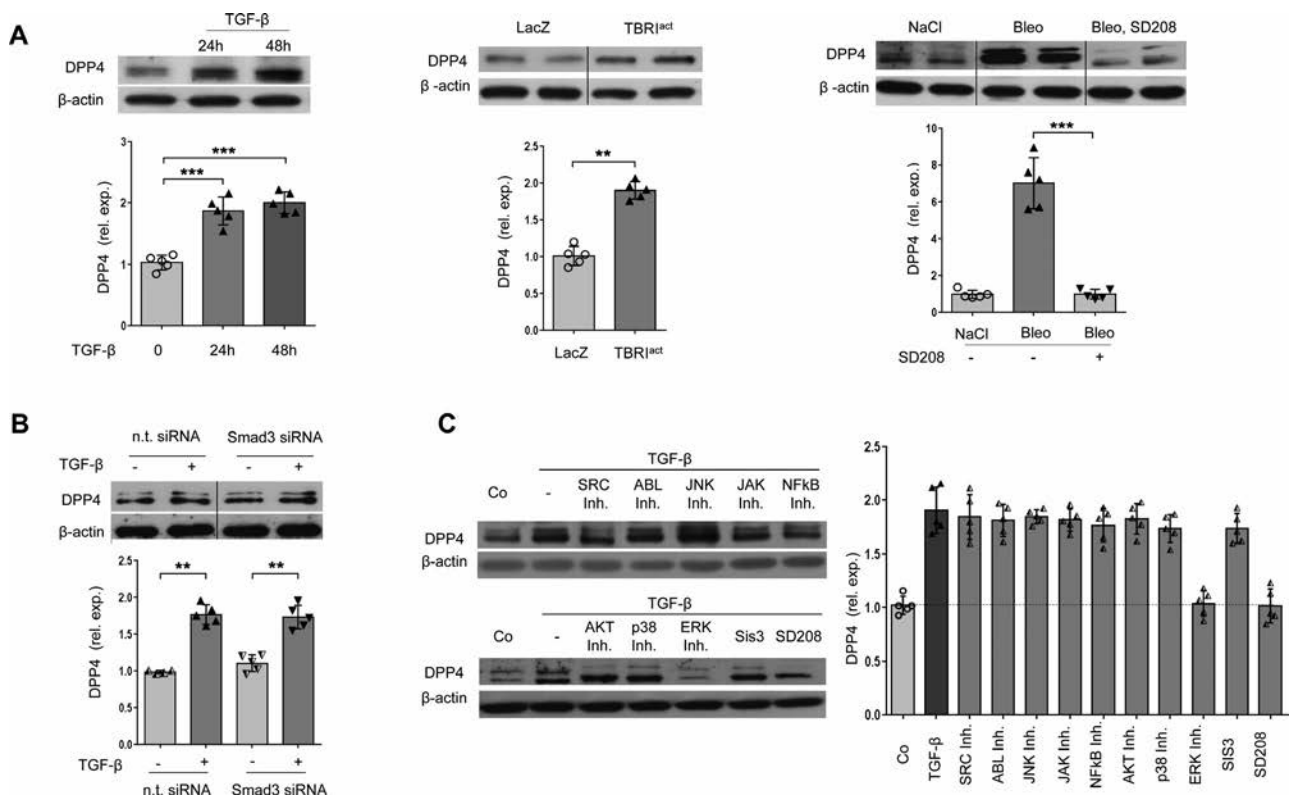
Figure 2. Induction of DPP-4 by transforming growth factor β (TGFβ). **A**, DPP-4 protein and gene expression in normal human dermal fibroblasts upon stimulation with TGFβ (left) and in murine skin overexpressing TGFβ receptor type I (TBRI[act]) (center), and effects of treatment with the selective TBRI inhibitor SD208 on DPP-4 protein and gene expression in mice with bleomycin-induced skin fibrosis (right) (n = 5 per group). **B**, Effects of Smad3 knockdown with small interfering RNA (siRNA) on TGFβ-induced expression of DPP-4 protein and gene in normal human dermal fibroblasts (n = 5 per group). Nontargeting (n.t.) siRNA was used as a control. **C**, TGFβ-induced DPP-4 protein expression in normal human dermal fibroblasts upon inhibition (Inh.) of noncanonical TGFβ pathways, including SRC, Abl, JNK, JAK, NF-κB, Akt, p38, ERK, and Smad (left), and effects of inhibition of noncanonical TGFβ pathways, the Smad inhibitor SIS3, and the TBRI inhibitor SD208 on DPP4 gene expression (right) (n = 5 per group). Symbols show individual samples; bars show the mean ± SEM. ** = $P \leq 0.001$; *** = $P \leq 0.0001$, by Mann-Whitney U test. Co = control (see Figure 1 for other definitions).

the stimulatory effects of TGFβ on DPP-4 expression, whereas inhibition of SRC, cABL, JAK, Akt, p38, NF-κB, and JNK did not interfere with TGFβ-induced DPP-4 expression in normal human dermal fibroblasts (Figure 2C).

Regulation of fibroblast activation and collagen release by DPP-4. To investigate the functional role of DPP-4 in fibroblast activation, we first sorted DPP-4–expressing and DPP-4–negative fibroblasts from the skin of mice (see Supplementary Figure 3A, available on the *Arthritis & Rheumatology* web site at http://onlinelibrary.wiley.com/doi/10.1002/art.41058/abstract) and analyzed the transcription of key profibrotic genes. DPP-4–expressing fibroblasts expressed higher levels of mRNA for

Col1a1, *Col1a2*, and *Acta2* (which encodes for α-SMA) compared to DPP-4–negative fibroblasts. Similar results were obtained when DPP-4–positive and DPP-4–negative fibroblasts were isolated from the lungs of mice (see Supplementary Figure 3B, http://onlinelibrary.wiley.com/doi/10.1002/art.41058/abstract).

Furthermore, we compared the fibrotic potential of fibroblasts isolated from DPP4-KO mice to that of fibroblasts isolated from WT control littermates. DPP4-KO mouse fibroblasts were less responsive to the stimulatory effects of TGFβ. The fibroblast-to-myofibroblast transition was impaired in DPP4-KO mouse fibroblasts, as indicated by the reduced expression of α-SMA and impaired formation of stress fibers upon stimulation with TGFβ as compared to that in control fibroblasts (Figure 3A). In addition, TGFβ
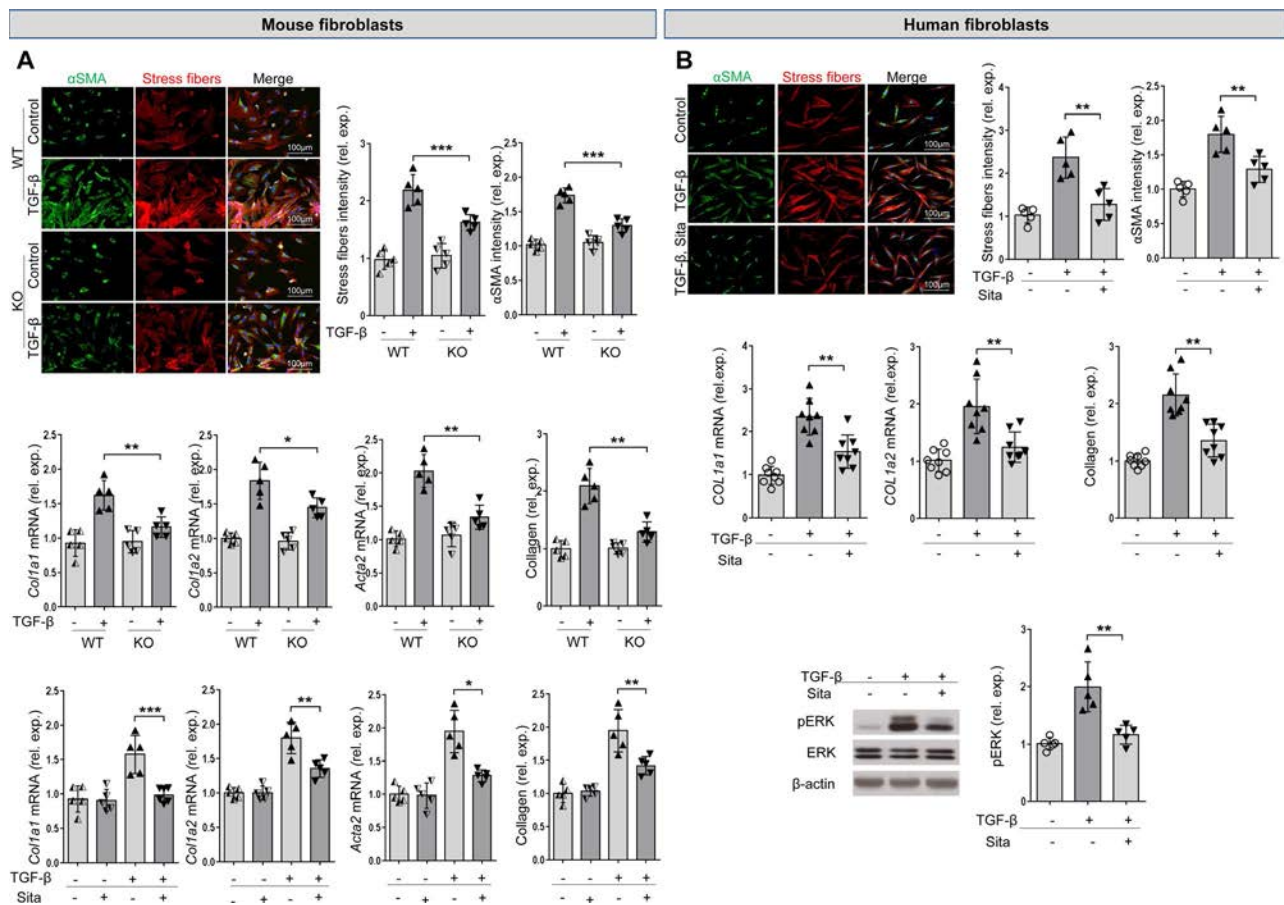
Figure 3. Inactivation of DPP4 inhibits fibroblast activation and collagen release. **A**, Top left, Immunohistochemical staining for α-SMA and stress fibers upon transforming growth factor β (TGFβ) stimulation of fibroblasts from a representative DPP4-knockout (DPP4-KO) mouse or wild-type (WT) control mouse. Nuclei were stained with DAPI (blue). Original magnification × 200. Top right, Intensity of stress fiber and α-SMA expression in mouse fibroblasts upon stimulation with TGFβ (n = 5 per group). Middle and Bottom, Levels of messenger RNA (mRNA) for *Col1a1*, *Col1a2,* and *Acta2* and collagen release in WT and DPP4-KO mouse fibroblasts upon stimulation with TGFβ, and effects of pharmaceutical inhibition of DPP4 with sitagliptin (Sita) (n = 5 per group). **B**, Top left, Immunohistochemical staining for α-SMA and stress fibers upon TGFβ stimulation of human dermal fibroblasts, and effects of treatment with sitagliptin. Representative images are shown (original magnification × 200). Top right, Intensity of stress fiber and α-SMA expression in human dermal fibroblasts upon stimulation with TGFβ, and effects of sitagliptin treatment (n = 5 per group). Middle, Effects of sitagliptin treatment on TGFβ-stimulated *COL1a1* and *COL1a2* mRNA levels and collagen protein release in human dermal fibroblasts (n = 8 per group). Bottom, Levels of phosphorylated ERK (pERK) in human dermal fibroblasts upon stimulation with TGFβ, and effects of sitagliptin treatment (n = 5 per group). Symbols show individual samples; bars show the mean ± SEM. * = $P \le 0.05$; ** = $P \le 0.001$; *** = $P \le 0.0001$, by Mann-Whitney U test. See Figure 1 for other definitions. Color figure can be viewed in the online issue, which is available at http://onlinelibrary.wiley.com/doi/10.1002/art.41058/abstract.

failed to induce an increase in the levels of mRNA for *Col1a1, Col1a2,* and *Acta2* or to increase the release of collagen in murine DPP4-KO fibroblasts (Figure 3A).

In scratch assays, DPP4-KO mouse fibroblasts demonstrated delayed closure of the gap as compared to control fibroblasts (see Supplementary Figure 4, available on the *Arthritis & Rheumatology* web site at http://onlinelibrary.wiley.com/doi/10.1002/art.41058/abstract). Furthermore, treatment with the DPP4 inhibitor sitagliptin consistently inhibited the stimulatory effects of TGFβ on murine fibroblasts (Figure 3A).

Overexpression of DPP4 in human dermal fibroblasts increased the levels of mRNA for *ACTA2*, *COL1A1,* and *COL1A2* and the levels of collagen protein secreted into the supernatant (see Supplementary Figure 5, available on the *Arthritis & Rheumatology* web site at http://onlinelibrary.wiley.com/doi/10.1002/art.41058/abstract). Incubation of SSc human dermal fibroblasts

with sitagliptin ameliorated the TGFβ-induced fibroblast-to-myofibroblast transition, prevented up-regulation of *COL1A1* and *COL1A2* mRNA by TGFβ, and reduced the release of collagen (Figure 3B).

We next aimed to characterize the molecular mechanisms through which DPP4 inhibition could interfere with TGFβ-induced fibroblast activation. We thus analyzed the effects of DPP4 inhibition on the canonical and noncanonical TGFβ pathways that have been implicated in the pathogenesis of fibrotic diseases. Treatment of human dermal fibroblasts with sitagliptin prevented the stimulatory effects of TGFβ on ERK signaling, leading to decreased levels of phosphorylated ERK in human dermal fibroblasts (Figure 3B). However, inhibition of DPP4 did not interfere with TGFβ-induced Smad3, STAT3, SRC, or Akt signaling or with cJun- and Fra2-mediated signaling of activator protein 1 (see Supplementary Figure 6, available on the
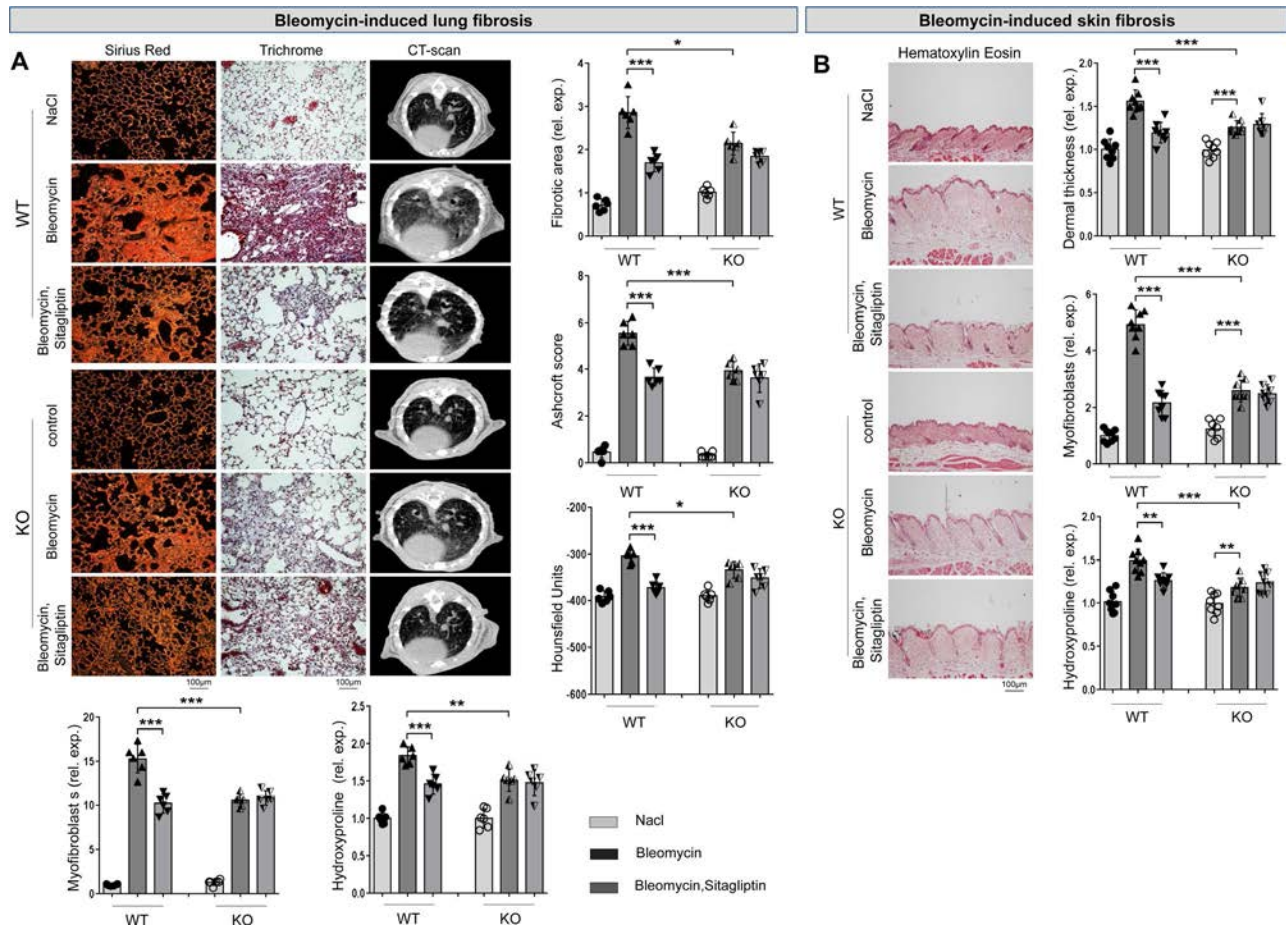
Figure 4. DPP4-knockout (DPP4-KO) mice are partially protected from experimental bleomycin-induced pulmonary and dermal fibrosis. **A,** Top left, Bleomycin-induced pulmonary fibrosis was assessed using sirius red and trichrome staining of lung tissue sections and high-resolution computed tomography (CT) scans of lungs from DPP4-KO and wild-type (WT) mice, and effects of sitagliptin treatment were assessed. Original magnification × 200. Top right, Mouse lungs were assessed for fibrotic area (relative expression [rel. exp.]), Ashcroft scores of lung fibrosis, and changes in lung density on CT scans (n = 6 per group). Bottom, Myofibroblast counts and hydroxyproline content were assessed in the mouse lungs (n = 6 per group). **B,** Left, Bleomycin-induced dermal fibrosis was assessed in hematoxylin and eosin–stained skin sections from DPP4-KO and WT mice. Original magnification × 200. Right, Dermal thickness, myofibroblasts, and hydroxyproline content were quantified in the mouse skin (n = 8 per group). Symbols show individual samples; show the mean ± SEM. * = $P \le 0.05$; ** = $P \le 0.001$; *** = $P \le 0.0001$, by Mann-Whitney U test. Color figure can be viewed in the online issue, which is available at http://onlinelibrary.wiley.com/doi/10.1002/art.41058/abstract.

Arthritis & Rheumatology web site at http://onlinelibrary.wiley.com/doi/10.1002/art.41058/abstract). The findings with regard to the pathways of DPP4 inhibition obtained in DPP4-KO mouse cells were consistent with these results (data not shown). Moreover, upon DPP4 overexpression, levels of phosphorylated ERK increased, whereas phosphorylated Smad3 levels did not change (see Supplementary Figure 7, available on the *Arthritis & Rheumatology* web site at http://onlinelibrary.wiley.com/doi/10.1002/art.41058/abstract), confirming the hypothesis that DPP-4 exerts part of its effects via noncanonical TGFβ signaling pathways.

Protection from experimental dermal and pulmonary fibrosis in DPP4-KO mice. To investigate whether the inhibitory effects of DPP4 inactivation on fibroblast activation in vitro would translate into antifibrotic effects in vivo, we evaluated the role of

genetic and pharmacologic inactivation of DPP4 in mice with bleomycin-induced pulmonary and dermal fibrosis. We found that DPP4-KO mice appeared phenotypically normal and that the histologic architecture of the lungs and the skin were not altered under homeostatic conditions (Figure 4A). However, DPP4-KO mice were less sensitive to bleomycin-induced fibrosis compared to their WT littermates. Pulmonary fibrosis induced by intratracheal injections of bleomycin was significantly ameliorated in DPP4-KO mice, as indicated by the reduced fibrotic area, decreased Ashcroft scores of lung fibrosis, less pronounced fibrotic changes on computed tomography scans, reduced myofibroblast counts, and decreased hydroxyproline content as compared to WT littermate controls (Figure 4A).

DPP4-KO mice were also protected from skin fibrosis induced by subcutaneous injections of bleomycin. We found
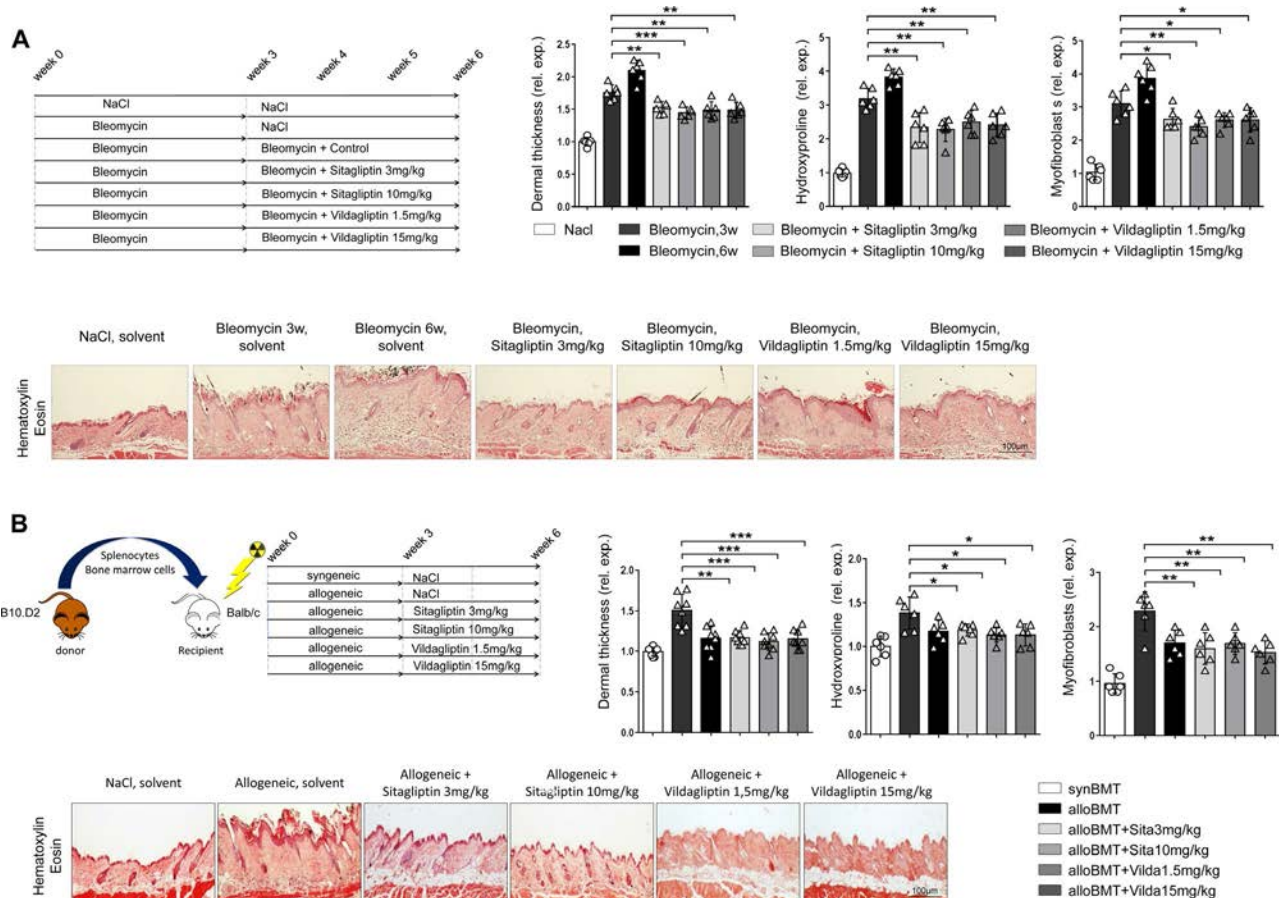
Figure 5. Pharmacologic inhibition of DPP4 induces the regression of fibrosis in mice with bleomycin-induced fibrosis and mice with chronic sclerodermatous chronic graft-versus-host disease (GvHD). **A**, Top left, Treatment scheme for bleomycin-induced dermal fibrosis in mice. Top right, Quantification (relative expression [rel. exp.]) of dermal thickness, hydroxyproline content, and myofibroblasts (n = 6 per group). Bottom, Representative images of hematoxylin and eosin (H&E)–stained mouse skin sections with or without sitagliptin (Sita) and vildagliptin (Vilda) treatment. Original magnification × 100. **B**, Top left, Experimental outline of sclerodermatous chronic GvHD in mice. Top right, Quantification of dermal thickness, myofibroblasts, and hydroxyproline content (n = 6 per group). Bottom, Representative images of H&E-stained mouse skin sections with or without sitagliptin and vildagliptin treatment. Original magnification × 100. Symbols show individual samples; bars show the mean ± SEM. * = $P \leq 0.05$; ** = $P \leq 0.001$; *** = $P \leq 0.0001$, by Mann-Whitney U test. synBMT = syngeneic bone marrow transplantation with 5×10^6 splenocytes and 1×10^6 bone marrow cells from BALB/c (H-2^d) mice into BALB/c (H-2^d) mice; alloBMT = allogeneic bone marrow transplantation with 5×10^6 splenocytes and 1×10^6 bone marrow cells from B10.D2 mice into BALB/c (H-2^d) mice. Color figure can be viewed in the online issue, which is available at http://onlinelibrary.wiley.com/doi/10.1002/art.41058/abstract.

that DPP4-KO mice had reduced dermal thickness, impaired myofibroblast differentiation, and decreased hydroxyproline content in comparison to WT littermates (Figure 4B).

In WT mice, preventive treatment with sitagliptin at a dose of 10 mg/kg, initiated together with the intratracheal or subcutaneous bleomycin challenge, also improved all measurements of fibrosis and strongly ameliorated bleomycin-induced pulmonary and dermal fibrosis. However, sitagliptin did not exert additional antifibrotic effects in DPP4-KO mice (Figures 4A and B), demonstrating that the antifibrotic effects of sitagliptin are indeed mediated by DPP4 inhibition and not by off-target effects.

Induction of regression of pre-established experimental fibrosis following pharmacologic inhibition of DPP4. Using a pharmacologic approach in murine SSc models, we first employed the murine model of bleomycin-induced skin fibrosis. We did not use preventive dosing schedules, but rather started treatment with the DPP4 inhibitors sitagliptin and

vildagliptin only after fibrosis had already been established in the mice (Figure 5A). Both DPP4 inhibitors, at both doses, strongly ameliorated bleomycin-induced dermal thickness, hydroxyproline content, and accumulation of myofibroblasts, as compared to vehicle-treated mice (Figure 5A). DPP4 inhibition also induced regression of pre-established fibrosis when all measures of fibrosis were compared to those at the pretreatment time point (Figure 5A). Furthermore, consistent with the in vitro data, phosphorylated ERK expression was reduced upon treatment with DPP4 inhibitors in bleomycin-challenged mice (see Supplementary Figure 8, available on the *Arthritis & Rheumatology* web site at http://online library.wiley.com/doi/10.1002/art.41058/abstract).

To further validate the antifibrotic effects of pharmacologic inhibition of DPP4, we next analyzed the effects of sitagliptin and vildagliptin in the B10.D2→Balb/c (H-2^d) mouse model of sclerodermatous chronic GvHD. Treatment with sitagliptin or vildagliptin, initiated after occurrence of the first clinical signs of disease, reduced chronic GvHD–induced dermal thickening, collagen
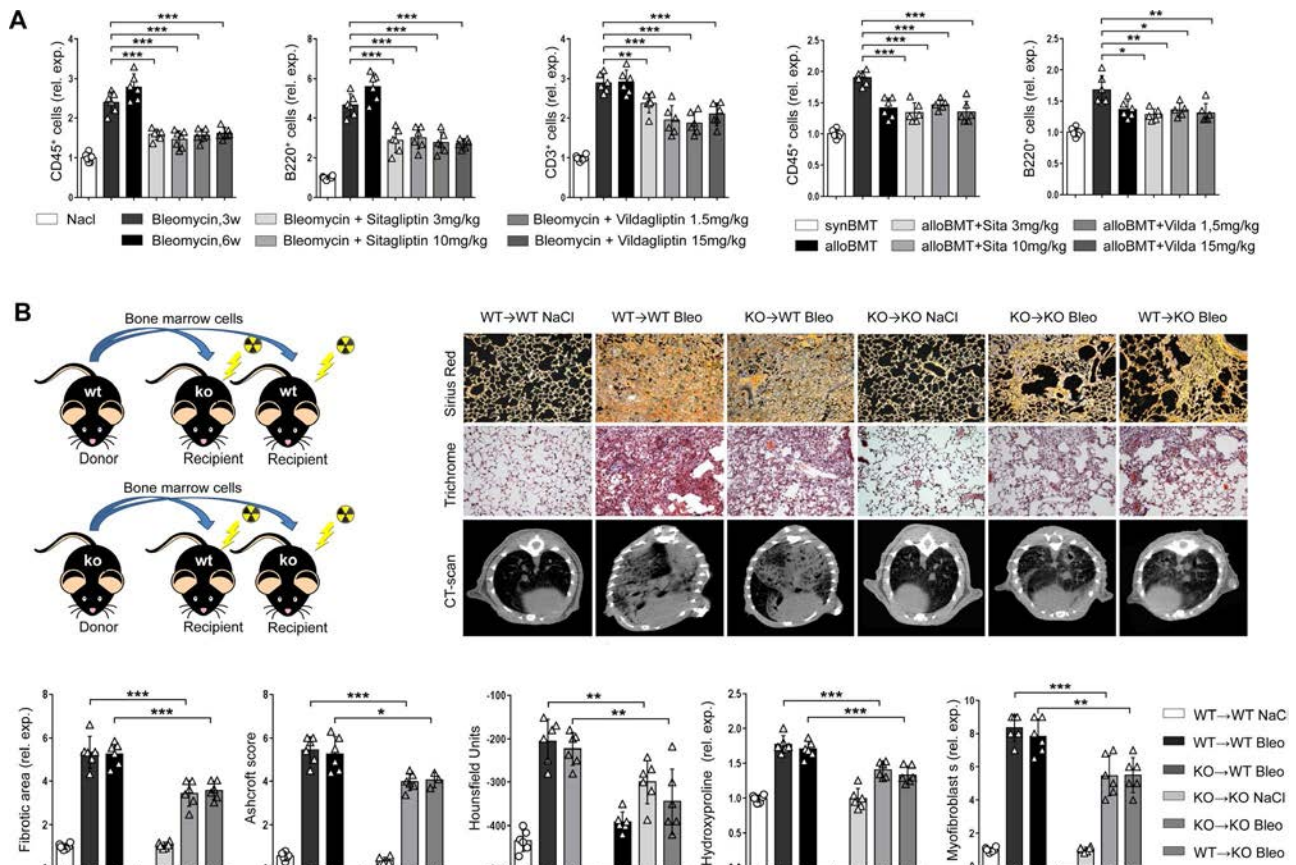
Figure 6. Antiinflammatory effects of DPP4 inhibition in mouse lungs. **A**, Numbers of CD45+, B220+, and CD3+ cells in bleomycin (Bleo)–challenged mice and mice with chronic GvHD treated with or without the DPP4 inhibitors sitagliptin and vildagliptin (n = 6 per group). **B**, Analysis of pulmonary fibrosis in chimeric mice. Top left, Generation of mixed bone marrow chimeras from DPP4-knockout (DPP4-KO) or wild-type (WT) mice. Top right, Representative images showing sirius red and trichrome staining of lung tissue sections and high-resolution computed tomography (CT) scans of the lungs of chimeric mice (n = 6 each). Bottom, Quantification of the fibrotic area, Ashcroft scores of lung fibrosis, fibrotic changes in lung density on CT scans, hydroxyproline content, and myofibroblasts (n = 6 each). Symbols show individual samples; bars show the mean ± SEM. * = $P \leq 0.05$; ** = $P \leq 0.001$; *** = $P \leq 0.0001$, by Mann-Whitney U test. See Figure 5 for other definitions. Color figure can be viewed in the online issue, which is available at http://onlinelibrary.wiley.com/doi/10.1002/art.41058/abstract.

deposition, and myofibroblast differentiation (Figure 5B). DDP4 inhibition also reduced chronic GvHD–induced weight loss (see Supplementary Figure 9, available on the *Arthritis & Rheumatology* web site at http://onlinelibrary.wiley.com/doi/10.1002/art.41058/abstract).

In addition to these 2 inflammation-driven models, we evaluated the antifibrotic effects of sitagliptin in the TSK1 mouse model of fibrosis, as a less inflammation-dependent model of SSc. Sitagliptin significantly ameliorated fibrosis in TSK1 mice, with DPP4 inhibition resulting in reductions in hypodermal thickness, myofibroblast counts, and hydroxyproline content as compared to vehicle-treated TSK1 mice. Treatment of TSK1 mice with sitagliptin also significantly reduced the levels of mRNA for *Col1a1*, *Col1a2*, and *Acta2* (see Supplementary Figure 10, available on the *Arthritis & Rheumatology* web site at http://onlinelibrary.wiley.com/doi/10.1002/art.41058/abstract).

Antiinflammatory effects of DPP4 inhibition. DPP4 expression has been shown to be implicated in the regulation of B and T cell activity (38). Treatment with sitagliptin and vildagliptin decreased the total leukocyte counts and reduced the numbers of B and T cells in the skin of mice with bleomycin-induced dermal fibrosis and mice with sclerodermatous chronic GvHD (Figure 6A), demonstrating that DPP4 inhibitors can also ameliorate inflammation in addition to exerting direct effects on fibroblasts.

We next aimed to characterize the contribution of DPP4 inactivation in leukocytes to the antifibrotic effects of DPP4 inhibition. To accomplish this, we generated chimeric mice by transplanting bone marrow from DPP4-KO mice to WT littermates (DPP4-KO→WT mice with selective knockout of DPP4 in bone marrow–derived cells such as leukocytes) and vice versa (WT→DPP4-KO mice with inactivation of resident, nonhematopoietic cells) (Figure 6B) and induced fibrosis by intratracheal or subcutaneous injections of bleomycin, respectively. While the extent of pulmonary and dermal fibrosis in DPP4-KO→WT mice was comparable to that in WT→WT control mice, fibrosis was strongly ameliorated in WT→DPP4-KO mice. Of note, all measurements of pulmonary and dermal fibrosis in WT→DPP4-KO mice were comparable to those in DPP4-KO→DPP4-KO mice (Figure 6B and Supplementary Figure 11 available on the *Arthritis & Rheumatology* web site at http://onlinelibrary.wiley.com/doi/10.1002/art.41058/abstract), thus characterizing resident cells such as fibroblasts as major target cells for the antifibrotic effects of DPP4 inhibitors.

DISCUSSION

In the present study we demonstrate that expression of DPP-4 is increased in skin fibroblasts from patients with SSc and in different murine models of skin fibrosis. We found no difference in the serum levels of DPP-4 between healthy controls and SSc patients, consistent with the findings of previous studies

(39,40), suggesting that DDP-4 expression is regulated locally in fibrotic tissues. Although DPP-4 is not specifically expressed in fibroblasts, costaining with fibroblast markers demonstrated that fibroblasts are the predominant cell type expressing DPP-4 in SSc skin, and that the majority of SSc fibroblasts in situ are positive for DPP-4. Of particular interest, we demonstrate that DPP-4 expression marks a population of activated fibroblasts. DPP-4–positive fibroblasts in SSc skin showed increased expression of the prototypical myofibroblast marker α-SMA as compared to DPP-4–negative cells. Moreover, dermal and pulmonary fibroblasts expressing DPP-4 demonstrated increased transcription of type I collagens and *Acta2* as compared to DPP-4–negative fibroblasts from the same mice. A recent landmark study by Rinkevich et al reported the presence of a DPP-4–positive fibroblast population in embryonic skin that possesses high fibroproliferative potential and that expands upon tissue injury to promote wound healing (20). The findings by Rinkevich et al, taken together with our present results, suggest that a subpopulation of DPP-4–positive fibroblasts expand to drive persistent tissue remodeling and tissue fibrosis in SSc. However, further studies with lineage-tracing experiments are required to further confirm this conclusion.

We provide evidence that TGFβ is a factor that may drive the expansion of DPP-4–positive fibroblasts. We demonstrate on multiple experimental levels that noncanonical TGFβ signaling is stimulating the expression of DPP-4, with the following evidence: 1) stimulation of cultured dermal fibroblasts with recombinant TGFβ up-regulated the expression of DPP-4 protein in normal human dermal fibroblasts; 2) DPP-4 levels were increased in SSc fibroblasts as compared to fibroblasts isolated from healthy individuals; 3) overexpression of TGFβ receptor type I increased DPP-4 expression in the skin of mice, thus confirming that TGFβ is sufficient to increase DPP-4 expression in fibroblasts in vitro and in vivo; 4) inhibition of the noncanonical TGFβ signaling mediator ERK inhibited the stimulatory effects of TGFβ on DPP-4 expression; and 5) selective inhibition of TGFβ signaling prevented the up-regulation of DPP-4 in murine experimental fibrosis, highlighting the notion that TGFβ signaling is required for the overexpression of DPP4 in mice with pulmonary or dermal fibrosis.

The up-regulation of DPP4 had direct functional consequences and promoted activation of certain noncanonical TGFβ pathways in fibroblasts. Inactivation of DPP4 reduced the TGFβ-induced activation of ERK signaling in cultured human dermal fibroblasts as well as in experimental fibrosis. ERK is an important intracellular mediator of TGFβ, which is activated in SSc, and targeted inhibition of ERK has been shown to ameliorate experimental fibrosis (41,42). Other intracellular cascades regulated by TGFβ were not affected by DPP4 inhibition. The molecular mechanisms underlying the selective regulation of ERK by DPP4 require further studies.

Consistent with the central role of TGFβ signaling in fibrogenesis, the inhibitory effects of DPP-4 on TGFβ signaling directly translated into inhibition of fibroblast activation. Inactivation of DPP4 blocked TGFβ-induced fibroblast-to-myofibroblast

differentiation and reduced the release of collagen in vitro. Genetic or pharmacologic inhibition of DPP4 also ameliorated experimental dermal and pulmonary fibrosis induced by bleomycin or in mice with sclerodermatous chronic GvHD. Moreover, a previous study demonstrated that inactivation of DPP4 ameliorated CCL4-induced liver fibrosis and cardiac remodeling after high-salt diet–induced heart failure (43–45). Targeted inhibition of DPP4 was also shown to reduce scar formation after cutaneous wounds. The potent antifibrotic effects of DPP4 inhibitors observed in the present study may have direct translational implications. We found that 1) pharmacologic inhibition of DPP4 not only prevented further progression of fibrosis, but also induced regression of pre-established fibrosis to below pretreatment levels; 2) potent antifibrotic effects were already observed with the lower doses of both DPP4 inhibitors in mice, implying that standard doses (as have already been used for the treatment of diabetes mellitus) could be effective in fibrotic diseases such as SSc; 3) antifibrotic doses of DPP4 inhibitors were well tolerated and their application was not limited by adverse events in our preclinical models; and 4) since DPP4 inhibitors are already being widely used for the treatment of diabetes, these findings support the need for further clinical studies to examine the use of potentially multiple drug candidates for the treatment of fibrosis in patients with SSc.

We provide evidence that DPP4 inhibition not only targets fibroblast activation directly, but also reduces inflammation. Treatment with DPP4 inhibitors reduced leukocyte counts and, in particular, T cell and B cell infiltration in 2 murine models of SSc, both of which are centrally involved in the pathogenesis of SSc (1,46). Indeed, DPP4 has been shown to regulate Th2 polarization and regulate B cell activation (47–50). Despite the potent effects on B cell and T cell infiltration into fibrotic tissues, our bone marrow transplantation experiments actually demonstrated that the profibrotic effects of DPP-4 required that DPP-4 be predominantly expressed in tissue-resident cells such as fibroblasts.

DPP4 inhibitors have, for more than 10 years, been in clinical use for the treatment of type 2 diabetes mellitus. The observed adverse effects have included, in particular, arthralgia or arthritis, but also hypersensitivity, skin-related reactions, and pancreatitis. The US Food and Drug Administration released a warning in 2015 that DPP4 inhibitors may cause joint pain. However, different studies showed no increased risk of arthritis in patients treated with DPP4 inhibitors compared to other second-line antidiabetic agents. Postmarketing events of hypersensitivity reactions, such as anaphylaxis and angioedema, have been reported in patients treated with DPP4 inhibitors. However, more detailed studies have revealed a similar incidence of angioedema between patients treated with sitagliptin and patients given placebo (51). Similar results with regard to adverse effects have also been reported for other DDP4 inhibitors such as saxagliptin (51). In our experiments, mice treated with DDP4 inhibitors did not show evidence of adverse events on clinical monitoring or on necropsy, including no evidence of arthritis or angioedema.

In summary, the results of the present study provide evidence that DPP-4 characterizes a population of activated fibroblasts in SSc. However, DPP-4 not only serves as an activation marker, but also is functionally required for fibroblast activation and tissue fibrosis. Targeted inactivation of DPP4 can exert potent antifibrotic effects in different mouse models of experimental dermal and pulmonary fibrosis. Based on the current clinical use of DPP4 inhibitors in patients with diabetes, these results may have direct translational implications for the treatment of fibrosis in patients with SSc.

ACKNOWLEDGMENTS

AUTHOR CONTRIBUTIONS

All authors were involved in drafting the article or revising it critically for important intellectual content, and all authors approved the final version to be published. Dr. J. H. W. Distler had full access to all of the data in the study and takes responsibility for the integrity of the data and the accuracy of the data analysis.
Study conception and design. Soare, Györfi, Matei, Dees, Rauber, Wohlfahrt, Chen, Ludolph, Horch, Bäuerle, von Hörsten, Mihai, O. Distler, Ramming, Schett, J. H. W. Distler.
Acquisition of data. Soare.
Analysis and interpretation of data. Soare, Schett, J. H. W. Distler.

REFERENCES

1. Gabrielli A, Avvedimento EV, Krieg T. Scleroderma. N Engl J Med 2009;360:1989–2003.

2. Ramming A, Dees C, Distler JH. From pathogenesis to therapy: perspective on treatment strategies in fibrotic diseases. Pharmacol Res 2015;100:93–100.

3. Mizoguchi F, Slowikowski K, Wei K, Marshall JL, Rao DA, Chang SK, et al. Functionally distinct disease-associated fibroblast subsets in rheumatoid arthritis. Nat Commun 2018;9:789.

4. Crowley T, O'Neil JD, Adams H, Thomas AM, Filer A, Buckley CD, et al. Priming in response to pro-inflammatory cytokines is a feature of adult synovial but not dermal fibroblasts. Arthritis Res Ther 2017;19:35.

5. Filer A, Ward LS, Kemble S, Davies CS, Munir H, Rogers R, et al. Identification of a transitional fibroblast function in very early rheumatoid arthritis. Ann Rheum Dis 2017;76:2105–12.

6. Buckley CD, Barone F, Nayar S, Bénézech C, Caamaño J. Stromal cells in chronic inflammation and tertiary lymphoid organ formation. Annu Rev Immunol 2015;33:715–45.

7. Neumann E, Lefèvre S, Zimmermann B, Gay S, Müller-Ladner U. Rheumatoid arthritis progression mediated by activated synovial fibroblasts. Trends Mol Med 2010;16:458–68.

8. Sorrell JM, Caplan AI. Fibroblasts: a diverse population at the center of it all. Int Rev Cell Mol Biol 2009;276:161–214.

9. Palumbo-Zerr K, Soare A, Zerr P, Liebl A, Mancuso R, Tomcik M, et al. Composition of TWIST1 dimers regulates fibroblast activation and tissue fibrosis. Ann Rheum Dis 2017;76:244–51.

10. Györfi AH, Matei AE, Distler JH. Targeting TGF-β signaling for the treatment of fibrosis. Matrix Biol 2018;68–9:8–27.

11. Gorrell MD, Gysbers V, McCaughan GW. CD26: a multifunctional integral membrane and secreted protein of activated lymphocytes. Scand J Immunol 2001;54:249–64.

12. Klemann C, Wagner L, Stephan M, von Hörsten S. Cut to the chase: a review of CD26/dipeptidyl peptidase-4's (DPP4) entanglement in the immune system. Clin Exp Immunol 2016;185:1–21.

13. Mulvihill EE, Drucker DJ. Pharmacology, physiology, and mechanisms of action of dipeptidyl peptidase-4 inhibitors. Endocr Rev 2014;35:992–1019.

14. Kim HJ, Kwak WY, Min JP, Sung SY, Kim HD, Kim MK, et al. Dipeptidyl peptidase-4 inhibitor with β-amino amide scaffold: synthesis, SAR and biological evaluation. Bioorg Med Chem Lett 2012;22:5545–9.

15. Dicker D. DPP-4 inhibitors: impact on glycemic control and cardiovascular risk factors. Diabetes Care 2011;34 Suppl 2:S276–8.

16. Lambeir AM, Durinx C, Scharpé S, De Meester I. Dipeptidyl-peptidase IV from bench to bedside: an update on structural properties, functions, and clinical aspects of the enzyme DPP IV. Crit Rev Clin Lab Sci 2003;40:209–94.

17. Forssmann U, Stoetzer C, Stephan M, Kruschinski C, Skripuletz T, Schade J, et al. Inhibition of CD26/dipeptidyl peptidase IV enhances CCL11/eotaxin-mediated recruitment of eosinophils in vivo. J Immunol 2008;181:1120–7.

18. Kameoka J, Tanaka T, Nojima Y, Schlossman SF, Morimoto C. Direct association of adenosine deaminase with a T cell activation antigen, CD26. Science 1993;261:466–9.

19. Kim SC, Schneeweiss S, Glynn RJ, Doherty M, Goldfine AB, Solomon DH. Dipeptidyl peptidase-4 inhibitors in type 2 diabetes may reduce the risk of autoimmune diseases: a population-based cohort study. Ann Rheum Dis 2015;74:1968–75.

20. Rinkevich Y, Walmsley GG, Hu MS, Maan ZN, Newman AM, Drukker M, et al. Skin fibrosis: identification and isolation of a dermal lineage with intrinsic fibrogenic potential. Science 2015;348:aaa2151.

21. Van den Hoogen F, Khanna D, Fransen J, Johnson SR, Baron M, Tyndall A, et al. 2013 classification criteria for systemic sclerosis: an American College of Rheumatology/European League Against Rheumatism collaborative initiative. Arthritis Rheum 2013;65:2737–47.

22. LeRoy EC, Medsger TA Jr. Criteria for the classification of early systemic sclerosis. J Rheumatol 2001;28:1573–6.

23. Marguet D, Baggio L, Kobayashi T, Bernard AM, Pierres M, Nielsen PF, et al. Enhanced insulin secretion and improved glucose tolerance in mice lacking CD26. Proc Natl Acad Sci U S A 2000;97:6874–9.

24. Liang R, Šumová B, Cordazzo C, Mallano T, Zhang Y, Wohlfahrt T, et al. The transcription factor GLI2 as a downstream mediator of transforming growth factor-β-induced fibroblast activation in SSc. Ann Rheum Dis 2017;76:756–64.

25. Chakraborty D, Šumová B, Mallano T, Chen CW, Distler A, Bergmann C, et al. Activation of STAT3 integrates common profibrotic pathways to promote fibroblast activation and tissue fibrosis. Nat Commun 2017;8:1130.

26. Matei AE, Beyer C, Györfi AH, Soare A, Chen CW, Dees C, et al. Protein kinases G are essential downstream mediators of the antifibrotic effects of sGC stimulators. Ann Rheum Dis 2018;77:459.

27. Uhl M, Aulwurm S, Wischhusen J, Weiler M, Ma JY, Almirez R, et al. SD-208, a novel transforming growth factor β receptor I kinase inhibitor, inhibits growth and invasiveness and enhances immunogenicity of murine and human glioma cells in vitro and in vivo. Cancer Res 2004;64:7954–61.

28. Palumbo-Zerr K, Zerr P, Distler A, Fliehr J, Mancuso R, Huang J, et al. Orphan nuclear receptor NR4A1 regulates transforming growth factor-β signaling and fibrosis. Nat Med 2015;21:150–8.

29. Distler A, Ziemer C, Beyer C, Lin NY, Chen CW, Palumbo-Zerr K, et al. Inactivation of evenness interrupted (EVI) reduces experimental fibrosis by combined inhibition of canonical and non-canonical Wnt signalling. Ann Rheum Dis 2014;73:624–7.

30. Zhang Y, Liang R, Chen CW, Mallano T, Dees C, Distler A, et al. JAK1-dependent transphosphorylation of JAK2 limits the antifibrotic effects of selective JAK2 inhibitors on long-term treatment. Ann Rheum Dis 2017;76:1467–75.

31. Soare A, Ramming A, Avouac J, Distler JH. Updates on animal models of systemic sclerosis. J Scleroderma Relat Disord 2016;1:266–76.

32. Zerr P, Palumbo-Zerr K, Distler A, Tomcik M, Vollath S, Munoz LE, et al. Inhibition of hedgehog signaling for the treatment of murine sclerodermatous chronic graft-versus-host disease. Blood 2012;120:2909–17.

33. Chen CW, Beyer C, Liu J, Maier C, Li C, Trinh-Minh T, et al. Pharmacological inhibition of porcupine induces regression of experimental skin fibrosis by targeting Wnt signalling. Ann Rheum Dis 2017;76:773–8.

34. Marquart S, Zerr P, Akhmetshina A, Palumbo K, Reich N, Tomcik M, et al. Inactivation of the cannabinoid receptor CB1 prevents leukocyte infiltration and experimental fibrosis. Arthritis Rheum 2010;62:3467–76.

35. Mallano T, Palumbo-Zerr K, Zerr P, Ramming A, Zeller B, Beyer C, et al. Activating transcription factor 3 regulates canonical TGFβ signalling in systemic sclerosis. Ann Rheum Dis 2016;75:586–92.

36. Huang J, Beyer C, Palumbo-Zerr K, Zhang Y, Ramming A, Distler A, et al. Nintedanib inhibits fibroblast activation and ameliorates fibrosis in preclinical models of systemic sclerosis. Ann Rheum Dis 2016;75:883–90.

37. Hübner RH, Gitter W, El Mokhtari NE, Mathiak M, Both M, Bolte H, et al. Standardized quantification of pulmonary fibrosis in histological samples. Biotechniques 2008;44:507–11, 514–7.

38. Waumans Y, Baerts L, Kehoe K, Lambeir AM, De Meester I. The dipeptidyl peptidase family, prolyl oligopeptidase, and prolyl carboxypeptidase in the immune system and inflammatory disease, including atherosclerosis [review]. Front Immunol 2015;6:387.

39. Wronkowitz N, Görgens SW, Romacho T, Villalobos LA, Sánchez-Ferrer CF, Peiró C, et al. Soluble DPP4 induces inflammation and proliferation of human smooth muscle cells via protease-activated receptor 2. Biochim Biophy Acta 2014;1842:1613–21.

40. Sinnathurai P, Lau W, Vieira de Ribeiro AJ, Bachovchin WW, Englert H, Howe G, et al. Circulating fibroblast activation protein and dipeptidyl peptidase 4 in rheumatoid arthritis and systemic sclerosis. Int J Rheum Dis 2018;21:1915–23.

41. Beyer C, Distler JH. Tyrosine kinase signaling in fibrotic disorders: translation of basic research to human disease. Biochim Biophys Acta 2013;1832:897–904.

42. Skhirtladze C, Distler O, Dees C, Akhmetshina A, Busch N, Venalis P, et al. Src kinases in systemic sclerosis: central roles in fibroblast activation and in skin fibrosis. Arthritis Rheum 2008;58:1475–84.

43. Kaji K, Yoshiji H, Ikenaka Y, Noguchi R, Aihara Y, Douhara A, et al. Dipeptidyl peptidase-4 inhibitor attenuates hepatic fibrosis via suppression of activated hepatic stellate cell in rats. J Gastroenterol 2014;49:481–91.

44. Esposito G, Cappetta D, Russo R, Rivellino A, Ciuffreda LP, Roviezzo F, et al. Sitagliptin reduces inflammation, fibrosis and preserves diastolic function in a rat model of heart failure with preserved ejection fraction. Br J Pharmacol 2017;174:4070–86.

45. Wang XM, Holz LE, Chowdhury S, Cordoba SP, Evans KA, Gall MG, et al. The pro-fibrotic role of dipeptidyl peptidase 4 in carbon tetrachloride-induced experimental liver injury. Immunol Cell Biol 2017;95:443–53.

46. Wohlfahrt T, Usherenko S, Englbrecht M, Dees C, Weber S, Beyer C, et al. Type 2 innate lymphoid cell counts are increased in patients

with systemic sclerosis and correlate with the extent of fibrosis. Ann Rheum Dis 2016;75:623–6.

47. Hatano R, Ohnuma K, Yamamoto J, Dang NH, Morimoto C. CD26-mediated co-stimulation in human CD8(+) T cells provokes effector function via pro-inflammatory cytokine production. Immunology 2013;138:165–72.

48. Tasic T, Bäumer W, Schmiedl A, Schwichtenhövel F, Pabst R, Raap U, et al. Dipeptidyl peptidase IV (DPP4) deficiency increases Th1-driven allergic contact dermatitis. Clin Exp Allergy 2011;41:1098–107.

49. Ohnuma K, Takahashi N, Yamochi T, Hosono O, Dang NH, Morimoto C. Role of CD26/dipeptidyl peptidase IV in human T cell activation and function. Front Biosci 2008;13:2299–310.

50. Yan S, Marguet D, Dobers J, Reutter W, Fan H. Deficiency of CD26 results in a change of cytokine and immunoglobulin secretion after stimulation by pokeweed mitogen. Eur J Immunol 2003;33:1519–27.

51. Karagiannis T, Boura P, Tsapas A. Safety of dipeptidyl peptidase 4 inhibitors: a perspective review. Ther Adv Drug Saf 2014;5:138–46.

Clinical Images: Catastrophic antiphospholipid syndrome–associated nephropathy in a systemic lupus erythematosus patient without lupus nephritis

The patient, a 35-year-old African American man with a history of seizures, presented with nausea, vomiting, abdominal pain, thrombocytopenia (platelet count 48,000 cells/mm^3), and acute renal failure (blood urea nitrogen:creatinine ratio 30:5.6). Urinalysis revealed mild proteinuria and microscopic hematuria. The patient was positive for antinuclear antibodies and anti–double-stranded DNA and had arthritis, thrombocytopenia, and hypocomplementemia, fulfilling the Systemic Lupus International Collaborating Clinics criteria for systemic lupus erythematosus (SLE) (1). Additionally, he was positive for cardiolipin antibodies, β_2-glycoprotein I, and lupus anticoagulant. ADAMTS-13 level was lower than normal, though not indicative of thrombotic thrombocytopenic purpura. Renal biopsy showed histologic lesions of acute and subacute thrombotic microangiopathy (TMA), characteristic of antiphospholipid antibody–associated nephropathy but without concomitant immune complex deposition in glomeruli, the sine qua non of lupus nephritis. Light microscopy (hematoxylin and eosin staining; original magnification × 400) showed an ischemic contracted glomerulus with apparent mesangial hypercellularity (suggestive of mesangiolysis), collapsed capillary loops, and an occluding fibrin thrombus in the afferent arteriole (**asterisk** in **A**, adjacent to a necrotic proximal tubule [**nT**]), an interstitial arteriole with an organizing thrombus perforated by recanalizing channels (**asterisks** in **B**), an interlobular artery showing fibromucoid intimal hyperplasia (**double asterisks** in **C**), and a fibrin thrombus within the residual slit-like lumen (**asterisk** in **C**). Electron microscopy (original magnification × 4,800) revealed a glomerulus with mesangial matrix collapse and resultant capillary loop collapse (**CL^b** in **D**), along with subendothelial electron-lucent widening (**dashed arrow** in **D**)—classic ultrastructural features of acute TMA and mesangiolysis (urinary space [**US**], mesangial cell nucleus [**MCN**], podocyte [**P**], and a normal capillary loop [**CL^a**] are also seen in **D**). Antiphospholipid antibody–associated nephropathy as pure TMA without concurrent lupus nephritis is rarely described in the literature (2,3). Further evaluation revealed mitral valvulitis with mitral regurgitation; right atrial thrombus; and thrombi in jugular, basilic, and brachial veins. Catastrophic antiphospholipid syndrome–associated nephropathy secondary to SLE was the final diagnosis (4).

1. Petri M, Orbai AM, Alarcón GS, Gordon C, Merrill JT, Fortin PR, et al. Derivation and validation of the Systemic Lupus International Collaborating Clinics classification criteria for systemic lupus erythematosus. Arthritis Rheum 2012;64:2677–86.

2. Daugas E, Nochy D, Huong DL, Duhaut P, Beaufils H, Caudwell V, et al. Antiphospholipid syndrome nephropathy in systemic lupus erythematosus. J Am Soc Nephrol 2002;13:42–52.

3. Tektonidou MG. Antiphospholipid syndrome nephropathy: from pathogenesis to treatment. Front Immunol 2018;9:1181.

4. Tektonidou MG, Sotsiou F, Moutsopoulos HM. Antiphospholipid syndrome (APS) nephropathy in catastrophic, primary, and systemic lupus erythematosus-related APS. J Rheumatol 2008;35:1983–8.

Rajib K. Gupta, MD (iD)
Eric Liu, MD, MPH
Eduardo Bonilla, MD
State University of New York Upstate Medical University
Syracuse, NY
Hind Elsaid, MD
United Health System Nephrology Group
Binghamton, NY

with systemic sclerosis and correlate with the extent of fibrosis. Ann Rheum Dis 2016;75:623–6.

47. Hatano R, Ohnuma K, Yamamoto J, Dang NH, Morimoto C. CD26-mediated co-stimulation in human CD8(+) T cells provokes effector function via pro-inflammatory cytokine production. Immunology 2013;138:165–72.

48. Tasic T, Bäumer W, Schmiedl A, Schwichtenhövel F, Pabst R, Raap U, et al. Dipeptidyl peptidase IV (DPP4) deficiency increases Th1-driven allergic contact dermatitis. Clin Exp Allergy 2011;41:1098–107.

49. Ohnuma K, Takahashi N, Yamochi T, Hosono O, Dang NH, Morimoto C. Role of CD26/dipeptidyl peptidase IV in human T cell activation and function. Front Biosci 2008;13:2299–310.

50. Yan S, Marguet D, Dobers J, Reutter W, Fan H. Deficiency of CD26 results in a change of cytokine and immunoglobulin secretion after stimulation by pokeweed mitogen. Eur J Immunol 2003;33:1519–27.

51. Karagiannis T, Boura P, Tsapas A. Safety of dipeptidyl peptidase 4 inhibitors: a perspective review. Ther Adv Drug Saf 2014;5:138–46.

Clinical Images: Catastrophic antiphospholipid syndrome–associated nephropathy in a systemic lupus erythematosus patient without lupus nephritis

The patient, a 35-year-old African American man with a history of seizures, presented with nausea, vomiting, abdominal pain, thrombocytopenia (platelet count 48,000 cells/mm^3), and acute renal failure (blood urea nitrogen:creatinine ratio 30:5.6). Urinalysis revealed mild proteinuria and microscopic hematuria. The patient was positive for antinuclear antibodies and anti–double-stranded DNA and had arthritis, thrombocytopenia, and hypocomplementemia, fulfilling the Systemic Lupus International Collaborating Clinics criteria for systemic lupus erythematosus (SLE) (1). Additionally, he was positive for cardiolipin antibodies, β_2-glycoprotein I, and lupus anticoagulant. ADAMTS-13 level was lower than normal, though not indicative of thrombotic thrombocytopenic purpura. Renal biopsy showed histologic lesions of acute and subacute thrombotic microangiopathy (TMA), characteristic of antiphospholipid antibody–associated nephropathy but without concomitant immune complex deposition in glomeruli, the sine qua non of lupus nephritis. Light microscopy (hematoxylin and eosin staining; original magnification × 400) showed an ischemic contracted glomerulus with apparent mesangial hypercellularity (suggestive of mesangiolysis), collapsed capillary loops, and an occluding fibrin thrombus in the afferent arteriole (**asterisk** in **A**, adjacent to a necrotic proximal tubule [**nT**]), an interstitial arteriole with an organizing thrombus perforated by recanalizing channels (**asterisks** in **B**), an interlobular artery showing fibromucoid intimal hyperplasia (**double asterisks** in **C**), and a fibrin thrombus within the residual slit-like lumen (**asterisk** in **C**). Electron microscopy (original magnification × 4,800) revealed a glomerulus with mesangial matrix collapse and resultant capillary loop collapse (**CL^b** in **D**), along with subendothelial electron-lucent widening (**dashed arrow** in **D**)—classic ultrastructural features of acute TMA and mesangiolysis (urinary space [**US**], mesangial cell nucleus [**MCN**], podocyte [**P**], and a normal capillary loop [**CL^a**] are also seen in **D**). Antiphospholipid antibody–associated nephropathy as pure TMA without concurrent lupus nephritis is rarely described in the literature (2,3). Further evaluation revealed mitral valvulitis with mitral regurgitation; right atrial thrombus; and thrombi in jugular, basilic, and brachial veins. Catastrophic antiphospholipid syndrome–associated nephropathy secondary to SLE was the final diagnosis (4).

1. Petri M, Orbai AM, Alarcón GS, Gordon C, Merrill JT, Fortin PR, et al. Derivation and validation of the Systemic Lupus International Collaborating Clinics classification criteria for systemic lupus erythematosus. Arthritis Rheum 2012;64:2677–86.

2. Daugas E, Nochy D, Huong DL, Duhaut P, Beaufils H, Caudwell V, et al. Antiphospholipid syndrome nephropathy in systemic lupus erythematosus. J Am Soc Nephrol 2002;13:42–52.

3. Tektonidou MG. Antiphospholipid syndrome nephropathy: from pathogenesis to treatment. Front Immunol 2018;9:1181.

4. Tektonidou MG, Sotsiou F, Moutsopoulos HM. Antiphospholipid syndrome (APS) nephropathy in catastrophic, primary, and systemic lupus erythematosus-related APS. J Rheumatol 2008;35:1983–8.

Rajib K. Gupta, MD iD
Eric Liu, MD, MPH
Eduardo Bonilla, MD
*State University of New York Upstate Medical University
Syracuse, NY*
Hind Elsaid, MD
*United Health System Nephrology Group
Binghamton, NY*

Effects of Conventional Uric Acid–Lowering Therapy on Monosodium Urate Crystal Deposits

Hanna Ellmann,[1] Sara Bayat,[1] Elizabeth Araujo,[1] Bernhard Manger,[1] Arnd Kleyer,[1] [iD] Alexander Cavallaro,[1] Michael Lell,[2] Hannah Schenker,[1] David Simon,[1] Koray Tascilar,[1] Herbert S. B. Baraf,[3] Georg Schett,[1] [iD] and Jürgen Rech[1] [iD]

Objective. Few studies have systematically and quantitatively addressed the impact of urate-lowering therapy on monosodium urate (MSU) deposits. This study was undertaken to analyze the effect of lifestyle measures and conventional urate-lowering therapy on MSU deposits in patients with gout.

Methods. In this prospective study, subjects with gout according to the American College of Rheumatology/ European League Against Rheumatism classification criteria and presence of MSU deposits seen on dual-energy computed tomography (DECT) scans received either lifestyle intervention or conventional urate-lowering therapy for a mean period of 18 months before a follow-up DECT scan. Detected MSU deposits were quantified by volumetric measurement and validated by semiquantitative scoring, and baseline and follow-up measurements were compared.

Results. Baseline and follow-up DECT scans were available for all 83 subjects. Six subjects discontinued treatment, and 77 subjects underwent a lifestyle intervention (n = 24) or were treated with allopurinol (n = 29), febuxostat (n = 22), or benzbromarone (n = 2) over the entire observation period. The mean serum uric acid (UA) level decreased from 7.2 to 5.8 mg/dl in the overall population. In patients who discontinued treatment, no change in MSU deposits or serum UA levels was observed. The burden of MSU deposits significantly decreased in patients undergoing lifestyle intervention (MSU volume $P = 0.007$; MSU score $P = 0.001$), and in patients treated with allopurinol (MSU volume and score $P < 0.001$) or febuxostat (MSU volume $P < 0.001$; MSU score $P = 0.001$). No significant decline in MSU deposits was noted in patients who discontinued treatment.

Conclusion. These data show that lifestyle intervention and xanthine oxidase inhibitors significantly decrease the MSU deposit burden. Hence, conventional gout therapy not only lowers serum UA levels, but also reduces pathologic MSU deposits.

INTRODUCTION

Gout is a musculoskeletal disease caused by an imbalance in purine metabolism (1,2). Due to impaired excretion, increased intake, or endogenous overproduction of purine, serum uric acid (UA) levels rise above the solubility concentration limit of 6.8 mg/dl, allowing the precipitation of monosodium urate (MSU) crystals in soft tissues and joints (3,4). This process triggers inflammation manifesting as arthritis and enthesitis (5). Identification of MSU crystals in synovial fluid is recognized as the gold standard for

the diagnosis of gout (6). However, direct identification of MSU crystals is often impossible due to the lack of fluid to be aspirated. Furthermore, it does not provide an estimate of the burden of MSU deposits. Therefore, techniques have been developed that allow visualization of MSU deposits in a noninvasive manner (7–10).

Dual-energy computed tomography (DECT) can noninvasively quantify the deposits of MSU crystals with high sensitivity and specificity (11,12). Automated volume measurement of MSU deposits is feasible by DECT, allowing quantification of MSU deposits (7,12).

A DECT-based scoring system for MSU deposits has been developed to cross-sectionally and longitudinally assess the distribution and severity of the MSU burden in anatomic regions most frequently affected by gout (13). Although DECT has been shown to reliably detect MSU deposits, data on how urate-lowering therapies affect MSU deposits are very limited. Therefore, we performed a longitudinal study to investigate the effect of different urate-lowering interventions on the MSU deposit burden using sequential DECT scanning followed by quantitative assessment of MSU deposits.

PATIENTS AND METHODS

Patients and evaluated characteristics. Patients were included consecutively in this prospective cohort study, if they had gout that fulfilled the 2015 American College of Rheumatology (ACR)/European League Against Rheumatism (EULAR) classification criteria (14) and had MSU deposits seen on the baseline DECT examination of both feet. Patients were recruited from the University Hospital Erlangen outpatient clinic after referrals from general, rheumatology, and orthopedic practices. All patients provided written informed consent. The study was approved by the Ethics Committee of the Medical University Erlangen-Nuremberg. All individuals received recommendations regarding lifestyle, which essentially followed the guidelines of the German Society of Rheumatology (15) and are in accordance with the EULAR recommendations for the management of gout (16). Briefly, patients were advised to avoid the consumption of alcohol, in particular beer (17), the ingestion of fructose-containing beverages, as well as the consumption of excessive meat and shellfish. Patients were also advised to use an online calculator for the energy (including purine) content of food, which is freely available in Germany (https://www.naehrwertrechner. de/naehrwerttabelle). It was recommmended that purine consumption be limited to 200 mg/day based on the published recommendations of the Technical University of Munich (www.mri.tum.de/sites/default/files/seiten/ernaehrungsempfehlung_gicht_2016.pdf).

In patients with recurrent gout attacks (≥2), additional pharmacologic therapy was initiated based on the ACR guidelines for the management of gout (18) and upon the decision of the treating physician and with the patient's consent. First choice was given to allopurinol, which was initiated at a dosage of 100 mg/day and titrated to a maximal dosage of 600 mg/day if a minimum target level of serum UA <6 mg/dl was not reached (18). Patients with symptomatic gout or serum UA levels >6 mg/dl who were already receiving treatment with allopurinol at baseline, or those who reported previous intolerability of allopurinol, were treated with febuxostat at a dosage of 80 mg/day, which was titrated up to 120 mg/day to reach the serum UA target level. In addition, 2 patients with contraindications to xanthine oxidase inhibitors were started on treatment with benzbromarone at 25 mg/day, which was titrated to a maximum dosage of 100 mg/day. At baseline, age, sex, and disease duration were recorded for all subjects, and serum UA levels were measured.

DECT scanning. All subjects underwent DECT scanning at baseline examination using a Somatom Definition Flash CT scanner (Siemens Healthcare). Follow-up examinations were done an average of 18 months following the initial scan. Scans were performed on the day of clinical and serologic investigation. For scanning, patients were placed in a supine position with dorsal extension of both feet during the examination. Scans were run axially in a caudocranial direction and covered a range of ~150 mm, including both feet and ankles. Regarding the setting of the scanner, tube A was run with Sn140kV/115 ref. mAs and tube B was run with 80kV/210 ref. mAs. DECT images were retrieved with commercial software (Syngo.via). MSU deposits were visualized and color-coded using the Syngo Dual Energy Gout clinical software application.

DECT image scoring. The urate volume in both feet was automatically calculated by the Siemens software application Syngo DE gout on a proprietary workstation (MultiModality Workspace). The urate ratio was set at 1.36 and the smoothing range was set at 4. Fluid was set at a minimum of 150 Hounsfield units for the 80kV/Sn140kV images. Artifacts such as beam hardening, submillimeter, nailbed, or skin were manually excluded from the calculation (19). In addition, a validated semiquantitative DECT scoring system was used to quantify the extent of MSU deposits (13). This scoring system includes 4 regions of MSU deposits: 1) first metatarsophalangeal (MTP1) joint; 2) toes (all distal and proximal interphalangeal joints, and metatarsophalangeal joints 2–5); 3) midfoot/ankle (tarsometatarsal joints, intertarsal joints, talocrural joints); and 4) soft tissue. MSU deposits were quantified in each region as follows: 0 = no deposit, 1 = single dot <2 mm, 2 = single deposits >2 mm, 3 = fused deposits. The subscores of each region were added, for a possible score range of 0–12. Baseline and follow-up DECT scans were evaluated by 2 independent readers (HE and SB) trained in both the automated volume measurement and the semiquantitative scoring system. The readers were unaware of the sequence of DECT scans and the identity of the patients. Interobserver reliability was assessed using the intraclass correlation coefficient (ICC). The smallest detectable change (SDC) was assessed as described by Bruynesteyn et al (20).

Statistical analysis. The data set was analyzed using IBM SPSS Statistics (version 23). Changes in serum UA level, MSU volume, and MSU score before and after treatment were analyzed by Wilcoxon's signed rank test. Differences between treatment groups were analyzed by the Kruskal-Wallis test. In the case of significance, Dunn's post hoc test for pairwise comparisons was performed. Characteristics related to changes in MSU volume were evaluated by Spearman's rank correlation. Interrater reliability was analyzed using the ICC (absolute agreement; two-way mixed). All tests were 2-tailed, and P values less than or equal to 0.05 were considered significant. Spaghetti plots were created using R (version 3.5.1). In
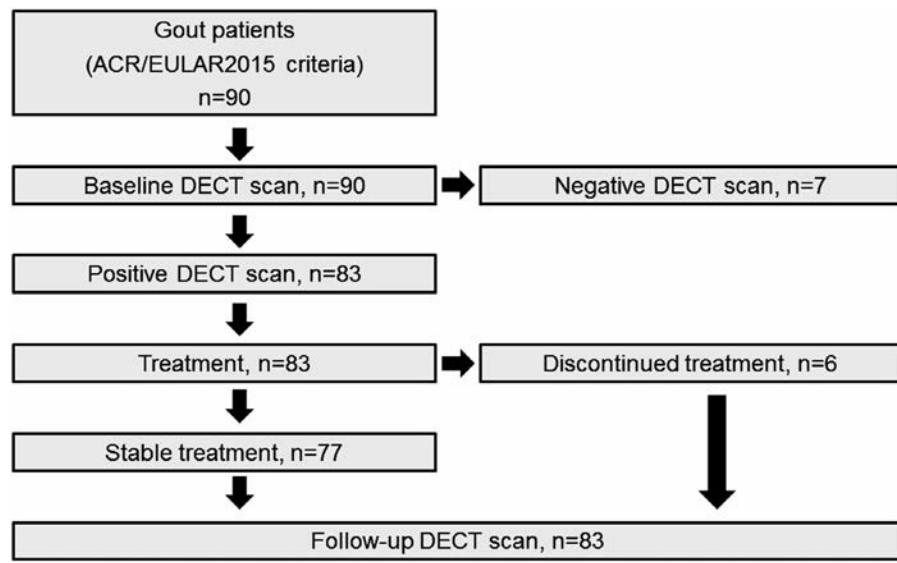
Figure 1. Disposition of patients in the prospective longitudinal observational study of dual-energy computed tomography (DECT) findings in patients with gout fulfilling the 2015 American College of Rheumatology/European League Against Rheumatism (ACR/EULAR) criteria. Patients received either lifestyle intervention only or additional treatment with allopurinol, febuxostat, or benzbromarone. Baseline and follow-up DECT scans were compared, and decreases in monosodium urate deposit volume and scores were documented.

order to reduce overplotting, small random noise was added to equal y values. Urate volume was displayed logarithmically, and an artificial 0 point was marked with an asterisk. As log(0) is not defined, 0.01 was added to all volume measurements.

RESULTS

Patient characteristics. Ninety consecutive patients with gout were screened (Figure 1). Seven patients were excluded because they did not show MSU deposits at the baseline DECT. In the remaining 83 patients, 166 DECT scans of the feet (83 at baseline and 83 at follow-up) were assessed. Of these 83 patients, 16 were female (19.3%) and 67 were male (80.7%), with a mean

± SD age of 59.4 ± 11.4 years (Table 1). The mean ± SD disease duration was 2.5 ± 6.3 years, and the time to follow-up was 18.7 ± 10.8 months. Seventy-seven of the 83 patients received continuous gout treatment between the baseline and follow-up DECT examinations, while 6 patients discontinued treatment on their own decision, i.e. due to noncompliance. Of the 77 patients treated continuously, 24 received lifestyle intervention only, 29 patients were treated with allopurinol (mean dosage 316 mg/day), 22 patients were treated with febuxostat (mean dosage 87 mg/day), and 2 patients were treated with benzbromarone. Age, sex, disease duration, and baseline serum UA levels were comparable among the groups.

Serum UA levels significantly decreased in the entire population (P <0.001) and in the subgroups treated with xanthine

Table 1. Demographic and disease-specific parameters and changes in serum UA levels*

	Total (n = 83)†	Lifestyle (n = 24)	Allopurinol (n = 29)	Febuxostat (n = 22)	Benzbromarone (n = 2)
Male, %	80.7	79.2	75.9	86.4	100
Age, years	59.4 ± 11.4	59.0 ± 9.2	59.0 ± 12.9	61.8 ± 12.6	62.5 ± 7.8
Chronic kidney disease, %	18.3	12.5	10.3	42.9	0
GFR, ml/minute	55.6 ± 10.4	59.1 ± 3.1	57.7 ± 6.5	48.6 ± 16.0	53.5 ± 9.2
Disease duration, years	2.5 ± 6.3	0.7 ± 2.0	2.0 ± 6.4	5.1 ± 8.8	1.0 ± 0.0
Months between baseline and follow-up DECT	18.7 ± 10.8	21.6 ± 10.9	18.0 ± 9.7	14.6 ± 9.0	11.4 ± 7.3
Recurrent gout attacks between baseline and follow-up, %	10.5	9.1	7.4	15.0	0
Baseline serum UA, mg/dl	7.2 ± 2.1	7.2 ± 1.7	7.0 ± 1.5	7.8 ± 3.0	5.9 ± 1.1
Follow-up serum UA, mg/dl	5.8 ± 2.2	6.7 ± 1.7	5.5 ± 1.8	5.1 ± 2.5	4.5 ± 0.8
Change in serum UA, mg/dl	1.4 ± 2.5	0.5 ± 2.0	1.3 ± 2.1	2.7 ± 2.9	1.4 ± 0.2
Tophaceous gout, %	65.1	54.2	58.6	81.8	100

* Except where indicated otherwise, values are the mean ± SD. UA = uric acid; GFR = glomerular filtration rate; DECT = dual-energy computed tomography.
† Includes 6 patients who discontinued treatment at some time during the follow-up period and whose data are not included within any of the 4 specific treatment groups.

Table 2. MSU volumes and scores before and after treatment, assessed by dual-energy computed tomography*

	Total (n = 83)†	Lifestyle (n = 24)	Allopurinol (n = 29)	Febuxostat (n = 22)	Benzbromarone (n = 2)
Volume-based assessment					
Baseline MSU volume, cm³	0.33 ± 1.48	0.07 ± 0.09	0.11 ± 0.15	0.99 ± 2.80	0.14 ± 0.18
Follow-up MSU volume, cm³	0.20 ± 1.10	0.05 ± 0.15	0.02 ± 0.04	0.64 ± 2.09	0.04 ± 0.04
Change in MSU volume, cm³	−0.14 ± 0.41	−0.02 ± 0.09	−0.09 ± 0.14	−0.35 ± 0.74	−0.11 ± 0.15
Follow-up MSU volume 0 cm³, no. (%)	34 (41.0)	14 (58.3)	12 (41.4)	6 (27.3)	0 (0.0)
P, baseline vs. follow-up‡	<0.001	0.007	<0.001	<0.001	0.317
Score-based assessment					
Baseline MSU score, units	4.2 ± 3.2	2.8 ± 2.0	3.6 ± 2.8	6.4 ± 3.9	5.0 ± 4.2
Follow-up MSU score, units	2.5 ± 3.1	1.5 ± 2.3	1.7 ± 2.1	4.3 ± 4.1	4.5 ± 5.0
Change in MSU score, units	−1.7 ± 2.0	−1.3 ± 1.4	−1.9 ± 2.0	−2.1 ± 2.6	−0.5 ± 0.7
Follow-up MSU score 0 units, no. (%)	26 (31.3)	10 (41.7)	12 (41.4)	2 (9.1)	0 (0.0)
P, baseline vs. follow-up‡	<0.001	0.001	<0.001	0.001	0.317

* Except where indicated otherwise, values are the mean ± SD. MSU = monosodium urate.
† Includes 6 patients who discontinued treatment at some time during the follow-up period and whose data are not included within any of the 4 specific treatment groups.
‡ By Wilcoxon's signed rank test.

Effects of treatment on the burden of MSU deposits. Next, we measured the extent of MSU deposits seen on DECT images, by volume measurement and semiquantitative scoring. Both MSU volume and MSU score significantly declined in the overall patient population. Mean ± SD MSU volume declined from 0.33 ± 1.48 to 0.20 ± 1.10 cm³ and semiquantitative score from 4.2 ± 3.2 to 2.5 ± 3.1 (both P <0.001) (Table 2). MSU deposits significantly decreased in the groups receiving lifestyle intervention (MSU volume P = 0.007; MSU score P = 0.001) or treatment with allopurinol (MSU volume and score P <0.001) or febuxostat (MSU volume P <0.001; MSU score P = 0.001). Absolute change in the extent of MSU deposits was higher in the febuxostat group than in the allopurinol group, which itself was higher than in the lifestyle intervention group. In contrast, patients who discontinued treatment did not show any decline in MSU deposits.

Regarding conversion from presence of MSU deposits to absence of MSU deposits, 58.3%, 41.4%, and 27.3% of patients undergoing lifestyle intervention, those receiving allopurinol treatment, and those receiving febuxostat treatment, respectively, were free of detectable MSU deposits after treatment. The likelihood of MSU absence at follow-up was associated with the baseline MSU burden, but not with the baseline serum UA level or the extent of decrease in serum UA level or other demographic factors (Table 3), indicating that it takes more time to reach complete resolution of MSU deposits if the baseline MSU burden is high.

Table 3. Characteristics of patients with and those without complete resolution of MSU lesions assessed by DECT*

	Follow-up MSU volume 0 cm³ (n = 34)	Follow-up MSU volume >0 cm³ (n = 49)
Male, no. (%)	24 (70.6)	43 (87.8)
Age, years	62.2 ± 11.2	57.5 ± 11.2
Disease duration, years	1.4 ± 5.5	3.4 ± 6.7
Months between baseline and follow-up DECT	19.0 ± 10.8	18.4 ± 11.0
Lifestyle intervention, no. (%)	14 (41.2)	10 (20.4)
Allopurinol, no. (%)	12 (35.3)	17 (34.7)
Febuxostat, no. (%)	6 (17.6)	16 (32.7)
Benzbromarone, no. (%)	0 (0.0)	2 (4.1)
Discontinuation, no. (%)	2 (5.9)	4 (8.2)
Baseline MSU volume, cm³	0.05 ± 0.06†	0.53 ± 1.90
Baseline total MSU score	2.3 ± 1.5†	5.6 ± 3.4
Baseline serum UA, mg/dl	6.6 ± 1.7	7.6 ± 2.2
Follow-up serum UA, mg/dl	5.5 ± 1.7	6.1 ± 2.4
Change in serum UA, mg/dl	1.1 ± 2.0	1.6 ± 2.7

* Except where indicated otherwise, values are the mean ± SD. DECT = dual-energy computed tomography; UA = uric acid.
† P < 0.05 versus patients without complete resolution of monosodium urate (MSU) lesions (volume >0 cm³), by Mann-Whitney U test.

Change in MSU volume was significantly related to baseline MSU volume ($r_S = 0.776$, $P < 0.01$) and baseline MSU score ($r_S = 0.499$, $P < 0.01$). There was a weaker but still significant correlation with the change in serum UA level ($r_S = 0.261$, $P < 0.05$), while there was no correlation with disease duration ($r_S = 0.016$, $P = 0.889$). Intraclass correlation coefficients were >0.99 for the total urate score and between 0.95 and 1.0 for the subscores. The SDC for the automated MSU volume measurement was 0.03 cm³. Spaghetti plots and DECT images depicting the decline in MSU deposits are shown in Figure 2.

Distribution of MSU deposits across anatomic regions. MSU deposits were most commonly found in the soft tissue (85.5% of all cases), followed by the toes (51.8%), MTP1 joint (47.0%), and the midfoot/ankle region (37.3%) (Table 4). Larger MSU deposits were most frequently found in the soft tissue, especially in the Achilles tendon, with the highest mean subscore (1.52) found in this region. The likelihood that MSU deposits completely dissolved differed among the regions, with 36.1% in soft tissue, 30.1% in the toes, 27.7% in the MTP1 joints, and 13.3% in the midfoot/ankle. New MSU deposits were found in the toes (4.8%), the soft tissues (3.6%), and the MTP1 joint or midfoot/ankle (1.2%). More detailed information on the local distribution of the MSU burden is provided in Table 4.

DISCUSSION

Understanding if and how MSU deposits resolve during treatment of gout is of seminal importance, since MSU deposits, as opposed to serum UA levels, are the central pathology in gout. Lowering the serum UA level without any impact on MSU deposits would reflect "laboratory cosmetics" rather than disease modification. Importantly, MSU deposits and serum UA levels are only weakly correlated (21), making it difficult to draw conclusions on the dynamics of MSU deposits by merely assessing serum UA levels. Such a concept suggests that state-of-the-art gout management would need to include the monitoring of resolution of the MSU deposits during treatment. In this longitudinal observational DECT study, we showed that implementation of relevant lifestyle measures and, even more pronounced, continuous treatment with xanthine oxidase inhibitors, lead to regression of MSU deposits. Our data also reveal that longitudinal DECT scanning is sensitive to change and allows monitoring of the regression of MSU deposits during therapeutic intervention. Both the volume and score of deposits significantly decreased during conventional gout treatment, supporting a disease-modifying effect of such intervention.

DECT is a highly sensitive diagnostic tool that can detect even very small MSU deposits and allows the testing of anatomic sites that cannot be assessed by joint aspiration, ultrasound, or clinical
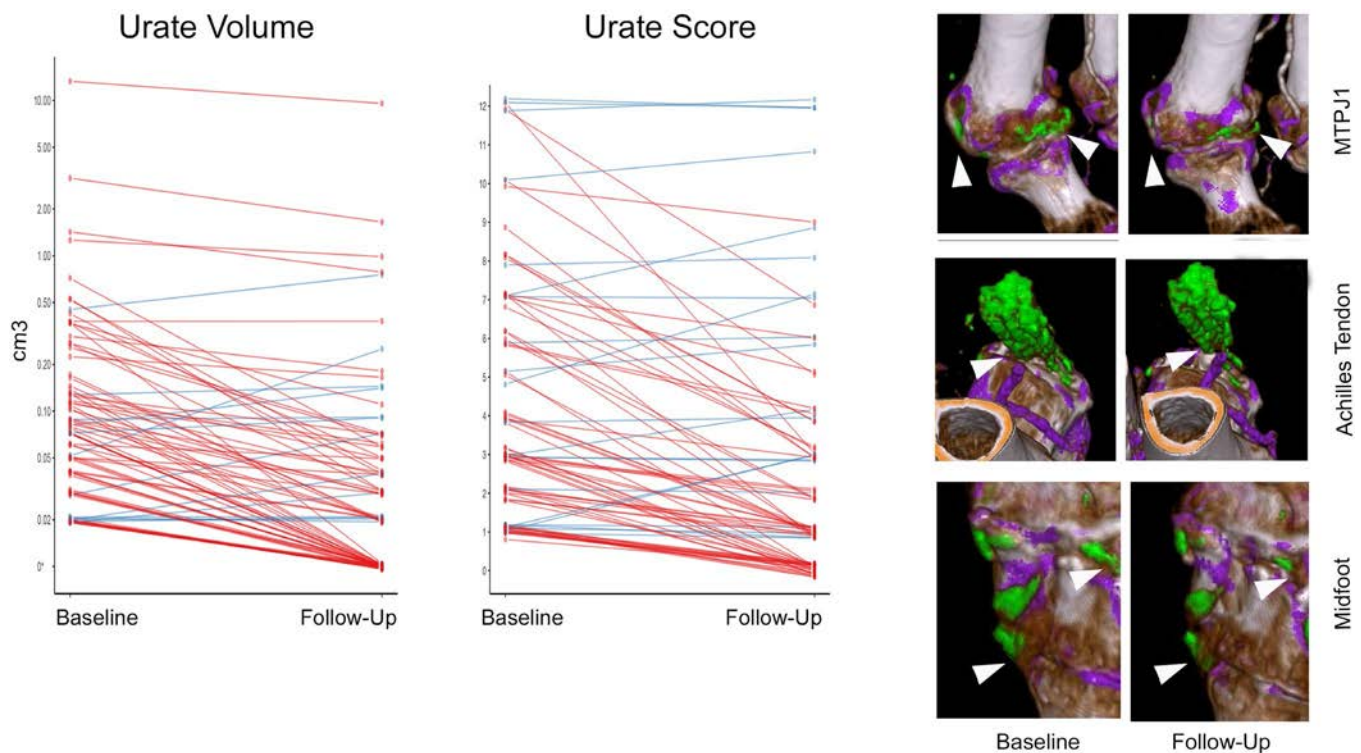
Figure 2. Change in monosodium urate (MSU) volume and score in individual patients with gout. Data shown on the spaghetti plots (left) represent the changes in MSU volume and MSU scores between baseline and follow-up. Dual-energy computed tomography images (right) show MSU deposits (**arrowheads**) in the first metatarsophalangeal joint (MTPJ1), the Achilles tendon, and the midfoot at baseline and the decline in MSU deposits with treatment.

Table 4. Distribution pattern of MSU crystals*

	MTP1	Toes	Midfoot/ankle	Soft tissue
Positive MSU score at baseline	39 (47.0)	43 (51.8)	31 (37.3)	71 (85.5)
Subscore at baseline, mean ± SD	0.92 ± 1.2	0.92 ± 1.1	0.89 ± 1.3	1.52 ± 1.1
Dots	17 (20.5)	22 (26.5)	7 (8.4)	40 (48.2)
Single deposit	7 (8.4)	9 (10.8)	5 (6.0)	7 (8.4)
Fused deposits	15 (18.1)	12 (14.5)	19 (22.9)	24 (28.9)
Positive MSU score at follow-up	17 (20.5)	22 (26.5)	21 (25.3)	44 (53.0)
MSU score 0 at follow-up	66 (79.5)	61 (73.5)	62 (74.7)	39 (47.0)
New deposits	+1 (1.2)	+4 (4.8)	+1 (1.2)	+3 (3.6)
Subscore at follow-up, mean ± SD	0.43 ± 1.0	0.55 ± 1.0	0.58 ± 1.1	0.95 ± 1.1
Dots	7 (8.4)	7 (8.4)	6 (7.2)	24 (28.9)
Single deposit	1 (1.2)	6 (7.2)	3 (3.6)	5 (6.0)
Fused deposits	9 (10.8)	9 (10.8)	12 (14.5)	15 (18.1)
P, baseline vs. follow-up†	<0.001	0.004	0.004	<0.001

* Except where indicated otherwise, values are the number (%). MSU = monosodium urate; MTP1 = first metatarsophalangeal joint.
† By Wilcoxon's signed rank test.

examination (12). Furthermore, DECT provides the opportunity to perform an automated volume measurement of MSU deposits, which allows the MSU burden to be quantified and compared between baseline and follow-up and provides information about sensitivity to change in lesions, which is considered essential as an outcome parameter (22). In addition to cumulative volume measurements, a semiquantitative score has been developed that takes into account the distribution and the extent of MSU deposits (13). Both instruments have been shown to allow measurement of the extent of MSU deposits in a cross-sectional setting (13).

Although MSU deposits also occur in asymptomatic hyperuricemia, such lesions are more frequent and larger in symptomatic gout (23). In order to evaluate the effects of urate-lowering treatment on MSU deposits, this study included only patients with symptomatic gout. To date, limited data are available on whether gout treatment affects the burden of MSU deposits and whether the DECT-based assessment of MSU deposits is sensitive to change. One case report (24) and 2 very small studies performed in 10 and 8 patients, respectively (13,25) showed a clear effect of intensified urate-lowering therapy on MSU deposits seen on DECT scans. Both studies, however, were performed in patients with gout treated with pegloticase, which led to a massive reduction in serum UA levels. The situation has been less clear in patients treated with conventional urate-lowering therapy. In a study by Rajan and colleagues, 62 patients receiving allopurinol were followed up, but neither a decrease in lesions shown on DECT nor a decrease in serum UA levels were found (21). Another small study showed a mild decrease in lesions seen on DECT in patients with gout treated with conventional therapy (26).

In the present longitudinal DECT study, we have now shown that both lifestyle intervention and continuous treatment with xanthine oxidase inhibitors lead to a significant decline in the volumes and the extent of MSU deposits. For patients treated with allopurinol, our data reflect recent findings by Dalbeth et al showing that appropriate dose-escalation of allopurinol treatment reduces MSU deposits (27). We additionally found that the

magnitude of the effect on MSU deposits is higher with xanthine oxidase inhibitor therapy than with lifestyle intervention, even though the interval between the 2 DECT scans was slightly higher in the lifestyle intervention group. However, it is interesting that lifestyle intervention per se also resulted in a consistent and significant reduction in MSU deposits over time. Furthermore, in the limited number of patients with gout who did not comply with treatment and discontinued xanthine oxidase inhibitor therapy and presumably also lifestyle measures, no reduction in MSU deposits was found. These latter data and the observation that the effect on MSU deposits was more pronounced with xanthine oxidase inhibitors than with mere lifestyle measures suggest that adherence to xanthine oxidase inhibitor therapy was good, although no formal surveillance of drug adherence was applied in this study.

Our study also showed that most MSU deposits are localized in soft tissue rather than in the toes or in the ankle joints. These findings highlight the importance of DECT as a diagnostic tool, as these locations are not accessible for joint aspiration. Use of the semiquantitative scoring system (13) also revealed that the regression of MSU deposits is faster in soft tissue than articular lesions, which suggests that urate-lowering treatment affects the various anatomic structures at different speeds. The likelihood of complete resolution of deposits depends on their anatomic distribution. Overall, MSU deposits may resolve more slowly with conventional treatment than with pegloticase (25), which yields very low serum UA levels and thus creates a larger gradient between circulating and tissue UA levels. In our cohort, serum UA levels reached <5 mg/dl, which is the treatment target suggested by EULAR (28), in only some of the patients. However, lesions seen on DECT significantly declined with lifestyle intervention and also with the xanthine oxidase inhibitors allopurinol and febuxostat.

In summary, this longitudinal DECT study showed that MSU deposits regress during gout management. Xanthine oxidase inhibitor treatment and, to a lesser extent, lifestyle intervention significantly reduced the burden of MSU deposits, suggesting

that lowering serum UA levels is accompanied by partial regression of the tissue lesions in gout. Conversion from presence to absence of MSU deposits occurs only in some individuals and is more likely if the initial MSU deposit burden is limited. This observation supports data obtained from a study by Dalbeth and colleagues, showing that a substantial proportion of patients treated with allopurinol still have lesions seen on DECT (29). Thus, longer follow-up will be necessary to demonstrate whether a complete resolution of MSU deposits indeed occurs in the majority of patients, if urate-lowering treatment is continuously received.

AUTHOR CONTRIBUTIONS

All authors were involved in drafting the article or revising it critically for important intellectual content, and all authors approved the final version to be published. Dr. Ellmann had full access to all of the data in the study and takes responsibility for the integrity of the data and the accuracy of the data analysis.
Study conception and design. Araujo, Manger, Schett, Rech.
Acquisition of data. Ellmann, Bayat, Araujo, Kleyer, Cavallaro, Lell, Schenker, Simon, Tascilar, Baraf, Schett, Rech.
Analysis and interpretation of data. Ellmann, Bayat, Araujo, Kleyer, Cavallaro, Lell, Schenker, Simon, Tascilar, Baraf, Schett, Rech.

REFERENCES

1. Eggebeen AT. Gout: an update. Am Fam Physician 2007;76:801–8.

2. Araujo EG, Manger B, Perez-Ruiz F, Thiele RG. Imaging of gout: new tools and biomarkers? Best Pract Res Clin Rheumatol 2016;30:638–52.

3. Martillo MA, Nazzal L, Crittenden DB. The crystallization of monosodium urate. Curr Rheumatol Rep 2014;16:400.

4. Chhana A, Lee G, Dalbeth N. Factors influencing the crystallization of monosodium urate: a systematic literature review. BMC Musculoskelet Disord 2015;16:296.

5. Czegley C, Gillmann C, Schauer C, Seyler L, Reinwald C, Hahn M, et al. A model of chronic enthesitis and new bone formation characterized by multimodal imaging. Dis Model Mech 2018;11:dmm034041.

6. Underwood M. Diagnosis and management of gout. BMJ 2006; 332:1315–9.

7. Choi HK, Al-Arfaj AM, Eftekhari A, Munk PL, Shojania K, Reid G, et al. Dual energy computed tomography in tophaceous gout. Ann Rheum Dis 2009;68:1609–12.

8. Grainger R, Dalbeth N, Keen H, Durcan L, Lawrence Edwards N, Perez-Ruiz F, et al. Imaging as an outcome measure in gout studies: report from the OMERACT gout working group. J Rheumatol 2015;42:2460–4.

9. McQueen FM, Doyle A, Dalbeth N. Imaging in gout—what can we learn from MRI, CT, DECT and US? [review]. Arthritis Res Ther 2011;13:246.

10. Perez-Ruiz F, Martin I, Canteli B. Ultrasonographic measurement of tophi as an outcome measure for chronic gout. J Rheumatol 2007;34:1888–93.

11. Manger B, Lell M, Wacker J, Schett G, Rech J. Detection of periarticular urate deposits with dual energy CT in patients with acute gouty arthritis [letter]. Ann Rheum Dis 2012;71:470–2.

12. Bongartz T, Glazebrook KN, Kavros SJ, Murthy NS, Merry SP, Franz WB III, et al. Dual-energy CT for the diagnosis of gout: an accuracy and diagnostic yield study. Ann Rheum Dis 2015;74:1072–7.

13. Bayat S, Aati O, Rech J, Sapsford M, Cavallaro A, Lell M, et al. Development of a dual-energy computed tomography scoring system for measurement of urate deposition in gout. Arthritis Care Res (Hoboken) 2016;68:769–75.

14. Neogi T, Jansen TL, Dalbeth N, Fransen J, Schumacher HR, Berendsen D, et al. 2015 gout classification criteria: an American College of Rheumatology/European League Against Rheumatism collaborative initiative. Arthritis Rheumatol 2015;67:2557–68.

15. Kiltz U, Alten R, Fleck M, Krüger K, Manger B, Müller-Ladner U, et al. S2e guidelines on gouty arthritis: evidence-based guidelines of the German Society of Rheumatology (DGRh). Z Rheumatol 2016 Suppl 2; 75:11–60.

16. Zhang W, Doherty M, Bardin T, Pascual E, Barskova V, Conaghan P, et al. EULAR evidence based recommendations for gout. Part II. Management: report of a task force of the EULAR Standing Committee for International Clinical Studies Including Therapeutics (ESCISIT). Ann Rheum Dis 2006;65:1312–24.

17. Choi HK, Atkinson K, Karlson EW, Willett W, Curhan G. Alcohol intake and risk of incident gout in men: a prospective study. Lancet 2004;363:1277–81.

18. Khanna D, Fitzgerald JD, Khanna PP, Bae S, Singh MK, Neogi T, et al. 2012 American College of Rheumatology guidelines for management of gout. Part 1. Systematic nonpharmacologic and pharmacologic therapeutic approaches to hyperuricemia. Arthritis Care Res (Hoboken) 2012;64:1431–46.

19. Mallinson PI, Coupal T, Reisinger C, Chou H, Munk PL, Nicolaou S, et al. Artifacts in dual-energy CT gout protocol: a review of 50 suspected cases with an artifact identification guide. AJR Am J Roentgenol 2014;203:W103–9.

20. Bruynesteyn K, Boers M, Kostense P, van der Linden S, van der Heijde D. Deciding on progression of joint damage in paired films of individual patients: smallest detectable difference or change. Ann Rheum Dis 2005;64:179–82.

21. Rajan A, Aati O, Kalluru R, Gamble GD, Horne A, Doyle AJ, et al. Lack of change in urate deposition by dual-energy computed tomography among clinically stable patients with long-standing tophaceous gout: a prospective longitudinal study. Arthritis Res Ther 2013;15:R160.

22. Dalbeth N, Aati O, Gao A, House M, Liu Q, Horne A, et al. Assessment of tophus size: a comparison between physical measurement methods and dual-energy computed tomography scanning. J Clin Rheumatol 2012;18:23–7.

23. Dalbeth N, House ME, Aati O, Tan P, Franklin C, Horne A, et al. Urate crystal deposition in asymptomatic hyperuricaemia and symptomatic gout: a dual energy CT study. Ann Rheum Dis 2015;74:908–11.

24. Bacani AK, McCollough CH, Glazebrook KN, Bond JR, Michet CJ, Milks J, et al. Dual energy computed tomography for quantification of tissue urate deposits in tophaceous gout: help from modern physics in the management of an ancient disease. Rheumatol Int 2012;32:235–9.

25. Araujo EG, Bayat S, Petsch C, Englbrecht M, Faustini F, Kleyer A, et al. Tophus resolution with pegloticase: a prospective dual-energy CT study. RMD Open 2015;1:e000075.

26. Sun Y, Chen H, Zhang Z, Ma L, Zhou J, Zhou Y, et al. Dual-energy computed tomography for monitoring the effect of urate-lowering therapy in gouty arthritis. Int J Rheum Dis 2015;18:880–5.

27. Dalbeth N, Billington K, Doyle A, Frampton C, Tan P, Aati O, et al. Effects of allopurinol dose escalation on bone erosion and urate volume in gout: a dual-energy computed tomography imaging study within a randomized controlled trial. Arthritis Rheumatol 2019;71:1739–46.

28. Richette P, Doherty M, Pascual E, Barskova V, Becce F, Castañeda-Sanabria J, et al. 2016 updated EULAR evidence-based recommendations for the management of gout. Ann Rheum Dis 2017;76:29–42.

29. Dalbeth N, Nicolaou S, Baumgartner S, Hu J, Fung M, Choi HK. Presence of monosodium urate crystal deposition by dual-energy CT in patients with gout treated with allopurinol. Ann Rheum Dis 2018;77:364–70.

Population Impact Attributable to Modifiable Risk Factors for Hyperuricemia

Hyon K. Choi,[1] [ID] Natalie McCormick,[2] [ID] Na Lu,[3] Sharan K. Rai,[4] Chio Yokose,[1] [ID] and Yuqing Zhang[1] [ID]

Objective. To examine modifiable risk factors in relation to the presence of hyperuricemia and to estimate the proportion of hyperuricemia cases in the general population that could be prevented by risk factor modification, along with estimates of the variance explained.

Methods. Using data obtained from 14,624 adults representative of the US civilian noninstitutionalized population, we calculated adjusted prevalence ratios for hyperuricemia, population attributable risks (PARs), and the variance explained according to the following 4 factors: body mass index (BMI; ≥25 kg/m^2), alcohol intake, nonadherence to a Dietary Approaches to Stop Hypertension (DASH) diet, and diuretic use.

Results. BMI, alcohol intake, adherence to a DASH-style diet, and diuretic use were all associated with serum urate levels and the presence of hyperuricemia in a dose-dependent manner. The corresponding PARs of hyperuricemia cases for overweight/obesity (prevalence 60%), nonadherence to a DASH-style diet (prevalence 82%), alcohol use (prevalence 48%), and diuretic use (prevalence 8%) were 44% (95% confidence interval [95% CI] 41%, 48%), 9% (95% CI 3%, 16%), 8% (95% CI 5%, 11%), and 12% (95% CI 11%, 14%), respectively, whereas the corresponding variances explained were 8.9%, 0.1%, 0.5%, and 5.0%. Our simulation study showed the variance nearing 0% as exposure prevalence neared 100%.

Conclusion. In this nationally representative study, 4 modifiable risk factors (BMI, the DASH diet, alcohol use, and diuretic use) could be used to individually account for a notable proportion of hyperuricemia cases. However, the corresponding serum urate variance explained by these risk factors was very small and paradoxically masked their high prevalences, providing real-life empirical evidence for its limitations in assessing common risk factors.

INTRODUCTION

Once considered to be a condition associated with a lifestyle of excess and overindulgence ("a disease of kings"), gout is now the most common form of inflammatory arthritis worldwide ("a disease of commoners"), with prevalence rising in many countries (1–3). Coinciding with the introduction of high-fructose corn syrup in the 1970s, increased consumption of sugar-sweetened beverages (4), expanding portion sizes (5), and the rising obesity epidemic in the US (4,6–8), both the incidence and prevalence of gout have more than doubled (2,6,9,10). Similarly, gout was previously rare in rural African communities where diets based on traditional agricultural products were consumed, but the prevalence in these regions is now increasing, most notably in urban communities (2,11,12). Increased serum urate levels, the causal precursor of gout, have been reported among Japanese immigrants who moved to the US, while elevated serum urate levels were not observed among those who continued to live in Japan (11,13). Moreover, the Tokelau Island migrant study showed that the incidence of gout between 1968 and 1982 was 9.0× higher in migrant men living in urban New Zealand than in nonmigrant men living in their isolated atoll homeland, with consistent serum urate level changes among men <55 years old (14). Finally, contemporary epidemiologic data from Canada, Europe, New Zealand, and China all suggest that gout incidence and prevalence are increasing (3,15–17), which correlates with obesity trends (2,7).

This historical background and epidemiologic data are at odds with a recent study that showed ≤0.3% of serum urate variance in the US to be explained by dietary components, particularly when compared with the variance explained by common genome-wide genes (i.e., genome-wide association study heritability estimate of 23.9%) (18). However, because the variance depends on the degree of variability of the exposure without incorporating the exposure's prevalence in the population, it can be highly misleading as a measure of relative importance among risk factors (19–21). This is particularly relevant when a risk factor is ubiquitous and its variability nearly 0%. In this case, the approach leads to almost none of the variance being explained, but with almost all cases being related to the risk factor (20). Studies using dietary exposures in the US would likely be examples of this, as most people have unhealthy, gout-prone diets. For example, an analysis of data from the Third National Health and Nutrition Examination Survey (NHANES-III) showed overwhelming noncompliance to the Dietary Approaches to Stop Hypertension (DASH) diet, a dietary regimen associated with lower levels of serum urate (18,22) and lower risk of gout (23). Less than 1% of the population with hypertension in the US was fully adherent to the DASH diet, and only 20% met half of the DASH nutrient targets (24,25).

To properly examine the theoretical population impact that can be attributed to modifiable risk factors (i.e., obesity, alcohol intake, diet, and diuretic use) for hyperuricemia in the US, thereby overcoming the critical limitations of the variance explained (18), we calculated the population attributable risk (PAR) percentage for each risk factor, assuming exposures were causal (26,27). The same approach has been used to estimate the population impact of lifestyle factors for myocardial infarction (28), hypertension (29), and type 2 diabetes mellitus (30), as well as for genetic factors discovered in genome-wide association studies on hyperuricemia (31,32) and gout (33). We also estimated the variance explained (18) for the same risk factors for illustration purposes.

SUBJECTS AND METHODS

Study population. The NHANES-III consisted of a representative sample of the US civilian, noninstitutionalized population between 1988 and 1994, who were selected using a multistage, stratified sampling design (34). We analyzed NHANES data for comparison purposes, as the same data were used in the recent study that demonstrated extremely low serum urate variance explained by dietary components (18). Our analysis was limited to adult participants (≥20 years old) who underwent a medical examination, and included the 14,624 participants with complete data on the target risk factors and covariates. We repeated our analyses on data from 14,187 participants after excluding those who self-reported gout or were taking allopurinol or uricosuric agents (n = 437).

As this was a secondary analysis of aggregated data, this study was exempt from institutional review board approval.

Uric acid measurement. Serum urate level was measured by oxidization with the specific enzyme uricase to form allantoin and H_2O_2 (Hitachi Model 737 Multichannel Analyzer; Boehringer Mannheim) (34).

Assessment of modifiable risk factors. Typical food intake was determined using responses to the food frequency questionnaire administered to participants to assess their normal consumption over the past month. We constructed a DASH diet score based on individual dietary elements that were emphasized or minimized in the DASH diet, focusing on the following components: high intake of fruits, vegetables, nuts and legumes, low-fat dairy products, and whole grains, and low intake of sodium, sweetened beverages, and red and processed meats (23,35,36). For each of the components, individuals were classified into quintiles according to their intake ranking. We then summed the component scores to obtain an overall DASH diet score (range 8–40). The DASH score has been successfully used in studies on serum urate levels (18), gout (23), cardiovascular disease (35), and kidney stones (37), and this quintile approach for dietary exposure has been used in PAR studies on cardiovascular–metabolic end points (28–30). The NHANES-III collected information on body measurements (including height and weight), medication use (including urate-lowering drugs and diuretics), and medical conditions.

Statistical analysis. The risk factors of interest were categorized as follows: BMI (<25.0 kg/m^2, 25.0–29.9 kg/m^2, 30.0–34.9 kg/m^2, and ≥35.0 kg/m^2), DASH diet score (quintiles 1–5), alcohol intake (0, 0.01–0.09, 0.1–0.49, 0.5–0.99, and ≥1.0 serving per day) (38), and diuretic use (yes or no). We evaluated the relationship between these modifiable risk factors and serum urate level using linear regression. We also estimated adjusted prevalence ratios for hyperuricemia, which was defined as a serum urate level of >417 μmoles/liter (7.0 mg/dl) in men and >340 μmoles/liter (5.7 mg/dl) in women, according to the NHANES-III laboratory definition (34). We used prevalence ratios instead of odds ratios in our primary analysis, given the relatively common frequency of hyperuricemia, as the odds ratio would overestimate the magnitude of the association when used as an approximation of relative risk. We examined the potential impact of an alternative definition of hyperuricemia (serum urate level >417 μmoles/liter [7.0 mg/dl]), regardless of sex (39). For all difference estimates and prevalence ratios, we calculated 95% confidence intervals (95% CIs). All P values are 2-sided.

For each risk factor, we calculated the PAR (28,30), which is an estimate of the percentage of hyperuricemia cases in this population that would have been avoided if the risk factor

exposure belonged to the corresponding lowest-risk group (BMI <25 kg/m², no alcohol consumption, adherence to a DASH-style diet, and no diuretic use), assuming a causal relationship between the risk factor and hyperuricemia (26,27). The evidence of causality of these 4 factors on serum urate levels and gout is summarized below and in the Supplementary Table, available on the *Arthritis & Rheumatology* web site at http://onlinelibrary.wiley. com/doi/10.1002/art.41067/abstract. The following is the PAR formula that was used:

$$\sum_{i=0}^{k} pd_i \left(\frac{RR_i - 1}{RR_i} \right) = 1 - \sum_{i=0}^{k} \frac{pd_i}{RR_i}$$

In this equation, pd_i represents the proportion of cases falling into ith exposure level, and RR_i refers to the relative risk comparing ith exposure level with unexposed group ($i = 0$) (26).

The PARs for individual risk factors accounted for covariates, using regression approaches (40). The individual (adjusted) PARs provided the following information: 1) the theoretical fraction of cases avoided by eliminating each individual factor from the US population, and 2) the relative importance among these factors. Adherence to a DASH-style diet was defined as the top quintile of DASH score, which corresponded to 50% compliance with the DASH nutrient targets among hypertensive patients in a previous NHANES analysis (24,25) and to 36% compliance in the current study population (n = 14,624). Furthermore, we explored the impact of changing the definition of adherence to 25%, 50%, and 75% compliance levels, corresponding to the top half, top

decile, and top percentile of DASH scores in the current study population. Finally we calculated the variance explained by each factor for comparison purposes, indicated by the partial R^2 obtained from linear regression models (18).

Simulation analyses. We conducted simulation analyses to evaluate the impact on PAR and variance explained when varying the prevalence of exposure by varying the proportion of target exposure group individuals in the study population. Using the parameters and variables from the current study population, including the adjusted prevalence ratios and covariates, we evaluated alcohol consumption (a lifestyle factor) and diuretic use (a drug) as examples.

RESULTS

Subject characteristics. The mean age of the study population was 47 years. The mean serum urate level was 319 μmoles/liter (5.36 mg/dl) (361 μmoles/liter [6.07 mg/dl] among men and 281 μmoles/liter [4.72 mg/dl] among women), and 20% were hyperuricemic (21% of men and 19% of women). The prevalence and distribution of risk factor categories are shown in Table 1.

Population attributable risk versus variance explained. The most important risk factor for hyperuricemia was BMI, with prevalence ratios of 1.85 (95% CI 1.69, 2.03), 2.72 (95% CI 2.48, 3.00), and 3.53 (95% CI 3.19, 3.91), respectively,

Table 1. Multivariable serum urate level differences and prevalence ratios for hyperuricemia, according to modifiable risk factors in the NHANES-III*

Risk factor	No. (%) of subjects	No. of hyperuricemia cases	Multivariable prevalence ratio for hyperuricemia (95% CI)†	Multivariable serum urate level difference, mg/dl (95% CI)†
BMI, kg/m²				
<25.0	5,789 (40)	607	1.0	0.0
25.0–29.9	5,133 (35)	1,090	1.85 (1.69, 2.03)	0.48 (0.44, 0.53)
30.0–34.9	2,378 (16)	729	2.72 (2.48, 3.00)	0.84 (0.78, 0.89)
≥35.0	1,324 (9)	508	3.53 (3.19, 3.91)	1.11 (1.04, 1.19)
DASH diet score				
1st quintile	2,602 (18)	544	1.0	0.0
2nd quintile	2,908 (20)	612	1.08 (0.98, 1.19)	0.01 (−0.06, 0.07)
3rd quintile	3,499 (24)	706	1.11 (1.00, 1.22)	0.04 (−0.02, 0.10)
4th quintile	3,075 (21)	593	1.16 (1.05, 1.29)	0.07 (0.01, 0.14)
5th quintile	2,540 (17)	544	1.22 (1.09, 1.37)	0.13 (0.05, 0.20)
Alcohol use, servings/day				
0	7,564 (52)	1,555	1.0	0.0
0.01–0.09	1,428 (10)	237	0.95 (0.85, 1.07)	0.00 (−0.07, 0.07)
0.1–0.49	3,398 (23)	637	1.18 (1.09, 1.28)	0.16 (0.11, 0.21)
0.5–0.99	1,313 (9)	284	1.37 (1.23, 1.53)	0.32 (0.25, 0.40)
≥1	921 (6)	221	1.40 (1.23, 1.58)	0.37 (0.29, 0.46)
Diuretic use				
No	13,388 (92)	2,280	1.0	0.0
Yes	1,236 (8)	654	2.24 (2.08, 2.41)	1.07 (1.00, 1.15)

* NHANES-III = Third National Health and Nutrition Survey; 95% CI = 95% confidence interval; BMI = body mass index; DASH = Dietary Approaches to Stop Hypertension.
† Mutually adjusted for the other risk factors in the table.

for individuals with a BMI of 25.0–29.9 kg/m^2, 30.0–34.9 kg/m^2, and ≥35 kg/m^2 compared with those with a BMI of <25.0 kg/m^2 (Table 1). In this population, 44% (95% CI 41%, 48%) of hyperuricemia cases were attributed to overweight or obesity (i.e., having a BMI of ≥25 kg/m^2) alone, whereas the serum urate variances explained by BMI as a categorical variable and as a continuous variable were 8.3% and 8.9%, respectively (Table 2).

The other 3 factors (i.e., a DASH-style diet, alcohol intake, and diuretic use) were also associated with the presence of hyperuricemia (Table 1). Those with the lowest levels of adherence to a DASH-style diet had scores that categorized them in the lowest quintile (quintile 5); they had a 22% higher prevalence of hyperuricemia (prevalence ratio 1.22 [95% CI 1.09, 1.37]) compared with those in the highest quintile (quintile 1). In the NHANES population, 9% of hyperuricemia cases (95% CI 3%, 16%) could have been prevented by following a DASH-style diet (i.e., by achieving a DASH diet score in the top quintile), whereas the corresponding variance explained was 0.1% (Table 2). When we set the reference group as subjects whose DASH diet scores were in the top half, top decile, and top percentile of scores, the PARs were 6%, 14%, and 40%, respectively (see Supplementary Figure 1, http://onlinelibrary.wiley.com/doi/10.1002/art.41067/abstract), whereas the corresponding variance explained remained at 0.1%. The adjusted serum urate level differences between the highest and lowest deciles and percentiles were 0.16 mg/dl and 0.44 mg/dl, respectively; the adjusted prevalence ratios between the extreme deciles and percentiles were 1.32 (95% CI 1.08, 1.61) and 2.11 (95% CI 1.18, 3.76).

A dose–response relationship was observed for alcohol intake categories, with those in the highest category (≥1 serving per day) showing the greatest prevalence ratio for hyperuricemia (1.40 [95% CI 1.23, 1.58]). In this population, 8% of hyperuricemia cases (95% CI 5%, 11%) could have been prevented by abstaining from alcohol consumption, whereas the corresponding serum urate variances explained as a categorial variable and as a continuous variable were 0.9% and 0.5%, respectively. The PAR of beer alone was 7%; when we used 0–0.09 servings per day as the reference group, the PAR remained nearly the same (8%). Subjects who took diuretics showed an increased risk of gout (prevalence ratio 2.24 [95% CI 2.08, 2.41]), with a PAR of 12% (95% CI 11%, 14%) and a serum urate variance explained of 5%.

The exclusion of patients with a self-reported history of physician-diagnosed gout or those who were taking medication to treat hyperuricemia did not materially alter our results; when they were excluded, PARs for overweight/obesity, nonadherence to a DASH-style diet, alcohol use, and diuretic use were 46%, 8%, 8%, and 12%, respectively. Similarly, an alternative definition of hyperuricemia (serum urate level >417 µmoles/liter [7.0 mg/dl], regardless of sex) did not materially alter these results (corresponding PARs using this alternative definition were 44%, 9%, 11%, and 16%).

Simulation study for varying prevalence of alcohol use and diuretic use. In our simulation study, where the prevalence of diuretic use increased from 8% (Table 1) to 100%, the PAR continued to increase as the prevalence increased, while the peak variance (6.3%) was observed at a prevalence of ~30% (Figure 1). The variance progressively declined after the prevalence reached 50% and approached zero when the prevalence was near 100%. Similarly, as the prevalence of alcohol use (≥1 serving per day) increased from 6% to near 100%, the PAR continued to increase, while the variance peaked at 1% when the prevalence was ~50% (Figure 2). As the prevalence further increased, the variance progressively declined and approached zero when the prevalence was nearly 100%.

DISCUSSION

In this national sample of US men and women, we found that overweight/obesity, gout-prone diet, alcohol consumption, and diuretic use could individually account for a substantial proportion of hyperuricemia cases. In contrast, the serum urate variance explained by these risk factors was very small. In particular, the serum urate variance explained by adherence to the DASH diet was very small (0.1%), similar to findings from a recent study that examined 5 US cohorts (variance ≤0.3%) (18).

How can dietary changes over time (together with a "Western lifestyle" of sedentary behavior and reduced physical activity) appear insignificant according to the variance measure, despite being associated with obesity (7,8) and gout epidemics (1,6)? This occurs because the variance measure does not incorporate how common the exposure is (i.e., its prevalence).

Table 2. Population attributable risk (PAR) of hyperuricemia and percent of serum variance explained according to modifiable risk factors in the NHANES-III

Modifiable risk factor	Exposure prevalence, %	PAR of hyperuricemia, % (95% CI)	Serum urate variance explained, %	Serum urate variance explained, %†
BMI ≥25 kg/m^2	60	44 (41, 48)	8.3	8.9
DASH diet score (bottom 4 quintiles)	82	9 (3, 16)	0.1	0.1
Alcohol use	48	8 (5, 11)	0.9	0.5
Diuretic use	8	12 (11, 14)	5.0	5.0

* See Table 1 for other definitions.
† Calculated based on continuous variables except for diuretic use.
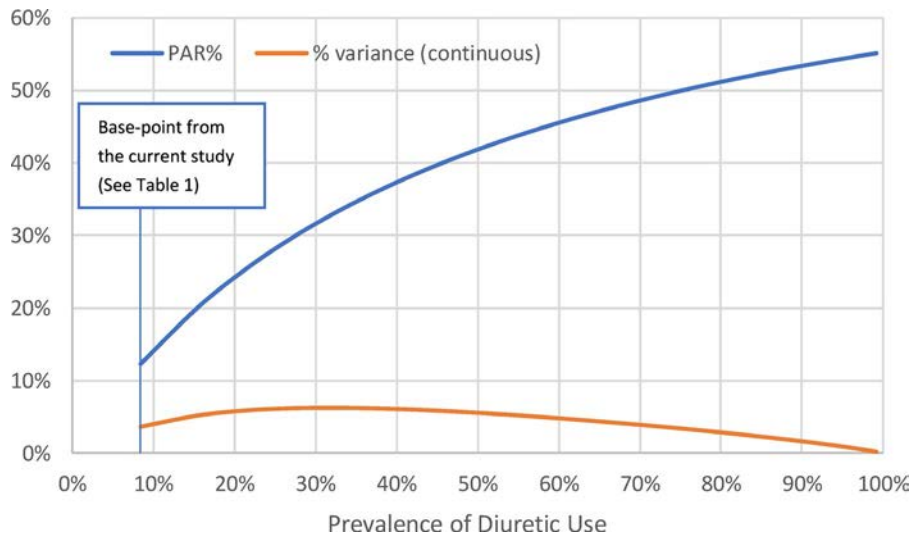
Figure 1. Population attributable risk (PAR) versus variance explained according to the prevalence of diuretic use.

As such, the proportion of the population variance explained can be highly misleading when used to assess which risk factor is more important (19), as previous studies and textbooks have demonstrated (i.e., the fallacy of employing the "proportion of population variance explained" as a measure of effect) (19–21,41). In a study of a population in which 90% of individuals were smokers (2,42), the proportion of variance in lung cancer explained by smoking was estimated to be <1% (with a PAR of 90%). Similarly, in our simulation analyses using the context of hyperuricemia, a 90% prevalence of taking diuretics or consuming alcohol (≥1 serving per day) corresponded to 1.6% and <1% of variance explained, respectively (Figures 1 and 2). These variance data appear counterintuitive, as one would expect a high level of contribution from these exposures, which are extremely prevalent in the population, provided that they have a strong causal effect. This is directly due to a low level of variability in exposure (e.g., 90% of the pop-

ulation takes diuretics or consumes alcohol), and the variance explained did not account for the high prevalence itself. Heuristically, this case can be best explained by the concept that "the most important causes of disease are invisible because they are everywhere" (2,20,42,43).

In contrast, the PAR correctly reflected the high level of exposure contribution by incorporating both its effect size and high prevalence (Figures 1 and 2). This is highly relevant to the potential population impact of dietary factors, as <1% of the US population is fully adherent to the DASH diet, and only 20% meet half of the DASH nutrient targets (24,25,44). These data collectively indicate that there is substantial room for improvement in modifying dietary factors to help prevent hyperuricemia and gout, in addition to preventing hypertension and related cardiovascular outcomes (24).

Furthermore, the continually worsening obesity epidemic in the US is largely driven by diet (including larger portion sizes [5]) and lifestyle changes that have occurred since the 1970s

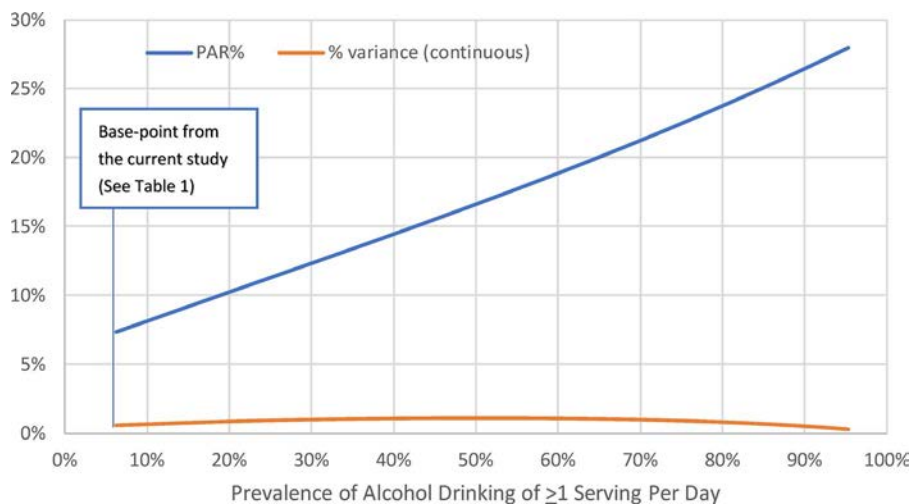**Figure 2.** Population attributable risk (PAR) versus variance explained according to the prevalence of alcohol consumption.

(7,8,42,45), which have coincided with the rising prevalence of hyperuricemia and gout (6,42). The current study also demonstrated that, among the 4 hyperuricemia risk factors examined, the most important factor was BMI, with a PAR of 44%. Because diet (along with physical activity) plays a critical role in the risk of obesity and the subsequent risk of hyperuricemia and gout (Figure 3), the net total effect of diet is greater than the PAR estimated for the isocaloric DASH diet alone (direct effect, measured independently of BMI), as shown in a previous study (18). To that end, the large PAR associated with BMI suggests large indirect effects of diet and exercise on the risk of hyperuricemia at the population level. Indeed, a previous prospective study on exercise demonstrated that both running distance and fitness performance were associated with a lower risk of gout; however, when the model was adjusted for BMI, the association disappeared, suggesting that the total effect of exercise was entirely through the indirect effect (i.e., BMI) (46). Although there is extensive evidence for the direct effect of isocaloric diet (discussed below), its expected impact is likely smaller than the indirect effect through BMI (47).

Obesity increases gout risk by raising the serum urate level, through both decreased renal urate excretion and increased urate production (48–53). Mendelian randomization studies have shown obesity to be causally associated with serum urate levels in the general population (54,55), and weight loss through bariatric surgery or lifestyle intervention leads to reductions in serum urate levels (56). Prompted by an interest in examining the strong biologic mechanism and plausibility of intake of purine, fructose, and alcohol, previous metabolic loading experiments examining these factors (57–65) have confirmed their serum urate–raising effects, whereas dairy products were shown to have urate-lowering effects in 3 experimental studies, including 2 randomized trials (66–68). The DASH diet discourages purine-rich red meat as well as fructose-rich foods, while encouraging dairy products, healthy protein, and fruits and vegetables (23,35). Indeed, a DASH diet trial analysis showed that the diet resulted in lower uric acid

levels compared with a typical American diet (the control diet), particularly among those with hyperuricemia. Adherence to the DASH diet resulted in lowering of serum urate levels by 0.4 mg/dl overall, by 1.0 mg/dl in subjects with a baseline serum urate level of ≥ 6 mg/dl, and by 1.3 mg/dl in subjects with a baseline serum urate level of ≥ 7 mg/dl (22). These findings, together with consistent epidemiologic data (from prospective cohort studies [23,69–71], ecologic studies [1], immigration studies [11,13], as well as correlating trends in food consumption and the obesity epidemic [1,2,4,6–10]) support the notion of a causal role of diet on hyperuricemia (directly or mediated by obesity) at the population level.

The increase in serum urate level caused by diuretics has been documented as occurring within a few days after the initiation of diuretic treatment (72–74). Accordingly, urate-lowering antihypertensive agents (e.g., calcium channel blockers or losartan) could be preferred, if hyperuricemia is a concern (74). These findings provide support for our assumptions that these associations are causal.

Strengths and limitations of our study deserve comment. This study was performed using a nationally representative sample of women and men in the US, so the findings are likely to be generalizable to the US adult population. Our individual (adjusted) PARs estimated the fraction of cases avoided by eliminating each of the individual factors from the population and assessing the relative importance of each of these factors. However, simply adding the individual PAR of each risk factor would be fallacious, because it would imply that each instance of disease is caused by a single factor and that ≥ 2 factors cannot collectively contribute to the same instance of disease. Measurement errors inherent in diet and alcohol exposures (unlike in BMI, diuretic use, or genes) would have underestimated their association with serum urate levels. Furthermore, the relatively small effect size was likely due to exposure status saturation in the US population, which made it difficult to detect differences between the quintiles of individual DASH
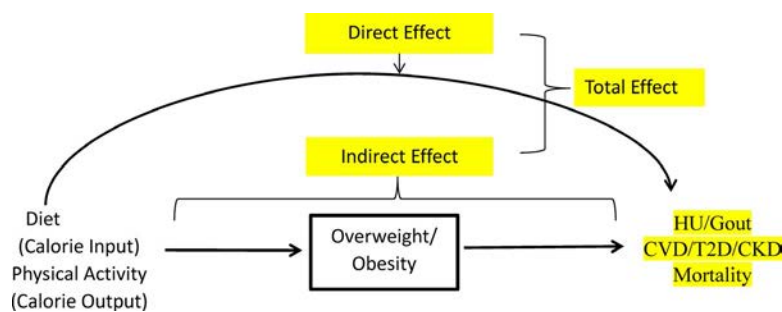
Figure 3. Causal pathways of modifiable factors on developing hyperuricemia (HU). Calorie input (diet) and calorie output (physical activity) are the modifiable determinants for overweight/obesity, which leads to hyperuricemia (indirect effect mediated by overweight/obesity). The other causal pathway for hyperuricemia is a direct effect, not mediated by overweight/obesity (e.g., isocaloric Dietary Approaches to Stop Hypertension diet or Western diet not affecting weight). The total effect of these lifestyle modifications is the combination of indirect and direct effects. Consistent with the large role that overweight/obesity plays in the risk of hyperuricemia, previous studies suggest that the indirect effect of these lifestyle factors (through overweight/obesity) is larger than their direct effect (46,47). CVD = cardiovascular disease, T2D = type 2 diabetes mellitus, CKD = chronic kidney disease. Color figure can be viewed in the online issue, which is available at http://onlinelibrary.wiley.com/doi/10.1002/art.41067/abstract.

food components or between the quintiles of the resulting diet score (see Supplementary Text, http://onlinelibrary.wiley.com/doi/10.1002/art.41067/abstract). Together, these mechanisms likely contributed to the observed small variance explained by the dietary scores. When a larger contrast with more stringent cutoffs was examined, the adjusted prevalence ratio increased as high as 2.11. This dose–response relationship provides further evidence of a causal role of the DASH diet. If there were no such relationship, PAR would not have increased, even with a more stringent choice of cutoffs.

Unlike prospective studies, a cross-sectional study design tends to leave uncertainty regarding the temporal sequence of exposure–outcome relationships and is also vulnerable to recall bias. However, if some participants modified lifestyle factors based on previously measured hyperuricemia, it would lead to an underestimation of the association between the corresponding factor and serum urate levels, making our findings too conservative. Furthermore, given the absence of existing conventional recommendations for the DASH diet for patients with hyperuricemia and gout at the time of study execution, it is unlikely that participants altered their adherence to the DASH diet based on previously identified hyperuricemia or gout. Moreover, exclusion of individuals with a self-reported history of physician-diagnosed gout or those who were taking medication to treat hyperuricemia did not materially alter our results. Finally, in the NHANES-III, the health examination component that included serum urate measurement (outcome) was performed after the household interview that inquired about dietary intake during the past month (exposure).

In conclusion, this nationally representative study indicates that modifiable risk factors (BMI, the DASH diet, alcohol consumption, and diuretic use) all have an important role in the primary prevention of hyperuricemia. Public health efforts to promote a healthy diet and prevent obesity would also help reduce the frequency of hyperuricemia and eventually the risk of gout in the general population. This includes encouraging individual behavioral changes as well as making broader policy changes targeting the obesogenic food environment (e.g., the implementation of a sugary beverage tax, menu labeling initiatives, and reforms to federal nutrition assistance programs) (75). Our findings also provide real-life empirical evidence that when the exposure is common, the variance explained is severely limited in assessing the relative importance among risk factors.

AUTHOR CONTRIBUTIONS

All authors were involved in drafting the article or revising it critically for important intellectual content, and all authors approved the final version to be published. Dr. Choi had full access to all of the data in the study and takes responsibility for the integrity of the data and the accuracy of the data analysis.
Study conception and design. Choi.
Acquisition of data. Choi.
Analysis and interpretation of data. Choi, McCormick, Lu, Rai, Yokose, Zhang.

REFERENCES

1. Kuo CF, Grainge MJ, Zhang W, Doherty M. Global epidemiology of gout: prevalence, incidence and risk factors. Nat Rev Rheumatol 2015;11:649–62.

2. Rai S, Zhang Y, Hu FB, Pearce N, Choi HK. The paradox of ubiquitous risk factors for gout. BMJ 2018;363:k3951.

3. Kuo CF, Grainge MJ, Mallen C, Zhang W, Doherty M. Rising burden of gout in the UK but continuing suboptimal management: a nationwide population study. Ann Rheum Dis 2015;74:661–7.

4. Bray GA, Nielsen SJ, Popkin BM. Consumption of high-fructose corn syrup in beverages may play a role in the epidemic of obesity. Am J Clin Nutr 2004;79:537–43.

5. Young LR, Nestle M. The contribution of expanding portion sizes to the US obesity epidemic. Am J Public Health 2002;92:246–9.

6. Zhu Y, Pandya BJ, Choi HK. Prevalence of gout and hyperuricemia in the US general population. Arthritis Rheum 2011;63:3136–41.

7. NCD Risk Factor Collaboration. Worldwide trends in body-mass index, underweight, overweight, and obesity from 1975 to 2016: a pooled analysis of 2416 population-based measurement studies in 128.9 million children, adolescents, and adults. Lancet 2017;390:2627–42.

8. Wang YC, McPherson K, Marsh T, Gortmaker SL, Brown M. Health and economic burden of the projected obesity trends in the USA and the UK. Lancet 2011;378:815–25.

9. Arromdee E, Michet CJ, Crowson CS, O'Fallon WM, Gabriel SE. Epidemiology of gout: is the incidence rising? J Rheumatol 2002;29:2403–6.

10. Lawrence RC, Felson DT, Helmick CG, Arnold LM, Choi H, Deyo RA, et al, for the National Arthritis Data Workgroup. Estimates of the prevalence of arthritis and other rheumatic conditions in the United States: part II. Arthritis Rheum 2008;58:26–35.

11. Johnson RJ, Rideout BA. Uric acid and diet—insights into the epidemic of cardiovascular disease. N Engl J Med 2004;350:1071–3.

12. Cassim B, Mody GM, Deenadayalu VK, Hammond MG. Gout in black South Africans: a clinical and genetic study. Ann Rheum Dis 1994;53:759–62.

13. Kagan A, Harris BR, Winkelstein W Jr, Johnson KG, Kato H, Syme SL, et al. Epidemiologic studies of coronary heart disease and stroke in Japanese men living in Japan, Hawaii and California: demographic, physical, dietary and biochemical characteristics. J Chronic Dis 1974;27:345–64.

14. Prior IA, Welby TJ, Ostbye T, Salmond CE, Stokes YM. Migration and gout: the Tokelau Island migrant study. Br Med J (Clin Res Ed) 1987;295:457–61.

15. Klemp P, Stansfield SA, Castle B, Robertson MC. Gout is on the increase in New Zealand. Ann Rheum Dis 1997;56:22–6.

16. Miao Z, Li C, Chen Y, Zhao S, Wang Y, Wang Z, et al. Dietary and lifestyle changes associated with high prevalence of hyperuricemia and gout in the Shandong coastal cities of Eastern China. J Rheumatol 2008;35:1859–64.

17. Rai SK, Aviña-Zubieta JA, McCormick N, De Vera MA, Shojania K, Sayre EC, et al. The rising prevalence and incidence of gout in British Columbia, Canada: population-based trends from 2000 to 2012. Semin Arthritis Rheum 2017;46:451–6.

18. Major TJ, Topless RK, Dalbeth N, Merriman TR. Evaluation of the diet wide contribution to serum urate levels: meta-analysis of population based cohorts. BMJ 2018;363:k3951.

19. Greenland S, Schlesselman JJ, Criqui MH. The fallacy of employing standardized regression coefficients and correlations as measures of effect. Am J Epidemiol 1986;123:203–8.

20. Pearce N. Epidemiology in a changing world: variation, causation and ubiquitous risk factors. Int J Epidemiol 2011;40:503–12.

21. Rothman KJ, Greenland S. Modern epidemiology. 2nd ed. Philadelphia: Lippincott Williams & Wilkins; 1998.

22. Juraschek SP, Gelber AC, Choi HK, Appel LJ, Miller ER III. Effects of the Dietary Approaches to Stop Hypertension (DASH) diet and sodium intake on serum uric acid. Arthritis Rheumatol 2016;68:3002–9.

23. Rai SK, Fung TT, Lu N, Keller SF, Curhan GC, Choi HK. The Dietary Approaches to Stop Hypertension (DASH) diet, Western diet, and risk of gout in men: prospective cohort study. BMJ 2017;357:j1794.

24. Steinberg D, Bennett GG, Svetkey L. The DASH diet, 20 years later. JAMA 2017;317:1529–30.

25. Mellen PB, Gao SK, Vitolins MZ, Goff DC Jr. Deteriorating dietary habits among adults with hypertension: DASH dietary accordance, NHANES 1988–1994 and 1999–2004. Arch Intern Med 2008;168:308–14.

26. Rockhill B, Newman B, Weinberg C. Use and misuse of population attributable fractions. Am J Public Health 1998;88:15–9.

27. Greenland S, Robins JM. Conceptual problems in the definition and interpretation of attributable fractions. Am J Epidemiol 1988;128:1185–97.

28. Stampfer MJ, Hu FB, Manson JE, Rimm EB, Willett WC. Primary prevention of coronary heart disease in women through diet and lifestyle. N Engl J Med 2000;343:16–22.

29. Forman JP, Stampfer MJ, Curhan GC. Diet and lifestyle risk factors associated with incident hypertension in women. JAMA 2009;302:401–11.

30. Hu FB, Manson JE, Stampfer MJ, Colditz G, Liu S, Solomon CG, et al. Diet, lifestyle, and the risk of type 2 diabetes mellitus in women. N Engl J Med 2001;345:790–7.

31. Yamagishi K, Tanigawa T, Kitamura A, Köttgen A, Folsom AR, Iso H, on behalf of the CIRCS Investigators. The rs2231142 variant of the ABCG2 gene is associated with uric acid levels and gout among Japanese people. Rheumatology (Oxford) 2010;49:1461–5.

32. Nakayama A, Matsuo H, Nakaoka H, Nakamura T, Nakashima H, Takada Y, et al. Common dysfunctional variants of ABCG2 have stronger impact on hyperuricemia progression than typical environmental risk factors. Sci Rep 2014;4:5227.

33. Woodward OM, Köttgen A, Coresh J, Boerwinkle E, Guggino WB, Köttgen M. Identification of a urate transporter, ABCG2, with a common functional polymorphism causing gout. Proc Natl Acad Sci U S A 2009;106:10338–42.

34. Centers for Disease Control and Prevention. National Health and Nutrition Examination Survey: reference manuals and report. URL: https://wwwn.cdc.gov/nchs/nhanes/nhanes3/ManualsAndReports.aspx.

35. Fung TT, Chiuve SE, McCullough ML, Rexrode KM, Logroscino G, Hu FB. Adherence to a DASH-style diet and risk of coronary heart disease and stroke in women. Arch Intern Med 2008;168:713–20.

36. Karanja NM, Obarzanek E, Lin PH, McCullough ML, Phillips KM, Swain JF, et al, for the DASH Collaborative Research Group. Descriptive characteristics of the dietary patterns used in the Dietary Approaches to Stop Hypertension Trial. J Am Diet Assoc 1999;99 Suppl:S19–27.

37. Taylor EN, Fung TT, Curhan GC. DASH-style diet associates with reduced risk for kidney stones. J Am Soc Nephrol 2009;20:2253–9.

38. Choi HK, Curhan G. Beer, liquor, and wine consumption and serum uric acid level: the Third National Health and Nutrition Examination Survey. Arthritis Rheum 2004;51:1023–9.

39. Choi JW, Ford ES, Gao X, Choi HK. Sugar-sweetened soft drinks, diet soft drinks, and serum uric acid level: the Third National Health and Nutrition Examination Survey. Arthritis Rheum 2008;59:109–16.

40. Benichou J. A review of adjusted estimators of attributable risk. Stat Methods Med Res 2001;10:195–216.

41. Rose G, Khaw KT, Marmot M. Rose's strategy of preventative medicine. Oxford: Oxford University Press; 2008.

42. Rai SK, Zhang Y, Hu BF, Pearce N, Choi HK. The fatalistic public health implication of flawed methodology. BMJ 2018;363:k951.

43. Rose G. Sick individuals and sick populations. Int J Epidemiol 2001;30:427–32.

44. Kim H, Andrade FC. Diagnostic status of hypertension on the adherence to the Dietary Approaches to Stop Hypertension (DASH) diet. Prev Med Rep 2016;4:525–31.

45. Hu FB. Genetic predictors of obesity. In: Hu F, editor. Obesity epidemiology. New York: Oxford University Press; 2008.

46. Williams PT. Effects of diet, physical activity and performance, and body weight on incident gout in ostensibly healthy, vigorously active men. Am J Clin Nutr 2008;87:1480–7.

47. Dessein PH, Shipton EA, Stanwix AE, Joffe BI, Ramokgadi J. Beneficial effects of weight loss associated with moderate calorie/carbohydrate restriction, and increased proportional intake of protein and unsaturated fat on serum urate and lipoprotein levels in gout: a pilot study. Ann Rheum Dis 2000;59:539–43.

48. Fam AG. Gout, diet, and the insulin resistance syndrome. J Rheumatol 2002;29:1350–5.

49. Emmerson BT. The management of gout. N Engl J Med 1996;334:445–51.

50. Emmerson BT. Alteration of urate metabolism by weight reduction. Aust N Z J Med 1973;3:410–2.

51. Modan M, Halkin H, Fuchs Z, Lusky A, Chetrit A, Segal P, et al. Hyperinsulinemia: a link between glucose intolerance, obesity, hypertension, dyslipoproteinemia, elevated serum uric acid and internal cation imbalance. Diabete Metab 1987;13:375–80.

52. Facchini F, Chen YD, Hollenbeck CB, Reaven GM. Relationship between resistance to insulin-mediated glucose uptake, urinary uric acid clearance, and plasma uric acid concentration. JAMA 1991;266:3008–11.

53. Yamashita S, Matsuzawa Y, Tokunaga K, Fujioka S, Tarui S. Studies on the impaired metabolism of uric acid in obese subjects: marked reduction of renal urate excretion and its improvement by a low-calorie diet. Int J Obes 1986;10:255–64.

54. Lyngdoh T, Vuistiner P, Marques-Vidal P, Rousson V, Waeber G, Vollenweider P, et al. Serum uric acid and adiposity: deciphering causality using a bidirectional Mendelian randomization approach. PLoS One 2012;7:e39321.

55. Oikonen M, Wendelin-Saarenhovi M, Lyytikäinen LP, Siitonen N, Loo BM, Jula A, et al. Associations between serum uric acid and markers of subclinical atherosclerosis in young adults: the cardiovascular risk in Young Finns study. Atherosclerosis 2012;223:497–503.

56. Nielsen SM, Bartels EM, Henriksen M, Wæhrens EE, Gudbergsen H, Bliddal H, et al. Weight loss for overweight and obese individuals with gout: a systematic review of longitudinal studies. Ann Rheum Dis 2017;76:1870–82.

57. Clifford AJ, Riumallo JA, Young VR, Scrimshaw NS. Effects of oral purines on serum and urinary uric acid of normal, hyperuricaemic and gouty humans. J Nutr 1976;106:428–34.

58. Clifford AJ, Story DL. Levels of purines in foods and their metabolic effects in rats. J Nutr 1976;106:435–42.

59. Zöllner N. Influence of various purines on uric acid metabolism. Bibl Nutr Dieta 1973;34–43.

60. Zöllner N, Griebsch A. Diet and gout. Adv Exp Med Biol 1974;41:435–42.

61. Stirpe F, Della Corte E, Bonetti E, Abbondanza A, Abbati A, De Stefano F. Fructose-induced hyperuricaemia [letter]. Lancet 1970;2:1310–1.

62. Emmerson BT. Effect of oral fructose on urate production. Ann Rheum Dis 1974;33:276–80.

63. Perheentupa J, Raivio K. Fructose-induced hyperuricaemia. Lancet 1967;2:528–31.

64. Dalbeth N, House ME, Gamble GD, Horne A, Pool B, Purvis L, et al. Population-specific influence of SLC2A9 genotype on the acute hyperuricaemic response to a fructose load. Ann Rheum Dis 2013;72:1868–73.

65. Gibson T, Rodgers AV, Simmonds HA, Toseland P. Beer drinking and its effect on uric acid. Br J Rheumatol 1984;23:203–9.

66. Garrel DR, Verdy M, PetitClerc C, Martin C, Brulé D, Hamet P. Milk- and soy-protein ingestion: acute effect on serum uric acid concentration. Am J Clin Nutr 1991;53:665–9.

67. Ghadirian P, Shatenstein B, Verdy M, Hamet P. The influence of dairy products on plasma uric acid in women. Eur J Epidemiol 1995;11:275–81.

68. Dalbeth N, Wong S, Gamble GD, Horne A, Mason B, Pool B, et al. Acute effect of milk on serum urate concentrations: a randomised controlled crossover trial. Ann Rheum Dis 2010;69:1677–82.

69. Choi HK, Atkinson K, Karlson EW, Willett W, Curhan G. Purine-rich foods, dairy and protein intake, and the risk of gout in men. N Engl J Med 2004;350:1093–103.

70. Choi HK, Curhan G. Soft drinks, fructose consumption, and the risk of gout in men: prospective cohort study. BMJ 2008;336: 309–12.

71. Choi HK, Willett W, Curhan G. Fructose-rich beverages and risk of gout in women. JAMA 2010;304:2270–8.

72. Leary WP, Reyes AJ, Wynne RD, van der Byl K. Renal excretory actions of furosemide, of hydrochlorothiazide and of the vaso- dilator flosequinan in healthy subjects. J Int Med Res 1990;18: 120–41.

73. Hunter DJ, York M, Chaisson CE, Woods R, Niu J, Zhang Y. Recent diuretic use and the risk of recurrent gout attacks: the online case- crossover gout study. J Rheumatol 2006;33:1341–5.

74. Choi HK, Soriano LC, Zhang Y, Rodríguez LA. Antihypertensive drugs and risk of incident gout among patients with hypertension: population based case-control study. BMJ 2012;344:d8190.

75. Gortmaker SL, Swinburn BA, Levy D, Carter R, Mabry PL, Finegood DT, et al. Changing the future of obesity: science, policy, and action. Lancet 2011;378:838–47.

AMERICAN COLLEGE
of RHEUMATOLOGY
Empowering Rheumatology Professionals

Activated M2 Macrophages Contribute to the Pathogenesis of IgG4-Related Disease via Toll-like Receptor 7/Interleukin-33 Signaling

Noriko Ishiguro,[1] Masafumi Moriyama,[1] [ID] Katsuhiro Furusho,[2] Sachiko Furukawa,[1] Takuma Shibata,[3] Yusuke Murakami,[3] Akira Chinju,[1] A. S. M. Rafiul Haque,[1] Yuka Gion,[4] Miho Ohta,[1] Takashi Maehara,[1] Akihiko Tanaka,[1] Masaki Yamauchi,[1] Mizuki Sakamoto,[1] Keita Mochizuki,[1] Yuko Ono,[1] Jun-Nosuke Hayashida,[1] Yasuharu Sato,[4] Tamotsu Kiyoshima,[1] Hidetaka Yamamoto,[5] Kensuke Miyake,[3] and Seiji Nakamura[1]

Objective. IgG4-related disease (IgG4-RD) is a unique inflammatory disorder in which Th2 cytokines promote IgG4 production. In addition, recent studies have implicated the Toll-like receptor (TLR) pathway. This study was undertaken to examine the expression of TLRs in salivary glands (SGs) from patients with IgG4-RD.

Methods. SGs from 15 patients with IgG4-RD, 15 patients with Sjögren's syndrome (SS), 10 patients with chronic sialadenitis, and 10 healthy controls were examined histologically. TLR family gene expression (TLR-1 through TLR-10) was analyzed by DNA microarray in the submandibular glands (SMGs). Up-regulation of TLRs was confirmed in SGs from patients with IgG4-RD. Finally, the phenotype of human TLR-7 (huTLR-7)–transgenic C57BL/6 mice was assessed before and after stimulation with TLR agonist.

Results. In patients with IgG4-RD, TLR-4, TLR-7, TLR-8, and TLR-9 were overexpressed. Polymerase chain reaction validated the up-regulation of TLR-7 in IgG4-RD compared with the other groups. Immunohistochemical analysis confirmed strong infiltration of TLR-7–positive cells in the SGs of patients with IgG4-RD. Double immunohistochemical staining showed that TLR-7 expression colocalized with CD163+ M2 macrophages. After in vitro stimulation with a TLR-7 agonist, CD163+ M2 macrophages produced higher levels of interleukin-33 (IL-33), which is a Th2-activating cytokine. In huTLR-7–transgenic mice, the focus and fibrosis scores in SMGs, pancreas, and lungs were significantly higher than those in wild-type mice ($P < 0.05$). Moreover, the concentration of serum IgG, IgG1, and IL-33 in huTLR-7–transgenic mice was distinctly increased upon stimulation with a TLR-7 agonist ($P < 0.05$).

Conclusion. TLR-7–expressing M2 macrophages may promote the activation of Th2 immune responses via IL-33 secretion in IgG4-RD.

INTRODUCTION

IgG4-related disease (IgG4-RD) is a recently described disease characterized by elevated serum IgG4 and marked infiltration of IgG4+ plasma cells with hyperplastic ectopic germinal centers (GCs) into multiple organs, including the pancreas, kidney, bile duct, lung, retroperitoneum, prostate, lacrimal glands, and salivary glands (SGs) (1–3). IgG4-RD patients frequently have a history of bronchial asthma and allergic rhinitis with severe eosinophilia and elevated serum IgE levels (4).

It is well known that allergic immune responses are induced by allergen-specific Th2 cytokines, such as interleukin-4 (IL-4), IL-10, and IL-13, which promote isotype switching to both IgG4 and IgE in B cells (5,6). Several studies have

indicated that Th2 cytokines such as IL-4 and IL-10 contribute to the IgG4 production of IgG4-related dacryoadenitis and sialadenitis (IgG4-DS) (7–9) and IgG4-related sclerosing pancreatitis and cholangitis (10). In addition, other adaptive immune cells, including Treg cells (11), follicular helper T cells (12), CD4+ cytotoxic T lymphocytes (13), and IgG4-producing plasmablasts (14), have recently received increasing attention with regard to the pathogenesis of IgG4-RD.

Innate immunity has also recently been shown to play a role in the initiation of IgG4-RD. We previously described the accumulation of CD163+ M2 macrophages in multiple organs from patients with IgG4-RD, indicating that these cells may contribute to the fibrosis associated with IgG4-RD through the production of profibrotic factors (CCL18 and IL-10) (15) and the activation of Th2 immune responses via IL-33 secretion (16). In addition, several studies have indicated that BAFF secreted by macrophages and basophils induces IgG4 production by B cells via activation of Toll-like receptors (TLRs) (17,18). Although BAFF was discovered originally as a cytokine that potentiates B cell maturation and immunoglobulin production (19), the BAFF-induced immunoglobulin subset was not restricted to IgG4; therefore, the immunopathogenesis of IgG4-RD via the TLR pathway remains unclear.

TLRs are a family of transmembrane receptors that play a crucial role in the activation of innate immunity against invading pathogens (20,21), as well as the development of antigen-specific acquired immunity (22,23). Interestingly, inappropriate signaling by TLRs triggers the polyclonal expansion of B cells that occurs after exposure to infectious agents and then exacerbates autoimmune diseases (24). In this study, we thus sought to characterize the expression of the TLR family in SGs from patients with IgG4-RD and the phenotype of TLR-transgenic mice to clarify the contribution of TLRs to the pathogenesis of IgG4-RD.

PATIENTS AND METHODS

Study participants. The study design and methods were approved by the Institutional Review Board of the Center for Clinical and Translational Research of Kyushu University Hospital (IRB serial nos. 25-287 and 26-86) and followed the tenets of the Declaration of Helsinki. The methods were carried out in accordance with the approved guidelines. All patients or their relatives gave their informed consent within the written treatment contract on admission and therefore prior to their inclusion in the study.

SG samples and peripheral blood mononuclear cells (PBMCs) were obtained from patients referred to the Department of Oral and Maxillofacial Surgery, Kyushu University Hospital between 2010 and 2016. The study included 15 patients with IgG4-RD (11 men and 4 women; mean ± SD age 63.6 ± 10.3 years), 15 patients with primary Sjögren's syndrome (SS) (15 women; age 54.3 ± 17.6 years), 10 patients with chronic sialadenitis (4 men and 6 women; age 49.1 ± 21.6 years), and 10 healthy controls (5 men and 5 women; age 62.1 ± 13.6 years). Clinical and serologic

profiles of the patients with IgG4-RD are available upon request from the corresponding author.

Patients with IgG4-RD and patients with SS underwent open SG biopsies, as described by Moriyama et al (25), while patients with chronic sialadenitis underwent an extraction of SGs. IgG4-RD was diagnosed according to both the "Comprehensive diagnostic criteria for IgG4-related disease" (26) and "Diagnostic criteria for IgG4-DS" (27). All patients with IgG4-RD showed characteristic histopathologic findings, including marked infiltration of IgG4-positive plasma cells, severe fibrosis, and formation of multiple ectopic GCs, and had never been treated with steroids or any other immunosuppressants. SS was diagnosed according to both the 1999 criteria for SS from the Research Committee of the Ministry of Health, Labour and Welfare of the Japanese Government (28) and the American College of Rheumatology/European League Against Rheumatism 2016 Classification Criteria for primary SS (29). All patients with SS had lymphocytic infiltration in the SGs, had no other autoimmune diseases, and had never been treated with steroids or any other immunosuppressants. There was no documented history of HIV, human T lymphotropic virus type 1, hepatitis B virus, or hepatitis C virus infection in any of the patients. None of the patients had evidence of malignant lymphoma at the time of the study. For comparison, tonsils and lymph nodes were obtained from patients with oral squamous cell carcinoma at tumor resection. These samples from patients with oral squamous cell carcinoma were histologically normal and lacked clinical evidence of metastasis and radiation therapy.

Extraction of RNA and synthesis of complementary DNA (cDNA). Total RNA was prepared from SGs by the acidified guanidinium–phenol–chloroform method as previously described (30). One microgram of total RNA was prepared and used for the synthesis of cDNA, and then RNA was incubated for 1 hour at 42°C with 20 units of RNase inhibitor (Promega), 0.5 μg of oligo-1218 (Pharmacia), 0.5 mM deoxyribonucleotide triphosphate (Pharmacia), 10 mM of dithiothreitol, and 100 units of RNA reverse transcriptase (Life Technologies).

Gene expression microarrays. According to the manufacturers' instructions, complementary RNA was amplified and labeled using a Low Input Quick Amp Labeling Kit (Agilent), and hybridized to SurePrint G3 Human Gene Expression Microarrays 8 60K v2 (Agilent) (DNA chip including 60,000 genes). All hybridized microarray slides were scanned using an Agilent scanner. Relative hybridization intensities and background hybridization values were calculated using Agilent Feature Extraction Software (version 9.5.1.1) as previously described (31).

Quantitative estimation of messenger RNA (mRNA) by real-time polymerase chain reaction (PCR). The resulting cDNA was amplified using LightCycler FastStart DNA Master mix SYBR Green III (Roche Diagnostics) in a LightCycler real-time

PCR instrument (version 3.5; Roche Diagnostics). The levels of mRNA for TLR-7, TLR-8, TLR-9, and IL-33 were analyzed. Target mRNA levels were expressed relative to β-actin as the housekeeping gene. Primer sequences used are available upon request from the corresponding author. All analyses were performed in triplicate.

Immunohistochemical analysis. Serial 4-μm sections were cut from formalin-fixed and paraffin-embedded SG tissue and stained with a conventional avidin–biotin complex technique as previously described (30). Antibodies used included anti-CD68 (catalog no. ab955; Abcam), anti-CD163 (catalog no. NCL-CD163; Leica Biosystems), anti-CD123 (catalog no. NCL-L-CD123; Leica Biosystems), anti–TLR-8 (catalog no. 85859; Abcam), anti–TLR-9 (catalog no. 134368; Abcam), and anti-IL-33 (catalog no. 54385; Abcam) mouse monoclonal antibodies; anti-CD11c (catalog no. 52632; Abcam), and anti–TLR-7 (catalog no. 124928; Abcam) rabbit monoclonal antibodies; anti-CD317 (catalog no. DDX0390p-100; Novus) rat monoclonal antibodies; and anti–TLR-10 (catalog no. 53631; Abcam), anti-CD206 (catalog no. AF2534; R&D Systems), and anti-IgG1 (catalog no. 97236; Abcam) goat polyclonal antibodies. Tissue sections were sequentially incubated with primary antibodies for 2.5 hours and then with biotinylated anti-mouse, anti-rabbit, anti-rat, or anti-goat IgG secondary antibodies (Vector), followed by avidin–biotin–horseradish peroxidase complex (Vector), and 3,3′-diaminobenzidine (Vector). Mayer's hematoxylin was used for counterstaining.

For double immunofluorescence analysis, formalin-fixed and paraffin-embedded sections of submandibular glands (SMGs) were stained using an Opal 4-Color Manual IHC Kit (catalog #NEL810001KT; PerkinElmer). The following primary antibodies were used: anti-CD163, anti-CD123, and anti–TLR-7. Photomicrographs were obtained using a light microscope equipped with a digital camera (BZ-9000 series; Keyence).

Cell culture and stimulation of human CD163+ M2 macrophages in vitro. PBMCs were obtained from a healthy donor, and CD14+ monocytes were isolated using an EasySep Human Monocyte Isolation Kit (StemCell Technologies). Cells (5 × 10^6 cells/ml) were cultured using a CellXVivo Human M2 Macrophage Differentiation Kit (R&D Systems) for 6 days in a humidified chamber with 5% CO_2 at 37°C. Differentiated M2 macrophages were dissociated and collected.

Next, collected cells were then counted and separated in three 15-ml tubes, followed by incubation with fluorescein isothiocyanate (FITC)–conjugated anti-human CD163 antibodies (BioLegend) for 10 minutes in the dark at 4°C. Samples were washed in MACS buffer (Miltenyi Biotec) and incubated with Anti-FITC MicroBeads (Miltenyi Biotec) for 15 minutes at 4°C. Samples were washed, and CD163+ cells were separated by manual magnetic-activated cell sorting procedure with a MiniMACS Starting Kit (Miltenyi Biotec), and were stimulated with R848. The supernatants were subjected to analysis.

Human TLR-7–transgenic/mouse TLR-7–deficient (huTLR-7–transgenic/mTLR-7^−/−) mice and in vivo treatment. The in vivo function of huTLR-7 was examined using TLR-7^−/− mice and huTLR-7–transgenic/mTLR-7^−/− mice on a C57BL/6 background. First, we generated Gt(ROSA)26Sor^huTLR7/+ mice (details are available upon request from the corresponding author). Briefly, CAG-STOP-eGFP-ROSA26TV Targeting vector (a kind gift from Yoshiteru Sasaki) with huTLR-7 coding sequence was electroporated into C57BL/6N mouse–derived JM8.A3N1 embryonic stem cells (ESCs). Neomycin-resistant ESC clones were screened by Southern blot analysis using a 5′ external probe and PCR using a 5′ external primer (5′-TCCTCA GAGAGCCTCGGCTAGGTAG-3′) and neomycin primer (5′- AA TGGCCGCTTTTCTGGATTCATC-3′), and then a homologous recombinant ESC clone was injected into C57/BL6N mouse–derived blastocysts to produce chimeric mice. Since the targeted allele enables CAG promoter–driven expression of human TLR-7 and green fluorescent protein (GFP) after removal of the floxed neomycin cassette by recombinases, male chimeric mice were crossed with female CAG-Cre–transgenic mice. Finally, Gt(ROSA)26Sor^huTLR-7/+ mice were crossed with mTLR-7^−/− mice, and mTLR-7^−/−/Gt(ROSA)26Sor^huTLR-7/+ (huTLR-7–transgenic) mice were subjected to in vivo experiments. For TLR-7 ligand treatment of mice, the skin on the ears was topically treated, 3 times weekly, with 100 μg of resiquimod (R848; ChemScene Chemicals) in 100 μl of acetone.

Histologic analysis in huTLR-7–transgenic/mTLR-7^−/− mice. Four-micron sections of mouse SMG, pancreas, kidney, lung, and liver were prepared and stained with hematoxylin and eosin (H&E) for conventional histologic examination. The degree of lymphocytic infiltration in the specimens was judged by focus scoring. The standardized score used is the number of focal inflammatory cell aggregates containing 50 or more mononuclear cells in each 4 μm^2 area of SG tissue (32,33).

Evaluation of the severity of fibrosis in huTLR-7–transgenic/mTLR-7^−/− mice. To evaluate fibrosis histologically, Masson's trichrome staining (Polysciences) was performed. Briefly, 4-μm formalin-fixed, paraffin-embedded sections were prepared and stained. Connective and fibrotic tissues were selectively stained blue, whereas nuclei were stained dark brown to black by Weigert's iron hematoxylin and the cytoplasm was stained red. The fibrosis scores in mouse SMGs, pancreas, kidney, lung, and liver were defined as the ratio of the fibrotic area (blue) to the whole stained area in a 4 μm^2 field of view, from 5 different areas.

Induction of bone marrow–derived macrophages. Bone marrow cells from mTLR-7^−/− and huTLR-7–transgenic mice on a C57BL/6 background were cultured with 100 ng/ml macrophage colony-stimulating factor (catalog no. 315-02; PeproTech) for 7 days.

Flow cytometric analysis. Prepared cells were subjected to flow cytometric analysis using an LSRFortessa X-20 system (Becton Dickinson). Bone marrow–derived macrophages were stained with anti-CD11b monoclonal antibody (clone M1/70). To detect GFP in bone marrow–derived macrophages (CD11b+), a blue laser was used. Flow cytometry data were analyzed using FlowJo software.
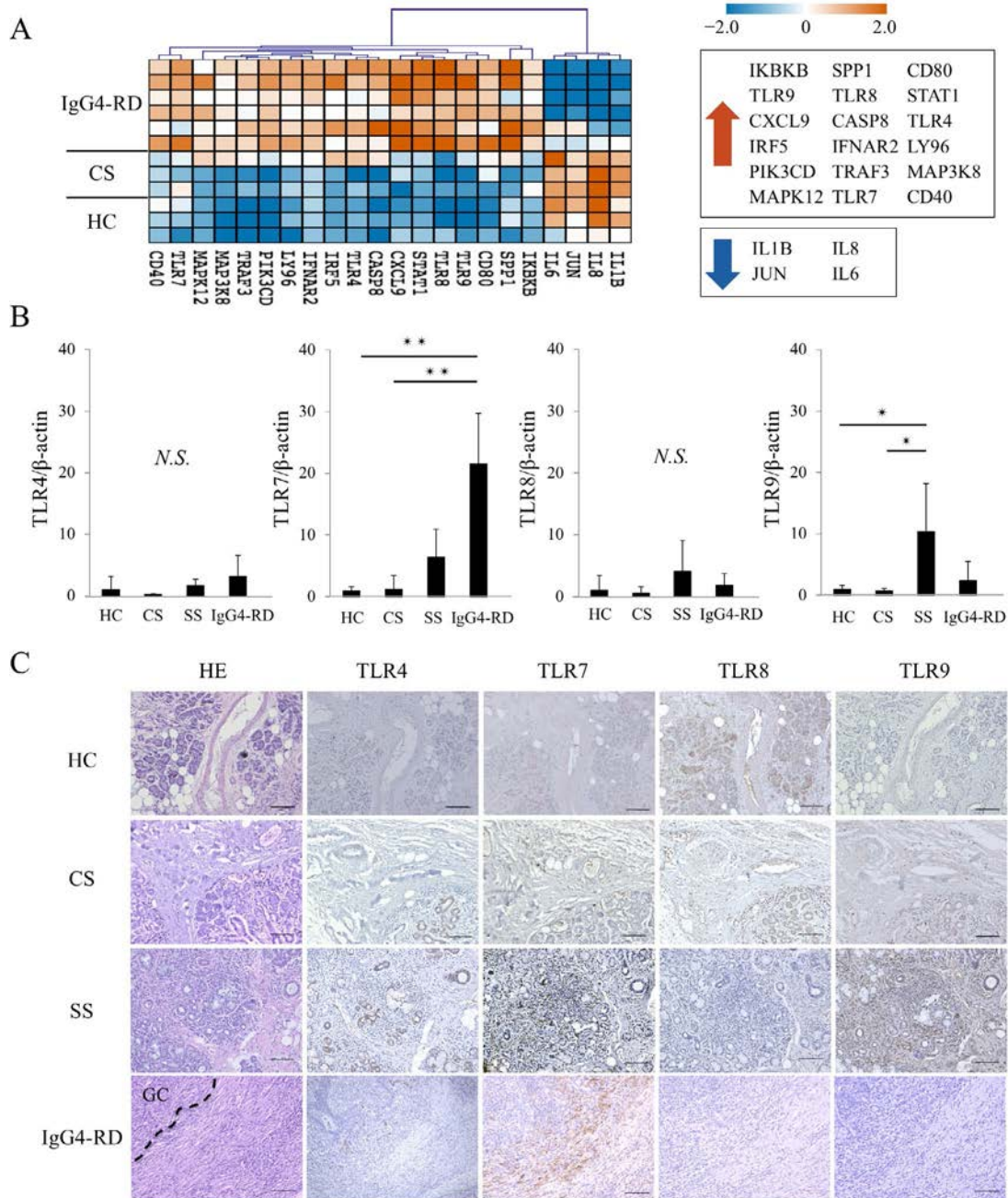
Figure 1. Toll-like receptor (TLR)–related gene expression patterns in salivary glands (SGs) from patients with IgG4-related disease (IgG4-RD). **A**, Heatmap depicting differentially expressed TLR-related genes in submandibular glands (SMGs) from patients with IgG4-RD (n = 6), patients with chronic sialadenitis (CS; n = 3), and healthy controls (HCs; n = 3). Only genes up-regulated or down-regulated by at least 2-fold are shown. **B**, Quantitative polymerase chain reaction analysis of TLR-4, TLR-7, TLR-8, and TLR-9 in SGs from healthy controls (n = 10), patients with chronic sialadenitis (n = 10), patients with Sjögren's syndrome (SS; n = 15), and patients with IgG4-RD (n = 15). Bars show the mean ± SD. * = $P < 0.05$; ** = $P < 0.01$ by Kruskal-Wallis test. NS = not significant. **C**, Distribution of candidate TLRs in SMGs from representative healthy controls and patients with chronic sialadenitis, patients with SS, and patients with IgG4-RD. Sections were stained with hematoxylin and eosin (H&E) and for TLR-4, TLR-7, TLR-8, and TLR-9. Outlined area indicates a germinal center (GC). Mayer's hematoxylin (blue) counterstained; bars = 100 μm.

Stimulation of bone marrow–derived macrophages. Bone marrow–derived macrophages (5 × 10⁴ cells/well) were seeded in 96-well plates and stimulated with R848 (catalog no. tlrl-r848; InvivoGen) for 24 hours. The culture supernatant was collected and subjected to enzyme-linked immunosorbent assay (ELISA) to detect cytokines.

ELISA. Serum levels of total IgG, IgG1, and IgG2a in mice were analyzed using a total IgG mouse uncoated ELISA kit with plates (catalog no. 88-50400-88; eBioscience), an IgG1 mouse uncoated ELISA kit with plates (catalog no. 88-50410-88; eBioscience), and an IgG2a mouse coated ELISA kit with plates (catalog no. ab133046; Abcam), respectively. IL-6, IL-12p40, and IL-33 in mice were detected by mouse IL-6 ELISA Ready-SET-Go! (catalog no. 88-7064-88; ThermoFisher Scientific), mouse IL-12p40 ELISA Ready-SET-Go! (catalog no. 88-7120-77; ThermoFisher Scientific), and IL-33 mouse uncoated ELISA kit plates (catalog no. GWB-SKR038; GenWay Biotech), respectively. IL-33 in humans was detected using a human IL-33 ELISA Kit (catalog no. ab223865; Abcam).

Statistical analysis. The significance of differences between groups was determined using chi-square test, Student's t-test, Mann-Whitney U test, and Kruskal-Wallis tests, and Spearman's rank correlation test was used to test correlations between groups. P values less than 0.05 were considered significant. All statistical analyses were performed using JMP software (V.8; SAS Institute).

RESULTS

Gene expression profiles of the TLR family in the SMGs. DNA microarray analysis was performed to compare gene expression profiles of SMG samples from healthy controls and patients with IgG4-RD or chronic sialadenitis. A heatmap was used to elucidate and visualize the differences in gene expression levels among patients with IgG4-RD, those with chronic sialadenitis, and controls (details are available upon request from the corresponding author). The differences in TLR-related gene expression between patients with IgG4-RD and those with chronic sialadenitis are shown in Figure 1A. The genes associated with TLR-4, TLR-7,
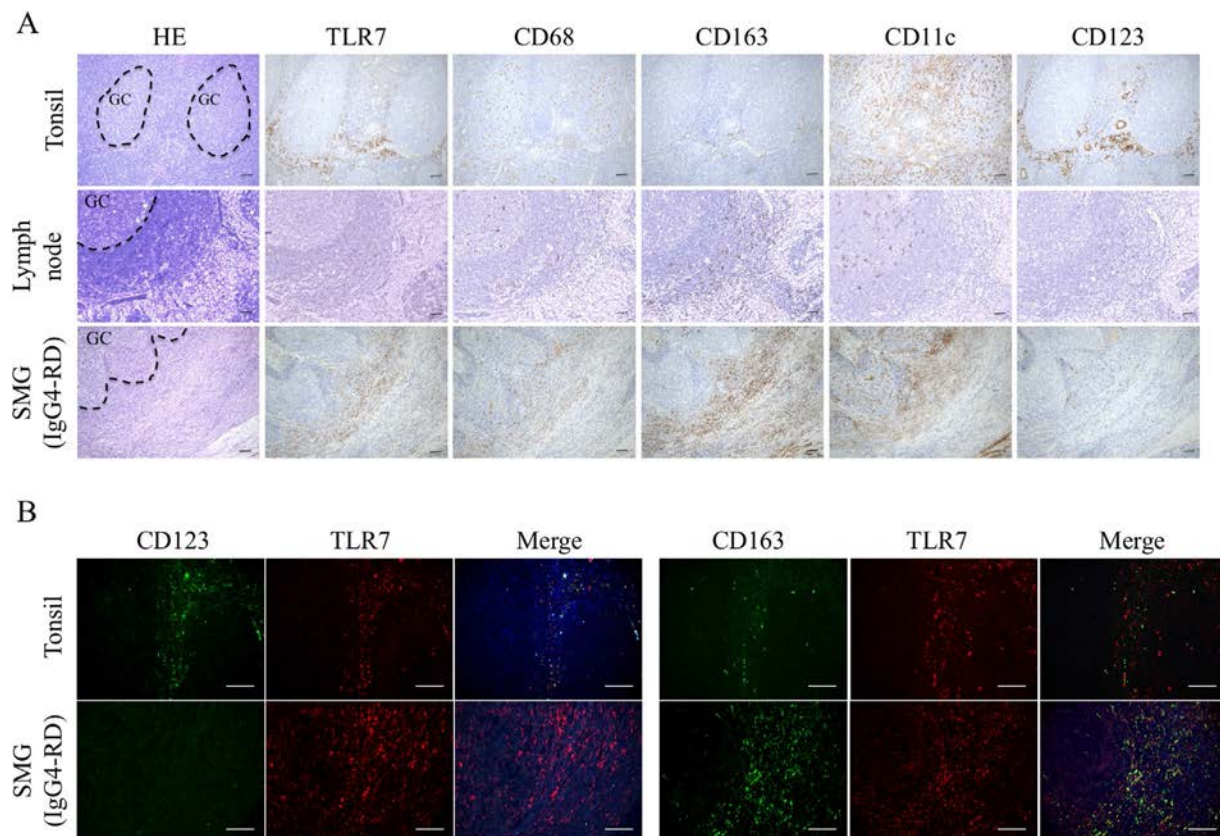
Figure 2. Identification of TLR-7–expressing cells in SMGs from patients with IgG4-RD and in normal secondary lymphoid organs from patients with oral squamous cell carcinoma. **A**, Staining of serial sections of normal tonsil, normal lymph node, and IgG4-RD SMGs with H&E, and for TLR-7, CD68 as a marker of both M1 and M2 macrophages, CD163 as a marker of M2 macrophages, CD11c as a marker of myeloid dendritic cells, and CD123 as a marker of plasmacytoid dendritic cells. Outlined areas indicate GCs. Mayer's hematoxylin (blue) counterstained; bars = 100 μm. **B**, Double immunostaining for TLR-7 (red), CD123 (green), and CD163 (green) in normal tonsil and SMGs from representative patients with IgG4-RD. DAPI (blue) counterstained; bars = 50 μm. See Figure 1 for definitions.

TLR-8, and TLR-9 were expressed to a higher extent in samples from IgG4-RD patients than those from patients with chronic sialadenitis or healthy controls. The expression of these candidate TLR genes was subsequently validated using quantitative real-time PCR by increasing the number of cases. As shown in Figure 1B, we found that the expression levels of mRNA for TLR-7 were significantly higher in SGs from patients with IgG4-RD compared with those from healthy controls or patients with chronic sialadenitis or SS.

Expression of candidate TLRs in the SGs. To evaluate the distribution of candidate TLRs, including TLR-4, TLR-7, TLR-8, and TLR-9, in SG specimens from patients with IgG4-RD, patients with chronic sialadenitis, patients with SS, and healthy controls, histologic analysis was carried out. Representative findings are shown in Figure 1C. Expression of TLR-7 was only detected in infiltrating inflammatory cells, identified morphologically in samples from patients with SS and patients with IgG4-RD but not those from patients with chronic sialadenitis or controls. In addition, patients with IgG4-RD showed strong infiltration of these positive cells around ectopic GCs compared with patients with SS. The other candidate TLRs were rarely seen in any of the samples.

Identification of TLR-7–expressing cells in the SMGs and normal secondary lymphoid organs. Since TLR-7 is expressed on macrophages and dendritic cells (DCs) in secondary lymphoid organs (34), we examined the distribution of macrophages (CD68+, CD163+), DCs (CD11c+, CD123+), and TLR-7 in the SMGs from patients with IgG4-RD and in normal secondary lymphoid organs such as lymph nodes and tonsils. Expression of CD68 and CD163 was strongly detected around ectopic GCs and fibrotic areas in IgG4-RD tissues. In the normal secondary lymphoid organs, expression of CD68 was also strongly detected in and around ductal ectopic GCs, whereas expression of CD163 was rarely detected around ectopic GCs. Expression of CD11c was strongly detected in and around ectopic GCs in both IgG4-RD tissues and normal secondary lymphoid organs. Expression of CD123 was rarely seen in IgG4-RD tissues, but CD123 was detected around ectopic GCs and in ductal epithelial cells in normal secondary lymphoid organs. Finally, expression of TLR-7 was strongly detected around ectopic GCs and fibrotic areas in IgG4-RD tissues, whereas expression of TLR-7 was detected only around ectopic GCs in normal secondary lymphoid organs (Figure 2A).

To clarify which cells expressed TLR-7 in IgG4-RD tissues, double immunofluorescence staining for TLR-7 (red) and CD163 or CD123 (green) was performed. Using this approach, TLR-7–positive cells mainly colocalized with CD123-positive cells in secondary lymphoid organs. In contrast, in IgG4-RD tissues, TLR-7–positive cells mainly colocalized with CD163-

positive cells (Figure 2B). This is consistent with macrophages, particularly M2 macrophages, expressing TLR-7 in IgG4-RD tissues.

Relationship between TLR-7 and IL-33 expression in the SGs. As mentioned above, our recent data indicate that M2 macrophages might contribute to aberrant activation of Th2 immune responses and fibrosis via production of IL-33 (15,16). IL-33 is a recently described cytokine and directly stimulates ST2-expressing immune cells, including Th2 cells, mast cells, eosinophils, and basophils, to secrete Th2 cytokines (35). Recently, in a mouse model where influenza infection acutely induces airway hyperreactivity, TLR-7 stimulation promoted IL-33 production by alveolar macrophages in the lung (36). In addition, TLR-7$^{-/-}$ mice developed a limited airway hyperreactivity response to influenza infection (37). Thus, we examined the association between IL-33 and candidate TLRs in IgG4-RD tissues. The expression levels of mRNA for IL-33 in SGs from patients with IgG4-RD were significantly higher than those in SGs from patients with chronic sialadenitis and controls (Figure 3A).

To evaluate the distribution of IL-33, SG specimens from patients with SS, patients with IgG4-RD, patients with chronic sialadenitis, and healthy controls were characterized immunohistochemically. Representative sections are shown in Figure 1C. Expression of IL-33 was detected in all samples in the ductal epithelial cells, while IL-33 was also detected in infiltrating inflammatory cells around ectopic GCs in patients with IgG4-RD (Figure 3B). Next, the relationships between expression levels of mRNA for IL-33 and candidate TLRs in SGs from patients with IgG4-RD were examined, and the expression of mRNA for IL-33 was positively correlated with expression of mRNA for TLR-7 but not with expression of mRNA for TLR-4, TLR-8, or TLR-9 (Figure 3C). Finally, CD163+ M2 macrophages isolated from PBMCs (Figure 3D) were found to enhance production of IL-33 in a dose-dependent manner after stimulation with TLR-7 agonist (Figure 3E). This suggested that activation of TLR-7 might induce the release of IL-33 from M2 macrophages.

Phenotype of affected organs in huTLR-7–transgenic/mTLR-7$^{-/-}$ mice. Since our current data suggest that TLR-7 might play a key role in the initiation of IgG4-RD, we examined the phenotype of Gt(ROSA)26Sor$^{huTLR-7/+}$/mTLR-7$^{-/-}$ mice (Figure 4A). Histologic examination was undertaken of organs relevant for IgG4-RD, including the SMGs, pancreas, kidney, lung, and liver, in huTLR-7–transgenic/mTLR-7$^{-/-}$ and wild-type (WT) mice. There were no significant differences in the weights of each organ between huTLR-7–transgenic/mTLR-7$^{-/-}$ mice and WT mice (Figure 4B). Representative histologic findings in each organ from huTLR-7–transgenic/mTLR-7$^{-/-}$ and WT mice are shown in Figure 4C. The degree of lymphocytic infiltration was evaluated by focus score, and the focus scores in the SMGs,
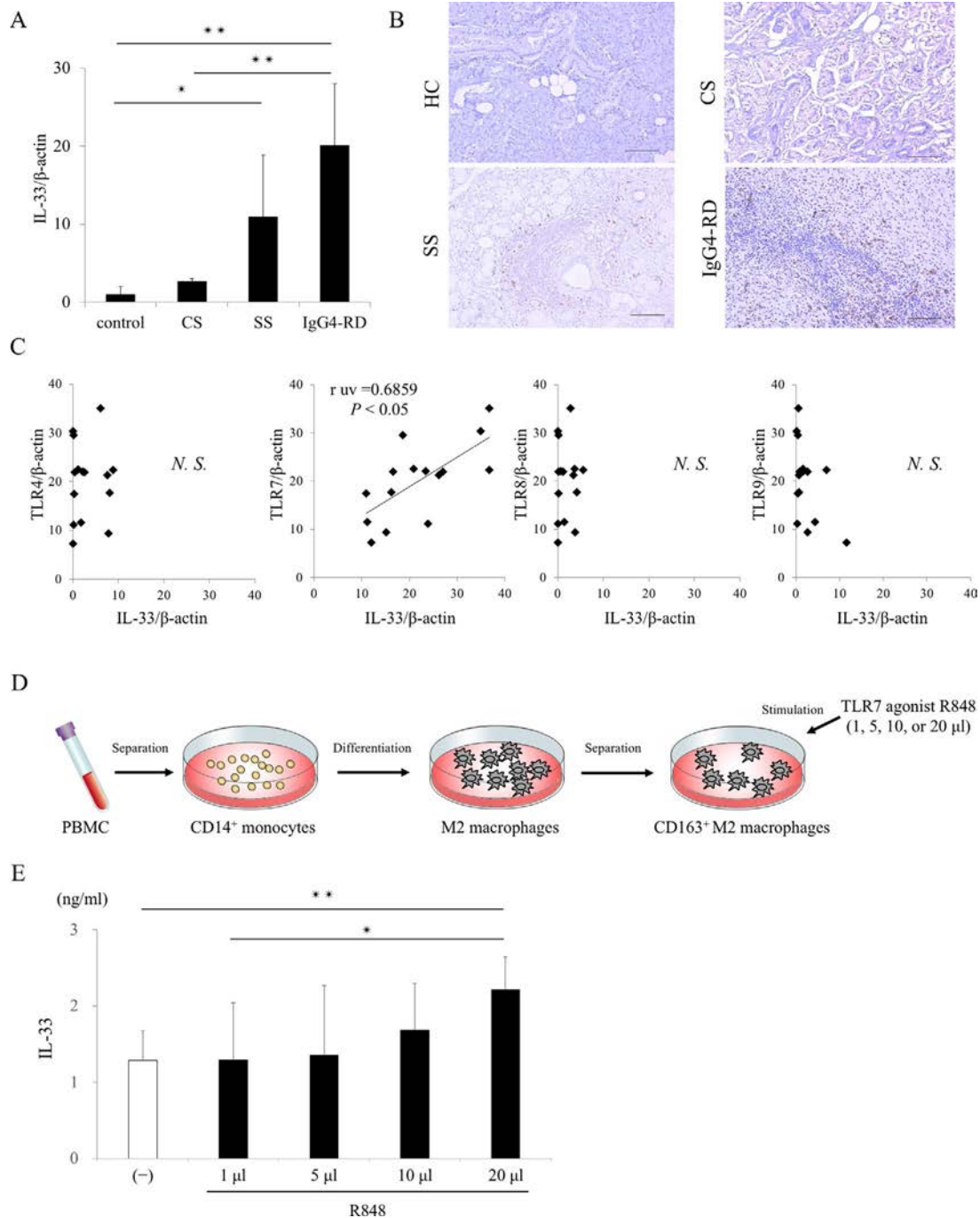
Figure 3. Expression of interleukin-33 (IL-33) and candidate TLRs in SGs from patients with IgG4-RD. **A**, Expression levels of mRNA for IL-33 in SGs from healthy controls (n = 10), patients with chronic sialadenitis (n = 10), patients with SS (n = 15), and patients with IgG4-RD (n = 15). **B**, Distribution of IL-33 in SGs from a representative healthy control, patient with chronic sialadenitis, patient with SS, and patient with IgG4-RD. Mayer's hematoxylin (blue) counterstained; bars = 100 μm. **C**, Correlation between expression levels of IL-33 mRNA and candidate TLRs in SGs from patients with IgG4-RD (n = 15), as determined by Spearman's rank correlation test. **D**, Schematic illustration of the extraction of CD163+ M2 macrophages stimulated with TLR-7 agonist R848. Cells were cultivated as described in Patients and Methods. PBMC = peripheral blood mononuclear cell. **E**, Production of IL-33 by CD163+ M2 macrophages stimulated with R848, as determined by enzyme-linked immunosorbent assay. IL-33 levels increased in a concentration-dependent manner. In **A** and **E**, bars show the mean ± SD. * = $P < 0.05$; ** = $P < 0.01$ by Kruskal-Wallis test. See Figure 1 for other definitions.

pancreas, and lungs from huTLR-7–transgenic/mTLR-7$^{-/-}$ mice were significantly greater than in WT mice (Figure 4D). In addition, to evaluate the degree of fibrosis in each organ, specimens were stained by Masson's trichrome staining. The huTLR-7–transgenic/mTLR-7$^{-/-}$ mice showed severe fibrosis in the lung and cordlike fibrosis in the SMGs and pancreas (Figure 4E).
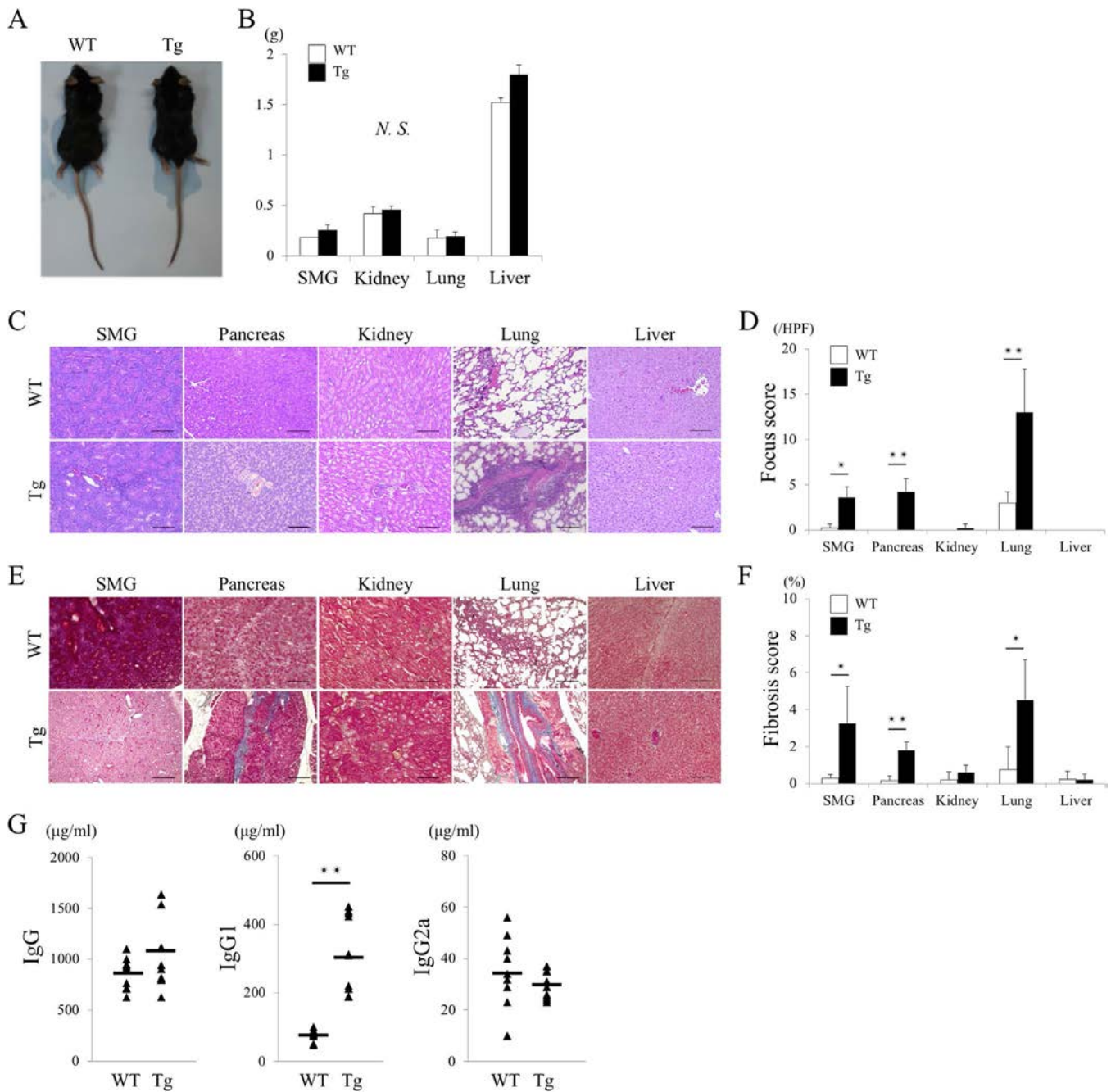
Figure 4. Pathologic and serologic findings in human TLR-7–transgenic/mouse TLR-7–deficient (huTLR-7–transgenic/mTLR-7⁻/⁻) mice on a C57BL/6 background. **A**, A wild-type (WT) C57BL/6 mouse and an huTLR-7–transgenic/mTLR-7–/– (transgenic [Tg]) mouse at 4 weeks old. **B**, Weight of SMGs, kidneys, lungs, and liver in 4-week-old WT mice (n = 5) and transgenic mice (n = 5). Bars show the mean ± SD. **C**, H&E-stained sections of SMGs, pancreas, kidneys, lungs, and liver from representative WT and transgenic mice. Bars = 100 μm. **D**, Focus score for each organ in WT mice (n = 5) and transgenic mice (n = 5). The focus score was estimated as described in Patients and Methods. Bars show the mean ± SD. HPF = high-power field. **E**, Masson's trichrome–stained sections of SMGs, pancreas, kidneys, lungs, and liver from representative WT and transgenic mice. Masson's trichrome was used to stain nuclei (purple), cytoplasm (red), and collagen (connective or fibrotic tissue; blue) Bars = 100 μm. **F**, Fibrosis score for each organ in WT mice (n = 5) and transgenic mice (n = 5). The fibrosis score was calculated from Masson's trichrome staining as described in Patients and Methods. Bars show the mean ± SD. **G**, Serum IgG, IgG1, and IgG2a levels in WT mice (n = 10) and transgenic mice (n = 10), as determined by enzyme-linked immunosorbent assay. Symbols represent individual mice; horizontal lines show the mean. * = $P < 0.05$; **= $P < 0.01$ by Mann-Whitney U test. See Figure 1 for other definitions.
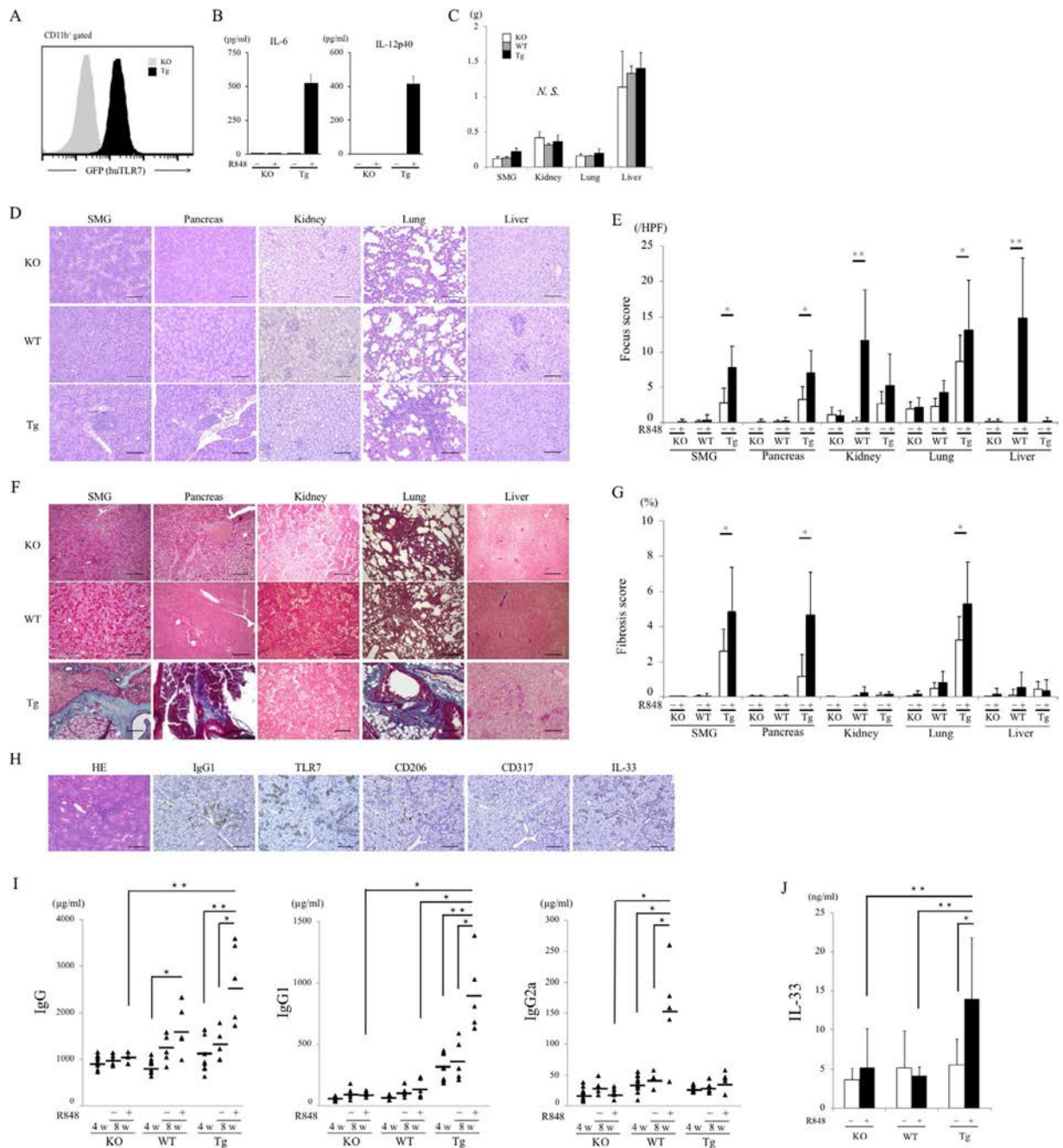
Figure 5. Effects of TLR-7 agonist R848 in transgenic mice. **A**, Detection of GFP in bone marrow–derived macrophages (BMMs) from mTLR-7–/– (knockout [KO]) mice and transgenic (Tg) mice by flow cytometric analysis, after staining with anti-CD11b antibody. At least 2 independent experiments were performed. **B**, Interleukin-6 (IL-6) and IL-12p40 levels in BMMs from knockout mice and transgenic mice left unstimulated or stimulated with R848. After 24 hours of incubation, IL-6 and IL-12p40 were detected in culture medium by enzyme-linked immunosorbent assay (ELISA). Results are from triplicate wells. At least 2 independent experiments were performed. **C**, Weight of SMGs, kidneys, lungs, and liver in 8-week-old knockout, wild-type (WT), and transgenic mice treated with topical R848 for 4 weeks (n = 8 per group). **D** and **F**, H&E-stained (**D**) and Masson's trichrome–stained (**F**) sections of SMGs, pancreas, kidneys, lungs, and liver from representative 8-week-old R848-treated knockout, WT, and transgenic mice. Bars = 100 μm. **E** and **G**, Focus score (**E**) and fibrosis score (**G**) for each organ in 8-week-old knockout, WT, and transgenic mice left untreated or treated with R848 (n = 8 per group). The fibrosis score was calculated from Masson's trichrome staining as described in Patients and Methods. HPF = high-power field. **H**, Serial sections of SMGs from a representative 8-week-old R848-treated transgenic mouse, stained with H&E and for IgG1, TLR-7, CD206, CD317, and IL-33. Mayer's hematoxylin (blue) counterstained; bars = 100 μm. **I**, Serum IgG, IgG1, and IgG2a levels in knockout, WT, and transgenic mice (n = 10 per group) before and after R848 treatment, as determined by ELISA. Symbols represent individual mice; horizontal lines show the mean. **J**, Serum IL-33 levels, determined by ELISA, in knockout, WT, and transgenic mice left untreated or treated with R848 (n = 10 per group). In **B**, **C**, **E**, **G**, and **J**, bars show the mean ± SD. * = $P < 0.05$; ** = $P < 0.01$ by Mann-Whitney U test in **E** and **G**; by Kruskal-Wallis test in **C**, **I** and **J**. See Figure 1 for other definitions.

The fibrosis scores for the SMGs, pancreas, and lungs from huTLR-7–transgenic/mTLR-7$^{-/-}$ mice were significantly higher than those in WT mice (Figure 4F).

Serum IgG1 levels in 4-week-old huTLR-7–transgenic/mTLR-7$^{-/-}$ mice were significantly higher than those in 4-week-old WT mice, while there was no significant difference in serum IgG or IgG2a levels between huTLR-7–transgenic/mTLR-7$^{-/-}$ and WT mice (Figure 4G).

Response to a TLR-7 agonist in huTLR-7–transgenic/mTLR-7$^{-/-}$ and WT mice. To test the in vivo responsiveness of huTLR-7–transgenic/mTLR-7$^{-/-}$ mice to an agonist of TLR-7, we applied the TLR-7 agonist R848 to their right ears, 3 times weekly for 4 weeks. Bone marrow–derived macrophages (CD11b+ cells) prepared from Gt(ROSA)26Sor$^{huTLR-7/+}$ TLR-7$^{-/-}$ mice expressed GFP (Figure 5A) and produced IL-6 and IL-12 p40 in response to the TLR-7 ligand R848 (Figure 5B), demonstrating that Gt(ROSA)26Sor$^{huTLR-7/+}$ TLR-7$^{-/-}$ mice enable us to study human TLR-7 responses in vivo. Once again, mouse SMGs, pancreas, kidney, lung, and liver were collected. There were no significant differences in the weights of the organs among 8-week-old R848-treated huTLR-7–transgenic/mTLR-7$^{-/-}$ mice, mTLR-7$^{-/-}$ mice, and WT mice (Figure 5C). Histologic examination of the SMGs, pancreas, and lung from R848-treated huTLR-7–transgenic/mTLR-7$^{-/-}$ mice revealed marked inflammation and fibrosis, while there was marked inflammation and fibrosis in the kidney and liver from R848-treated WT mice (Figures 5D and F). In R848-treated huTLR-7–transgenic/mTLR-7$^{-/-}$ mice, the focus score and fibrosis score for the SMGs, pancreas, and lung were significantly increased after R848 stimulation (Figures 5E and G). In contrast, in R848-treated WT mice, the focus scores for the kidney and liver were significantly increased after R848 stimulation (Figure 5E), but the fibrosis score remained unchanged for all organs (Figure 5G). Immunohistochemical analysis demonstrated focal accumulation of CD206+ cells (marker for M2 macrophages in mice), IgG1+ plasma cells, and IL-33+ cells around ectopic GCs in the SMGs, while there were no CD317+ cells (marker for plasmacytoid DCs in mice) in the SMGs (Figure 5H).

Beginning 4 weeks after topical R848 treatment, serum IgG, IgG1, and IgG2a levels in knockout mice remained unchanged. Interestingly, serum IgG2a levels were significantly elevated only in WT mice, while serum IgG and IgG1 levels were significantly elevated only in huTLR-7–transgenic/mTLR-7$^{-/-}$ mice (Figure 5I). Mouse IgG1 is considered a functional equivalent of human IgG4. Moreover, serum IL-33 levels were significantly elevated only in huTLR-7–transgenic/mTLR-7$^{-/-}$ mice (Figure 5J). Thus, huTLR-7 activation through topical TLR-7 agonist treatment might lead to the manifestation of IgG4-RD.

DISCUSSION

M2 macrophages are typically degenerated by stimulation with the Th2 cytokines IL-4 and IL-13 (38). Notably, in allergic regions, infiltrating inflammatory monocytes can differentiate into M2 macrophages via basophil-derived IL-4 (39). Moreover, it has been found that basophils produce a large amount of IL-4 in response to various stimulants, including IgE plus antigens, cytokines (IL-3, IL,18, and IL-33), and TLR ligands (40). Watanabe et al (17,18) demonstrated that TLR signaling in monocytes/macrophages and basophils might enhance the abnormal innate immune responses observed in IgG4-RD. A recent study showed infiltration of activated TLR-2+ and/or TLR-4+ basophils in the pancreas tissue of patients with autoimmune pancreatitis (41). Although the relationship between TLRs and innate immunity has recently received increasing attention with regard to the initiation of IgG4-RD, the detailed mechanism of pathogenesis by TLR signaling remains to be completely elucidated. Therefore, we performed gene expression microarray analysis to identify TLR-related molecules using SMG samples from patients with IgG4-RD and patients with chronic sialadenitis.

Microarray of SMGs demonstrated significant increases in TLR-7–, TLR-8–, and TLR-9–related genes in patients with IgG4-RD compared with patients with chronic sialadenitis and controls. In addition, overexpression of TLR-7 in SMGs from patients with IgG4-RD compared with the patients with chronic sialadenitis and controls was validated by real-time PCR and immunohistochemistry.

TLR-7 recognizes single-stranded RNA from viruses. Chang et al (37) observed IL-33 production by alveolar macrophages in virus-infected lungs after in vitro stimulation with an agonist of TLR-7, consistent with our results showing the positive correlation between TLR-7 and IL-33 only in IgG4-RD tissue. In addition, several studies have indicated that TLR-7 is important not only for the activation of antiviral responses but also for the induction of adaptive immunity (34). Activation of TLR-7–expressing plasmacytoid DCs in mice causes diseases such as lupus nephritis or arthritis (42), suggesting that TLR-7 has a risk of responding to endogenous ligands in the disease state. Notably, Yokogawa et al (43) showed that WT BALB/c mice treated with the TLR-7 agonist imiquimod for 4 weeks had an accumulation of plasmacytoid DCs at the epidermal–dermal junction and elevated serum IgG2a levels, but unchanged serum IgG1 levels. These results were consistent with our results in the present study (Figure 5I). Mouse IgG2a is the most prominent IgG subclass involved in inducing autoimmunity. Thus, Yokogawa et al suggested that mTLR-7 activation of plasmacytoid DCs in WT BALB/c mice leads to lupus-like systemic autoimmune disease.

On the other hand, Fukui et al (44), and the findings of the present study, showed a predominant infiltration of TLR-7+CD163+ M2 macrophages in the pancreas and SMGs from patients with IgG4-RD, while TLR-7+CD123+ plasmacytoid DCs were rarely seen in IgG4-RD tissues. Interestingly, the normal human secondary lymphoid organs, including lymph nodes and tonsils, showed a predominant infiltration of TLR-7+CD123+ plasmacytoid DCs. In huTLR-7–transgenic/mTLR-7$^{-/-}$ mice, fibrosis and lymphocytic
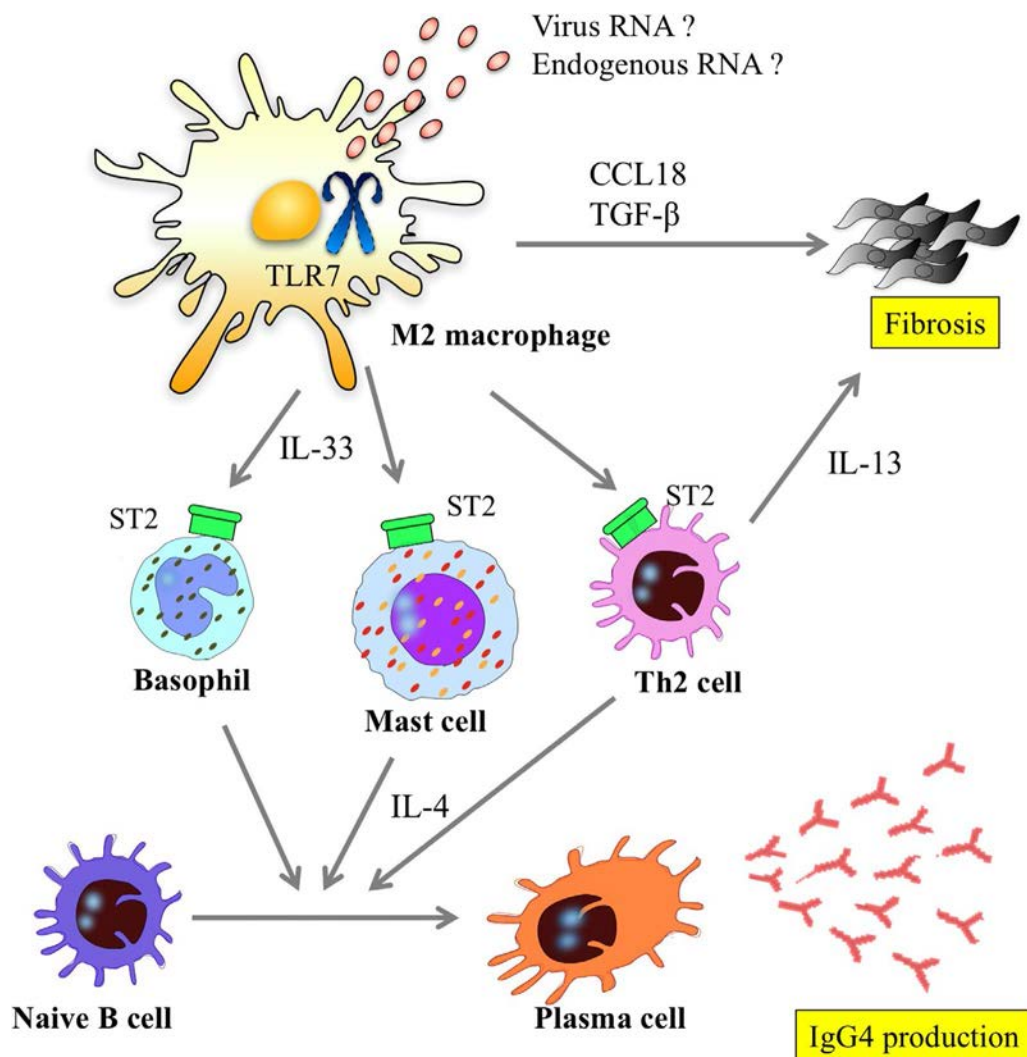
Figure 6. Schematic model of the role of Toll-like receptor 7 (TLR-7)–positive M2 macrophages in the initiation of Ig4-related disease. TLR-7 expressed on M2 macrophages recognize some RNA viruses or self RNA from apoptotic cells. Activated M2 macrophages secrete interleukin-33 (IL-33) and promote production of Th2 cytokines that lead to IgG4 class-switching and fibrosis. TGFβ = transforming growth factor β.

infiltration were notably increased in multiple organs compared with WT mice. Moreover, we confirmed elevated serum IgG and IgG1 levels in huTLR-7–transgenic/mTLR-7$^{-/-}$ mice after topical treatment with TLR-7 agonists. In contrast, Arai et al (45) reported that CD123+CD303+ plasmacytoid DCs were easily detected in pancreas tissues from patients with autoimmune pancreatitis. In addition, increased interferon-α production by plasmacytoid DCs promotes pancreatic inflammation in a murine model of autoimmune pancreatitis (MRL/Mp mice treated with the TLR-3 ligand poly[I–C]). These contradictions with the findings of previous studies are thought to reflect differences in TLR-7–expressing cells in each organ or in the function of mTLR-7 and huTLR-7.

This study is the first to demonstrate that huTLR-7 activation through topical TLR-7 agonist treatment in huTLR-7–transgenic/mTLR-7$^{-/-}$ mice leads to an IgG4-RD phenotype. Furthermore, after topical treatment with TLR-7 agonists, fibrosis and lymphocytic infiltration in affected organs was notable. A schematic

model for the initiation of IgG4-RD is shown in Figure 6. M2 macrophages recognize some RNA viruses or self RNA from apoptotic cells in affected organs via TLR-7, which causes activated M2 macrophages to secrete IL-33 and promote production of Th2 cytokines by various immune cells that lead to IgG4 class-switching and severe fibrosis.

Since TLR-7 is considered to induce production of inflammatory cytokines (tumor necrosis factor, IL-1β, IL-12, and interferon-α) as well as IL-33, we are currently examining the association of novel T cell subsets, including CD4+ cytotoxic T cells and T follicular helper cells, with TLR-7 downstream signals other than IL-33 in both huTLR-7–transgenic/mTLR-7$^{-/-}$ mice and patients with IgG4-RD. A more thorough understanding of the role of TLR-7+CD163+ M2 macrophages in IgG4-RD could lead to the establishment of a mouse model of IgG4-RD and to the eventual development of novel pharmacologic strategies to interrupt TLR-7 or TLR-7 downstream

signals as a further means of inhibiting disease initiation or progression.

REFERENCES

1. Hamano H, Kawa S, Horiuchi A, Unno H, Furuya N, Akamatsu T, et al. High serum IgG4 concentrations in patients with sclerosing pancreatitis. N Engl J Med 2001;344:732–8.

2. Umehara H, Okazaki K, Masaki Y, Kawano M, Yamamoto M, Saeki T, et al. A novel clinical entity, IgG4-related disease (IgG4RD): general concept and details. Mod Rheumatol 2012;22:1–14.

3. Stone JH, Zen Y, Deshpande V. IgG4-related disease. N Engl J Med 2012;366:539–51.

4. Nirula A, Glaser SM, Kalled SL, Taylor FR. What is IgG4? A review of the biology of a unique immunoglobulin subtype. Curr Opin Rheumatol 2011;23:119–24.

5. Finkelman FD, Boyce JA, Vercelli D, Rothenberg ME. Key advances in mechanisms of asthma, allergy, and immunology in 2009. J Allergy Clin Immunol 2010;125:312–8.

6. Meiler F, Klunker S, Zimmermann M, Akdis CA, Akdis M. Distinct regulation of IgE, IgG4 and IgA by T regulatory cells and Toll-like receptors. Allergy 2008;63:1455–63.

7. Maehara T, Moriyama M, Nakashima H, Miyake K, Hayashida JN, Tanaka A, et al. Interleukin-21 contributes to germinal centre formation and immunoglobulin G4 production in IgG4-related dacryoadenitis and sialoadenitis, so-called Mikulicz's disease. Ann Rheum Dis 2012;71:2011–9.

8. Tanaka A, Moriyama M, Nakashima H, Miyake K, Hayashida JN, Maehara T, et al. Th2 and regulatory immune reactions contribute to IgG4 production and the initiation of Mikulicz disease. Arthritis Rheum 2012;64:254–63.

9. Tsuboi H, Matsuo N, Iizuka M, Tsuzuki S, Kondo Y, Tanaka A, et al. Analysis of IgG4 class switch-related molecules in IgG4-related disease. Arthritis Res Ther 2012;14:R171.

10. Zen Y, Fujii T, Harada K, Kawano M, Yamada K, Takahira M, et al. Th2 and regulatory immune reactions are increased in immunoglobin G4-related sclerosing pancreatitis and cholangitis. Hepatology 2007;45:1538–46.

11. Moriyama M, Tanaka A, Maehara T, Furukawa S, Nakashima H, Nakamura S. T helper subsets in Sjögren's syndrome and IgG4-related dacryoadenitis and sialoadenitis: a critical review. J Autoimmun 2014;51:81–8.

12. Akiyama M, Suzuki K, Yamaoka K, Yasuoka H, Takeshita M, Kaneko Y, et al. Number of circulating follicular helper 2 T cells correlates with IgG4 and interleukin-4 levels and plasmablast numbers in IgG4-related disease. Arthritis Rheumatol 2015;67:2476–81.

13. Maehara T, Mattoo H, Ohta M, Mahajan VS, Moriyama M, Yamauchi M, et al. Lesional CD4+ IFN-γ+ cytotoxic T lymphocytes in IgG4-related dacryoadenitis and sialoadenitis. Ann Rheum Dis 2017;76:377–85.

14. Mattoo H, Mahajan VS, Della-Torre E, Sekigami Y, Carruthers M, Wallace ZS, et al. De novo oligoclonal expansions of circulating plasmablasts in active and relapsing IgG4-related disease. J Allergy Clin Immunol 2014;134:679–87.

15. Furukawa S, Moriyama M, Tanaka A, Maehara T, Tsuboi H, Iizuka M, et al. Preferential M2 macrophages contribute to fibrosis in IgG4-related dacryoadenitis and sialoadenitis, so-called Mikulicz's disease. Clin Immunol 2015;156:9–18.

16. Furukawa S, Moriyama M, Miyake K, Nakashima H, Tanaka A, Maehara T, et al. Interleukin-33 produced by M2 macrophages and other immune cells contributes to Th2 immune reaction of IgG4-related disease. Sci Rep 2017;7:42413.

17. Watanabe T, Yamashita K, Fujikawa S, Sakurai T, Kudo M, Shiokawa M, et al. Involvement of activation of Toll-like receptors and nucleotide-binding oligomerization domain-like receptors in enhanced IgG4 responses in autoimmune pancreatitis. Arthritis Rheum 2012;64:914–24.

18. Watanabe T, Yamashita K, Sakurai T, Kudo M, Shiokawa M, Uza N, et al. Toll-like receptor activation in basophils contributes to the development of IgG4-related disease. J Gastroenterol 2013;48:247–53.

19. Mackay F, Browning JL. BAFF: a fundamental survival factor for B cells. Nat Rev Immunol 2002;2:465–75.

20. Janeway CA Jr, Medzhitov R. Innate immune recognition. Annu Rev Immunol 2002;20:197–216.

21. Beutler B, Rietschel ET. Innate immune sensing and its roots: the story of endotoxin. Nat Rev Immunol 2003;3:169–76.

22. Medzhitov R. Toll-like receptors and innate immunity. Nat Rev Immunol 2001;1:135–45.

23. Akira S, Takeda K, Kaisho T. Toll-like receptors: critical proteins linking innate and acquired immunity. Nat Immunol 2001;2:675–80.

24. Hwang IY, Park C, Harrison K, Kehrl JH. TLR4 signaling augments B lymphocyte migration and overcomes the restriction that limits access to germinal center dark zones. J Exp Med 2009;206:2641–57.

25. Moriyama M, Furukawa S, Kawano S, Goto Y, Kiyoshima T, Tanaka A, et al. The diagnostic utility of biopsies from the submandibular and labial salivary glands in IgG4-related dacryoadenitis and sialoadenitis, so-called Mikulicz's disease. Int J Oral Maxillofac Surg 2014;43:1276–81.

26. Umehara H, Okazaki K, Masaki Y, Kawano M, Yamamoto M, Saeki T, et al. Comprehensive diagnostic criteria for IgG4-related disease (IgG4-RD), 2011. Mod Rheumatol 2012;22:21–30.

27. Masaki Y, Sugai S, Umehara H. IgG4-related diseases including Mikulicz's disease and sclerosing pancreatitis: diagnostic insights. J Rheumatol 2010;37:1380–5.

28. Fujibayashi T, Sugai S, Miyasaka N, Hayashi Y, Tsubota K. Revised Japanese criteria for Sjögren's syndrome (1999): availability and validity. Mod Rheumatol 2004;14:425–34.

29. Shiboski CH, Shiboski SC, Seror R, Criswell LA, Labetoulle M, Lietman TM, et al, and the International Sjögren's Syndrome Criteria Working Group. 2016 American College of Rheumatology/European League Against Rheumatism classification criteria for primary Sjögren's syndrome: a consensus and data-driven methodology involving three international patient cohorts. Arthritis Rheumatol 2017;69:35–45.

30. Moriyama M, Hayashida JN, Toyoshima T, Ohyama Y, Shinozaki S, Tanaka A, et al. Cytokine/chemokine profiles contribute to

understanding the pathogenesis and diagnosis of primary Sjögren's syndrome. Clin Exp Immunol 2012;169:17–26.

31. Ohta M, Moriyama M, Maehara T, Gion Y, Furukawa S, Tanaka A, et al. DNA microarray analysis of submandibular glands in IgG4-related disease indicates a role for MARCO and other innate immune-related proteins. Medicine (Baltimore) 2016;95:e2853.

32. Greenspan JS, Daniels TE, Talal N, Sylvester RA. The histopathology of Sjögren's syndrome in labial salivary gland biopsies. Oral Surg Oral Med Oral Pathol 1974;37:217–29.

33. Chisholm DM, Mason DK. Labial salivary gland biopsy in Sjögren's disease. J Clin Pathol 1968;21:656–60.

34. Baenziger S, Heikenwalder M, Johansen P, Schlaepfer E, Hofer U, Miller RC, et al. Triggering TLR7 in mice induces immune activation and lymphoid system disruption, resembling HIV-mediated pathology. Blood 2009;113:377–88.

35. Schmitz J, Owyang A, Oldham E, Song Y, Murphy E, McClanahan TK, et al. IL-33, an interleukin-1-like cytokine that signals via the IL-1 receptor-related protein ST2 and induces T helper type 2-associated cytokines. Immunity 2005;23:479–90.

36. Louten J, Rankin AL, Li Y, Murphy EE, Beaumont M, Moon C, et al. Endogenous IL-33 enhances Th2 cytokine production and T-cell responses during allergic airway inflammation. Int Immunol 2011;23:307–15.

37. Chang YJ, Kim HY, Albacker LA, Baumgarth N, McKenzie AN, Smith DE, et al. Innate lymphoid cells mediate influenza-induced airway hyper-reactivity independently of adaptive immunity. Nat Immunol 2011;12:631–8.

38. Paul WE, Zhu J. How are T_H2-type immune responses initiated and amplified? Nat Rev Immunol 2010;10:225–35.

39. Egawa M, Mukai K, Yoshikawa S, Iki M, Mukaida N, Kawano Y, et al. Inflammatory monocytes recruited to allergic skin acquire an anti-inflammatory M2 phenotype via basophil-derived interleukin-4. Immunity 2013;38:570–80.

40. Yamanishi Y, Karasuyama H. Basophil-derived IL-4 plays versatile roles in immunity. Semin Immunopathol 2016;38:615–22.

41. Yanagawa M, Uchida K, Ando Y, Tomiyama T, Yamaguchi T, Ikeura T, et al. Basophils activated via TLR signaling may contribute to pathophysiology of type 1 autoimmune pancreatitis. J Gastroenterol 2018;53:449–60.

42. Deane JA, Pisitkun P, Barrett RS, Feigenbaum L, Town T, Ward JM, et al. Control of Toll-like receptor 7 expression is essential to restrict autoimmunity and dendritic cell proliferation. Immunity 2007;27:801–10.

43. Yokogawa M, Takaishi M, Nakajima K, Kamijima R, Fujimoto C, Kataoka S, et al. Epicutaneous application of Toll-like receptor 7 agonists leads to systemic autoimmunity in wild-type mice: a new model of systemic lupus erythematosus. Arthritis Rheumatol 2014;66:694–706.

44. Fukui Y, Uchida K, Sakaguchi Y, Fukui T, Nishio A, Shikata N, et al. Possible involvement of Toll-like receptor 7 in the development of type 1 autoimmune pancreatitis. J Gastroenterol 2015;50:435–44.

45. Arai Y, Yamashita K, Kuriyama K, Shiokawa M, Kodama Y, Sakurai T, et al. Plasmacytoid dendritic cell activation and IFN-α production are prominent features of murine autoimmune pancreatitis and human IgG4-related autoimmune pancreatitis. J Immunol 2015;195:3033–44.

AMERICAN COLLEGE
of RHEUMATOLOGY
Empowering Rheumatology Professionals

Proinflammatory Histidyl–Transfer RNA Synthetase–Specific CD4+ T Cells in the Blood and Lungs of Patients With Idiopathic Inflammatory Myopathies

Angeles S. Galindo-Feria,[1] [iD] Inka Albrecht,[1] Cátia Fernandes-Cerqueira,[1] Antonella Notarnicola,[1] Eddie A. James,[2] Jessica Herrath,[1] Maryam Dastmalchi,[1] Tatyana Sandalova,[3] Lars Rönnblom,[4] Per-Johan Jakobsson,[1] Maryam Fathi,[5] Adnane Achour,[3] Johan Grunewald,[1] Vivianne Malmström,[1] and Ingrid E. Lundberg[1]

Objective. Autoantibodies targeting histidyl–transfer RNA synthetase (HisRS; anti–Jo-1) are common in the idiopathic inflammatory myopathies (IIMs) and antisynthetase syndrome. This study was undertaken to investigate immunity against HisRS in the blood and lungs of patients with IIM/antisynthetase syndrome.

Methods. Bronchoalveolar lavage (BAL) fluid, BAL fluid cells, and peripheral blood mononuclear cells (PBMCs) from patients with IIM/antisynthetase syndrome (n = 24) were stimulated with full-length HisRS protein or a HisRS-derived peptide (HisRS$_{11-23}$). BAL fluid and PBMCs from patients with sarcoidosis (n = 7) and healthy subjects (n = 12) were included as controls. The CD4+ T cell response was determined according to levels of CD40L up-regulation and cytokine expression using flow cytometry. Anti–Jo-1 autoantibody responses in the serum and BAL fluid were assessed by enzyme-linked immunosorbent assay. Lung biopsy samples from patients with IIM/antisynthetase syndrome (n = 14) were investigated by immunohistochemistry.

Results. In BAL fluid, CD4+ T cells from 3 of 4 patients with IIM/antisynthetase syndrome responded to stimulation with HisRS protein, as measured by the median fold change in CD40L expresssion in stimulated cells compared to unstimulated cells (median fold change 3.6, interquartile range [IQR] 2.7–14.7), and 2 of 3 patients with IIM/antisynthetase syndrome had the highest responses to HisRS$_{11-23}$ (median fold change 88, IQR 27–149). In PBMCs, CD4+ T cells from 14 of 18 patients with IIM/antisynthetase syndrome responded to HisRS protein (median fold change 7.38, IQR 2.69–31.86; $P < 0.001$), whereas a HisRS$_{11-23}$ response was present in 11 of 14 patients with IIM/antisynthetase syndrome (median fold change 3.4, IQR 1.87–10.9; $P < 0.001$). In the control group, there was a HisRS$_{11-23}$ response in 3 of 7 patients with sarcoidosis (median fold change 2.09, IQR 1.45–3.29) and in 5 of 12 healthy controls (median fold change 2, IQR 1.89–2.42). CD4+ T cells from patients with IIM/antisynthetase syndrome displayed a pronounced Th1 phenotype in the BAL fluid when compared to the PBMCs ($P < 0.001$), producing high amounts of interferon-γ and interleukin-2 following stimulation. Anti–Jo-1 autoantibodies were detected in BAL fluid and germinal center (GC)–like structures were seen in the lung biopsy samples from patients with IIM/antisynthetase syndrome.

Conclusion. The results of this study demonstrate a pronounced presence of HisRS-reactive CD4+ T cells in PBMCs and BAL fluid cells from patients with IIM/antisynthetase syndrome as compared to patients with sarcoidosis and healthy controls. These findings, combined with the presence of anti–Jo-1 autoantibodies in BAL fluid and GC-like structures in the lungs, suggest that immune activation against HisRS might take place within the lungs of patients with IIM/antisynthetase syndrome.

INTRODUCTION

Idiopathic inflammatory myopathies (IIMs) represent a group of chronic autoimmune disorders that are characterized by muscle weakness and systemic extramuscular manifestations in the joints, skin, heart, and, particularly, the lungs (1). The identification of autoantibodies unique to IIMs, also known as myositis-specific autoantibodies (MSA), has allowed recognition of correlations with distinct clinical phenotypes (2,3). Among the MSA, anti–Jo-1 autoantibodies targeting histidyl-transfer RNA synthetase (HisRS) are the most common (found in 25–35% of patients with IIM) (4–6) and are associated with interstitial lung disease (ILD) and antisynthetase syndrome (3,7).

Insights from studies of several autoimmune diseases have placed the presence and presentation of the autoantigen in the lung, where innate immunity and genetics play important roles in the initiation of the autoimmune response, as seen in rheumatoid arthritis (RA) (8–10), sarcoidosis (11), and multiple sclerosis (MS) (12). Several genetic and experimental findings support the role of adaptive immunity in anti–Jo-1 autoantibody formation. Thus, HLA–DRB1*03 has been found to be strongly associated with anti–Jo-1 autoantibodies (13–15). Furthermore, observations of gene–environment interactions suggest an additional risk of anti–Jo-1 autoantibodies in HLA–DRB1*03–positive patients who are ever smokers (14), indicating the importance of environmental exposures in the development of anti–Jo-1 autoantibodies. In addition, the presence of class switching, epitope spreading, and affinity maturation of anti–Jo-1 autoantibodies points toward a significant contribution of antigen-specific T cells in the development of these antibodies (16–19).

A question that has been difficult to elucidate is, how might HisRS, a ubiquitous cytoplasmic protein, induce an autoimmune reaction? The high expression of HisRS in specific microenvironments, such as in normal lung tissue (20), combined with altered expression of HisRS and/or an enriched conformation of highly sensitive HisRS in response to granzyme B cleavage in the lung (21), supports the role of the lung as a potential site where immune tolerance could be broken. A previous study demonstrated the presence of T cells reactive to both intact HisRS protein and HisRS fragments, most of which were ~150 amino acids in length, in peripheral blood mononuclear cells (PBMCs) from patients with IIM as well as PBMCs from healthy controls (22). Other observations revealed that both intact and granzyme B–cleaved HisRS, corresponding to residues 1–48, can drive specific immune responses, including recruitment of CD4+ and CD8+ T cells, as well as immature dendritic cells and activated monocytes (23). This finding, together with identification of a B cell epitope among the 60 amino acids of the N-terminal region of the HisRS protein, makes this region an attractive part of the protein to search for T cell–reactive peptides.

An additional question is, in which body compartment might HisRS-reactive T cells be triggered? An interesting possibility is that such immune activation may take place in the lungs, as indicated by the detection of expanded T cell clones in bronchoalveolar lavage (BAL) fluid and peripheral blood from patients with IIM-associated interstitial pneumonitis (24), and the finding of expansions in BAL fluid CD4+ and CD8+ T cells and corresponding biased T cell receptor V-gene usage in the muscle of patients with IIM (25). These observations suggest the involvement of a shared antigen–driven immune response in the inflammatory process between the lungs and muscles of these patients. However, antigen-specific T cell responses in cells derived from the lungs of patients with IIM have hitherto not been demonstrated.

The present study aimed to address T cell specificity and triggering in anti–Jo-1+ patients with IIM/antisynthetase syndrome. Specifically, we aimed to investigate 1) T cell reactivity and phenotype upon stimulation with full-length HisRS protein and an HLA–DRB1*03 binding HisRS-derived peptide in PBMCs from anti–Jo-1+ patients with IIM/antisynthetase syndrome, 2) whether such antigen-specific T cells are present in the lungs of anti–Jo-1+ patients with IIM/antisynthetase syndrome, and 3) whether immune activation and the presence of anti–Jo-1 autoantibodies can be assessed in the lungs of anti–Jo-1+ patients with IIM/antisynthetase syndrome.

PATIENTS AND METHODS

Patients and selection criteria. Samples were collected between November 2010 and June 2013 at the Rheumatology Unit and Respiratory Medicine Unit of Karolinska University Hospital (Stockholm, Sweden). Patients with IIM fulfilled the criteria for definite, probable, or possible polymyositis or dermatomyositis according to the Bohan and Peter criteria (26,27). The diagnosis of ILD, meeting the American Thoracic society criteria (28), was based on findings from chest radiography/high-resolution computed tomography and/or pulmonary function tests. The diagnosis of antisynthetase syndrome was based on the presence of anti–Jo-1 autoantibodies in addition to one of the following features: ILD, myositis, arthritis, Raynaud's phenomenon, fever, or mechanic's hands (7).

Sample collection. PBMCs were obtained from anti–Jo-1+ patients with IIM/antisynthetase syndrome (n = 15; 6 male and 9 female) and anti–Jo-1– patients (n = 3; all female) (corresponding to patients P1–P18 in Table 1).

Address correspondence to Angeles S. Galindo-Feria, MD, Karolinska University Hospital, Karolinska Institutet, Department of Medicine, Division of Rheumatology, Center for Molecular Medicine, L8:04 SE-171 76 Stockholm, Sweden. E-mail: angeles.galindo.feria@ki.se.

Table 1. Clinical and laboratory characteristics of the 24 patients with idiopathic inflammatory myopathy/antisynthetase syndrome according to type of experiment*

| Patient | Diagnosis | T cell reactivity† | | | | Muscle inflammatory infiltrates | Anti-Jo-1 status | | HLA–DRB1 genotype | |
| | | PBMCs | | BAL fluid | | | | | | |
		Full-length protein	HisRS$_{11-23}$	Full-length protein	HisRS$_{11-23}$		Serum	BAL fluid	Allele 1	Allele 2
P1	PM/antisynthetase syndrome	+	Not tested	Nonviable cells	Nonviable cells	Present	Positive‡§¶	Negative‡	04	15
P2	Antisynthetase syndrome/ILD	++	++	++	++	Absent	Positive‡	Positive‡	01	13
P3	Antisynthetase syndrome/ILD	++	+++	+	+++	Absent	Positive‡§¶	Positive‡	NA	NA
P4	DM	++	+++	–#	–#	Present	Negative‡§	Negative‡	09	13
P5	PM	+++	Not tested	+++	+#	Present	Negative‡	Negative‡	03	10
P6	DM/ILD	–	+	Nonviable cells	Not tested	Absent	Negative‡	NA	03	03
P7	Antisynthetase syndrome/ILD	+++	+	NA	Nonviable cells	Absent	Positive‡	NA	14	15
P8	Antisynthetase syndrome/ILD	++	++	NA	NA	Absent	Positive‡§¶	Positive‡	03	13
P9	Antisynthetase syndrome/ILD	+++	+	NA	NA	Absent	Positive‡	Positive‡	03	04
P10	Antisynthetase syndrome/ILD	++	++	NA	NA	Present	Positive‡§¶	NA	03	15
P11	Antisynthetase syndrome/ILD	++	–	NA	NA	Present	Positive‡§¶	NA	03	13
P12	Antisynthetase syndrome/ILD	+++	++	NA	NA	Present	Positive‡	NA	03	04
P13	Antisynthetase syndrome/ILD	+++	+	NA	NA	Present	Positive‡§¶	NA	03	04
P14	Antisynthetase syndrome/ILD	+++	–	NA	NA	Present	Positive‡§¶	NA	03	04
P15	Antisynthetase syndrome	+	Not tested	NA	NA	Absent	Positive‡¶	NA	01	03
P16	Antisynthetase syndrome/ILD	–	Not tested	NA	NA	Present	Positive§	NA	03	15
P17	Antisynthetase syndrome/ILD	–	–	NA	NA	Absent	Positive‡¶	NA	03	15
P18	DM	–	–	NA	NA	Present	Positive‡	NA	03	13
P19	Antisynthetase syndrome/ILD	NA	NA	NA	NA	Present	Positive‡§¶	Positive‡	01	11
P20	DM/ILD	NA	NA	NA	NA	Present	Negative‡§¶	Negative‡	03	15
P21	DM	NA	NA	NA	NA	Absent	Negative‡§¶	Negative‡	04	07
P22	PM	NA	NA	NA	NA	Present	Negative‡§¶	Negative‡	01	16
P23	DM/ILD	NA	NA	NA	NA	Absent	Negative‡	Negative‡	03	04
P24	PM/antisynthetase syndrome	NA	NA	NA	NA	Present	Positive‡¶	Positive‡	03	03

* HisRS$_{11-23}$ = histidyl–transferase RNA synthetase peptide 11–23; PM = polymyositis; ILD = interstitial lung disease; NA = not available; DM = dermatomyositis.
† In peripheral blood mononuclear cells (PBMCs) and bronchoalveolar lavage (BAL) fluid cells, + = low reactivity, ++ = medium reactivity, +++ = high reactivity, and – = nonreactive.
‡ Detected by enzyme-linked immunosorbent assay.
§ Detected by immunoprecipitation.
¶ Detected by line blotting.
# Analysis of BAL fluid cells with short-term stimulation (1 day), and in low-viability cells with long-term stimulation (5 days).

From 6 of these patients, paired BAL fluid and BAL fluid cell pellets were obtained by bronchoscopy (from 3 anti–Jo-1+ patients and 3 anti–Jo-1– patients [patients P1–P6 in Table 1]) (29). Additional cell-depleted BAL fluid samples were obtained from 4 anti–Jo-1+ patients with IIM/antisynthetase syndrome (1 male and 3 female) and 4 anti–Jo-1– patients (1 male and 3 female) (patients P8 and P9 and P19–P24 in Table 1). All samples were stored at –80°C at the Human Laboratory Area of the Center for Molecular Medicine (Solna, Stockholm, Sweden). In addition, serum samples were obtained from anti–Jo-1+ patients with IIM/antisynthetase syndrome (n = 17; 6 male and 11 female) and anti–Jo-1– patients (n = 7; 1 male and 6 female) (patients P1–P24 in Table 1).

Patients included in the experiments were clustered in groups according to the availability of samples. Group 1 included patients with available PBMCs, BAL fluid, BAL fluid cell pellets, and paired serum samples (patients P1–P6). Group 2 included patients with available PBMCs and paired serum samples (patients P7–P18). Group 3 included patients with serum samples and cell-depleted BAL fluid samples (patients P8 and P9 and P19–P24). T cell experiments included patients from group 1 and group 2. Anti–Jo-1 antibody experiments included patients from group 1 and group 3. For technical reasons (low cell numbers, low cell viability of BAL fluid cells, or low volume of BAL fluid), some samples were excluded. Details regarding the distribution of patients according to the type of analysis, degree of T cell reactivity, presence or absence of muscle inflammatory infiltrates, antibody status, and HLA genotyping are provided in Table 1.

Lung tissue specimens from patients with IIM/antisynthetase syndrome (n = 14; 4 anti–Jo-1+ and 10 anti–Jo-1–) and from comparator cases (patients with chronic obstructive lung disease [COPD]; n = 10) were retrieved from regional biobanks.

Age, sex, smoking status, diagnosis, disease duration from onset of symptoms, clinical manifestations, anti–Jo-1 antibody status, and treatment at the time of blood/BAL fluid sampling are summarized in Table 1 and Supplementary Table 1 (available on the *Arthritis & Rheumatology* web site at http://onlinelibrary.wiley.com/doi/10.1002/art.41075/abstract). Features of the muscle biopsy specimens obtained at the time of disease onset from patients with IIM/antisynthetase syndrome, as detailed in pathology reports, are summarized in Supplementary Table 2 (http://onlinelibrary.wiley.com/doi/10.1002/art.41075/abstract).

Control groups. For the disease control T cell experiments, paired PBMCs and BAL fluid cell pellets were retrieved from patients with sarcoidosis (n = 7; 6 male and 1 female) (patients Sarc1–Sarc7 in Supplementary Table 3, available at http://onlinelibrary.wiley.com/doi/10.1002/art.41075/abstract), since this disease is characterized by the presence of autoimmune features along with ILD, and is associated with HLA–DRB1*03:01. For detection of anti–Jo-1 autoantibodies, additional control patients with sarcoidosis and with avail-

able paired serum samples and cell-depleted BAL fluid were collected (n = 9; 4 male and 5 female). All samples were provided by the Respiratory Medicine Unit, according to a published protocol (29). Descriptions of the lung and lymph node biopsy samples from patients with sarcoidosis, as detailed in pathology reports, are presented in Supplementary Table 4 (available at http://onlinelibrary.wiley.com/doi/10.1002/art.41075/abstract).

For the healthy control T cell experiments, fresh PBMCs were isolated from buffy coats and were obtained from healthy donors who expressed at least one copy of the HLA–DRB1*03 allele (n = 12; 3 male and 9 female). Blood samples from healthy subjects were provided by Uppsala Bioresource at Uppsala University Hospital in Sweden. For the autoantibody analysis, additional paired serum and cell-depleted BAL fluid from healthy controls (n = 18; 8 male and 10 female) were provided by the Respiratory Medicine Unit.

Ethics. The study was approved by the Regional Ethics Committee of Stockholm at Karolinska Institutet and Uppsala University, and performed in accordance with the Declaration of Helsinki guidelines on studies with human subjects. All subjects provided written informed consent prior to any study procedure.

Functional T cell assay. Fresh samples were used for all analyses. PBMCs were obtained from heparinized blood and were prepared by centrifugation over Ficoll-Hypaque gradients. PBMCs were resuspended in 96-well plates in RPMI 1640 medium supplemented with 10% heat-inactivated fetal bovine serum (1×10^6 cells/well) according to an adapted protocol (30). Cells were incubated for 5 days with recombinant human full-length HisRS (20 μg/ml; Bio Supply), with the candidate peptide HisRS$_{11–23}$ (20 μg/ml, sequence VKLQGERVRGLKQ; GenScript) or with RPMI medium as a negative control. Cells were restimulated on day 5 for 8 hours, and brefeldin A (10 μg/ml; Sigma-Aldrich) was added for the last 6 hours. Stimulation with staphylococcal enterotoxin B (10 μg/ml, Sigma-Aldrich) was used as a positive control.

Following stimulation, cells were stained with Live/Dead Fixable Green Dead Cell Stain as well as with antibodies toward CD14, CD3, CD4, CD40L, interferon-γ (IFNγ), interleukin-2 (IL-2), and IL-17A. In some experiments, blocking antibodies for HLA–DR or HLA–DQ or staining with anti-CXCR3, anti-CCR5, and anti-CCR6 antibodies were used. Details on the antibodies used are specified in Supplementary Materials and Methods and Supplementary Table 5 (available at http://onlinelibrary.wiley.com/doi/10.1002/art.41075/abstract).

Flow cytometry. Cells were run on a Gallios Analyzer (Beckman Coulter), and data were analyzed using FlowJo software, version 7.5.1 (Tree Star). The gating strategy is specified in Supplementary Materials and Methods and Supplementary

Figure 1 (available at http://onlinelibrary.wiley.com/doi/10.1002/art.41075/abstract).

Identification of the HisRS T cell epitope. The prediction of a CD4+ T cell epitope was based on the crystal structure of the HLA–DRB1*03:01 molecule in complex with class II–associated invariant chain peptide, which reveals the binding pockets of HLA and how the anchor residues are docking into HLA (31). Prior motif studies established that HLA–DRB1*03:01 epitopes most commonly contain an aliphatic residue in position 1, an acidic or polar residue in position 4, and either a basic residue at position 6 paired with a small residue at position 9 (submotif 1) or a nonbasic residue at position 6 paired with a large residue at position 9 (submotif 2) (32). In this way, a theoretical prediction of CD4+ T cell epitopes can be made from any antigen. In our case, the sequence of the first 60 amino acids of HisRS (UniProtKB identifier P12081) was examined to predict peptides that can bind DRB1*03:01; residues 11–23 (HisRS$_{11-23}$) contained 2 such motifs and therefore had a high probability of containing a bona fide DRB1*03:01 epitope. Thus, HisRS$_{11-23}$ peptide was selected for further functional assays (Figure 1A).

BAL fluid and serum samples for detection of anti–Jo-1 autoantibodies. Anti–Jo-1 IgG and total IgG were measured by enzyme-linked immunosorbent assay (ELISA) in BAL fluid and serum from patients with IIM/antisynthetase syndrome, control patients with sarcoidosis, and healthy controls. Details on the protocol used are presented in Supplementary Materials and Methods (http://onlinelibrary.wiley.com/doi/10.1002/art.41075/abstract).

Immunohistochemistry and histopathology. Paraffin-embedded lung tissue from patients with IIM/antisynthetase syndrome and patients with COPD were analyzed by immunohistochemistry according to a previously published protocol (33). The primary antibodies used were anti-CD3, anti-CD138, anti-CXCR3, and anti-CCR5 or the isotype controls IgG, IgG2b, and IgG1. Details on the protocol and antibodies used for ELISAs and immunohistochemistry are specified in Supplementary Materials and Methods, Supplementary Table 6, and Supplementary Figure 2 (available at http://onlinelibrary.wiley.com/doi/10.1002/art.41075/abstract). Whole sections were evaluated independently by 2 investigators (AGF and CFC) on coded slides by semiquantitative scoring for the extent of immunohistochemical staining on a 4-point scale, where 0 = none, 1 = low, 2 = intermediate, and 3 = high amount of staining. Results are expressed as the mean of 2 observations.

Statistical analysis. Continuous variables are expressed as the median with interquartile range (IQR; 25th–75th percentiles) or minimum and maximum values. Categorical variables are presented as frequencies and percentages. Differences between groups were analyzed using Mann-Whitney U test. For comparison of the percentage of CD40L up-regulation between different stimulation conditions, Wilcoxon's signed-rank test was used. Two-tailed *P* values less than 0.05 were considered significant. Up-regulated expression of CD40L in T cells was normalized to the value in unstimulated cells, and presented as the median fold change according to the following categories: low (<3-fold), intermediate (3–10-fold), or high (>10-fold). The analyses were performed using Prism 5 software (Graph Pad) and IBM SPSS Statistics, version 25.

RESULTS

Clinical characteristics of the patients and controls. A total of 17 anti–Jo-1+ and 7 anti–Jo-1– patients with IIM/antisynthetase syndrome were included in our analyses (Table 1). The anti–Jo-1+ patients (median age 55 years [IQR 53–55 years]) had a longer disease duration and higher frequency of ILD compared to the anti–Jo-1– patients (median age 57 years [IQR 54–57 years]) (*P* = 0.033 and *P* = 0.021, respectively). There was no difference in sex, age, or smoking status between the 2 groups of patients (*P* = 0.625, *P* = 0.425, and *P* = 0.724, respectively). A comparison of the characteristics of the 2 groups of patients is presented in Supplementary Table 7 (available at http://onlinelibrary.wiley.com/doi/10.1002/art.41075/abstract).

Group 1 (T cell group, patients P1–P6) had a median disease duration of 5 months (IQR 1–48 months). Five patients in this group were untreated and 1 patient was receiving immunosuppressive treatment. Group 2 (T cell group, patients P7–P18) had a median disease duration of 64 months (IQR 1–193 months), and 9 of 12 patients were receiving immunosuppressive treatment. Group 3 (antibody group, patients P19–P24) had a median disease duration of 13 months (IQR 4–60 months), and 4 of 6 patients were receiving immunosuppressive treatment (see Supplementary Table 1 [http://onlinelibrary.wiley.com/doi/10.1002/art.41075/abstract]).

The control patients with sarcoidosis and healthy controls assessed in T cell and antibody analyses had a median age of 55 years (IQR 43–62 years) and 33 years (IQR 28–49 years), respectively. Detailed clinical information on the patients with sarcoidosis is presented in Supplementary Table 3 (http://onlinelibrary.wiley.com/doi/10.1002/art.41075/abstract).

Presence of HisRS-T cell reactivity in the peripheral blood of patients with IIM/antisynthetase syndrome. To identify the potential presence of antigen-specific T cells against HisRS in the blood of patients with IIM/antisynthetase syndrome, we assessed the up-regulation of CD40L in CD4+ T cells following stimulation with HisRS protein or HisRS$_{11-23}$ in patients from group 1 and group 2. After stimulation of PBMCs with HisRS protein, we identified up-regulation of CD40L on CD4+ T cells in 14 of 18 patients with IIM/antisynthetase syndrome, with a median fold change of 7.38 (IQR 2.69–31.86) relative to unstimulated cells (*P* = 0.0002).

High (>10-fold) up-regulation of CD40L in CD4+ T cells following stimulation with the HisRS protein was observed in 6 of 14
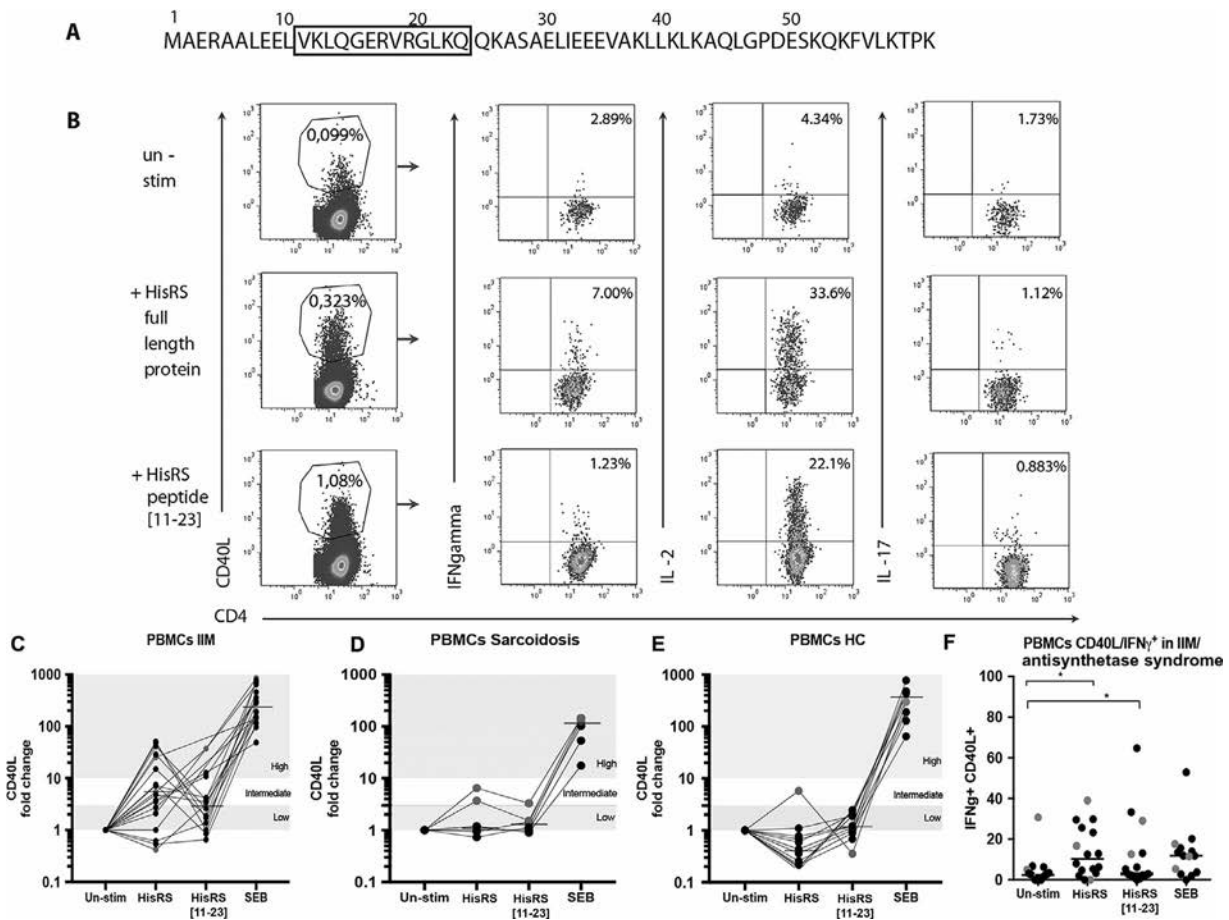
Figure 1. Anti–histidyl–transfer RNA synthetase (HisRS)–specific T cells are enriched in the blood of patients with idiopathic inflammatory myopathy (IIM)/antisynthetase syndrome. **A**, A 13-mer peptide within the first 60 amino acids of HisRS was predicted to represent a potential T cell epitope, HisRS$_{11-23}$. **B**, Representative plots from fluorescence-activated cell sorter analysis (gated on lymphocytes and CD4+CD3+ T cells, with exclusion of dead cells and monocytes) show up-regulation of CD40L in CD4+ T cells as well as production of interferon-γ (IFNγ), interleukin-2 (IL-2), and IL-17 on peripheral blood mononuclear cells (PBMCs) from an anti–Jo-1+ patient with IIM/antisynthetase syndrome, in unstimulated (un-stim) conditions or after stimulation with full-length HisRS protein or HisRS$_{11-23}$. **C–E**, Up-regulation of CD40L expression was examined on CD4+ T cells in PBMCs from anti–Jo-1+ patients with IIM/antisynthetase syndrome (n = 18) (patients P1–P18 in Table 1) (**C**), patients with sarcoidosis (n = 6) (**D**), and HLA–DRB1*03–positive healthy controls (HCs) (n = 12) (**E**). Solid symbols in **C–E** represent the median fold change in PBMCs from these groups, while gray-shaded symbols represent the median fold change in PBMCs from anti–Jo-1– patients (**C**), patients with sardoidosis who showed reactivity toward HisRS protein and HisRS$_{11-23}$ (**D**), and a healthy control subject who showed reactivity to HisRS protein (**E**). Categories of fold change were low (<3-fold), intermediate (3–10-fold), or high (>10-fold). Cells were left unstimulated or stimulated with full-length HisRS protein, HisRS$_{11-23}$, or staphylococcal enterotoxin B (SEB) as a positive control. **F**, IFNγ production was assessed on CD40L+CD4+ T cells in PBMCs from patients with IIM/antisynthetase syndrome. Solid symbols represent anti–Jo-1+ patients and gray-shaded symbols represent anti–Jo-1– patients; horizontal lines show the median. Cells were left unstimulated or stimulated with full-length HisRS recombinant protein, HisRS$_{11-23}$, or SEB. * = $P < 0.05$ by 2-tailed Wilcoxon's matched-pairs signed rank test.

patients with IIM/antisynthetase syndrome (5 anti–Jo-1+ and 1 anti–Jo-1–), with a median fold change of 35 (IQR 22.76–48.53) relative to unstimulated cells (Figures 1B and C). The highest responses were present in the PBMCs from patients with IIM/antisynthetase syndrome, specifically those who expressed at least one copy of the HLA–DRB1*03 allele and were anti–Jo-1+ as compared to anti–Jo-1+ patients without the HLA–DRB1*03 allele (mean fold change in CD40L expression relative to unstimulated cells 16.05 versus 7.57; P not significant) (see Supplementary Figures 3A and C, available at http://onlinelibrary.wiley.com/doi/10.1002/art.41075/abstract).

After stimulation of PBMCs with HisRS$_{11-23}$, we detected up-regulation of CD40L on CD4+ T cells in 11 of 14 patients with IIM/antisynthetase syndrome, with a median fold change of 3.4 (IQR 1.87–10.9) relative to unstimulated cells ($P = 0.0012$). The highest response toward HisRS$_{11-23}$ (>10-fold change versus unstimulated cells) was observed in 3 of 11 patients with IIM/antisynthetase syndrome (2 anti–Jo-1+ and 1 anti–Jo-1–), with a median fold change of 12.75 (IQR 10.9–37) (Figures 1B and C).

In the sarcoidosis group, up-regulation of CD40L was detected in PBMCs from 2 of 7 patients after stimulation with HisRS protein, with a median fold change of 5.08 (IQR

Figure 2. HisRS reactivity is restricted to HLA–DR. **A**, Representative plots from fluorescence-activated cell sorter analysis show up-regulation of CD40L on CD4+ T cells in PBMCs from anti–Jo-1+ patients w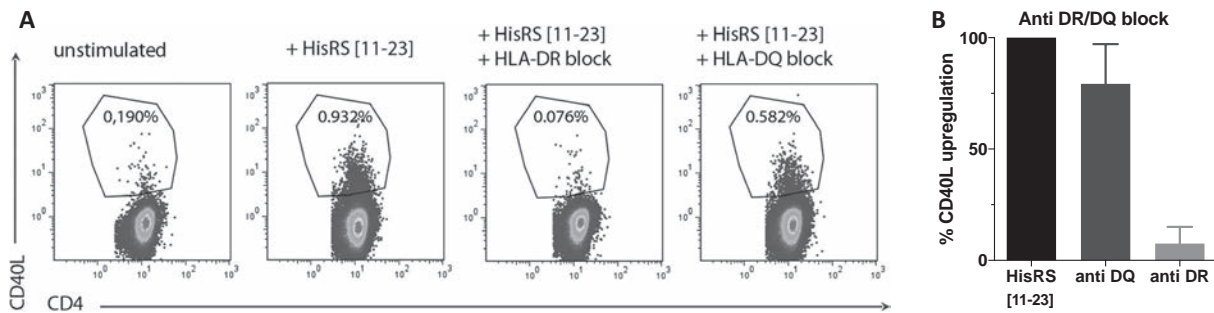ith IIM/antisynthetase syndrome after stimulation with $HisRS_{11-23}$ compared to unstimulated cells. This up-regulation was abolished in the presence of anti–HLA–DR but not in the presence of anti–HLA–DQ blocking antibodies. **B**, Effects of anti–HLA–DQ and anti–HLA–DR blocking antibodies on CD40L up-regulation by $HisRS_{11-23}$ were quantified in PBMCs from anti–Jo-1+ patients with IIM/antisynthetase syndrome (n = 2; patients P2 and P12 in Table 1). Bars show the median percentage change (with upper limit of maximum range) relative to $HisRS_{11-23}$ (set at 100%). See Figure 1 for definitions.

3.7–6.47) relative to unstimulated cells, and detected in 3 of 7 patients following stimulation with $HisRS_{11-23}$, with a median fold change of 2.09 (IQR 1.45–3.29) relative to unstimulated cells (Figure 1D). The HisRS-reactive patients with sarcoidosis were positive for either HLA–DRB1*04/*15 or HLA–DRB1*01/*03 and were former smokers (see Supplementary Table 3 [http://online library.wiley.com/doi/10.1002/art.41075/abstract]).

In the healthy control group who were positive for HLA–DRB1*03, up-regulation of CD40L was observed in PBMCs stimulated with HisRS protein in 1 of 12 subjects (5-fold change relative to unstimulated cells). After stimulation of PBMCs with $HisRS_{11-23}$, up-regulation of CD40L was observed in 5 of 12 healthy controls, with a median fold change of 2 (IQR 1.89–2.42) relative to unstimulated cells (P = 0.06) (Figure 1E).

We next evaluated the proinflammatory effector functions of HisRS-specific T cells by examining cytokine production within the CD4+CD40L+ T cell population. The HisRS-specific CD4+CD40L+ T cells in peripheral blood mainly produced IL-2 and IFNγ. In the patients with IIM/antisynthetase syndrome, a median of 12% (IQR 5.39–25.6%) of CD4+CD40L+ T cells produced IFNγ after antigenic stimulation with HisRS protein, and a median of 4% (IQR 2–18%) produced IFNγ after stimulation with $HisRS_{11-23}$ (P = 0.0084 and P = 0.02 respectively, compared to unstimulated cells) (Figure 1F).

To confirm an HLA–DR dependency of the observed T cell responses, PBMCs from 2 anti–Jo-1+ patients were stimulated with $HisRS_{11-23}$ in the presence of anti–HLA–DR or anti–HLA–DQ blocking antibodies. Anti–HLA–DR blocking efficiently abrogated the up-regulation of CD40L upon stimulation with $HisRS_{11-23}$, while anti–HLA–DQ blocking did not (Figures 2A and B), thereby indicating that the $HisRS_{11-23}$ epitope is presented by HLA–DR.

Presence of HisRS-specific T cells in the lungs of patients with IIM/antisynthetase syndrome display a pronounced Th1 phenotype as compared to PBMCs. To investigate whether the presence and functionality of antigen-specific CD4+ T cells may vary in different compartments, we

selected BAL fluid cells and corresponding PBMCs from anti–Jo-1+ patients with IIM/antisynthetase syndrome (n = 2) and anti–Jo-1− patients (n = 2) (group 1, patients P2–P5 [Table 1]) and patients with sarcoidosis (n = 7) (see Supplementary Table 3 [http://onlinelibrary.wiley.com/doi/10.1002/art.41075/abstract]), and stimulated the cells with either HisRS protein or $HisRS_{11-23}$.

A CD40L response of BAL fluid cells stimulated with HisRS full-length protein was present in 3 of 4 patients with IIM/antisynthetase syndrome (patients P2, P3, and P5), with a median fold change in CD40L expression of 3.6 (IQR 2.68–14.7) relative to unstimulated cells. The corresponding CD4+ T cells from PBMCs had a similar up-regulation of CD40L in response to the HisRS protein in all 4 patients tested (patients P2–P5), with a median fold change of 4.58 (IQR 3.25–25.36) relative to unstimulated cells (Figures 3A and B).

When the response to $HisRS_{11-23}$ stimulation was analyzed in the lung compartment of patients with IIM/antisynthetase syndrome, we identified a high CD40L up-regulation in BAL fluid cells from 2 of 3 patients (patients P2 and P3) when compared to unstimulated conditions, with a median fold change of 88 (IQR 27–149). Furthermore, the CD40L responses in PBMCs were also high in all 3 patients evaluated (patients P2–P4), with a median fold change of 12.7 (IQR 4.18–37) relative to unstimuated cells.

Moreover, the highest frequencies of CD4+CD40L+ T cells were found in BAL fluid after stimulation with $HisRS_{11-23}$, with a median fold change of 7.83% (IQR 1.37–29.9%), whereas in PBMCs, the median fold change was 0.38% (IQR 0.02–5.89%), suggesting an enrichment of antigen-specific T cells in the lung compartment (see Supplementary Table 8, available at http://online library.wiley.com/doi/10.1002/art.41075/abstract). In addition, the highest reactivity to $HisRS_{11-23}$ was seen in the 2 anti–Jo-1+ patients with IIM/antisynthetase syndrome, whereas BAL fluid cells from 1 anti–Jo-1− patient (patient P4) showed no response upon $HisRS_{11-23}$ stimulation.

In order to characterize the phenotype of CD4+ T cells in BAL fluid and PBMCs, we selected unstimulated, paired CD4+ T cells from both compartments, obtained from 3 anti–Jo-1+
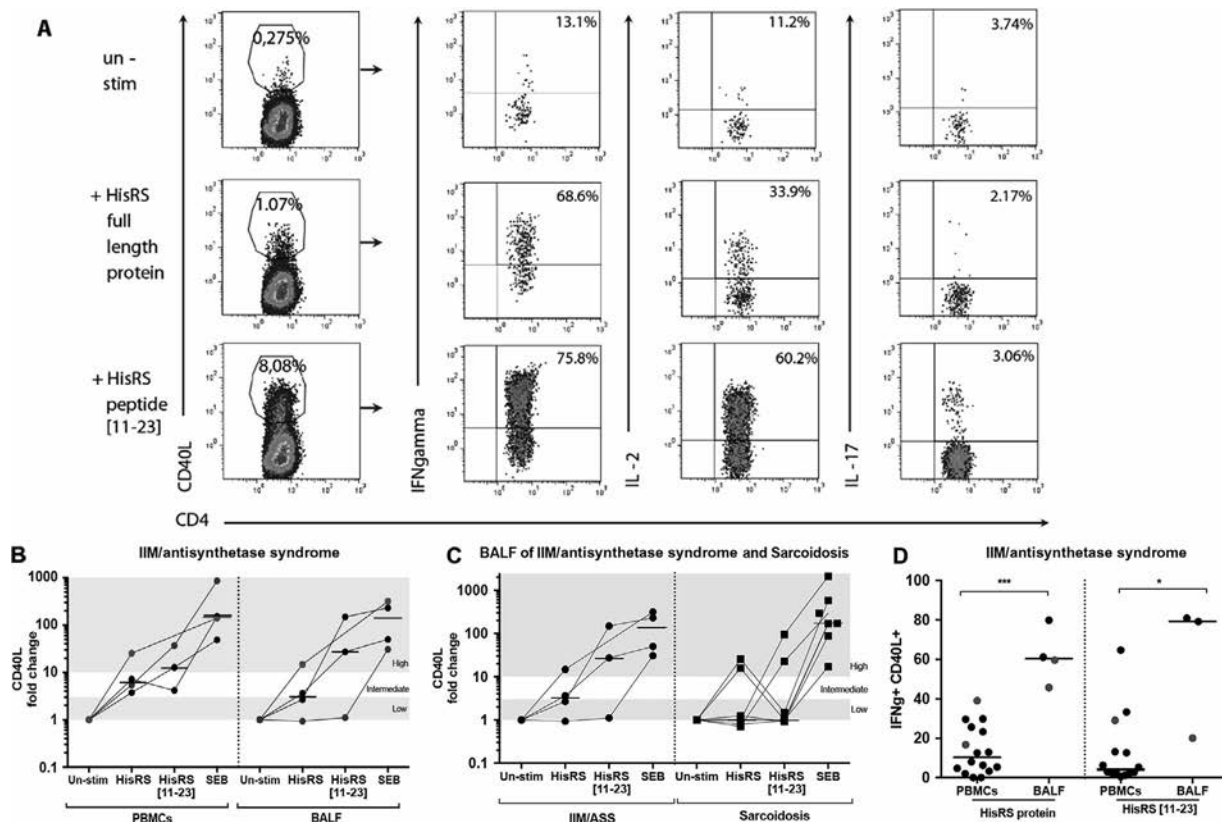
Figure 3. Anti–HisRS–specific T cells are detected in the lungs of patients with IIM/antisynthetase syndrome. **A**, Representative plots from fluorescence-activated cell sorter analysis (gated on lymphocytes and CD4+CD3+ T cells, with exclusion of dead cells and monocytes) show up-regulation of CD40L as well as production of IFNγ, IL-2, and IL-17 on CD4+ T cells obtained from bronchoalveolar lavage (BAL) fluid (BALF) from an anti-Jo-1+ patient with IIM/antisynthetase syndrome. BAL fluid T cells were left unstimulated or stimulated with full-length HisRS recombinant protein or HisRS$_{11-23}$. **B** and **C**, CD40L up-regulation on CD4+ T cells, relative to unstimulated cells, was compared between BAL fluid cells and corresponding PBMCs from patients with IIM/antisynthetase syndrome (n = 4; patients P2–P5 in Table 1) (**B**) and in BAL fluid CD4+ T cells between patients with IIM/antisynthetase syndrome (n = 4) and patients with sarcoidosis (n = 7) (**C**). Cells were left unstimulated or stimulated with full-length HisRS protein, HisRS$_{11-23}$ peptide, or SEB for 5 days. Solid symbols represent the median fold change in individual anti-Jo-1+ patients with IIM/antisynthetase syndrome or patients with sarcoidosis; gray-shaded symbols represent the median fold change in anti-Jo-1− patients. Categories of fold change were low (<3-fold), intermediate (3–10-fold), or high (>10-fold). **D**, IFNγ production on CD40L+CD4+ T cells was compared between BAL fluid cells and corresponding PBMCs from anti-Jo-1+ patients with IIM/antisynthetase syndrome after stimulation with full-length HisRS recombinant protein or HisRS$_{11-23}$. Solid symbols represent anti-Jo-1+ patients and gray-shaded symbols represent anti-Jo-1− patients; horizontal lines show the median. * = $P < 0.05$; *** = $P < 0.001$, by 2-tailed Mann-Whitney U test. See Figure 1 for definitions.

patients with IIM/antisynthetase syndrome (patients P1–P3) and 2 anti-Jo-1− patients (patients P4 and P5). Almost all of the CD4+ T cells in BAL fluid were positive for the Th1-associated chemokine receptors CXCR3 (97%) (Figure 4A) and CCR5 (93%) (Figure 4B), compared to 46% and 50% of PBMCs, respectively ($P < 0.01$ and $P < 0.05$, respectively). Moreover, ~60% of the BAL fluid T cells expressed CCR6, compared to 20% of PBMCs ($P < 0.01$) (Figure 4C). In BAL fluid, >90% of CCR6+CD4+ T cells were positive for CXCR3, indicating that CD4+ T cells in BAL fluid had a Th1/Th17 phenotype in anti-Jo-1+ and anti-Jo-1− patients.

Furthermore, HisRS-specific BAL fluid CD4+CD40L+ T cells presented a pronounced proinflammatory Th1 phenotype that was characterized by an increased production of IFNγ, when compared to the corresponding CD4+CD40L+ T cells from PBMCs, in both anti-Jo-1+ and anti-Jo-1− patients. On average, 60% of the

CD4+CD40L+ T cells from BAL fluid produced IFNγ in response to antigenic stimulation with either HisRS full-length protein or HisRS$_{11-23}$, compared to 10% of the CD4+CD40L+ T cells in the corresponding blood samples ($P < 0.001$ and $P < 0.05$, respectively) (Figure 3D).

In the disease control group of patients with sarcoidosis, BAL fluid cells from 2 of 7 patients with sarcoidosis (patients Sarc1 and Sarc4) displayed a high (>10-fold) CD40L response to the HisRS protein, with a median fold change of 20 (IQR 15.75–25.5) relative to unstimulated cells. Two other control patients with sarcoidosis (of the 7 tested) presented high CD40L up-regulation in response to HisRS$_{11-23}$ (patients Sarc3 and Sarc7), with a median fold change of 59 (IQR 22.7–95) relative to unstimulated conditions (Figure 3C). CD40L up-regulation in BAL fluid cells from the group of patients with sarcoidosis who responded to HisRS full-length protein was 4 times higher compared to that in the corresponding PBMCs (Figure 1D
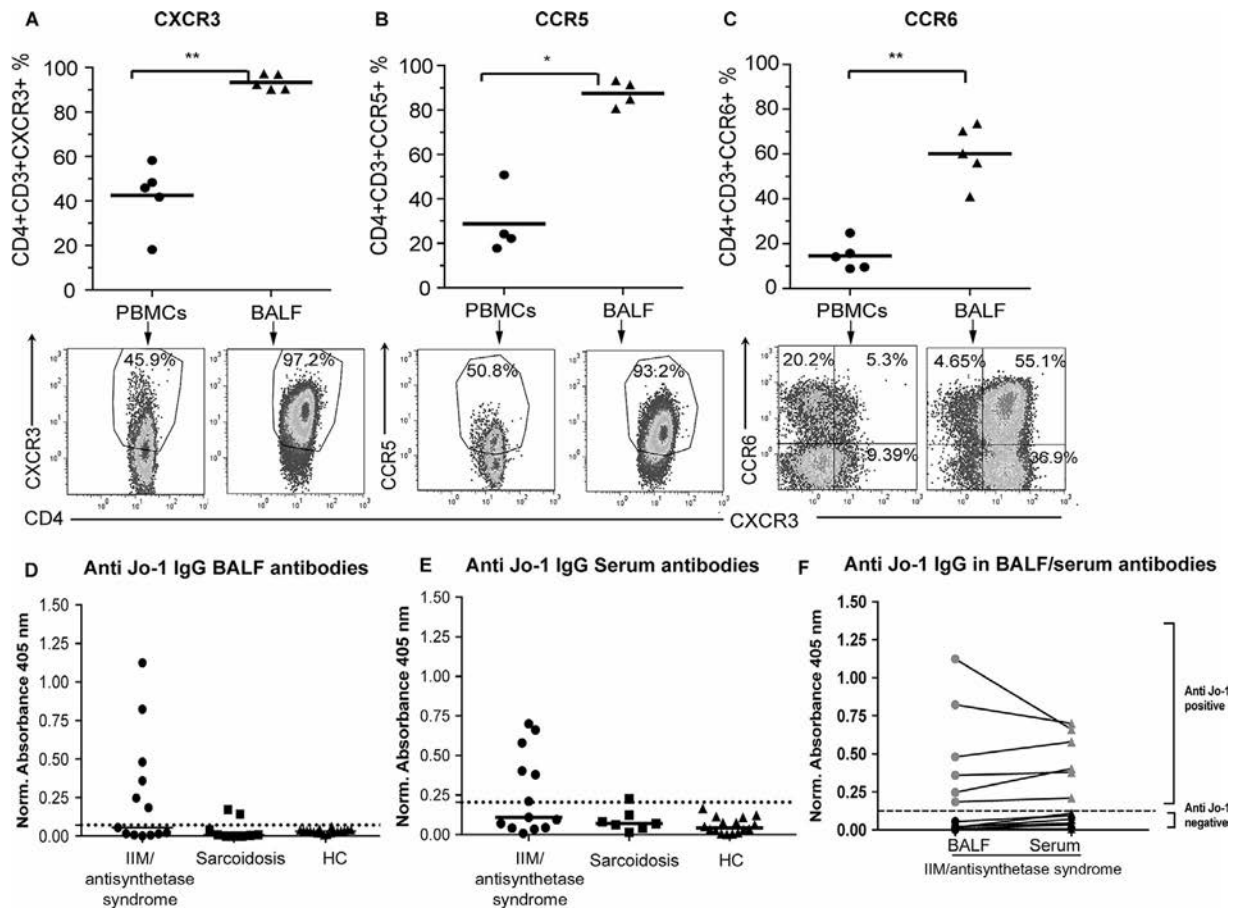
Figure 4. Th1 cells and anti–Jo-1 antibodies are present in the lungs of patients with IIM/antisynthetase syndrome. **A–C**, Representative plots from fluorescence-activated cell sorter analysis (bottom) and quantification of the results (top) show the percentage of CD4+CD3+CXCR3+ T cells (**A**), CD4+CD3+CCR5+ T cells (**B**), and CD4+CD3+CXCR3+CCR6+ T cells (**C**) in PBMCs and bronchoalveolar lavage (BAL) fluid (BALF) cells from patients with IIM/antisynthetase syndrome (n = 5). **D** and **E**, Presence of anti–Jo-1 autoantibodies was analyzed by enzyme-linked immunosorbent assay (ELISA) in the BAL fluid (**D**) and corresponding serum (**E**) of patients with IIM/antisynthetase syndrome, patients with sarcoidosis, and healthy controls. The broken horizontal line indicates the cutoff value for positivity, calculated using the values in healthy controls (mean absorbance in healthy controls + 3SD). Results are expressed as the normalized (Norm.) values for the absorbance at 405 nm (optical density ratio of anti–Jo-1 IgG to total IgG in the BAL fluid and serum). Symbols in **A–E** show individual subjects; horizontal lines show the mean. **F**, Presence of anti–Jo-1 IgG autoantibodies was compared between the BAL fluid and serum of anti–Jo-1+ (n = 6) and anti–Jo-1– (n = 7) patients with IIM/antisynthetase syndrome, assessed by ELISA with values normalized to the total IgG levels in corresponding compartments. Patients were classified as anti–Jo-1+ if they were seropositive by at least one method (ELISA, immunoprecipitation, or line blotting, as described in Table 1). The broken horizontal line indicates the cutoff value for seropositivity. * = P < 0.05; ** = P < 0.01, by 2-tailed Mann-Whitney U test. See Figure 1 for definitions.

and Figure 3C). The frequencies of CD4+CD40L+ T cells in patients with IIM/antisynthetase syndrome, control patients with sarcoidosis, and healthy controls are presented in Supplementary Table 8 (http://onlinelibrary.wiley.com/doi/10.1002/art.41075/abstract).

Anti–Jo-1 autoantibodies in BAL fluid. To further dissect the HisRS-specific immune response in the lung compartment, cell-depleted BAL fluid samples from patients with IIM/antisynthetase syndrome (n = 13), corresponding to group 1 and group 3 (patients P1–P5 in group 1, and patients P8 and P9 and P19–P24 in group 3), patients with sarcoidosis (n = 9), and healthy controls (n = 18) were analyzed for the presence of anti–Jo-1 autoantibodies. We detected anti–Jo-1 IgG autoan-

tibodies in BAL fluid from 6 of 7 anti–Jo-1+ patients and in 2 of 9 patients with sarcoidosis, but not in healthy controls or in anti–Jo-1– individuals (Figure 4D). After normalizing the amount of anti–Jo-1 autoantibodies to the values for total IgG, all of the anti–Jo-1+ patients who showed reactivity in the BAL fluid were also reactive in the serum (Figures 4E and F).

Infiltration of lung tissue by T cells and plasma cells in patients with IIM/antisynthetase syndrome. Germinal center (GC)–like structures characterized by T cells and surrounding plasma cells were observed in the lung tissue from 2 of 4 anti–Jo-1+ patients with IIM/antisynthetase syndrome but in none of the lung tissue samples from anti–Jo-1– patients
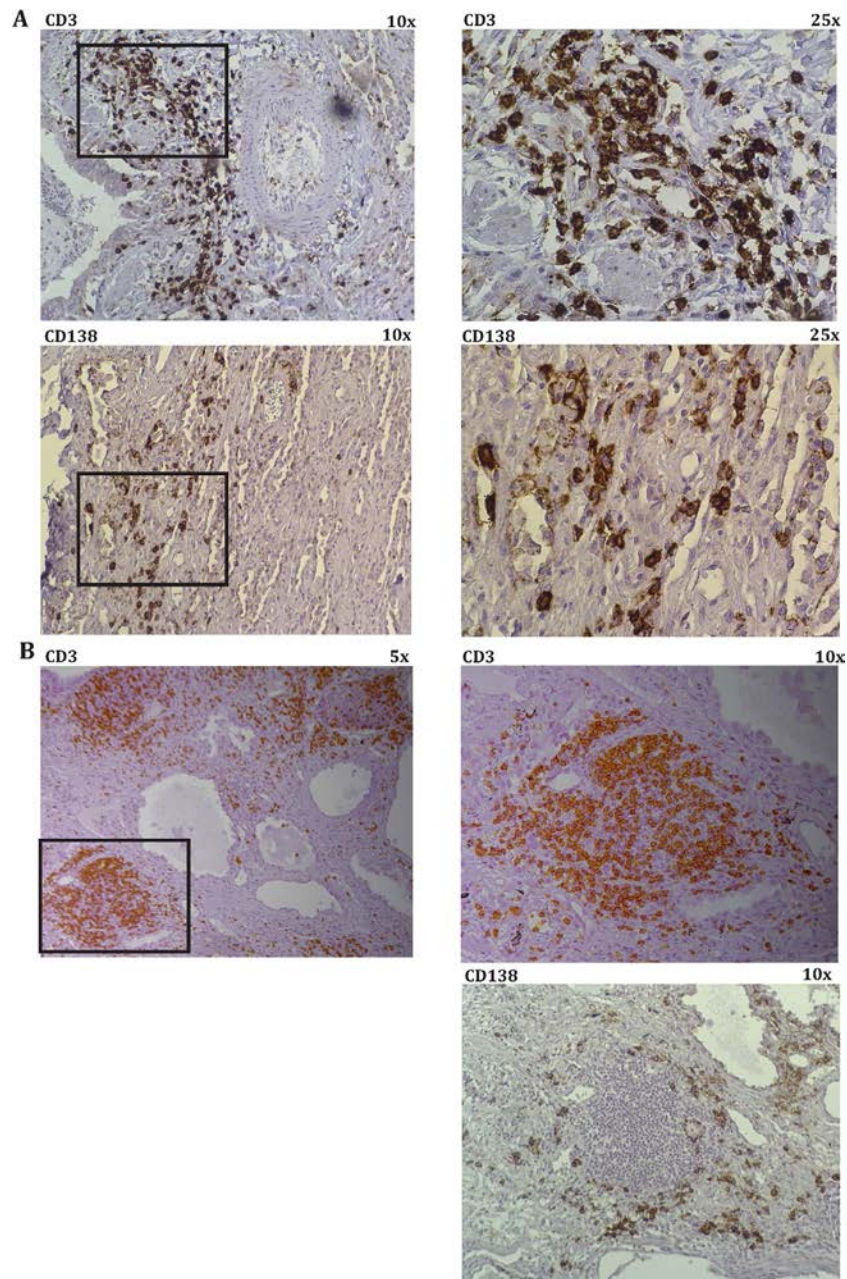
Figure 5. Histologic examination of the lungs of a representative anti–Jo-1+ patient with idiopathic inflammatory myopathy/antisynthetase syndrome and interstitial lung disease. **A**, Immunohistochemical analysis of the lung tissue sections reveals T cell infiltrates (CD3 staining) (upper panels) and infiltration of plasmablasts (CD138 staining) (lower panels). Boxed areas in the left panels are shown at higher magnification on the right. Original magnification × 10 on left; × 25 on right. **B**, Immunohistochemical staining of the lung tissue shows several germinal center–like formations on CD3 staining (left and upper right panels) and CD138 staining (lower right panel). Boxed area in the left panel is shown at higher magnification on the upper right. Original magnification × 5 on left; × 10 on right. Isotype controls for CD3, CCR5, and CXCR3 with semiquantitative analysis are presented in Supplementary Figure 2 (http://onlinelibrary.wiley.com/doi/10.1002/art.41075/abstract).

or patients with COPD (Figures 5A and B). In addition, we observed infiltrating CD3+ T cells in all patient groups (patients with IIM/antisynthetase syndrome and patients with COPD), with a higher number of infiltrating CD3+ T cells in patients with COPD than in patients with IIM/antisynthetase syndrome ($P = 0.009$). No differences between groups were seen for CD138+ plasma cell expression ($P = 0.37$) (see Supplementary Figures 2A and C, available at http://onlinelibrary.wiley.com/doi/10.1002/art.41075/abstract). There was no difference in the expression of CXCR3 and CCR5 between anti–Jo-1+ and anti–Jo-1– patients (staining not performed in lung biopsy samples from patients with COPD). Transbronchial lung biopsy samples from patients with sarcoidosis did not show the presence of GC formation (see Supplementary Table 4).

DISCUSSION

In this study, we describe activation of antigen-specific CD4+ T cells in peripheral blood and BAL fluid cells from patients with IIM/antisynthetase syndrome by an HLA–DRB1*03-associated T cell epitope corresponding to the stretch of residues 11–23 within the HisRS protein. The stimulation of CD4+ T cells with the full-length HisRS protein and the $HisRS_{11-23}$ peptide induced up-regulation of CD40L in CD4+ T cells in both the lung and blood compartments, indicating the presence of HisRS-specific T cells in patients with IIM/antisynthetase syndrome.

To our knowledge, the phenotype of T cells involved in the immune reactivity toward a specific peptide in IIM/antisynthetase syndrome has not been previously addressed. The present description of T cell reactivity is directed against a candidate HisRS-derived peptide ($HisRS_{11-23}$) that we selected based on binding predictions to HLA–DRB1*03:01. The high reactivity observed in patients with IIM/antisynthetase syndrome compared to patients with sarcoidosis and healthy controls indicates that the $HisRS_{11-23}$ epitope is an important target for autoreactive T cells in IIM/antisynthetase syndrome. Furthermore, our results demonstrate that the activation of HisRS-specific T cells was abrogated by blocking HLA–DR but not by blocking HLA–DQ. We thus demonstrate a T cell activation bias in HLA–DRB1*03:01–positive patients toward $HisRS_{11-23}$. These findings confirm previous results demonstrating T cell proliferation following stimulation with substantially larger fragments of HisRS in T cell cultures (22).

Nevertheless, the observed T cell activation was not entirely limited to the anti–Jo-1+ subset of patients with IIM/antisynthetase syndrome, but occurred in some anti–Jo-1– patients, although to a substantially lower degree. While the genetic association between IIM with anti–Jo-1 antibody positivity and HLA–DRB1*0301 is well established, we find it interesting that patients with other class II major histocompatibility complex alleles could also be implicated in the presentation of HisRS-derived peptides.

Our findings of an increased reactivity against the HisRS protein, and in particular the HisRS-derived peptide $HisRS_{11-23}$ in lung-derived T cells compared to blood-derived cells, are, in our opinion, striking, and despite the limited number of cases with BAL fluid–derived T cells, this observation may point to the lung as a potential site of primary activation of T cells against HisRS, similar to what has been proposed in other autoimmune diseases such as RA (8,9,34) and MS (12). We also identified the presence of anti–Jo-1 autoantibodies in BAL fluid as well as GC-like structures in lung tissue from anti–Jo-1+ patients, supporting the hypothesis of the lungs as a potential site for immune activation and anti–Jo-1 autoantibody production. As some patients displayed reactivity to the HisRS full-length protein but not to the $HisRS_{11-23}$ epitope, other HisRS-derived peptides are likely to be implicated.

Interestingly, 2 patients with sarcoidosis with the highest HisRS T cell reactivity were former smokers, indicating a possible

gene–environment interaction. In this context, the previously described higher expression of HisRS in lung tissue compared to other types of tissue is interesting (20). Also, a granzyme B–sensitive form of HisRS has been identified exclusively in the lung (21). Therefore, increased amounts of granzyme B triggered by proinflammatory environmental stimuli, such as infections or smoke exposure (35), may contribute to the release of N-terminal HisRS fragments and the formation and enhanced processing of neoepitopes that can be recognized by HisRS-reactive T cells in patients with IIM/antisynthetase syndrome (21,36).

The N-terminal HisRS fragments have chemotactic properties that can induce migration of CCR5-expressing lymphocytes, activated monocytes, and immature dendritic cells (23). The aforementioned mechanism suggests that the HisRS protein or fragments released from damaged lungs may be involved in the recruitment of activated T cells, including HisRS-activated cells to inflammatory sites in the lungs, thereby providing costimulatory signals to B cells and antigen-presenting cells. In this hypothesis, the muscle might become targeted in later stages of the disease (20).

Consistent with previous reports (37–40), the present study demonstrated high expression of the chemokine receptors CCR5 and CXCR3 (markers of Th1 cells) and CCR6 (Th17 marker) in nearly 100% of CD4+ T cells isolated from the BAL fluid of both anti–Jo-1+ and anti–Jo-1– patients. The enriched expression of these chemokine receptors in BAL fluid T cells compared to peripheral blood T cells was not unexpected, as several studies have shown that these receptors are known to regulate antigen-induced T cell homing in lung diseases, such as asthma (41,42), COPD (43), and sarcoidosis (44), and can even be found in healthy smokers (45). Moreover, the identification of a Th1/Th17 phenotype (Th17.1 cells) in BAL fluid from patients with IIM/antisynthetase syndrome, characterized by an excessive secretion of IFNγ, has also been reported in patients with chronic sarcoidosis (38,46,47) and in other autoimmune diseases such as Crohn's disease (48) and arthritis (49).

The design of the present study has a number of limitations. One limitation was the low availability of paired samples from BAL fluid and PBMCs from untreated patients with inflammatory active IIM/antisynthetase syndrome. Acquiring BAL fluid samples requires an invasive procedure, and it may be unethical to delay the start of treatment until the bronchoscopy can be performed. Nevertheless, the results obtained from this small number of patients were consistent, contributing to the significance of our observations.

In conclusion, the results of the present study indicate that specific HisRS-derived peptides in HLA–DRB1*03–positive individuals, including the $HisRS_{11-23}$ peptide investigated herein, may be presented to locally available T cells, which become activated and subsequently adopt a proinflammatory phenotype. These T cells may promote B cell maturation and activation, GC-like structure formation, and subsequent production of anti–Jo-1

autoantibodies. One possible site for the initial activation of the immune system could be in the lungs, where environmental factors such as smoking or infections may cause an unspecific inflammation in the lung tissue, leading to granzyme B release and HisRS cleavage that may then lead to the recruitment of T cells. Further studies on other relevant peptides with a broader coverage of the antigenic sites of HisRS, as well as studies on the phenotypes of locally infiltrating T cells, in patients with IIM/antisynthetase syndrome remain a priority.

ACKNOWLEDGMENTS

AUTHOR CONTRIBUTIONS

All authors were involved in drafting the article or revising it critically for important intellectual content, and all authors approved the final version to be published. Dr. Galindo-Feria had full access to all of the data in the study and takes responsibility for the integrity of the data and the accuracy of the data analysis.

Study conception and design. Galindo-Feria, Albrecht, Fernandes-Cerqueira, Notarnicola, James, Dastmalchi, Rönnblom, Jakobsson, Fathi, Grunewald, Malmström, Lundberg.

Acquisition of data. Galindo-Feria, Albrecht, Fernandes-Cerqueira, Notarnicola, Herrath, Dastmalchi, Fathi, Lundberg.

Analysis and interpretation of data. Galindo-Feria, Albrecht, Fernandes-Cerqueira, Notarnicola, James, Dastmalchi, Sandalova, Fathi, Achour, Grunewald, Malmström, Lundberg.

ADDITIONAL DISCLOSURES

Author Albrecht is currently an employee of Sanofi Genzyme. Author Herrath is currently an employee of Pfizer.

REFERENCES

1. Marie I. Morbidity and mortality in adult polymyositis and dermatomyositis. Curr Rheumatol Rep 2012;14:275–85.

2. McHugh NJ, Tansley SL. Autoantibodies in myositis. Nat Rev Rheumatol 2018;14:290–302.

3. Betteridge Z, Tansley S, Shaddick G, Chinoy H, Cooper RG, New RP, et al. Frequency, mutual exclusivity and clinical associations of myositis autoantibodies in a combined European cohort of idiopathic inflammatory myopathy patients. J Autoimmun 2019;101:48–55.

4. Brouwer R, Hengstman GJ, Vree Egberts W, Ehrfeld H, Bozic B, Ghirardello A, et al. Autoantibody profiles in the sera of European patients with myositis. Ann Rheum Dis 2001;60:116–23.

5. Aggarwal R, Cassidy E, Fertig N, Koontz DC, Lucas M, Ascherman DP, et al. Patients with non-Jo-1 anti-tRNA-synthetase autoantibodies have worse survival than Jo-1 positive patients. Ann Rheum Dis 2014;73:227–32.

6. Hervier B, Devilliers H, Stanciu R, Meyer A, Uzunhan Y, Meau A, et al. Hierarchical cluster and survival analyses of antisynthetase syndrome: phenotype and outcome are correlated with anti-tRNA synthetase antibody specificity. Autoimmun Rev 2012;12:210–7.

7. Connors GR, Christopher-Stine L, Oddis CV, Danoff SK. Interstitial lung disease associated with the idiopathic inflammatory myopathies: what progress has been made in the past 35 years? Chest 2010;138:1464–74.

8. Reynisdottir G, Karimi R, Joshua V, Olsen H, Hensvold AH, Harju A, et al. Structural changes and antibody enrichment in the lungs are early features of anti–citrullinated protein antibody–positive rheumatoid arthritis. Arthritis Rheumatol 2014;66:31–9.

9. Catrina AI, Ytterberg AJ, Reynisdottir G, Malmström V, Klareskog L. Lungs, joints and immunity against citrullinated proteins in rheumatoid arthritis. Nat Rev Rheumatol 2014;10:645–53.

10. Willis VC, Demoruelle MK, Derber LA, Chartier-Logan CJ, Parish MC, Pedraza IF, et al. Sputum autoantibodies in patients with established rheumatoid arthritis and subjects at risk of future clinically apparent disease. Arthritis Rheum 2013;65:2545–54.

11. Kinloch AJ, Kaiser Y, Wolfgeher D, Ai J, Eklund A, Clark MR, et al. In situ humoral immunity to vimentin in HLA-DRB1*03+ patients with pulmonary sarcoidosis. Front Immunol 2018;9:1516.

12. Hedström AK, Sundqvist E, Bäärnhielm M, Nordin N, Hillert J, Kockum I, et al. Smoking and two human leukocyte antigen genes interact to increase the risk for multiple sclerosis. Brain 2011;134:653–64.

13. O'Hanlon TP, Carrick DM, Targoff IN, Arnett FC, Reveille J, Carrington M, et al. Immunogenetic risk and protective factors for the idiopathic inflammatory myopathies: distinct HLA-A, -B, -Cw, -DRB1, and -DQA1 allelic profiles distinguish European American patients with different myositis autoantibodies. Medicine (Baltimore) 2006;85:111–27.

14. Chinoy H, Adimulam S, Marriage F, New P, Vincze M, Zilahi E, et al. Interaction of HLA-DRB1*03 and smoking for the development of anti-Jo-1 antibodies in adult idiopathic inflammatory myopathies: a European-wide case study. Ann Rheum Dis 2012;71:961–5.

15. Rothwell S, Chinoy H, Lamb JA, Miller FW, Rider LG, Wedderburn LR, et al. Focused HLA analysis in Caucasians with myositis identifies significant associations with autoantibody subgroups. Ann Rheum Dis 2019;78:996–1002.

16. Goldstein R, Duvic M, Targoff IN, Reichlin M, McMenemy AM, Reveille JD, et al. HLA–D region genes associated with autoantibody responses to histidyl–transfer RNA synthetase (Jo-1) and other translation-related factors in myositis. Arthritis Rheum 1990;33:1240–8.

17. Miller FW, Waite KA, Biswas T, Plotz PH. The role of an autoantigen, histidyl-tRNA-synthetase, in the induction and maintenance of autoimmunity. Proc Natl Acad Sci U S A 1990;87:9933–7.

18. Ascherman DP. Role of Jo-1 in the immunopathogenesis of the antisynthetase syndrome. Curr Rheumatol Rep 2015;17:56.

19. Miller FW, Twitty SA, Biswas T, Plotz PH. Origin and regulation of a disease-specific autoantibody response: antigenic epitopes, spectrotype stability, and isotype restriction of anti-Jo-1 autoantibodies. J Clin Invest 1990;85:468–75.

20. Casciola-Rosen L, Nagaraju K, Plotz P, Wang K, Levine S, Gabrielson E, et al. Enhanced autoantigen expression in regenerating muscle cells in idiopathic inflammatory myopathy. J Exp Med 2005;201:591–601.

21. Levine SM, Raben N, Xie D, Askin FB, Tuder R, Mullins M, et al. Novel conformation of histidyl–transfer RNA synthetase in the lung: the target tissue in Jo-1 autoantibody–associated myositis. Arthritis Rheum 2007;56:2729–39.

22. Ascherman DP, Oriss TB, Oddis CV, Wright TM. Critical requirement for professional APCs in eliciting T cell responses to novel fragments of histidyl-tRNA synthetase (Jo-1) in Jo-1 antibody-positive polymyositis. J Immunol 2002;169:7127–34.

23. Howard OM, Dong HF, Yang D, Raben N, Nagaraju K, Rosen A, et al. Histidyl-tRNA synthetase and asparaginyl-tRNA synthetase, autoantigens in myositis, activate chemokine receptors on T lymphocytes and immature dendritic cells. J Exp Med 2002;196:781–91.

24. Chino Y, Murata H, Goto D, Matsumoto I, Tsutsumi A, Sakamoto T, et al. T cell receptor BV gene repertoire of lymphocytes in bronchoalveolar lavage fluid of polymyositis/dermatomyositis patients with interstitial pneumonitis. Int J Mol Med 2006;17:101–9.

25. Englund P, Wahlström J, Fathi M, Rasmussen E, Grunewald J, Tornling G, et al. Restricted T cell receptor BV gene usage in the lungs and muscles of patients with idiopathic inflammatory myopathies. Arthritis Rheum 2007;56:372–83.

26. Bohan A, Peter JB. Polymyositis and dermatomyositis (first of two parts). N Engl J Med 1975;292:344–7.

27. Bohan A, Peter JB. Polymyositis and dermatomyositis (second of two parts). N Engl J Med 1975;292:403–7.

28. American Thoracic Society, European Respiratory Society. American Thoracic Society/European Respiratory Society International multidisciplinary consensus classification of the idiopathic interstitial pneumonias. Am J Respir Crit Care Med 2002;165:277–304.

29. Karimi R, Tornling G, Grunewald J, Eklund A, Skold CM. Cell recovery in bronchoalveolar lavage fluid in smokers is dependent on cumulative smoking history. PLoS One 2012;7:e34232.

30. Snir O, Bäcklund J, Boström J, Andersson I, Kihlberg J, Buckner JH, et al. Multifunctional T cell reactivity with native and glycosylated type II collagen in rheumatoid arthritis. Arthritis Rheum 2012;64:2482–8.

31. Ghosh P, Amaya M, Mellins E, Wiley DC. The structure of an intermediate in class II MHC maturation: CLIP bound to HLA-DR3. Nature 1995;378:457–62.

32. James EA, Moustakas AK, Bui J, Nouv R, Papadopoulos GK, Kwok WW. The binding of antigenic peptides to HLA-DR is influenced by interactions between pocket 6 and pocket 9. J Immunol 2009;183:3249–58.

33. Zickert A, Oke V, Parodis I, Svenungsson E, Sundström Y, Gunnarsson I. Interferon (IFN)-λ is a potential mediator in lupus nephritis. Lupus Sci Med 2016;3:e000170.

34. Klareskog L, Stolt P, Lundberg K, Källberg H, Bengtsson C, Grunewald J, et al, and the Epidemiological Investigation of Rheumatoid Arthritis Study Group. A new model for an etiology of rheumatoid arthritis: smoking may trigger HLA–DR (shared epitope)–restricted immune reactions to autoantigens modified by citrullination. Arthritis Rheum 2006;54:38–46.

35. Hodge S, Hodge G, Nairn J, Holmes M, Reynolds PN. Increased airway granzyme B and perforin in current and ex-smoking COPD subjects. COPD 2006;3:179–87.

36. Casciola-Rosen L, Andrade F, Ulanet D, Wong WB, Rosen A. Cleavage by granzyme B is strongly predictive of autoantigen status: implications for initiation of autoimmunity. J Exp Med 1999;190:815–26.

37. Shimizu S, Yoshinouchi T, Niimi T, Ohtsuki Y, Fujita J, Maeda H, et al. Differing distributions of CXCR37- and CCR37-positive cells among types of interstitial pneumonia associated with collagen vascular diseases. Virchows Arch 2007;450:51–8.

38. Ramstein J, Broos CE, Simpson LJ, Ansel KM, Sun SA, Ho ME, et al. IFN-γ-producing T-helper 17.1 cells are increased in sarcoidosis and are more prevalent than T-helper type 1 cells. Am J Respir Crit Care Med 2016;193:1281–91.

39. Acosta-Rodriguez EV, Rivino L, Geginat J, Jarrossay D, Gattorno M, Lanzavecchia A, et al. Surface phenotype and antigenic specificity of human interleukin 17-producing T helper memory cells. Nat Immunol 2007;8:639–46.

40. Sallusto F, Lanzavecchia A, Mackay CR. Chemokines and chemokine receptors in T-cell priming and Th1/Th2-mediated responses. Immunol Today 1998;19:568–74.

41. Campbell JJ, Brightling CE, Symon FA, Qin S, Murphy KE, Hodge M, et al. Expression of chemokine receptors by lung T cells from normal and asthmatic subjects. J Immunol 2001;166:2842–8.

42. Thomas SY, Banerji A, Medoff BD, Lilly CM, Luster AD. Multiple chemokine receptors, including CCR42 and CXCR42, regulate antigen-induced T cell homing to the human asthmatic airway. J Immunol 2007;179:1901–12.

43. Forsslund H, Yang M, Mikko M, Karimi R, Nyrén S, Engvall B, et al. Gender differences in the T-cell profiles of the airways in COPD patients associated with clinical phenotypes. Int J Chron Obstruct Pulmon Dis 2016;12:35–48.

44. Kaiser Y, Lakshmikanth T, Chen Y, Mikes J, Eklund A, Brodin P, et al. Mass cytometry identifies distinct lung CD4$^+$ T cell patterns in Löfgren's syndrome and non-Löfgren's syndrome sarcoidosis. Front Immunol 2017;8:1130.

45. Brozyna S, Ahern J, Hodge G, Nairn J, Holmes M, Reynolds PN, et al. Chemotactic mediators of Th1 T-cell trafficking in smokers and COPD patients. COPD 2009;6:4–16.

46. Broos CE, Koth LL, van Nimwegen M, In 't Veen JC, Paulissen SM, van Hamburg JP, et al. Increased T-helper 17.1 cells in sarcoidosis mediastinal lymph nodes. Eur Respir J 2018;51:1701124.

47. Kaiser Y, Eklund A, Grunewald J. Moving target: shifting the focus to pulmonary sarcoidosis as an autoimmune spectrum disorder. Eur Respir J 2019;54:1802153.

48. Annunziato F, Cosmi L, Santarlasci V, Maggi L, Liotta F, Mazzinghi B, et al. Phenotypic and functional features of human Th17 cells. J Exp Med 2007;204:1849–61.

49. Nistala K, Adams S, Cambrook H, Ursu S, Olivito B, de Jager W, et al. Th17 plasticity in human autoimmune arthritis is driven by the inflammatory environment. Proc Natl Acad Sci U S A 2010;107:14751–6.

AMERICAN COLLEGE
of RHEUMATOLOGY
Empowering Rheumatology Professionals

CONCISE COMMUNICATION

Myositis autoantibodies: a comparison of results from the Oklahoma Medical Research Foundation Myositis Panel to the Euroimmun Research Line Blot

The ability to accurately assay a broad range of well-defined autoantibody specificities in myositis patients is imperative for clinical phenotyping and patient care. In myositis research, the systematic serotyping of patient cohorts is often performed using various research assays, and understanding the relationship between research testing and clinical testing is paramount to advancing the field of myositis. An increasingly popular research multiplex antibody assay platform was developed by Euroimmun (Euroline Autoimmune Inflammatory Myopathies 16 Ag IgG) for myositis-specific and associated autoantibodies. Prior research has suggested that the interrater reliability of Euroline compared to in-house immunoprecipitation methods (considered the gold standard) is reasonable, with the possible exception of transcription intermediary factor 1γ (TIF1γ) (1–4). In this communication, we share our experience comparing serologic results obtained for clinical purposes with a commercial myositis autoantibody panel (the traditional Oklahoma Medical Research Foundation [OMRF] myositis panel) and serologies obtained for research purposes using the Euroline myositis panel.

The OMRF myositis autoantibody panel utilizes several different assays to detect antibodies. These include immunodiffusion, indirect immunofluorescence (for antinuclear antibodies), immunoprecipitation of ^{35}S-methionine–labeled proteins from cell extracts, and RNA immunoprecipitation. The assay is performed at the Clinical Immunology Laboratory in Oklahoma City. It tests for autoantibodies recognizing Jo-1, Mi-2, signal recognition particle (SRP), PM/Scl, PL-7, PL-12, Ku, EJ, and OJ. Results are provided as negative, positive, or weak positive/indeterminate. Weak positive and indeterminate results were excluded from this analysis (10 values). The Euroline Autoimmune Inflammatory Myopathies 16 Ag IgG platform tests for Mi-2α, Mi-2β, PM/Scl-75, PM/Scl-100, Ku, Jo-1, SRP, PL-7, PL-12, EJ, OJ, TIF1γ, melanoma differentiation–associated protein 5 (MDA-5), NXP-2, anti–small ubiquitin-like modifier activating enzyme (SAE), and Ro52. Based on the Euroimmun package insert, different thresholds of 8–14, ≥15 or +, ≥36 or ++, and ≥71 or +++ correspond with borderline, low positive, moderately positive, and strongly positive results, respectively. Borderline Euroline results were considered negative for this analysis. Intraassay reproducibility was previously established by Euroimmun and at our own laboratory

with excellent agreement. Sensitivity and specificity were subsequently calculated for the OMRF and Euroline platforms, along with the mean ± SD of Cohen's kappa statistic in order to measure interrater agreement (using Stata version 14).

We performed Euroline testing on serum samples from all patients in the Johns Hopkins Myositis Cohort who provided written informed consent. This group of patients (with dermatomyositis, polymyositis, or immune-mediated necrotizing myopathy; n = 281) was subsequently analyzed using clinical OMRF myositis autoantibody testing performed on a serum sample obtained on the same day as that used for Euroline testing. The importance of matching the date on which samples are obtained has become increasingly recognized, with studies showing a change in autoantibody titers over time (5–7). At the time of antibody testing, the mean ± SD age of the patients was 52 ± 14 years, and the majority of patients were female (71%). The racial composition of the cohort was 72% white, 13% African American, 4% Asian, and 11% unknown. The mean ± SD disease duration from symptom onset to antibody testing was 3.9 ± 5.1 years, and most patients were treated with immunosuppressants at the time of antibody testing.

A total of 154 patients (55% of samples tested) had at least 1 antibody specificity by Euroline using the standard positivity cutoff of ≥15. Of note, this low prevalence of seropositive patients is likely explained by the fact that several other prominent myositis antibody specificities, such as hydroxymethylglutaryl-coenzyme A reductase, TIF1γ, SAE, NXP-2, and MDA-5, were not included in this study (see below). Using the cutoff of ≥15 on Euroline, 15 patients had more than 1 autoantibody (excluding copositivity for Mi-2α and Mi-2β, or for PM/Scl-75 and PM/Scl-100). The number of patients tested, the number of positive results by each assay, and the corresponding sensitivities, specificities, and kappa statistics are presented in Table 1. The interassay agreement using different cutoffs for the Euroline assay was calculated using kappa statistics and was found to be highest overall for the moderate positivity cutoff (mean ± SD 0.73 ± 0.18, 0.78 ± 0.13, and 0.71 ± 0.27 for thresholds of ≥15/+, ≥36/++, and ≥71/+++, respectively). The lowest threshold for positivity (≥15/+) resulted in the best kappa statistic for anti–Jo-1, anti–Mi-2α, anti–Mi-2β, anti–PM/Scl-100, and anti-Ku autoantibodies. The moderate positivity threshold (≥36/++) resulted in the best kappa statistic for anti-SRP, anti-EJ, and anti–PL-12. The highest cutoff (≥71/+++) had the best kappa statistic for anti–PM/Scl-75 and anti–PL-7.

To better understand discordant results (patients who were positive by the Euroline assay but negative using the OMRF

Table 1. Results obtained with the Euroline antibody assay in comparison to the OMRF assay*

Autoantibody (no. patients tested/no. OMRF positive)	Cutoff ≥15/+				Cutoff ≥36/++				Cutoff ≥71/+++			
	No. Euroline positive	Sensitivity	Specificity	κ	No. Euroline positive	Sensitivity	Specificity	κ	No. Euroline positive	Sensitivity	Specificity	κ
Jo-1 (281/29)	31	96.6	98.6	0.93	27	89.7	99.6	0.92	24	79.3	99.6	0.85
Mi-2 (280/20)												
Mi-2α (280)	20	94.7	99.6	0.94	11	55.0	100.0	0.69	2	10.5	100.0	0.18
Mi-2β (280)	30	85.0	95.0	0.65	18	60.0	97.7	0.60	8	40.0	100.0	0.55
Mi-2α or Mi-2β (280)	33	100.0	94.9	0.73	22	80.0	97.6	0.74	8	40.0	100.0	0.55
Mi-2α and Mi-2β (280)	17	80.0	99.6	0.85	7	35.0	100.0	0.50	2	10.0	100.0	0.17
SRP (280/18)	27	94.4	96.2	0.74	20	94.4	98.6	0.89	13	70.6	99.6	0.79
PM/Scl (279/12)												
PM-75 (279)	26	83.3	94.0	0.50	13	75.0	98.5	0.71	7	58.3	100.0	0.73
PM-100 (279)	15	83.3	98.1	0.73	10	66.7	99.2	0.72	4	25.0	99.6	0.36
PM-75 or PM-100 (279)	33	100.0	92.1	0.50	16	83.3	97.7	0.70	8	58.3	99.6	0.69
PM-75 and PM-100 (279)	8	66.7	100.0	0.79	7	58.3	100.0	0.73	3	25.0	100.0	0.39
PL-7 (280/5)	15	100.0	96.4	0.49	9	100.0	98.5	0.71	5	100.0	100.0	1.00
PL-12 (281/3)	7	100.0	98.6	0.59	4	100.0	99.6	0.86	4	100.0	99.6	0.86
Ku (279/3)	5	100.0	99.3	0.75	5	100.0	99.3	0.75	5	100.0	99.3	0.75
EJ (281/2)	3	100.0	99.6	0.80	2	100.0	100.0	1.00	2	100.0	100.0	1.00
OJ (281/0)	2	NA	NA	NA	0	NA	NA	NA	0	NA	NA	NA

* All Oklahoma Medical Research Foundation (OMRF)–positive patients were also Euroline positive (≥15). SRP = signal recognition particle; NA = not applicable.

assay), the clinical phenotype of 19 patients who had antisynthetase antibodies is shown in Table 2. Among these 19 Euroline-positive patients, only 5 (26%) had a clinical picture consistent with the antisynthetase syndrome, and those who did were often positive for other antibody specificities. Interestingly, many of these patients had amyopathic dermatomyositis.

Our findings will enable researchers to correctly interpret serologies acquired by research testing using the Euroline platform. Our study highlights the importance of carefully defined cutoffs for assigning positive antibody status. That is, different autoantibody specificities may require different thresholds to define a positive result. The sensitivity of the Euroline assay readout appears to depend on the defined cutoff value. It is also possible that the increased sensitivity may come from measuring different epitopes that are not tested for by OMRF. However, data in Table 2 suggest that this increased sensitivity does not translate to clinically meaningful results. One important distinction between the OMRF and Euroline assays is that Euroline reports antibody specificity to individual subunits for Mi-2 (α/β) and PM/Scl (75/100), while the

OMRF assay does not. The OMRF utilizes immunoprecipitation of ^{35}S-methionine–labeled lysate proteins for both anti–Mi-2 and anti-PM/Scl. Analysis of these immunoprecipitates by fluorography shows a series of multiple, distinctive protein bands that are readily recognizable to an experienced investigator. The presence of multiple bands with these autoantibodies (since both antigens are multiprotein complexes) allows definitive identification of the autoantibody (Targoff I: personal communication).

A limitation of these data is the inability to assess some of the more common myositis autoantibodies that were not consistently ordered at our center as part of the comprehensive OMRF panel (anti-TIF1γ, anti–NXP-2, and anti–MDA-5). Furthermore, this study included too few patients with some autoantibodies (e.g., anti–PL-7, anti–PL-12, anti-EJ, and anti-OJ) to make any robust conclusions about the performance of the assays. Based on these results, we conclude that the same threshold may not be appropriate for determining a positive antibody result for all specificities tested using the Euroline panel and that sensitivity analyses should be conducted with different titer cutoffs.

Table 2. Clinical features of patients positive by Euroline testing (at a cutoff of ≥15) but negative by OMRF testing*

Autoantibody (no. patients Euroline positive but OMRF negative)	Inflammation on muscle biopsy	Fever (>100.4°F)	ILD	Mechanic's hands	RP	Inflammatory arthritis	Additional antibody specificities observed by Euroline testing (no. patients)
PL-7 (10)	5 (50)	1 (10)	3 (30)	3 (30)	6 (60)	2 (20)	Jo-1 (3), PL-12 (1), Ku (1)
PL-12 (4)	2 (50)	0 (0)	2 (50)	1 (25)	2 (50)	2 (50)	Jo-1 (2), PL-7 (1)
OJ (2)	0	0	0	0	0	0	SRP (1)
Jo-1 (2)	0	0	0	0	0	0	SRP (1), Ku (1)
EJ (1)	1 (100)	0	0	0	0	1 (100)	SRP (1)

* Values are the number (%) of patients. OMRF = Oklahoma Medical Research Foundation; ILD = interstitial lung disease; RP = Raynaud's phenomenon; SRP = signal recognition particle.

ACKNOWLEDGMENT

We thank Dr. Ira Targoff for his assistance in describing OMRF laboratory methodology.

Christopher A. Mecoli, MD, MHS [iD]
Jemima Albayda, MD [iD]
Eleni Tiniakou, MD
Julie J. Paik, MD, MHS
Umar Zahid, MBBS
Sonye K. Danoff, MD, PhD
Livia Casciola-Rosen, PhD [iD]
Johns Hopkins University School of Medicine
Baltimore, MD
Maria Casal-Dominguez, MD, PhD
Katherine Pak, MD
Iago Pinal-Fernandez, MD, PhD
Andrew L. Mammen, MD, PhD
National Institute of Arthritis and Musculoskeletal and Skin
  Diseases, NIH
Bethesda, MD
  and Johns Hopkins University School of Medicine
  Baltimore, MD

Lisa Christopher-Stine, MD, MPH [iD]
Johns Hopkins University School of Medicine
Baltimore, MD

1. Rönnelid J, Barbasso Helmers S, Storfors H, Grip K, Rönnblom L, Franck-Larsson K, et al. Use of a commercial line blot assay as a screening test for autoantibodies in inflammatory myopathies. Autoimmun Rev 2009;9:58–61.

2. Ghirardello A, Rampudda M, Ekholm L, Bassi N, Tarricone E, Zampieri S, et al. Diagnostic performance and validation of autoantibody testing in myositis by a commercial line blot assay. Rheumatology (Oxford) 2010;49:2370–4.

3. Cavazzana I, Fredi M, Ceribelli A, Mordenti C, Ferrari F, Carabellese N, et al. Testing for myositis specific autoantibodies: comparison between line blot and immunoprecipitation assays in 57 myositis sera. J Immunol Methods 2016;433:1–5.

4. Espinosa-Ortega F, Holmqvist M, Alexanderson H, Storfors H, Mimori T, Lundberg IE, et al. Comparison of autoantibody specificities tested by a line blot assay and immunoprecipitation-based algorithm in patients with idiopathic inflammatory myopathies [letter]. Ann Rheum Dis 2019;78:858–60.

5. Matsushita T, Mizumaki K, Kano M, Yagi N, Tennichi M, Takeuchi A, et al. Antimelanoma differentiation-associated protein 5 antibody level is a novel tool for monitoring disease activity in rapidly progressive interstitial lung disease with dermatomyositis. Br J Dermatol 2017;176:395–402.

6. Abe Y, Matsushita M, Tada K, Yamaji K, Takasaki Y, Tamura N. Clinical characteristics and change in the antibody titres of patients with anti-MDA5 antibody-positive inflammatory myositis. Rheumatology (Oxford) 2017;56:1492–7.

7. Aggarwal R, Oddis CV, Goudeau D, Koontz D, Qi Z, Reed A, et al. Autoantibody levels in myositis patients correlate with clinical response during B cell depletion with rituximab. Rheumatology (Oxford) 2016;55:991–9.

AMERICAN COLLEGE
of RHEUMATOLOGY
Empowering Rheumatology Professionals

LETTERS

Circulating interferon-α measured with a highly sensitive assay as a biomarker for juvenile inflammatory myositis activity: comment on the article by Mathian et al

To the Editor:

We read with interest the report by Dr. Mathian and colleagues in which they suggested that direct serum interferon-α (IFNα) determination with a highly sensitive assay might be useful for disease activity monitoring in systemic lupus erythematosus (SLE) (1). More generally, the identification of reactive biomarkers is highly desirable in many disease states, including idiopathic inflammatory myopathies (IIMs). Various monitoring tools are currently available for the evaluation of IIM, including clinical assessment, determination of myositis-specific autoantibodies, histopathologic investigation of muscle and skin, and laboratory testing of blood. However, few studies have made use of validated indices (2). Despite the longstanding implication of type I IFNs in the pathology of IIMs (2,3), few data are available relating to the use of type I IFN as a tool in the stratification of IIM patients or the prediction of disease evolution. Herein, we show for the first time that IFNα protein measurements obtained by digital enzyme-linked immunosorbent assay (ELISA) are correlated with disease activity not only in SLE, but also in juvenile dermatomyositis (DM) and juvenile overlap myositis (OM).

At our National Reference Center for Rare Rheumatic and Systemic Autoimmune Diseases in Children (RAISE), serum IFNα was longitudinally measured in 64 children, 46 with juvenile DM (72%) and 18 with juvenile OM (28%). The median follow-up duration was 18.6 months (range 10.9–32.0), and 206 serum samples (1–24 samples per patient) were collected. Serum was also collected from healthy controls. Clinically inactive disease was defined according to the modified Paediatric Rheumatology International
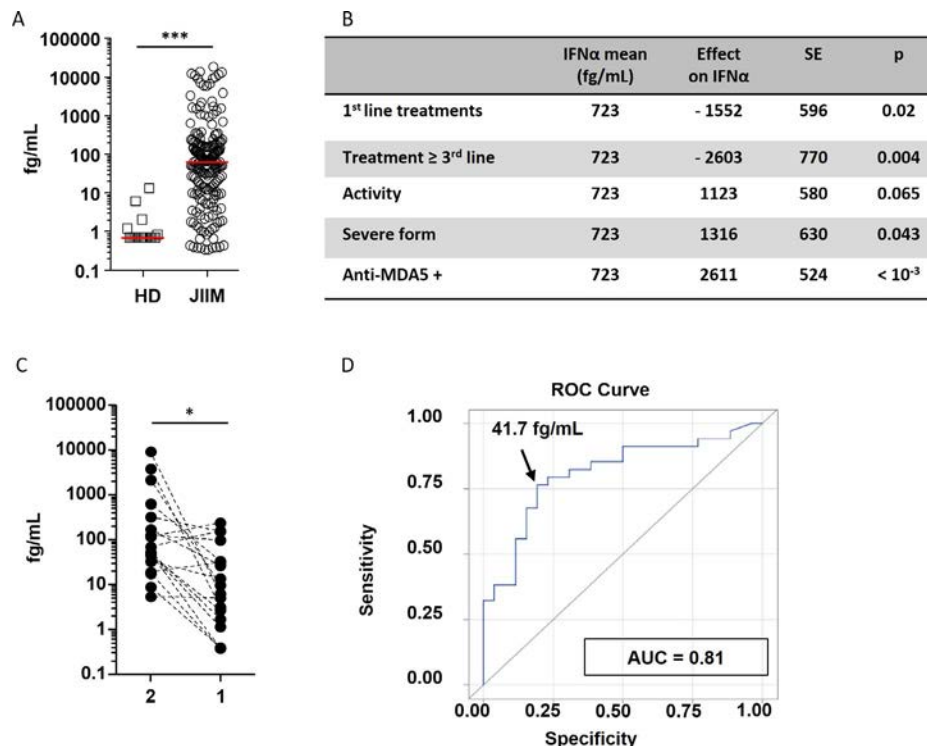
Figure 1. Serum interferon-α (IFNα) concentrations according to disease activity in patients with juvenile idiopathic inflammatory myopathies (JIIMs; IIMs). **A**, Serum IFNα concentrations in patients with juvenile IIM versus healthy donors (HDs). Symbols represent individual samples; horizontal lines show the median. *** = $P < 0.0001$. **B**, Multivariate analysis results of the effects of receiving a first treatment, receiving ≥3 types of treatment, disease activity, disease severity, and anti–melanoma differentiation–associated protein 5 (anti–MDA-5) positivity on IFNα concentrations. Effect on IFNα is the mean estimated difference of IFNα levels in patients with a given characteristic compared to other patients (evaluated by mixed models). **C**, IFNα concentrations (in femtograms [fg]/ml) among 18 juvenile IIM patients who were tested both during inactive disease (group 1) and during active disease (group 2). * = $P < 0.0077$. **D**, Receiver operating characteristic (ROC) curve of IFNα concentration as a discriminator for active juvenile IIM versus inactive juvenile IIM. AUC = area under the curve.

Trials Organisation criteria (4) as well as inactive skin disease at the time blood was drawn (4). Patients were divided into 2 subpopulations, with group 1 consisting of patients with inactive disease and group 2 consisting of patients with active disease. Severe disease course was defined as the need for >2 types of treatment (treatment beyond steroids, disease-modifying antirheumatic drugs, and intravenous immunoglobulin), and/or a requirement for intensive care, and/or death. Clinical characteristics of the patients analyzed in our study are provided in Supplementary Tables 1 and 2, available on the *Arthritis & Rheumatology* web site at http://onlinelibrary.wiley.com/doi/10.1002/art.41096/abstract.

Patient groups were compared using Fisher's exact test and Mann-Whitney U test for categorical and continuous variables, respectively. The diagnostic performance of the Simoa assay (Quanterix) predicting juvenile IIM disease activity was determined by analysis of receiver operating characteristic (ROC) curves, with active disease as the gold standard. Optimal thresholds were determined using a compromise among the maximum correct classification rate, the minimum distance to the upper left corner of the ROC curve, the minimum difference between sensitivity and specificity, and the Youden index. All analyses were performed with SAS software, version 9.4. Serum IFNα concentrations were determined with an ultrasensitive Simoa digital ELISA utilizing high-affinity autoantibodies (isolated from autoimmune polyendocrinopathy–candidiasis–ectodermal dystrophy patients) that recognize all human IFNα subtypes (5). Ethical approval for this study was obtained from a French research ethics committee (Comite de Protection Des Personnes Ile-de-France IX no. 12-009; ID-RCB/EudraCT database no. 2014-A01017-40).

The level of circulating IFNα was significantly higher in juvenile IIM patients than controls (Figure 1A). Taking into account all samples (n = 206) and using bivariate mixed models, IFNα concentrations (median 66 femtogram [fg]/ml [range 15–173]) were significantly higher in group 2 versus group 1 in the overall cohort (median 77.66 fg/ml [range 0.34–17809.31]; $P < 0.0001$) as well as in the juvenile DM subgroup (median 71.55 fg/ml [range 0.34–9100.7]; $P < 0.0001$) and the juvenile OM subgroup (median 1,701.5 fg/ml ([range 0.38–17809.31]; $P = 0.0088$). In multivariate analysis, IFNα concentrations were significantly correlated with disease severity and inversely correlated with treatment (Figure 1B). Additionally, there was a trend toward a correlation with disease activity. In patients with available Simoa measurements from consecutive time points spanning an active to inactive status, low concentrations of IFNα (<10 fg/ml) were found in 2 patients (11%) during active disease, versus 10 patients (56%) during inactive disease (median concentrations 61 fg/ml versus 8 fg/ml; $P = 0.0077$) (Figure 1C). The area under the ROC curve for IFNα concentration as a discriminator of active versus inactive juvenile IIM was 0.81 (95% confidence interval 0.70–0.92) (Figure 1D). This value is close to the value of 0.83 previously described in

SLE patients by Mathian et al (1). To distinguish active versus inactive juvenile IIM, the optimal cutoff threshold for IFNα concentration was 41.7 fg/ml, with a sensitivity and specificity of 76% and 81%, respectively (Youden index 0.57).

In conclusion, IFNα dosage measured with Simoa may have clinical utility in non-monogenic interferonopathies other than SLE and address a currently unmet need in patient stratification. A future challenge to clinical implementation would be assay standardization across medical centers. Most importantly, the specificity of the antibody pairs used in the assay for each IFNα subtype would likely have an impact on clinical practice. Comparison of various assays on larger cohorts of patients with IFN-related diseases is needed so that a common assay can be selected to be used in routine clinical practice across laboratories.

Isabelle Melki, MD, PhD [iD]
Imagine Institute, RAISE
 Robert Debré & Necker Hospital (AP-HP)
Paris, France
Hervé Devilliers, MD, PhD
Centre Hospitalier Universitaire de Dijon
 CIC, INSERM 1432
Dijon, France
Cyril Gitiaux, MD, PhD
Reference Centre for Neuromuscular Diseases
 Necker Hospital (AP-HP 5)
Paris, France
Vincent Bondet, PhD
Institut Pasteur, INSERM U1223
Paris, France
Alexandre Belot, MD, PhD
Hôpital Femme Mère-Enfant
 RAISE, FAI2R, INSERM U1111
Lyon, France
Christine Bodemer, MD, PhD
MAGEC, Necker Hospital (AP-HP 5)
 Imagine Institute, Paris University
Paris, France
Pierre Quartier, MD
Imagine Institute, Paris University
 RAISE, Necker Hospital (AP-HP 5)
Paris, France
Yanick J. Crow, MD, PhD
Imagine Institute
Paris, France
 and IGMM, University of Edinburgh
 Edinburgh, UK
Darragh Duffy, PhD
Institut Pasteur, INSERM U1223
Mathieu P. Rodero, PhD [iD]
Imagine Institute, Université Paris Descartes
 CBMIT, CNRS, UMR8601
Paris, France
Brigitte Bader Meunier, MD
Imagine Institute, Paris University
 RAISE, Necker Hospital (AP-HP 5)

1. Mathian A, Mouries-Martin S, Dorgham K, Devilliers H, Barnabei L, Ben Salah E, et al. Monitoring disease activity in systemic lupus erythematosus with single-molecule array digital enzyme-linked immunosorbent assay quantification of serum interferon-α. Arthritis Rheumatol 2019;71:756–65.

2. Wienke J, Deakin CT, Wedderburn LR, van Wijk F, van Royen-Kerkhof A. Systemic and tissue inflammation in juvenile dermatomyositis: from pathogenesis to the quest for monitoring tools. Front Immunol 2018;9:2951.

3. Gitiaux C, Latroche C, Weiss-Gayet M, Rodero MP, Duffy D, Bader-Meunier B, et al. Myogenic progenitor cells exhibit type I interferon–driven proangiogenic properties and molecular signature during juvenile dermatomyositis. Arthritis Rheumatol 2018;70:134–45.

4. Lazarevic D, Pistorio A, Palmisani E, Miettunen P, Ravelli A, Pilkington C, et al. The PRINTO criteria for clinically inactive disease in juvenile dermatomyositis. Ann Rheum Dis 2013;72:686–93.

5. Rodero MP, Decalf J, Bondet V, Hunt D, Rice GI, Werneke S, et al. Detection of interferon α protein reveals differential levels and cellular sources in disease. J Exp Med 2017;214:1547–55.

Reply

To the Editor:

We thank Dr. Melki and colleagues for their interest in our work on IFNα assessment in SLE. In their correspondence, they show that IFNα protein measurement by digital ELISA is also correlated with disease activity in other IFN-dependent autoimmune diseases, and in this case, juvenile IIMs.

Since IFNs (especially IFNα) are involved in the pathogenesis of several autoimmune diseases such as SLE, myositis, Sjögren's syndrome, and systemic sclerosis (Muskardin TL, Niewold TB. Type I interferon in rheumatic diseases. Nat Rev Rheumatol 2018;14:214–28), monitoring their presence in the circulation of patients might help physicians to better evaluate disease activity and/or predict future flares. However, until recently, clinicians lacked a robust and standardized method for the measurement of IFNs in serum because IFN concentrations are usually very low and often not detectable with the use of classic immunoassays. Tools for indirect measurement of IFNα activity through an IFN gene expression score have a very low availability. These scores are not only notoriously difficult to standardize but are also less sensitive to change than direct measurement of IFNα. The advent of the ultrasensitive Simoa digital ELISA technology now makes it possible to reliably measure very low concentrations of IFNα (Rodero MP, Decalf J, Bondet V, Hunt D, Rice GI, Werneke S, et al. Detection of interferon α protein reveals differential levels and cellular sources in disease. J Exp Med 2017;214:1547–55). The studies by Melki et al and ourselves show that direct measurement of IFNα might improve monitoring of clinical activity in myositis and SLE, respectively.

Of note, the area under the ROC curve value of 0.81 for IFNα concentration as a discriminator between active versus inactive juvenile IIM determined by Melki and colleagues is similar to the value of 0.83 that we had previously reported in SLE. In Melki and colleagues' study, the optimal cutoff threshold of IFNα concentration permitting the ability to distinguish active from inactive juvenile IIM was 42 fg/ml, which is not only substantially lower than the value observed in our study (266 fg/ml) as being optimal to distinguish active from inactive SLE, but also lower than the value (136 fg/ml) calculated as the threshold below which IFNα values are within the range of those in healthy controls. The discrepancy between the 2 studies might be explained by the different types of antibodies used in the digital IFNα ELISAs, the different types of disease studied, as well as by age and demographic differences between the patient populations. It is therefore clear that the implementation of the digital IFNα ELISA to meet clinical grade standards still requires further investigation. Moreover, the determination of the specific roles of type I IFNs versus type II and type III IFNs in the pathogenesis of various autoimmune diseases will be facilitated by the use of this highly sensitive digital ELISA technology that enables the measurement of cytokines at physiologic concentrations.

The prognostic value of elevated levels of IFNs in the prediction of a disease flare also remains to be studied. It is therefore important that this technology be developed for the measurement of other types of IFNs, particularly the IFNβ and IFNλ subtypes. In conclusion, the translation of digital ELISA technology into the clinical laboratory setting will enhance the potential for routine measurement of IFNα in the monitoring of several "nonmonogenic" interferonopathies.

Alexis Mathian, MD, PhD
Suzanne Mouries-Martin, MD, MSc
Karim Dorgham, PhD
Hans Yssel, PhD
Zahir Amoura, MD, MSc
Sorbonne Université, AP-HP
  Hôpital Pitié–Salpêtrière
  French National Referral Center for Systemic
  Lupus Erythematosus, Antiphospholipid Antibody
  Syndrome and Other Autoimmune Disorders
  Service de Médecine Interne 2, Institut E3M
  INSERM UMRS, CIMI-Paris
Paris, France

Is a small meniscal radial tear equivalent to a radial posterior root tear in destabilizing the meniscus? Comment on the article by Driban et al

To the Editor:

We read with interest the article by Driban and colleagues (1), in which they described characteristic magnetic resonance imaging findings characteristic in subjects exhibiting accelerated

onset of knee osteoarthritis (KOA), defined as a Kellgren/Lawrence grade of <2 at baseline progressing to grade 3 or 4 within 48 months. Driban et al reported that accelerated KOA is characterized by destabilizing meniscal tears (root tears, radial tears, or complex tears), which almost always include a radial component and miscellaneous pathologic changes (attrition, acute ligamentous or tendinous injuries, subchondral insufficiency fractures, and other incidental findings). They also found that at the index visit, destabilizing meniscal tears or miscellaneous pathologic changes were 3 times more common in adults with accelerated KOA (49%) than in adults with typical KOA (15%) or those with no KOA (6%). The topic itself is of high clinical and research relevance, as meniscal tears are important features in the onset and progression of KOA. We would like to comment, however, on the potential relevance of different tear morphologies.

The definition of destabilizing meniscal tear used by Driban et al seems somewhat arbitrary and challenging to follow. It is known that root tears markedly compromise joint biomechanics, resulting in a 25% increase in peak contact pressure in the medial compartment compared with that found in the intact state (2)—a loading profile similar to that of the total meniscectomized knee—and that root tears are associated with incident and progressive medial tibiofemoral cartilage loss in OA (3). Yet the evidence for other tear types and their effect on joint mechanics has not been thoroughly investigated. For example, it seems unclear why a small radial tear of the meniscal body should be considered destabilizing. Indeed, from multiple large epidemiologic studies, we have learned that partial or complete meniscal maceration (i.e., substance loss) is highly relevant to disease onset and progression, despite not being destabilizing per se (4,5). The relevance of other tear types to accelerated KOA is less clear. Moreover, Englund et al found that meniscal tears are commonly present in the general population, including radial tears with or without pain (6), which indicates the relatively benign nature of such radial tears.

Furthermore, Driban and colleagues analyzed miscellaneous pathologic changes, which included attrition, acute ligamentous or tendinous injuries, subchondral insufficiency fractures, and other incidental findings. Summarizing all these pathologic entities under one category seems problematic, given their varying clinical significance and uncertain contribution to accelerated KOA. For example, attrition (i.e., flattening or remodeling of the articular surface) is commonly found in knee OA, including in the early stages of the disease process (7,8). While it seems reasonable to assume that a complete ligament tear such as a cruciate or collateral ligament disruption may increase risk of accelerated KOA due to instability of the knee joint, this seems unlikely for minor ligamentous sprains. The logic of including other incidental findings remains somewhat elusive, as there is no detailed explanation regarding the specific pathologic entities included in this subcategory.

Daichi Hayashi, MD, PhD [iD]
Stony Brook Medicine
State University of New York
Stony Brook, NY
  and Boston University School of Medicine
  Boston, MA
Ali Guermazi, MD, PhD
Boston University School of Medicine
Boston, MA
  and VA Boston Healthcare System
  West Roxbury, MA

1. Driban JB, Davis JE, Lu B, Price LL, Ward RJ, MacKay JW, et al. Accelerated knee osteoarthritis is characterized by destabilizing meniscal tears and preradiographic structural disease burden. Arthritis Rheumatol 2019;71:1089–100.
2. Allaire R, Muriuki M, Gilbertson L, Harner CD. Biomechanical consequences of a tear of the posterior root of the medial meniscus: similar to total meniscectomy. J Bone Joint Surg Am 2008;90:1922–31.
3. Guermazi A, Hayashi D, Jarraya M, Roemer FW, Zhang Y, Niu J, et al. Medial posterior meniscal root tears are associated with development or worsening of medial tibiofemoral cartilage damage. Radiology 2013;268:814–21.
4. Jarraya M, Roemer FW, Englund M, Crema MD, Gale HI, Hayashi D, et al. Meniscus morphology: does tear type matter? Semin Arthritis Rheum 2017;46:552–61.
5. Antony B, Driban JB, Price LL, Lo GH, Ward RJ, Nevitt M, et al. The relationship between meniscal pathology and osteoarthritis depends on the type of meniscal damage visible on magnetic resonance images: data from the Osteoarthritis Initiative. Osteoarthritis Cartilage 2017;25:76–84.
6. Englund M, Guermazi A, Gale D, Hunter DJ, Aliabadi P, Clancy M, et al. Incidental meniscal findings on knee MRI in middle-aged and elderly persons. N Engl J Med 2008;359:1108–15.
7. Hernandez-Molina G, Neogi T, Hunter DJ, Niu J, Guermazi A, Reichenbach S, et al. The association of bone attrition with knee pain and other MRI features of osteoarthritis. Ann Rheum Dis 2008;67:43–37.
8. Reichenbach S, Guermazi A, Niu J, Neogi T, Hunter DJ, Roemer FW, et al. Prevalence of bone attrition on knee radiographs and MRI in a community-based cohort. Osteoarthritis Cartilage 2008;16:1005–10.

Reply

To the Editor:

We thank Drs. Hayashi and Guermazi for their valuable insight, and we appreciate the opportunity to further elaborate on our definitions of destabilizing meniscal tears and miscellaneous pathologic changes.

We defined destabilizing meniscal tear as a root tear, radial tear, or complex tear, which almost always features a radial component. As Drs. Hayashi and Guermazi noted, root tears

compromise joint biomechanics and are associated with incident and progressive tibiofemoral cartilage loss. Furthermore, a large radial tear compromises the circumferential collagen bundles of a meniscus, which enables it to resist hoop stresses experienced with normal weight bearing (1,2). This results in radial tears of the medial or lateral meniscus leading to a decrease in contact area and an increase in contact pressures, similar to a root tear (1,3,4). For this reason, radial tears are risk factors for OA (5). Given this rationale, we grouped root tears with radial tears and complex tears, which typically included a radial component, as destabilizing meniscal tears.

While 80% of the destabilizing tears analyzed in our study were in the posterior horn, there is less known about how size and location of a radial tear may influence outcomes. A partial radial tear, defined as comprising 50% of the meniscal width in the anterior half of a medial meniscus, impedes the function of a meniscus with reduced strain in the anterior horn but increased strain in the posterior horn when loaded to 3 times the body weight of the donor knee (6). Furthermore, a radial tear that affects at least 33% of the width of a meniscus was associated with incident KOA over the subsequent 2 years (5). However, if smaller radial tears are insignificant, then this would have led us to underestimate the true association between destabilizing tears and accelerated KOA.

We respectfully disagree that just because something is common in the general population, it must be benign. Based on similar logic, we would also assume that obesity is benign, given its high prevalence of 40%, affecting 93 million US adults. On the contrary, however, obesity is viewed by the Centers for Disease Control and Prevention and the National Institutes of Health as a serious concern, given its association with death and lower quality of life. Although Englund et al (7) found that meniscal tears are common, they also found that among those without radiographic evidence of OA, meniscal tears were more common in those with knee pain (32% versus 23%) for an adjusted prevalence ratio of 1.43 (1.08–1.90). Additionally, in a follow-up study using a different cohort, Englund et al found that patients with meniscal tears who did not have surgery were at 5.7 times increased risk of developing incident KOA over a 30-month follow-up period, supporting the critical nature of meniscal tears in OA pathology (7).

We defined miscellaneous pathologic changes as attrition, acute ligamentous or tendinous injuries, subchondral insufficiency fractures, and other incidental findings to ensure there was sufficient statistical power for analyses (Table 1). We also provided information regarding the frequency of attrition and the other findings separately by group and time in Table 2 in our article to help clarify the frequency of these findings and to highlight that statistical analyses were impossible because only 1 or 2 adults with typical or no KOA had these results. These findings highlight the fact that while other pathologies occur among people with accelerated KOA, they do not represent a large proportion of the group,

Table 1. Detailed breakdown of miscellaneous pathologic features observed in adults with accelerated KOA, typical KOA, or no KOA*

Variable, visit	No. (%) of subjects with variable		
	Accelerated KOA	Typical KOA	No KOA
Subchondral insufficiency fractures			
Visit −2	2 (2)	0 (0)	0 (0)
Visit −1	0 (0)	0 (0)	0 (0)
Index visit	3 (3)	0 (0)	0 (0)
Visit 1	0 (0)	0 (0)	0 (0)
Visit 2	0 (0)	0 (0)	0 (0)
Acute ligamentous injuries			
Visit −2	2 (2)	1 (2)	1 (1)
Visit −1	2 (2)	1 (1)	1 (1)
Index visit	2 (3)	1 (1)	1 (1)
Visit 1	0 (0)	2 (2)	1 (1)
Visit 2	0 (0)	1 (1)	0 (0)
Acute tendinous injuries			
Visit −2	0 (0)	0 (0)	0 (0)
Visit −1	1 (1)	0 (0)	0 (0)
Index visit	1 (1)	0 (0)	0 (0)
Visit 1	1 (1)	0 (0)	0 (0)
Visit 2	1 (3)	0 (0)	0 (0)
Other incidental findings			
Visit −2	1 (1)†	0 (0)	0 (0)
Visit −1	1 (1)‡	0 (0)	0 (0)
Index visit	1 (1)‡	0 (0)	1 (1)§
Visit 1	1 (1)‡	0 (0)	0 (0)
Visit 2	0 (0)	0 (0)	0 (0)

* Index visit is the visit at which the criteria for accelerated knee osteoarthritis (KOA) or typical KOA were met (or a matched time point for subjects with no KOA).
† Popliteus strain.
‡ Osteochondral lesion.
§ Tibial contusion.

and support our focus on destabilizing meniscal tears in the presence of a joint with greater preradiographic disease burden than subjects with typical KOA.

Jeffrey B. Driban, PhD [iD]
Matthew S. Harkey, PhD [iD]
Robert J. Ward, MD
Tufts Medical Center
Boston, MA
Grace H. Lo, MD, MSc
Baylor College of Medicine
Houston, TX
James W. MacKay, MRCP, FRCR
University of Cambridge
Cambridge, UK
Timothy E. McAlindon, MD, MPH
Tufts Medical Center
Boston, MA

1. Bedi A, Kelly N, Baad M, Fox AJ, Ma Y, Warren RF, et al. Dynamic contact mechanics of radial tears of the lateral meniscus: implications for treatment. Arthroscopy 2012;28:372–81.

2. Bedi A, Kelly NH, Baad M, Fox AJ, Brophy RH, Warren RF, et al. Dynamic contact mechanics of the medial meniscus as a function of radial tear, repair, and partial meniscectomy. J Bone Joint Surg Am 2010;92:1398–408.

3. LaPrade CM, Jansson KS, Dornan G, Smith SD, Wijdicks CA, LaPrade RF. Altered tibiofemoral contact mechanics due to lateral meniscus posterior horn root avulsions and radial tears can be restored with in situ pull-out suture repairs. J Bone Joint Surg Am 2014;96:471–9.

4. Padalecki JR, Jansson KS, Smith SD, Dornan GJ, Pierce CM, Wijdicks CA, et al. Biomechanical consequences of a complete radial tear adjacent to the medial meniscus posterior root attachment site: in situ pull-out repair restores derangement of joint mechanics. Am J Sports Med 2014;42:699–707.

5. Badlani JT, Borrero C, Golla S, Harner CD, Irrgang JJ. The effects of meniscus injury on the development of knee osteoarthritis: data from the Osteoarthritis Initiative. Am J Sports Med 2013;41:1238–44.

6. Jones RS, Keene GC, Learmonth DJ, Bickerstaff D, Nawana NS, Costi JJ, et al. Direct measurement of hoop strains in the intact and torn human medial meniscus. Clin Biomech (Bristol, Avon) 1996;11:295–300.

7. Englund M, Guermazi A, Gale D, Hunter DJ, Aliabadi P, et al. Incidental meniscal findings on knee MRI in middle-aged and elderly persons. N Engl J Med 2008;359(11):1108–15.

Assessing cardiovascular risk in patients with antineutrophil cytoplasmic antibody–associated vasculitis: comment on the article by Wallace et al

To the Editor:

In a post hoc analysis of the Rituximab for Antineutrophil Cytoplasmic Antibody (ANCA)–Associated Vasculitis (RAVE) trial, Wallace and colleagues evaluated changes in serum lipid levels following initiation of remission induction therapy in 142 patients with ANCA-associated vasculitis (AAV) (1). Levels of total cholesterol, low-density lipoprotein, and apolipoprotein B increased significantly from baseline to month 6. These changes were independent of treatment with either rituximab or cyclophosphamide/azathioprine, did not correlate with glucocorticoid exposure, and were observed among newly diagnosed and proteinase 3 (PR3)–ANCA–positive subjects but not among patients with relapsing disease or myeloperoxidase (MPO)–ANCA positivity. The authors suggested that changes in lipid profile in AAV may vary according to disease phase (e.g., new versus relapsing) as well as ANCA type and may reflect differences in inflammatory states between the subsets of patients.

An increased risk of cardiovascular disease (CVD) in patients with AAV is well established. A recent meta-analysis of observational studies comprising almost 14,000 AAV patients showed an increase in relative risk of 65% for all CV events, 60% for ischemic heart disease, and 20% for cerebrovascular accidents (2). Inflammation plays a key role in all stages of atherosclerosis (3) and apparently contributes to CV morbidity and mortality in patients with AAV and other inflammatory disorders. Moreover, the Canakinumab Antiinflammatory Thrombosis Outcome Study clearly demonstrated a direct benefit of targeting inflammation on outcomes among patients with established atherosclerotic disease who have already survived a myocardial infarction (4).

Nevertheless, the negative impact of inflammation on CV risk in patients with AAV should not be overestimated, particularly in view of currently available treatments. Intensive immunosuppressive therapy rapidly results in complete or near-complete resolution of inflammatory activity, and prolonged remission maintenance treatment prevents disease relapses in the majority of patients. In this setting, the accumulation of traditional risk factors induced by prolonged glucocorticoid exposure seems to offer a more plausible explanation for an increased incidence of CVD in patients with AAV.

In a cross-sectional study, Houben et al conducted a comprehensive assessment of CV risk in 144 patients with established AAV (mean disease duration 7.0 years) (5). The mean estimated 10-year risk for CVD (as identified in the Framingham Heart Study) was 19%. Hypertension and dyslipidemia were present in 72% and 69% of patients, respectively. Of note, 25% of the patients had an indication for lipid-lowering or antihypertensive therapy but were either not treated or not treated to a target level.

In our cohort of 268 patients with AAV (mean disease duration 5 years), dyslipidemia and other CV risk factors such as arterial hypertension, overweight/obesity, and smoking history were also highly prevalent, both in PR3-ANCA–positive and MPO-ANCA–positive patients with AAV (Table 1). There was a trend toward a higher prevalence of dyslipidemia in patients with PR3-ANCA compared to those with MPO-ANCA. However, this difference was clinically insignificant given the high occurrence of lipid disorders in both groups and could also be explained by confounding factors, such as a longer disease duration or a higher prevalence of obesity in PR3-ANCA–positive patients. Therefore, in the long term, MPO-ANCA–positive and PR3-ANCA–positive patients showed a similar predisposition to lipid profile changes.

Suppiah et al reviewed CV outcomes during a long-term follow-up of 535 AAV patients in 4 European Vasculitis Study Group trials (6). In that study, PR3-ANCA was associated with a reduced CV risk compared to MPO-ANCA or negative ANCA status (odds ratio 0.39 [95% confidence interval 0.20–0.74]). Therefore, in the study by Wallace and colleagues (1), changes in lipid parameters during remission induction therapy that were limited to PR3-ANCA–positive patients and newly diagnosed patients did not indicate that future dyslipidemia or CV events would be avoided in MPO-ANCA–positive patients or in those with relapsing disease.

In summary, Wallace and colleagues' study illustrated an important association between disease activity, ANCA specificity, and changes in lipid levels in patients with AAV. However, previous outcome data from randomized controlled trials in patients with AAV showed that CVD was one of the leading causes of death only after the first year of follow-up, and that within the first year of follow-up, patients usually died of infection and active vasculitis

Table 1. Prevalence of cardiovascular risk factors in patients with antineutrophil cytoplasmic antibody–associated vasculitis*

Characteristic	Overall (n = 268)	PR3-ANCA (n = 161)	MPO-ANCA (n = 107)	P†
Male sex	94 (35.1)	62 (38.5)	32 (29.9)	0.150
Age at onset, mean ± SD years	45.3 ± 16.9	45.1 ± 16.4	45.6 ± 17.9	0.820
Duration of follow-up, median (IQR) months	62 (21–99)	71 (29–106)	48 (15–95)	0.023
GPA	163 (60.8)	133 (82.6)	30 (28.0)	–
MPA	80 (29.9)	24 (14.9)	56 (52.3)	–
EGPA	25 (9.3)	4 (2.5)	21 (19.6)	–
BVAS at diagnosis, median (IQR)	18 (11–23)	18 (11–25)	16 (12–21)	0.240
Dyslipidemia‡	159 (59.3)	103 (64.0)	56 (52.3)	0.075
Hypertension	171 (63.8)	111 (68.9)	60 (56.1)	0.038
Current or past smoker	44 (16.4)	30 (18.6)	14 (13.1)	0.240
BMI, mean ± SD kg/m^2	26.8 ± 5.6	26.7 ± 5.3	26.0 ± 6.1	0.150
BMI 25–29.9 kg/m^2	69 (25.7)	50 (31.1)	19 (17.8)	0.016
BMI ≥30 kg/m^2	52 (19.4)	35 (21.7)	17 (15.9)	0.270

* Except where indicated otherwise, values are the number (%). Proteinase 3 = PR3; ANCA = antineutrophil cytoplasmic antibody; MPO = myeloperoxidase; IQR = interquartile range; GPA = granulomatosis with polyangiitis; MPA = microscopic polyangiitis; EGPA = eosinophilic granulomatosis with polyangiitis; BVAS = Birmingham Vasculitis Activity Score; BMI = body mass index.
† By Fisher's 2-tailed exact test, Mann-Whitney U test, or *t*-test as appropriate.
‡ Defined as total cholesterol >5 mmoles/liter and/or treatment with statins.

(7). It seems that short-term changes in lipid parameters that are reversible in a proportion of cases do not pose an immediate threat to a patient. We suggest that CV risk be stratified during remission of AAV, when persistence of dyslipidemia and/or other risk factors would more realistically estimate the probability of future CV outcomes and the need for prolonged (lifelong) lipid-lowering treatment. This is particularly true in young patients with AAV who have low risk of CVD. Notably, venous thromboembolic events in patients with AAV are clearly related to inflammation and usually develop during periods of disease activity (8).

Sergey Moiseev, MD (iD)
*Sechenov First Moscow State Medical University
   and Lomonosov Moscow State University*
Pavel Novikov, MD
Nikolai Bulanov, MD
Sechenov First Moscow State Medical University
Anastasiia Zykova, MD
*Sechenov First Moscow State Medical University
   and Lomonosov Moscow State University*
Elizaveta Safonova, MD
*Lomonosov Moscow State University
Moscow, Russia*

1. Wallace ZS, Fu X, Liao K, Kallenberg CG, Langford CA, Merkel PA, et al. Disease activity, antineutrophil cytoplasmic antibody type, and lipid levels in antineutrophil cytoplasmic antibody–associated vasculitis. Arthritis Rheumatol 2019;71:1879–87.
2. Houben E, Penne EL, Voskuyl AE, van der Heijden JW, Otten RH, Boers M, et al. Cardiovascular events in anti-neutrophil cytoplasmic antibody-associated vasculitis: a meta-analysis of observational studies. Rheumatology (Oxford) 2018;57:555–62.
3. Libby P, Okamoto Y, Rocha VZ, Folco E. Inflammation in atherosclerosis: transition from theory to practice. Circ J 2010;74:213–20.
4. Ridker PM, Everett BM, Thuren T, MacFadyen JG, Chang WH, Ballantyne C, et al, for the CANTOS Trial Group. Antiinflammatory therapy with canakinumab for atherosclerotic disease. N Engl J Med 2017;377:1119–31.
5. Houben E, Mendel A, van der Heijden JW, Simsek S, Bax WA, Carette S, et al. Prevalence and management of cardiovascular risk factors in ANCA-associated vasculitis. Rheumatology (Oxford) 2019. E-pub ahead of print.
6. Suppiah R, Judge A, Batra R, Flossmann O, Harper L, Höglund P, et al. A model to predict cardiovascular events in patients with newly diagnosed Wegener's granulomatosis and microscopic polyangiitis. Arthritis Care Res (Hoboken) 2011;63:588–96.
7. Flossmann O, Berden A, de Groot K, Hagen C, Harper L, Heijl C, et al, for the European Vasculitis Study Group. Long-term patient survival in ANCA-associated vasculitis. Ann Rheum Dis 2011;70:488–94.
8. Novikov P, Makarov E, Moiseev S, Meshkov A, Strizhakov L. Venous thromboembolic events in systemic vasculitis. Ann Rheum Dis 2015;74:e27.

Reply

To the Editor:

We thank Dr. Moiseev and colleagues for their comments regarding lipid levels in AAV. We would like to further discuss the assessment of CV risk in AAV as well as the need for more studies in this field. We agree that there are multiple factors that contribute to the increased risk of CVD in AAV, including inflammation and comorbidities associated with treatment (e.g., hypertension, diabetes). However, the relative impact of inflammation versus comorbidities on excess CVD risk in AAV is unknown, and we do not believe either factor can be overestimated.

We agree that contemporary treatment regimens often lead to effective control of AAV, but it is unknown what effect severe acute inflammation, even over a short time period, has on long-term CVD risk. Moreover, many patients with AAV face delays in diagnosis and treatment initiation, which may leave them exposed to inflammation for prolonged periods of time (1,2). As such, inflammation may play a more important role in CVD risk than suggested by Moiseev et al.

Moiseev and colleagues cite their work and that of others highlighting the burden of CVD risk factors (e.g., hypertension, diabetes, dyslipidemia) in AAV cohorts. We agree that managing these comorbidities is important for improving long-term outcomes in AAV. However, additional studies are needed to understand how these factors differ between patients with and those without AAV and how the differences in risk factor burden might explain the excess risk of CVD associated with AAV.

Given the increased risk of CVD associated with AAV, there are recommendations to periodically estimate this risk using available calculators (e.g., the Framingham Risk Score) (3). However, these risk calculators have not been validated in AAV patients and are known to underestimate risk in patients with other inflammatory conditions (e.g., rheumatoid arthritis) (4). They should be used with caution in AAV pending further studies to assess their performance in this population.

Our study provides important context for the interpretation of lipid measurements in AAV during remission induction. The changes in lipid measurements that occur during remission induction likely make any single lipid measurement during this period an unreliable indicator of future CVD risk (5). Moiseev et al suggest that lipids should be assessed during remission. However, it is unknown whether lipid measurements during remission accurately reflect CVD risk. It is also unknown if lipid metabolism normalizes during AAV remission, either with or without immunosuppression.

Finally, we would like to clarify the potential significance of changes in lipid measurements. The reduction in lipids such as low-density lipoprotein (LDL) cholesterol during acute inflammation does not suggest a reduced risk of CVD. Rather, the association of total cholesterol and LDL cholesterol levels with CVD risk may be "J-shaped," such that lower levels are actually associated with relatively greater CVD risk compared with mid-range levels (5,6). As such, the lack of change in lipid levels in MPO-ANCA–positive patients during remission induction should not be interpreted as suggesting that MPO-ANCA–positive patients are at a lower risk of CVD. Our results are not inconsistent, therefore, with the work published by Suppiah and colleagues (7).

As immunosuppressive regimens for AAV become increasingly effective, attention must shift toward addressing the complications of the disease and its treatment. CVD is a leading cause of death in AAV, so efforts to understand the relative impact of inflammation and comorbidities on CVD outcomes are critical to further improving outcomes.

Zachary S. Wallace, MD, MSc [iD]
John H. Stone, MD, MPH
Massachusetts General Hospital
and Harvard Medical School
Boston, MA

1. Poulton CJ, Nachman P, Hu Y, McGregor JG, Jennette JC, Falk RJ, et al. Pathways to renal biopsy and diagnosis among patients with ANCA small-vessel vasculitis. Clin Exp Rheumatol 2013;31 Suppl 75:S32–7.
2. Abdou NI, Kullman GJ, Hoffman GS, Sharp GC, Specks U, McDonald T, et al. Wegener's granulomatosis: survey of 701 patients in North America: changes in outcome in the 1990s. J Rheumatol 2002;29:309–16.
3. Yates M, Watts RA, Bajema IM, Cid MC, Crestani B, Hauser T, et al. EULAR/ERA-EDTA recommendations for the management of ANCA-associated vasculitis. Ann Rheum Dis 2016;75:1583–94.
4. Arts EE, Popa C, Den Broeder AA, Semb AG, Toms T, Kitas GD, et al. Performance of four current risk algorithms in predicting cardiovascular events in patients with early rheumatoid arthritis. Ann Rheum Dis 2015;74:668–74.
5. Myasoedova E, Crowson CS, Kremers HM, Roger VL, Fitz-Gibbon PD, Therneau TM, et al. Lipid paradox in rheumatoid arthritis: the impact of serum lipid measures and systemic inflammation on the risk of cardiovascular disease. Ann Rheum Dis 2011;70:482–7.
6. Liao KP, Liu J, Lu B, Solomon DH, Kim SC. Association between lipid levels and major adverse cardiovascular events in rheumatoid arthritis compared to non–rheumatoid arthritis patients. Arthritis Rheumatol 2015;67:2004–10.
7. Suppiah R, Judge A, Batra R, Flossmann O, Harper L, Höglund P, et al. A model to predict cardiovascular events in patients with newly diagnosed Wegener's granulomatosis and microscopic polyangiitis. Arthritis Care Res (Hoboken) 2011;63:588–96.

ACR Announcements

ACR Meetings

Winter Rheumatology Symposium
    January 25–31, 2020, Snowmass

State-of-the-Art Clinical Symposium
    March 27–29, 2020, New Orleans

Pediatric Rheumatology Symposium
    April 29–May 2, 2020, New Orleans

For additional information, contact the ACR office.

ACR 2020 Winter Rheumatology Symposium

The 2020 Winter Rheumatology Symposium boasts a carefully crafted program that provides a unique blend of world-class lectures and interactive sessions in an intimate setting, allowing for quality interactions with peers and experts in the field. The symposium will provide attendees with a well-rounded view of the latest advances in the discipline. Highlights for this annual event include the interactive panel discussion on therapy, with Bonnie Bermas, MD, Christopher Ritchlin, MD, MPH, Joel Kremer, MD, and Michael Weinblatt, MD. Back by popular demand will be the Points-on-Joints session, presented in the "thieves' market" format and providing a series of interesting, difficult, or puzzling rheumatologic cases via 10-minute summaries followed by audience discussion. Registration and housing for the 2020 Winter Rheumatology Symposium are limited, so be sure to register by the advance deadline of January 8, 2020, and book your hotel room by December 15, 2019. For additional information and to register, visit www.rheumatology.org/Learning-Center/Educational-Activities.

ACR 2020 State-of-the-Art Clinical Symposium

Join the ACR in New Orleans for rheumatology's premier weekend symposium, complete with cutting-edge clinical best practices and emerging trends, without taking time from work! What's new in 2020? The first full day of the 2020 meeting kicks off with a wellness yoga session to help you avoid physician burnout and get a healthy jumpstart to the weekend. Cap off the day in New Orleans style with Cocktails & Cases, an event designed to encourage discussion and networking. You'll also be able to participate in a lively panel discussion after each group session. Experience the exceptional educational programs yourself, March 27–29 in New Orleans, LA. Early-bird registration ends January 9, and advance registration ends March 11. After March 11, you may register on-site. To take advantage of special housing rates, reserve your room by March 6. Visit rheumatology.org/Learning-Center/Educational-Activities to learn more and register.

ACR 2020 Pediatric Rheumatology Symposium

Join your pediatric colleagues from across the country at the Pediatric Rheumatology Symposium (PRSYM), a scientific meeting dedicated exclusively to pediatric rheumatology. In 2020, PRSYM is being held in New Orleans for the first time ever! The most cutting-edge pediatric rheumatology research will be on display in the poster hall, where a variety of abstracts will provide enlightening content to bring back to your team. Get an interactive learning experience with panel discussions, as well as several key networking opportunities. Take part in the exciting educational programs, April 29–May 2 in New Orleans. Register by March 4 for early-bird rates or by April 15 for advance registration rates, or register on-site. Reserve your room early to take advantage of special rates (until April 8). Visit rheumatology.org/Learning-Center/Educational-Activities to learn more and register.

Education Programs

6th Systemic Sclerosis World Congress. March 5–7, 2020, Prague, Czech Republic. The Systemic Sclerosis World Congress boasts an eclectic mix of interactive opportunities for attendees, including hands-on workshops; lectures, and discussions between physicians, medical staff, and patients; oral presentations; and satellite sessions. Lectures will be given in English but will be translated into major audience languages, and some topics will be covered in different languages in smaller groups. The broad scope of the Congress includes, among other topics, developments in scleroderma treatments, an update on major research projects, and how to treat pain in digital ulcers. Smaller groups will examine more specific topics, including juvenile scleroderma and the impact of scleroderma on sexual life. Registration fees are €760 (December 3–February 17) and €830 (February 18–onsite) for physicians; €300 (December 3–February 17) and €365 (February 18–onsite) for fellows, basic scientists, and health professionals; and €180 (December 3–February 17), and €240 (February 18–onsite) for students. For additional information, e-mail worldssclerodermafoundation@gmail.com or visit the web site http://worldsclerofound.org/systemic-sclerosis-world-congress/.